TP 15546E

Characterization of Canadian Marine Vessel Operational Profiles and Hybrid Electric Propulsion System Modelling Tool Improvement for GHG and Ship Noise Reduction

Prepared for
Innovation Centre of Transport Canada

Prepared by
UVic Clean Transportation and Glas Ocean Research Teams

Zuomin Dong (PI)
Department of Mechanical Engineering
Institute for Integrated Energy Systems
University of Victoria

December 31, 2019

TP 15546E

Characterization of Canadian Marine Vessel Operational Profiles and Hybrid Electric Propulsion System Modelling Tool Improvement for GHG and Ship Noise Reduction

Prepared by

UVic Clean Transportation and Glas Ocean Research Teams

Zuomin Dong (PI)

Department of Mechanical Engineering

Institute for Integrated Energy Systems

University of Victoria

December 31, 2019

This report reflects the views of the authors and not necessarily the official views or policies of the Transportation Innovation Centre of Transport Canada or the co-sponsoring organizations.

The Transport Canada's Innovation Centre and the co-sponsoring agencies do not endorse products or manufacturers. Trade or manufacturers' names appear in this report only because they are essential to its objectives.

Since some of the accepted measures in the industry are imperial, metric measures are not always used in this report.

PROJECT TEAM:

- **Principal Investigator**: Zuomin Dong
- **Principal Researcher**: Peter Oshkai and Sue Molloy
- **Team Members**: Helen Bailey, Kevin Andersen (now at Seaspan), Lily Li Chen, Huachao Dong, Yanbiao Feng, Michael Grant, Dylan Iverson, Jiajun Liu, Duncan William McIntyre, Babak Manouchehrinia, Mostafa Rahimpour, Anthony Truelove, Alex Haijia Zhu, and Hubert Hongbo Zhu (now at AVL).

Transport Canada Transports Canada

PUBLICATION DATA FORM

1. Transport Canada Publication No.	2. Project No.	3. Catalogue No.	4. ISBN
TP 15546E	-	T89-20/2022E-PDF	978-0-660-46120-5

5. Title and Subtitle	6. Publication Date
Characterization of Canadian Marine Vessel Operational Profiles and Hybrid Electric Propulsion System Modelling Tool Improvement for GHG and Ship Noise Reduction	December 2019
	7. Performing Organization Document No. --
8. Author(s)	9. Transport Canada File No.
Zuomin Dong, Peter Oshkai, etc. and Sue Molloy (GOE)	--
10. Performing Organization Name and Address	11. PWGSC File No.
Department of Mechanical Engineering University of Victoria Victoria, BC, Canada, V8W 2Y2 Tel: 250-721-8693 Fax: 250-721-6051 Email: zdong@uvic.ca	--
	12. PWGSC or Transport Canada Contract No. T8156-160094
13. Sponsoring Agency Name and Address	14. Type of Publication and Period Covered Final
Innovation Centre 330 Sparks Street Ottawa, Ontario K1A 0N5	15. Project Officer J. O'Reilly

16. Supplementary Notes (Funding programs, titles of related publications, etc.)

17. Abstract

This report summarizes the work carried out by the University of Victoria (UVic) Clean Transportation Research Team and Glas Ocean Ltd. (under a subcontract) between November 1, 2016, and March 31, 2018. First, the joint team has completed the development of operation profiles for representative Canadian coastal vessels, including passenger and vehicle ferry ships, tugboats, and fishing boats using information and data drawn from dedicated data acquisition systems, ship sensors, controller area bus, etc. Based upon these operation profiles, the fuel consumption, greenhouse gas emissions, and lifecycle cost reduction potentials of diesel/natural gas engine hybrid electric and pure electric propulsion systems were identified. These quantitative analyses have been carried out through eight comprehensive case studies on the targeted marine vessels, using our integrated hybrid electric marine propulsion system modelling tools. Extensions of these integrated modelling tools include additions of natural gas engine efficiency and emission models for new integrated NG engine hybrid electric propulsion system, battery performance degradation model for lifecycle cost modelling and analyses, models of key hybrid powertrain components, model of marine weather state (MWS), and models of AC and DC power buses. The report also includes improvements to the induced propeller cavitation noise models by including experimental validation, and model simplification efforts to incorporate ship noise considerations into propulsion system design and operation control.

18. Key Words	19. Distribution Statement
Marine Vessel Operational Profiles, Hybrid Electric Propulsion System, Integrated Modelling Tools, NG Hybrid, Ship Noise Modelling and Reduction	Digital Copy

20. Security Classification (of this publication)	21. Security Classification (of this page)	22. Declassification (date)	23. No. of Pages	24. Price
Unclassified	Unclassified	—	xxiv, 82, apps	-

Canada

Transports Canada Transport Canada

FORMULE DE DONNÉES POUR PUBLICATION

1. No de la publication de Transports Canada	2. Nº de l'étude	3. Nº de catalogue	4. No de catalogue du destinataire / ISBN
TP 15546E	-	T89-20/2022E-PDF	978-0-660-46120-5

5. Titre et sous-titre	6. Date de la publication
Caractérisation des profils opérationnels des navires canadiens et amélioration des outils de modélisation des systèmes de propulsion électrique hybride pour la réduction des GES et du bruit des navires	décembre 2019
	7. No de document de l'organisme exécutant --
8. Auteur(s)	9. No de dossier - Transports Canada
Zuomin Dong, Peter Oshkai, etc. and Sue Molloy (GOE)	--
10. Nom et adresse de l'organisme exécutant	11. No de dossier - TPSGC
Department of Mechanical Engineering University of Victoria Victoria, BC, Canada, V8W 2Y2 Tel: 250-721-8693 Fax: 250-721-6051 Email: zdong@uvic.ca	--
	12. No de contrat - TPSGC ou Transports Canada T8156-160094
13. Nom et adresse de l'organisme parrain	14. Genre de publication et période visée
Centre d'innovation de Transports Canada 800 René Lévesque Blvd. West Suite 600 Montreal, Quebec H3B 1X9	Finale
	15. Agent de projet J. O'Reilly

16. Remarques additionnelles (programmes de financement, titres de publications connexes, etc.)

17. Résumé

Ce rapport résume le travail entrepris par l'équipe de recherche sur le transport propre de l'Université de Victoria (UVic) et de Glas Ocean Ltd. (sous-traitance), qui s'est déroulé entre le 1er novembre 2016 et le 31 mars 2018. Premièrement, l'équipe de recherche a terminé l'élaboration de profil d'exploitation pour des navires côtiers canadiens représentatifs (tels que des transbordeurs de passagers et de véhicules, des remorqueurs, et des bateaux de pêche) à l'aide d'informations et de données extraites de systèmes d'acquisition de données spécialisés, de capteurs, de bus de données CAN, etc. Sur la base de ces profils d'exploitation, la consommation de carburant, les émissions de gaz à effet de serre et les potentiels de réduction des coûts reliés aux cycles de vies des systèmes de propulsion exclusivement électriques et hybrides électriques-diesel/gaz naturel (GN) ont été identifiés. Ces analyses quantitatives ont été réalisées au moyen de huit études de cas complètes sur les navires ciblés à l'aide de nos outils de modélisation de systèmes de propulsion hybrides électriques intégrés. Les extensions de ces outils de modélisation intégrés incluent des ajouts de modèles d'efficacité et d'émissions pour le nouveau système de propulsion hybride électrique-GN, un modèle de dégradation des performances d'une batterie pour la modélisation et l'analyse du coût du cycle de vie, des modèles de composants clés du groupe propulseur hybride, un modèle de l'état de la météo marine et des modèles de bus d'alimentation en courant alternatif et continu. Les améliorations apportées aux modèles de bruit de cavitation d'hélice des navires incluent leurs efforts de validation expérimentale et de simplification des modèles afin d'intégrer la prise en compte du bruit des navires dans la conception et le contrôle de l'exploitation des systèmes de propulsion.

18. Mots clés	19. Diffusion
Profils opérationnels des navires, système de propulsion électrique hybride, outils de modélisation intégrés, GN hybride, modélisation et réduction du bruit des navires.	Copie numérique

20. Classification de sécurité (de cette publication)	21. Classification de sécurité (de cette page)	22. Déclassification (date)	23. Nombre de pages	24. Prix
Non classés	Non classés	-	xxiv, 82, apps	--

Canada

ACKNOWLEDGEMENTS

The work is part of our continuing research supported by the Clean Transportation Initiative of Transport Canada, as well as our on-going research collaborations with BC Ferris, Robert Allan Ltd, Seaspan, and several other leading Canadian marine engineering and service providers.

The work would not be possible without strong support from the Transportation Development Centre of Transport Canada. Tabitha Takeda, Research Development Officer, has provided treasured guidance, advice and continuous support; and Jordan O'Reilly, Project Officer and Engineer, and Denis Tran, Co-op Intern, have provided valuable inputs to the improvements of this report. Financial supports from Transport Canada are gratefully acknowledged.

Many industrial and institutional collaborators have also provided extensive assistance to this work through special arrangements, and by sharing their expertise and experiences. They include Bruce Paterson, William Russell, Bob Kearney, Andre Bosveld, François Cambron, Dan Scott, Wayne Fu, and Cliff Provost at BC Ferries; Vince den Hertog, Brendan Smoker and Robin Stapleton at Robert Allan Ltd.; Ryan Nicoll at Dynamic Systems Analysis; Michaël Gagné at Techsol Marine; Michele Viviani at University of Genoa; and the Nova Scotia Boat Builders Association.

Kevin Andersen, a previous member of the team and now working at Seaspan, has done the groundwork on ship operation pattern and integrated marine propulsion system modelling, and tutored many team members.

EXECUTIVE SUMMARY

This report summarizes the work carried out by the University of Victoria (UVic) Clean Transportation Research Team and Glas Ocean Ltd. (under a subcontract), between November 1, 2016, and March 31, 2018, under a research contract from Public Works (Innovation Centre of Transport Canada).

Operation profiles were developed for three types of representative coastal vessels: passenger and vehicle ferries, tugboats, and fishing boats. These operation profiles were developed using information and data drawn from both dedicated data acquisition systems and vessel documentation. The work has also focused on improvements and extensions of the new integrated hybrid electric marine vessel model based design and optimization tool (HEMV-MBDOT) platform. Specifically, these major extensions include modularization of different functional modules of the integrated system model, additions of many key hybrid electric powertrain component models, the ability to model various powertrain system architectures with DC or AC power buses, and incorporation of system design and control optimization using the integrated hybrid electric marine propulsion system model. Furthermore, model validations using experimental data have been carried out to improve model accuracy; this includes validation of the propeller cavitation noise and ship propulsion models. Full-scale Computational Fluid Dynamics (CFD) simulation models have been validated using experimental data. Among the many newly added powertrain system component models, this work includes the addition of ground-breaking power performance, energy efficiency, and emission models for heavy-duty diesel and natural gas (NG) diesel dual-fuel engines, as well as performance degradation and life-cycle cost models for the Lithium-ion battery. The work made high-fidelity performance, emission, and life cycle cost modelling, as well as design optimization of diesel/NG hybrid and pure-electric vessels, possible.

Using the expanded integrated hybrid electric marine propulsion system modelling tools, as well as the newly introduced vessel operation profile models, the performance, fuel consumption, greenhouse gas emission, and life-cycle cost improvement potentials of various clean marine propulsion solutions have been examined through eight case studies based on real marine vessels and their operation data. These clean marine propulsion solutions include hybrid electric and plug-in hybrid electric powertrains with diesel or NG engines in series and parallel configurations, and pure-electric vessels using stored energy from the power grid. Traditional marine propulsion technologies using diesel-mechanical or diesel-electric powertrains were used as benchmarks for these studies.

The generation of optimized control rules for the hybrid electric powertrain system, as well as the optimal sizing of key powertrain components, was carried out using dynamic programming and advanced global optimization tools developed by the UVic team. This undertaking resulted in the creation of several effective methods for applying optimization to electrified marine propulsion system development in particular.

This work provides a better understanding of a systematic approach to, and essential enabling techniques for designing and developing cleaner marine propulsion systems.

SOMMAIRE

Ce rapport résume les travaux réalisés par l'équipe de recherche sur les transports propres de l'Université de Victoria (UVic) et Glas Ocean Ltd. (en sous-traitance), entre le 1er novembre 2016 et le 31 mars 2018, dans le cadre d'un contrat de recherche de Travaux publics (Centre d'innovation de Transports Canada).

Des profils d'exploitation ont été élaborés pour trois types de navires côtiers représentatifs : les traversiers pour passagers et véhicules, les remorqueurs et les bateaux de pêche. Ces profils d'exploitation ont été élaborés à l'aide de renseignements et de données provenant à la fois de systèmes spécialisés et de la documentation relative aux navires. Dans leurs travaux, l'équipe de recherche s'est également concentrée sur des façons d'améliorer et de renforcer le modèle pour les navires hybrides électriques en fonction de l'outil de conception et d'évaluation (HEMV-MBDOT). L'équipe s'est entre autres penchée sur l'établissement de différents modules fonctionnels pour le modèle de système intégré, l'ajout de nombreux modèles de composants clés de groupes motopropulseurs électriques hybrides, la possibilité de modéliser diverses architectures de groupes motopropulseurs avec des circuits d'alimentation en courant continu ou alternatif, et l'optimisation de la conception et du contrôle du système à l'aide du modèle de système de propulsion marine électrique hybride intégré. En outre, des vérifications ont été effectuées à partir de données expérimentales afin d'améliorer la précision des modèles, notamment la validation des modèles relatifs au bruit des hélices et à la propulsion des navires. Les modèles de simulation grandeur nature de la dynamique des fluides ont été validés à l'aide de données expérimentales. L'équipe a aussi ajouté des modèles novateurs d'évaluation du rendement, de l'efficacité énergétique et des émissions pour les moteurs diesel lourds et les moteurs bicarburants au gaz naturel (GN), ainsi que des modèles d'évaluation de la dégradation du rendement et de calcul du coût du cycle de vie pour les batteries lithium-ion. Les travaux réalisés par l'équipe ont permis de modéliser avec précision le rendement, les émissions et les coûts des différents moteurs durant l'ensemble de leur cycle de vie, ainsi que d'améliorer la conception des navires hybrides diesel/gaz naturel et des navires purement électriques.

À l'aide des outils intégrés de modélisation des systèmes de propulsion marine hybrides et électriques, ainsi que de nouveaux modèles de profil d'exploitation des navires, l'équipe s'est penchée sur les améliorations possibles pour ce qui est du rendement, de la consommation de carburant, des émissions de gaz à effet de serre et du coût du cycle de vie de diverses solutions de propulsion marine propre dans le cadre de huit études de cas basées sur des navires réels et leurs données d'exploitation. Les solutions de propulsion marine propre comprennent des groupes motopropulseurs électriques hybrides et hybrides rechargeables avec des moteurs diesel ou au gaz naturel dans des configurations en série et en parallèle, ainsi que des navires purement électriques utilisant l'énergie stockée du réseau électrique. Les technologies traditionnelles de propulsion marine utilisant des groupes motopropulseurs diesel-mécaniques ou diesel-électriques ont servi de référence pour ces études.

L'élaboration de règles de contrôle optimisées pour le système de propulsion électrique hybride, ainsi que le calibrage optimal des principaux composants du groupe motopropulseur, ont été réalisés par l'équipe de l'UVic à l'aide de la programmation dynamique et d'outils avancés. Cette initiative a mené à la création de plusieurs méthodes efficaces d'application de solutions optimisées, en particulier pour le développement de systèmes de propulsion électrique.

Les travaux effectués permettent de mieux comprendre l'approche systématique et les techniques essentielles à la conception et au développement de systèmes de propulsion marine plus propres.

CONTENTS

L. Case Study for Skeena Queen - Optimal Design of Series Hybrid Marine Propulsion System with Li-ion Battery Performance Degradation and Life Cycle Cost Model

M. Case Study for Skeena Queen - Design of Parallel Hybrid Propulsion System

N. Case Study on BC Ferries' Tachek - Hybrid Electric Propulsion System Designs for Fuel Economy and Emission Improvements

O. Case Study for Klitsa - Modelling and Simulation of Hybrid Electric Ships with AC Power Bus

P. Case Study for Klitsa - Modelling and Simulation of Hybrid Electric Ships with DC Power Bus

Q. Case Study on Tugboats - Operation Profile Modelling and Benefits of Hybrid Electric Propulsion

R. Case Study on Fishing Boats - Emission and Life-Cycle Cost Analysis of Hybrid and Pure Electric Propulsion Systems

S. Generating Representative Drive/Load Cycles for Arbitrary Surface Vessels

T. UVic Global Optimization Program Toolbox

LIST OF FIGURES

LIST OF TABLES

GLOSSARY OF ACRONYMS AND ABBREVIATIONS

ABC	Artificial Bee Colony
ABS	American Bureau of Shipping
ADVISOR	Advanced Vehicle Simulator
AES	All Electric Ship
AMS	Alarm Monitoring System
AMT	Automatic Manual Transmission
ANL	Argonne National Laboratory
AC/DC	Alternating Current and Direct Current (Inverter / Rectifier)
ADN	Active Distribution Network
ARSM	Adaptive Response Surface Method
AVR	Automatic Voltage Regulators
BA	Bat Algorithm
BAS	Battery Alternator Starter
BCFS	British Columbia Ferry Services Inc.
BC Ferries	British Columbia Ferry Services Inc.
BESS	Battery Energy Storage System
BEV	Battery Electric Vehicle
BMS	Battery Management System
BSFC	Brake Specific Fuel Consumption
BV	Bureau Veritas
CAC	Criteria Air Contaminants
CAD	Computer-Aided Design
CAN	Controller Area Network
CC-CV	Constant Current – Constant Voltage
CFD	Computational Fluid Dynamics
CI	Compression Ignited
CIMarE	Canadian Institute of Marine Engineering
CiSMART	Canadian National Network for Innovative Shipbuilding/Marine Research and Training
CNC	Computer Numerical Control
CO	Carbon Monoxide

CO_2	Carbon Dioxide
CO_{2e}	Carbon Dioxide Equivalent
COG	Center of Gravity
COSIA	Canada's Oil Sands Innovation Alliance
CPM	Collaboration Pursuing Method
CPP	Controllable Pitch Propeller
CS	Cuckoo Search
DA	Data Acquisition
DBD	Disk Brake Design
DC/DC	Direct Current and Direct Current Converter
DE	Differential Evolution
DFN	Doyle-Fuller-Newman'
DG	Distributed Generation
DIRECT	Dividing Rectangles
DITEN	Department of Electrical, Electronic, Telecommunication Engineering and Naval Architecture
DOD	Depth of Discharge
DOE	Design of Experiment
DOF	Degree of Freedom
DOH	Degree of Hybridization
DP	Dynamic Programming
DR	Demand Response
DRE	Distributed Renewable Energy
DSA	Dynamic Systems Analysis
EBOP	Expensive Black-box Optimization Problem
ECM	Engine Control Module
ECMS	Equivalent Consumption Minimization Strategy
ECU	Electronic Control Unit
EEA	Energy and Environmental Analysis Inc.
EFD	Experimental Fluid Dynamics
EGR	Exhaust Gas Recirculation
EIS	Electrochemical Impedance Spectroscopy

EM	Electric Machines
EMV	Electric Marine Vessel
EP	Evolutionary Programming
EPA	Environmental Protection Agency (US)
EPC	Electric Power Converter
EREV	Extended Range Electric Vehicles
e-CVT	electronically controlled, continuous variable transmission
ES	Evolution Strategy
ESS	Energy Storage System
EV	Electric Vehicle
FB	Free Board
FCM	Fuel Consumption Map
FFA	Firefly Algorithm
FPA	Flower Pollination Algorithm
FOWT	Floating Offshore Wind Turbine
GA	Genetic Algorithm
GC	Geometric Container function
GDP	Gross Domestic Product
GHG	Greenhouse Gas
GN	Griewank Function
GNS	Graphene Nano-Sheets
GO	Global Optimization
GOE	Glas Ocean Engineering
GO Tools	Global Optimization Tool Library
GP	Goldstein and Price Function
GPS	Global Positioning System
GSA	Gravitational Search Algorithm
GTI	Gas Technology Institute
GTO	Gate Turn-off Thyristors
GWI	Global Warming Impact
GWO	Grey Wolf Optimization
GWP	Global Warming Potential

HAM	Hybrid Adaptive Metamodelling
HAMT	Hybrid Automated Manual Transmission
HC	Hydrogen Carbon
HDSR	Hierarchical Design Space Reduction
HEMV	Hybrid Electric Marine Vessel
HES	Hybrid Electric Ship
HESS	Hybrid Energy Storage System
HEV	Hybrid Electric Vehicle
HPDI	High-Pressure Direct Injected
HSOSR	Hybrid Surrogate-based Optimization using Space Reduction
ICE	Internal Combustion Engine
IES	Integrated Energy System
IGBT	Insulated Gate Bipolar Transistors
IGS	ICE-generator set
IMO	International Maritime Organization
IPCC	International Panel on Climate Change
IPS	Integrated Power System
ITTC	International Towing Tank Conference
K-BA	Kriging-Bat Algorithm
KMOO	Kriging-based multi-objective optimization
KPI	Key Performance Indicators
LCC	Life Cycle Cost
LFP	Lithium-iron phosphate
Li-ion	Lithium-Ion Battery
LMO	Lithium-Manganese Oxide
LNG	Liquefied NG
LTO	Lithium Titanate Oxide
MARPOL	International Convention for the Prevention of Pollution from Ships
MBD	Model Based Design
MBD-O	Model Based Design and Optimization
MBDOT	Model Based Design and Optimization Tool
MBGO	Metamodel-Based Global Optimization

MCC	Motor Control Center Units
MCU	Motor Control Unit
MDO	Marine Diesel Oil
M/G	Motor and/or Generator
MGO	Marine Gas Oil
MOGA	Multi-Objective Genetic Algorithms
MOSFET	Metal-Oxide-Semiconductor Field-Effect Transistor
MOO	Multi-Objective Optimization
MPS	Mode Pursuing Sampling
MSSE	Mixed Surrogates and Design Space Exploration
MSSR	Multi-Start Space Reduction
MWS	Marine Weather State
NCA	Nickel-Cobalt-Aluminum
Ni-MH	Nickel Metal Hydride Battery
NFE	Number of Function Evaluation
NG	Natural Gas
NMC	Nickel-Manganese-Cobalt
NO_x	Nitrogen Oxide
NRC	National Research Council
NREL	National Renewable Energy Laboratory
NURBS	Non-Uniform Rational Basic Spline
OCRE	Ocean, Coastal and River Engineering
OCV	Open Circuit Voltage
OEM	Original Equipment Manufacturer
OPTIP	Optimization Toolkit for Computationally Intensive Problems
PDOL	Product Design and Optimization Lab
PHEMV	Plug-in Hybrid Electric Marine Vessel
PHES	Plug-in Hybrid Electric Ship
PHEV	Plug-in Hybrid Electric Vehicle
PEMFC	Proton-Exchange Membrane Fuel Cell
PEMV	Pure Electric Marine Vessel
PEV	Pure Electric Vehicle

PID	Proportional–Integral–Derivative
PLM	Product Lifecycle Management
PM	Particulate Matter
PMS	Power Management System
PMSM	Permanent Magnet Synchronous Motors
PNGV	Partnership for a New Generation of Vehicle
P-Q	Active and Reactive Power
PSAT	Powertrain Systems Analysis Toolkit
PSO	Particle Swarm Optimization
PSP	Pareto Set Pursuing Method
PTI	Power Take-In
PTO	Power Take-Off
PV	photovoltaic
PVD	Pressure Vessel Design
RA	Robot Arm
RAL	Robert Allan Ltd.
RAO	Response Amplitude Operator
Raptures	Robert Allan Ltd: Powering Tugs for Real Energy Savings
RC	Resistor and Capacitor
RMS	Root-Mean-Squared
RP	Rectangular Parallelepiped
RPM	Revolutions per Minute
RTM	Rear Traction Motor
QRS	Quadratic Response Surface
SA	Simulated Annealing
SAE	Society of Automotive Engineers
SC	Supercapacitor
SCF	Six-hump Camel-back Function
SCR	Source Voltage Reverses
SEI	Solid Electrolyte Interphase
SEUMRE	Space Exploration and Unimodal Region Elimination
SFC	Specific Fuel Consumption

SG	Smart Grid
SKQ	Skeena Queen
SOx	Sulphur oxides
SOC	State of Charge
SOCE	Surrogate-based Optimization with Clustering-based Space Exploration
SOFC	Solid Oxide Fuel Cell
SPM	Single Particle Model
SRD	Speed Reducer Design
SS	Sea State
SSB	Ship Stability Book
TBD	Two-bar truss design
TO	Target Object
TSD	Tension / Compression Spring Design
UC	Ultracapacitor
UNFCCC	United Nations Framework Convention on Climate Change
US DOE	The U.S. Department of Energy
UVic	University of Victoria
VDR	Voyage Data Recorder
V-F	Voltage and Frequency
VFD	Variable-Frequency Drive
VSC	Voltage Source Converters
VSI	Voltage Source Inverter
VSP	Voith Schneider Propellers
WBD	Welded Beam Design
WCWI	West Coast Wave Initiative
WED	Canadian Western Economic Diversertification
WHO	World Health Organization

1 INTRODUCTION

1.1 Context

In recent years, all-electric and hybrid electric propulsion systems for marine vessels have seen increased levels of adoption. This trend has been driven by regulatory caps on emissions in harbours and offshore waters, with these regulations coming from regional and national governments and the International Maritime Organization (IMO), as well as fluctuating oil prices. Additional benefits that have encouraged adoption by industry include improved energy conversion efficiency, reduced Greenhouse Gas (GHG) emissions and ship induced noise, and in many cases, superior performance over traditional diesel propulsion systems.

Over the past decade, hybrid electric propulsion system technology has been developed and widely used to improve operation performance, energy efficiency, and GHG emissions reductions for ground vehicles. The hybrid vehicle's propulsion power demands are met by both an internal combustion engine (ICE) combined with an electric motor/generator (M/G) with a large battery energy storage system (ESS). These are coordinated by dedicated controls in the system controller, allowing the ICE and M/G to operate at their highly efficient operating points and to deliver the needed power through interconnected mechanical and electric drives. The system design and operation control of a hybrid electric propulsion system have an enormous range of possible solutions due to the mutual influence among key powertrain components and the different operation modes. This challenge led to the creation of standard vehicle driving cycles and integrated system modelling, or Model Based Design (MBD), methodology and industrial practice. Furthermore, the need to search for the optimal design and control solutions to achieve the best energy efficiency and emissions reduction of hybrid electric propulsion led to the further extension of MBD, to Model Based Design and Optimization (MBDO), which has been extensively studied by the Clean Transportation research team at the University of Victoria (UVic) in close collaborations with leading automotive and marine propulsion technology developers.

Marine propulsion presents some similarity to the propulsion of ground vehicles, but the application has its unique characteristics and challenges.

- Firstly, the operation profiles of marine vessels are much more diversified, since their propulsion power and energy demands do not only depend upon the travelling speed-based driving cycles of road vehicles. The more flexible sailing routes, different hull shapes and propulsion selection, varying displacement under changing cargo loads, and fluctuating marine weather conditions (ocean current, wave, wind and tides) lead to substantial variations in the needed propulsion power. The industry has recognized that one of the major factors that hinder the easy adoption of advanced propulsion technologies is the lack of representative load cycle data for different classes of vessels. Unlike the automotive industry, standardized marine drive cycles have not yet been developed, primarily because each vessel and its operating conditions are significantly different. However, it should be possible to develop common load characteristics for vessels in the same category, to serve as fundamental design requirements for developing the electric and hybrid electric propulsion systems and their controls.

- Secondly, the resistance and propulsion forces of a marine vessel are determined by hydrodynamic phenomena that are much more complex and variant than the drag and propulsion forces of road vehicles.
- Thirdly, many larger ships require considerable energy for propulsion and hotel loads, and several ICEs and M/Gs to meet these power demands, thus requiring an electric power generation and distribution network to operate. Optimized design and operation of the electric power bus in Alternating Current (AC) and/or Direct Current (DC) and AC/DC or DC/DC converters become important.
- Fourthly, the heavy-duty operation and/or large size of marine vessels have significant fuel consumption and produce a huge amount of emissions, making them ideal candidates for conversion to clean fuels, such as natural gas (NG), with conventional or hybrid electric propulsion. However, these lead to significant investment costs. The ability to predict accurate lifecycle cost and payback time of the new or retrofitted system and the quantitative assessment of fuel cost savings and emission reduction becomes essential for the wide commercialization of vessel electrification. Therefore, special technologies are needed to ensure the low-emission operation of an NG engine and to predict the performance degradation/operation life of a battery ESS under different use patterns. At present, NG engines suffer a number of weaknesses, including surged hydrocarbon (HC) emissions at low speed and load; and the performance degradation of batteries cannot be accurate predicted.
- Finally, ship induced ocean noise presents an additional form of transportation pollution, causing potential severe harm to marine life if not properly monitored and controlled. The predominant source of ship induced noise is the cavitation noise caused by cavitation on the ship's propeller at its off-design working conditions. In recent years, considerable efforts have been devoted to the monitoring and measurement of ship induced noise, but effective methods for predicting the occurrence of this noise, and reducing/eliminating it through proper ship propulsion system design and operation control have not yet been developed.

The marine industry has fallen behind the automotive industry in adopting clean propulsion technologies, due to the encountered complexity and uncertainties previously discussed. This is due to the huge technical challenges in solving these problems, and the heavy investment costs needed to build clean propulsion systems and to change the vessels' design and operation practices. Marine vessels are considerably different from each other, and made in very small batches. Unlike road vehicles with lower single-vehicle cost and mass production in millions, there is often no margin for design mistakes and no opportunity for *design-prototype-redesign* iterations. The design of the vessel's propulsion system and development of its operation control strategies have to be done correctly, ideally with optimal results, the first time and at each time.

1.2 Objective and Scope of the Project

The objective of this contract research is to address the issues stated in Section 1.1 and establish a new path for an innovative and technological robust solution. This is performed through the detailed study of representative marine vessels, development of essential software modelling analysis and simulation tools for hybrid and electric marine propulsion system design and control operations, validation and improvement of cavitation noise predicting models, and demonstration

of the benefits of clean propulsion solutions for representative marine vessels using these newly developed tools. Specifically, the planned and completed work consists of the following elements:

1) Introduction of operation pattern models for representative Canadian coastal vessels, including ferries, tug boats and fishing boats, based on field acquired vessel operation data.
2) Further development of the Hybrid Electric Marine Vessel - Model Based Design and Optimization Tool (HEMV-MBDOT) platform by adding a number of new and critical capabilities to HEMV-MBDOT, including
    a) ability to model all variations of hybrid electric marine propulsion systems;
    b) ability to accurately model natural gas (NG) engine fuel efficiency and various emissions, including carbon dioxide (CO_2), hydrocarbon (HC), and carbon monoxide (CO) at different engine operation speed and torque, since the HC and CO emissions are major concerns of NG engines and form the foundation for optimizing the design and control of NG hybrid powertrain system;
    c) ability to model the performance degradation/lifecycle costs of Li-ion batteries under different operation conditions accurately. (These types of model are the missing key elements for electrified powertrain systems at present, blocking reliable battery size optimization, optimal energy management, and electrified powertrain life-cycle prediction);
    d) ability to model vessel electric power system with AC power bus (DC bus modelled previously in our work);
    e) ability to develop quasi-optimal control strategies for the rule-based controller through Dynamic Programming (DP) based global optimization over a complete routine trip, defined by the established vessel operation pattern models, to accomplish the optimal propulsion system energy efficiency and life-cycle;
    f) ability to carry out design optimization of the propulsion system on the optimal sizing of key powertrain system components, including engines, M/Gs, and battery ESS, as well as with different powertrain types and architectures.
3) Experimental validation and further improvements of propeller cavitation models in collaboration with the ship propeller cavitation noise laboratory at the University of Genoa, Italy, an internationally leading group in this area, and in connection with several leading Canadian ocean noise research groups;
4) Detailed case studies on the pros and cons of different propulsion alternatives for the three representative types of coast vessels, ferry ships, tug boats, and fishing boats. These studies will identify the performance and efficiency improvement as well as emissions and operation cost reduction potentials of various clean propulsion solutions.

1.3 Accomplishments of the Project

1.3.1 Generic Outcomes

During this contract research, the UVic Clean Transportation team has addressed these five critical issues introduced in Section 1.1 and completed the tasks/objectives summarized in Section 1.2. These include:

1) Gained a better understanding of the energy efficiency, emissions, and ship induced noise problems in marine propulsion, and identified and verified the solutions to these problems;
2) Introduced and improved a new integrated system modelling and optimization approach to the optimal design and control of hybrid electric marine propulsion systems for improved performance, energy efficiency, emissions and ship-induced noise;
3) Acquired operation data and developed the representative operation patterns based on the load characteristics of representative Canadian coastal vessels in three different categories, including ferries, tugboats and fishing boats, to provide fundamental design requirements for developing electric and hybrid electric propulsion system and its controls, and examining variations of these operation patterns under different load conditions;
4) Developed high fidelity, compact and computation-efficient ship drag, propulsor thrust, and propeller cavitation noise models that can be used in the integrated marine propulsion system model, to support the integrated and synchronized design and optimization at the system level in the MATLAB/Simulink environment. These include the completed reduced-order hydrodynamic models as defined in the contract, and the additional low-order hydrodynamic models with no need of complex Computational Fluid Dynamics (CFD) work, currently under development;
5) An extension of the existing and additional high fidelity and computation-efficient system and component models of the hybrid electric powertrain and AC/DC power system suited for electrified marine vessels. These are in the MATLAB/Simulink environment, including the key NG engine efficiency and emission models, and the Li-ion battery performance degradation and life-cycle cost models;
6) Verified and improved ship-induced propeller cavitation noise models using experimental results through collaborated research, and using full-scale CFD simulations on Compute Canada's supercomputer. A method was developed to incorporate these cavitation noise models into the propulsion system modelling. Further collaborations with other ocean-noise research groups in Canada have been initiated;
7) Application of the newly developed models, modelling tools, and system optimization methods to representative marine vessels through a series of case studies. These tested and verified the feasibility, accuracy and benefits of the newly introduced methodology, models and modelling tools. These case studies were on representative ferry ships, tugboats and fishing boats and produced quantitative comparisons on vessel performance, energy efficiency/fuel costs, and GHG emissions of conventional and electrified marine propulsion systems, including diesel-mechanical, diesel-electric, series/parallel hybrid electric, NG-diesel dual-fuel engine hybrid electric, plug-in hybrid electric, and pure electric powertrain system designs;

8) Produced and tested all MATLAB software modules of the HEMV-MBDOT platform, and the advanced global optimization tools in UVic Global Optimization Tool Library (GO Tools), and developed detailed users' instructions of the GO Tools.

9) Passed on the new learning and case study results from this research to collaborating marine engineering and service companies, and presented this Transport Canada supported work to the Canadian and international marine engineering and service communities, demonstrating the benefits of Clean Transportation techniques and solutions. These ventures included the 2018 Canadian Institute of Marine Engineering (CIMarE) Annual Conference, *Mari-Tech 2018*, the Green Marine 11th Annual Conference, *GreenTech 2018*, and the Electric & Hybrid Marine World Expo 2018, Amsterdam, The Netherlands.

1.3.2 Specific Results

The finished project work has fully accomplished the original objectives, summarized in Section 1.2, and completed all planned research and development tasks. Specifically, the completed work includes the following:

- Operation Data Acquisition and Vessel Operation Pattern Modelling

  A set of vessel operation data collection projects have been completed that characterize the mission cycles of representative vessels of Canada's East and West Coast maritime fleets. The field acquired vessel operation data has been used to form the operation pattern models for representative Canadian coastal vessels, including ferries, tugboats and fishing boats/commercial boats.

  The vessel operation pattern models were then used as inputs in a series of clean marine propulsion technology case studies for each class of vessels. This enabled studies on the technical feasibility and economic/environmental benefits of ship electrification, and tests on the functionality of the HEMV-MBDOT modelling methods and platform.

  The collected vessel operation data were also used to verify the modelling results and validate the HEMV-MBDOT modelling tools.

- Key Extensions and Applications of HEMV-MBDOT Platform

  The HEMV-MBDOT platform was introduced to allow designers to evaluate various ship electrification solutions, choose and optimise powertrain components of the new electric or hybrid propulsion system, and develop appropriate controls for the electrified vessel. The HEMV-MBDOT platform was developed and validated using comprehensive vessel information and operation data collected during this work. New additions to the modelling platform include:

  a) Modularization of the integrated system models to convert the modelling platform into building blocks of independent function modules for ease of use on different vessels and diversified applications;

  b) Addition of a number of new and critical capabilities, including the ability to model all variations of hybrid electric marine propulsion systems, and the ability to accurately model battery performance degradation/lifecycle costs, and natural gas (NG) engine

fuel efficiency and emissions under different operation conditions, which are the missing key powertrain component models at present worldwide;

c) Addition of design optimization and optimal control capability to support the reduction of ship operation costs, GHG emissions and noise reduction; and,

d) System tests through detailed case studies on the pros and cons of different propulsion alternatives and the efficiency improvement, emission reduction and cost-saving potentials of various clean propulsion solutions for representative marine vessels, including ferry ships, tug boats, and fishing boats.

The studies using HEMV-MBDOT have demonstrated the methods for modelling, evaluating and optimizing different electrified marine propulsion systems. The work was done using newly introduced battery and hybrid energy storage system (ESS) performance and life-cycle cost models, NG engine/generator fuel economy and emission models, AC and DC power bus models, marine weather state (or Metocean conditions) models, and ship-induced (propeller cavitation) noise models.

The generic HEMV-MBDOT platform presents a new MBD-O methodology and consists of a series of different software models and programs in modular form. The use of these models and programs are documented in Appendix D to Appendix R. Close collaboration of our research team and engineers from the industrial partners is needed to combine and use these tools for their new marine applications, and to form a customized design tool for a specific application area. The technical documents serve as road maps and instructions.

- Incorporated Ship-induced Noise Model to HEMV-MBDOT Platform

Propeller cavitation is the dominant source of ship-induced underwater noise, particularly in abnormal or off-design operating conditions, including speed reduction and docking maneuvers. This portion of our project, documented in detail in Appendix H and I, is aimed at developing the capability to predict the level of noise for given ship operation profiles and propulsion system designs to guide the design of electric or hybrid propulsion systems and finding solutions in propulsion operation controls.

Propeller cavitation noise has a low-frequency spectrum that peaks at around 50 Hz, and it comes with almost all vessels independent of their type. The level of the noise is found to be heavily speed-dependent [12][13]. The study has thus focused on the propeller in-flow speed that is a result of the speed and direction of the vessel, ocean current, Z-drive/rudder angle, and the propeller (rotation) speed. The study has proceeded in three related areas:

a) Introducing the modelling method for predicting cavitation noise using full-scale Computational Fluid Mechanics (CFD) simulations for a given propeller under different water in-flow speed and propeller shaft speed. Additionally, methods were developed for validating the CFD simulation results using experimental data obtained from water-tank experiments and cavitation noise measurements;

b) Improving and simplifying the introduced propeller cavitation noise models, and identifying a way to use these models in hybrid electric system design and operation control;

c) Developing an effective method to calculate the propeller in-flow water speed under given vessel speed and ocean current to predict possible cavitation noise. This, in turn, supports design and operation changes to reduce cavitation noise.

To simplify the complex full-scale CFD dependent cavitation noise modelling and simulation methods, a new semi-empirical numerical modelling approach based on the "panel method" for cavitation modelling have been studied. This avoids complex CFD simulations so the model can be more easily used in propeller selection and vessel control.

- Completed Case Studies of Hybrid Electric/Electric Marine Propulsion Systems for Representative Ferry, Tug and Fishing Vessels

  The detailed case studies on different propulsion alternatives, from conventional to advanced clean propulsion, for the three representative types of coast vessels, ferry ships, tugboats, and fishing boats have been completed. These studies have identified the performance and efficiency improvements as well as emissions and operation cost reduction potentials of various clean propulsion solutions and presented the associated costs.

  The case studies also tested the ability of the expanded HEMV-MBDOT platform to serve the industry-wide needs, and prepared these tools to be used for the optimal design of clean marine vessels in the next phase of industrial collaboration, with existing and newly identified marine partners during this contract work.

1.3.3 New Marine Propulsion System Design Methods

The new hybrid electric propulsion system is characterized by a large onboard battery ESS, the optimal power and energy control strategies in system controllers or the Electronic Control Unit (ECU), and the introduction of the NG-diesel dual-fuel engine. This advantageous combination, however, demands fundamental changes to be made to the traditional and present marine propulsion system design practice.

In carrying out the planned extensions of the HEMV-MBDOT platform, and in clean-propulsion case studies using these tools, innovative new marine propulsion system design methods have been introduced in the following areas:

1) Using the time-series power profile to replace the traditional power-spectrum power profile as the foundation to size the powertrain system components and to develop the system control algorithms. This method allows for multiple power sources and the added ESS which change the power supply and use relations of these vessels;

2) Using advanced global optimization methods to design the hybrid propulsion system and to determine the control strategies used in the system's controller, considering both energy efficiency and life-cycle cost, specifically:

   a) Using energy efficiency, emissions, and life-cycle cost models as objectives and constraints of a Dynamic Programming (DP) global control optimization problem to identify the optimal control parameters and benchmark vessel performance for a given operation profile/trip, for forming the control rules in the system controller;

b) Using vessel performance, energy efficiency, emissions, and life-cycle cost models as design objectives and constraints of a global design optimization problem to determine the optimal sizes of key powertrain components for given vessel operation profile and corresponding rule-based controls. The formulated optimization problems are solved using UVic's advanced global optimization tools in the GO Tool library;

3) Using new, dedicated control strategies of the hybrid electric propulsion system to overcome the current drawbacks of NG-diesel dual-fuel engines to obtain improved power performance, ease of engine operation control, and significant reduction of hydrocarbon (HC) emissions.

These new and optimization-based marine propulsion system design methods represent innovative and original research contributions, essential for the conducted work, but beyond the original scope of this contract.

1.4 Organization of this Report and Its Appendices

This report first summarizes the research objectives, completed data collection and modelling tool improvement work and the major results and learning. It later outlines our present and emerging industrial/institutional partnerships on various related issues, as well as the on-going and future directions of the work.

The report provides an outline of the completed work and relations among different portions of the comprehensive work. The details of the technical work are summarized in Appendix A to Appendix T, referred and attached to this report. Each of these appendices focused on a specific technical aspect of the completed work. Specifically, this summary and its appendices cover the following:

- Representative ship operational profiles with a detailed driving cycle, load cycle, sailing route, ocean conditions, ship operation data, ship hull and propeller geometries, for vessels located at the west and east coasts of Canada.
- Case study results of different technical aspects of the representative ships. Including the technical and economic feasibility and benefits of various ship electrification solutions, considering their functional performance, fuel efficiency, emissions, and ship noise.
- Detailed documentation on the functionality, use and simulation study results of the HEMV-MBDOT platform, particularly the newly added features and capabilities.
- Detailed explanations on how the results of the case studies were obtained for the given ship operation profiles

This report contains technical materials that can be divided into three main areas as outlined in the following subsections.

1.4.1 An Overview of the Representative Marine Vessels Studied in this Work

This part of the report identifies the key characteristics of three types of representative Canadian coastal marine vessels, including vehicle and passenger ferry ships, seaport tugboats, fishing and small commercial boats. Three vessels have been selected from each of these three categories. In addition to a generic outline, the detailed technical data of these vessels and their acquisition guidelines are documented in three appendices:

- Appendix A. All Studied Marine Vessels
- Appendix B. Guidelines for Preparing Ship Hull & Propeller CFD Models
- Appendix C. List of Required Tasks and Preferred Ship Operation Data

1.4.2 Improvements of the HEMV-MBDOT platform with extended functionalities

The integrated modelling tool platform, HEMV-MBDOT, has been improved and expanded. These improvements can be summarized in the following five areas.

a) Additions of energy efficiency and emission models of many key hybrid electric powertrain components – these additions are essential for modelling the energy efficiency and greenhouse gas (GHG) or carbon dioxide equivalent (CO_{2e}) emissions in which other harmful emissions, such as CO, HC, etc., are converted into the equivalent amount of CO_2 emissions based on their impacts to the environment. These components include diesel engines, natural gas (NG) engines, and generic DC/DC power converter. In addition to a generic summary, detailed technical information is documented in two appendices:

   - Appendix D. Model Library for Diesel and Natural Gas Engines
   - Appendix E. DC/DC Converter Power Loss Data Modelling Tool

b) Addition of the performance and lifecycle cost models of Li-ion battery energy storage system (ESS) and battery-supercapacitor (SC) hybrid ESS. The cost of battery ESS constitutes a large portion of the vessel electrification/hybridization cost, it is thus important to accurately model this cost. However, the operation life of the battery heavily depends upon the way the batteries are used and relatively short battery life leads to likely battery replacements. Modelling battery performance degradation and life under different use patterns is thus essential for accurately predicting battery lifecycle cost, and supporting the economics analysis for vessel electrification. These models are also essential to the optimization of battery size and its optimal energy management. In addition to a generic outline, detailed technical information is documented in Appendix F Li-ion Battery and Battery-UC Hybrid ESS Performance and Lifecycle Cost Models.

c) Research progress and improvements made on the reduced-order hydrodynamic and ship propulsion model – these improvements consist of three parts:

   i) Modularization of the system model to allow easy model expansion and improvement;
   ii) Documented generation procedure and method for the reduced-hydrodynamics model, and the on-going expansion of the ship propulsion model with two additional degrees of freedom (DOF); and
   iii) Introduction of ship-specific, low-order regression model. This is done to avoid the computation-intensive full-scale CFD work for generating the hydrodynamic coefficients in the present reduced-order hydrodynamic ship propulsion model. Detailed work is documented in Appendix G. Improvement of the Reduced-Order Hydrodynamic and Ship Propulsion Model.

d) Research progress and improvements made on the modelling of vessel propeller introduced cavitation noise – these include the propeller cavitation noise experiments conducted in collaboration with the University of Genoa, the obtained data and new learning, the use of the obtained data for the validation of numerical simulations, and comparison of the results.

In addition to a generic summary in the report, more detailed discussions are provided in two appendices:

- Appendix H. Experimental Investigation of Cavitation-induced Propeller Noise
- Appendix I. Improvements of Propeller Cavitation Noise Model

e) Initial investigation on the incorporation of weather and seasonal variations of ocean current, wave and wind into the marine vessel operation pattern models. This addition is beneficial to improve modelling accuracy on several fronts: vessel speed, energy use, emissions, propeller cavitation condition (ocean noise), and to combine these research efforts with the broad ocean science and ocean energy research to benefit the marine industry. Details of the proposed methodology and results are given in Appendix J: Marine Weather State (MWS) or Metocean Loads.

1.4.3 Case Studies on Benefits of Vessel Hybridization and Electrification

In this part, comparative studies have been carried out to compare various clean marine transportation solutions, including:

a) Hybrid electric propulsion systems of series and parallel powertrain architectures,

b) Plug-in hybrid electric propulsion system,

c) NG-diesel dual-fuel engine with conventional diesel-mechanical and diesel-electric powertrains,

d) NG-diesel dual-fuel engine with hybrid electric powertrain and special control strategies,

e) Pure electric propulsion system powered by battery, comparing with the traditional marine propulsion technologies of diesel-mechanical and diesel-electric powertrains.

These different clean and electrified marine transportation solutions suit the diverse needs of different marine vessels, based on their size, sailing route, and operation patterns. These comparative studies quantitatively demonstrate the pros and cons of each option. Studies have been done for ferry ships, tugboats and fishing/commercial boats using their vessel and operation data. For the ferries with different and unique characteristics, more modelling and analyses have been carried out. In addition to a short summary of the work, the technical details are documented in nine appendices, six for ferry ships (Appendix K-P), one for tugboat (Appendix Q), and one for fishing boat (Appendix R), Appendix S outlines a new, more generic approach for modelling vessel's power demands.

a) BC Ferry Ships:

- Appendix K. Case Study for Skeena Queen - LNG Series Hybrid
- Appendix L. Case Study for Skeena Queen - Optimal Design of Series Hybrid Propulsion
- Appendix M. Case Study for Skeena Queen - Design of Parallel Hybrid Propulsion System
- Appendix N. Case Study for Tachek - Alternative Hybrid Electric Propulsion Designs
- Appendix O. Case Study for Klitsa - Model of Hybrid Electric Ships with AC Power Bus
- Appendix P. Case Study for Klitsa - Model of Hybrid Electric Ships with DC Power Bus

The Appendixes L and M cover two different types of hybrid electric powertrain architectures, series and parallel for BC Ferries' Skeena Queen, and the Appendix N discusses the hybrid electric powertrain system design for another ferry ship, Tachek. The Appendixes O and P present two different types of electric power systems with AC and DC power bus. Appendix K emphasizes NG engine adoption, and Appendix L discusses the use of a Li-ion battery performance degradation model in design optimization of the hybrid electric propulsion system.

b) Tugboats are unique; their workloads are not determined only by the hydrodynamic drag as other vessels, rather on their working duties. Their operation patterns are modelled using data from both public literature and acquired operation data. The detailed technical information is documented in Appendix Q: Case Study for Tugboat - Their Operation Profile - Benefits of Hybrid Powertrain.

c) Lobster fishing boats also present different and unique operation patterns. Detailed comparative studies have been carried out through modelling of both traditional mechanical and new electrified propulsion systems, considering their emissions and lifecycle cost. The detailed technical information and results are documented in Appendix R: Case Study for Fishing Boats - Emission Reduction and Lifecycle Costs of Hybrid Electric and Pure Electric Powertrains. The commercial boat from the east coast, studied in this work, is of a similar size and operation pattern as the lobster fishing boats.

d) To better guide the case studies and to produce clean energy propulsion solutions for each specific class of marine vessels, a new area of research on a generic vessel classification technique has been initiated. The method considers vessel sizes, sailing routes, operation patterns, and other unique characteristics, from the perspective of energy demand, emission and noise constraints, and cost sensitivity. The research will incorporate intelligent pattern recognition using fuzzy pattern clustering and recognition techniques. Part of this initial work is outlined in Appendix S: Generic Ship Classification and Modelling Method

The report summarizes completed contract work, discusses on-going efforts based on the new learning throughout this project, and outlines new initiatives in collaboration with several new industrial partners in a number of key areas.

2 TECHNICAL REVIEW OF RELATED WORK

Due to the broad areas covered by this research work and the distinct nature of each of the detailed studies, the technical background and literature reviews on related work are organized into the detailed technical reports in the appendices of this report.

3 OVERVIEW OF THE INTEGRATED MODELLING TOOLS

3.1 Function of Integrated Propulsion System Modelling

The function of the integrated propulsion system modelling tools, HEMV-MBDOT, is to support the design and control optimization of marine propulsion systems. For hybrid electric marine propulsion systems, the multiple propulsion power sources and onboard ESS lead to a complex

and multiple degrees of freedom (DOF) system that demands an integrated system design and control approach to achieve the best system performance, energy efficiency and emission/noise reductions. The HEMV-MBDOT methodology has been developed to support hybrid propulsion system design and control development on an integrated platform. The function of this platform is illustrated in Figure 1.

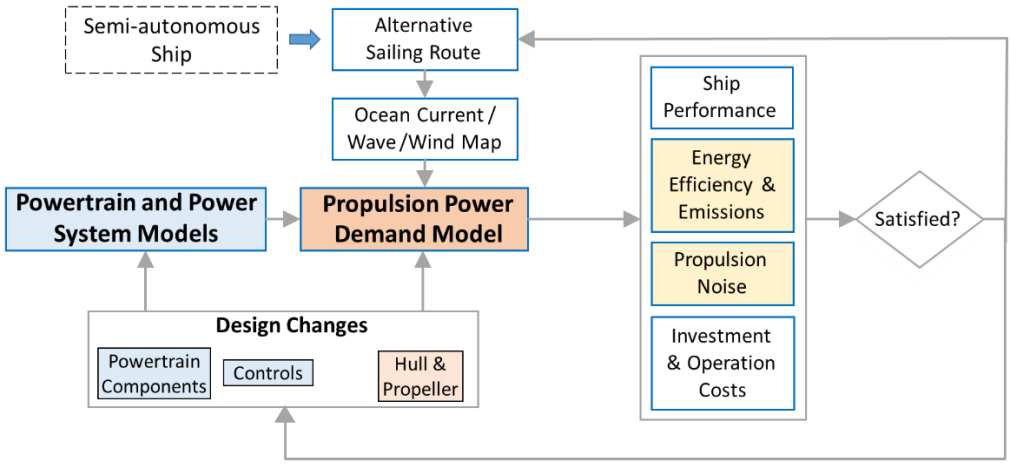

Figure 1 Propulsion System Design Requirements and Activities

The propulsion system is to be designed to produce enough power to meet the power demands of the vessel under different operation conditions, including hydrodynamic drag, ocean current/wave and wind, the variation of routes and cargo loads. The "quality" of the hybrid propulsion system includes power performance, energy efficiency, emissions and vessel introduced ocean noise. This quality is associated with a certain level of investment/conversion and operation costs. There also exist many alternative powertrain system solutions to produce the propulsion power to the propulsor shaft(s) and produce propulsion force using different types of propulsor(s). The powertrain system, and associated power system for larger vessels, can have different architectures, sizes of key components, and system control/power management strategies. The combination of these leads to different "quality" and costs. This work, and the development of the HEMV-MBDOT, is to support the accurate and quantitative evaluations of different hybrid propulsion system designs and their associated costs, to allow the vessel designer and operator to identify the optimized design and operation control. The work was done based on the most recently developed MBDO techniques and in the context of real marine vessels and operation data.

3.2 Architecture of the HEMV-MBDOT Platform and Its Key Components

The HEMV-MBDOT platform consists of four functional components: (a) model of vessel propulsion power demands; (b) model of drag force from hull-water interaction; (c) model of propulsion force from propulsor and potential cavitation noise; and, (d) model of powertrain system and power system. Details of these major function components at three different levels of complexity, used in this work, are discussed in the following subsections.

3.3 Three Different Levels of Propulsion Power Modelling

The HEMV-MBDOT platform presents three different levels of complexity and comprehension, for different types of marine vessels with different individual levels of technical complexity and at different stages of design and development.

Traditionally hull drag and propeller thrust models follow two different techniques:

- Generic Empirical Equations – the empirical data-driven equations, documented in marine engineering textbooks, have a relatively simple form. However, parameters of these equations are vessel dependent, leading to inaccurate modelling results for new vessels.
- Full-scale CFD – the approach used widely at present by industry in designing new ships can accurately simulate the tow tank experiments. However, it requires intensive computation in the CFD simulation. It is thus impossible to be incorporated into the integrated hybrid electric marine propulsion system.

To address these issues, high fidelity, reduced-order hydrodynamics models for vessel hull drag and propeller thrust have been introduced to predict the ship's hydrodynamic behaviour within the integrated marine propulsion system modelling tools. In this work, the previously introduced modelling tools have been modularized to support its flexible use in various applications. Three different levels of propulsion power modelling, which can be used to support the integrated marine propulsion system modelling and simulation work, are discussed in this section.

3.3.1 With Reduced-order Hydrodynamic Hull Drag and Propeller Thrust Models

The most comprehensive form of the integrated system model is based on the reduced-order hydrodynamic hull resistance and propeller thrust models to replace the conventional computation-intensive, full-scale CFD based hydrodynamic hull resistance and propeller thrust simulations, also called soft tow-tank and water-tank simulations. In this approach, the hull and propeller coefficient matrices are obtained using the full-scale CFD simulations first. The compact and easy to calculate parameter based reduced-order models with the obtained hull and propeller coefficient matrices are then embedded into the integrated system model in MATLAB/Simulink codes. These parameter-based models can be executed quickly in Simulink with accurate results. Verification of the calculated results showed resistance and propulsion force prediction errors at about 5 percent. Components of the integrated system models are shown in Figure 2.

(1) Ship Operation Data Collection

In this work, extensive vessel operation data has been collected for a number of reasons: (a) to better understand the operation patterns of different categories of vessels, (b) to serve as data inputs for the case studies using the HEMV-MBDOT, (c) to validate the results from the integrated system model, and (d) to support future research and development work. Parts (b) and (c) are illustrated clearly in Figure 2.

Collection of vessel operation data involved the following activities:

- Design, construction, and lab testing of equipment
- Installation planning and equipment procurement
- Installation, commissioning, and monitoring
- Post-collection data analysis and processing
- Decommissioning

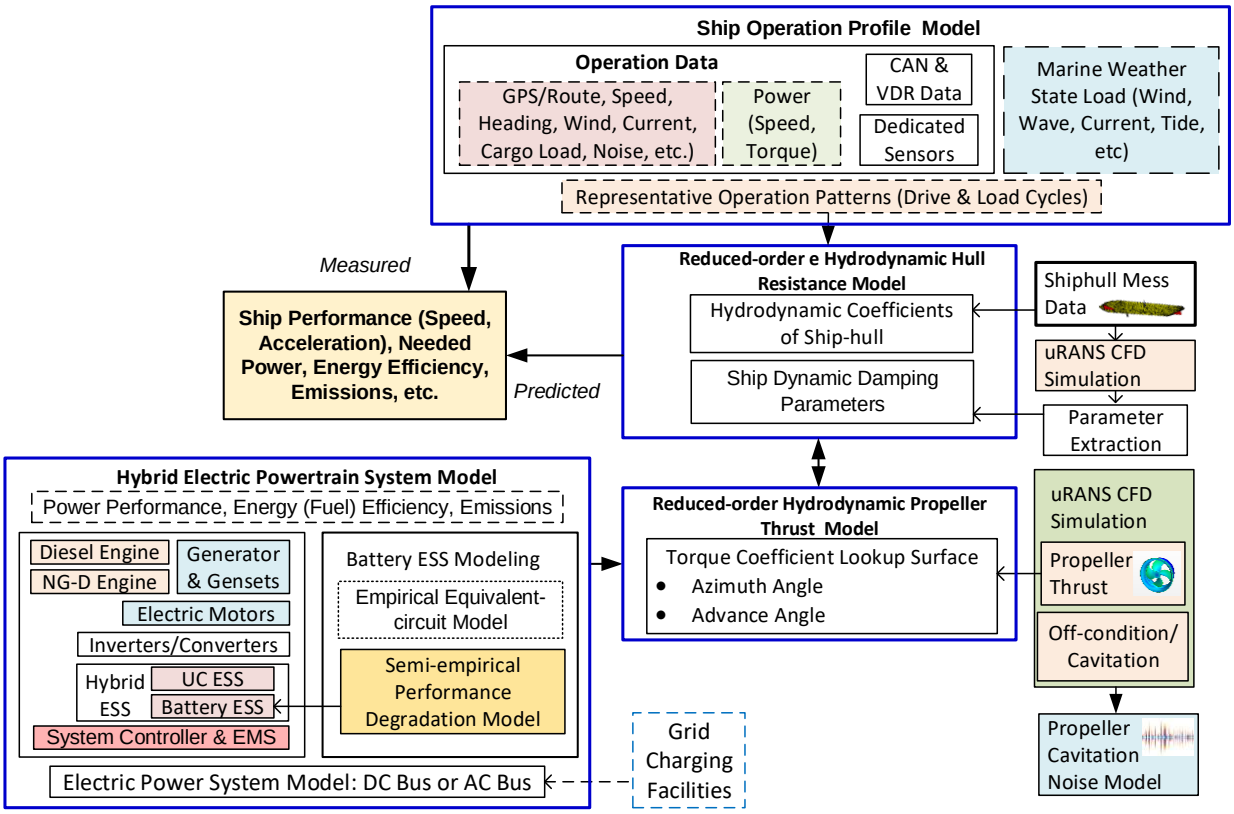

Figure 2 HEMV-MBDOT Platform with Reduced-order Hydrodynamic Models

(2) Building the Reduced-Order Hull/Propeller Hydrodynamic Models

This model configuration is particularly suitable for a new vessel and vessels for which the actual power use cannot be measured. The following preparation work is needed to determine the model parameters of the reduced-order hull drag and propeller thrust models, including:

- Geometric (CAD) Modelling of Ship Hull and Propeller – used to form the mesh data for CFD simulations.
- Full-scale CFD Simulations to obtain parameters of the Reduced-Order Models - CFD analyses of the bare hull, rear propellers, bow thruster, self-propelled vessel, and wake fraction and thrust deduction analysis.
- Vessel Dynamics – carried out using a number of tools and methods, including ShipMo3D analysis, maneuvering model parameterization, rudder model, and surge resistance decomposition.

The reduced-order model introduced in this work covers the full six DOFs of the vessel movements. At present, the model used for propulsion system design is implemented as a 1-DOF, quasi-static, power-loss model that is enough for the propulsion system design task, as is common practice in the automotive industry. However, for the dynamic maneuvering of the vessel during turning and docking, more complex and accurate dynamic models with at least

three DOFs will be needed. This part of the modelling work has been initiated at the end of this project.

(3) Powertrain System and Power System Modelling

Modelling of different types of vessel's powertrain systems, including conventional, hybrid electric, plug-in hybrid electric and pure electric, is similar to the modelling of vehicle powertrain system with two major exceptions. These two differences are: (a) different type and size of powertrain components, and (b) the need to use multiple engines, generators, and propulsion motors in the form of a micropower grid to meet the much higher power and energy demands of larger marine vessels.

At present, existing automotive powertrain system modelling tools are only designed to handle vehicles of similar size and capability, such as passenger cars, light trucks, or at most city buses. The difference of marine vessel sizes and power demands in this work is much larger, including small fishing boats, power-thirsty tugs, and large ferries. Their powertrain architecture and electric power system designs are considerably different.

To address this issue, considerable efforts have been devoted in this contract work to introduce new plant models and modelling methods for various key powertrain and electric power system components. These models covered their energy efficiency, different types of emissions, and performance degradations at different operating conditions. The controls of these components, including off-line optimal control planning using Dynamics Programming (DP) and real-time implementation using DP result-based rule-based system have been developed for each representative architectures.

To evaluate the life-cycle cost of alternative propulsion system solutions, the investment, replacement, maintenance, and operation costs of these powertrain/power system components have been modelled when possible.

3.3.2 Using Low-Order Hull Drag and Propeller Thrust Models

At the later stage of this contract, an effort has been made to further reduce the needed computation work in generating the vessel hull drag and propeller thrust models, and this led to the creation of the low-order hull drag and propeller thrust models. This work, however, is not part of the original contract; and it is to be completed in the future research. The primary focus and challenge of this part of work is to introduce proper model parameters to ensure modelling accuracy, and to verify the obtained results.

In this approach, the full-scale CFD simulations used to generate the model parameters of the hull and propeller have been replaced by simple, one pass CFD simulation. The former needs professional CFD codes, such as StarCCM, and ideally a supercomputer to execute, while the later can be carried out using regular CAD workstations and common CAD/CAE software. Parameters of the reduced-order hull drag can be obtained from the existing vessel's Stability Book, or obtained using one-pass vessel stability CFD simulations. The initial tests showed results with acceptable accuracy. Since this work was beyond the scope of the current contract, further development and tests are needed. Nevertheless, this approach is illustrated in Figure 3.

3.3.3 Directly Using Propulsion Power Data Inputs

For an existing marine vessel, if the actual power demands of the vessel can be accurately measured during its routine operations; various vessel propulsion system designs can be tested. These can use the direct power demand data without the need of hull drag and propeller thrust models to predict the power demand. This led to a further simplified integrated system model architecture as shown in Figure 4. This direct approach is particularly suitable for existing vessels with a complete set of operation data. It can be applied to all of the ferries, tugs, and fishing boats studied in this contract work. The method has been used in several case studies.

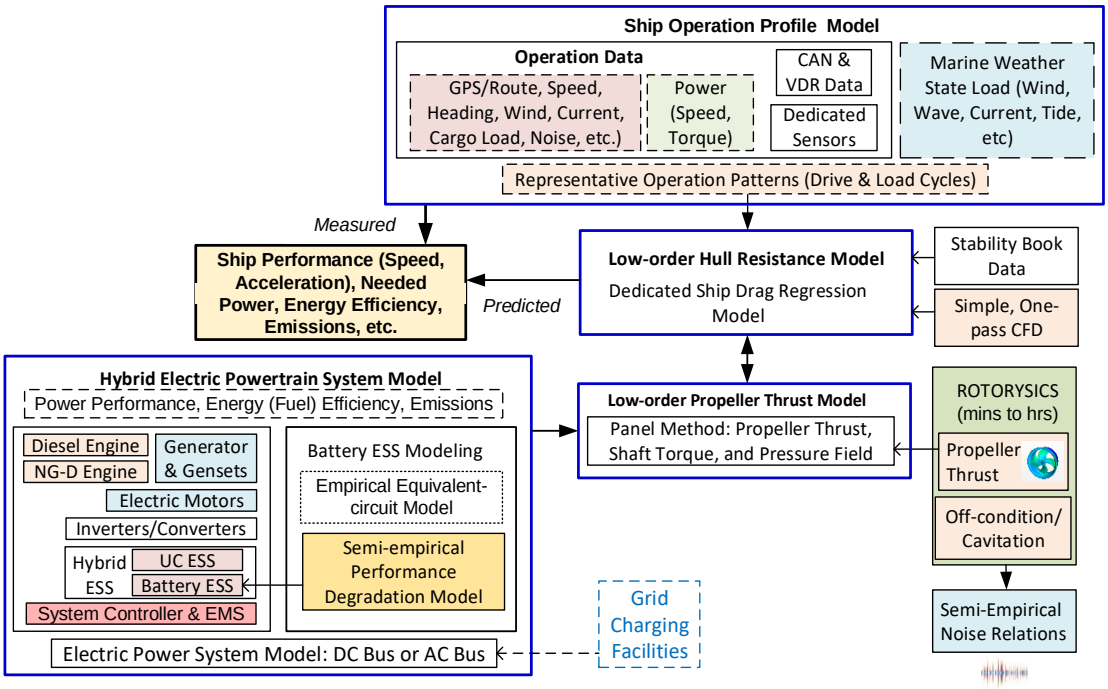

Figure 3 HEMV-MBDOT Platform with Low-order Hydrodynamic Models

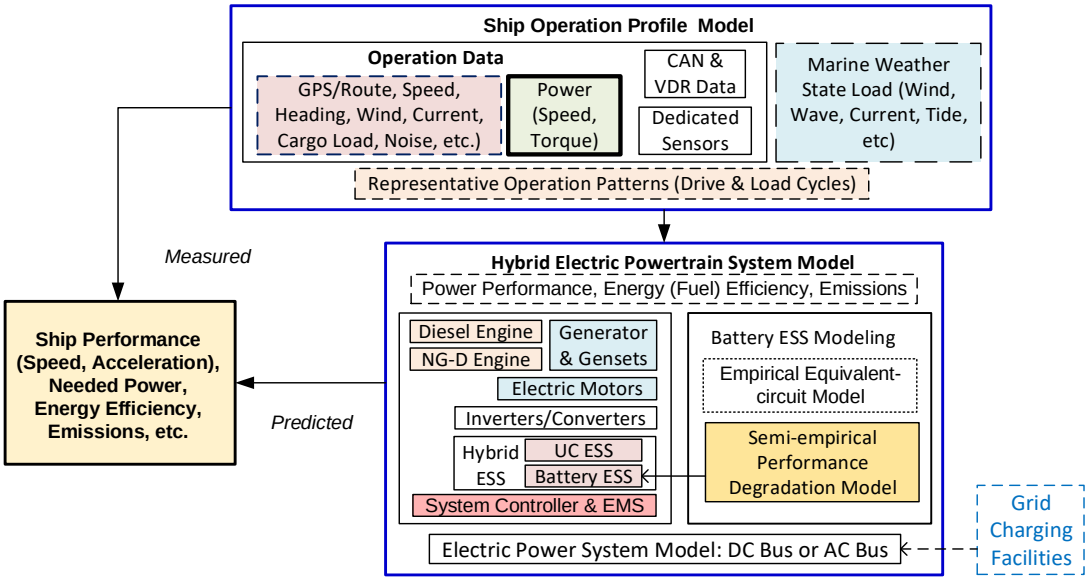

Figure 4 HEMV-MBDOT Platform with Direct Power Demand Data Model

For example, the case study on fishing boats, documented in Appendix R, has been carried out using this approach.

4 SHIP OPERATION DATA AND ACQUISITION

4.1 Background

As discussed previously, the operation profiles of marine vessels are quite diversified and standardized marine drive cycles have not yet been developed. Although the vessels' propulsion power and energy demands do not only depend upon the travelling speed-based driving cycles as road vehicles, it should be possible to develop common load characteristics for vessels in the same category. Thus serving as fundamental design requirements for developing the hybrid electric propulsion systems and their controls. Meanwhile, the recorded vessel velocities under different loads and propulsion power are used to calibrate and validate the integrated marine propulsion system models introduced in this work.

This section is devoted to the Ship Operation Profile Model block, introduced in the system overview of Section 3.3 and Figures 2, 3 and 4.

4.1.1 Scope of Ship Operation Pattern Modelling

The integrated hybrid electric marine propulsion system and ship-induced noise modelling tools, introduced in this work, are generally applicable to all types of marine vessels to form a commonly applicable technology platform. However, to better understand the types and operation patterns of Canadian marine vessels, and to test the newly introduced modelling techniques and software tools, typical and representative coastal marine vessels in three different categories are studied in this work. These vessels have different sizes (displacement), operation patterns, and routes.

4.1.2 Representative Canadian Coastal Vessels

The selected representative marine vessels include:

- larger vehicle and passenger ferries in British Columbia,
- medium size tug boats in west coast seaports,
- smaller lobster fishing boats and commercial boats in the maritime province of Nova Scotia

Complete technical information, hull and propeller computer models and a broad scope of operation data of each of these vessels are collected and acquired using dedicated data collection apparatus and through interfaces to the vessels Controller Area Network (CAN) data bus or operation data logger.

The characteristics of these marine vessels are briefly overviewed in this section. The detailed information and collected data of these vessels are given in Appendix A: All Studied Marine Vessels.

4.2 Passenger and Vehicle Ferry Ships

British Columbia Ferry Services Inc. (BC Ferries) provides all major passenger and vehicle ferry services for coastal and island communities in British Columbia (BC), Canada. With a fleet of 35 vessels, serving 47 locations on the BC coast, BC Ferries is the largest passenger ferry line in North America and the second largest in the world. In this work, three ships from BC Ferries have been selected:

- M. V. Skeena Queen – BC Ferries operates a number of these short crossing, commute ships, and plans to replace many of them in the near future. Outcomes of the study on this ferry will have more potential to influence the new ferry design in the future. The ferry ship is shown in Figure 5.

Figure 5 M. V. Skeena Queen from BC Ferries

- M. V. Tachek – This ferry has been retrofitted with a hybrid electric drive system with an added onboard battery ESS to assist the ferry to dock and depart. Studies on this ferry will produce a better understanding of its operation pattern and explore the potentials of adopting a new hybrid electric propulsion system design and optimized controls. In addition, the ferry operates in open water with varying marine weather conditions. The

acquired operation data will support future research on sailing route optimization and semi-autonomous sailing to reduce fuel consumption, emissions, and ship-induced noise.

- M.V. Klitsa – this smaller passenger and vehicle ferry ship has been studied previously at the early stage of the integrated hybrid electric marine system modelling tool development. Kevin Andersen has done the early research work on this ferry, including ship operation data acquisition, operation pattern modelling, reduced-order hull and propeller hydrodynamic modelling, and a feasibility study on pure electric ship propulsion system design using DC powertrain components. Details of this previous work have been documented in [1]. During this project, further studies have been carried out on a number of more complex issues using data from M.V. Klitsa.

The acquired operation pattern data of these three ferries are used in the case studies documented in Appendixes K, L and M (for Skeena Queen), Appendix N (for Tachek) and Appendixes O and P (for Klitsa). These studies compared the conventional gasoline/diesel powertrain versus cleaner hybrid electric, and pure electric propulsion system designs on their energy efficiency, GHG emissions, and life cycle cost to explore the feasibility and benefits of each alternative, and to identify the most beneficial design solution. Uses of the integrated modelling and simulation tools in these comparative studies are also discussed. New propulsion systems, either with a natural gas (NG) engine or with NG engine/hybrid electric powertrain/special controls are also studied in detail to explore the advantages of these technologies, as documented in detail in Appendix K.

4.3 Tugboats

Tugboats (Figure 6) are important tools in ports and harbours to assist large ships to and from their berths. Today, multi-purpose tugs are designed to perform various jobs such as offshore support, salvage, icebreaking, etc. Some key parameters that define the performance of a tugboat include the bollard pull capacity, maximum free-running speed, time taken to achieve maximum free-running speed from rest, distance covered to crash stop, time taken to complete a 360° turn on its own axis, and soundproofing of machinery spaces.

Figure 6 Tugboats in British Columbia

Tugboats can be classified into the following three major categories based on the type of work they perform.

(1) Harbour tugs - Harbour tugs are required to assist large ships on and off a berth by pushing and pulling. Since the navigation of a large ship is confined in restricted water, tugs are

necessary tools in the harbour to safely handle the ships while entering or leaving a port. Some special applications of harbour tugs with more rigid hull and fender construction are for inland sea transportation and coastal shipping.

(2) Escort tugs - Escort towing tugs are designed to provide emergency steering and braking functions to tankers in critical or confined coastal areas. Due to the accidents that have happened in the past that caused oil leakage from tankers, it is required by a jurisdiction that tankers within specific waters must be 'escorted' by a tugboat. A towrope is connected to the vessel being assisted from the towing winch in tug. Tugs need to generate the required ship control forces for steering and braking by carefully balancing all force from their propulsion drive units and ship hull hydrodynamic forces.

(3) Seagoing tugs - Seagoing tugs are generally larger and capable of performing good sea keeping characteristics to ensure that vessels can provide required power in any rough sea weather. They can perform various operations including assisting ships in ports as well as at sea.

Harbour tugboats form a unique category of marine vessels. The power load and energy requirements of tugboats are not determined by the hydrodynamic drug as other marine vessels but determined by its working load cycles during the manipulations (push and pull) of a large ship.

In this study, harbour tugboats have been studied using the tug operation data acquired from public literature and Robert Allan Ltd. (RAL) of Vancouver, BC. Proprietary data has been removed. The tugboats produced by Robert Allan Ltd (RAL) are used to produce an overview of the architectural features of a tugboat and the challenges faced by tugboat design and operations. The advanced hybrid electric tugboats and liquefied NG (LNG) (or NG and diesel dual fuel) powered escort and ship-handling tugboats have been illustrated.

General tugboat operation data was collected from all sources, including generic ship handling profile, normal tug operation profile, Canadian tug operation profile, harbour duty profile, ocean towing profile, and tug power requirements.

The acquired operation pattern data are used in the case study, documented in Appendix Q. This compares conventional gasoline/diesel powertrain versus cleaner hybrid electric, and pure electric propulsion systems on their energy efficiency, GHG emissions, and life cycle cost to explore the feasibility and benefits of each option, and to identify the most beneficial design solution. Uses of the integrated modelling and simulation tools are also discussed.

4.4 Fishing Boats and Commercial Boats

In the Atlantic Maritime Provinces of Canada, a large number of marine vessels are in the form of small lobster fishing boats, as shown in Figure 7, and commercial tourist boats. In this work, the unique operation profiles of representative lobster fishing boats and tourist boats are modelled using the ship operation data, acquired using dedicated data acquisition systems developed in this project.

Figure 7 A Typical Fishing Boat

The fishing boats studied in this work include the following:

- Boat #1: Lobster Fishing Boat I
- Boat #2: Lobster Fishing Boat II
- Boat #3: Commercial Boat I

The specific names of these boats have been removed but acquired representative operation pattern data of these boats are given in Appendix A and are used in the case study documented in Appendix R.

Modelling and simulations of a typical fishing boat with conventional gasoline/diesel powertrain versus cleaner hybrid electric and pure electric propulsion system has been done to evaluate their energy efficiency, GHG emissions, and life-cycle cost. The method is used to explore the feasibility and benefits of each powertrain option, and to identify the most beneficial design solution.

4.5 Ship Operation Data

To derive the operation patterns of different categories of marine vessels, and to prepare for the modelling of ship power demands and propulsion system, the following data have been collected. This was collected using the ship operation profile module as shown at the top of Figure 2.

4.5.1 Engine/Propeller Shaft Speed and Torque Data

Propeller shaft speed and torque measurements to obtain the actual vessel propulsion power data are normally made at sea trials of a new or overhauled vessel. These speed and torque sensors are commonly removed afterwards. In this work, portable data acquisition systems were installed for all vessels to acquire the needed propeller shaft speed and torque data. The systems used include:

- BEETECH Multiple Channel Shaft Speed and Torque Acquisition System – Special shaft torque and speed sensors have been mounted on the engine shafts of the studied marine vessels.
- Operation Data Recording and Remote Data Acquisition – Special data recording devices have been incorporated and/or developed for ship operation data acquisition.

4.5.2 Hull Dimensions and Geometry

Information is collected from ship stability books, manufacturing data sheets and other related sources. Using the original CAD models or scanned data, the geometric models of the vessel hull has been built or reconstructed to support the CFD hydrodynamic hull drag simulation. A typical example of the created hull model for BC Ferries' Skeena Queen is shown in Figure 8 (a).

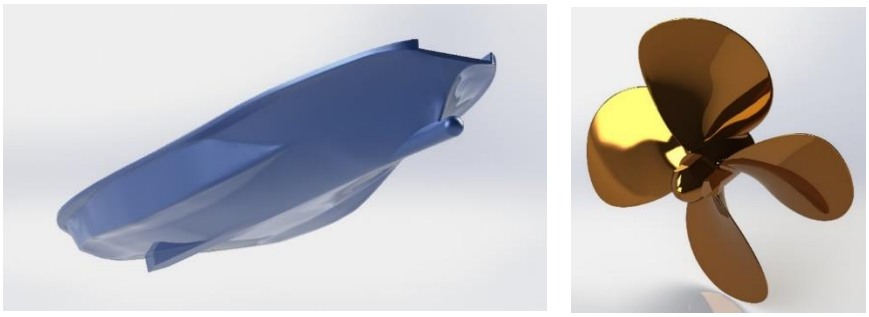

(a) (b)

Figure 8 Representative Geometric Models of Ship Hull and Propeller

4.5.3 Propeller Parameter and Geometry

Information on the propeller is collected from manufacturing data sheets and other related sources. Geometric models of the propeller have been built or reconstructed to support CFD hydrodynamic propeller thrust and cavitation (noise) simulations. A typical example of a created propeller model for BC Ferries' Skeena Queen is shown in Figure 8(b).

4.5.4 Log Book – Case Dependent

Information is acquired from vessel operators, including:

- Cargo Load
- Fuel Tank Readings (manually taken records)

4.6 Operation Data for Larger and Fleet Vessels

Larger marine vessels have their own operation data acquisition and control system networks. A considerable amount of ship operation data can be obtained in real-time and/or from recorded data. Examples of these included the following systems on BC Ferries' Skeena Queen and Tachek.

4.6.1 Controller Area Network (CAN) Bus System Data

A message-based protocol for component status data and control signals, used during ferry data acquisition as a supplemental source of information.

4.6.2 Voyage Data Recorder (VDR) Data

All vessels required by International Maritime Organization (IMO)'s requirements to collect data from various sensors on board, used during recent ferry data acquisition as a supplemental source of information.

4.7 Guideline Documentation

During this project, detailed guidelines for collecting the technical information and operation data of a marine vessel in the following three areas have been produced:

- Guidelines for Ship Operation Data Collection
- Ship Operation Data - Signal List
- Guidelines for Generating Ship Hull and Propeller CFD CAD Models

The specific requirements in each area are documented in Appendix B Guidelines for Preparing Ship Hull & Propeller CFD Models and Appendix C List of Required Tasks and Preferred Ship Operation Data.

4.8 Marine Weather State (Sea State)

Traditionally, sea state is used to describe the general condition of the ocean considering wind waves and swell at a given location and moment. Sea states of calm, smooth, moderate, rough, high, etc. grades present differing levels of challenge to marine operations and are recorded as statistical data in oceanography. However, the hydrodynamic hull resistance and propeller thrust models are normally based on calm water, and sea state does not directly translate to vessel propulsion loads. The ocean science community also uses the term "Metocean" to describe ocean wind, wave, etc. Metocean data are considered as an important and highly useful category of oceanographic and marine data that comprises observed measurements of the current, wave, sea level and meteorological data. It has not yet been decided whether to use Metocean conditions directly due to its less direct connection to ocean current that is not caused by wind.

The vessel propulsion resistance is directly related to current, wind, and waves. In this work, we re-name the load to Marine Weather State (MWS) load from Sea State (SS) load used previously. Specifically, the major influences to marine vessel propulsion resistance are divided into two major components: MWS Load and Cargo Load. The MWS load adds to the propulsion resistance of the vessel from the pure hydrodynamic load during its travelling in calm wind and calm water. The cargo load changes the submerged hull volume and mass of the vessel, and alters the hull drag force from their norm.

The detailed discussions and obtained MWS data are given in Appendix J Marine Weather State (MWS) or Metocean Loads**.**

5 IMPROVEMENTS OF HULL DRAG, PROPELLER THRUST AND CAVITATION-NOISE MODELS

As discussed previously in Section 3, the unique feature and capability of this work is integrated propulsion system modelling in the MATLAB/Simulink environment, and the reduced-order hydrodynamic models. These models accurately calculate the drag force of the vessel's hull and the propulsion thrust force of the propulsor(s), which made this approach feasible. In addition to addressing the issue of ship induced ocean noise, primarily caused by propeller cavitation, the propeller cavitation and cavitation noise predication models have been introduced through hydrodynamic simulations. Considerable improvements have been made in these models, as outlined in this section.

This section is devoted to the Reduced-order Hydrodynamic, Low-order Hull Resistance and Propeller Thrust Model blocks introduced in the system overview of Section 3.3 and Figures 2 and 3.

5.1 Improvements in Driving Cycle, Load Cycles, and Ship Operation Models

To better understand the operation pattern of different types of marine vessels, extensive amounts of vessel information and operation data have been acquired. These data in the form of power load cycles were used in the case studies documented in Appendices K to R. During this project, more data have been collected for the larger and more sophisticated passenger and vehicle ferries. This will serve as inputs for designing new vessels, and provide benchmarks to validate our vessel hull drag, propeller drag and cavitation (noise) models. Specifically, the collected data include the following:

- Driving Cycle and Power Load Cycle
    - Ship Sailing Route and Speed GPS Data (Installed GPS and Ship GPS)
    - Engine and Propeller Shaft Torque and Speed (Measured Using Dedicated Equipment and Verified with Recorded Data if available from VDR)
- Cargo Load Cycles
    - Cargo Load (Vehicle Counts from BC Ferries' Records)
- Ship Operation Model (from Vessel Operators and VDR)
    - Use of Engines
    - Ship Maneuver (docking and departure)
    - Heading/Route

5.2 Improvement of the Reduced-Order Hydrodynamic and Ship Propulsion Model

In an effort to improve the modelling accuracy of the reduced-order hydrodynamics simulation, the model's parameterization procedures were altered and several of the simulation's subsystems were revised. Noteworthy changes to the model include a) revised formulation of the propeller torque coefficient and thrust coefficient lookup surfaces, b) a revised process for estimation of the propeller thrust deduction factor, c) the augmentation of CFD bare hull resistance with appendage resistance, and d) accounting for effects of current and wind loading through ProteusDS simulation. To assess the accuracy of the revised hydrodynamic and propulsion subsystems, the following procedure was developed:

1) Input time-varying propeller shaft speed from recorded ship data
2) Determine the corresponding propeller speed and use CFD generated lookup surfaces to estimate the propeller thrust force. Thrust is influenced by wake fraction, thrust deduction and ship velocity.
3) Send estimated propeller thrust force to the ship-maneuvering software module that contains the hull resistance and propeller thrust models and calculate the predicted ship velocity. Hydrodynamic calculations are parameterized by CFD analysis and are affected by wind/current loading.

4) Send the predicted ship velocity back to the propulsion module in a feedback loop. The velocity feedback affects the next value of estimated thrust force due to advance velocity and wake fraction effects
5) Compare the model's predicted ship velocity with the actual recorded speed throughout the voyage and determine model accuracy

Simulation results showed satisfactory prediction accuracy when comparing the predicted ship velocity with the recorded ship velocity. As shown in Figure 9, the error between recorded speed and predicted speed was reduced to approximately 5-7% during the transiting portion of the voyage of the vessel studied.

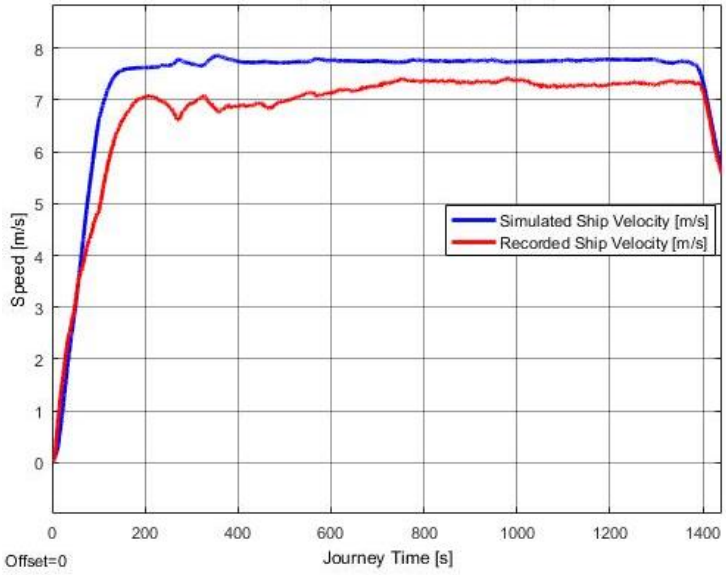

Figure 9 Recorded Ship velocity vs. Simulated Ship velocity

5.2.1 Revised Procedure for Getting Thrust and Torque Coefficient Lookup Surfaces

It is well documented in the literature [2] that propeller thrust, *T*, and propeller torque, *Q*, can be represented in terms of their respective torque and thrust coefficients K_T and K_Q such that

$$T = K_T \rho n^2 D^4 \quad (1)$$

$$Q = K_Q \rho n^2 D^5 \quad (2)$$

where n is propeller's angular velocity, ρ is the density of fluid, *D* is the diameter of the propeller and the coefficients K_T and K_Q are both functions of advance ratio *J* and incident flow angle α, which is the angle between the incoming flow stream and the angle of the azimuth drive, as shown in Figure 10.

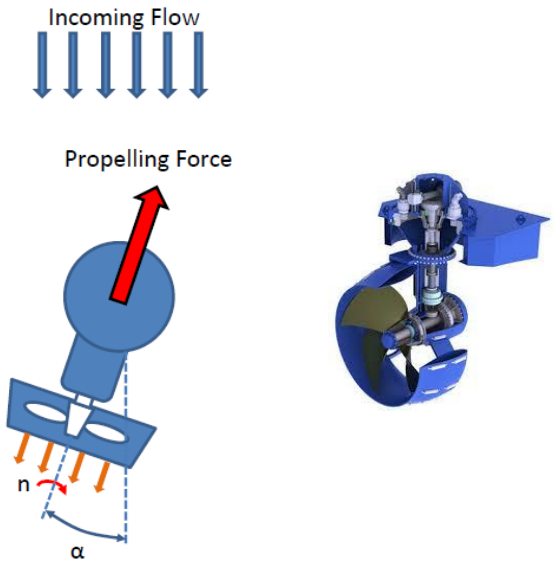

Figure 10 Incident Flow Angle of the Propeller

The motivation for the construction of K_T and K_Q lookup surfaces for use in simulation is to provide a fast and computationally efficient way of solving for thrust force and torque at every instance of the simulation, given that ρ, n, D, J *and* α are always known quantities.

The coefficients $K_T = f(\alpha, J)$ and $K_Q = f(\alpha, J)$ are both functions of the incident angle and advance ratio. The advance ratio J is given by

$$J = \frac{V_a}{nD} \tag{3}$$

where V_a is the advance velocity.

Due to non-finite values of J when $n = 0$, the lookup surfaces for $K_T = f(\alpha, J)$ and $K_Q = f(\alpha, J)$ are remapped to become functions of incident angle α and thrust quadrant angle β, or $K_T = f(\alpha, \beta)$ and $K_Q = f(\alpha, \beta)$ where the thrust quadrant angle β is defined as

$$\beta = \tan^{-1}\left(\frac{V_a}{0.7\pi nD}\right) \tag{4}$$

and β is asymptotically limited to $\frac{\pi}{2}$ when $n = 0$.

To obtain the K_T and K_Q lookup surfaces, CFD experiments (Figure 11) are repeated at incident angles of $\alpha = 0°$ through to $\alpha = 180°$ in 15-degree increments. CFD results for K_T vs β at $\alpha = 0$ and $\alpha = 180$ are illustrated in Figure 12 and Figure 13, respectively. These two figures show the CFD simulation obtained values of coefficient K_T with respect to different thrust quadrant angle β at incident angle α = 0° and 180°. Continuous variation of α and β results in a pre-calculated look-up table or model surface for coefficient K_T.

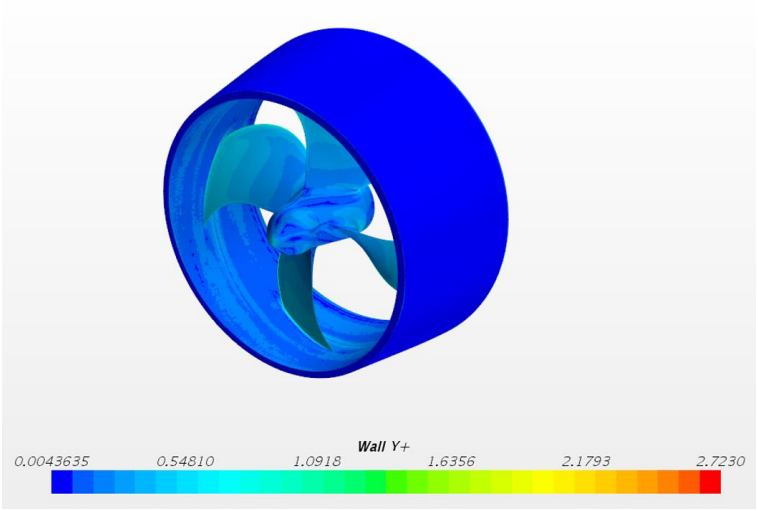

Figure 11 Propeller CFD Study Visualization

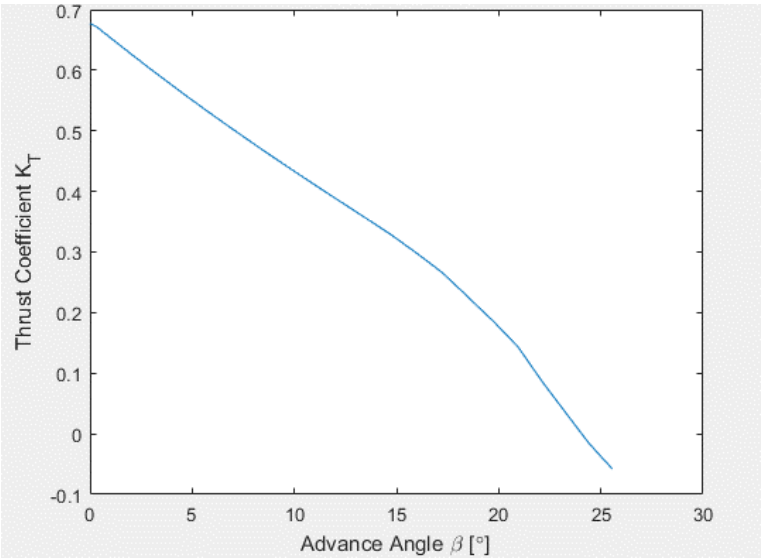

Figure 12 CFD results $\boldsymbol{K_T}$ vs $\boldsymbol{\beta}$ at $\boldsymbol{\alpha = 0^o}$

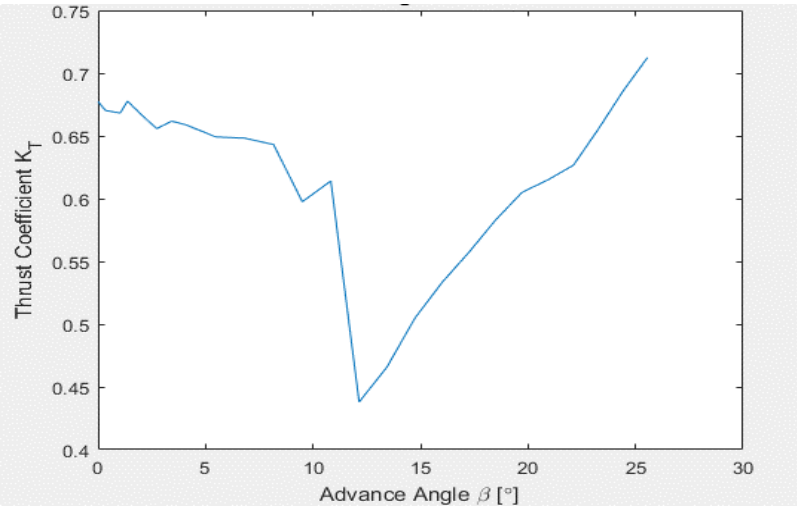

Figure 13 CFD Results $\boldsymbol{K_T}$ vs $\boldsymbol{\beta}$ at $\boldsymbol{\alpha = 180^0}$

After CFD results have been obtained, the discrete lookup table data is fit with polynomial functions as shown in Figure 14 and Figure 15.

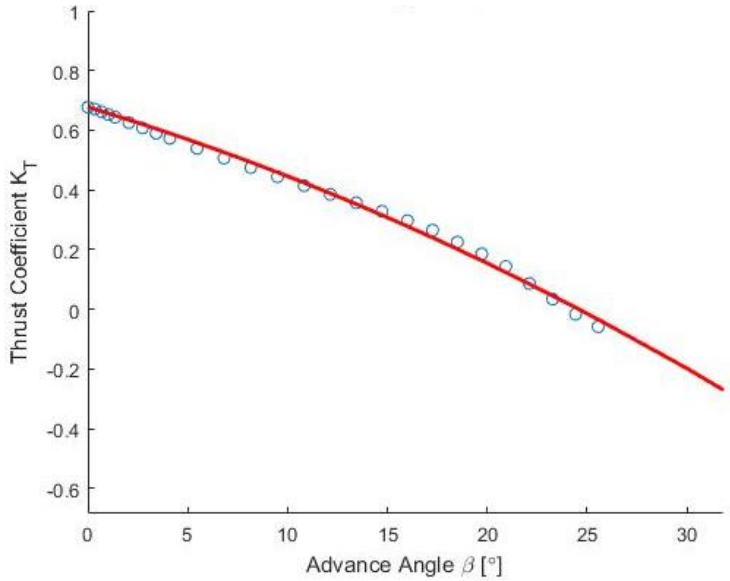

Figure 14 Fitted $\boldsymbol{K_T}$ vs $\boldsymbol{\beta}$ at Angle $\boldsymbol{\alpha = 0^0}$

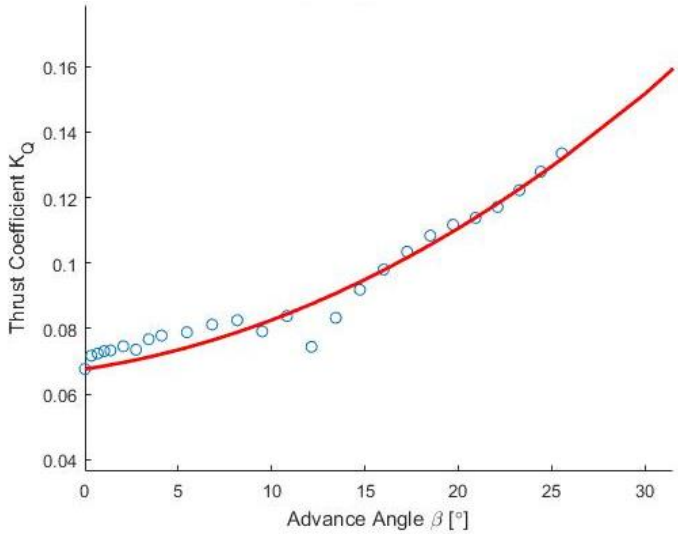

Figure 15 Fitted $\boldsymbol{K_Q}$ vs $\boldsymbol{\beta}$ at Angle $\boldsymbol{\alpha = 180^0}$

Repeating the curve fitting process at all angles of α, the K_T and K_Q lookup surfaces can be constructed as shown in Figure 16 and Figure 17.

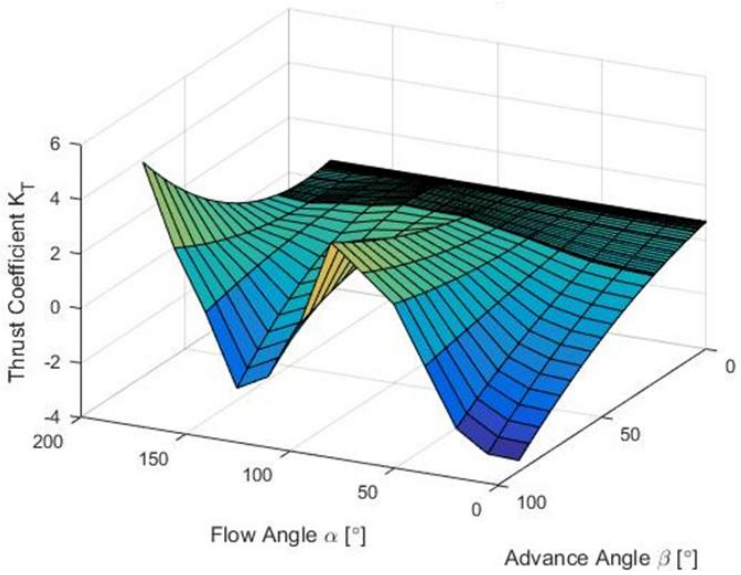

Figure 16 Fitted $\boldsymbol{K_T}$ Lookup Surface

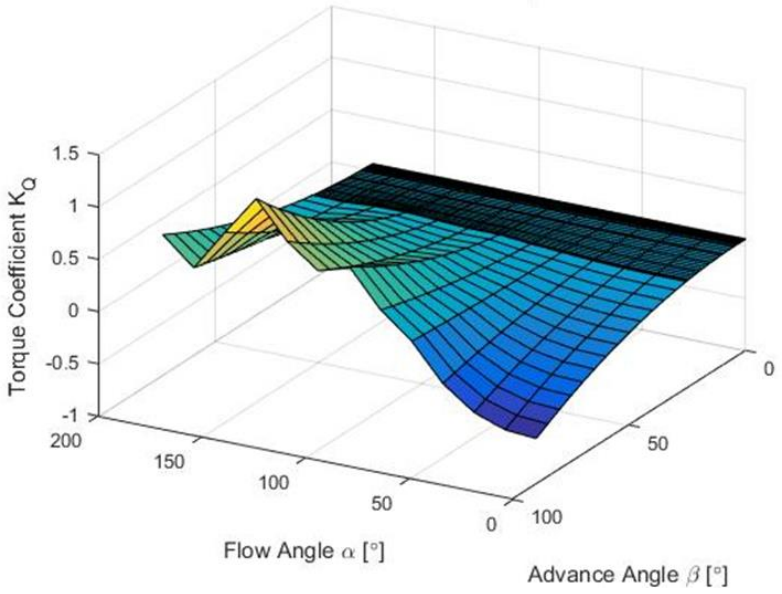

Figure 17 Fitted $\boldsymbol{K_Q}$ Lookup Surface

Once the lookup surfaces have been constructed, they are integrated into the propulsion module providing an efficient method to obtain propeller thrust T and torque Q at each iteration of the simulation in MATLAB/Simulink.

5.2.2 Revised Process for Thrust Deduction Factor

Due to numerical instabilities encountered during CFD analysis, the studies of propeller thrust and hull resistance are currently completed independently of each other. The presence of a rotating propeller near the hull causes a propeller-hull interaction that alters the local pressure fields around the hull [3]. This interaction has the effect of reducing propeller thrust according to

$$R = T(1 - t) \tag{5}$$

where R is the bare hull towed resistance, T is the required thrust and t is the thrust deduction factor.

As traditional naval architecture relies heavily on tow tank tests of bare hulls, empirical relations that quantify the expected thrust deduction effects are available for nearly all hull and propeller combinations.

As an example, the ship used in case studies detailed in Appendices L-M to validate the model employed the use of podded propulsion for which Flikkema *et al*. [4] proposed the empirical relation of

$$t = 0.21593 + 0.099768C_B - 0.56056\frac{D}{\sqrt{BF}} \tag{6}$$

where C_B is the box coefficient, D is the propeller diameter, B is the ship beamwidth, and F is the ship's draft.

5.2.3 Revised Process for Hull Resistance Parameterization

The process for hull resistance parameterization with corrections for appendage drag and wake fraction was revised to improve accuracy and augment the simulation model with previously unaccounted for sources of resistance. Fossen [5], proposes a modified equation for hull resistance in the surge that produces more accurate resistance at low speed

$$F_{Drag} = \underbrace{X_u u_r}_{\substack{Linear \\ Force}} - \underbrace{\frac{1}{2}\rho S|u_r|u_r(1+k)\cdot\left[C_F(u_r{}^{max}) + \left(\frac{A_x}{S}C_X - C_F(u_r{}^{max})\right)e^{-(\mu\cdot u_r{}^2)}\right]}_{\substack{Non-Linear \\ Force}} \quad (7)$$

where A_x is the projected frontal wetted area, S is the wetted surface, u_r is the ship velocity in surge, $C_F(u_r{}^{max})$ is the hull friction coefficient at design speed, and X_u, k, C_X, and μ are four parameters that are fitted to the bare hull resistance results, F_{Drag}, through regression methods as shown in Figure 18.

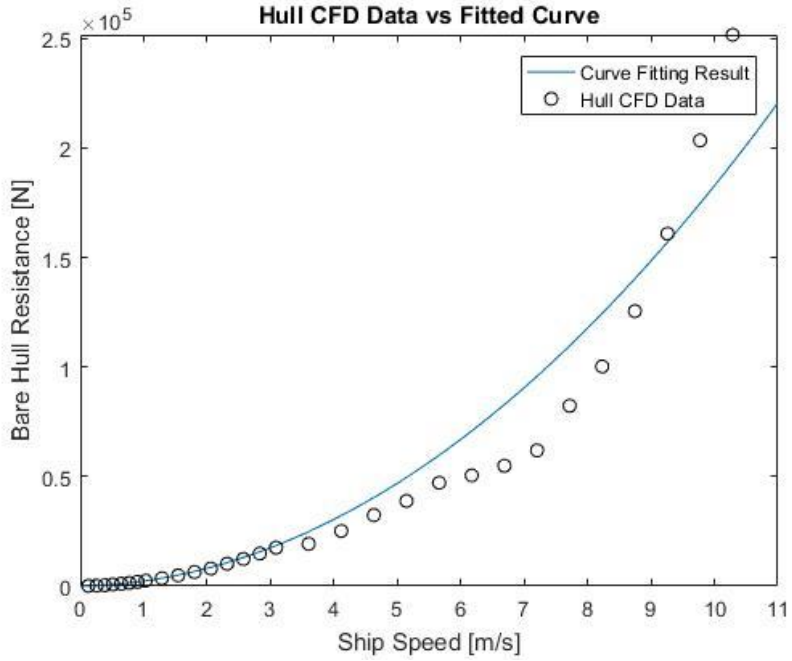

Figure 18 – Curve Fitting of CFD Bare Hull Resistance

Once the equation for hull resistance has been parameterized from bare hull CFD results, the bare hull resistance is then augmented with appendage drag resistance using available empirical relations according to the ship being studied. A study of a ship with podded propulsion for example, may reference Abdul Ghani *et al.* [6], where it was concluded that podded propulsion modules increase ship's total resistance by approximately 20% over bare hull resistance values obtained from tow tank tests and CFD analyses.

In addition to modifying the hull surge resistance, it is essential to capture the hull propeller interaction known as wake fraction. Due to the geometry of the hull and its effect on the flow field, the advance velocity of the fluid into the propeller is not always equal to the ship's forward velocity. Advance velocity is provided by

$$V_a = (1 - w)u_r \tag{8}$$

where w is the wake fraction parameter and u_r is the ship velocity in surge.

To obtain estimates for wake fraction, velocity probes were inserted in the bare hull CFD studies and placed at the locations where the propellers would have been. Advance velocities were measured and values for wake fraction were obtained for a range of forwarding ship velocities as shown in Figure 19. These results are used in the vessel proportion force model to take care of the effects caused by the wake at different vessel speeds.

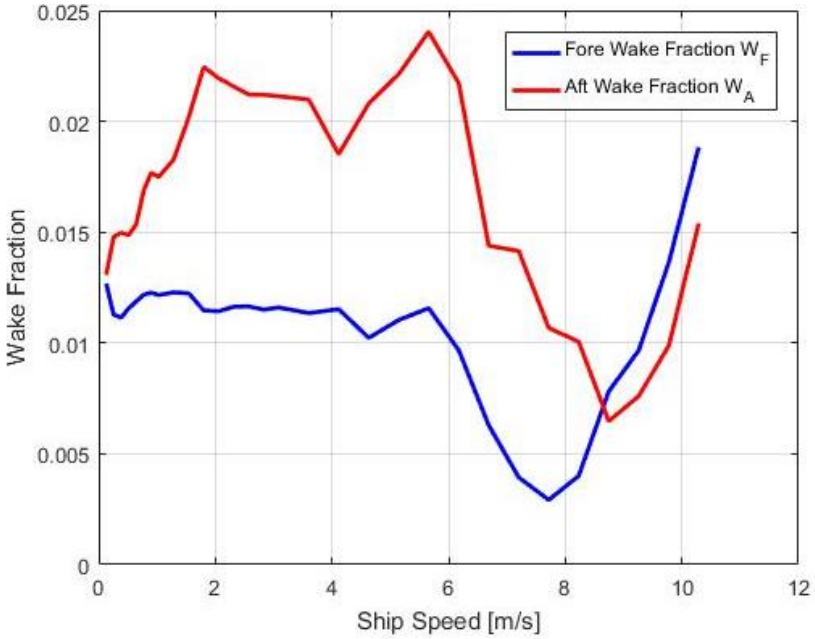

Figure 19 – Wake Fraction

The wake fraction curves and augmented bare hull resistance were then integrated into the model to account for these effects.

5.2.4 Ocean Current and Wind Loading Estimates through ProteusDS Simulations

To account for ocean current and wind forces on the hull and superstructure, simulations in ProteusDS software were conducted. ProteusDS is a full-featured dynamic analysis software capable of simulating vessels, structures, lines, and technologies in harsh marine environments, produced by Dynamic Systems Analysis (DSA) - an ocean engineering consultancy and software company based in Victoria, British Columbia. DSA is a close industrial collaborator of UVic's ocean energy and green ship research teams. The use of ProteusDS can effectively model ocean current and wave variations and their resulting forces. For this process, both current and wind velocity data were obtained from weather buoys near the route being studied. A 3D mesh representing the hull and superstructure was loaded into ProteusDS (see Figure 20) and the software calculates the total loading forces through the summation of the force from each panel of the mesh using

$$F = \frac{1}{2}\rho C_d A \tag{9}$$

where ρ is the density of the fluid (seawater for current forces, or air for wind forces), C_d is a marine structure related coefficient, and A is the frontal surface area of the vessel.

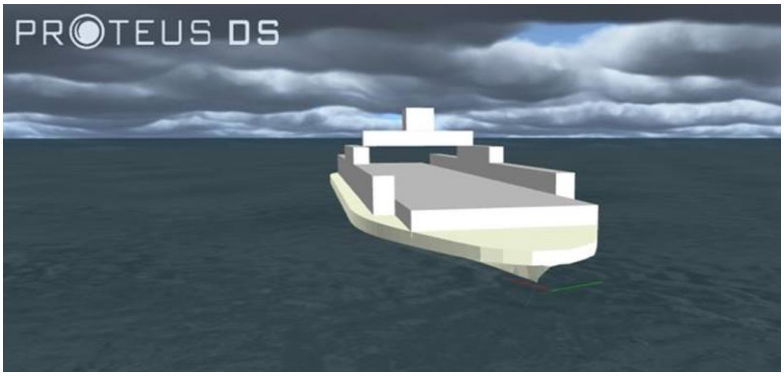

Figure 20 Ocean Current Loading Study above Waterline View

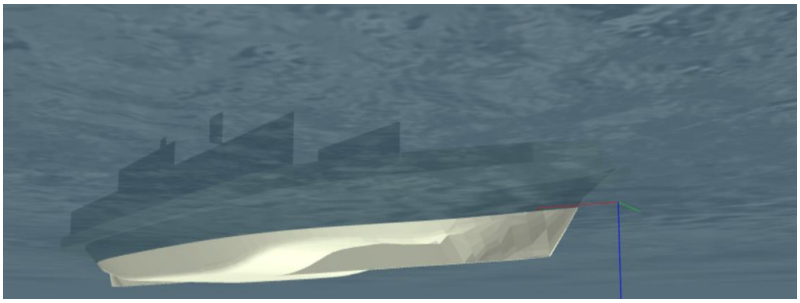

Figure 21 Ocean Current Loading Study below Waterline View

Simulation parameters, and resulting current and wind loads from a case study on the Skeena Queen are presented in Table 1.

Table 1 Ocean Current and Wind Loading Study

Ship velocity (m/s)	7.0
Ship Heading (deg)	13
Current Direction	80
Current speed (m/s)	1.03
Wind Direction	100
Wind Speed (m/s)	2.78
Wind loading - x Direction (N)	1.46E+02
Wind loading - y Direction (N)	4.30E+02
Current loading - x direction (N)	1.20E+04
Current loading - y direction (N)	1.10E+05

While current and wind loading is presently approximated as constant for the duration of short voyages, the capability to vary wind and current velocities over the course of a voyage is being implemented by adjusting the relative speed of the vessel in the water.

This work is also documented as a separate document in Appendix G. Improvement of the Reduced-Order Hydrodynamic and Ship Propulsion Model.

5.2.5 Improved Reduced-order Hydrodynamics Model

In our previous and present work, the full mathematical formulations of the reduced-order hydrodynamic propulsion model - a 6 Degree of Freedom (DOF) dynamic model with ship hydrodynamic parameters obtained from full-scale CFD simulations have been introduced. This model is capable of supporting new ship design, serving as a benchmark, and capturing the dynamic behaviours of the vessel. However, the full implementation and parameterization of these six DOF models are very complex and unnecessary for evaluating the hybrid electric powertrain system design. In this work, a 1-DOF longitude direction, motion model along the direction of ship movement has been implemented and verified in MATLAB/Simulink, as well as used in all case studies. The model met the basic requirements for evaluating and comparing different vessel propulsion solutions in terms of speed performance, energy efficiency, fuel consumption, and emissions.

The work to further implement the other two key influencing DOFs of ship motions, in the directions perpendicular to the direction of ship movement and the ship turning has been initiated. This work, however, needs complex, close-loop dynamic vessel operation controls to be added to the reduced-order hydrodynamics model, thus requiring more time and effort to complete. This is part of our future work beyond the scope of the present contract. The benefit of this addition is the ability to introduce dynamic operation control of the vessel. This can improve the propulsion force/energy calculation and propeller cavitation/noise prediction during the dynamics maneuvers of the vessels, including during sharp turns and docking operations. The present quasi-static modelling tools developed during this contract work have relatively large errors for those dynamic vessel operations.

5.3 Modularization of the Developed Modelling Tools

To improve the usability of the HEMV-MBDOT platform, the modelling tools have been modularized in this work to support versatile marine applications, and to allow different functional elements of the modelling platform and different powertrain component models to serve as flexible building blocks of the integrated system model, depending upon the vessel and propulsion system to be modelled.

5.3.1 System Modularization Work

The intention of using a modularized modelling method for green ship simulations in MATLAB/Simulink environment is to partition a complicated ship model into several sub-systems. By categorizing all the components into different modules, it is much easier to integrate them together, after building and verifying simulation models for each module. The complexity and computational time could also be reduced by identifying the inputs and outputs signals between modules instead of tangling all the components signals together. The BC Ferries' Skeena Queen, discussed in Section 4.2, is used as an example to illustrate how the modularized green ship model works. Details of the hybrid electric ship propulsion system design are given in Appendix M Case Study for Skeena Queen.

As complicated as a bulk ship can be, the ship simulation model can be separated into four main modules, as shown in Figure 22. In this figure, the travelling velocity of the vessel is marked as, `V_ship`, and `P_req` represents the required propulsion power of the vessel to travel at the given velocity.

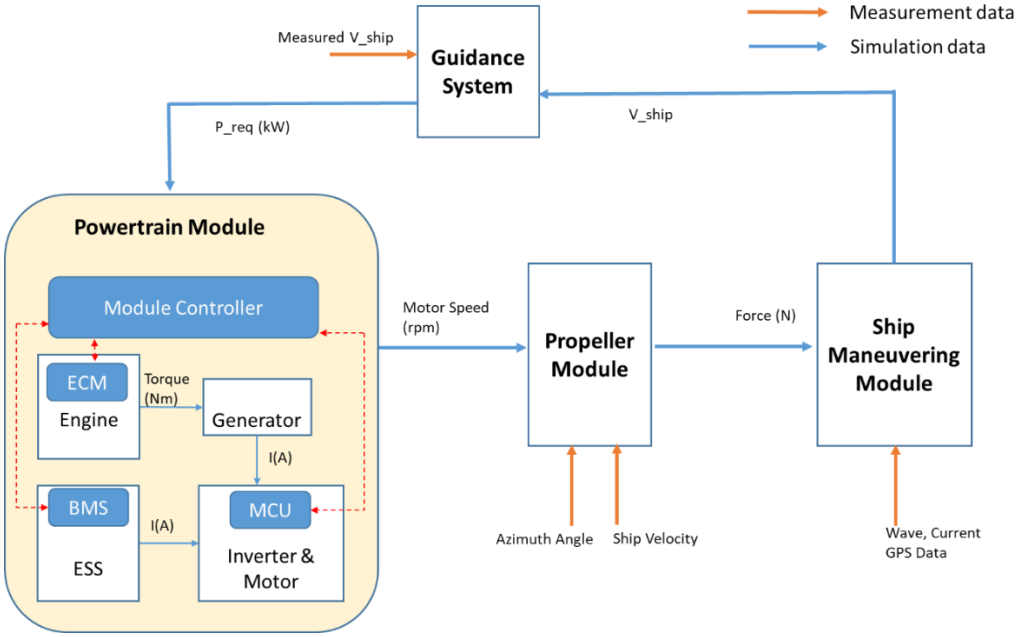

Figure 22 Modularized Ship Simulation Model

The powertrain module is the power supply system that consists of all the prime movers in the ship. Depending on the propulsion system, it could be purely mechanical, pure electric, or hybrid propulsion. In Figure 22, the vessel propulsion system has a series hybrid electric propulsion architecture. Engines, battery energy storage system (ESS), motors and converters are all included in this powertrain system module. Inside this module, a module controller, or supervisory controller, collects all the signals from the engine control module (ECM), the battery management system (BMS) and the motor control unit (MCU), to generate a high-level control strategy for power distribution between the engines and the battery ESS.

The propeller module takes the motor speed signal from the powertrain module, as well as data measurements of azimuth angle and ship velocity, for the purpose of propeller simulation. The thrust forces would be the output signal from the propeller module after the calculation.

The ship-maneuvering module accepts the thrust force signal and other measurement data, such as wave, wind, and current data to calculate the ship hydrodynamic performance.

The ship guidance system takes the simulated ship velocity signal and compares it with measured ship velocity to give instructions to the powertrain module and eliminate any errors.

Besides taking ship velocity as a control variable, it could have other control methods such as using motor speed for the controller in the powertrain module. The modularized integrated system model is thus separated into several independent function modules connected by key system state and control variables. Replacements of powertrain system, propeller, or ship maneuvering

elements would be very straightforward without the need to re-develop the complete integrated system model.

5.3.2 Modular Simulation and Validation

The suggested modelling method is to build the model and validate each module separately. By doing this, the complete green ship model can be integrated easily and maintain clean signals between components. The likelihood of success is increased since all modules have been individually tested to be accurate and robust.

The propulsion system of a vessel can be modelled using a backward-facing modelling method, or a forward-facing modelling method. The backward-facing modelling method models the behaviour of the propulsion system using a vessel's velocity profile as the system input and tracing back to the skipper's "throttle" command through inversed speed transmission and power flow in the powertrain. The approach assumes that the power and velocity required by the vessel's operation can always be met by the vessel's powertrain plant. The forward-facing modelling method, on the other hand, models the propulsion system using the skipper's "throttle" command as the system input, tracing the power flow from the power plant to the propeller, and calculating the resulting ship velocity. The difference between the target ship velocity and the calculated ship velocity is then fed back to the skipper's model for adjusting the "throttle" command to reduce this difference through a series of control operations in closed-loop control. The backward-facing modelling method is easy to execute without the need for complex closed-loop velocity control and is appropriate for quick system design and parameter determination. The method is particularly advantageous for powertrain component size optimization that requires many loops of system simulations. The more accurate and more realistic forward-facing modelling method is used in developing the control system of the vessel, and in obtaining more accurate simulation results.

Among all electrified ship propulsion systems, the pure electric powertrain, as shown in Figure 23, has the simplest form, consisting of a battery ESS, a DC/DC converter, and electric motor(s). No diesel engine(s) and complex hybrid electric powertrain control are involved. The powertrain includes a PID controller that control the motor/propeller speed and resulting propulsion force.

During normal operation, a vessel needs to follow a given GPS route at a prespecified velocity, or target velocity. The Ship Maneuvering Module of the modelling tool predicts ship velocity, heading and trajectory changes under the propulsion force produced by the vessel's propulsion system, and loads of wind, wave and current. The calculated ship velocity, heading and trajectory are used as the "measured" velocity, heading and trajectory in the simulation. The PID controller in the Powertrain Module, shown in Figure 23, compares the target and "measured" ship velocities and GPS routes, and adjusts the propulsion system control to minimize the error, thus allowing the vessel to operate as expected. Vessel velocity is actually controller by varying the motor current to adjust the speed of the propulsion motor in the Powertrain Module.

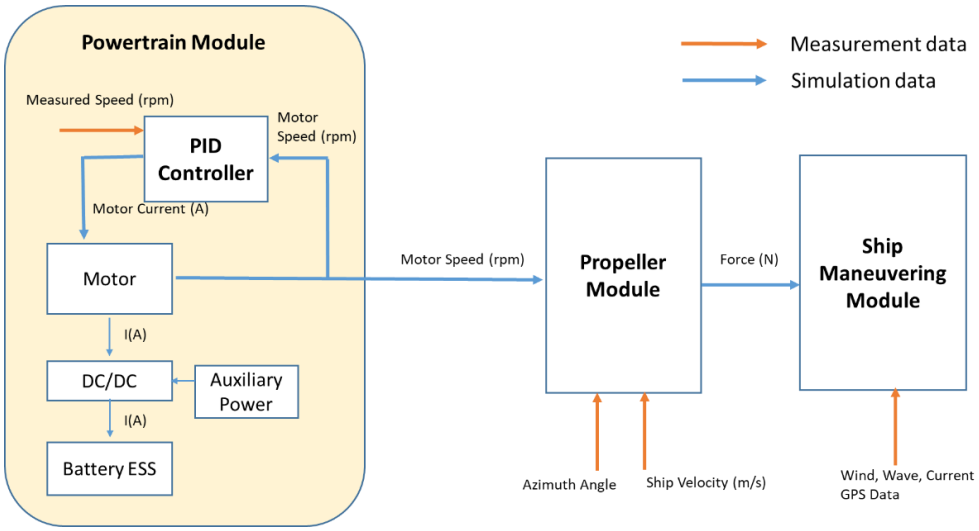

Figure 23 Pure Electric Powertrain System

Figure 24 demonstrates a backward-facing model with the propeller and ship maneuvering modules. The input signals are the previously acquired vessel velocity and GPS data. The vessel velocity is used as input to the ship propulsion simulation. The difference between the expected or targeted vessel speed and the predicted vessel speed is calculated to find the needed propulsion power adjustment. The resulting power output of the simulation model is compared with the actually measured vessel propulsion power for model validation, as discussed in Section 4. It is now easier to focus on building an accurate, functional sub-system module and verifying it without the interactions and couplings from other modules.

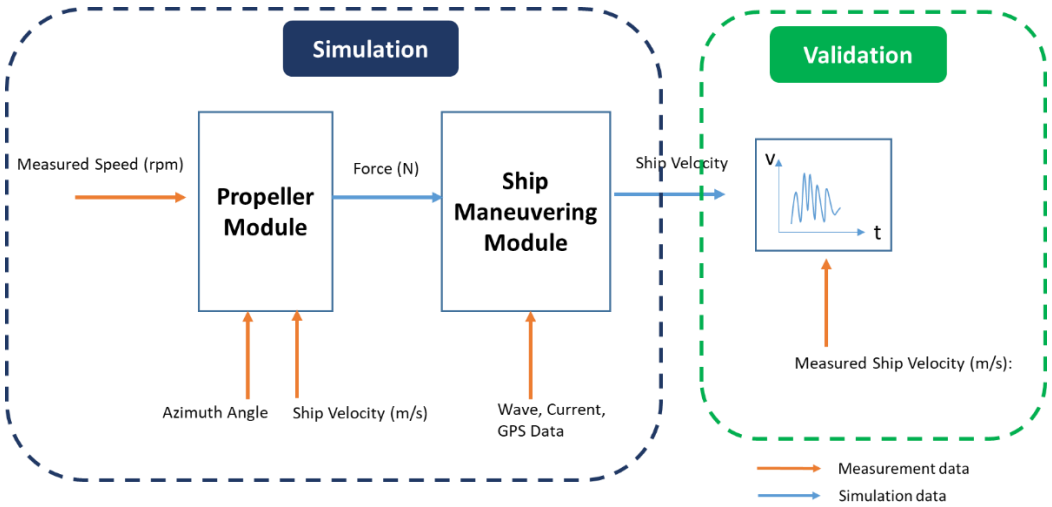

Figure 24 Backward-facing Modelling for Propeller and Ship Maneuvering Modules

The forward-facing model can also be built after acquiring an accurate propeller and ship-maneuvering model, as showed in Figure 25. The simulated ship velocity is a control signal in the module controller to determine if the propulsion system can meet the thrust demand from the ship hull to follow the prespecified vessel velocity that was measured and recorded from routine operations. The powertrain system controller, acting as the brain of the skipper, compares the difference between the targeted ship velocity and actual velocity, and produce corrections to the

skipper's "throttle" or power input. At each instance of time, several iterations of the simulation are needed before the actual velocity of the vessel meets the targeted velocity, at this single time point of a long driving cycle. This approach is consistent with the experience of operating a vessel but requires many more simulations and higher computational time requirements.

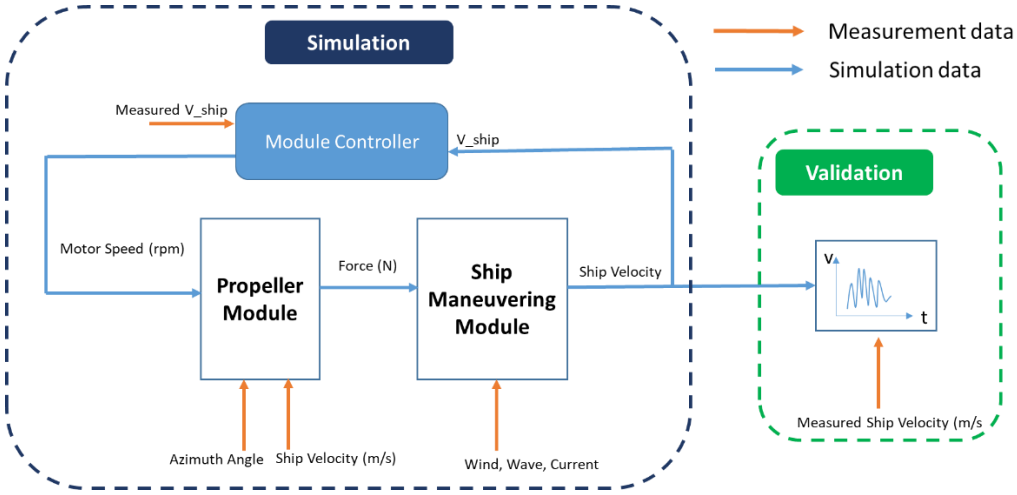

Figure 25 Forward-facing Modelling for Propeller and Ship Maneuvering Module

A pure electric powertrain can be modelled using a simple, one-pass backward-facing model illustrated in Figure 26, in which the measured propulsion motor speed is used to calculate the needed operation speed and torque of the electric motor in the powertrain module, regardless of its ability to operate at these reversely calculated speed and torque.

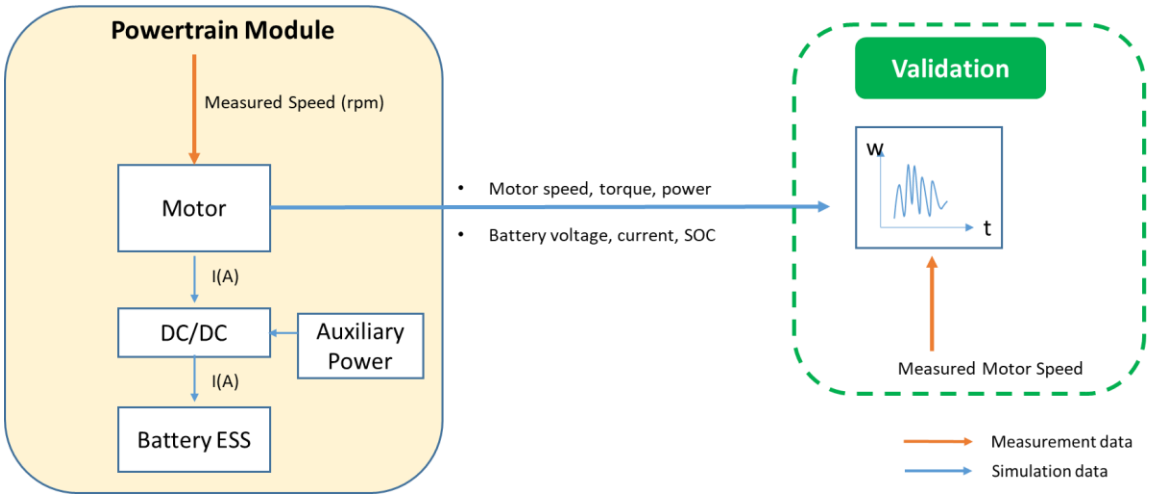

Figure 26 Backward-facing Modelling for Pure Electric Powertrain Module

5.3.3 Integrated System Model of Marine Propulsion System

A more realistic forward-facing model of the pure electric powertrain is shown in Figure 27. The powertrain module controller controls the speed and torque of the electric motor in the powertrain module by reducing the difference between the measured and actual propulsion motor speeds, which correspond to the expected and simulated ship velocities, through many adjustments of the control loop. The measured motor speeds were acquired simultaneously with the expected vessel

velocity during vessel operation data acquisition. The integrated propulsion system model was built using the powertrain system component models based on the experiential data from the manufacturers and the validated propulsion drag and thrust models. A supervisory powertrain module controller of the propulsion system is needed to control the flow of all signals from sub-systems and issue instructions to sub-controllers, according to the developed system control algorithms. A forward-facing pure electric powertrain system model with module controller is shown in Figure 27.

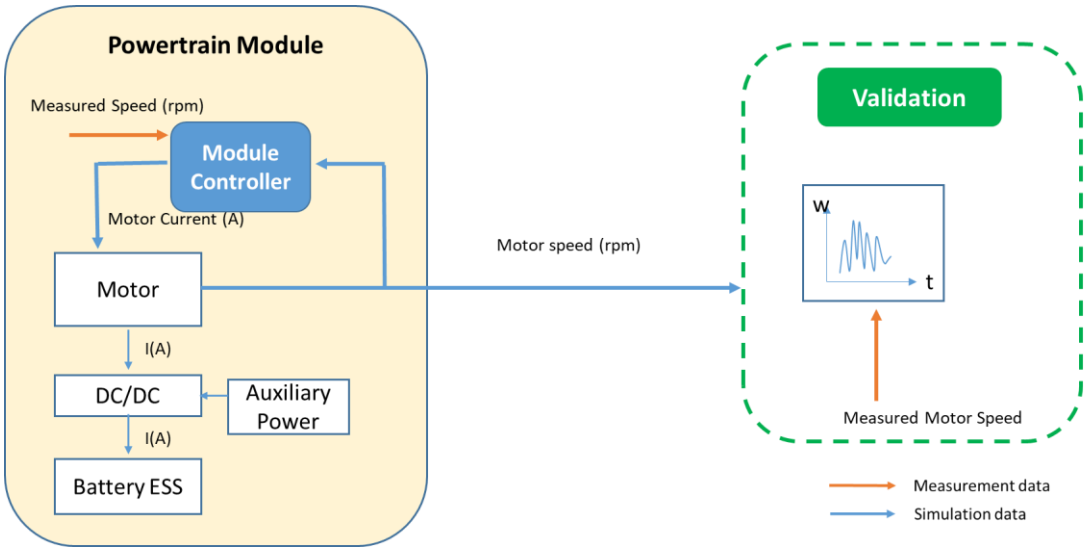

Figure 27 Forward-facing Modelling for Pure Electric Powertrain Module

Depending on the complexity level of plant modelling, each module can have several different forms, such as a simpler power loss model, or a more detailed multi-physics model. The simple power loss models are normally built using empirical data from the plant and stored in the form of lookup tables of plant outputs vs. inputs. The composition and connection of the functional modules of the integrated system model are shown in Figure 28.

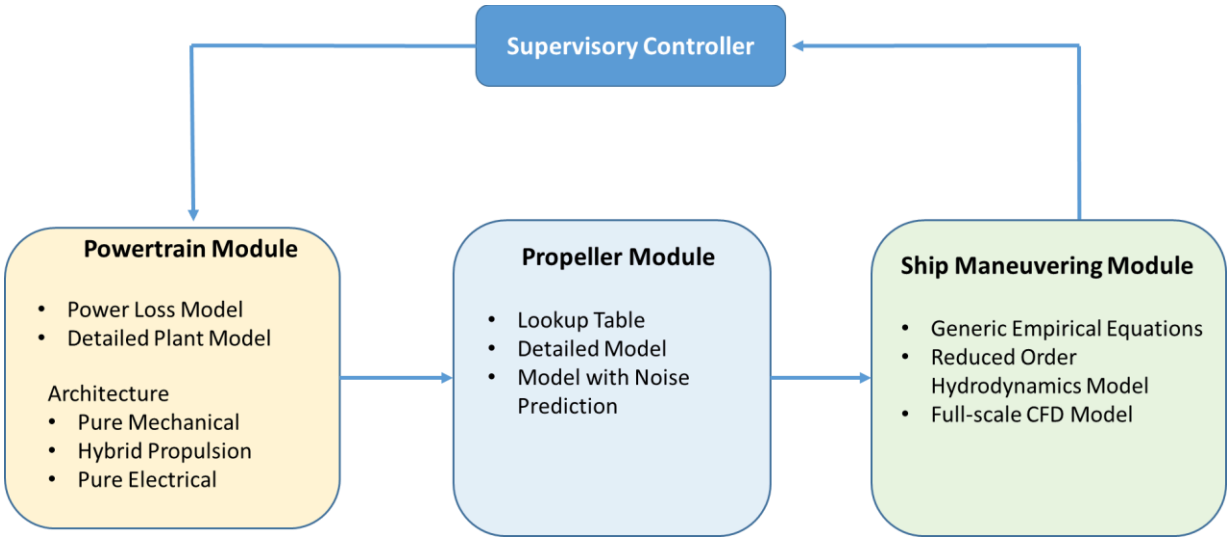

Figure 28 Integrated Vessel propulsion System Model

5.4 New Low-Order Hull Drag Regression Modelling Method

In section 3.3.2, the needs of low-order hull drag and propeller thrust models and their functions have been introduced. Although this work was not in the original plan, preliminary research has been carried out on this subject, leading to promising results, as reported in this sub-section.

Specifically, research efforts have been made to introduce a semi-static hull drag model that is built directly using data from the Ship Stability Book (SSB) of an existing marine vessel. The SSB is generated when the ship is developed through sea trials, or obtained using simple, one-path CFD simulations. In this work, another function of the SSB data has been found and put into use to generate the low-order hull resistance model of the existing marine vessel. This learning is acquired through the collaborative work with BC Ferries on their ferry ships.

The stated one-path CFD simulation can be carried out using regular CFD software and workstation, eliminating the need of computational intensive full-scale CFD and simulations on a supercomputer. This is largely the motivation for our work, as it allows the developed modelling tools to be used by average marine companies.

The low-order hull resistance prediction model, based on statistical regression methods, has long been the subject of marine propulsion research, which resulted in methods for predicting the trial performance of single- and twin-screw merchant ships. Among them, is the regression-based method of Holtrop and Mennen 1982 [2]. The key challenge in using this model is to obtain accurate model inputs for new hull design, or for older vessels with only limited technical information. In this section, the Holtrop/Mennen model and method for obtaining its inputs are discussed. Combining this regression model with the method of obtaining the model inputs for a specific vessel form, leads to the new Dedicated Hull Drag Regression Modelling Method. The hull resistance modelling results of a representative BC ferries' ship are compared with the results from full CFD simulation to validate the new low-order modelling method.

5.4.1 Dedicated hull drag regression modelling method

In Holtrop and Mennen [2], the total hull resistance is subdivided into the following parts:

$$R_T = R_F\,(1+K_1) + R_{APP} + R_W + R_B + R_{TR} + R_A \qquad (10)$$

where, R_T is the total resistance, R_F is the friction resistance, $1+K_1$ is the hull form factor, R_{APP} is the resistance of appendages force, R_W is the wave-making and wave-breaking resistance, R_B is the additional pressure resistance of a bulbous bow near the water surface, R_{TR} is the additional pressure resistance of immersed transom stern, and R_A is the model-ship correlation resistance.

5.4.2 Inputs for hull resistance

The inputs for calculating the hull resistance of the Holtrop and Mennen's method includes:

- Length on the waterline (LWL)
- Length between perpendiculars (L_{pp}) (length of a ship along the waterline from the forward surface of the stem)
- Breadth moulded (B)
- Average moulded draft (T)
- Displacement volume moulded (V_d)

- Longitudinal centre of buoyancy (*LCB*) (forward +, aft -)
- Draft moulded on F.P. (T_f)
- Draft moulded on A.P. (T_A)
- Transverse bulb area (A_{bt})
- Centre of bulb area above keel (h_b)
- Midship section area (A_{mid})
- Waterplane area (A_w)
- Transom area (A_t)
- Wetted area of the hull (S)
- Wetted area appendages (S_{app})
- Bow thruster tunnel diameter (d_{bto})
- Bow thruster tunnel openings coefficient (C_{bto})

These values are dependent on the hull geometry as well as the loading conditions, which determine the draft and the longitudinal center of buoyancy. These, in turn, influence other variables, e.g. length of the waterline, displacement volume moulded, midship section area and waterplane area.

If the draft and the longitudinal center of buoyancy are known (as for most existing and operational vessels), the rest of the parameters can be obtained readily using the CAD model of the hull on most 3D CAD systems. An example hull model of BC Ferries' M.V. Klitsa, shown in Figure 29 has been used to obtain the hull parameters, including *LWL*, L_{pp}, midship section area, waterplane area, and wetted area.

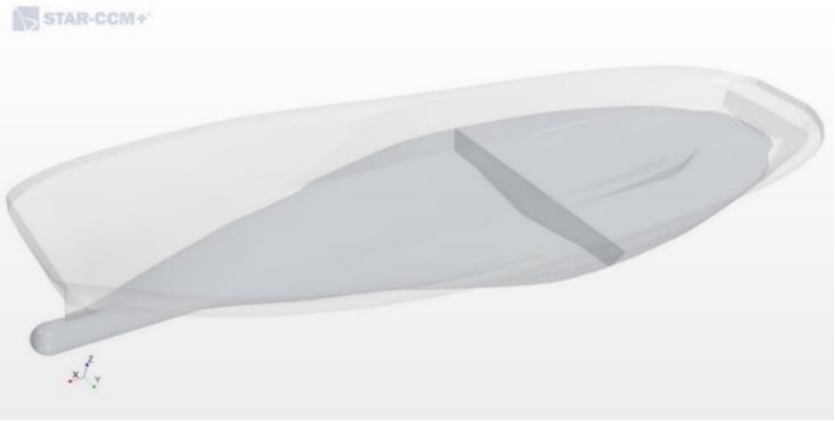

Figure 29 CAD model of M.V. Klitsa for hull geometry analysis

For most operational vessels, the draft and the longitudinal center of buoyancy, for different loading conditions, are available in the SSB. For a new hull geometry or design, these variables under different loading conditions can be obtained by conducting CFD simulations on the floating hull, as numerical tow tank experiments with zero inflow velocity. The simulation will also yield the hydrostatic position of the vessel. In comparison with the full-scale, hull resistance CFD studies, this one-pass CFD analysis requires considerably less computational time and a courser mesh, as shown in Figure 30.

5.4.3 Model validation

The input parameters, obtained for BC Ferries' M.V. Klitsa as shown in

Table 2, have been used to validate the proposed low-order hull resistance model. The predicted hull resistance results are compared with the hull resistance results obtained from CFD simulations as shown in Figure 31, showing excellent agreement.

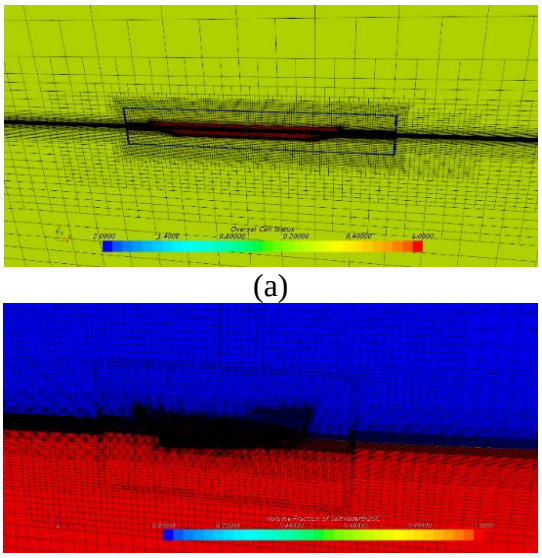

(a)

(b)

Figure 30 Examples of the one-pass CFD mesh for calculating the input parameters (a) MV Skeena Queen ferry, (b) Cape Islander fishing boat

Table 2 Input parameters of the dedicated ship drag regression method for M.V. Klitsa

Density, kg/m^3	1024.8103
Viscosity	0.001077
Ship velocity, knots	From GPS recordings
LWL, m	46.1568
Lpp, m	44.42
B, m	13
T, m	2.46835
Vd, m^3	690.78
LCB	-3.65
T_f, *m*	2.46835
T_a, *m*	2.46835
A_{bt}, m^2	1.3607
h_b, *m*	1.05
A_{mid}, m^2	22.0566
A_w, m^2	429.1799
A_t, m^2	0.8772

S_{Skeg}, m^2	26.5243
d_{bto}, m	0.125
C_{bto}	0.003
C_{stern}	0

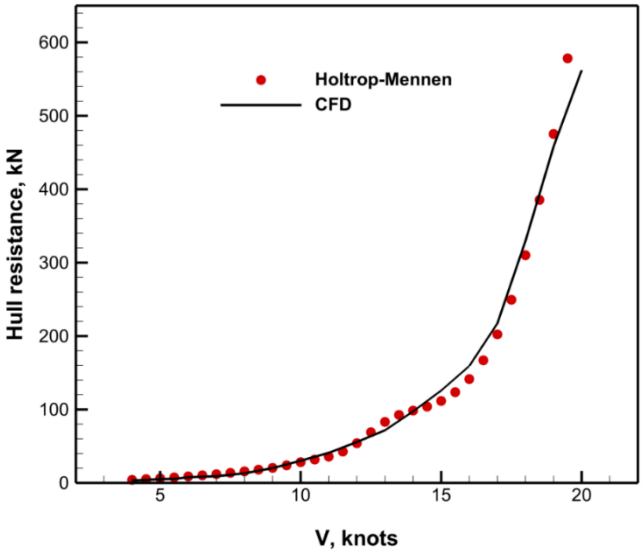

Figure 31 Comparison between the dedicated ship drag regression and numerical results

5.5 New Low-Order Propeller Thrust and Cavitation (Noise) Models

As discussed previously in section 5.2, traditionally hull drag and propeller thrust models follow two different techniques, generic empirical equations and full-scale CFD. Both of these two approaches have their drawbacks and limitations, particularly for the integrated marine propulsion system modelling tools. To address these issues, high fidelity, reduced-order hydrodynamic models for calculating propeller thrust and methods for predicting propeller cavitation and mapping propeller cavitation to cavitation noise have been introduced in our previous work and further improved during this contract research.

For the same reasons discussed in Section 5.4, to reduce the dependence on computation-intensive CFD simulations to get the model parameters of the reduced-order hydrodynamic models, studies on new, alternative semi-empirical propeller torque-thrust and cavitation models have been initiated. This work is beyond the scope of the contract and will be fully engaged in future work, but the promising preliminary studies and results are worthy of a brief overview of this report.

5.5.1 Propeller modelling and design tool – ROTORYSICS

At the core of the propulsion system, design and analysis lay hydrodynamic modelling of propellers themselves. Accurate knowledge of propeller operation physics is fundamental to both hybrid propulsion system design and acoustic noise generation; both of which are core aspects of this contract work. Many tools exist to model propeller performance, of varying complexity and accuracy, from rudimentary actuator disk theory to high-resolution CFD simulations. A satisfactory balance of accuracy and computational expense is provided by a panel method

approach [3], as found in the software package used by researchers working on propeller modelling and design, ROTORYSICS (formally PROPELLA, 1999-2015). Specifically, ROTORYSICS is a low order source-doublet, steady/unsteady time domain panel method code that has been developed to predict the hydrodynamic performance of screw propellers and extensively validated against experimental data. The panel method originated from earlier panel codes introduced in the late 1960s for determining fluid velocity, and subsequently the pressure distribution on an object. Panel codes gained popularity with the advance of computing capability, and were replaced with higher-order panel methods and subsequently CFD [3]. However, the panel codes and panel method are still used for preliminary aerodynamic analysis, as the time required for an analysis run is significantly less due to a decreased number of elements comparing with the CFD simulation.

ROTORYSICS is being used by the UVic Green Ship team to quantify propeller performance under the influence of many parameters. The code capably models the flow physics of a ship's propeller under the influence of pods, nozzles, rudders, ice-blockage, non-uniform hull-wake profiles, blade surface cavitation, and any combination of these parameters. Unlike fully resolved CFD approaches, ROTORYSICS does not require supercomputing resources but rather runs on common computing devices. The low computational expense of the panel method allows a large number of numerical tests to be completed in a reasonable timeframe. ROTORYSICS, therefore, facilitates batch execution, covering a large parametric space for database development and performance optimization. As an example, the range of operating conditions that represent a vessel's operating route can be calculated in an automated manner. Alternatively, propeller geometries can be optimized provided a set of constraints to minimize acoustic emissions or maximize propulsive efficiency.

The ROTORYSICS codes are capable of predicting sheet cavitation occurring on the propeller blades. The size of the cavitation sheet can be related to net noise emissions of the propeller. The cavitation event is modelled within the software by means of a sophisticated semi-empirical scheme that models "chop-off and fill-in" of pressure near cavitating regions. Time-varying cavity volume changes can also be calculated, which are responsible for a large portion of the generated acoustic noise spectrum. The panel method approach is limited to computing sheet cavitation only. Other forms of cavitation, such as tip vortex cavitation and bubble cavitation, are not accurately estimated by these approaches but occur less commonly [13].

The planned research is to test and modify the ROTORYSICS codes, and to use it as the propeller thrust prediction and cavitation detection module. This module will interface with the propeller driving system module at the front and the cavitation to ocean noise mapping function module at the end. This "low-order" propeller thrust and cavitation noise prediction module can thus replace the present reduced-order hydrodynamic model module and avoid the full CFD modelling and simulations needed to obtain the model parameters for the reduced-order hydrodynamic model.

5.5.2 Validation of Propeller Thrust and Cavitation Noise Models

All propeller thrust and cavitation noise models, in reduced-order, in low-order, or by full-scale CFD, need to be validated against measured data. The propeller thrust has been verified directly using acquired vessel operation data, while the more challenging validation of cavitation noise and more accurate thrust measurements have been completed in collaborating a world-leading research laboratory on propeller cavitation noise. The laboratory is led by Professor Michele Viviani of the

Naval Architecture Group in the Department of Electrical, Electronic, Telecommunication Engineering and Naval Architecture (DITEN), University of Genova, Italy.

Specifically, validation of hull resistance and propeller thrust models were conducted using the acquired vessel operation data, including the measured propulsion power and vessel speed. The propulsion power was obtained from the speed and torque readings from the propeller shaft, and the vessel speed was retrieved from the vessel's GPS data. On the other hand, validations of propeller cavitation and cavitation noise were carried out experimentally using a scaled propeller model in the pressurized cavitation tunnel at the University of Genoa, Italy, through our collaborative work in March 2017. Details of the experimental setup, the obtained results and their comparisons to results from full-scale CFD simulations are documented in Appendix H. Experimental Investigation of Cavitation-induced Propeller Noise, and [13].

The full-scale CFD models and simulation results validated using vessels' operation data and cavitation tunnel experiments are later used to verify results from the reduced-order hydrodynamic models as part of the contract work. The verified full-scale CFD models and simulations are also used as generic validation tools for other simplified modelling methods, including the low-order hull resistance and propeller thrust models, as well as the reduced-order propeller cavitation model using the panel method.

5.5.3 Experimental Model Validation with New Canadian Collaborators

An alternative validation method is to use the ocean noise measurement directly on passing marine vessels. Collaboration with JASCO Applied Sciences has been initiated and planned. The work is aimed at improving the ability to model noise sources and establishing a real-world ship noise validation method. The work will be carried out in the following stage of this research.

Efforts have been made to initiate possible collaboration with the Ocean, Coastal and River Engineering (OCRE) Laboratory of NRC through the connection with Dr. Shameem Islam to update OCRE's cavitation research facilities for propeller acoustic noise measurements. The UVic Green Ship research team would provide design specifications for the facility modifications and the instrumentation, as well as the experimental procedures for dynamic scaling the propellers and for cavitation/noise imageing measurements. The OCRE would be responsible to carry out the facility updates. This joint effort, if successfully completed, would produce a new and unique experimental facility in Canada. The work is to be carried out in the future, pending available research funding.

6 IMPROVEMENTS OF HYBRID POWERTRAIN AND INTEGRATED POWER SYSTEM MODELS

This section is devoted to the Hybrid Electric Powertrain System Model block introduced in the system overview of Section 3.3 and Figures 2, 3 and 4.

Extensions of the integrated hybrid electric marine propulsion system modelling tools with additional modelling capabilities are summarized in this section. These include:

a) broader hybrid electric powertrain component selections;
b) different electric power bus types, AC and DC;

c) addition of Natural Gas (NG) engine efficiency and emissions models to support the replacement of diesel engines and introduction of the new integrated NG engine hybrid electric propulsion technology;
d) new battery performance degradation model for ESS size optimization and optimal energy management; and
e) powertrain system design and control optimizations.

Details of these technological developments are documented in the detailed subject reports Appendixes D to F and case studies Appendixes K to R.

6.1 Building Marine Hybrid Powertrain Component Model Library

The marine powertrain system is considered the marine propulsion system without the propeller. It is similar in form to the vehicular powertrain system, but different in component size, capability, and pattern of use. The key components of a generic powertrain system consist of the following:

- Power Plants
  - Diesel or Gasoline Engines – diesel is the typical international combustion engine (ICE) for marine applications, while smaller boats also use gasoline engines.
  - NG Engine – At present, large NG engines are often NG and Diesel Dual-fuel Compression Ignition Engines, using liquefied or compressed NG. Smaller NG engines can be spark ignited with no need for diesel pilot fuel.
  - Diesel generators, or diesel gensets – these are used in diesel-electric propulsion systems to generate electric power for the electric drive of the vessel. It has largely replaced the old hydraulic drive.
  - Hydrogen Fuel Cell Systems – Proton Exchange Membrane Fuel Cells (PEMFC) and Solid Oxide Fuel Cells (SOFC) are two possible future power plant options that are beyond the scope of this report.
- Electric Machines (EM) – Electric motors and generators of different types are used in the electrified marine propulsion system. These are discussed in detail in the vessel-by-vessel case studies (Appendixes K to R).
- Energy Storage Systems (ESS)
  - Fuel tank (diesel, gasoline, NG, or hydrogen)
  - Lithium-ion Battery – commonly used, of several varieties
  - Nickle-metal hydride battery
  - Supercapacitor or ultracapacitor
- Electric Power Systems
  - AC Power Bus – used in traditional electric propulsion systems
  - DC Power Bus – used in most recently developed electric propulsion systems
  - Bidirectional DC/DC Converter – regulating and supporting electric power flow at different DC voltages (generators, motors and ESS)
  - Bidirectional AC/DC Inverter - regulating and supporting electric power flow between AC/DC sources and at different voltages (generators, motors and ESS)
- Mechanical Gear Box and Clutch

An adequate model library, or collection, of these key powertrain components, is essential for building a functional powertrain system or propulsion system model. The model of each component should have its torque, speed (or voltage, current), power characteristics, energy

efficiency, and levels of emissions at different operation states. This library should contain different types and sizes of these components, or appropriate techniques to produce models of different types and sizes. This is a major challenge to the modelling work in hybrid and electrified marine propulsion systems. In the past, present and continuous research of the UVic Clean Transportation research team, considerable efforts have been devoted to this foundation work, through close collaborations with the OEMs and extensive studies of literature from different sources.

In the past, the US Department of Energy (DOE) has made an effort to systematically model commonly used powertrain system components, including various ICEs, Electric Machines, transmissions, etc. and included them in the vehicle modelling and simulation tool - ADvanced VehIcle SimulatOR (ADVISOR), developed by National Renewable Energy Laboratory (NREL). These models have later been incorporated into the more advanced MATLAB/Simulink based vehicle modelling and simulation tool, Powertrain Systems Analysis Toolkit (PSAT) and AUTONOMIE, developed by the Argonne National Laboratory (ANL). AUTONOMIE is actively in use today and distributed by Siemens.

6.1.1 Fuel Efficiency and Emissions Modelling of Diesel and NG Engines

Heavy-duty transportation applications, including marine vessels, mining trucks, and locomotives, prefer to use a diesel engine as its primary power source due to its higher power, efficiency and reliability. In this work, engine performance data from the ADVISOR/AUTONOMIE libraries have been used in conjunction with this methodology to scale these fuel economy and emission models properly to meet the needs of marine propulsion. Data from research literature are also used and their sources are given in the detailed technical report of Appendixes D, E, F and K to R.

Since NG contains less carbon than diesel fuel, NG fueled engines have seen increased applications in recent years for their near-zero-emissions of Particulate Matter (PM) and lower emissions of CO_2. Additionally, due to the carcinogenicity of diesel engine emissions, many world legislative directives or organizations have launched severe diesel fuel regulations and emission standards [7]. In the past several decades, considerable efforts have been devoted to the development of diesel engine models, including thermodynamic models, multidimensional models, and averageing value models, to support their performance and emission evaluation without performing the demanding engine dynamometer tests. These models can accurately predict the engine dynamic characteristics, including transient torque response, intake/outtake manifold volume efficiency, noise emission, and torque fluctuation during combustion, providing excellent tools for engine control and diagnostics. However, all of these engine-modelling methods are time-consuming and computationally intensive.

In this work, the fuel consumption and emission maps of diesel engines at different operation speeds and torques have been collected, as listed in Table 3. A representative fuel consumption and CO emission maps (brake-specific fuel consumption) are illustrated in Figure 32 and Figure 33, respectively. The shown engine fuel consumption data and CO emission data are for the Caterpillar 3126E diesel engine under the European Stationary Cycle test. Sources of some of these data sets were not given.

Using these “engine maps”, the fuel efficiency and emissions of the diesel engine operating at different speeds and output torques can be accurately calculated. Additional emission maps for nitrogen oxide (NOx), carbon monoxide (CO), and hydrocarbons (HC) are also available for many

common diesel engines, and these maps are generated through extensive engine dynamometer tests. The carbon dioxide (CO_2) emissions are proportional to the fuel consumption and the type of the fuel.

Table 3 AUTONOMIE ready-to-use diesel engine list

Year	Model	Manufacturer	Emission Map	Efficiency Map	Rated Power/kW	Speed Range/rpm
1998	-	-		x	37	1500-5000
1998	-	-		x	54	1000-5000
2001	-	Mercedes	x	x	60	1200-4200
1999	-	Volkswagen	x	x	67	800-4400
1998	-	Audi		x	88	1000-4500
2002	OM611	Mercedes	x	x	92	1250-4250
1998	-	-		x	119	1000-3500
2000	Powerstroke	Navistar T444E	x	x	163	700-2800
1999	-	-		x	171	650-2300
1999	-	-		x	205	650-2100
2002	3126E	Caterpillar	x	x	205	700-2500
1998	-	Cummins		x	246	650-2000
2002	DM4840 02	Caterpillar		x	250	650-2100
2001	DM6006 02	Caterpillar		x	321	650-2100
2002	DM4908 01	Caterpillar		x	324	650-2100
1998	Series 60	Detroit Diesel		x	330	1200-2100

In some cases, the engine performance characteristic data, provided by an industrial partner, such as Detroit Diesel, have been used directly to get results that are more accurate. The details of the model are documented in Appendix P.

The complete list of these diesel, gasoline and NG engine maps and detailed discussions on their sources and use in this work are given in Appendix D. Model Library for Diesel and NG Engines.

6.1.2 Modelling of Various Electric Machines (Motors/Generators)

Similarly, to the use of a scaled engine performance map, the motor/generator performance data from the ADVISOR/AUTONOMIE libraries is also used in this work. Proper scaling of the performance data model is done to accommodate different motor/generator sizes. In other cases, motor/generator performance characteristic data, provided by industrial partners, such as TM4 in Quebec, have been used directly for more accurate results, as in case studies documented in Appendix P. Detailed discussions on the modelling of these motors and generators are given in the case studies documented in Appendixes K to R.

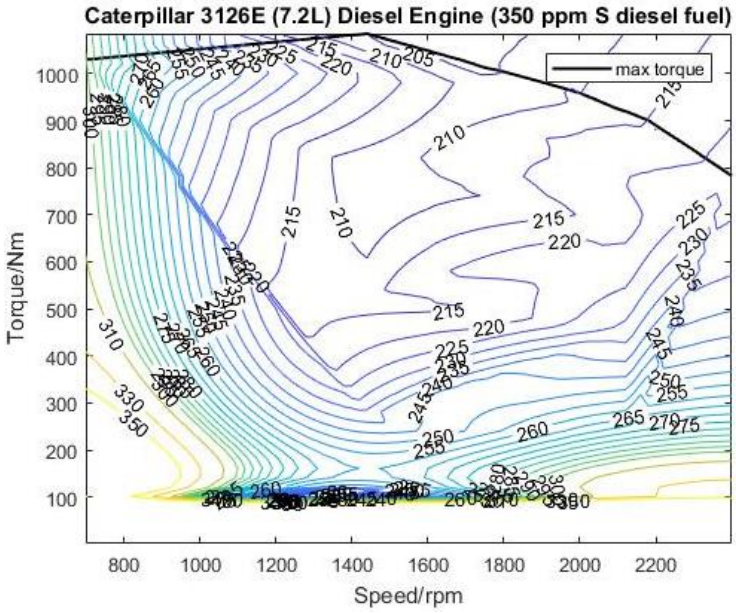

Figure 32 Caterpillar 3126E Diesel engine fuel consumption map (*g* per *kWh*)

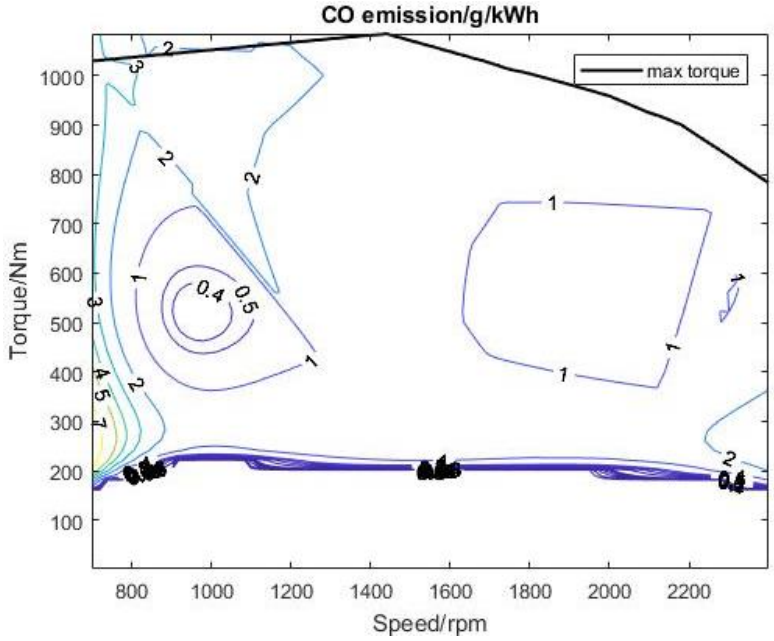

Figure 33 Caterpillar 3126E Diesel engine CO emission map (*ppm*)

6.1.3 Modelling Tool for Power Converter/Inverter Performance and Power Loss

Presently, DC/DC converters and AC/DC inverters are normally designed for a specific application, and they are important components of the hybrid electric powertrain or hybrid ESS. The functions to support bi-directional current flow in the electric power system and the power losses in them at different operation states need to be modelled.

The purpose of developing a generic converter model is for generating different power loss models of various DC/DC converters in ships. The powertrain of DC hybrid series architecture uses many electrical conversions besides its mechanical energy conversion. This electrical conversion is the key technology for reaching high efficiency in hybrid architectures. Generally, converters can be divided into four types as shown in Table 4.

Table 4 Types of converter systems.

Type of conversion	Converter system	Function
AC-to-DC	RECTIFIERS (Uncontrolled) (Diodes)	Fixed AC to Fixed DC (Line Commutation)
	RECTIFIERS (Controlled) (SCRs, IGBTs, MOSFETs, GTOs ...)	Fixed AC to Fixed or Variable DC (Line or Forced Commutation)
DC-to-DC		Fixed (or variable) DC to Variable (or fixed) DC
DC-to-AC	Inverters (Uncontrolled)	Fixed voltage DC to Fixed AC
	Inverters (Controlled)	Fixed (or variable) DC to Variable AC
AC-to-AC	AC Voltage Controllers	Fixed to variable AC
	Cycle Converters	Fixed AC to variable voltage & frequency (usually less than input frequency)

The methodology for building a model is consistent across all modelling methods. The steps for developing converter models are:

1) Select a suitable converter topology based on given conditions and the state of the art technology.
2) Analyse converter operation and develop a simulation model.
3) Implement variables (from datasheet) and use an appropriate method to estimate the unknown parameters in the model.
4) Validate the converter model to assess its adequacy.
5) Develop an efficiency map for the converter.

When the parameters are implemented into a simulated model, the model is carefully assessed to see if the underlying assumptions of power rating, conversion efficiency, voltage variation range and operating temperature are acceptable. If the assumptions seem valid, the converter model can be used in the power loss simulation at different operating conditions. A converter efficiency map at different input/output voltages and currents can be obtained using appropriate interpolation methods. In many cases, the DC/DC converters are built into the controllers of the electric machines and battery pack, and a separated DC/DC converter model is no longer needed.

DC/DC converters are required in a ship power system in order to chop DC voltage for other DC loads such as engine and generator controls, instrumentation, navigation equipment, engine room automation etc. Directional DC/DC converters can be divided into two categories: boost converters and buck converters. In boost converters, the output voltage is higher than the input voltage while in a buck converter the output is less than the input voltage.

In this work, a generic, parametric converter model has been introduced for use in various applications, including the hybrid ESS model in Appendix F and the case studies documented in Appendix K to R. A voltage-doubler boost converter is modelled in order to develop an accurate power loss model. The developed model needs to be computationally efficient so that it can be used in different modelling and design optimization functional modules. For this purpose, the

high-frequency dynamic behaviours of the converters are ignored, and this omission has little impact on the effectiveness of the model since the major concern of this modelling approach is on the power loss and energy efficiency. Details of the newly developed simulation tool are included in Appendix E. DC-DC Converter Power Loss Data Modelling Tool.

Bi-directional DC/AC converters are used to incorporate the battery ESS into the three-phase AC power system. It is also prominent for optimal energy management in a hybrid AC power system. Several methods have been developed to derive the model of this power converter including detailed switching models and average-value models. Detailed switching models are more complicated and require very small sample time, thus, these models are extremely computationally expensive for large power system simulation. Average models can be used to make the system-level simulation faster while preserving the average voltage dynamics. Details on this bi-directional DC/AC converter model and its use are documented in Appendix O - Case Study for Klitsa - Modelling and Simulation of Hybrid Electric Ships with AC Power Bus. It has not yet been built as a generic simulation tool due to its relatively limited applications in this work.

6.1.4 Modelling Battery ESS with Performance Degradation and Lifecycle Cost

Lithium-ion (Li-ion) batteries have been largely used within electrified transportation as a rechargeable energy storage system (ESS). In recent years, graphite, lithium Titanate (LTO), and new materials such as transition-metal oxides or graphene nanosheets (GNS) were invented as negative materials for Li-ion batteries. Positive electrodes include a variety of lithium metal oxide compounds. Lithium-iron phosphate (LFP), lithium-nickel-cobalt-aluminum (NCA), lithium-nickel-manganese-cobalt (NMC) and lithium-manganese oxide (LMO) are the most prominent materials in automotive applications. By melting Nickle, Cobalt and Manganese, manufacturers are trying to achieve higher voltage and capacity, as well as maintain a safe working condition. Details on various types of Li-ion batteries are provided in Appendix F. The performance degradation of Li-ion batteries under different operation conditions directly determines their operation life and lifecycle cost. These two closely related issues are thus discussed together in this section.

Along with the massive production of commercial Li-ion batteries, the price of this popular type of batteries has reduced dramatically during the last ten years, from above US $1,000 per kWh in 2007 to about US $250 per kWh in 2014. Moreover, this cost could fall to about US $200 per kWh by 2020 and about $160 per kWh by 2025 according to an analysis report [8]. However, it would be hard to compete with internal combustion engines (ICE) in cost if the battery packs could not fall below US$150 per kWh, considering the lifecycle ownership cost without government incentive programs and the present fuel price.

At present, estimation on the approximate cost of a battery pack is around US $300 ~ $500 per kWh, given the manufacturing volume of the battery cells and the pack assembly cost of the propulsion system battery OEMs as discussed in Appendix R Case Study for Fishing Boats - Emission Reduction and Lifecycle Costs of Hybrid Electric and Pure Electric Powertrains. A simple model of projected battery cost for the years to come for calculating the projected lifecycle cost of the electrified vessel, considering multiple battery replacements during the vessel's lifecycle, has been presented in detail in this Appendix.

Besides the price and manufacturing barriers, batteries' performance deterioration may aggravate the total cost of ownership to customers. The ageing phenomena caused by charging and

discharging microscopic electrochemical reactions inside every single cell are increased by cycling numbers and affected by temperature and current. A Battery management system (BMS) is very important to ensure good performance during driving. Failure to accurately calculate battery terminal voltage and state-of-charge (SOC) will induce inappropriate usage.

The ability to accurately predict the performance degradation of the battery under a specific load pattern is essential to determine the life of a battery ESS of a given size under a particular use pattern of the battery. This model can be used to determine the life-cycle cost of the battery ESS, thus supporting the accurate prediction of the life-cycle cost of the electrified or hybridized marine vessel. The model is also key to optimize the size of the battery ESS with minimum lifecycle cost, since a smaller battery ESS with less investment cost will have a shorter life, needing frequent replacements, leading to a potentially increased lifecycle cost.

The battery model is used within the dynamic simulation of the hybrid power system, and it should accurately represent the I-V performance and state-of-charge (SOC) without the excessive computational expense. There are three different types of battery models. The simple, less accurate and seldom-used mathematical battery model was discussed in Appendix O. The widely used electrical battery /equivalent circuit model was used in Appendix P. The electrochemical models with increasing model complexity and capability were discussed in Appendices F and L. In this work, all three types of battery models were tested. The widely used equivalent circuit model was used to for battery performance prediction with a new performance degradation extension. The modelling of battery performance degradation was also done using the electrochemical model. The accuracy and precision of battery models would determine the usefulness of the battery life-cycle cost model and affect the system control strategy since effective control strategies will not only help reduce driving consumption and emission but also prolong the battery life. The commonly used equivalent circuit models and the more accurate electrochemical models are further discussed in this section.

- Electric Battery Model/Equivalent Circuit Model

  The most commonly used battery model by the automotive industry at present is the electrical equivalent circuit model. The model is a theoretical model that simplifies a physical battery to an electrical source with some passive elements. Empirically, a DC voltage source combined with an internal resistor and two resistor-capacitor parallel elements would be sufficient to simulate a Li-ion battery cell. Most researchers normally use a one-dimensional equivalent circuit model for rechargeable batteries. Sometimes multi-dimensional equivalent circuit models were built to serve multi-purpose applications. For instance, as shown in Figure 34, an open-circuit voltage (V_{oc}) with an internal resistor (R_i) and two Resistor and Capacitor (RC) parallel circuits are adopted for battery performance modelling. The terminal voltage V_t and SOC were calculated as outputs from this model.

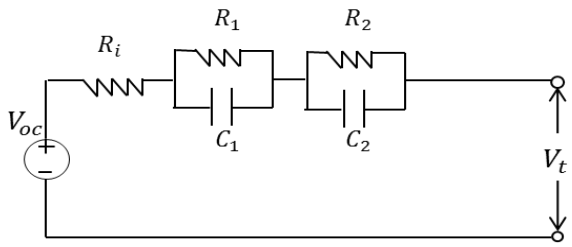

Figure 34 Equivalent Circuit Model.

The terminal voltage was determined by Kirchhoff laws:

$$V_t = V_{oc} - V_i - V_1 - V_2 \tag{11}$$

where V_i, V_1, V_2 are voltage drops caused by the resistors.

The estimates to V_1 and V_2 are calculated by:

$$\dot{V_1} = \frac{I_{c1}}{C_1} = -\frac{V_1}{R_1 C_1} + \frac{I}{C_1} \tag{12}$$

$$\dot{V_2} = \frac{I_{c2}}{C_2} = -\frac{V_2}{R_2 C_2} + \frac{I}{C_2} \tag{13}$$

where I_{c1} and I_{c2} are current flowing through the two capacitors.

SOC estimation was based on Coulomb counting which equals the integral over time of the ratio between current (I) and nominal capacity (Q) (positive current was discharging).

$$\dot{SOC} = -\frac{I}{Q} \tag{14}$$

The model was implemented in Simulink. A constant current – constant voltage (CC-CV) charging protocol was developed to maximally fulfill its capacity without causing overcharging, as shown in Figure 35.

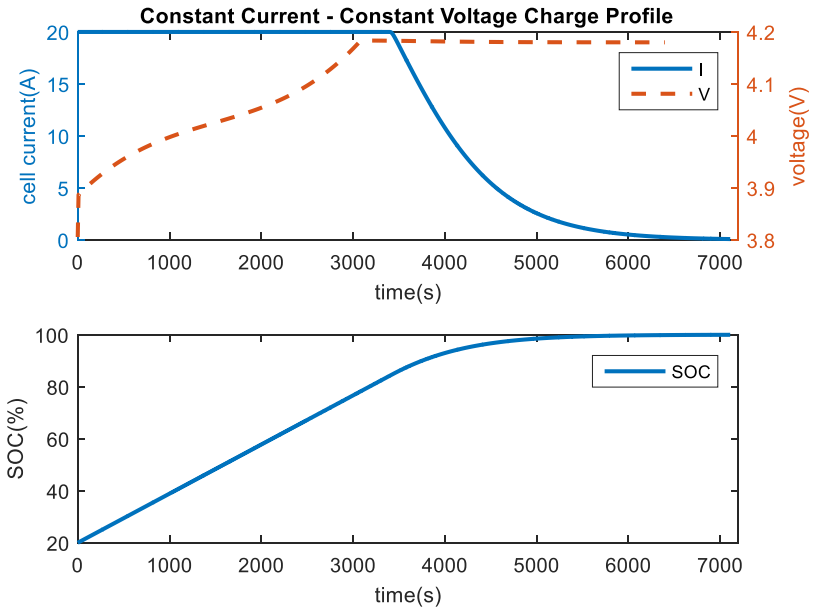

Figure 35 CC-CV Charging Profile.

- Electrochemical Model

Considerable efforts were placed, in this work, on an electrochemical model to seek an accurate simulation result for battery ageing performance. This model is much more complex with many parameters associated with different properties and phenomena of the battery's negative and positive electrodes. To reduce its computational complexity, simplifications have been made,

and a so-called 'Single Particle Model' (or SPM) was developed to use only one carbon particle and one lithium metal oxide particle to represent the responses on the negative and positive electrode. Our battery performance and performance degradation model was introduced based on this model.

In this work, the form of the battery performance degradation model and the simulation program in Simulink have been introduced. The complete model with all model parameters for the A123's Li-ion battery has been introduced and validated, as documented in Appendix F - Li-Ion Battery and Battery-UC Hybrid ESS Performance and Lifecycle Cost Models. As an industrial partner of the UVic Clean Transportation team, A123 has provided some battery performance data. The Li-ion batteries from A123 have also been widely studied by many organizations in recent years, providing sources of useful data, as documented in detail in Appendix F. Sets of these data have been used to determine the model parameters of the newly introduced model, and others have been used in the model validation.

The technical details of this single-particle based battery performance degradation model are provided in the first part of Appendix F. Li-Ion Battery and Battery-UC Hybrid ESS Performance and Lifecycle Cost Models. The application of this model is presented in Appendix L Case Study for Skeena Queen - Optimal Design of Series Hybrid Propulsion System.

Meanwhile, experimental data of the battery at different charge/discharge current, depth of charge, frequency of charge/discharge, at different stage of life of the battery (new, middle life and end life), and of different materials are needed to determine all model parameters, while many of our collaborating battery and battery pack manufacturers only have provided test data on fresh batteries, and battery samples. To address this critical issue, actions have been made at two fronts. Firstly, collaboration agreements have been made with three major leading battery testing labs: the battery modelling group at the US DOE's National Renewable Energy Laboratory (NREL), the Air-battery Research Lab at NRC-Vancouver, and the Beijing National EV Battery Testing and Certification Laboratory. All have first-class battery testing facilities and extensive experiences in this area. Secondly, working with other UVic colleagues on Ocean Energy Modelling, a new and complete battery testing facility, specially designed and set up for battery cell performance degradation tests, has been acquired through major funding support from the Canadian Western Economic Diversification (WED) Funds. The facility will be operational in November 2018.

A much simpler empirical battery performance model that uses an empirically obtained performance drop term to the equivalent circuit model has also been studied in this work. The model is limited to the specific type of battery under limited working conditions. Nevertheless, the model can support the proof-of-concept research on battery life-cycle cost evaluation and size optimization as documented in detail in the second part of Appendix F.

6.1.5 Modelling Battery-UC Hybrid ESS - Performance and Lifecycle Cost

Ultracapacitors (UCs) (or supercapacitors (SC)) contain two-conductor electrodes, an electrolyte, and a porous membrane separator, which only permits the ion mobility but prevents electric contact. The major advantages of UCs are long cycle times (more than 500,000 cycles) and high cycle efficiency (84-97%) and power density. However, they also have a number of drawbacks, including a high self-discharge rate (5-40%) and low energy density (10-30 W h/L).

A hybrid energy storage system (HESS) that combines batteries and UCs presents unique electric energy storage capabilities over traditional ESS made of pure batteries or UCs. As a critical powertrain component, the performance and life of the ESS dominate the performance and life cycle cost of the pure electric marine vessel (PEMV) and plug-in hybrid electric marine vessel (PHEMV) due to the large size of their ESS. Different from traditional power density and energy density considerations, the use of battery and UC HESS today is more geared toward the use of UCs to take over the high frequency, dynamics charge and discharge to ensure quick system response and to extend battery life by reducing its frequent charge and discharge [9].

In this work, a review of the recent advance of HESS and relevant technologies, the state-of-the-art battery ESS and modelling method has been carried out [9]. The study also considered the modelling of battery performance degradation under different use patterns, and the performance and power loss of UCs and DC/DC converter in the HESS. Effective energy management methods of HESS have also been introduced to make appropriate energy split strategies between the batteries and UCs. The new HESS model module has been discussed in detail in Appendix F. Extending from the completed contract research, applications of the new HESS model and methods for HESS design and control optimization for tug boats with dynamic load changes are studied in the UVic teams' present and future work.

6.2 Natural Gas (NG) Hybrid Electric Propulsion System Models

6.2.1 NG and NG-Diesel Dual Engines

In recent years, NG-diesel dual-fuel engines became more popular for heavy-duty transportation applications, due to the significant and widely acknowledged cost and CO_2 emission reduction advantages of NG fuel. The smaller amount of diesel fuel used in these engines serves as pilot fuel. Presently, there are some power performance, fuel efficiency and emissions (CO, CO_2, NO_x, HC, PM, etc.) information for diesel engines, but a limited amount of information and data on NG engines. In this contract work, an array of power performance, fuel efficiency and emissions models for both diesel and NG fueled engines have been introduced for the energy efficiency and emissions of the hybrid propulsion system involving these types of engines. The completed task forms the foundation for improving the integrated marine propulsion system modelling tools (Appendix D) and for a clean propulsion vessel case study discussed in detail in Appendix K.

While the substitution of NG fuel is a readily acknowledged solution to fuel cost and CO_2 emission reduction, there are also inherent drawbacks to NG-diesel dual-fuel engines that must be addressed. These include:

- An NG fueled engine (or an NG-diesel dual-fuel engine) usually produces less power than a neat diesel operation engine. Although a pre-mixture system and high-pressure direct-injected (HPDI) systems have made considerable progress in recent years a 5-35% peak power gap still exists [10,11].
- There are difficulties in using NG in a diesel compression-ignition engine as NG's higher auto-ignition temperature and lower flame velocity make it harder to ignite. Mixed diesel and NG fuel at the different ratios with complex control is needed depending upon the engine load [14].

- Despite the potential for an NG engine with much lower overall emissions at its ideal operating torque and speed, the hydrocarbon (HC) emissions may be up to an order of magnitude higher at low and high engine load. The reduced emissions on CO_2, NO_x, CO, and PM can be offset by the sharp increase of HC, leading to marginal or no improvement in GHG emission [15][16].

6.2.2 Modelling of NG Engine Fuel Efficiency and Emissions

The efficiency and emission data (maps) for diesel engines were based on the vehicle modelling and simulation tools ADVISOR and PSAT/AUTONOMIE from US DOE's National Renewable Energy Laboratory (NREL) and Argonne National Laboratory (ANL), and engine scaling techniques. Comparing with the diesel engines, the efficiency and emission data (map) for an NG engine is very limited and is based on research literature [10, 11]. The details of these models are included in Appendix D Model Library for Diesel and Natural Gas Engines. The use of the NG engine model is illustrated in Appendix K - Case Study for Skeena Queen: Integrating NG Engine and Hybrid Electric Powertrain with Special Controls for Fuel Cost and Emission Reductions, and the use of the diesel engine model can be found in all case studies.

6.2.3 Overcoming Drawbacks of NG Engine by Hybrid Powertrain and Control

The inherent problems associated with NG fueled engine discussed in the previous subsection can be effectively overcome with the introduction of the hybrid electric powertrain system. The addition of electric drive, battery ESS and dedicated controls will:

a) Provide enough power to eliminate the power gap and response delay that would otherwise exist between the NG fueled engine and the original diesel engine.
b) Serve as either a power supplement source or excessive power storage, depending on need. This allows the NG fueled engine to operate within its ideal speed and torque operation range that provides optimum fuel efficiency, performance and decreased emissions. The approach can help eliminate the increase in HC emissions.

The new method to integrate NG fueled, compression ignited (CI) engine, hybrid electric powertrain and dedicated controls, introduced in this work and related UVic research, will ensure the NG engine to operate in ideal conditions with much-improved energy efficiency and emissions. The study used a representative marine vessel, its real-life operation patterns, available NG CI engine efficiency data, and lithium-ion (Li-ion) battery cost/life data from the literature to introduce a straightforward hybrid electric powertrain retrofitting design and associated control solution. The modelling and simulation results with the integrated system showed significant reductions of fuel cost, GHG, and other harmful emissions from a conventional diesel-fueled vessel. The detailed work is presented in Appendix K. Case Study for Skeena Queen: Integrating NG Engine and Hybrid Electric Powertrain with Special Controls for Fuel Cost and Emission Reductions. The investigation forms the foundation for further research in this area.

6.3 Alternative Power System Architectures

Traditionally, marine vessels are propelled using ICE, mostly diesel engines, through a mechanical powertrain. Gasoline engines are used for smaller vessels, such as fishing boats and most small recreational boats. Diesel-hydraulic and diesel-electric propulsion systems have also been popular

choices in the past and at present to provide high propulsion torque at low-speed operation, and to decouple the constantly changing and relatively low operation speed of the propeller shaft and the preferred stable and high operation speed of a diesel engine.

6.3.1 Diesel-electric Drive

With the advance of the electric power system, power electronics, and electric machine technologies, the diesel-electric drive has almost completely replaced the pure mechanical drive and diesel-hydraulic drive with much-improved efficiency, controllability and powertrain layout in heavy-duty transportation applications. The diesel-electric marine propulsion system is very similar to the diesel-electric drive system of a large mining truck, as shown in the following Figure 36, replacing the wheels with propellers. The ICE, or diesel engine, and generator combination is called a diesel-generator set, or simply genset.

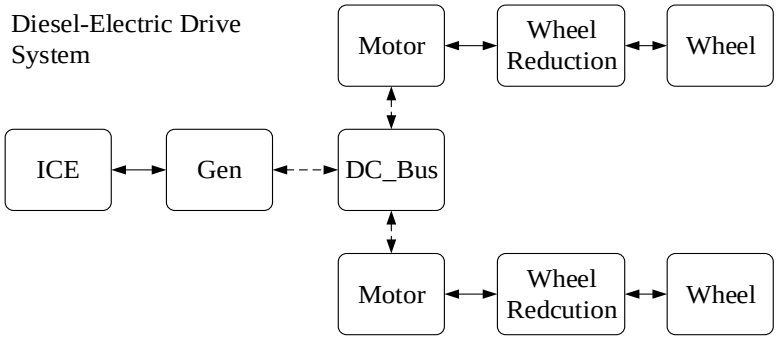

Figure 36 Diesel-electric drive for large mining truck with DC power bus

The difference between a diesel-electric propulsion system and a series hybrid electric propulsion system is the lack of an electric ESS in the former. In the hybrid electric powertrain, the excessive energy produced by the genset can be temporally stored in the ESS and the stored energy can be retrieved from the ESS to fill the power gap between the genset and the required propulsion power during quick accelerations and power intensive operations. This ensures efficient, steady genset operation to meet the dynamic propulsion power needs.

Conversion of a diesel-electric propulsion system into a series hybrid electric propulsion system is the least expensive powertrain retrofitting method, and an ideal solution for applications with dynamically changing power loads [17].

6.3.2 Hybrid Electric Propulsion with Diesel/NG Engine(s)

Hybrid powertrain architectures can be classified into two fundamental categories, series and parallel hybrid. In series hybrid architecture the energy sources are coupled electrically through an electric power bus. While in parallel hybrid architecture, the energy sources are coupled mechanically through certain mechanical coupling methods such as drive chain. In order to gain the advantages from both series and parallel, many series-parallel hybrid electric powertrains have been developed for a large portion of vehicular applications.

A hybrid electric propulsion system has the inherent advantage of dual power plants with built-in power redundancy, often demanded or preferred by marine applications. In case of failure of the

engines or the battery ESS, the other can still propel the vessel. The parallel powertrain is safer due to the completely redundant mechanical and electric drives.

- Series Hybrid Electric Powertrain

  The layout of a series hybrid electric powertrain system is as shown in Figure 37. It consists of an engine, a generator (G), an ESS, power electronics consisting of a power converter and system controller, and an electric traction motor (M). A series hybrid electric ship (HES) transforms the power from the engine into electric energy through the generator. The ESS works as a buffer to store the energy and supply power to the electric motor. Only the motor provides the torque to drive the propeller using electric energy from the ESS, the genset or both. By de-coupling the mechanical connection, the engine can operate at its highest efficiency with steady speed and torque, and avoid idling. The architecture is particularly suitable for applications with constantly changing propulsion power needs, such as operations with frequent speed-ups and slow-downs.

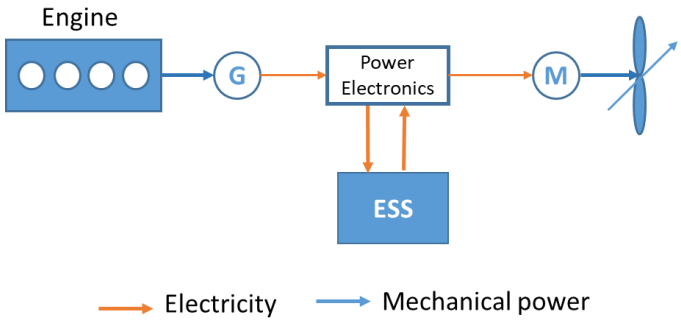

Figure 37 Series hybrid electric powertrain system

However, for medium-sized marine vessels with a constant propulsion power load, this architecture has to continuously convert between mechanical, electrical and electrochemical energies, causing a significant amount of unnecessary energy conversion losses. The architecture is thus less efficient than the parallel powertrain in which mechanical power from the engine can be directly transmitted via a propeller shaft with no energy conversion loss. For large marine vessels, multiple gensets and propellers are used, forming a local electric power generation and distribution network. The gain of grid operation efficiency is potentially able to offset the energy conversion loss.

The other disadvantage of a series hybrid powertrain is that it requires a dedicated electricity generator and a dedicated electric propulsion motor, and the system requires a larger ESS and traction motor to accommodate the entire propulsion power for the overall system.

- Parallel Hybrid Electric Powertrain

  A parallel hybrid electric powertrain system with parallel mechanical and electrical power flow consists of an engine, one or more electric motor/generators, an ESS, a propulsion power-merging gearbox, and a system controller as shown in Figure 38.

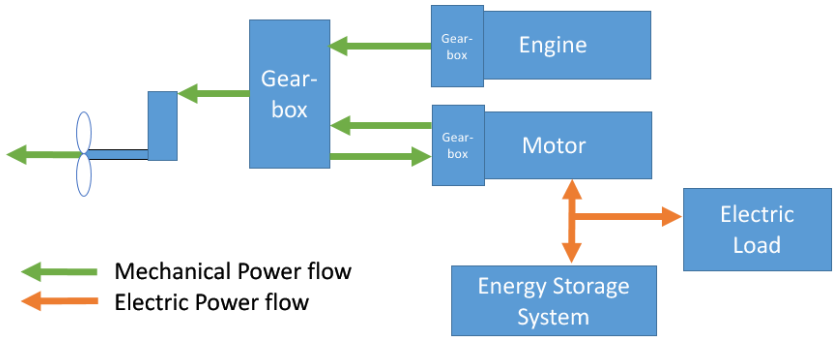

Figure 38 Parallel hybrid electric powertrain system

The mechanical and electrical drive can be merged at a fixed speed ratio using a co-axial arrangement or a gearbox at a designed speed ratio. The propeller shaft can be driven by the engine, by the electric motor, or by both. The engine and the motor are connected in parallel through a mechanical coupling and transmission. The parallel operation mechanism of the engine and electric motor allows torque blending such that the engine provides most of the constant speed cruising torque and the motor provides accelerating torque. There are many possible ways to connect the engine, motor and transmission systems. For instance, the engine and the electric machine as a motor can drive the propeller simultaneously, or the engine can drive the propeller and the electric machine as a generator, draw electric energy from or provide electric energy to the ESS following system control algorithms.

- Series-Parallel Hybrid Electric Powertrain

  The series-parallel hybrid powertrain may be viewed as a combination of series hybrid and parallel hybrid architecture. It is commonly used in light vehicles and trucks in the form of Hybrid Electric Vehicle (HEV) and Plug-in HEV (PHEV) with a special electronically controlled, continuous variable transmission (e-CVT), or using both front and rear wheel drives, as shown in Figure 39. This four-wheel-drive vehicle has a large battery alternator starter (BAS) motor, a large rear traction motor (RTM) and an automatic manual transmission (AMT). In this powertrain architecture, the engine output is divided into two paths. One is a mechanical transmission path directly connected to a driveshaft functioning as the parallel architecture. The other is an electrical transmission path through a generator that is similar to the series architecture. The series-parallel hybrid powertrain is usually called a power-split architecture that requires one ICE and at least two electric machines. This architecture found wide applications in HEV and PHEV due to its ability to meet both static driving load (highway driving) and dynamically changing driving load (city driving). The essential feature of the power-split architecture is that it requires the eCVT or front/rear drives as power split devices. However, the commonly used planetary gear set based e-CVT for passenger cars has very limited torque and power capacities, and is not suitable for marine applications with high torque demands, and partially loaded, redundant propellers are less efficient. A new design of Hybrid Automated Manual Transmission (HAMT) has been introduced in our recent research and patented. The e-CVT and HAMT have numerate different variations and are beyond the

scope of this contract work. Application of the new HAMT design for hybrid marine applications will be one of the areas of our research in the near future.

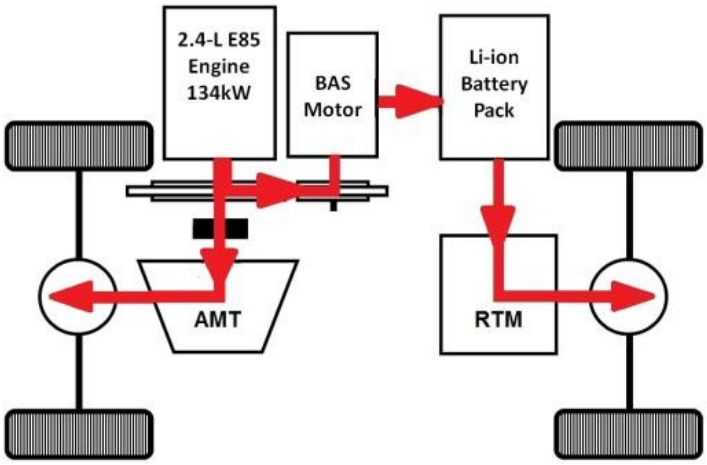

Figure 39 Series-Parallel Powertrain of a Four Wheel Drive Hybrid Electric Vehicle

6.3.3 Pure Electric Propulsion

The straightforward pure electric propulsion system only consists of a battery ESS and electric propulsion motor. A large ESS is essential to obtain enough electric charge from the shore power grid to support the required operation range. The battery ESS also provides the vessel's hotel load and requires a DC/AC converter if an AC induction motor is used. A typical system is illustrated in Figure 40.

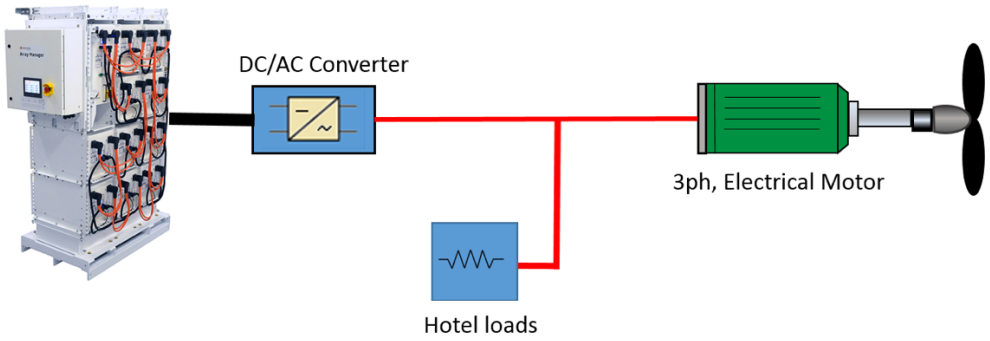

Figure 40 Pure battery electric propulsion system.

Appropriate charge infrastructure is needed to meet the power demand and to reduce battery charge time. At present, high battery ESS cost, limited energy density, and reduced battery life have limited the use of pure electric propulsion to smaller vessels with shorter ranges or frequent change opportunities. When these conditions are met, pure electric propulsion does present a clean and low lifecycle cost solution, as identified in one of our case studies documented in Appendix R. Case Study for Fishing Boats - Emission Reduction and Lifecycle Costs of Hybrid Electric and Pure Electric Powertrains.

6.3.4 Plug-in Hybrid Electric Propulsion

Plug-in hybrid electric propulsion system is the combination of the previously discussed series or parallel hybrid electric powertrain systems with a large onboard ESS and grid ESS charging capability. An example plug-in hybrid electric propulsion system, designed in our previous work for a research ship, is shown in Figure 41. With a large battery ESS, the system can obtain a significant portion of its required stored energy from the electric charge from the shore power grid. The hybrid electric propulsion system uses the engine power to operate in its hybrid mode to extend the operation range when the state of charge (SOC) of the ESS drops to a predefined lower level. This system enjoys a much longer operation range, security of power redundancy, and lower investment cost due to its much smaller battery ESS.

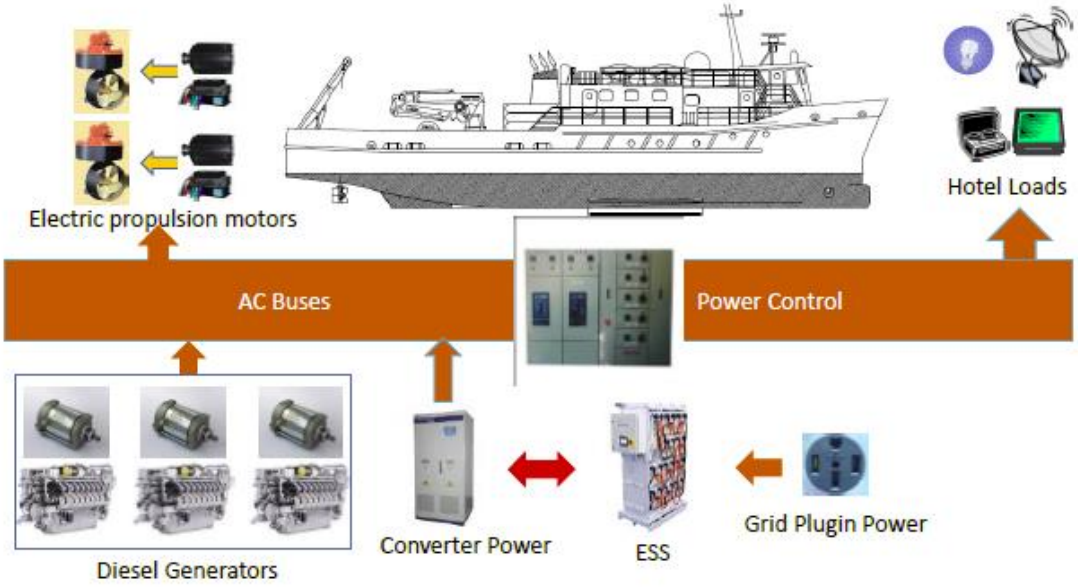

Figure 41 Plug-in hybrid electric propulsion system

6.4 Integrated Power System (IPS) Models

As shown in Figure 41, the hybrid electric propulsion system for a large vessel involves multiple generators and electric motors, hotel loads, and grid connections, sharing a common electric power bus. The complete electric power supply and demand system form a small, local power network, or an integrated power system.

6.4.1 AC Bus Based Modelling

At present, the terms of all-electric ships or electrified ships are referring to ships with electric propulsion, including diesel-electric ships, hybrid electric ships and pure electric ships. These electrified ships can provide reduced fuel consumption, maintenance, and emissions as well as improved reliability and responsiveness, particularly the hybrid and pure electric ships. Today, many of these electrified ships operate on an AC power bus. Due to the complexity of the electric propulsion system, effective modelling and simulation tools are essential for the design, analysis, optimization and evaluation of the ship's propulsion system. In this project, a dynamic model of

a shipboard AC hybrid power system has been introduced. The AC power system is composed of seven major components: three diesel-generator sets, a battery Energy Storage System (ESS), an AC power source synchronizer and a bi-directional DC/AC power converter, as shown in Figure 42. The study used the BC Ferries' Klitsa ferry ship as the modelling platform using its operation data acquired in the earlier work conducted at UVic. The power converter is modelled as a nonlinear dynamic average-value model to suit system-level studies. Each of the component models is parameterized using the data sheet provided information from the manufacturers. A rule-based supervisory controller is proposed to coordinate power-sharing among diesel-generator sets and the ESS.

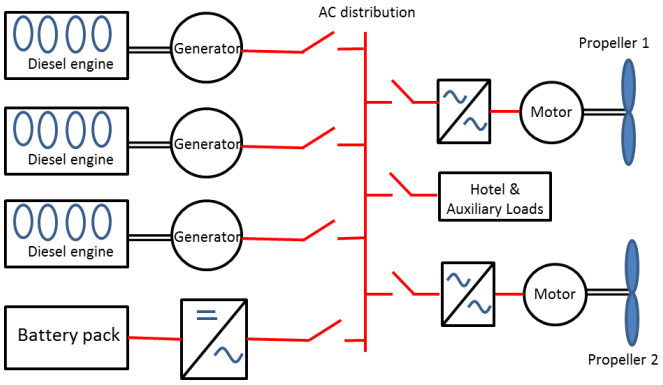

Figure 42 Series hybrid electric propulsion system with an AC power bus on M.V. Klitsa

Using the acquired load profile of the ferry, simulation results obtained using the introduced modelling tool present power-sharing solutions among four power sources in four operation modes with voltage and frequency stabilization of the system AC bus. The details of the modelling and simulation are documented in Appendix O - Case Study for Klitsa - Modelling and Simulation of Hybrid Electric Ships with AC Power Bus**.**

6.4.2 DC Bus Based Modelling

Traditionally, the diesel-electric propulsion systems for heavy-duty transportation applications, including locomotive, marine and mining vehicles, are powered by AC generators, propelled by large AC induction motors, and connected by an AC power bus. Large transformers and induction motors are readily available at reasonable costs.

Due to the rapid technological advancements in power electronics and electric drive, as well as the addition of large ESS with DC input and output, a DC power bus has been now used in various electrified consumer vehicles. This is due to its higher efficiency, ease of control and integration with battery ESS. With the rapidly increased power capability and reduced cost of permanent magnet synchronous motors (PMSM) and their controllers with built-in DC/DC converting power electronics, a DC power bus now also presents a more efficient power bus arrangement for heavy-duty transportation applications, including marine transportation. Some of the newly developed all-electric ships are now equipped with a DC power bus. Compared to the AC power system, a DC power system has some obvious benefits, including improvement of generator and motor efficiency; reduction of weight; reduced required space; transmission loss; simplified parallel connection of generators; and ease of connection to ESS. The challenges associated with the DC power bus technology include high short-circuit currents and needed DC protection and high

power electronics. These, however, are being resolved with the wide adoption of new technologies. The modelling and simulation of hybrid electric ships are primarily carried out using a common DC power bus in this work.

In our case study using BC Ferries' Klitsa, a short-range car deck ferry, as the modelling platform, a series hybrid electric powertrain system with a battery ESS has been studied. An actual diesel engine fuel consumption map (FCM), modelled using data from the engine manufacturer, was used. The optimal engine and battery size were determined through powertrain design optimization using the advanced global optimization (GO) search program, Hybrid Adaptive Metamodelling (HAM). HAM is one of the advanced GO algorithms developed by the research team previously and documented in the Appendix T Overview of the UVic Global Optimization Toolbox. The cost-benefit and GHG emission analysis showed that the series hybrid electric propulsion system, as illustrated in Figure 43, could outperform the original diesel-electric counterpart while keeping the vessel cost almost the same over a 10-year period. Detailed modelling, simulation, and result analyses are given in Appendix P. Case Study for Klitsa - Modelling and Simulation of Hybrid Electric Ships with DC Power Bus**.** This hybrid electric propulsion system has two generator sets and two propellers. The diesel engines and PMSM motors have been modelled using data provided by collaborating manufacturers.

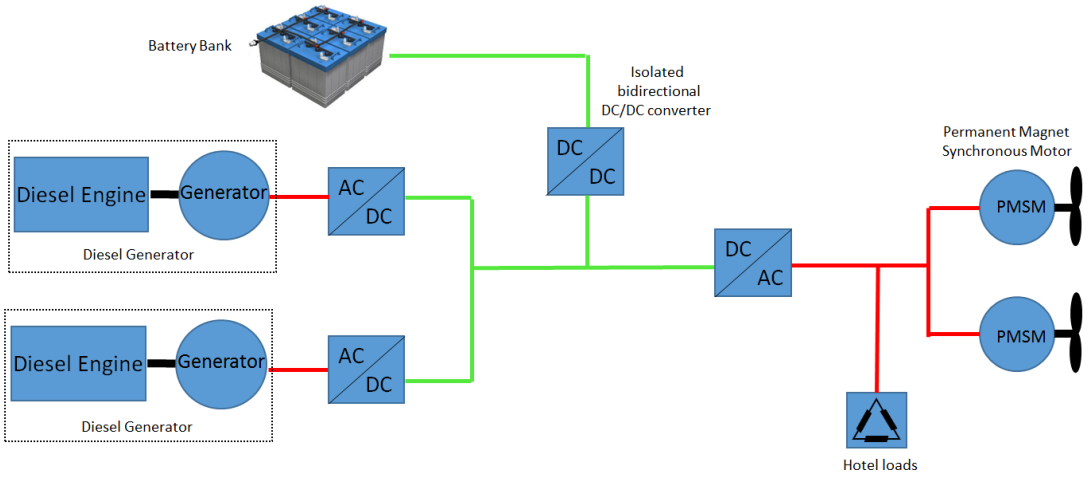

Figure 43 Series hybrid electric propulsion system with a DC power bus on M.V. Klitsa

7 CASE STUDIES ON VARIOUS CLEAN PROPULSION SOLUTIONS

Based upon the newly introduced vessel operation profile models for ferries, tugboats and fishing boats, the fuel consumption, GHG emissions, and life cycle cost reduction potentials of different electrified marine propulsion systems are evaluated, including diesel hybrid electric, NG engine hybrid electric, and pure electric. Detailed modelling, simulation and analyses are presented in several case studies. The traditional diesel-mechanical and diesel-electric powertrain systems were used as benchmarks for comparison. These quantitative analyses contained the simulation results from eight case studies on the focused marine vessels, using our improved, integrated hybrid electric marine propulsion system modelling tools.

In Sections 5 and 6, the pros and cons of various clean propulsion solutions have been briefly discussed. To quantitatively compare these promising solutions, modelling, simulations and analyses were conducted on these different marine propulsion systems using the vessel operation pattern data acquired from the representative marine vessels, as discussed in Section 4.

The objective and scope of these case studies and the major findings are briefly summarized in this section. The technical details of the work and obtained results are documented in the following eight separate appendices attached to the report.

- Appendix K. Case Study for Skeena Queen - LNG Series Hybrid
- Appendix L. Case Study for Skeena Queen - Design of Series Hybrid Propulsion System
- Appendix M. Case Study for Skeena Queen - Parallel Hybrid Propulsion System
- Appendix N. Case Study BCF Tachek - Analysis of Hybrid Propulsion Designs
- Appendix O. Case Study for Klitsa - Model of Hybrid Electric Ships with AC Power Bus
- Appendix P. Case Study for Klitsa - Model of Hybrid Electric Ships with DC Power Bus
- Appendix Q. Case Study for Tugboat - Operation Profile - Benefits of Hybrid Powertrain
- Appendix R. Case Study for Fishing Boats - Emission Reduction and Lifecycle Costs of Hybrid Electric and Pure Electric Powertrains

7.1 Subjects of the Case Studies - Three Types of Vessels

Three representative types of marine vessels have been studied: passenger and vehicle ferries, tug boats, and fishing boats.

7.1.1 Case Studies on Passenger and Vehicle Ferries

Ferries are essential transportation tools for the west coast residents of Canada, as well as for about 10% of the world's population, who live on islands. However, the ferry fleet with large amounts of marine diesel fuel consumption bears high fuel costs and produces heavy GHG emissions, including PM, NO_x, SO_2, CO_2 and HC, emitted from the old cumbersome marine diesel engines.

BC Ferries, one of the industrial partners of this project, has been providing transportation services for passengers and vehicles between various islands and the mainland in British Columbia since 1960. As the largest passenger ferry company in North America, BC Ferries owns 47 operation lines, which has consumed 115.4 million litres of marine diesel at a cost of CAD$103.3 million in fiscal 2016. To reduce fuel cost and GHG emissions, BC Ferries has been seeking new technologies for its future ships.

This work focuses on the new propulsion system designs of three vessels operated by BC Ferries:

a) Skeena Queen - one of the typical middle size ferries, running between Salt Spring Island and Vancouver Island, a category of vessels for clean energy propulsion technology adoption;
b) Klitsa – one of the smaller ferries with short crossing time, a good candidate for pure electric or plug-in hybrid electric propulsion system; and

c) Tachek – the first ferry retrofitted with a hybrid electric propulsion assist system and a good candidate for full hybridization study. This vessel is fitted with modern data acquisition and control system and operated on the Quadra Island – Cortes Island route with dynamically changing ocean conditions.

7.1.2 Case Studies on Tugboats

Tugboats (or Tugs) are important tools in harbours to assist large ships to and from their berths. Today multi-purpose tugboats are designed to perform various jobs such as offshore support, salvage, icebreaking, etc. Some key parameters that define the performance of a tugboat include the bollard pull capacity, maximum free-running speed, time taken to achieve maximum free-running speed from rest, distance covered to crash stop, time taken to complete a 360 turn in its own axis, soundproofing of machinery spaces, etc. According to the type of work they perform, tugs can be categorized into three major groups: harbour tugs, escort tugs and ocean-going tugs. Tugs form a different type of marine vessel, for which the forces needed to propel itself is often just a small portion of its operation loads, while the primary loads come from its ship handling duty cycles.

Robert Allan Ltd. (RAL) of British Columbia, another industrial partner of this project, is a leading tug design company with extensive experiences on the development of different types of tugboats and one of the pioneers in adopting new, clean energy to tug boats.

7.1.3 Case Studies on Fishing and Commercial Boats

Commercial fishing is an important part of the Canadian economy, playing a vital role in the economic well-being of the coastal communities along the east and west coasts of Canada.

Traditionally, these smaller low-tech fishing boats and commercial boats use less-efficient engines and collectively produce considerable amounts of pollutions. Commercial fishing boats are capable of hauling a catch of thousands of kilograms of fish per voyage. Larger fishing boats that operate in higher water depth have advanced equipment and facilities where the fish can be prepared and stored for sale. These vessels are also equipped with some amenities for workers for long stays on the ocean and they can do the job of several smaller boats.

Fishing boats have a dynamic load profile. The location of fishing, method of capture and duration of the trip can also vary significantly each trip. Glas Ocean Electric of Halifax, NS, the subcontracting team of this project, has been working with the east coast fishing communities in seeking clean energy fishing-boat propulsion solutions to reduce fuel cost and GHG emissions for the industry. In this work, the operations of lobster fishing boats have been selected for detailed study, including data acquisition, modelling, and simulations on various alternative propulsion system designs.

7.2 Case Study for BC Ferries' Skeena Queen: Integrating NG Engine and Hybrid Electric Powertrain with Special Controls for Fuel Cost and Emission Reductions (Details in Appendix K)

The use of liquefied NG (LNG) to replace diesel fuel presents a feasible and attractive fuel cost and emission reduction solution for heavy-duty transportation applications, particularly for large marine vessels. To overcome the shortcomings of present NG engine in comparison to its replaced diesel counterpart, including less peak power, slower response, complexity of different NG-diesel pilot fuel ratios under varying load, and surge of hydrocarbon (HC) emissions at low and high loads, hybrid electric powertrains with specialized controls have been introduced in this work.

The model of a specially designed hybrid electric powertrain system has been introduced with important new developments on its three key powertrain components. First, the NG engine model contains detailed fuel economy and emissions maps, including HC, to support the consideration of engine carbon dioxide equivalent (CO_{2e}) emissions to effectively control and reduce the overall emissions of an NG engine. Secondly, the performance degradation and life-cycle cost considerations of the Lithium-ion (Li-ion) battery ESS have been added using a new battery performance degradation model to support battery size optimization and optimal energy management. Thirdly, special control strategies for the series hybrid electric powertrain system have been introduced to address the issues associated with the present NG engine, as stated in Section 6.2.1, to ensure it operates in the ideal torque and speed region identified in this work.

The work uses the acquired operation and power load patterns of the BC Ferries' Skeena Queen as a case study to demonstrate the fuel cost and emission reduction potentials of the newly proposed technology by comparing results from three powertrain alternatives: traditional diesel engine, NG (or NG-diesel dual fuel) engine, and series hybrid electric with NG engine and dedicated controls. The results showed that the combination and optimization of NG engine, hybrid electric powertrain, and special controls could significantly reduce both fuel cost and harmful emissions. The series hybrid electric powertrain system has been targeted in this work due to its relatively small powertrain architecture difference from the traditional diesel-electric powertrain, and the ease of control development.

7.3 Case Study for BC Ferries' Skeena Queen - Optimal Design of Series Hybrid Marine Propulsion System with Li-ion Battery Performance Degradation and Life Cycle Cost Model (Details in Appendix L)

This study adds to the research outlined previously in Section 7.2, and focuses on the performance degradation of the battery ESS of electrified ferries. Besides the traditional mechanical propulsion architecture, hybrid and pure electric propulsion systems were proposed and compared with the original design.

Specifically, the diesel-LNG dual-fuel engine and rechargeable Li-ion battery have been adopted in the new designs. The battery ESS can provide extra energy to allow the engines to operate at their most efficient speed and torque to reduce emission. However, depending upon the designed capacity and the use pattern of the ESS, the Li-ion batteries may reach their end of operation life quickly and cause costly and even frequent replacements and interruption of service.

In this work, a semi-empirical battery life prediction model under different use patterns has been introduced to predict the life degradation of the battery ESS, considering the impacts of battery state of charge variation (ΔSOC) and discharge current rate (C-rate). These are determined by the operation pattern of the ferry, the size of the battery and the battery management system (BMS). The new model made optimization on battery ESS size and BMS possible, as demonstrated in this case study.

7.4 Case Study for BC Ferries' Skeena Queen - Design of Parallel Hybrid Marine Propulsion System (Details in Appendix M)

The series hybrid electric powertrain system is closer in architecture to the traditional diesel-electric powertrain system, its control development is more straightforward, and retrofitting cost is lower. However, many ferries, such as Skeena Queen, travel on calm water with relatively steady power loads, except the short docking operations at berths. The advantage of series hybrid powertrain to handling dynamics loads is less useful, while the constant mechanical-electrical-mechanical and battery ESS energy conversions present unavoidable and unnecessary energy and efficiency loss. This study adds to the research outlined previously in Sections 7.2 and 7.3, to focuses on the adoption of parallel hybrid electric powertrain systems and the resulting benefits.

The advance of the marine propulsion system went from diesel-mechanical drive to diesel-hydraulic drive, and to diesel-electric drive with electric propulsion. Natural development is to add a battery-electric ESS and powertrain system control to make it a hybrid electric system with a series powertrain architecture. This series hybrid electric powertrain system will allow the diesel (or gasoline or NG) generator to operate at its ideal speed and torque zone with the highest efficiency, regardless of the speed change of the ship, thus increasing the energy efficiency and reducing emissions.

As proved in-ground vehicle applications, this series hybrid electric powertrain architecture is superior for heavy-traffic city driving with constant decelerations and accelerations. However, for highway driving at static speed, the inherent mechanical to electrical and electric to mechanical energy conversion loss of the architecture is considerably less energy efficient than the parallel hybrid electric powertrain in which mechanical power from the engine can directly flow to the propulsion wheels. The acquired operation and propulsion power patterns of the ferry ships have confirmed that a large portion of the ferry's power demand and travelling speed remain constant during the crossing, as shown by the recorder speed a short-crossing ferry (Figure 9). It is thus worthwhile to examine the feasibility and benefits of parallel hybrid electric propulsion systems, as even the design, retrofitting, and control of the system is more complex.

Specifically, two cases are used to illustrate the concept of parallel hybrid electric ship modelling and improvement compared to a mechanically propelled ship: NG parallel hybrid and diesel parallel hybrid propulsion systems. A mechanically propelled ship is also modelled and simulated based on Skeen Queen's powertrain configuration to serve as the baseline for this study. The detailed ship configuration and information are documented in Appendix A - All Studied Marine Vessels. Details of the hybrid powertrain modelling, the model implementation and the definition of the control problem have been discussed in Appendix M Case Study for Skeena Queen - Design of Parallel Hybrid Marine Propulsion System

7.5 Case Study BC Ferries' Tachek - Modelling and Analysis of Hybrid Electric Propulsion Designs for Fuel Economy and Emission Improvements (Details in Appendix N)

The vehicle and passenger ferry, MV Tachek, operated by BC Ferries was built in 1969 in Vancouver. In 2013, a life extension project was applied on this ship to add a part-time hybrid electric propulsion system. At present, the benefits and room for improvement of the hybrid electric propulsion system of MV Tachek have not yet been systematically investigated. In this work, three different types of ship propulsion systems are simulated to illustrate the different levels of fuel economy and emission improvements, including a diesel engine and mechanical propelled benchmark powertrain system, the present part-time hybrid electric powertrain system, and a redesigned hybrid electric powertrain with more capable operations.

7.6 Case Study for BC Ferries' Klitsa - Modelling and Simulation of Hybrid Electric Ships with AC Power Bus (Details in Appendix O)

Today many electrified ships operate on an AC power bus. As a well-proven technology and extensively adopted in shipboard, the AC distribution will be still dominant for the shipboard power system in the near future. Combined with a battery ESS through a bi-directional DC/AC power converter, diesel generator sets of hybrid AC power systems can also operate at their maximum efficiency point at different load levels. Compared with conventional diesel-electric ship power systems, hybrid AC power systems offer higher fuel economy, reliability, responsiveness, and reduction in emissions and maintenance costs. However, these systems do not have the notable fault protection challenge inherent in a hybrid DC power system.

This work focused on the dynamic modelling and simulation of the shipboard hybrid AC power system. Well-known dynamic models of each powertrain component are used and put together including three diesel-generator sets, a bi-directional DC/AC converter, a battery ESS, and an AC power source synchronizer.

Due to the complexity of the system, effective modelling and simulation tools are essential for the design, analysis, optimization and evaluation of the hybrid electric propulsion system. The power converter is modelled as a nonlinear dynamic average-value model to suit system-level studies. Each component model is parameterized using datasheet information from the manufacturers. The PID controllers are implemented for diesel engine speed governors, synchronous generators, Automatic Voltage Regulators (AVR), and the power converter controller. A rule-based supervisory controller is proposed to coordinate power-sharing among diesel-generator sets and the ESS.

The research used a load profile acquired from M.V. Klitsa as the testing platform. With the new models and control methods introduced in this work, power-sharing solutions among four power sources for four operation modes and voltage and frequency stabilization of the system AC bus have been generated. The simulation results demonstrated the benefits of hybrid electric propulsion using conventional AC power bus and powertrain components.

7.7 Case Study for BC Ferries' Klitsa - Modelling and Simulation of Hybrid Electric Ships with DC Power Bus (Details in Appendix P)

Recently, research has picked up a pace in the area of ship electrification. Shipowners are now keen to deploy ESS and electric propulsion in order to increase the overall efficiency and availability of their vessels.

In this work, hybrid series and battery-electric power architectures are developed and investigated for a short-range car deck ferry. Due to a lack of standardized drive cycles for marine vessels, real data was collected from BC Ferries MV Klitsa and compared with the simulation results. An actual diesel engine fuel consumption map (FCM) was implemented in the model, and the optimal engine and battery size were obtained using the hybrid adaptive meta-modelling (HAM) optimization algorithm. The proposed ship propulsion system is based on a DC power bus due to the extensive knowledge and experiences of DC bus based HEV/EV research, the more straightforward interface between DC power bus to larger battery ESS, and the availability of power electronic devices for this relatively smaller vessel. The cost-benefit and GHG emission analyses showed the benefits of the electrified ship proportion technologies.

7.8 Case Study on a Representative Tugboat - Operation Profile Modelling and Hybrid Electric Propulsion Benefits (Details in Appendix Q)

In this work, the critical load profiles of various tugboats are first introduced. These statistical load profiles, rather than the hull resistance, determine the actual power demands of these tugboats. The unique energy demand time-shift characteristics of a hybrid electric propulsion system with onboard ESS has fundamentally changed the type of load profiles to be used to guide the tugboat propulsion system design.

Traditionally, the fuel efficiency and emissions of tugboats have been evaluated based on the generic load profiles of the tugboats working at different function modes. In this work, we have chosen a representative tugboat load profile (or a very similar version) that has been used by multiple organizations in tugboat power analysis and design to carry out the fuel efficiency and emission simulations using our marine propulsion system model. Considering different tugboats may have different load profiles unique to their routine duties, a timescale load profile has been generated based on collected data from the literature for a typical harbour tugboat as an alternative power demand input in analyzing tugboat energy efficiency and emissions. This timescale load profile can be obtained by recording the actual power load data of a tugboat, serving as the statistical driving/load cycles, similar to ground vehicles. The higher resolution of power demand records and the time history provide a better load profile for the modelling, design optimization and optimal operation control of a tugboat with a hybrid electric propulsion system. The addition of the battery ESS for the hybrid electric or plug-in hybrid electric tugboats allows peak power shift in the time domain, a timescale, load power demand profile thus becomes essential in designing the hybrid propulsion system.

In this work, fuel consumption and emission simulations using both traditional duty-divided and our new time-scale load profiles have been carried out in alternative propulsion system analyses and designs. To ensure consistency, the newly proposed, standard time-scale load profile produces an identical duty-divided load profile, used in the study.

The preliminary study showed that the proposed hybrid electric propulsion system could lead to an 18% fuel consumption reduction and significantly lower emissions compared with the conventional propulsion system. Results from duty-divided and time-scale load profiles are presented and compared, showing the need and benefit of acquiring statistical time-scale power load data for a specific tugboat.

To build on this progress, the lifecycle cost of the hybridized tugboat will be further studied in our future and continuing work to consider both the additional investment costs of the added battery ESS and power electronics, and the fuel cost saving gained by improved fuel economy. The work is supported by our new battery performance degradation/lifecycle cost model under different ESS use patterns and by the newly proposed time-scale tugboat load profile model. The study will produce an accurate prediction of the payback time of the vessel electrification and hybridization, facilitate the selection of propulsion system architecture and optimization of hybrid electric powertrain components, and support accurate cost estimation for a specific application. Additional hybrid powertrain architectures, including plug-in hybrid, best suited for different tugboat load profiles will also be investigated.

The battery performance degradation model will be used in system design to evaluate battery lifecycle cost and optimize the size of the battery ESS and engine. The use of the LNG-diesel dual-fuel engine will be investigated with different propulsion system architectures in comparison to traditional diesel-mechanical and diesel-electric drivetrains for fuel cost and emission reductions.

7.9 Case Study for a Representative Fishing Boat - Emission and Life-Cycle Cost Analysis of Hybrid and Pure Electric Propulsion Systems (Details in Appendix R)

In recent years, progress on electrification of marine vessels has been made; however, the pace has been impacted by the different operational requirements of each type of vessel, relatively small batch of production, longer or varied lifetime, and complex design optimizations of the vessels' electric propulsion system and energy storage system (ESS). In this work, the hybrid electric and pure electric propulsion system designs for lobster fishing boats are studied based on in-field acquired operation data. A new integrated marine propulsion system modelling and simulation method and software tools, and a dedicated mobile data acquisition system have been introduced. These support the quantitative analyses of energy efficiency, emission reductions, and life-cycle costs of a new or retrofitted fishing boat with hybrid electric and pure electric powertrains, compared with the traditional ICE-powered benchmark. Following the automotive industry's MBD approach, modelling and simulation of electrified fishing ships under the acquired operation profile in MATLAB/Simulink have been carried out. Series hybrid electric and pure electric powertrain system designs with powertrain component models and rule-based system control, including properly sized electric ESS with SC or battery, have been studied. The total GHG emissions and life-cycle costs of various new, electrified boat propulsion system designs have been quantitatively evaluated against conventional ICE-powered boats with both gasoline and diesel engines. The life-cycle costs of the competing powertrain systems include the investment costs, operation/energy-consumption costs, and the replacement costs of key powertrain components over a projected ten-year operation life. Both of the new hybrid electric and battery-powered pure electric boat designs showed considerable GHG emissions reduction and favourable life-cycle cost

saving. The study presents superior clean propulsion system solutions for lobster fishing boats with quantitative justification and detailed powertrain system and control system designs, forming the foundation for further research and development.

8 OPTIMAL DESIGN AND OPERATION OF HYBRID ELECTRIC PROPULSION SYSTEM

A hybrid electric powertrain is a complex propulsion system with inherent multiple degrees of freedom in its control operations, due to the existence of at least one ICE, multiple electric machines, and the ESS. The benefits of hybrid electric propulsion can only be realized through some level of optimized operation. Control algorithms for the optimal operation of the powertrain system resided in the ECU, is an integrated part of the powertrain system. Design optimization is also critical for the proper sizing of key powertrain components, and selection of the preferred architecture. Optimal control at different levels has been implemented in all hybrid electric powertrain systems studied in this work. In some cases, powertrain component size optimization has also been carried out to obtain a fair cost-benefit comparison to the conventional powertrains. Advanced global optimization search algorithms and codes, developed earlier and during this project, have been used in the design and control optimizations.

8.1 Design Optimization

The design optimization of the hybrid electric propulsion system includes three closely related areas: powertrain system architecture, powertrain component sizes, and powertrain system control. Although case dependent, the objective of the design would include minimum life-cycle cost and/or maximum emission reduction, while maintaining required power performance and controllability. Design constraints include class and Transport Canada safety regulations, emissions, and ship-induced noise.

8.1.1 Optimization of Powertrain Architecture

The optimization of powertrain architecture is aimed at identifying the ideal powertrain architecture for a given application. The possible candidates include pure mechanical (traditional), diesel-electric, pure electric, hybrid electric, plug-in hybrid electric powertrains.

The hybrid electric and plug-in hybrid electric powertrains can be at different levels of hybridization measured by the percentage of electric propulsion power: light (3~10%), mild (10-20%), medium (20-30%) and full (≥30%); can use a diesel, gasoline, pure NG (spark-ignited), and NG-diesel dual-fuel (compression-ignited); and can have a series, parallel, or series-parallel (power blend) architectures.

The pros and cons of each powertrain architecture have been briefly discussed previously in Sections 6.3.2, 7.3 and 7.4, and their suitability/advantages for a specific vessel and its operation pattern are discussed in detail in Appendixes L and M.

8.1.2 Optimization of Key Powertrain Component Sizes

Proper sizing of key powertrain components, including engine, generator, motor, battery/UC ESS, and power converters, as well as the number, type and size of the propellers, are critical in determining the power performance, energy efficiency, emissions, and induced noise of the vessel. Among those, the selection of the engine and battery ESS are most critical, since the engine is the major source of emissions, and the large battery ESS is the most expensive and short-living powertrain component. The optimization requires accurate modelling on the performance degradation and replacement cost of these components, which is very difficult for batteries, leading to a major area of our research efforts, as discussed in detail in Appendix F.

8.1.3 Optimization of Powertrain Controller and ESS Energy Management

Different from traditional pure mechanical and electric systems, today's hybrid electric powertrain system operates on its own system controller and energy management controller. The design optimization includes the optimizations of these controllers and control algorithms. Although simplified to support real-time operation, these controllers have to reflect the optimal operation of the system based on the plant model. Optimal control at different levels has been implemented in all hybrid electric powertrain systems studied in this work. This is shown in all vessel-based case studies, including Appendixes K to R.

8.1.4 Dynamics Programming (DP) and Its Use

The addition of the ESS has fundamentally changed the way energy is provided and used in the propulsion system. Different from a traditional propulsion system in which energy is converted by the ICE to produce the power to meet the exact power demand for driving the vessel, the ESS in a hybrid electric powertrain allows stored energy to be used to assist or replace the ICE to meet the power demand for driving the vessel. Not all of the energy converted by the ICE at each time instance needs to be used for the propulsion, part or all of it can be stored in the ESS for later use. This change is adding considerable flexibility and challenges to control optimization. Dynamics programming, as a global optimization technique, can exhaustively examine various operation combinations and find the best energy conversion and utilization solution – the optimized plan for the EMS. Since this optimization needs to cover the entire "trip" to ensure balanced ESS state of charge (SOC), the DP based optimization method is time-consuming and computation intensive. It served as an excellent benchmark producing technique for generating optimal control targets under a given vessel operation pattern in this work. The actually implemented control rules are based on the DP optimizations. These are discussed in detail in the vessel-based case studies, documented in Appendix L to Q.

8.2 Current Rule-based Power Control and Energy Management Method

Some type of optimized control for the hybrid electric powertrain is essential to best utilize the powertrain system hardware to produce the best energy efficiency and emission reduction, from straightforward rule-based system to more advanced real-time intelligent control system. In this project, the rule-based controllers using the control rules derived from the DP optimization in the controller design process have been implemented in all vessel-based case studies, discussed in detail in Appendixes K to R.

The rule-based systems encompass "if-then" type decisions to control system behaviour. Typically, the rules are based on human intelligence, heuristics, or DP-based system efficiency maximization. A complex set of rules can be generated in order to obtain the specified goals of low fuel consumption, but also for desirable traits of drivability, safety, and component life. Rule-based systems are inherently rigid, and in general, are unable to adapt to conditions not accounted for during the rulemaking process. In addition, tuning of a rule-based system for a particular driving condition or drive cycle may make it behave sub-optimally for operation cycles with different behaviour. Rule-based systems are easy to implement, and as such, it is frequent that rule-based systems are used as a starting point for control strategy development, and for comparing the pros and cons of different powertrain system designs. As an ideal fit to the objectives of this work, the rule-based control strategy has been used in all case studies.

8.3 Future Real-time Optimal Power Control and Energy Management

Research on more advanced optimal control algorithms, including adaptive control, predictive control, and intelligent control using pattern-recognition, has been initiated. These aim to improve the energy-saving and emission reduction capability of marine vessels and to deal with the dynamically changing cargo and marine weather condition variations. These, however, are beyond the scope of the present contract work and will be studied in the following research.

Specifically, future research will cover two areas:

a) Real-time optimal power control that optimally allocates the speeds and torques for all-electric motors/generators and engines, depending upon the net degree of freedom (DOF) of the designed powertrain system; and

b) Real-time optimal energy management that determines the charge/discharge regimes of the battery ESS, including when and how quickly the stored energy is used.

Preliminary study on adaptive and intelligent optimal control and energy management has begun.

Although the operation patterns of representative coastal vessels have been obtained and used in various case studies completed in this project, the operations of all vessels are subject to changes due to variations of marine weather state load and cargo loads. The operation routes of these vessels are also subject to changes. To address this issue, a multiple-step procedure is proposed, including:

a) automatic recognition of vessel operation patterns from massive operation data,

b) creation of the optimal operation control plans for all recognized patterns and form a knowledge base,

c) developing the mechanism for quickly recognizing the best match vessel operation pattern during vessel operation, and applying the stored optimal control plan of this operation pattern to vessel operation control in real-time, and

d) continuously learning new operation patterns and finding the corresponding best control strategy.

These procedures will form the core of the adaptive and intelligent optimal control and energy management for our continuous research in the coming years.

8.4 Advanced Metamodel-based Global Optimization Search Tools

Design optimization of hybrid electric marine propulsion systems leads to complex global optimization problems. The design objective and constraint functions of these global optimization problems are computation-intensive MATLAB/Simulink numerical simulation models. These are a typical implicit, black box, non-unimodal, and computation-intensive functions. The design variables are mixed with integer and real variable types. Traditional unimodal optimization algorithms cannot solve these problems. Classical global optimization algorithms are not appropriate due to their lengthy computation time and slow convergence.

Over the past many years, the UVic Green Transportation research team has conducted extensive research on this subject, and developed many advanced, metamodel-based global optimization search algorithms for solving this type of complex global optimization problems. As discussed in the various case studies, these advanced global optimization tools have been used in determining the powertrain system design. An overview of this updated toolbox is attached in Appendix T Overview of the UVic Global Optimization Program Toolbox, GO Tools.

9 EXPANDED PARTNERSHIP AND FUTURE WORK

The reported contract research allowed us to gain a much better understanding of the electrified marine propulsion problem, developed the unique capability and experiences to identify appropriate clean marine transportation solutions with optimized hybrid electric marine propulsion system design and controls. The work led to expanded research and industrial partnership, and form the foundation for coming research that will address the bottle-neck problems currently faced by the marine industry in designing and building the next generation of energy efficient and pollution reduced (including ocean noise) marines vessels, including ferry ships, tugboats, and fishing boats. The previously developed, and recently improved and tested functional modules of the HEMV-MBDOT Platform can be used directly in the coming green ship developments.

9.1 Expanded Industrial Partners and Collaborators

During this project, the UVic Clean Transportation research team has collaborated effectively and productively with our research partner (and subcontractor), Glas Ocean Ltd, which conducted the planned work on the operation data acquisition and modelling of east coast fishing and commercial boats.

Extended industrial and research partnerships have also been built to expand the scope and depth of the reported R&D work and to apply the new learning and modelling tools that we have acquired during this work to various targeted applications in the future. These new developments are briefly summarized in this section

9.1.1 Marine Service and Fleet Operators

- BC Ferries – based upon the extensive studies on three ferries, the new learning and much improved modelling tools, we will further study a number of key BC Ferries' sailing routes and identify the most beneficial propulsion solutions for replacement ferry ships.

- Seaspan Ferries – based upon the extensive studies on three ships from BC Ferries, the new learning and much improved modelling tools, the new learning will be applied to Seaspan NG-diesel dual-fuel cargo ferries.
- Seaspan Marine (Vancouver Harbour Tug) – possible collaborative will be on real-time operation data acquisition for the port tug in Vancouver to examine low emission and noise solutions, with possible reduction of operation costs.

9.1.2 Marine Engineering and Technology Firms

1) Robert Allan Ltd. (RAL) – Testing and developing tug design and cost projection tool using the integrated hybrid electric propulsion modelling tools, propeller cavitation modelling tools, as well as acquired tug operation data and learnings from the case studies.
2) Seaspan/Washington Co. – generic collaborative work on NG-hybrid electric propulsion system technology for marine and mining transportation operations.
3) Dynamic Systems Analysis (DSA) – applying DSA's dynamic ship/marine structure modelling tool to simplify the hull reduced-order hydrodynamics model, and seeking new applications
4) Techsol Marine – the UVic team has worked with Techsol on UVic Green Research Ship in 2010 and BC Ferry Tachek in 2017. Future collaborative work will be on the next series NG hybrid cargo ships for Seaspan Ferries
5) JASCO – agreements have been researched on collaborative work to better trace the measured ocean noise to a different class of ships and serve as a means for better ocean noise regulation. In addition, using JASCO's ocean-noise measurement setups to verify the models of ship-induced noise from vessels from BC Ferries, Seaspan, RAL, and east coast fishing boats is going to be planned.
6) Vard Marine – as a consulting naval architecture and marine engineering company with Canadian operations located in Vancouver, Vard has engineered the development of the Seaspan NG hybrid cargo ferry. The initial work will be a case study on the completed NG hybrid cargo ferry, and our collaboration will be in this area.
7) Corvus Power – research agreement and initial work has been done on battery performance degradation and life cycle cost modelling (LG Chemical battery).
8) Shanghai Automotive (SAIC Motor) – Battery performance degradation and life cycle cost modelling (A123 battery class).
9) dSPACE – Hardware-in-Loop simulation and modelling of heavy-duty diesel engines and hybrid electric marine propulsion system. The company has agreed for more collaborative work on diesel and NG engine modelling.
10) Siemens PLM Software (MIS, Belgium) – modelling tools for hybrid electric marine propulsion systems.

9.2 Expanded Collaborating Academic and Research Institutions

1) NRC-OCRE (St John's) – Developing Canadian Propeller Test Facilities (with U Genova)

2) NRC (Vancouver/Ottawa) – Battery Performance Degradation and Life-cycle Cost Modelling
3) Western Economic Diversification Canada (WD) – to establish battery performance degradation experiment facilities at UVic in July 2018 to obtain the missing empirical data for establishing battery lifecycle cost model and for optimal energy management of battery.
4) Gas Technology Institute (GTI) – our collaborative work with this Chicago-based, non-profit research institute will be on NG engine modelling and transportation applications, which are the focuses of the institute.
5) COSIA (Canada's Oil Sands Innovation Alliance) – NG engine modelling and transportation applications. GTI is presently COSIA's lead on NG engine research.
6) Canadian Urban Transit Research and Innovation Consortium – seeking joint work nationally for clean transportation in marine and on road.
7) CiSMART (Canadian National Network for Innovative Shipbuilding/Marine Research and Training – initiatives on clean marine research and education through National Centre of Excellences. The UVic team will contribute in green ship and propulsion system, better use of ocean energy, emission and ship noise reduction, better propulsion efficiency.
8) University of Genoa – experimental verification of marine propeller cavitation noise model, and joint-work with NRC-OCRE to build Canadian propeller experiment capabilities.
9) Nova Scotia Boat Builders Association – through Glas Ocean Ltd, to look into clean propulsion solutions for fishing boats and small commercial boats
10) School of Port & Transportation Engineering, Zhejiang Ocean University, China – this institute has specialties in two areas: a) diesel and NG engine test laboratory that can produce valuable NG engine efficiency and emission data, and b) a large amount of vessel sea trials data to recognize and verify vessel operation pattern.
11) National Centre for Maritime Engineering and Hydrodynamics, Australian Maritime College, University of Tasmania, Australia – our team has used their ROTORYSICS codes to quantify propeller performance under the influence of many parameters, to seek the use of time-domain panel method to predict the hydrodynamic performance of screw propellers on common computing devices.

9.3 Planned Continuous Work

The reported work is part of our continuous research on the development of enabling technologies for clean marine transportation and our research collaborations with BC Ferries, Robert Allan Ltd, Seaspan, and several other leading Canadian marine engineering and service providers.

9.3.1 Focused Study on Plug-in Hybrid Electric Marine Propulsion System

Our previous studies have successfully demonstrated the superior energy efficiency, CO_{2e} emission, and lifecycle cost reduction of hybrid, plug-in hybrid, and electric propulsion technologies for various coastal vessels. Among these clean energy propulsion options, the plug-in hybrid electric propulsion technology inherently possesses the features of 2-3 different types of

vessels: ICE hybrid electric; pure electric; (and pure ICE in extreme case). The technology presents a number of unique features and advantages:

- The availability of dual power sources from both ICE and grid-charged battery to ensure the power plant redundancy for marine safety
- The ability to utilize low-cost, grid energy from renewable energy sources during a portion of the operation, which can be supported by the available charge time. The approach also allows different levels of initial battery ESS and charge infrastructure investment, and later expansion with added investment.
- The technology is compatible with NG-diesel dual-fuel engine, and support engine upgrade with a simple change to the control system.
- The technology supports a progressive transition from hybrid electric to full electric propulsion operation at a pace compatible with the developments of renewable energy power generation and battery technology (cost reduction).

The application of the Plug-in Hybrid Electric Marine Propulsion technology is of present interest to BC Ferries, BC Hydro, Seaspan, and very likely the east coast fishing community due to these stated, unique advantages of the technology. The versatile technology has tremendous value to Canada with clean electric power at a lower cost.

9.3.2 Improvements of Key Powertrain System Components

1) Generic and more accurate performance, energy efficiency, and emissions data of NG-diesel dual-fuel engine, through collaborative work with:
   - Research Institutes:
     - Gas Technology Institute (GTI) – planned collaborative work with this Chicago-based, non-profit research institute will be on NG engine modelling and transportation applications, which are the focuses of the institute.
     - School of Port & Transportation Engineering, Zhejiang Ocean University, China – NG engine test laboratory to obtain NG engine efficiency and emission data
   - Engine manufacturers:
     - Caterpillar (through the connection of GTI of Chicago and Teck Resources Ltd of BC, both Caterpillar NG engine users)
     - Westport (smaller NG engine)
     - dSPACE – diesel and NG engine model

BC Ferries, RAL, COSIA and Teck are involved as NG engine users.

2) Expanded battery performance degradation and life-cycle model
   - Battery and battery ESS manufacturers
     - Corvus Power – formally agreed to collaborate on battery performance degradation and life cycle cost modelling. Batteries will be used by both BC Ferries and Seaspan
     - Shanghai Automotive (SAIC Motor) – formally agreed on a collaboration to allow us to get battery test data for battery performance degradation and life cycle cost modelling.
   - Research Institutes:

- NRC (Vancouver/Ottawa) – obtain more battery test data and carrying testing on large battery modules for battery performance degradation and life-cycle cost modelling with Corvus Power collaboration
- Western Economic Diversification Canada (WD) – to complete the battery performance degradation experiment facilities at UVic for acquiring missing empirical data in establishing battery lifecycle cost model and for optimal energy management of battery.
- UVic Clean Energy Lab – obtain additional (missing) battery test data and carrying out testing on small battery cells for battery performance degradation and life-cycle cost modelling
- Potential collaboration with – NREL and ANL's battery modelling teams

3) Improving the Converter (AC/DC) model into a generic modelling tool – producing a generic, power loss model similar to the DC/DC converter modelling tool developed in this work.
4) Implementation of the software modelling tools onto dSPACE Hardware-in-Loop (HIL) simulation and testing platform for more accurate experimentation validation.

9.3.3 Application Specific Modelling and Designs Using Manufacturers' Equipment Data

During this contract research, the capability of the integrated hybrid electric marine propulsion system tools has been expanded. The integrated modelling tools in different forms have been applied to investigate the energy efficiency and emission/noise reduction improvement potentials of different clean transportation solutions. These integrated modelling tools are assembled through different combinations of the developed system function modules, and the operation data acquired from real marine vessels are used to form the load profiles of these vessels.

These operating vessel derived models and resulting case studies, using advanced model based design and optimization methodology, have built additional confidence on marine industry partners, and attracted considerable attentions from many other leading Canadian marine industry players. The logical next step is to apply these new learning and tools to seek clean energy marine propulsion solutions for a number of unfolding Canadian applications.

1) BC Ferries are planning to replace 12 shuttle ferry ships over the next 12 years, with 50 and 100 vehicle-carrying capabilities, for its various sailing routes. Ideally, these ferries can be built with optimized plug-in hybrid electric powertrain designs for their routine sailings. Detailed case studies for these routes will be needed to identify the optimal size of the ferry, as well as the optimal powertrain architecture and the size of engines and battery ESS. Detailed case studies using the route and BC hydro's power grid inputs will produce more energy efficient and cost effective solutions with much reduced emissions and ship induced noise.

2) As the port tugboats operator and designer, Seaspan Marine and Robert Allan Ltd (RAL) are interested in developing high fidelity, integrated hybrid electric propulsion modelling tools that can be used to predict fuel economy, GHG emissions, and propeller cavitation noise for new tug design and controls with this project team. The ability to generate a reliable cost projection tool for the battery ESS, and to obtain the optimal hybrid propulsion system for a given tug operation profile is very important to improve the ability for the company to compete well internationally.

3) The Nova Scotia Boat Builders are planning to proceed with fishing boat electrification. Dedicated hybrid electric and electric boat designs and case studies, using the data of the LiNMC batteries supplied by Torqeedo, can optimize the design and its operation controls.

4) Seaspan Ferries, Techsol and Vard Marine are in the process of developing next generation NG hybrid cargo ferries. Similarly, these ferries can be built ideally with optimized plug-in hybrid electric powertrain designs for their routine shipping tasks. Detailed case studies for these routes will be needed to identify the optimal size of the ferry, as well as the optimal powertrain architecture and the size of NG engines and battery ESS. Detailed case studies using the routes and BC hydro's power grid inputs will produce more energy efficient and cost effective solution with much reduced emissions and ship-induced noise.

The industrial partners have all expressed their intentions to collaborate closely with the project team to put the new clean propulsion system modelling and design optimization technologies into real applications. New hybrid electric powertrain system components, which can be used in the new hybrid electric vessels to be produced by these industrial partners, need to be modelled using data acquired from their OEMs. Following the same process, these more accurate, dedicated powertrain component models, rather than the generic models used in our present contract work, can better support the design and control developments for these real marine vessels.

9.3.4 Continuous Research Work

All research activities defined in the contract proposal and plan have been successfully completed. The UVic Clean Transportation team would like to work on the following tasks continuously due to the urgent need and for the continuity of the research program.

1) Improving the ship dynamics and maneuver reduced-order hydrodynamics model.

   This 3-DOF model implementation will reveal the accurate propeller inflow-stream speed, thus: a) improving vessel energy consumption modelling during docking and departing processes; and b) accurately predicting propeller cavitation and cavitation-noise.

   The present 1-DOF reduced-order hydrodynamics model worked very well in steady sailing along the longitudinal direction, and the modelling error from experimental data is about 5-7%. However, when the lateral and yaw motions of the ship are involved the error increases considerably. Although the lateral and yaw motions only contribute a very small part of vessel motion, it has a higher chance of making the propeller work outside its design specification, thus creating cavitation noise. Extended 3-DOF implementation work to improve the model has been started. Dynamic Systems Analysis (DSA)'s dynamic ship/marine structure modelling tool will be used to simplify the hull reduced-order hydrodynamics model, and to test on new applications.

2) Working with the West-Coast-Wave-Initiative and Ocean Canada research teams to model the Marine Weather State (MWS) conditions along Canadian coasts, and incorporating MWS considerations into the modelling of vessel operation profiles.

   The work will form the foundations for

   a) Producing more accurate best, worst, and season medium propulsion power estimations to address the dynamic variations of the ocean environment,

b) Combining MWS and vessel sailing speed to accurately predict propeller in-flow stream speed to assess the risk of cavitation and cavitation noise; and

c) Supporting semi-autonomous sailing or automatic piloting to minimize propulsion energy use, emissions and cavitation noise.

3) Completing the vessel stability book-based regression model of hull resistance; and the panel method-based semi-empirical propeller thrust and cavitation model.

   Efforts in these two areas are both aimed at introducing new, accurate and ease to solve numerical models to obtain hull resistance, propeller thrust and cavitation noise without the need of full-scale CFD simulations on a supercomputer. The acquired experimental data from vessel operation and the full-scale CFD simulation can be reserved as means for modelling result validation.

4) Better trace the measured ocean noise to different class of ships and identify the speed threshold of cavitation noise

   Working with JASCO – agreements have been reached on collaborative work to trace the measured ocean noise to an individual ship, and to use the method for better ocean noise regulation. In addition, using JASCO's ocean-noise measurement setups to verify the models of ship-induced noise from vessels from BC Ferries, Seaspan, RAL, and east coast fishing boats is going to be planned.

5) Identifying new area of research through interactions with world leading hybrid electric marine technology developers

   - Presenting our new research results to the hybrid electric marine R&D community
   - Renewing our connections with leading groups in this area, including Siemens PLM Software (MIS, Belgium), Norwegian Institute of Marine Research, and ABB, and Wärtsilä.

6) Introducing Canadian propeller cavitation noise measurement facility

   Working with NRC-OCRE (St John's) to develop Canadian Propeller Test Facilities. University of Genoa will participate in this work to setup experimental verification equipment and procedures.

REFERENCES

[1] Andersen, K. (2016) *Development of a Time-Domain Modelling Platform for Hybrid Marine Propulsion Systems*, M.A.Sc. Thesis, University of Victoria.

[2] Holtrop, J. and Mennen, G.G. (1982), An approximate power prediction method, *International Shipbuilding Progress*, 29 (335), 166-170.

[3] Carlton, J. (2012), *Marine propellers and propulsion,* Butterworth-Heinemann.

[4] Flikkema, M. B., J. Holtrop and T. J. C. Van Terwisga, (2006) "Aparametric power prediction model for tractor pods," in *Proceedings of Second International Conference on Advances in Podded Propulsion*, Brest.

[5] Fossen, T. I. (2011) *Handbook of Marine Craft Hydrodynamics and Motion Control,* Chichester: John Wiley & Sons Ltd., 2011.

[6] Abdul Ghani, M. P., O. Yaakob, N. Ismail, A. S. A. Kader and A. F. Ahmad Sabki, (2014) "Experimental Analysis of Podded Propulsor on Naval," *TransNav*, 8 (1), pp. 153-156.

[7] Wei, L., and P. Geng. (2016) "A review on natural gas/diesel dual-fuel combustion, emissions and performance." Fuel Processing Technology 142 pp. 264-278.

[8] Hensley, R. J. Newman, M. Rogers, and M. Shahinian (2012) "Battery technology charges ahead," *McKinsey Quarterly*, vol. 3, pp. 5-50.

[9] Liu, J., Z. Dong, T. Jin, and L. Liu (2018) “Recent Advance of Hybrid Energy Storage Systems for Electrified Vehicles,” *Proceedings of 14th IEEE/ASME International Conference on Mechatronic and Embedded Systems and Applications*, July 2 - 4, Oulu, Finland.

[10] Wei, L. and P. Geng (2016) "A review on natural gas/diesel dual-fuel combustion, emissions and performance." *Fuel Processing Technology* 142, pp. 264-278

[11] Cheenkachorn, K., C. Poompipatpong, and C. G. Ho (2013) "Performance and emissions of a heavy-duty diesel engine fueled with diesel and LNG" *Energy* 53, pp. 52-57.

[12] Dong, Z., P. Oshkai, O. Barannyk, M. Rahimpour and K. Andersen, “Review of the Sources of Flow-Induced Ship Noises, Their Modelling and Mitigation Using Hybrid Electric Ship Propulsion System Modelling Tool,” Technical (Contract) Report to Transport Canada, T8156-150105/A, 2016.

[13] Rahimpour, M., D. Iverson, D. W. McIntyre, G. Tani, F. Miglianti, M. Viviani, Z. Dong, and P. Oshkai, “Semi-Empirical Approach to Predicting Cavitation-Induced Acoustic Noise from Marine Propellers,” *Proceedings of 9th International Symposium on Fluid-Structure Interactions, Flow-Sound Interactions, Flow-Induced Vibration & Noise*, July 8-11, 2018, Toronto, Canada.

[14] Wei, Lijiang, and Peng Geng. "A review on natural gas/diesel dual-fuel combustion, emissions and performance." Fuel Processing Technology 142 (2016): 264-278. 21

[15] Cheenkachorn, Kraipat, Chedthawut Poompipatpong, and Choi Gyeung Ho. "Performance and emissions of a heavy-duty diesel engine fueled with diesel and LNG (liquid natural gas)." Energy 53 (2013): 52-57. 19

[16] Namasivayam, A. M., et al. "Biodiesel, emulsified biodiesel and dimethyl ether as pilot fuels for natural gas fueled engines." Applied Energy 87.3 (2010): 769-778. 22

[17] Feng, Y., Z. Dong, J. Yang and R. Cheng, “Performance Modelling and Cost-benefit Analysis of Hybrid Electric Mining Trucks,” *Proceedings of the 12th IEEE/ASME International Conference on Mechatronic and Embedded Systems and Applications*, August 29-31, 2016, Auckland, New Zealand.

Appendix A. All Studied Marine Vessels

A1. BC FERRIES MV SKEENA QUEEN

Figure A - 1: MV Skeena Queen

Table A - 1: MV Skeena Queen Profile

Built	1997, Vancouver
Overall Length	110 metres (360'8")
Maximum Displacement	2942 tonnes
Car Capacity	100
Passenger & Crew Capacity	450
Gross tonnage	2453 tonnes
Service Speed	14.5 knots (16.7 mph; 26.9 km/h) at 3500 bhp
Maximum Speed	17.3 knots
Power	4500 kW
Amenities	Car deck lounges, vending machines, accessible washrooms
Route	Fulford Harbour-Swartz Bay
Builder	Allied Shipbuilders Ltd., North Vancouver

The MV Skeena Queen is a ferry built in 1997 and named after the Skeena River. It was intended to be part of a class of Spartan, utilitarian ferries, in the "Century ferry class", designed by McLaren

and Sons naval architects. In 1994, the 10-year plan of BC Ferries called for construction of three Century class ferries, to service the busier Gulf Island routes in British Columbia operated by BC Ferries. The name for the class was derived from the capacity, which is approximately 100 cars. However, the only ferry of the class actually built was the Skeena Queen. It runs solely on the Swartz Bay-Salt Spring Island (at Fulford Harbour) route (except for a brief four-day trial on the Horseshoe Bay to Bowen Island run from April 23 to April 26, 1998).

The original four propulsion engines of the Skeena Queen had major problems following commission, including excessively high noise levels and cylinder cracking during high-speed operation. On April 15, 2002, Skeena Queen was removed from service and its four high-speed Mitsubishi S12R diesel engines were replaced with four Mitsubishi medium-speed engines, model S6U. The Skeena Queen has very little cabin space because the Century ferry class was intended to be used on short commuter runs of less than a half-hour duration where most of the passengers stay in their vehicles. The Skeena Queen operates solely on the route between Swartz Bay and Fulford Harbour, which is a 35-minute crossing.

Skeena Queen is one of the typical middle size ferries operating between southern gulf islands and Vancouver Island by BC Ferries. It has been chosen as a study case to analyze fuel consumptions and emissions for different applied technologies. The capacity of Skeena Queen can accommodate about 92 vehicles and 450 passengers. With a total maximum 45,000 kW propulsion power from four diesel engines, it can sail as fast as 17.3 knots in the ocean (other information was showed in Figure 1: Sailing Route and General Information about Skeena Queen).

Skeena Queen	
Overall Length:	110 metres
Maximum Displacement:	2,942 tonnes
Car Capacity:	92
Passenger & Crew Capacity:	450
Maximum Speed:	17.3 knots
Horsepower:	6,000
Route:	Fulford Harbour-Swartz Bay
Corssing Time:	35 mins
Distance:	5 nautical miles

Figure A - 2: Sailing Route and General Information about Skeena Queen

As the only ship running between Fulford Harbour, Salt Spring Island and Swartz Bay, Vancouver Island, Skeena Queen has a very tight schedule. It runs 16 times on weekdays and 18 times on Saturday with only 10 to 35mins resting and loading time at terminals after each voyage. With four Mitsubishi heavy industry diesel engine and two auxiliary genset working on board, the total diesel fuel consumption for one day could be more than 8,000 Liters with full load at certain ocean conditions. The lay out of the ship's propulsion system is shown in Figure A - 3 and Figure A - 4. A photo of the ship at Victoria's Dry Dock is shown in Figure A - 5.

A1.1. Skeena Queen Propulsion System

The detailed CAD models of Skeena Queen's ship hull and propeller have been regenerated using acquired rough design data. The models were used to create the smooth surface files (.SL) for the detailed CFD modelling and hydrodynamics (Soft Towing Tank) Flow Simulation.

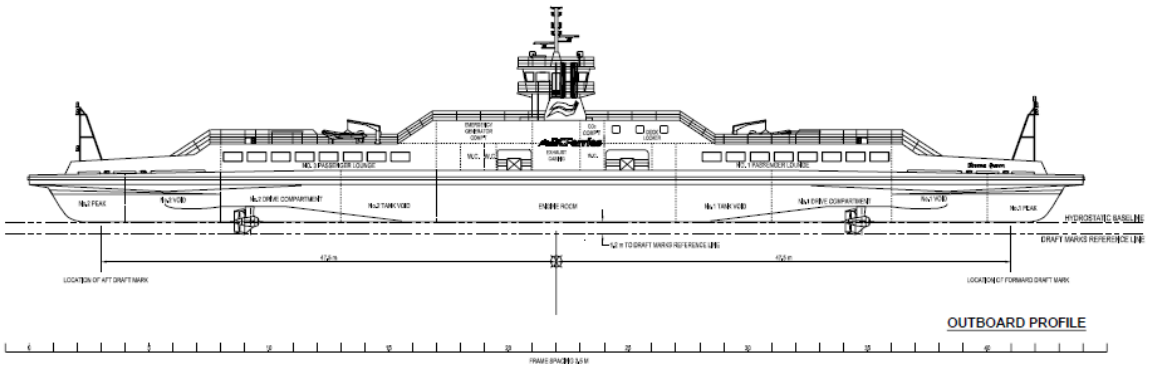

(a)

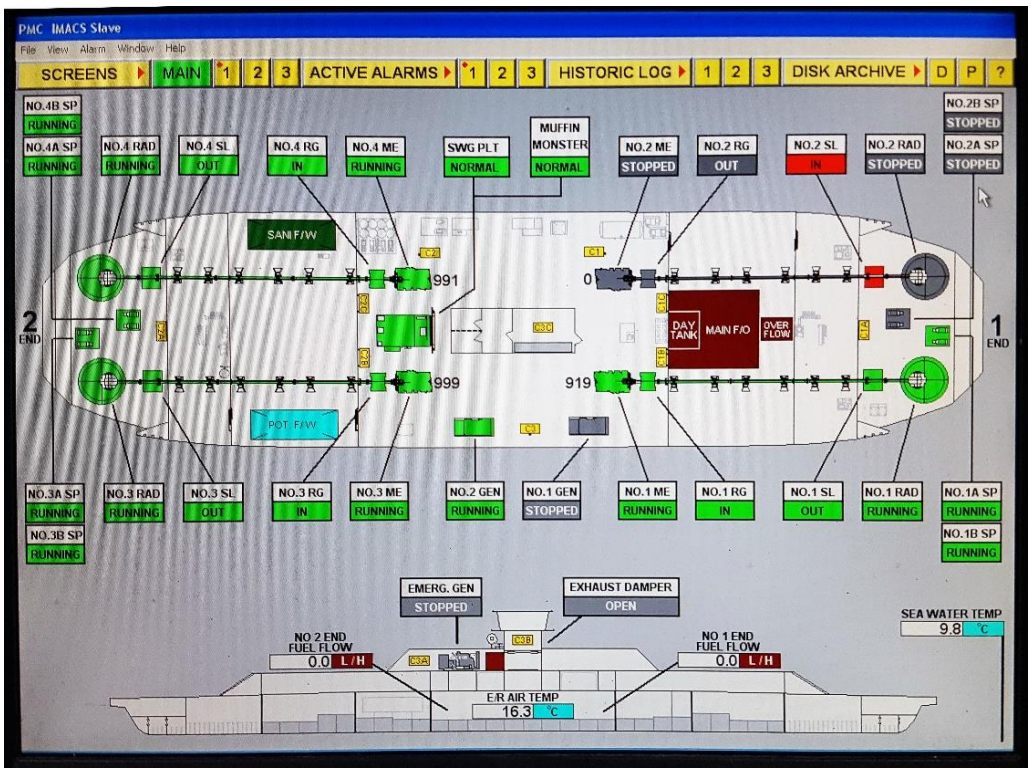

(b)

Figure A - 3: Skeena Queen's Hull and Propeller (4) Models\Layout of Present Ship Propulsion System

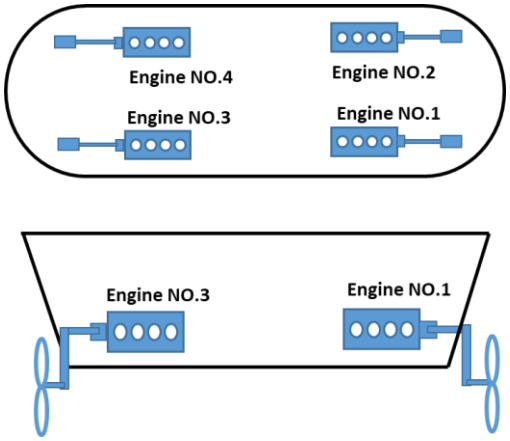

Figure A - 4: Illustration for Skeena Queen Propulsion System Architecture

The gear ratios of the engine to shaft gearbox and the RAD (shaft to propeller), and the engine and propeller speed ratio are given in Table A - 1.

Table A - 2: RPM Ratios

Gearbox:	1.226
RAD:	2.797
Engine/Prop ratio:	3.429

Shaft RPM	Engine RPM	Prop RPM
500	613	179
750	920	268
850	1042	304
865	1060	309

A1.1.1. Skeena Queen Project - Work Requirements

a) CFD Analysis for Model Parameterization
- CFD analysis of bare hull
- CFD analysis of rear propellers
- CFD analysis of bow thruster
- CFD self-propelled
- Wake fraction and thrust deduction analysis

b) Vessel Dynamics
- ShipMo3D analysis
- Maneuvering model parameterization
- Rudder model
- Surge resistance decomposition

c) CAD Modelling
- Develop 3D CAD model of hull and propellers for CFD

d) Data Collection System
   - Design, construction, and lab testing of equipment
   - Installation planning and equipment procurement
   - Installation, commissioning, and monitoring
   - Post-collection data analysis and processing
   - Decommissioning

e) Generic Powertrain System Component Modelling for Case Studies
   - Component information gathering
   - Model of Diesel Engine (Performance, Fuel Economy and Emissions)
   - Model of Natural Gas Engine (Performance, Fuel Economy and Emissions)
   - Modelling of Induction Generator and Electric Motor
   - Modelling of DC/DC converter
   - Modelling of Battery ESS with Performance Degradation and Life-cycle Cost

f) Real-time Control of Power Management
   - Analysis of current power management system
   - Existing Operational Analysis
     - Energy efficiency analysis and actual utilization of existing components
     - Study of alternate powertrain architectures for ferry load profile
   - Real-time power management control system and optimization of ship
   - Optimization of battery size for the acquired operation pattern and design life

g) Data acquisition system installed on the ship
   - Four sets of engine speed and torque sensors and wireless data recording
   - Other operation data from CAN and VDR

A considerable amount of data acquisition equipment was installed when the ship came to the Victoria Dry Dock for repair work. Ship operation data have been acquired both during after service sea trials and routine ferry operations.

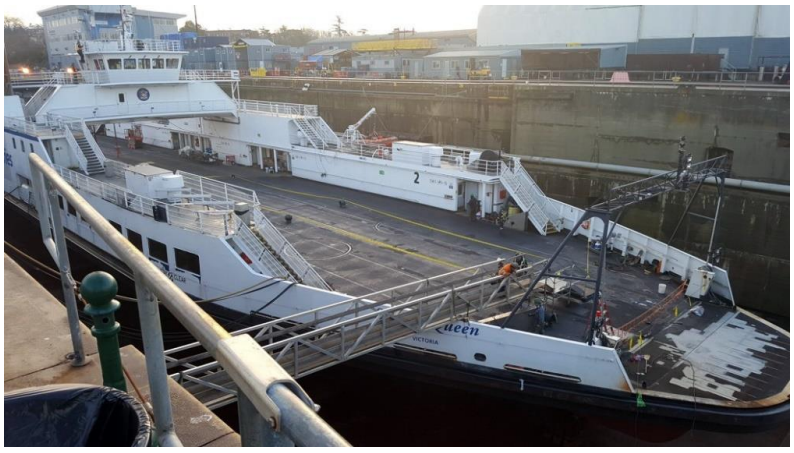

Figure A - 5: Skeena Queen at Victoria's Dry Dock

Figure A - 6: Skeena Queen's Hull and Propeller (4) Models

The ships operation data have been acquired from several channels, including

a) Speed and torque sensors mounted on the four engine/propeller shafts, as shown in the bottom of Figure 5. We have used the BeeTech shaft speed and torque data acquisition system with shaft mounted strain gauge torque and speed sensors. Wireless data transmitters and used to send signals to a data recorder with PC interfaces.
b) The MV Skeena Queen Trim and Stability Booklet (from BCFS).
c) Ship operation data acquired from the BC Ferries (Voyage Data Recorder) VDR Computer (as shown at top of Figure 5).
d) 1997 Propulsion Control Trails and the new sea trials conducted after the installation of our shaft sensors in April 2017.

Figure A - 7: Ferry Operation, VDR, Engine/Propeller Shaft and Mounted Sensors

The VDR data from BCFS's database may contain the data listed in Table A - 3. Not all ships have data recorded in every category. The typical operation speed profile on a Saturday, acquired by

our data acquisition system, was showed in Figure A - 8 (relatively stable between each voyage). The ferry faces different traffic demands and patterns during weekdays and weekend days.

Data on variable cargo (car) load and sea state (current, tide, wave and wind) load have been acquired from ship's operation logbook (William Russell, Senior Chief Engineer, Skeena Queen).

Table A - 3 Data List from BC Ferries (Voyage Data Recorder) VDR Computer

Compass	Rate of Turn
	Heading, True
Hull	Depth below transducer
	Depth Below Surface
	Depth below keel
	Heading – Deviation & Variation
Unknown	Furuno device message
	Furuno device message
GPS	Track Made Good and Speed Over Ground
	Recommended minimum specific GPS/Transit data
	UTC day, month, and year, and local time zone offset
	Global Positioning System Fix Data
	Datum reference information
	Geographic Position, Latitude/Longitude Data
Weather Station	Wind Direction and Speed, with respect to north
	Wind Speed and Angle, in relation to the vessel's bow/centerline.
	Track Made Good and Speed Over Ground
Speed logger	Distance Traveled through Water
	Speed Through Water and Speed Over Ground
	Acknowledge alarm
	AIS Alarm Messages
Rudder	Rudder order status
	Rudder angle
Propeller	Engine order

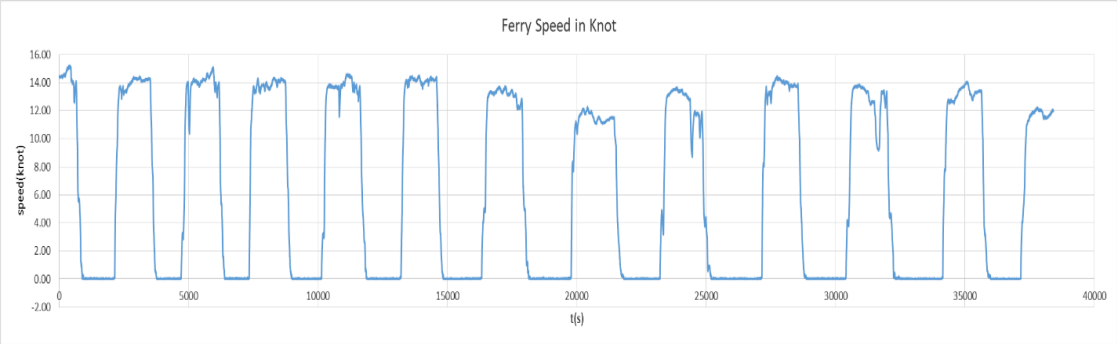

Figure A - 8 Ferry Speed Profile

A2. BC FERRIES MV TACHEK

Figure A - 9 MV Tachek

Table A - 4 MV Tachek Profile

Built	1969, Vancouver
Overall Length	49.53 metres (162'6")
Maximum Displacement	807 tonnes
Length	49.53 m (162 ft 6 in)
Beam	14.63 m (48 ft 0 in)
Installed power	1,300 kW (1700 hp)
Car Capacity	30
Passengers	143
Crew	7
Maximum Speed	12.5 knots
Amenities	None
Route	Denman Island-Hornby Island

BC Ferries operates two T class ferries for use on small inter-island routes. They have raised bows, which make it easier for the ships to travel in the rough seas often found on British Columbia's central coast. The ferries carry 30 cars and 143 passengers. Both were built in 1969. They were originally owned and operated by BC's Ministry of Transportation and Highways until 1985, when the Ministry's saltwater ferries and routes were transferred to BC Ferries, including the T-Class. The two T-class ferries are Tachek and Quadra Queen II.

MV Tachek was built in 1969 in Vancouver, BC by Allied Shipbuilders. She was originally named Texada Queen and was used on the Powell River-Blubber Bay route, serving her namesake Texada Island. She was renamed Tachek in 1977, and continued serving Texada Island until 1979 when the larger North Island Princess replaced her. Since then, she has served as an auxiliary vessel, providing additional capacity where demand is needed and serving as a backup ferry when other ferries are out of service. As of 2013, she is used on the route between Denman Island and Hornby Island from mid-fall to mid-spring, and serves as a backup vessel for the rest of the year, tied up at Blubber Bay when not in use. On 15 December 2012, Tachek was removed from service to undergo a nine-month life-extension project[1].

Figure A - 10 MV Tachek

Field Trip Travel between Victoria and Campbell River: 2h 57 min and 265 km; Campbell River – Quadra Island (10 min); Quadra Island (Heriot Bay) – Cortes Island (45 min) in Heriot Bay on Quadra island at 08:30 am or the next docking there will be 10:30 am.

A2.1. Operation Profile Generation and Modelling

A2.1.1. BC Ferries Original Intent for Hybridization

Part of the project to extend the life of the 44-years-old vessel was to rebuild the ferry's propulsion and mechanical systems. The objectives set by BC Ferries required us to develop a range of unique and custom technical solutions. The ultimate goal was to create a vessel that would provide an effective service to the existing routes with reduced fuel consumption and environmental emissions. The recent integration of the hybrid system improved the performance resulting in major fuel savings. Techsol Marine's integrated hybrid battery system, provided by Super B, makes it one of the most innovative and environmentally friendly vessels in BC Ferries' fleet.

Main Features:

Improved fuel efficiency, reduced power lose and power generation is achieved with active front-end drive technology and PTO motors

- Reduced carbon footprint system eligible for carbon credits
- Lower vibration and noise for increased comfort of the crew and passengers
- Lower maintenance cost on generators due to reduced usage and loads

A2.2. Tachek Project – Work Requirements

a) CFD Analysis for Model Parameterization
   - CFD analysis of bare hull
   - CFD analysis of rear propellers
   - CFD analysis of bow thruster
   - CFD self-propelled
   - Wake fraction and thrust deduction analysis

b) Vessel Dynamics
   - ShipMo3D analysis
   - Maneuvering model parameterization
   - Rudder model
   - Surge resistance decomposition

c) CAD Modelling
   - Develop 3D CAD model of Tachek propellers for CFD

d) Data Collection System
   - Design, construction, and lab testing of equipment
   - Installation planning and equipment procurement
   - Installation, commissioning, and monitoring
   - Post-collection data analysis and processing
   - Decommissioning

e) Plant Modelling
   - Component information gathering
   - Model SuperB 114kW energy storage system
   - Modelling of Induction Generator
   - Modelling of Variable-Speed Generation Power Electronics
   - Modelling of DC/AC converter
   - Modelling of DC/DC converter model

f) Real-time Control of Power Management
   - Analysis of current power management system
   - Existing Operational Analysis
     - Energy efficiency analysis and actual utilization of existing components
     - Study of alternate powertrain architectures for ferry load profile
   - Real-time power management control system and optimization of ship

g) Tachek Supply
   - Main and Emergency Switchboards
   - Power Management System (PMS)
   - Low harmonic (common DC bus) Drives for PTO (Power Take-Off)
   - Bow thruster motors and DC Battery banks
   - Alarm Monitoring System (AMS)
   - Wheelhouse and ECR consoles

- PTO (Power Take-Off) motors
- Motor Control Center Units (MCC)
- Distribution Panels

A2.3. Powertrain Architecture

The present powertrain architecture of the ship is illustrated in Figure A - 11.

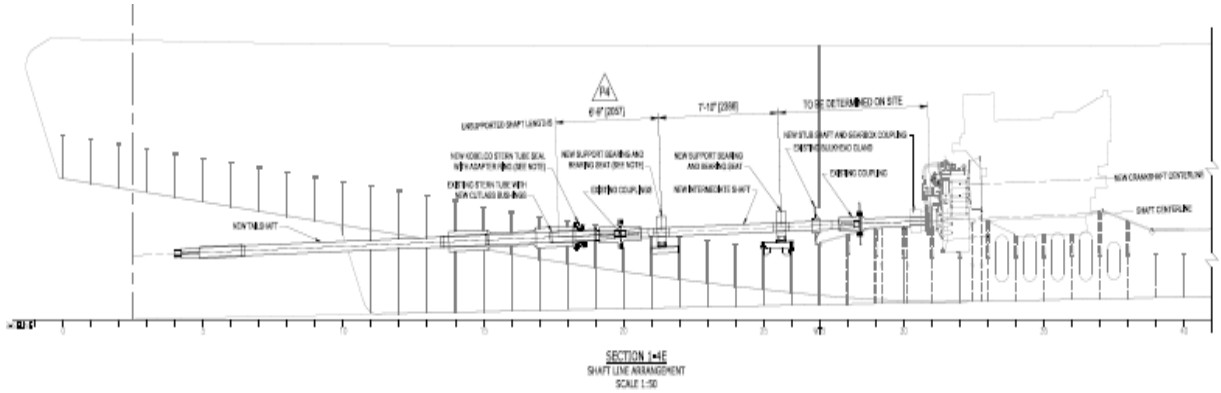

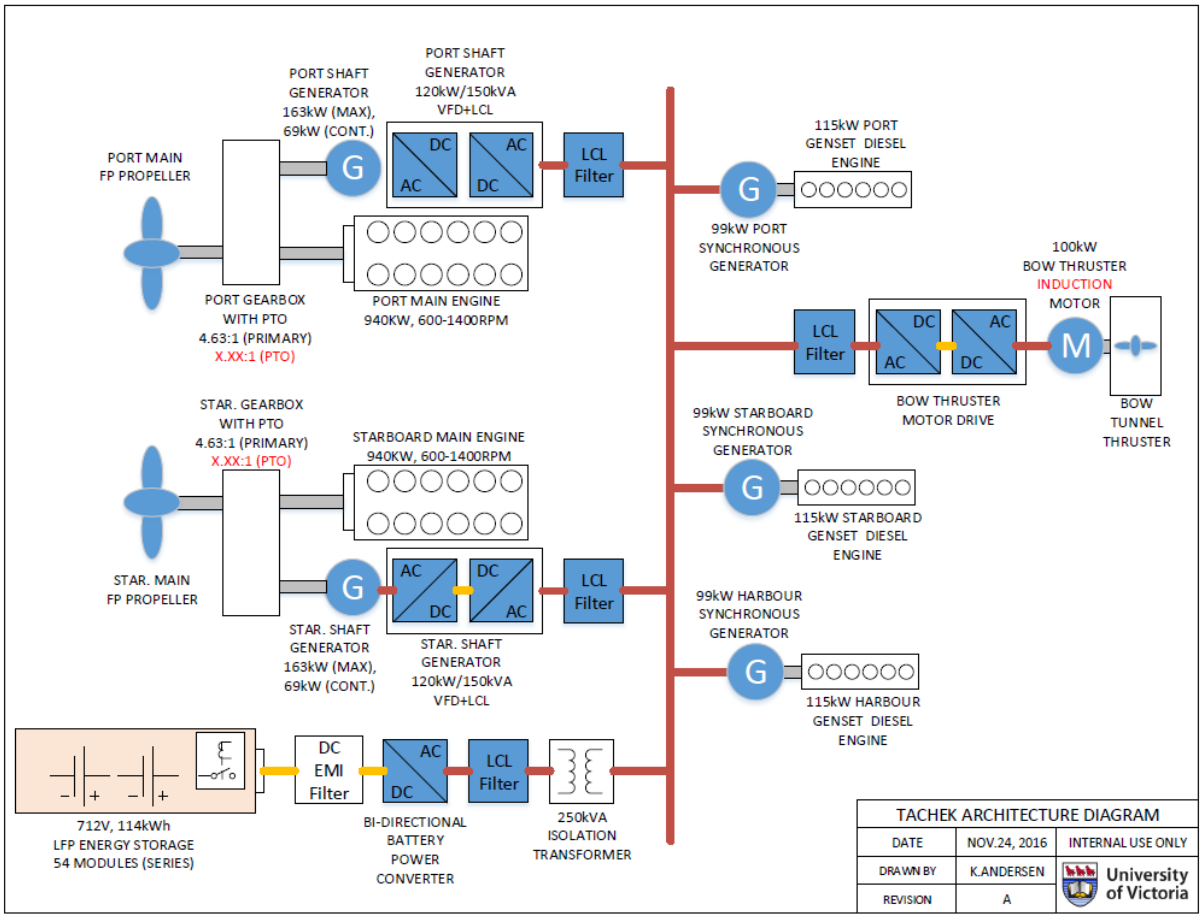

Figure A - 11 Propulsion System Architecture and Mechanical Drive

A2.4. Data Acquisition (DA) System

The unique architecture of Tachek makes the DA system quite different compared to the Skeena Queen (SKQ). We have divided the data acquisition tasks into two portions: from the propulsion system and from the navigation system.

Tachek has a Modbus TCP/IP network on the ship. This a Modbus variant used for communications over TCP/IP networks. With this network, we can connect to various equipment on the ship, and manipulate the information flow in the network:

- Generator: 2 sets - Frequency, power, power factor
- Shaft generator: 2 sets - Frequency, power, power factor
- Emergency generator: 1 set - Frequency, power, power factor
- Bow thruster: 1 set - Speed, power
- Gearbox: 2 sets - Electric generator, diesel engine, and propeller shaft speeds
- ESS: 1 set - DC current, DC voltage, DC/AC power output

The ship's data acquisition system is shown in Figure A - 13.

To collect and store ship operation data, a custom program was developed (by Michael Grant). The program was designed to acquit data at a frequency of 2 Hz, the data is stored in an excel file. The program runs on a Windows-based laptop. The user interface (UI) of the program is shown in Figure A - 14.

The Tachek's hybrid control system developer, TECHSOL, built the ESS system using Super B's 2V160E lithium-ion phosphate (LiFePO4) batteries. CANopen is used to communicate between the battery pack and BMS. By installing a CANlogger, as shown in Figure A - 15, we have recorded the communication data between the batteries and its BMS to the .eds files. These data contain cell temperature, cycle count, current and voltage, and SOC. The data recording was done in the engine room as shown in Figure A - 16. The orange wire in Figure A - 17 is the CAN bus cable, and the white box with LEDs on is the gateways of the isolator.

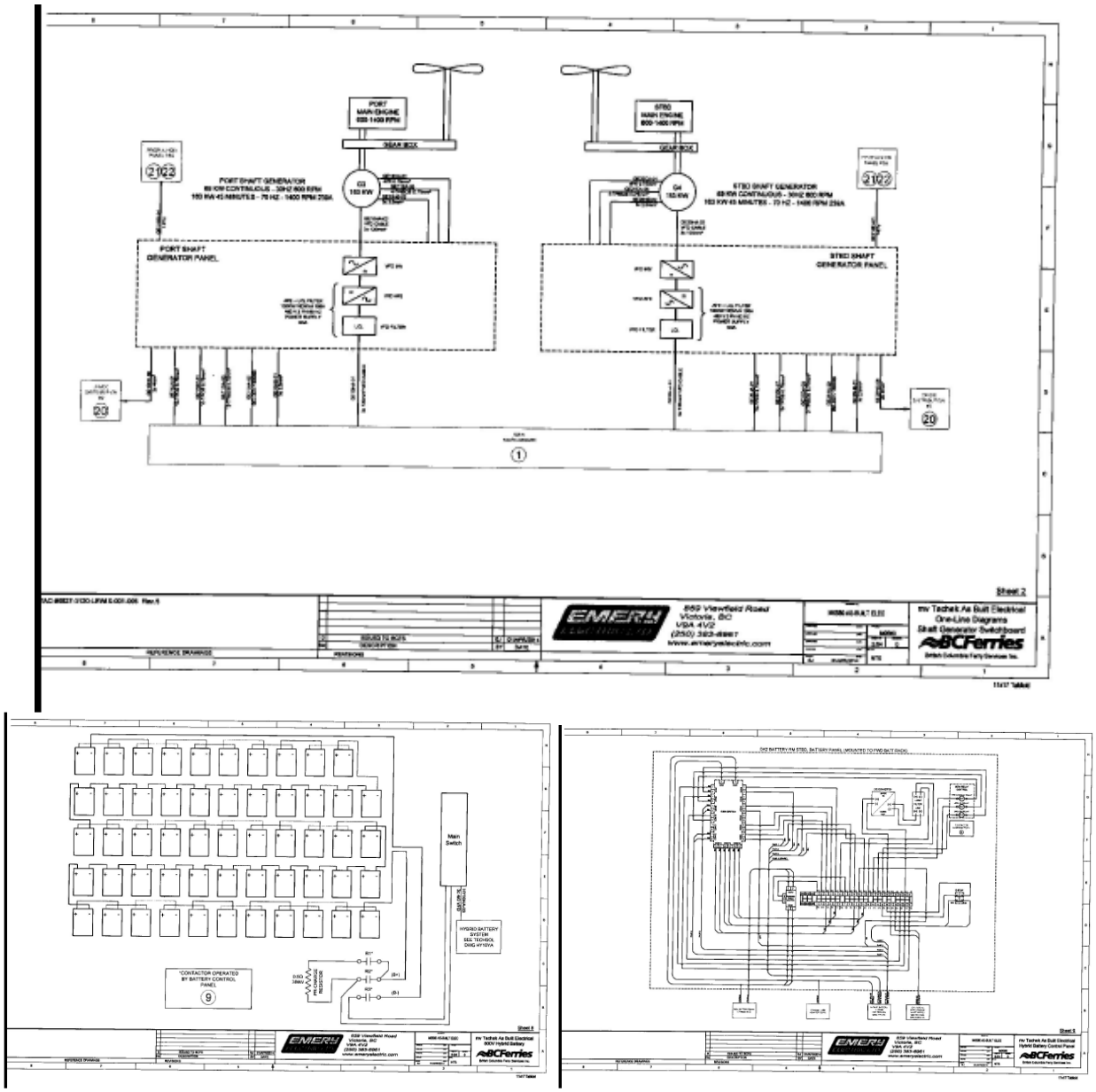

Figure A - 12 Battery and Electric Propulsion System

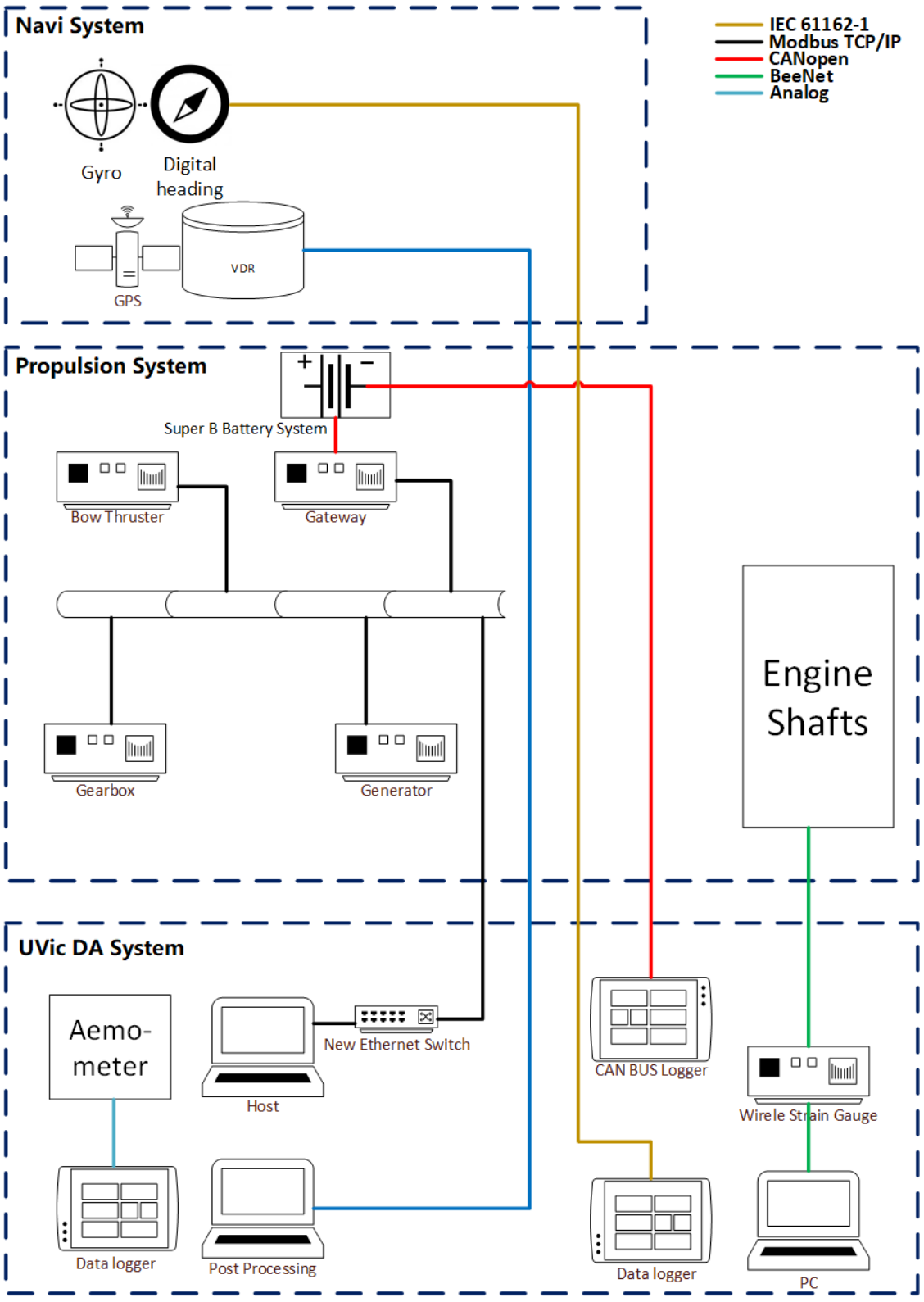

Figure A - 13 Data Acquisition System Architecture

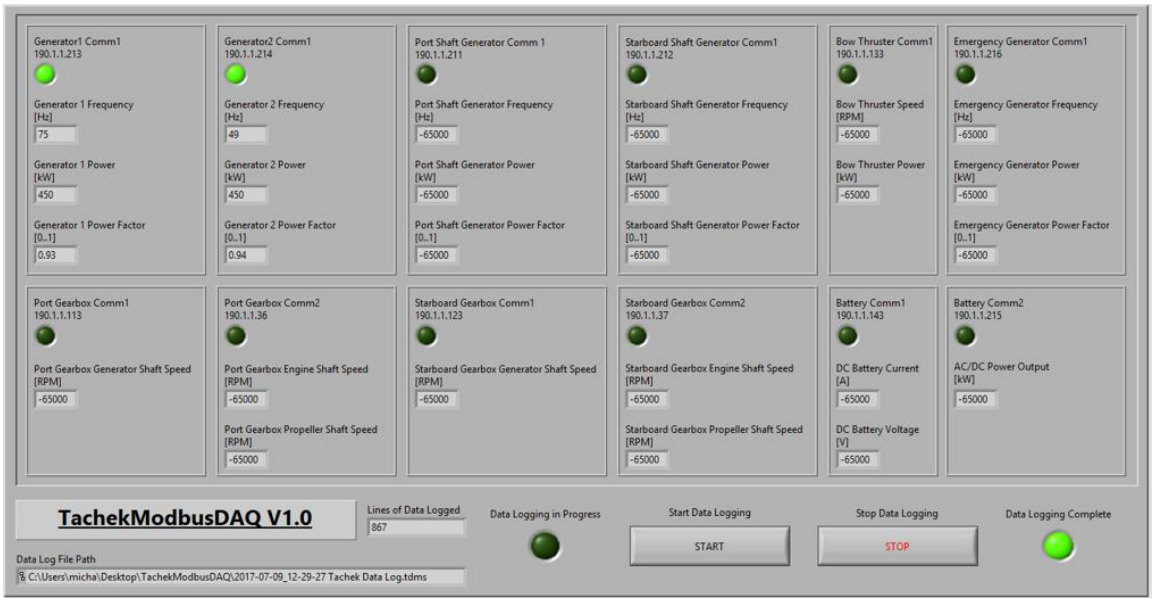

Figure A - 14 Modbus TCP/IP logger Modbus TCP/IP logger

Figure A - 15 CrossChasm C5

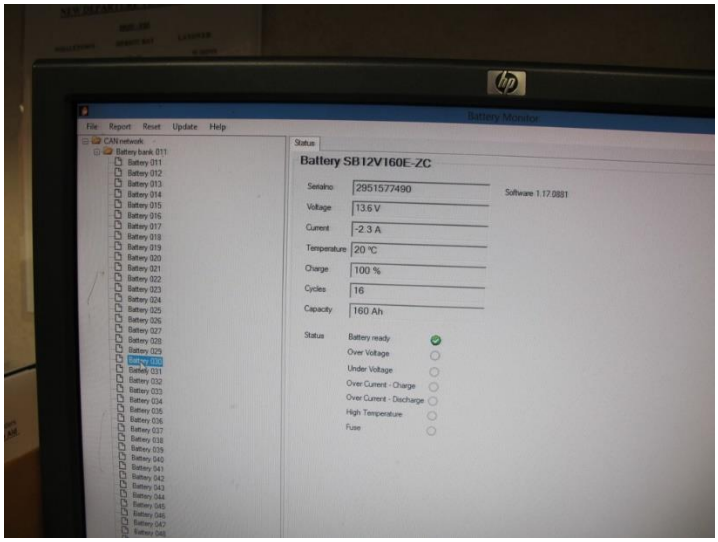

Figure A - 16 Battery Status Information in the Engines' Room

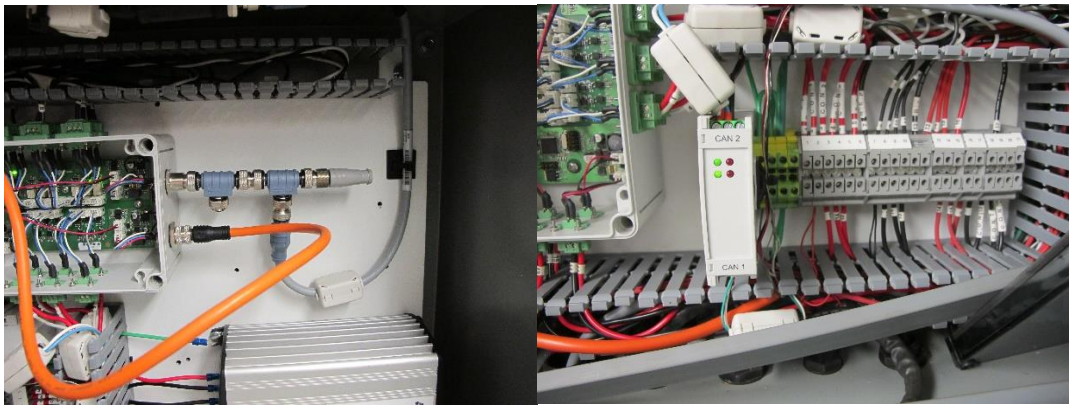

Figure A - 17 CAN Bus Network Junction Box

As for the engine power, we will continue using the wireless strain gauge that we used on the Skeena Queen. We will also develop a rapid battery replacement device for Tachek as this could save lots of time to replace a new battery. The engine fuel-power curve is available now.

The onboard VDR records the GPS information such as UTC time, ship speed, GPS coordinate and some of the ship operation information such as the propeller speed (we also collect this using BeeTech's wireless strain gauge) and rudder angle. VDR will store the data for quite a long period (On SKQ, 30 days), and we are able to copy them using a portable drive afterwards.

All the subsystem will collect data automatically.

A2.5. Tachek Hull and Propeller Models

The detailed CAD models of Tachek's ship hull and propeller have been regenerated using acquired rough design data. The models were used to create the smooth surface files (.SL) for the detailed CFD modelling and hydrodynamics (Soft Towing Tank) Flow Simulation.

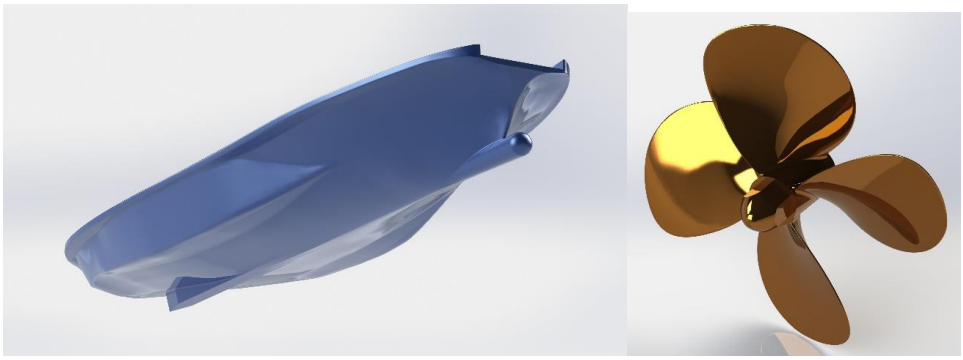

Figure A - 18 Hull and Propeller Models

A3. M.V. KLITSA

Klitsa sails between Brentwood Bay and Mill Bay close to Victoria, BC. We have studied this smaller BCFS passenger and vehicle ferry ship previously at the early stage of the integrated hybrid electric marine system modelling tool development. Kevin Andersen has done the pioneer work around this ferry on ship operation data acquisition, operation pattern modelling, reduced-order hull and propeller hydrodynamic modelling, and feasibility study on pure electric ship propulsion

system design using DC powertrain components. Details are documented in his MASc thesis from the University of Victoria - Development of a Time-Domain Modelling Platform for Hybrid Marine Propulsion Systems, 2016.

During this project, further studies have been carried out using the acquired ship operation data, including:

- Model developments and case studies of hybrid electric and pure ship propulsion system with commonly used AC power bus (Appendix O);
- Model developments and case studies of hybrid electric and pure ship propulsion system with AC powertrain components and advanced DC power bus, considering GHG emission reduction and life-cycle cost saving (Appendix O and Appendix P)

These extensions provide comparable results with ship propulsion and power system models and designs, closer to present marine operations.

Figure A - 19 M.V. Klitsa and Its Sailing Route

Built	1972, Vancouver
Overall Length	47.55 metres (156')
Beam, Moulded	12.04 (metres)
Depth (to Baseline)	2.97 (metres)
Maximum Displacement	450 tonnes
Car Capacity	23 (2m x 8 m)
Passenger & Crew Capacity	196
Maximum Speed	10.0 knots
Power	525 kW (700 hp)
Amenities	Accessible car deck lounge
Route	Brentwood Bay-Mill Bay
Engine (x2)	Detroit Diesel Series 60, 260kW @ 1800 rpm
Marine Genset (x2)	Deutz 912 Marine Diesel Generator, 50 kW

A3.1. Other Operation Information

Table A - 5 Main Engine Characteristics

MAIN ENGINE CHARACTERISTICS, **Speed vs RPM** - Trial Conditions	
Engine RPM (both)	Speed (*kt*)
Idle (650)	3.8
1200	7.2
1400	8.3
1600	9.6
1800 (WOT)	10.0

Table A - 6 Manoeuvring Characteristics

Turning Circles - 35 degree helm - P&S. Bow #1 End		
	Port Turn	Starboard Turn
Drive Angle (deg.)	35	35
Time 0 to 35 deg. (sec)	3	3
Initial Speed (knots)	10.2	9.5
Tactical Diameter (nmi)	0.022	0.031
Rate of Turn (Deg./sec)	230	186

Accelerating Turn – Helm Hard Over (deep water) – P&S	
- In hard over (90 deg.) turns, vessel spins on own axis.	
Time to 90 deg. (sec)	12s
Time to rotate 360 deg. (sec). [P/S]	98 P
	67 S

Table A - 7 Lateral Thruster Capabilities

Lateral Thruster Capabilities - P&S, Bow 1 – RADs @ 90 deg.		
Engine RPM (both)	Speed to Port (kt)	To Starboard (kt)
1200	3.2	2.7
1400	3.6	3.4
1800 (WOT)	4.3	3.3

Table A - 8 Stopping And Speed Control Test Result

STOPPING AND SPEED CONTROL CHARACTERISTICS (DEEP WATER)					
Stopping Ability - Crash Stop					
Both RADs rotated opposite directions (Trial Condition)					
Bow/Rotation	Initial Speed (kts)	Initial RPM	Rotation Time (s)	Time to Stop (s)	Distance to Stop (m)
#1 End/Inward	10.1	1800	12	37	69.2
#2 End/Outward	10.2	1800	19	37	59.8

Bow/Rotation	Initial Speed (kts)	Initial RPM	Idle RPM	Rotation Time (s)
#1 End/Inward	10.1	1800	650	25
#2 End/Outward	10.2	1800	650	25
Bow/Rotation	Initial Speed (kts)	Initial RPM	Rotation Time (s)	
#2 End/Inward	9.5	1800	10	
#1 End/Outward	10.1	1800	13	

A3.2. KLITSA Propulsion System and Cad Modelling

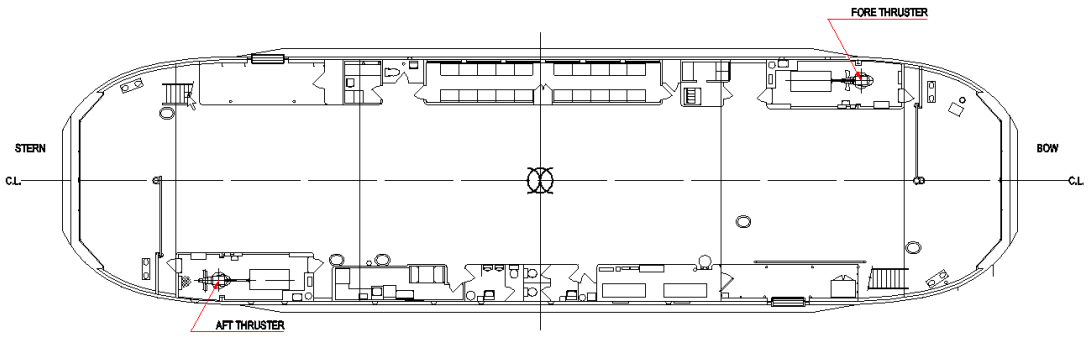

Figure A - 20 Thruster Configuration on the M.V. Klitsa

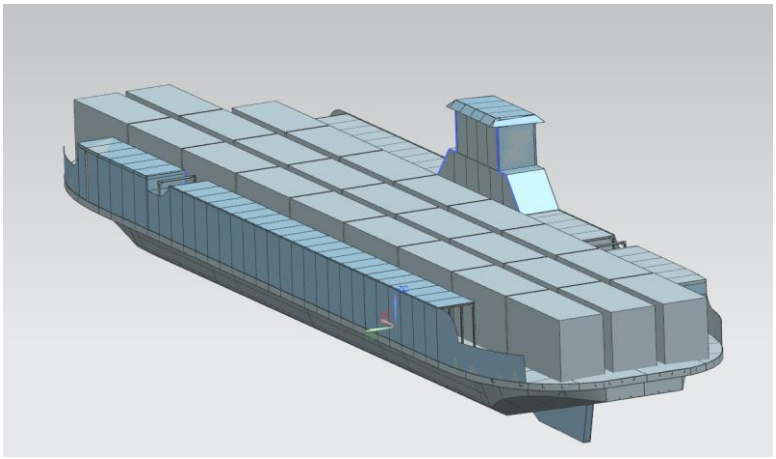

Figure A - 21 3D CAD Image of the Klitsa Used to Determine Inertial Properties1

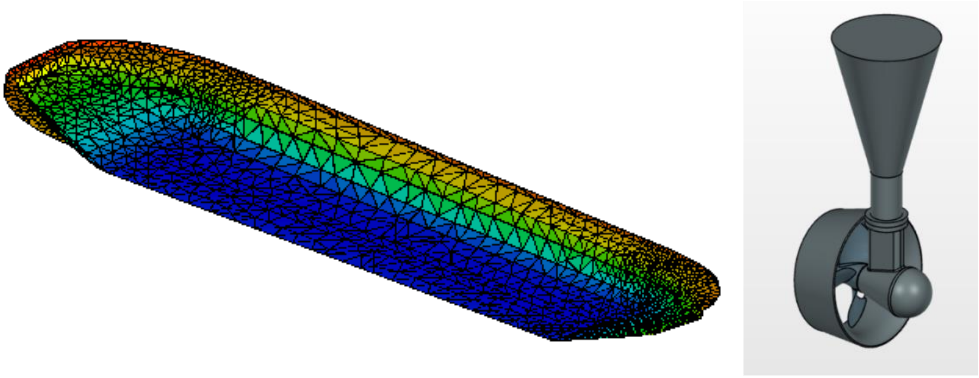

Figure A - 22 Panelled Hull in ShipMo3D and Propeller Model

A3.3. KLITSA Operation Data Acquisition Study

The data acquisition system made use of the onboard J1587/J1708 serial communication bus for the engines, and the NMEA183 serial bus from the azimuth angle thruster systems. Custom serial converters were developed to read from the onboard serial buses to broadcast the data over the CAN network. CAN traffic was logged using the Cross-Chasm data logger, which also contains an integrated GPS system that was used for tracking vessel position and speed. The system was designed to operate autonomously using an enable message to trigger all nodes to begin broadcasting. The enable was triggered by sensing Engine 1's serial communication bus activity. A schematic of the instrumentation and communication network layout is provided in Figure A - 23 and data acquired are listed in Table A - 9.

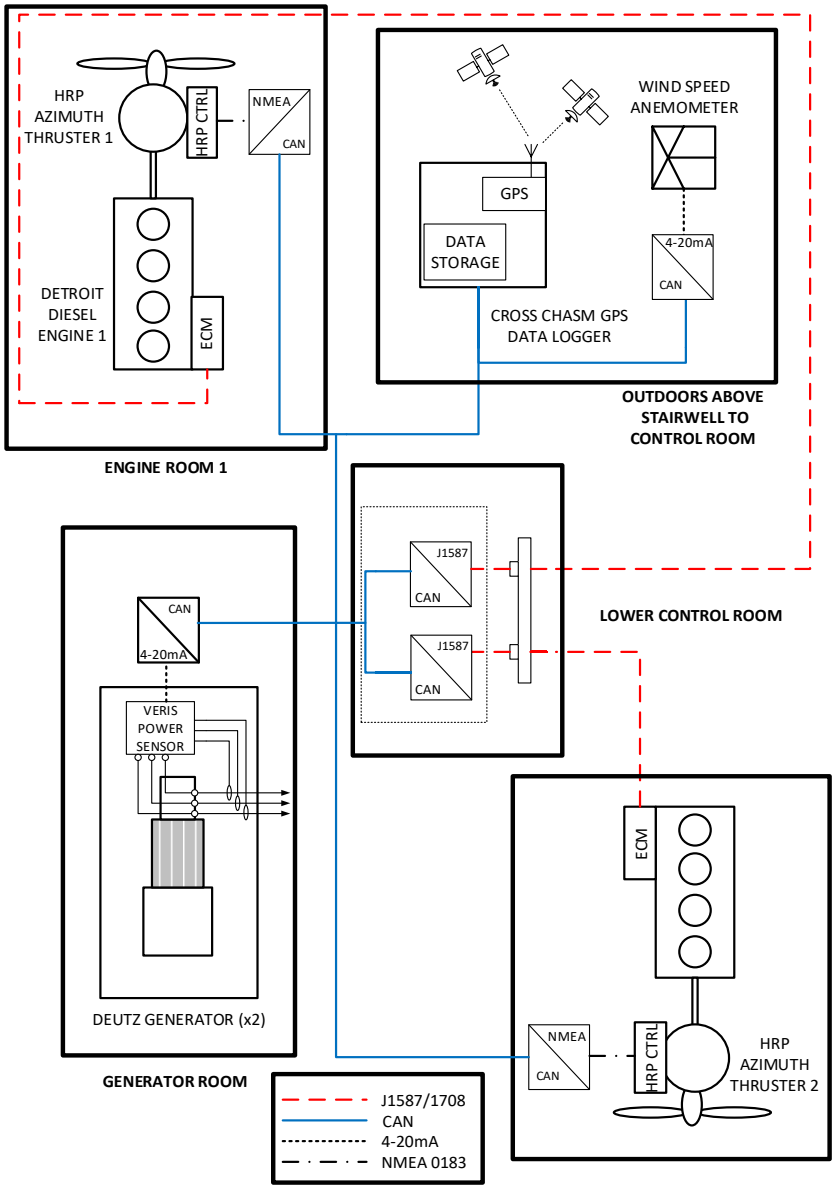

Figure A - 23 CAN Network Schematic and General Arrangement for DAQ Study

A3.4. Development of Load Profiles from Operational Data

Extracted and developed into a set of representative load profiles of differing power outputs. The primary parameters required for validation of the model are as follows:

- Propulsion System Load: Torque/Speed vs. Time
- Hotel Loads: Electrical Power vs. Time
- Propeller Position: Azimuth Angle vs. Time
- Vessel Speed vs. Time

Table A - 9 Summary of Acquired Parameters in Data Acquisition Study

Description	Physical Parameter	Transducer Signal Source
GPS Data	Position (NED)	Cross Chasm GPS Logger
	Vessel Speed	Cross Chasm GPS Logger
Engine 1 Data	Engine Load	J1587/J1708 Serial Bus
	Engine Speed	J1587/J1708 Serial Bus
	Engine Torque	J1587/J1708 Serial Bus
	Throttle Demand	J1587/J1708 Serial Bus
Engine 2 Data	Engine Load	J1587/J1708 Serial Bus
	Engine Speed	J1587/J1708 Serial Bus
	Engine Torque	J1587/J1708 Serial Bus
	Throttle Demand	J1587/J1708 Serial Bus
Azimuth Propeller 1	Azimuth Angle Position	HRP NMEA0183 Serial Bus
	Thruster Position Reference	HRP NMEA0183 Serial Bus
Azimuth Propeller 2	Azimuth Angle Position	HRP NMEA0183 Serial Bus
	Thruster Position Reference	HRP NMEA0183 Serial Bus
Generator Output	3-Phase Power	Veris H8043-0300-2 Power Sensor
Wind Data	Wind Speed	Campbell Scientific 05103LK Wind Monitor
	Direction	Campbell Scientific 05103LK Wind Monitor
Heading/Attitude	Heading Direction	Maretron SSC200 Fluxgate Gyrocompass
	Pitch Angle	Maretron SSC200 Fluxgate Gyrocompass
	Roll Angle	Maretron SSC200 Fluxgate Gyrocompass
	Turn Rate	Maretron SSC200 Fluxgate Gyrocompass

The two main diesel engines and the auxiliary generator supply all of the energy required for the ship, and are thus the most important for computing energy demands for the BEIPS. The load

information from the engines was captured from the ECM units, which are not known to have very high precision. The measured engine load can be compared against the published propeller data in the first quadrant as a sanity check. The azimuth angle time-series position data will serve as a model input to simulate the actions of the operator in the system-level simulation.

The present objective is to develop a set of standard driving cycles that represent the variability of the ship's operation described by low, medium, and high output conditions. The data were surveyed to assess the variability in the load profiles observed over the two months of data collected. A maximum operational speed of just over 9 knots was observed in some instances, but normal operating speed typically hovered around 7.5 knots when the ship was on schedule. Based on these observations, three representative mission profiles were identified as being good representations for use as standardized cases. The acquired time series data are presented in Figure A - 24, Figure A - 25 and Figure A - 26.

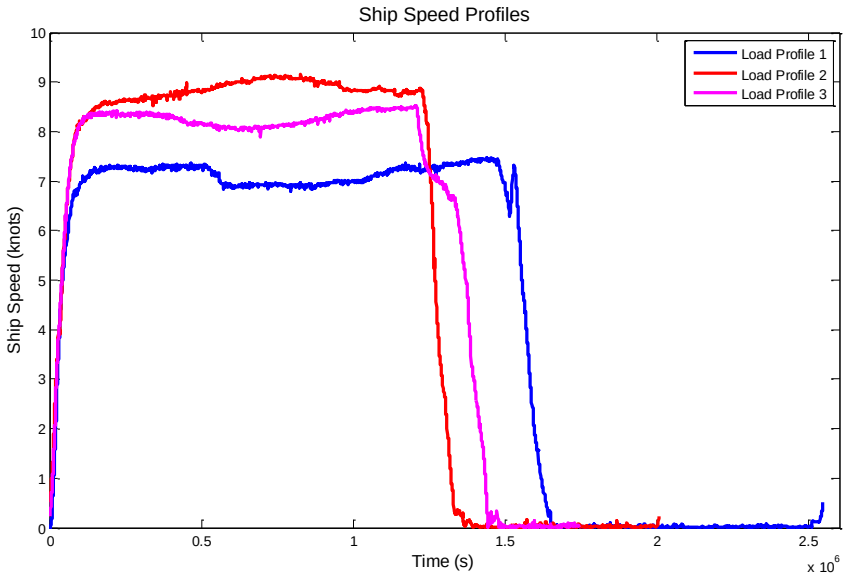

Figure A - 24 Plot of Ship Speed vs. Time for 3 Load Profiles

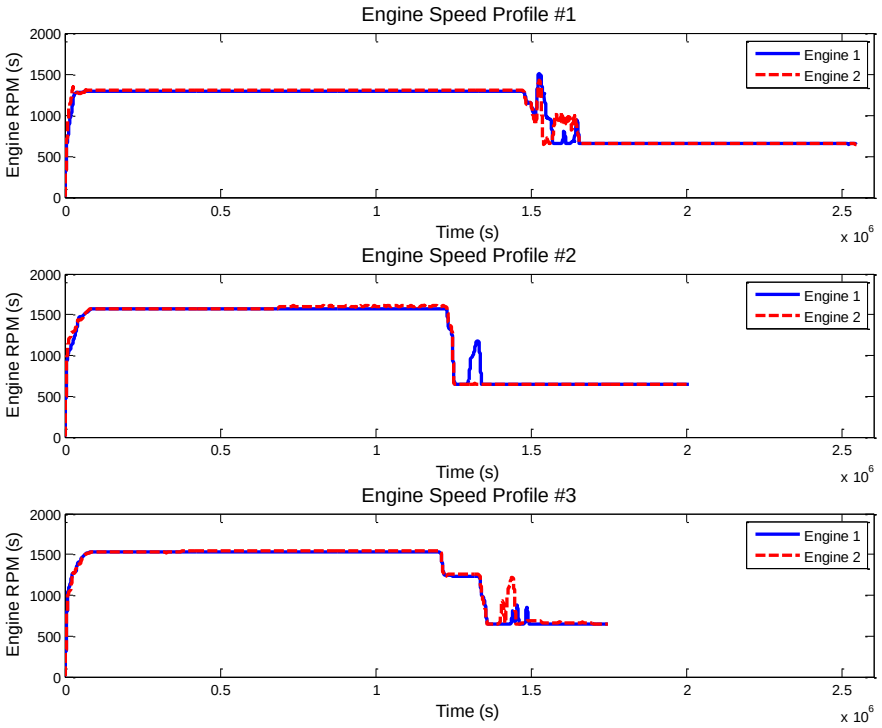

Figure A - 25 Engine Speed Profiles

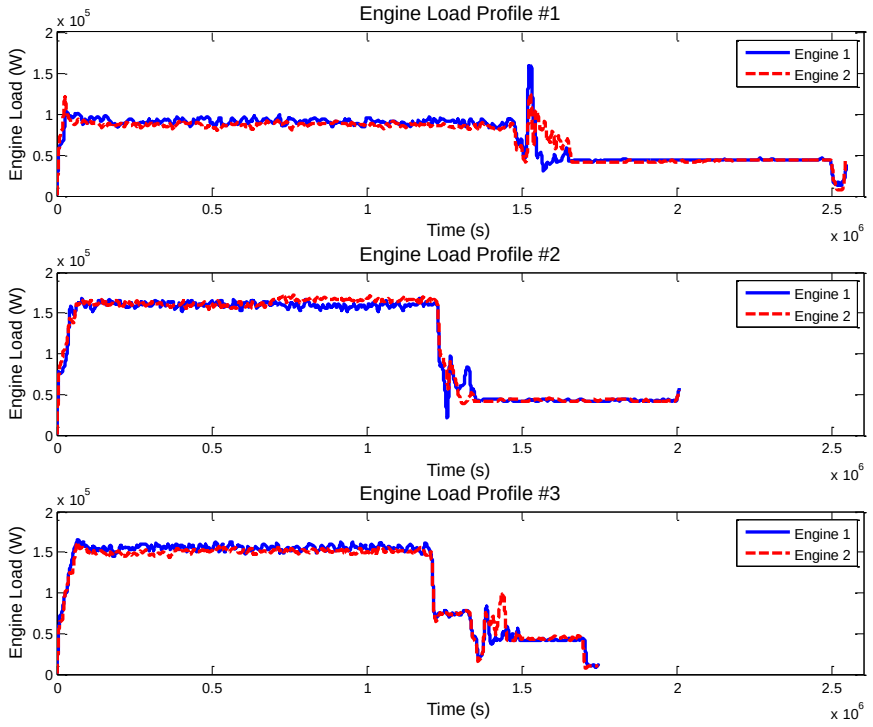

Figure A - 26 Engine Load Profiles

A4. PORT TUGBOATS

A4.1. Tug Category

Tugs are important tools in harbours to assist large ships to and from their berths. Today multi-purpose tugs are designed to perform various jobs such as offshore support, salvage, icebreaking, etc.

Some key parameters that defining the performance of a tugboat including: the bollard pull capacity, maximum free running speed, time taken to achieve maximum free running speed from rest, distance covered to crash stop, time taken to complete a 360 turn in its own axis, sound proofing of machinery spaces, etc. [2]. According to the type of work they perform, tugs can be categorized as below.

a) Harbour tugs

Harbour tugs are required to assist large ships onto and off a berth by pushing and pulling. Since the navigation of a large ship is confined in restricted water, tugs are necessary tools in harbour to safely handle the ships while entering or leaving a port. Some special application of harbour tugs with more rigid construction of hull and fender are for inland sea transportation and coastal shipping.

b) Escort tugs

Escort towing tugs are designed to provide emergency steering and braking functions to tankers in critical or confined coastal areas. Due to the oil leakage accidents happened in the past, tankers within specific waters are required be escorted by tugboat.

Escorting is more challenging than regular ship-handling because it takes place at higher speed [3]. A towrope will be connected to the vessel being assisted from the towing winch of the tug. Tugs need to generate the required ship control forces for steering and braking by carefully balancing all forces from their propulsion drive units and ship hull hydrodynamic forces.

c) Seagoing tugs

Seagoing tugs are generally larger and capable of performing good sea keeping characteristics to ensure that vessels can provide required power in any rough sea weather conditions. They can perform a variety of operations, including assisting ships in ports as well as at sea.

- Terminal support tug: terminal support tugs are typically larger and more sea-capable to work at large oil or gas terminals. They frequently include capacity for fire-fighting and spill response. These tugs are normally equipped with dynamic positioning system to prevent drift off position to waves, wind and currents.
- Offshore support tug: It is typically larger and more powerful to perform anchor-handling, cargo transfer, tail-back duties etc.
- Offshore rescue / Salvage: These tugs are designed for fast response speed, long-distance towing capability and the best possible seakeeping for crew safety in rough sea conditions.
- Coastal towage tug: Coastal towing tugs are used to provide sustainable pulling power to barges between coastal ports. It is specially designed to handle more severe ocean weather.
- Deep-sea towage: help tow ships in any sea area and any period of the year without restrictions.

A4.2. Representative Tug Boats from Robert Allan Ltd

One of the world-leading Canadian tugboat designers is Robert Allan Ltd (RAL). The company is an independent, privately-owned firm of Consulting Naval Architects and Marine Engineers, established since 1930 in Vancouver, Canada. Over the past many years, the company has designed and developed many tugboats of different types for a variety of tasks in the categories listed below. However, the most common and representative tugboats are the Escort, Ship-Handling and Terminal Support tugs, such as the Vancouver Harbour Tugboats operated by Seaspan Marine. Robert Allan Ltd. has designed the world's first hybrid-powered tug, the RApport-2400-Carolyn-Dorothy-1440x960, and many tugs with LNG or diesel-LNG dual-fuel systems, such as the ART-80-32-RT-Evolution-1440x960. The company has also developed a powerful analytical tool, the ***RAptures program*** to enable a thorough analysis of the relative merits and efficiency of a variety of hybrid or conventional powering options, whether diesel-mechanical, diesel-electric or any combination thereof.

Figure A - 27 RApport 2400 Mk II (Courtesy of RAL)

Figure A - 28 RT Evolution – Advanced Rotor tug (Courtesy of RAL)

The RANGLer series of LNG (or dual fuel) powered escort and ship-handling tugs take maximum advantage of the space available for LNG systems and look at tug design configurations with fresh eyes.

A4.2.1. Bollard Pull Tugs (65 Tonne)

The Bollard Pull Tugs is a 65 tonne boat with 4320 operating hours per year. It has about 4175 kW nominal system rated power. Other specification of the tug includes those listed in Table A - 10.

Table A - 10 Tug Specifications

Power Demand				
Z-Drive Power Demand (Pz) [kW]	Hotel Electric Power Demand [kW]	Deck Mach. Electric Power Demand [kW]	Total Power [kW]	% of Installed Power
0	60	0	60	1
74	60	0	209	5
144	60	0	347	8
339	60	0	739	18
1012	60	0	2083	50
175	60	20	430	10
690	60	40	1481	35
1271	60	60	2663	64
1960	60	80	4060	97

Operation Patterns (% of Time)		
	Harbour	Ship Assist
Idle	35%	10%
6.6 kts transit	25%	20%
8 kts transit	0%	0%
10 kts transit	10%	0%
12.5 kts transit	0%	50%
20% Bollard	15%	10%
50% Bollard	8%	5%
75% Bollard	5%	3%
100% Bollard	2%	2%
Total	100%	100%

A4.2.2. RANGLer - LNG powered escort and ship-handling tugs[4]

The *RANGLer* series of LNG (or dual fuel) powered escort and ship-handling tugs (introduced in 2014) were conceived to take maximum advantage of the very limited space available for LNG

fuelled systems in tugs. The unique RANGLer design places the gas tank forward and oriented vertically for maximum advantage as shown below.

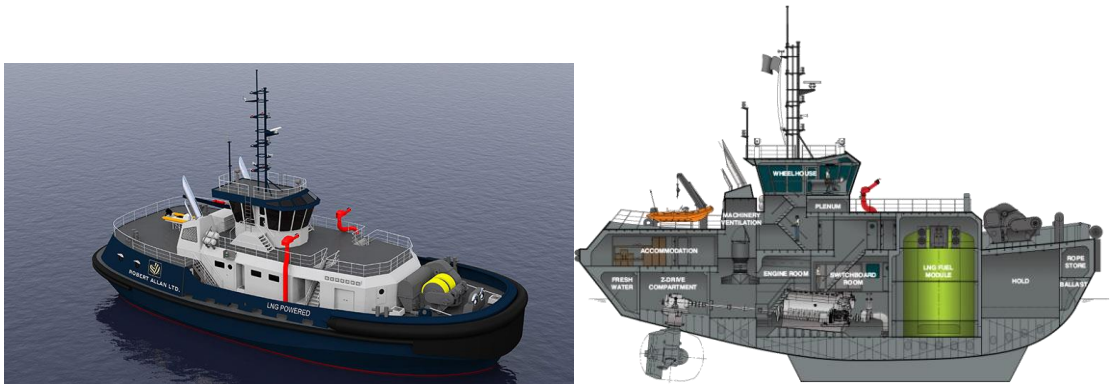

Figure A - 29 RANGLer 3D Model and Concept

Working closely with both Bureau Veritas (BV) and the American Bureau of Shipping (ABS) on the LNG safety aspects of the design, Robert Allan Ltd has announced that the RANGLer 3600 Class concept has received Approval in Principle from both classification societies for either single gas fuel or dual-fuel engines. The particulars of this new LNG tug design are as following in Table A - 11.

Table A - 11 LNG Tug Boat Profile

Length, Overall	36.5 m
Beam, Moulded	15.4 m
Depth, Least Moulded	7.1 m
Draft, Navigational	5.8 m (above bottom of drives)
Installed Power	2 x 2430 kW
Complement	up to 10 crew
LNG Capacity	80 m^3 (gross)
Vessel Speed, ahead	14 knots, approx.
Bollard Pull, ahead	80 tonnes, approx.

A4.3. Review of Alternative Propulsion for Tugboat

Today, tugs are most powered by diesel main engines coupled to propellers, azimuthing propulsors (Z-drives), or Voith Schneider Propellers (VSP drives)[5]. Electric power for hotel and auxiliary requirements is typically supplied by one or more small generator sets. The heavy fuel cost and greenhouse gas (GHG) emissions from tugs have laid great stress on operators. Tugboat operators are looking for ways to make their vessels more efficient and clean to the environment. However, the direct connection between engine and propulsor is hard for emission control. Alternative propulsion configurations have gained more interest recently for their potential in fuel-saving and emission-reducing.

The world's first hybrid harbour tug, the Carolyn Dorothy, was built by Foss Maritime Company and started to operate in 2009 to reduce emissions and fuel consumption. Moreover, a sister tug, the Campbell Foss, was joined the operation in 2012 by converting a conventionally powered tug to a hybrid at the Foss shipyard in Rainier. Foss hybrid tugboat used a combination of smaller main diesel engines and larger diesel-generator sets (as compared to a conventional Dolphin tug), main shaft-driven motor/generators, batteries and state-of-the-art power conversion and control technology [6]. The boat can operate in direct-diesel, diesel-electric, and electric configurations. The benefits of this hybrid tugboat including emissions reduction (about 73% for particulate matter, 51% for nitrogen oxides and 27% for fuel related pollutants such as sulfur oxide and carbon emissions); fuel consumption reducing by 20-30%; reducing main engine maintenance costs by about 50% through decreased operating hours; reducing noise pollution by using batteries and generators; improving safety by effectively removing any chance of power loss with multiple system redundancies[6].

Inspired by Foss hybrid tug, Europe's first hybrid ship handling tug E-KOTUG was converted from traditional tug named RT Adrian and entered into service in 2012 by KOTUG fleet in Rotterdam, Netherlands[7]. It was retrofitted with a 78kWh lithium polymer battery pack to provide pure electric drive at low speed. The main engines only start when demands are made for high bollard pull situations. It showed a 50% reduction in harmful emissions of CO2, NOx, and PM2.5.

The world's first hybrid offshore platform supporting vessel, Viking Princess, was designed by Finland's Company - Wärtsilä. It also is the world's first hybrid ship with a dynamic positioning system. This vessel has completed sea trials and handed over to customer Ediesvik Offshore in Norway in October 2017. The vessel was originally built in 2003 with four LNG engine generator sets as the world's first offshore supply vessel powered by LNG fuel. Now, by replacing one LNG gen-set with a 533 kWh Li-ion based energy storage system (ESS) provided by Corvus Energy, it can reduce fuel consumption by up to 30% in various operations. CO2 emissions can also be reduced.

Robert Allan Ltd. has developed a design tool named Raptures (Robert Allan Ltd: Powering Tugs for Real Energy Savings) to analyze a wide range of hybrid or conventional powering options for typical harbour tug propulsion systems, including diesel-mechanical, diesel-electric or any combinations [5]. With inputs of basic tug power and an operating profile, the fuel consumption, emissions and installed costs can be calculated. Cost comparisons included equipment capital costs, fuel operation cost and equipment maintenance cost. A net present cost method was used for a 20 years evaluation. Four powering configurations: diesel-mechanical, series diesel-mechanical/electrical, diesel electric-running standby, diesel electric-cold standby, were compared based on the tugboat Ramparts 2800 designed by Robert Allan Ltd for both harbour and ship assist duties. The design with a series diesel-mechanical/electrical configuration showed lower fuel consumption, emissions and cost.

Researchers at Nanyang Technological University published several papers for a new design of electric tugboat[8]–[10]. In [8] and [9], the author presented optimal power management to split the power supply from engines and batteries in response to the load demand, while minimizing the engine fuel consumption and maintaining the battery life. The cost function includes power load demand tracking engine fuel consumption and change of battery SOC. A load prediction method was introduced to anticipate the load demand based on a typical tugboat operation profile provided by ABB Singapore. In [10] equivalent consumption minimization strategy (ECMS) control method

was adopted in a hybrid all-electric tugboat for power management, and showed 17.6% of fuel saving compared to the use of conventional rule-based control strategies.

MacPherson and Boyd [11] presented an optimal design approach for a tugboat through computational analysis of alternative propulsions. Instead of using traditional single design measure, such as bollard pull or cruising speed, this paper optimizes the propulsion system components by using the all-inclusive duty cycle profiles of multi-role service (as a harbour tug and in long haul ocean barge towing). Variables include main engines and gearboxes (gear reduction ratio), propellers (type, blade count, and blade area ratio), and speed (mode operational speed). The cost function is to minimize propulsion fuel consumption over a typical transit voyage or operational duration. Key performance indicators (KPI) were used for qualitative comparisons of different design options. Three different consumption index forms were used in the analyses: fuel, energy and power. By replacing the original open propeller with high-efficiency ducted propeller and increasing the gear reduction ratio, the tugboat can gain 29% overall fuel reduction in harbour duty profile and 19% in ocean towing duty profile.

Researchers at the Marine Science and Technology of Tokyo University have published several papers on fuel consumption reduction for a tugboat, using a new hybrid propulsion system without a large battery ESS. A new hybrid propulsion system with the additions of two motor generators (M/G) and three electric power converter (EPC) to the conventional two main diesel engine propulsion system has been introduced [12]. A DC bus was built with one EPC connected to auxiliary diesel generator and two EPCs connected to M/G with main engines respectively. A changeover gear is installed to one of the main engine to adjust load torque so that the main engine can mechanically drive and electrically drive. The fuel consumption of the tug was calculated by considering the overall efficiency with all apparatus in different energy flow paths. The new hybrid system used 20% less fuel than the conventional powertrain when tugboat was in waiting and out of service modes. However, the fuel consumption was higher for the hybrid electric system when demanded power was high in the service mode, due to system efficiency loss.

Different control strategies for energy management of the hybrid tugboat when it is not in service have been compared, and a number of efficiency data sets of powertrain components have been used for evaluating these control strategies [13]. Three control patterns were evaluated in terms of controllability, redundancy and efficiency, although the threshold to shift between EPA1 and EPA3 was arbitrarily chosen. The more efficient control strategy is obtained only considering the no service state; it is not necessarily optimal for the entire tugboat operation.

Völker [14] presented hybrid propulsion designs for two cases: a harbour tugboat and a motor ferry. For harbour tugs, a DC-bus with two main engine-generators and a large battery pack was designed to support two thrusters.

Lindstad and Sandaas [15] provided hybrid propulsion design for offshore support vessels with 10,000 kW installed engine power, and compared emissions with traditional 4 diesel generator sets propulsion. Two battery packages of 500 kWh with a total 1000 kWh was chosen to sufficiently power the vessel at full installed engine power for 5 mins and 20 mins at calm water. Three alternative fossil fuels were used: marine diesel oil (MDO) with a sulfur content up to 0.5%, marine gas oil (MGO) with a sulfur content up to 0.1% and LNG in dual-fuel engines with high-pressure and low-pressure systems. Region-specific global warming potentials (GWPs) was used to evaluate each emission species with time length of 20 and 100 years. The global warming impact (GWI) has been developed for each of the options for non-Arctic (average for four regions: East

Asia, Europe and North Africa, North America, and South Asia), and Arctic (in the Barents Sea) operations, respectively. The hybrid systems reduces CO_2 emissions by 5%. When all emissions are counted and represented as CO_2 equivalents (CO_{2e}), the hybrid system reduces CO_{2e} by 10-25% for operations in non-Arctic regions and 25-40% in Arctic regions with GWI 20 years. Different fuels present different environment impacts at different regions. In non-Arctic region, MDO used in the hybrid option gives the lowest climate impact, while in Arctic region, LNG hybrid option gives 25-60% less emissions comparing to others.

In conclusion, the main methods that can be adopted to improve tugboat fuel economy and reduce emission include using LNG dual-fuel engines, using large battery package for peak power shaving, and using hybrid electric propulsion system to achieve the optimal engine efficiency.

A4.4. General Tugboat Operation Data

Tugboat operation data collection is the first step for designing an alternate propulsion system. Seven different tugboat operation profile data sets have been obtained from literatures, and through collaboration with leading naval architect firm specializing on tugboat design.

The operation profile of a harbour tug is given below. The bollard pull harbour ship-handling tug is a 24 m long and 50 tonne. Total operating hours per year is about 2400 h. Main engines are 2x1500 *bkW*. Gensets are 2x99 *ekW*. Average electric load is about 60 *ekW*.

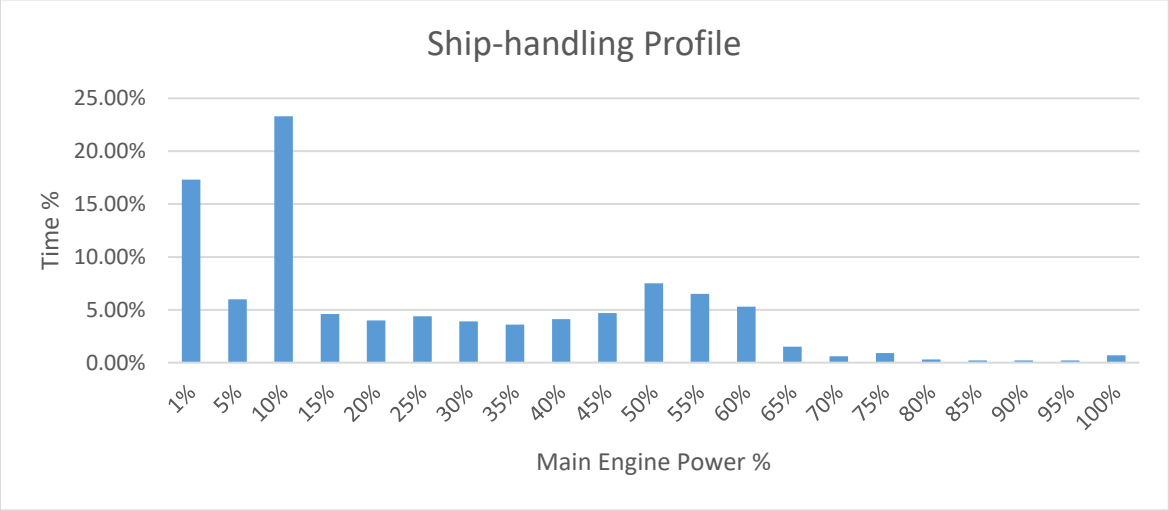

Figure A - 30: Ship-handing Profile

Below is another harbour tug profile with 24 m long, 75 tonne bollard pull. It represents a general idea of normal operation. Total operating hours per year is about 2500 h. Main engines are 2x2240 bkW. Gensets are 2x75 ekW.

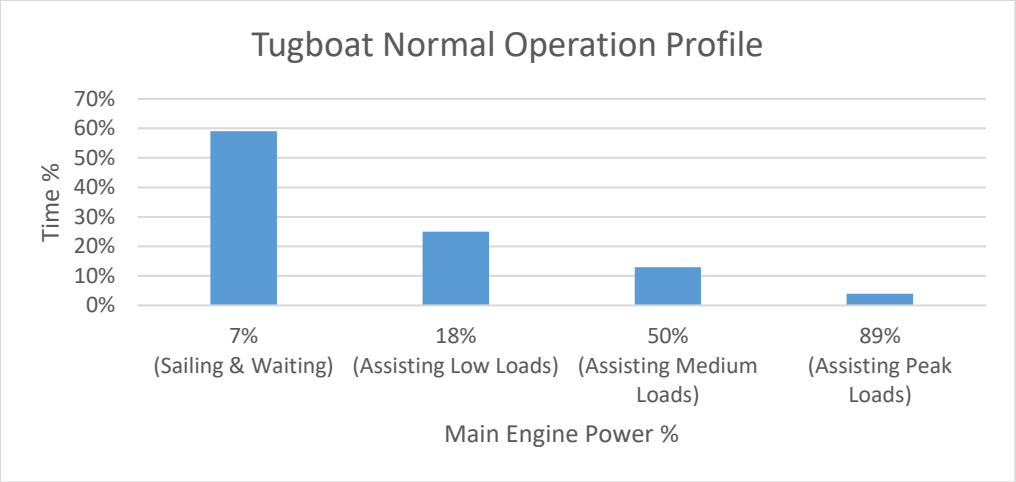

Figure A - 31: Tugboat Normal Operation Profile

Below is a harbour tug profile from a Canadian operator. The tug is 24 m long, 55 tonne bollard pull. Operating hours are 4500 h per year. Main engines are 2x1600 bkW, and gensets are 2x99 bkW.

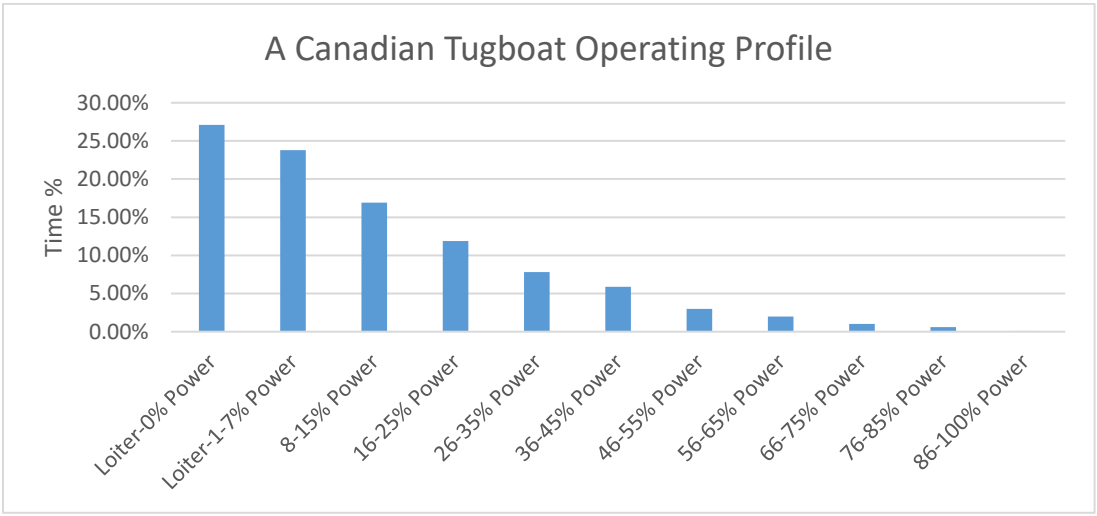

Figure A - 32 A Canadian Tugboat Operating Profile

Another 65-tonne bollard pull tug profile is showed below. It has 4300 h operating hours per year, 4175 nominal system rated power

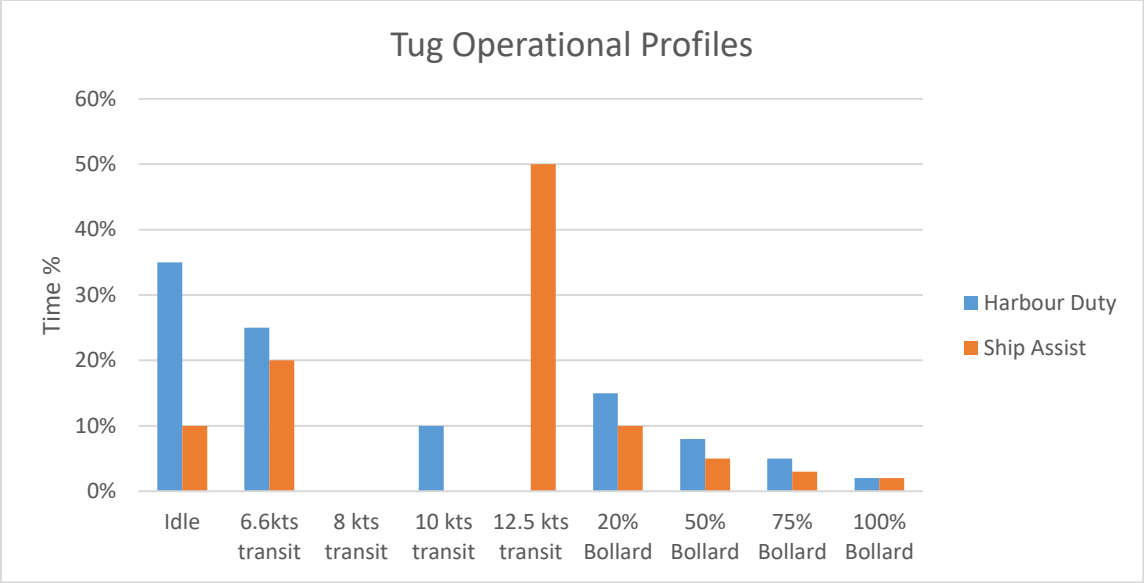

Figure A - 33 Tug Operational Profiles

Some general tugboat operation data can be obtained from published papers.

Nanyang Technological University in Singapore has presented a tugboat profile in [8], showed below.

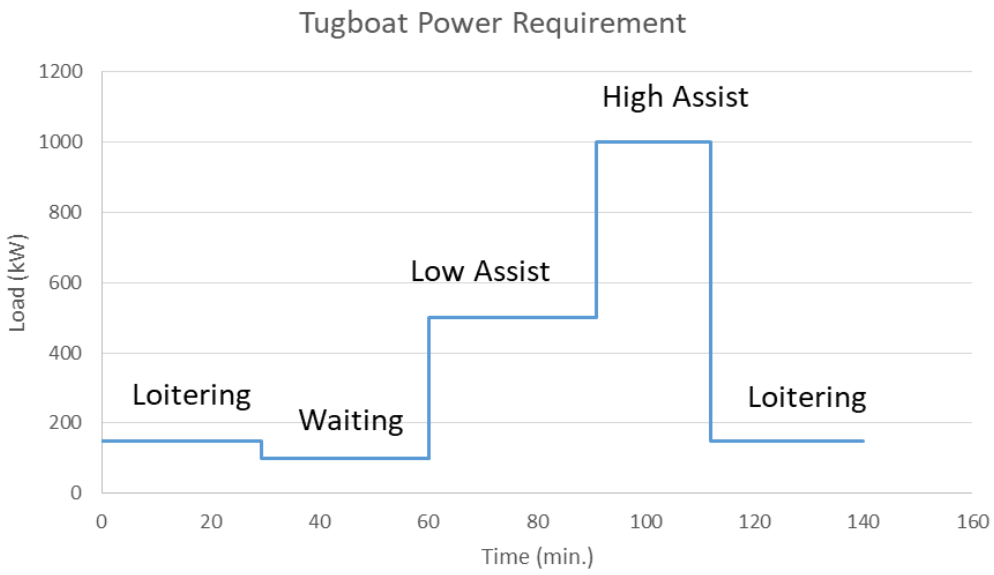

Figure A - 34 Tugboat Power Requirements

MacPherson and Boyd [11] showed two different tugboat operational profiles in their paper, as shown in Figure A – 35.

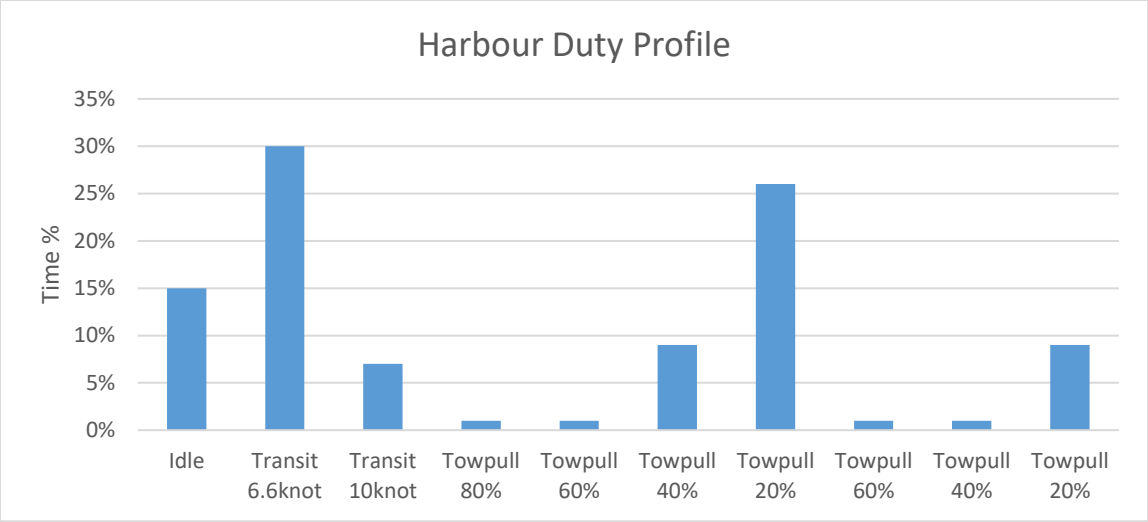

Figure A - 35 Harbour Duty Profile

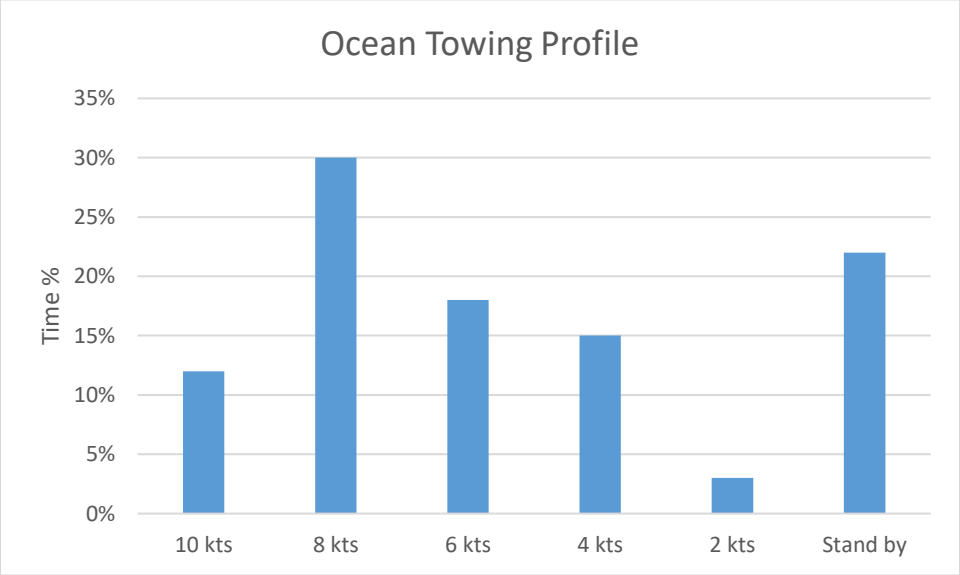

Figure A - 36 Ocean Towing Profile

A4.5. Future Research Plan

After a thorough study and comparison of the tugboat operating profile and generic duty cycle, our future work will be focused on the optimal design of hybrid electric propulsion systems according to the characteristics of each different operational duty cycle for tugboats.

A5. LOBSTER FISHING BOAT I

Table A - 12 Boat specifications of Lobster Fishing Boat I

	Boat #1
Boat Model	Cape Islander
Builder	Stanley Greenwood
Operation	Lobster
Length	12.2 m
Beam	5.18 m
Height	3.66 m
Displacement	15 Tonnes
Engine Make/Model	1986 Cummins Big Cam 4
Horsepower	400
Max Speed	14 kt
Cruise Speed	10 kt
Fuel Usage at Cruise	36 L/hr
Fuel Usage at Full Power	95 L/hr
Propeller	5 blade 30"x26"
Gear Reduction	2.1:1
Time at Dock/Day	18 hr
Time Spent at Sea / Day	6 hr
Cruise Time to Fishing zone	15 m
Distance to Fishing zone	2 NM
Cruise Time Back to Dock	10 m
Distance Back to Dock	1.5 NM
Typical Departure Time	5:00 AM
Batteries	5 x 8D
Gas / Oil powered Devices	Diesel stove
Electrically Powered Devices	Vacuum Cleaner, 4x plotters, Inverter, sounder, 2 VHF, 2 GPS, stereo, radar, lights, 3 bilge pumps
Hydraulically Powered Devices	power steering, 2x trap haulers

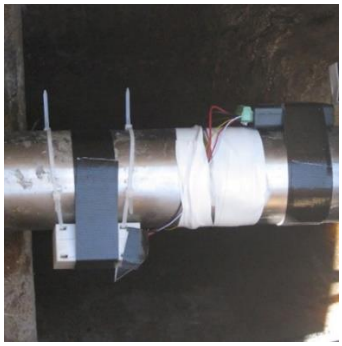

Figure A - 37 Strain Gauge Installation on Propeller Shaft

A5.1. Power Usage

Commercial lobster boats use mechanical, hydraulic, and electrical transmission from the main engine to power various appliances aboard the vessel. These typically include:

- propulsion
- trap-haulers (winches)
- power steering
- water pumps
- navigation electronics
- lights, and
- heaters

A5.2. Operation Routine

In general, the vessels follow a route from the dock to the most distant trap. This typically is 2-5nm depending on the placement of traps and takes about 15 minutes. Once at the fishing zone, the boat proceeds through the zone, stopping at each trap in the zone using low power. Then the deck crew winches the trap to the surface using the trap-hauler, empties its catch and returns the trap to the bottom. The captain then steams to the next trap and the process is repeated for all of the traps in their zone. In most cases, the trip ends at the trap nearest the dock.

Hauling, emptying and replacing all traps typically takes 6 hours including the time spent steaming from trap to trap. This distance also depends on the placement of traps, but typically takes about 15 minutes.

The captain docks at a loading and unloading zone to bring their catch ashore before returning the boat to its berth at the home wharf. Reverse power is used to stop and position the boat whenever docking.

A5.3. Collected Data

A torque sensor was used for the preliminary testing work and additional items that were required and supplied by Glas Ocean Engineering (GOE) are listed in Table 3. Torque and revolutions per minute (rpm) data were sampled at a 10 Hz frequency and files with 1 Hz extracted data.

Table A - 13 Materials Used in Testing

Item	Use
Strain gauge	Measure strain on prop shaft
BEETECH Torque sensor	Convert strain to torque and measure rpm
BEETECH Wireless ports	Communication between torque sensor and laptop
12V DC power supply	Power wireless port
Magnets	Activate rpm sensor in torque sensor
Communication cables	Attach wireless ports and laptop
9V battery leads	Power torque sensor
400 watt power inverter	powering laptop computer and wireless receiver for sensor data
25 watt Soldering iron	making repairs to electronic equipment when needed
3 oz rosin core solder	making repairs to electronic equipment when needed
20 g gorilla brand super glue	bonding a strain gauge to the propeller shaft of boats
32 GB SD card	taking and storing pictures of boats participating in the study

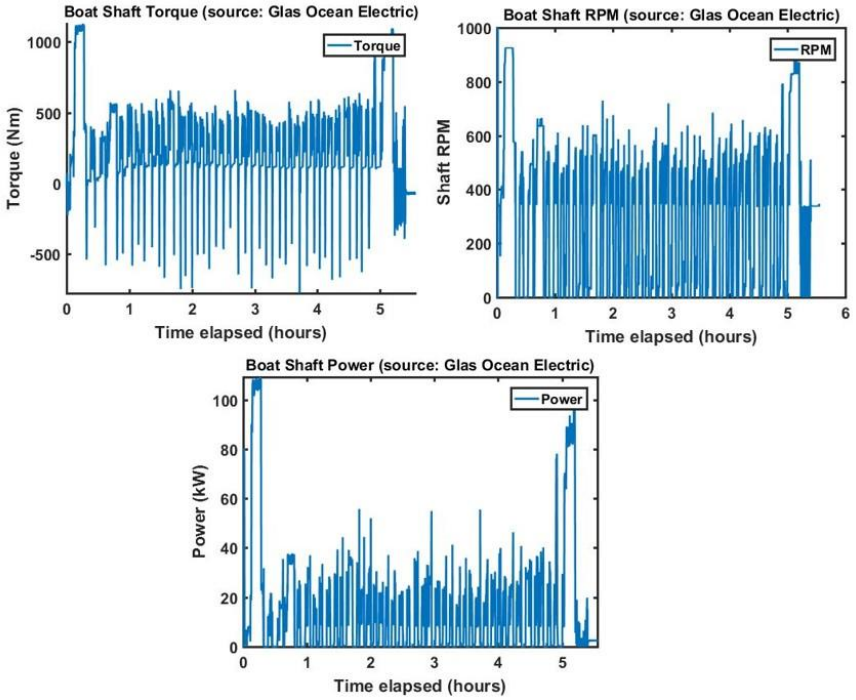

Figure A - 38 Data Collected and Calculated from Fishing Boat #1

After consultation with local fishers and boat building companies we have found that the majority of Cape Islander style vessels found in the NS fishing fleet (including the vessels GOE recorded data from) were built at local boat building facilities that keep minimal to no records of line drawings or other detail for hull shape. The boats are typically constructed using methods similar to past models and constructed in a way that is less formal than in large shipyards. Due to this fact, it has been difficult to acquire line drawings, CAD files or other technical information on the boats, a local naval architect was hired to develop 3D models of each boat from the provided particulars.

A5.4. CAD Models of Hull and Propeller

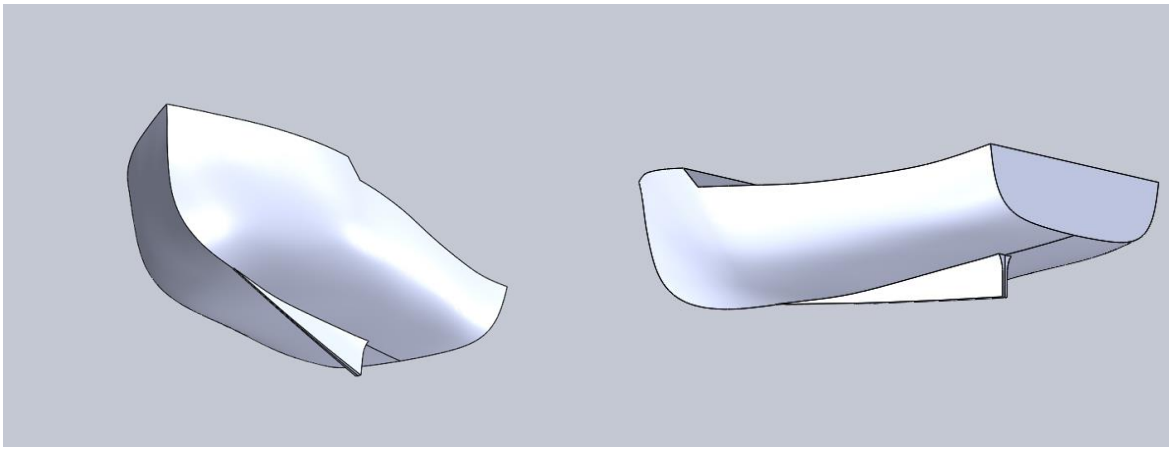

Figure A - 39 Model hull based on the style of Lobster Fishing Boat I

Due to the similarity, the same propeller geometry has been applied to all modelled fishing boats.

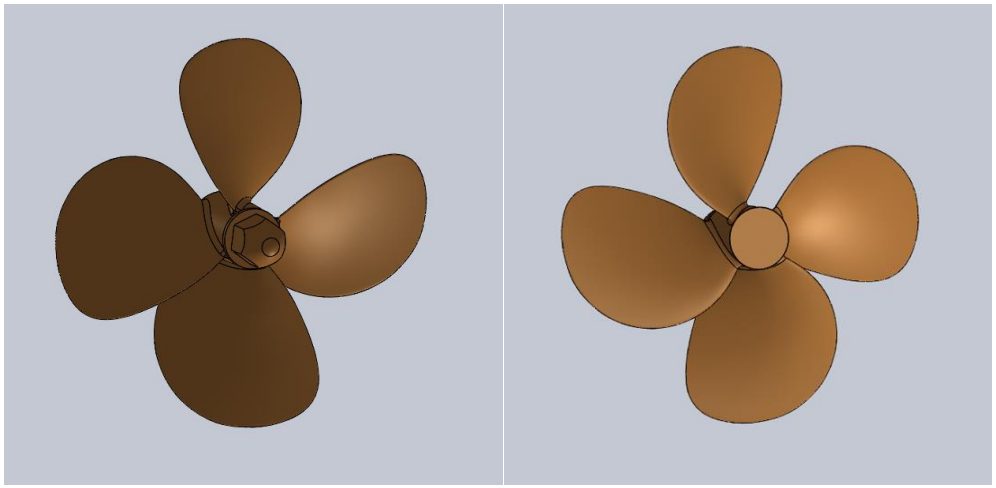

Figure A - 40 Generic Propeller Used on Lobster Fishing Boat I Style Vessels

A6. LOBSTER FISHING BOAT II

Table A - 14 Boat Specifications of Lobster Fishing Boat II

Boat Model	Miramichi
Builder	Gusmond
Operation	Lobster
Length	13.7 m
Beam	3.66 m
Height	3.66 m
Displacement	13 Tonnes
Engine Make/Model	John Deere 300
Power	244 kW (325 hp)
Max Speed	16 kt
Cruise Speed	13 kt
Fuel Usage at Cruise	12 L/h
Fuel Usage at Full Power	59.1 L/h
Propeller	4 blade 24"x26"
Gear Reduction	unavailable
Time at Dock/Day	18 hr
Time Spent at Sea / Day	6 hr
Cruise Time to Fishing zone	15 m
Distance to Fishing zone	4-5 NM
Cruise Time Back to Dock	15 m
Distance Back to Dock	4-5 NM
Typical Departure Time	6:00 AM
Batteries	2 x 8D
Gas / Oil powered Devices	
Electrically Powered Devices	VHF, lights, radio, CD player, 3 bilge pumps
Hydraulically Powered Devices	power steering, trap hauler

Figure A - 41 Strain Gauge Installed on Lobster Fishing Boat II

Table A - 15 Additional information regarding participants

Data logging date Engine model	June/2017
Engine power	John Deere 300 (22+ years old) 325 hp
Approximate fuel cost	30 Liters / day
Majority of operation time	Starting and stopping
Daily operation time	6 hours

A6.1. Power Usage

Commercial lobster boats use power through means of mechanical, hydraulic, and electrical transmission from the main engine to various appliances aboard the vessel. These typically include:

- propulsion
- trap-haulers (winches)
- power steering
- water pumps
- navigation electronics
- lights, and
- heaters

A6.2. Operation Routine

In general, the vessels follow a route from the dock to the most distant trap. This typically is 2-5 Nautical Miles depending on the placement of traps and takes about 15 minutes. Once at the fishing zone, the boat proceeds through the zone, stopping at each trap in the zone using reverse power. Then the deck crew winches the trap to the surface using the trap-hauler, empties its catch and returns the trap to the bottom. The Captain then steams to the next trap and the process is repeated for all of the traps in their zone. In most cases, the trip ends at the trap nearest the dock.

Hauling, emptying and replacing all traps typically takes 6 hours including the time spent steaming from trap to trap. This distance also depends on the placement of traps, but typically takes about 15 minutes.

The Captain first docks at a loading and unloading zone to bring their catch ashore before returning the boat to its berth at the home wharf. Reverse power is used to stop and position the boat whenever docking.

A6.3. Collected Data

Examples of the propeller shaft torque, speed, and power data are shown in Figure A - 42.

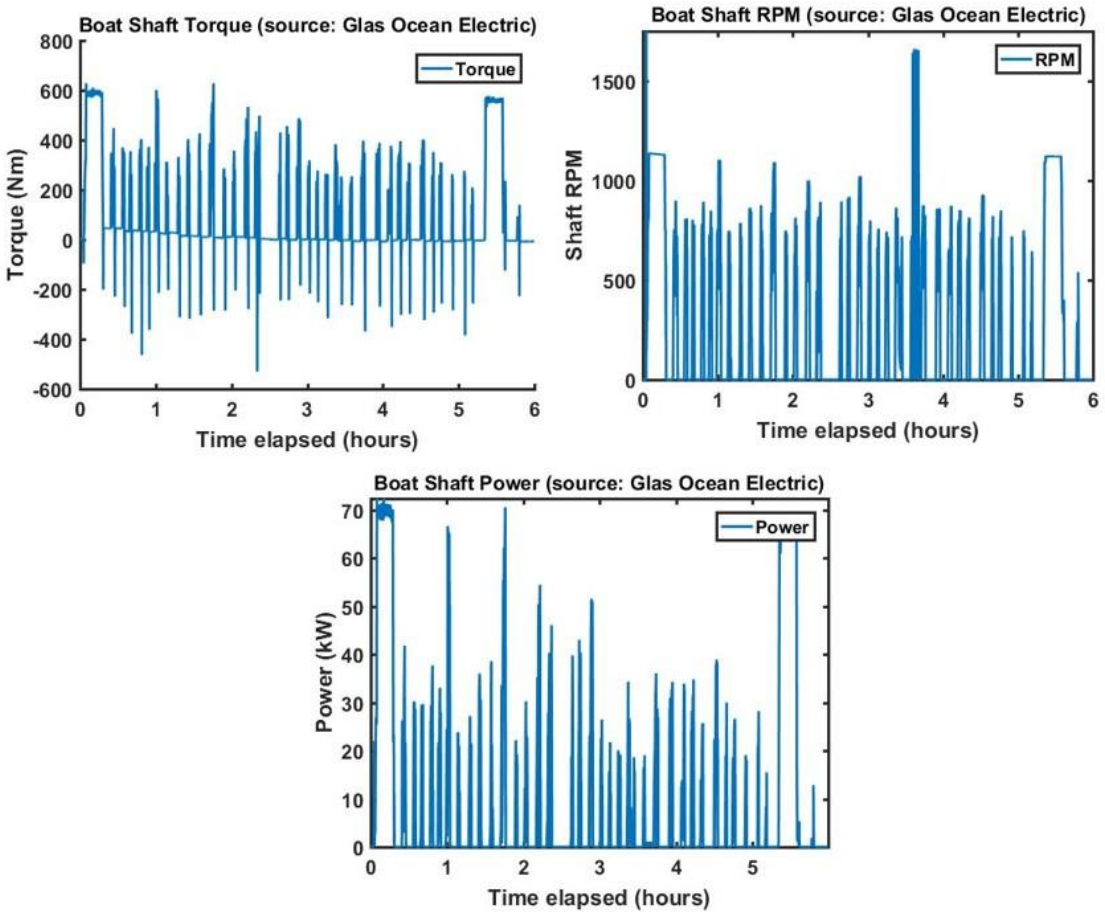

Figure A - 42 Processed Collected Data from Lobster Fishing Boat II

A6.4. Boat Hull

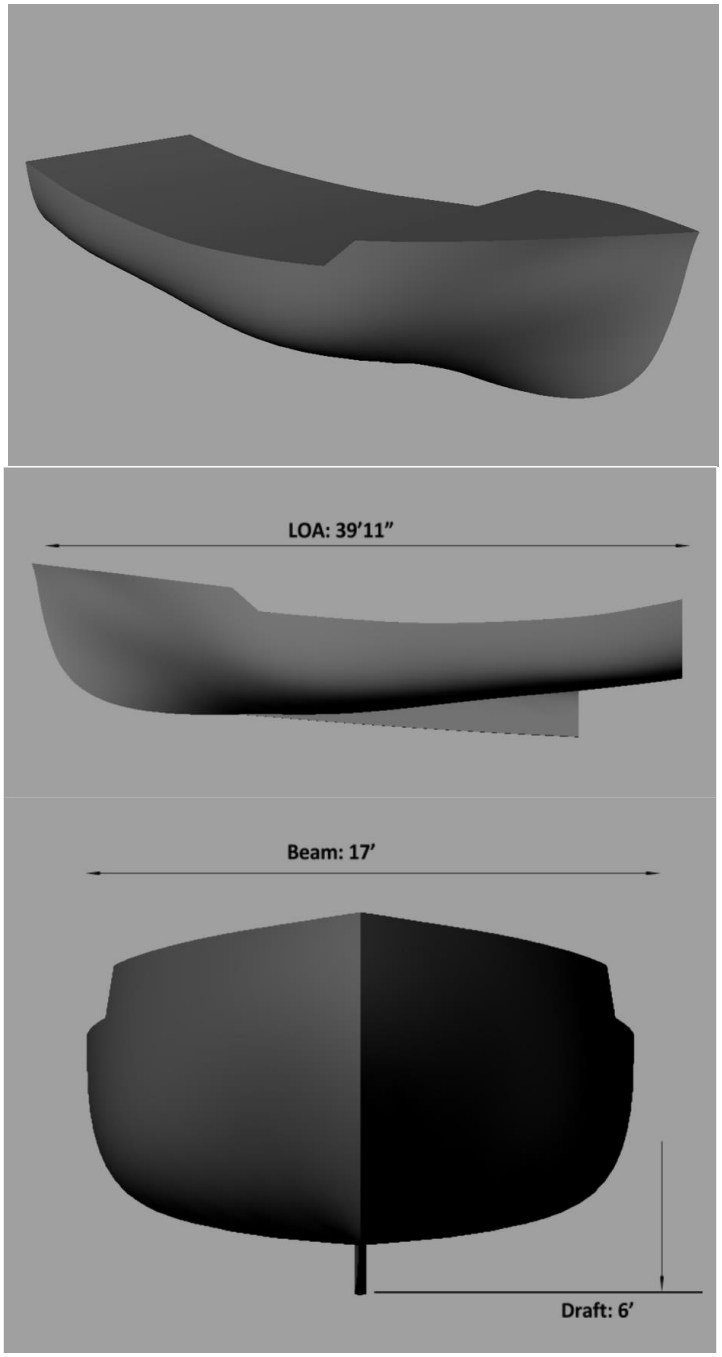

Figure A - 43 3D Boat Hull Model

A7. FISHING BOAT III

Table A - 16 Specifications of Fishing Boat III

Boat Model	Cape Island Fat 40
Builder	Doug Mood
Operation	Lobster
Length	12 m
Beam	7.4 m
Height	4.9 m
Displacement	15 Tonnes
Engine Make/Model	Doosan MD196TI
Power	240 kW (320 hp)
Max Speed	10 kt
Cruise Speed	8.5 kt
Fuel Usage at Cruise	36.6 L/hr
Fuel Usage at Full Power	58.6 L/hr
Propeller	4 blades 42"x38"
Gear Reduction	3.1:1
Time at Dock/Day	14 hr
Time Spent at Sea / Day	10 hr
Cruise Time to Fishing zone	1 hr
Distance to Fishing zone	8 NM
Cruise Time Back to Dock	1.5 hr
Distance Back to Dock	12 NM
Typical Departure Time	4:00 AM
Batteries	4 x 8D
Gas / Oil powered Devices	Gas stove
Electrically Powered Devices	fridge, microwave, 2x bus heaters, radar, plotter, sounder, autopilot, stereo, lights, TV, play station, VHF, Inverter, 3 bilge pumps
Hydraulically Powered Devices	power steering, trap hauler, pole master

A7.1. Collected Data

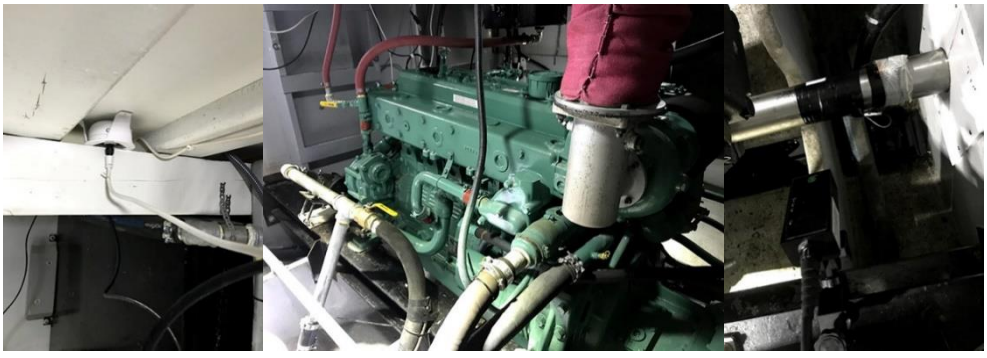

Figure A - 44 Boat Engine Room and Installed Torque and Speed Sensors

A7.2. Boat Hull

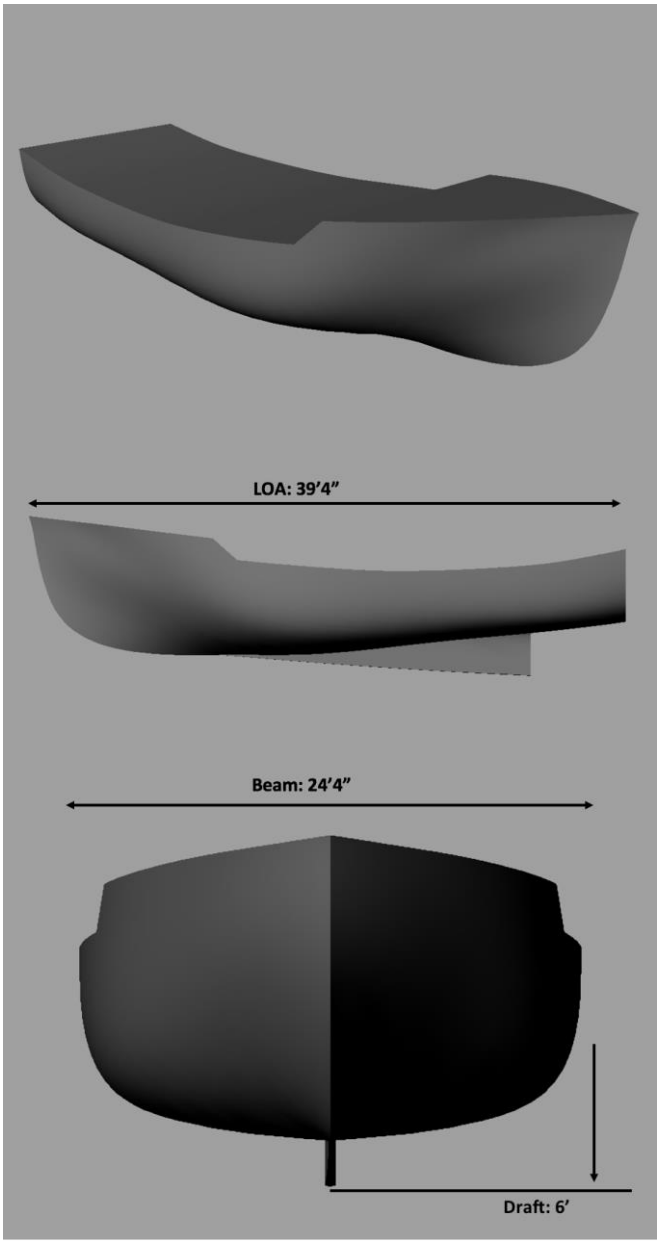

Figure A - 45 3D Boat Hull Model

A8. TOUR VESSEL

Table A - 17 Particulars and Specifications of Studied Tour Vessel

Boat Model	unknown
Builder	unknown
Operation	whale watching/fishing tours
Length	12.3 m
Beam	3.60 m
Height	3.66 m
Displacement	15 Tonnes
Engine Make/Model	Cummins 6CTA
Power	323 kW (430 hp)
Max Speed	15 kt
Cruise Speed	12 kt
Fuel Usage at Cruise	54.4 L/hr
Fuel Usage at Full Power	96 L/hr
Propeller	4 blade 30"
Gear Reduction	2.1.1
Time at Dock/Day	unknown
Time Spent at Sea / Day	unknown
Cruise Time to Fishing zone	unknown
Distance to Fishing zone	unknown
Cruise Time Back to Dock	unknown
Distance Back to Dock	unknown
Typical Departure Time	unknown
Batteries	2 x 8D
Gas / Oil powered Devices	none
Electrically Powered Devices	power steering
Hydraulically Powered Devices	unknown

Figure A - 46 Hardware installation on tour boat

A8.1. Collected Data

A8.1.1. August 16th, 2017 Data

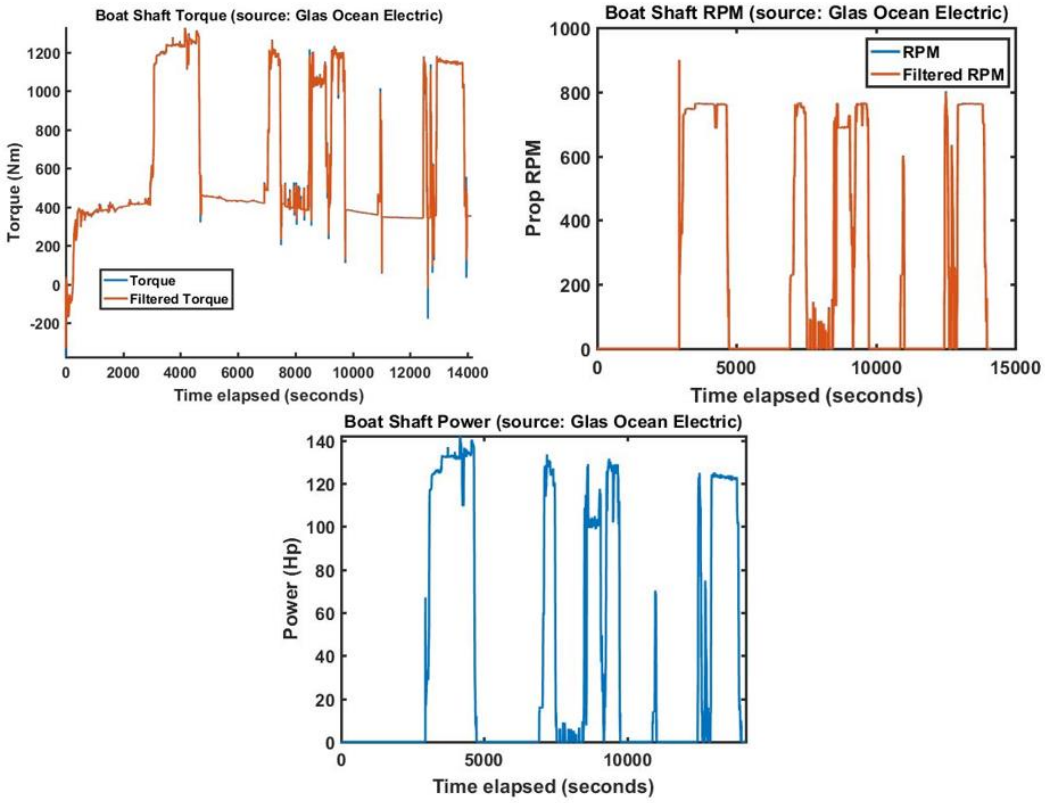

Figure A - 47 Torque, Shaft Speed, and Power Data from the Tour Vessel (I)

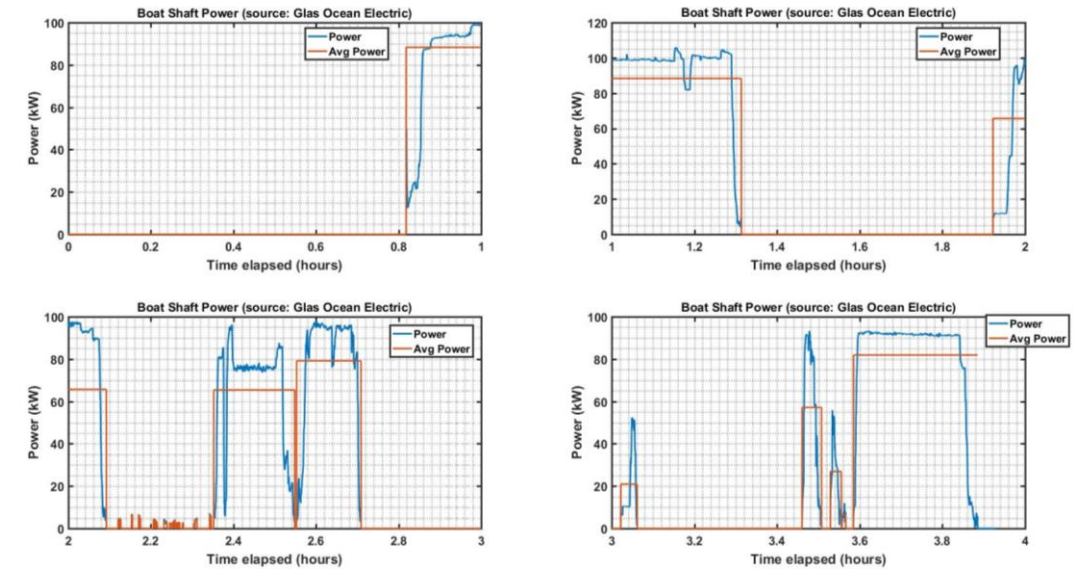

Figure A - 48 Integrated Energy Using Average Power Values

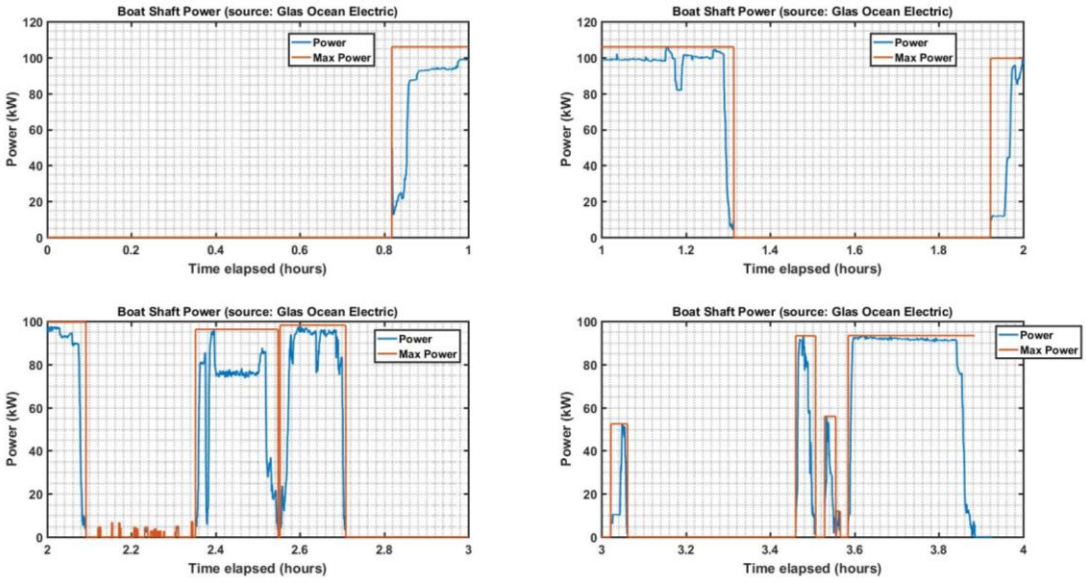

Figure A - 49 Integrated Energy Using Maximum Power Values

A8.1.2. August 17th, 2017 Data

The following sub-section will display the data from Aug. 17 in the same format as displayed for Aug. 16 in the previous sub-section

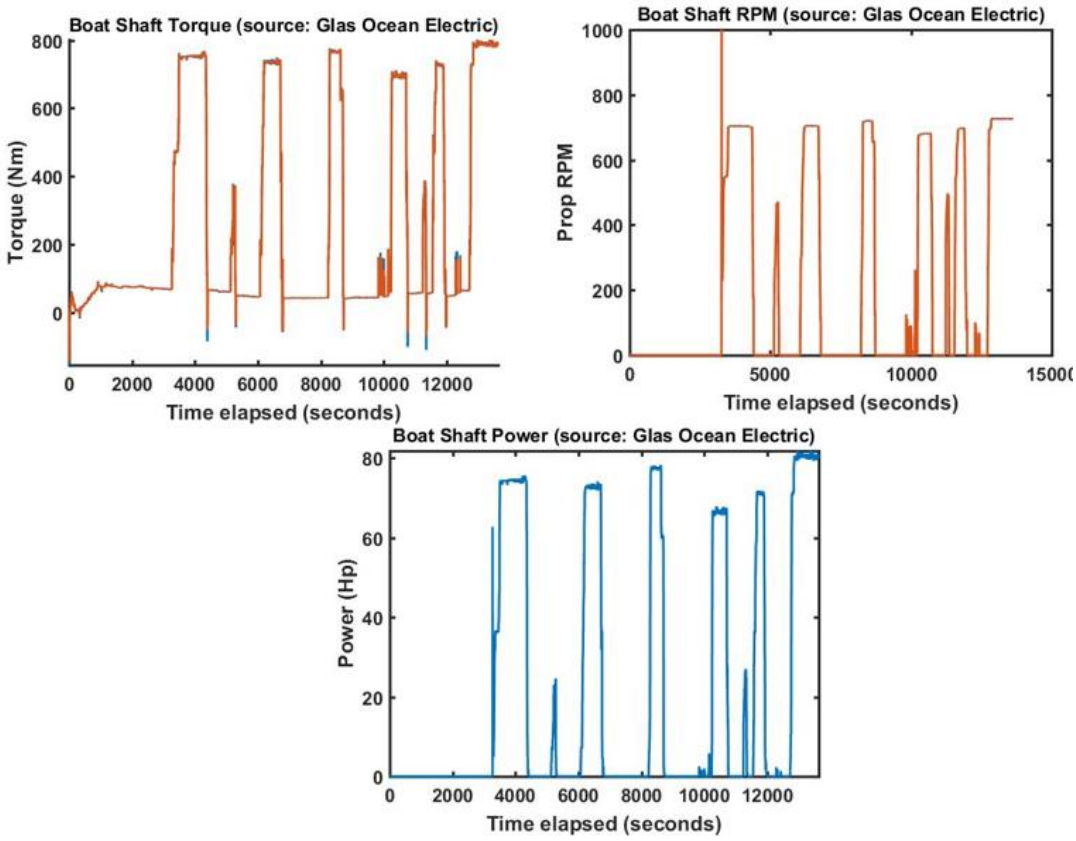

Figure A - 50 Torque, Shaft Speed, and Power Data Collected from Tour Vessel (II)

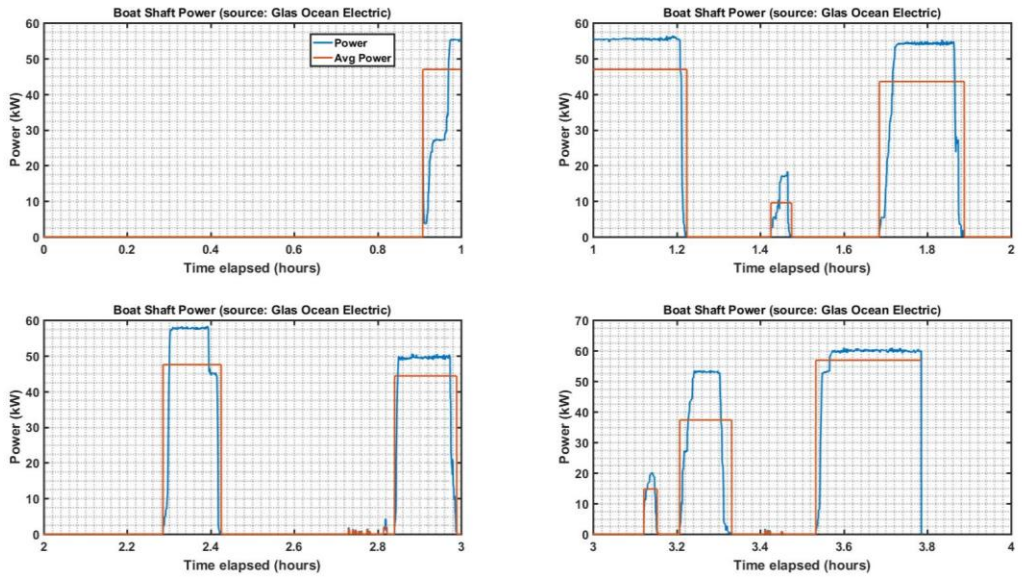

Figure A - 51 Integrated Energy Using Average Power Values

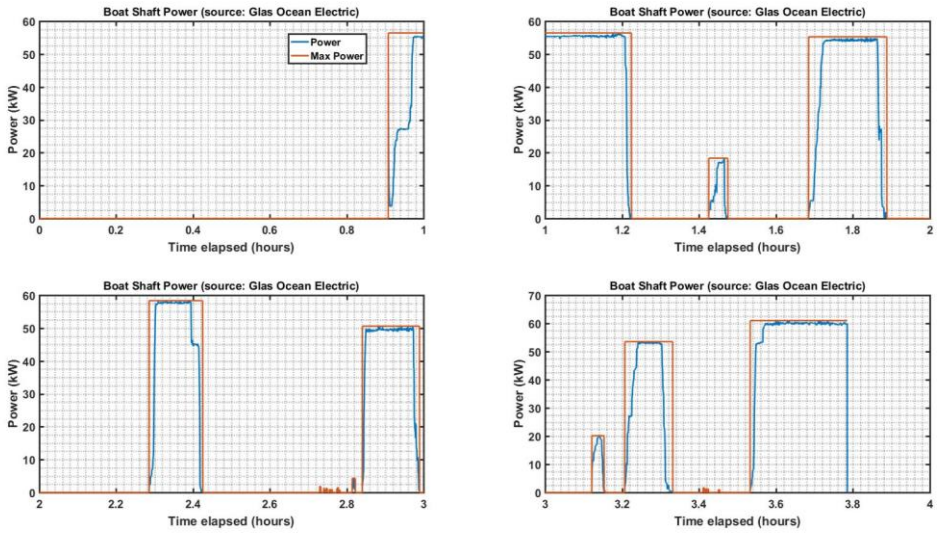

Figure A - 52 Integrated Energy Using Maximum Power Values

A8.2. Ship Hull

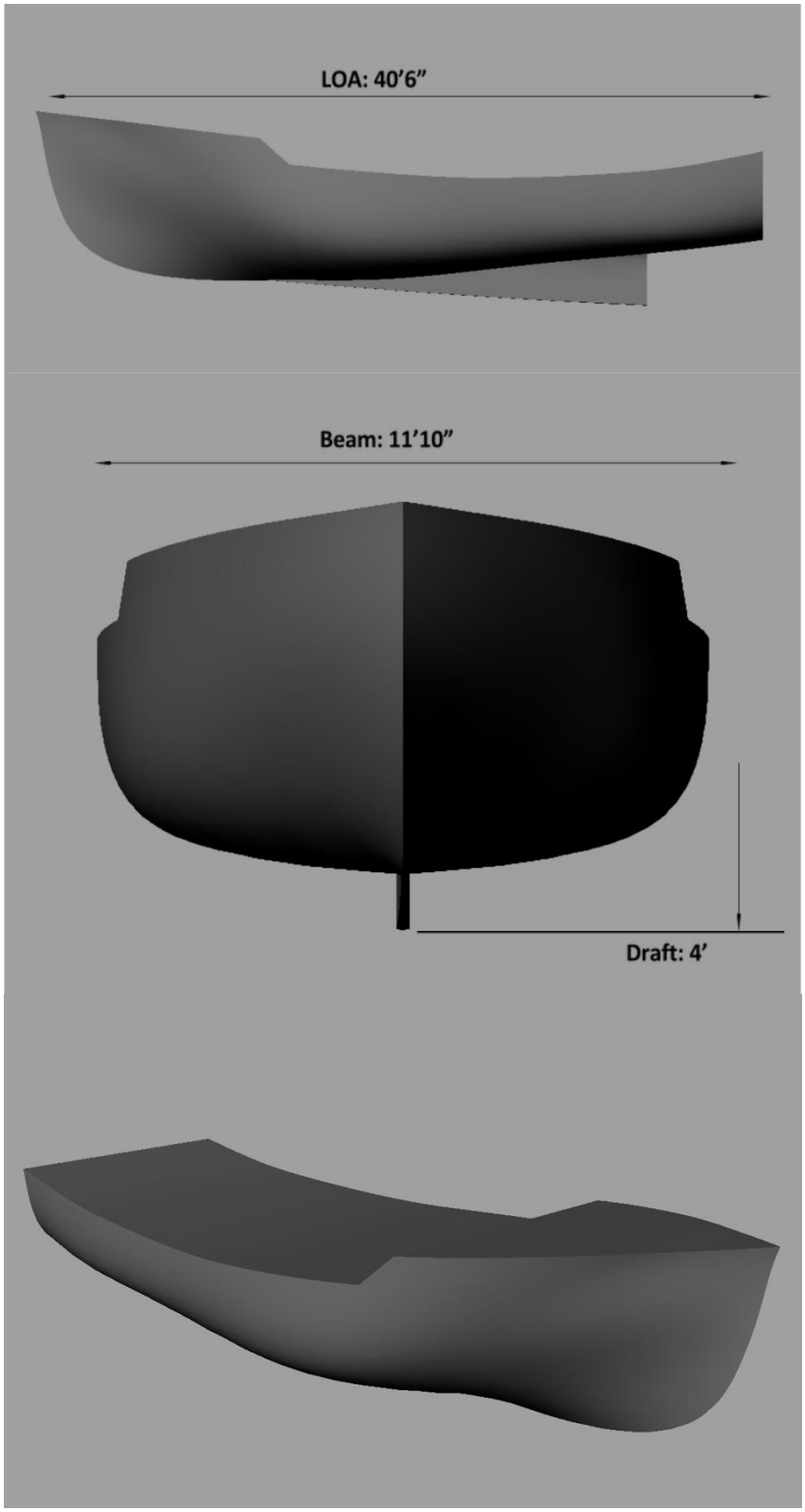

Figure A - 53 3D Hull Model on Style of Studied Tour Vessel

REFERENCE

[1] "MV Tachek Life-Extension Project." [Online]. Available: http://www.bcferrycommission.ca/regulations-probes/probes/mv-tachek-life-extension-update/.

[2] P. K. Balakrishnan and S. Sasi, "Technological and Economic Advancement of Tug Boats," *IOSR J. Mech. Civ. Eng.*, p. 10.

[3] "Tug and Workboat Design Guide," *Tug And Workboat Design Guide.* [Online]. Available: http://ral.ca/.

[4] "RANGLer," *Robert Allan Ltd.*.

[5] R. A. Ltd, "RAptures: Resolving the Tugboat Energy Equation," p. 14.

[6] "The Hybrid Tug," *Foss*. [Online]. Available: https://www.foss.com/foss-innovation/the-hybrid-tug/. [Accessed: 14-Aug-2018].

[7] "Corvus-Energy-CASE-STUDY_RT-ADRIAAN_-MAY-2015.pdf." [Online]. Available: http://corvusenergy.com/. [Accessed: 14-Aug-2018].

[8] T. L. Vu, J. S. Dhupia, A. A. Ayu, L. Kennedy, and A. K. Adnanes, (2014) "Optimal power management for electric tugboats with unknown load demand," in *2014 American Control Conference*, pp. 1578–1583.

[9] T. L. Vu, A. A. Ayu, J. S. Dhupia, L. Kennedy, and A. K. Adnanes, (2015) "Power Management for Electric Tugboats Through Operating Load Estimation," *IEEE Trans. Control Syst. Technol.*, Vol. 23, No. 6, pp. 2375–2382.

[10] L. C. W. Yuan, T. Tjahjowidodo, G. S. G. Lee, R. Chan, and A. K. Ådnanes, (2016) "Equivalent Consumption Minimization Strategy for hybrid all-electric tugboats to optimize fuel savings," in *2016 American Control Conference (ACC)*, pp. 6803–6808.

[11] S. Evans, "Understanding and Optimizing Vessel Propulsive Power and Fuel Use Using Duty Cycle Analysis Computations," pp.13.

[12] H. Kifune and T. Nishio, (2015) "A Study of Fuel Consumption Model Using Tugboat's Propulsion System," マリンエンジニアリング, vol. 50, no. 4, pp. 527–534.

[13] H. Kifune and T. Nishio, (2017) "Fuel Saving Effect of Hybrid Propulsion System-Case: Tugboat is not in Service," *Mar. Eng.*, Vol. 52, No. 6, pp. 811–817.

[14] T. Völker, "Hybrid propulsion concepts on ships," (2015).

[15] H. E. Lindstad and I. Sandaas, "Emission and Fuel Reduction for Offshore Support Vessels through Hybrid Technology," Nov-2016. [Online]. Available: https://www.ingentaconnect.com/content/sname/jspd/2016/00000032/00000004/art00001.

Appendix B. Guidelines for Preparing Ship Hull and Propeller CFD Models

ABSTRACT

This document summarizes the general requirements and processes for preparing the 3D CAD solid and surface models that are used to form the data input models for Computation Fluid Dynamics (CFD) simulations. The CFD simulations are used to generate the model parameters for the reduced-order hydrodynamics hull resistance and propeller thrust force models that are used in the integrated hybrid electric marine propulsion system model.

The full-scale CFD simulations are also used as a validation tool for the stated integrated system model, and for investigating propeller cavitation noise at different states of vessel operation.

B1MODEL REQUIREMENTS AND PROCESS

B1.1 Requirements on the CAD Models

- CAD files can be created using any 3D modelling package such as (Siemens NX, Catia, ProE, SolidWorks, etc.)
- CAD files should be as smooth as possible and be created with the fewest number of surfaces as possible
- CAD files should be "water-tight" i.e. the surface(s) should form a closed volume
- CAD files should not contain any intersecting surfaces
- Hull CAD files should include a coordinate system at the center of gravity
- CAD files should be saved in ".stl" format for import into the CFD software used at UVic (For hull files, a coordinate system located at the COG should be used as the ".stl" file coordinate system)
- Hull CAD files should be accompanied with a value(s) for the vessels Moment of Inertia (Calculated or Estimated)

B1.2 CAD Model Building Process

The following is a description of some methods used at UVic to obtain the required hull and propeller models.

B1.1.1 Hull Surfacing

The UVic team was fortunate to be able to obtain hull files containing the required hull profiles that detail the contours of the ship (See Figure B - 1 below).

Note that, as shown in Figure B - 2, some hull profile curves contained. In order to resolve this issue, curves were fitted to each hull profile curve to form a smooth contour and remove the irregularities.

Furthermore, if a hull profile file is unavailable, these hull profiles could possibly be obtained using a hull scan, or a hull profile drawing, if the spacing between the hull profiles is known (See Figure B - 3)

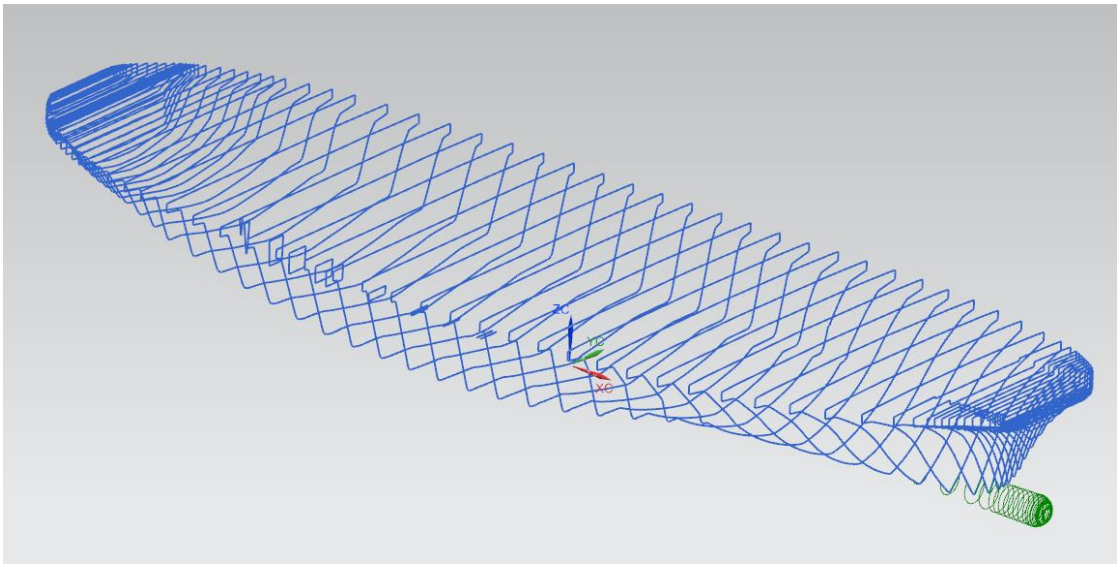

Figure B - 1 Hull profile.

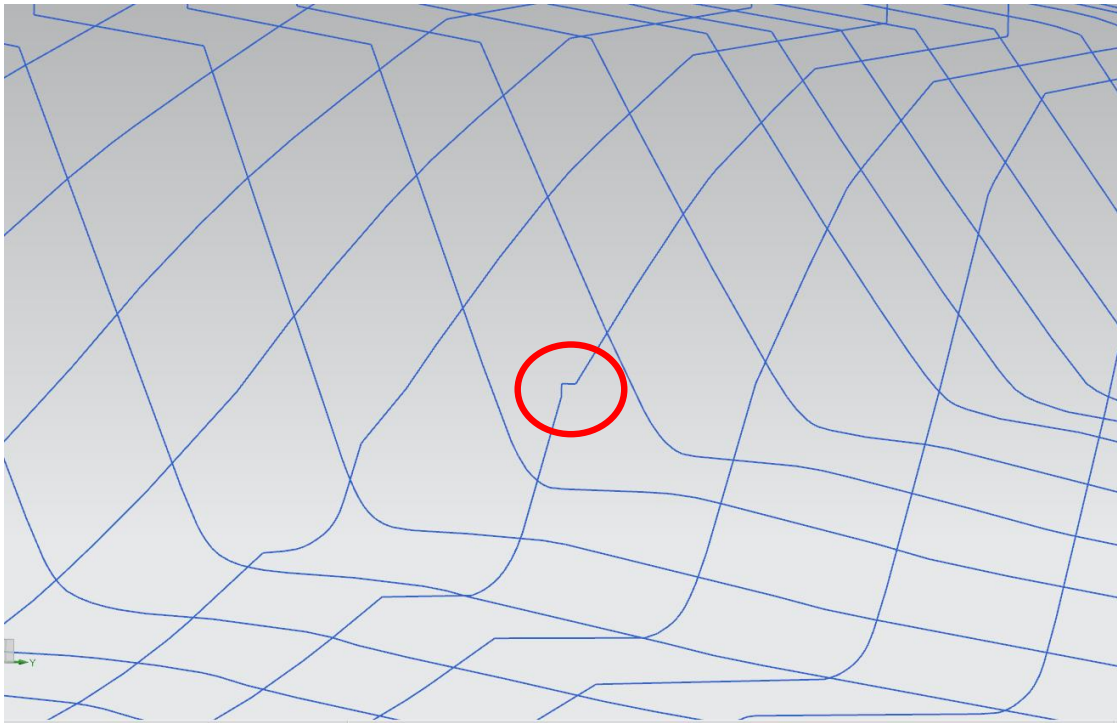

Figure B - 2 Hull profile irregularity.

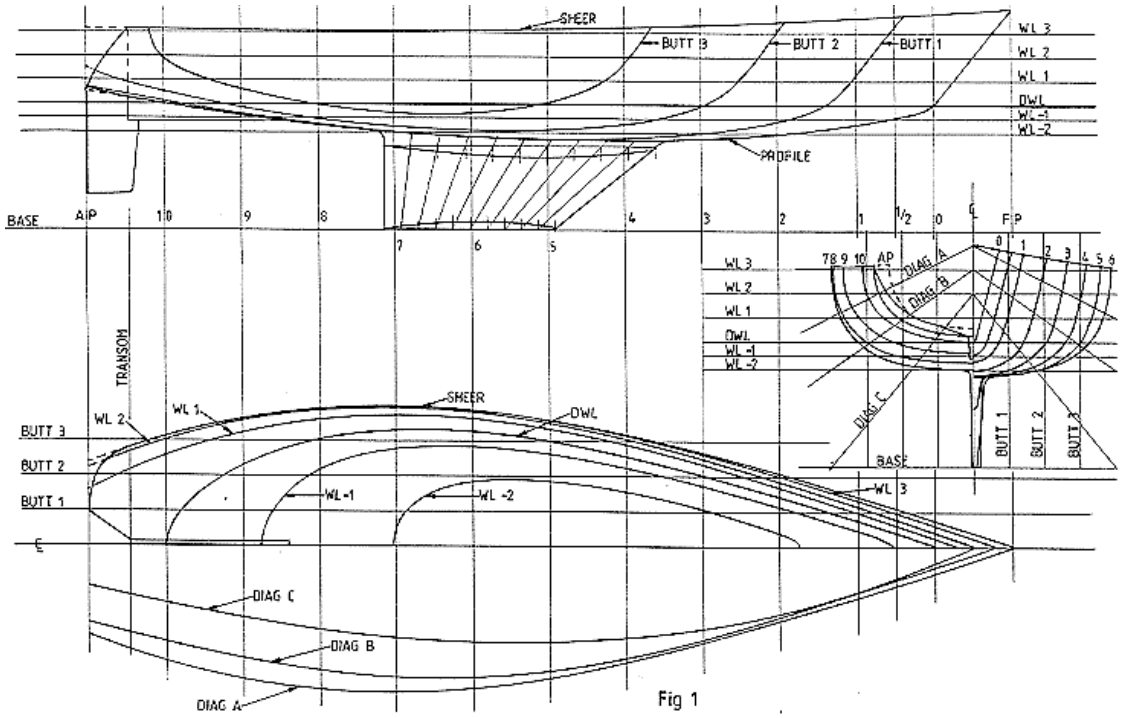

Figure B - 3 Hull profile drawing [1].

Using a 3D CAD program, as shown in Figure B - 4, UVic used a surfacing feature to create a smooth continuous surface over the hull profiles.

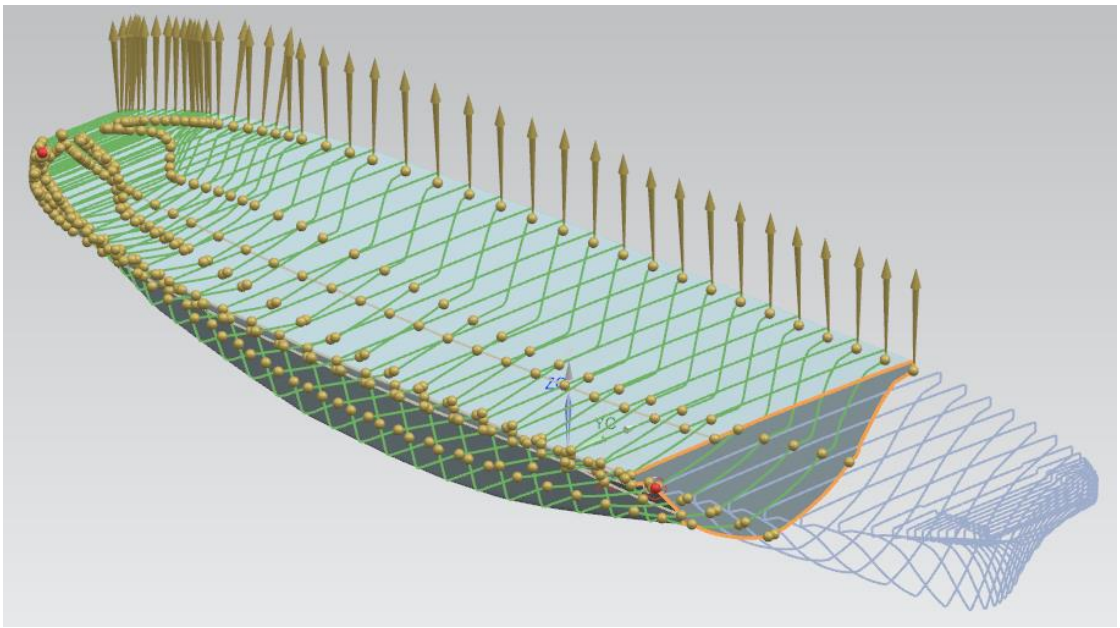

Figure B - 4 Forming hull surface using Siemens NX.

Next, The UVic team added any additional appendages and united them with the hull while ensuring surfaces had a smooth transition. It is noteworthy that:

- UVic obtained the center of gravity of vessels from supplied stability books. A coordinate system at the estimated center of gravity is required in the CAD file.
- The hull file was then exported to a ".stl" file format that is compatible with CFD software used at UVic.
- UVic obtained the mass of vessels from supplied stability books.
- In the current build of the simulation, the mass of the vessel remains static for the duration of the simulation and one representative mass needs to be chosen. For example, if a ferry makes several crossings in a day with a varying number of cars and passengers, a mass is chosen that best represents the combined mass of the ferry and cargo during the majority of its crossings.
- UVic calculated the ships moment of inertia using the mass and center of gravity of the ship and the mass and center of gravity of all major components, passengers, and loads on the ship (in this document a major mass can be defined as a mass >= 1% of a lightship mass).

If creating a list of components including their masses and locations relative to the COG is deemed too difficult to obtain, the moments of inertia can be estimated using the following approximation:

(Radius of Gyration) [m] K_x = (0.35 to 0.40) * Beam
(Radius of Gyration) [m] K_y = (0.2 to 0.25) * Length
(Radius of Gyration) [m] K_z = (0.2 to 0.25) * Length

(Moment of Inertia) [kg*m^2] $I_{xx} = K_x^2$ * mass
(Moment of Inertia) [kg*m^2] $I_{yy} = K_y^2$ * mass
(Moment of Inertia) [kg*m^2] $I_{zz} = K_z^2$ * mass

Products of inertia must be assumed negligible in this case

B1.1.2 Propeller Surfacing

UVic was able to obtain 2D propeller drawings containing the required propeller information to construct a 3D model of a propeller (See Figure B - 5). UVic used the theory described in [2] to develop a process to translate the information from a 2D propeller drawing to a 3D model. The following steps describe the process step-by-step:

1) Equations from the literature [2] were used to find points on the generator line, the leading edge locus, and the trailing edge locus, at each of the radial steps on the 2D propeller drawing (See Figure B - 6).
2) Three curves were fit to define the generator line, leading-edge locus, and the trailing edge locus using the points from the previous step
3) A semi-circular surface was created at each radial step from the drawing. In addition, a plane that is tangent to the semi-circular surface and normal to the generator line was added (See Figure B - 7).

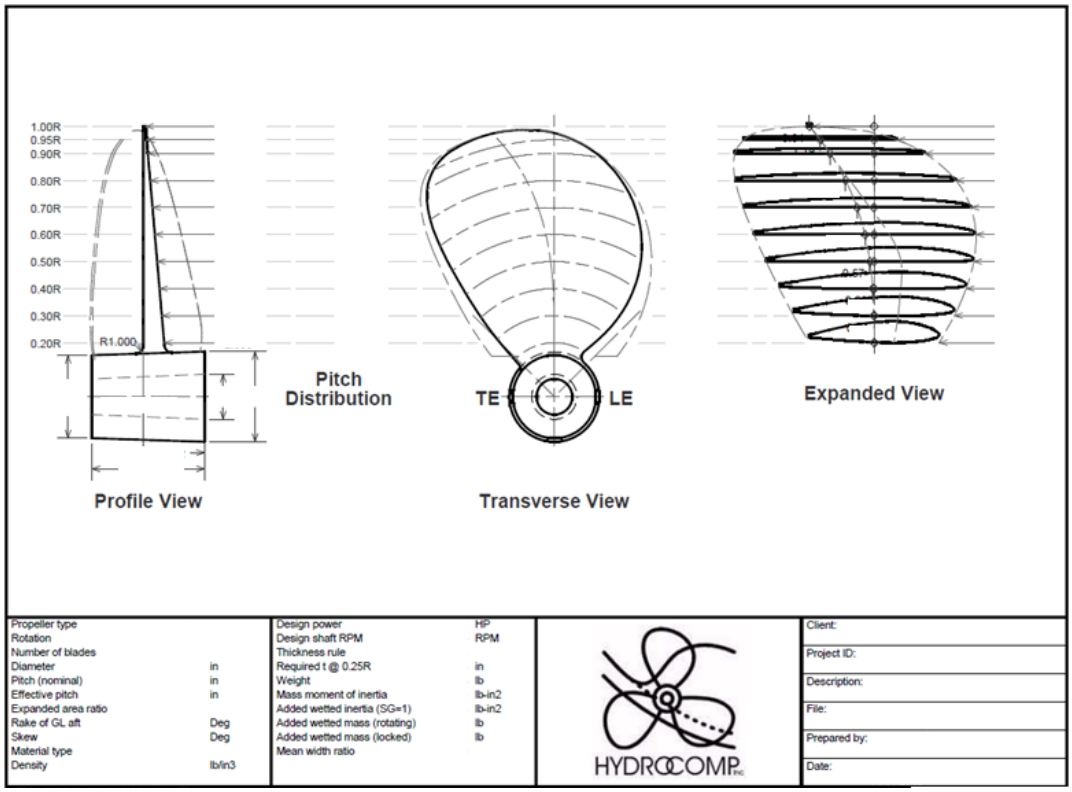

Figure B - 5 Two-dimensional propeller drawing (dimensions removed).

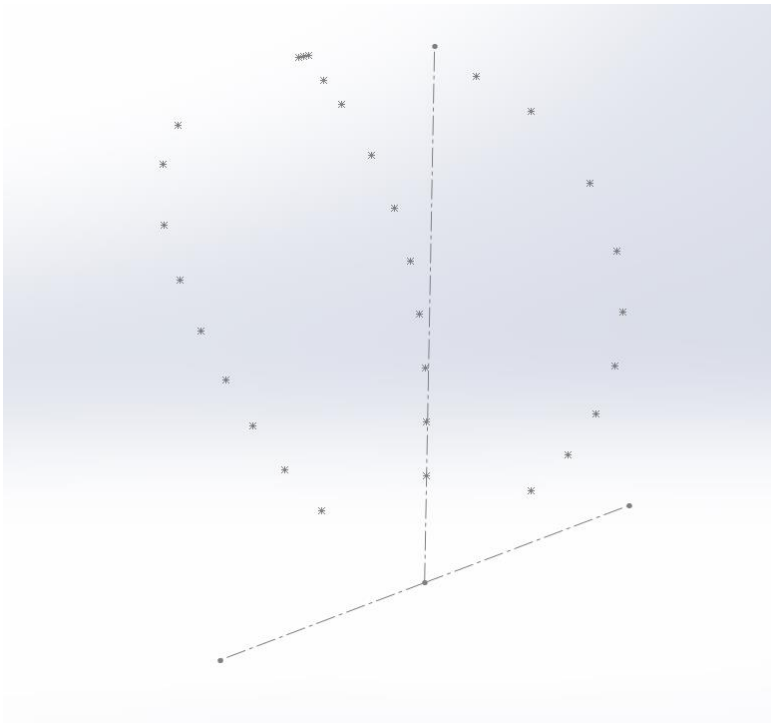

Figure B - 6 Points on the generator, leading edge, and trailing edge curves.

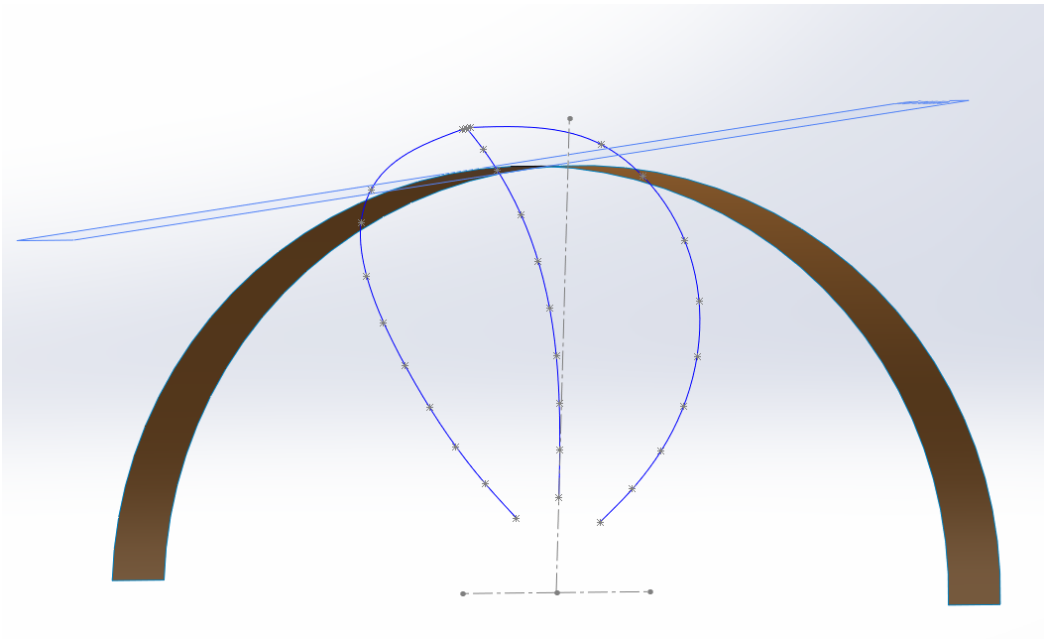

Figure B - 7 Semi-circle and plane.

4) Next, a sketch was started on each of the planes created in the step above. A 2D image of the corresponding cross-sectional propeller profile for each individual radial step was inserted into each sketch.
    - Ensure to rotate the angle of the cross-section according to the calculations for rake and skew.
    - NOTE: If the 2D propeller drawing is not from a drafting program (i.e. AUTOCAD) and is in a form such as PDF, you can insert a picture from the PDF into the sketch, scale it to size, and create the contour using a continuous spline.
5) Next, a command such as Wrap (SolidWorks) was used to wrap the cross-sectional contour onto the semi-circular surface for that radial step (See Figure B - 8).
6) Trim away the remaining semi-circular material leaving only the cross-sectional contours at each radial step (See Figure B - 9):
7) A propeller blade surface was created by using a surfacing command with the radial contours as inputs (See Figure B - 10):
8) Finally, the propeller hub and any other features defined on the 2D propeller drawing were added. The blade was blended to the hub and the blade was circularly patterned to create as many instances of the blade as required (See Figure B - 11):
    - The propeller model was exported to ".stl" file format to be compatible with the CFD software used at UVic.

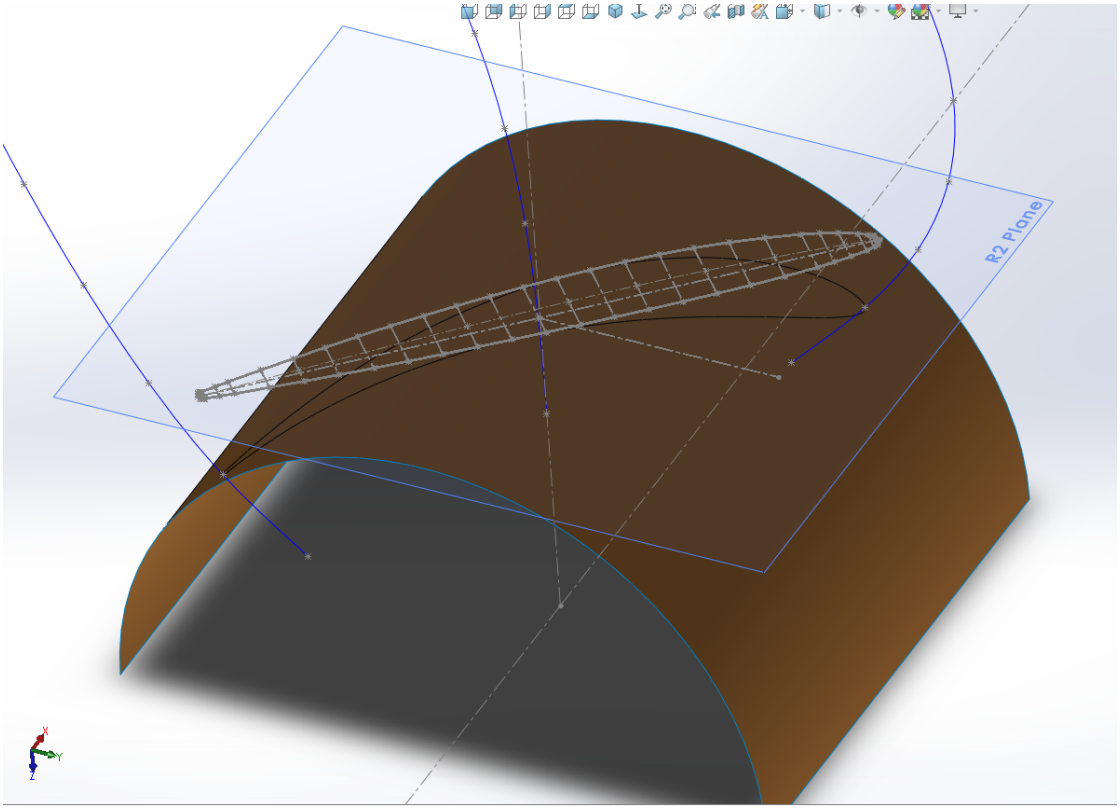

Figure B - 8 Cross-sectional contour and wrap.

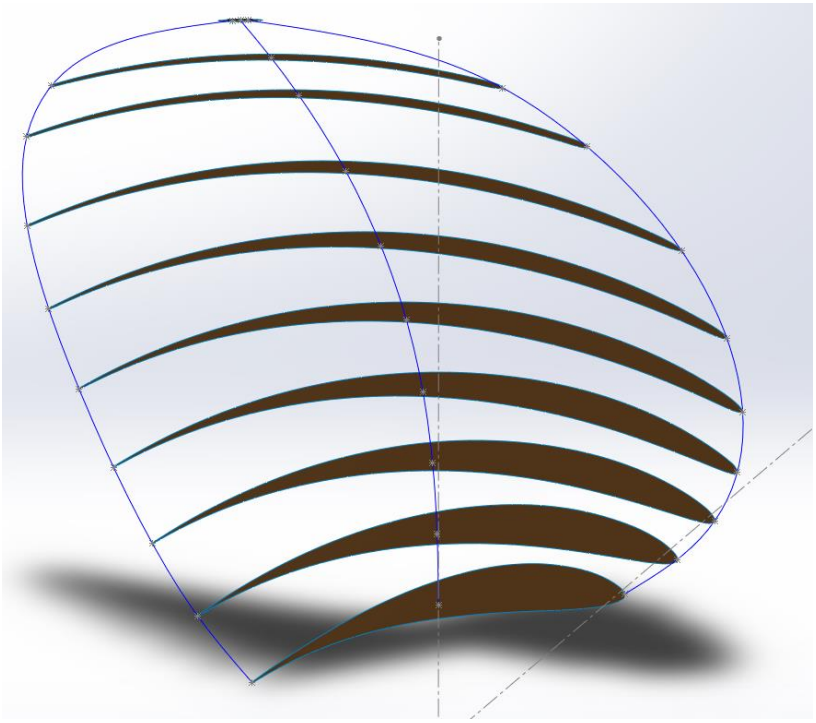

Figure B - 9 Radial contours.

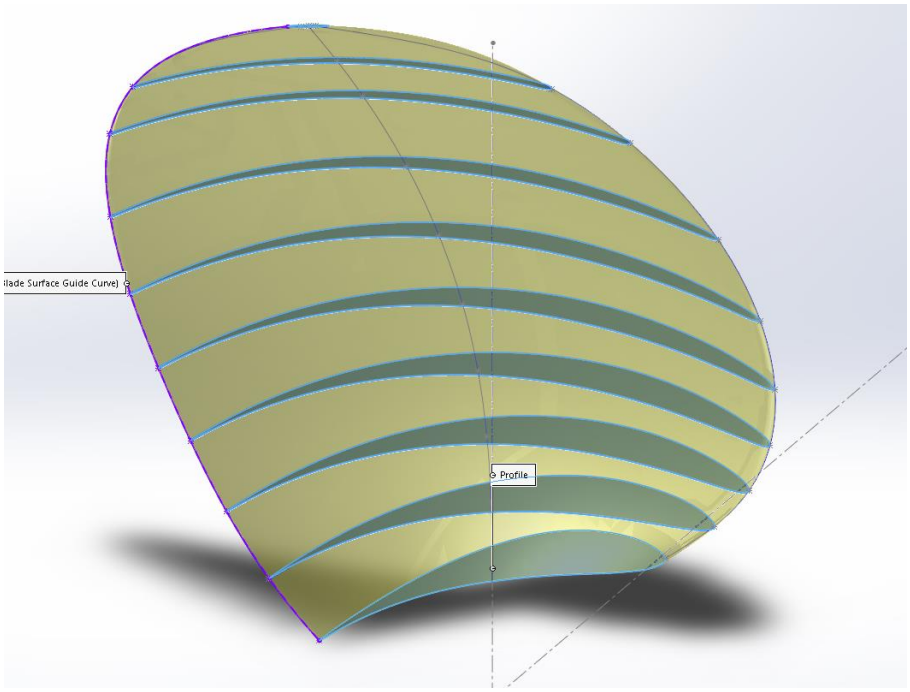

Figure B - 10 Propeller blade surfacing.

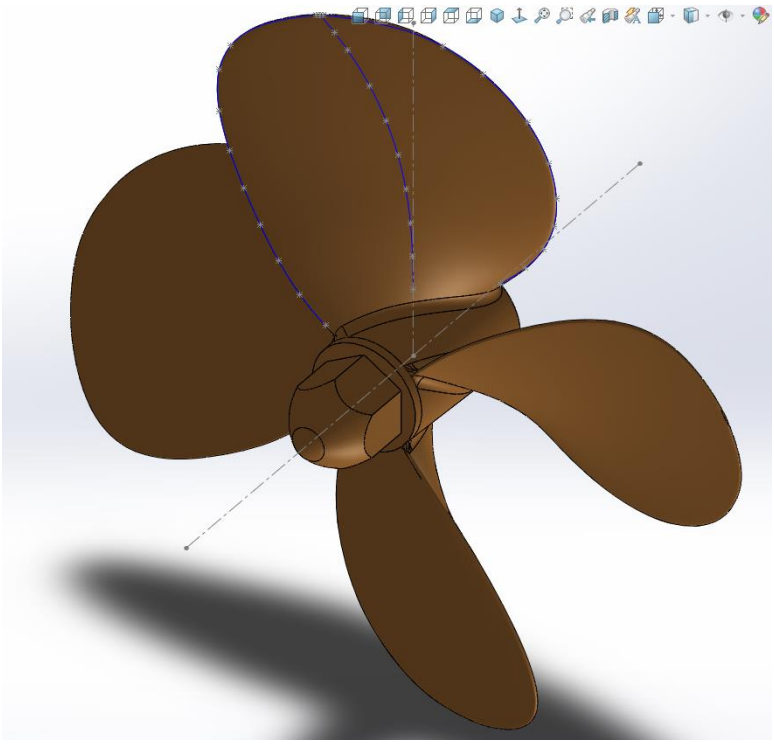

Figure B - 11 Completed propeller.

B1.3 Examples of Acceptable CAD Models

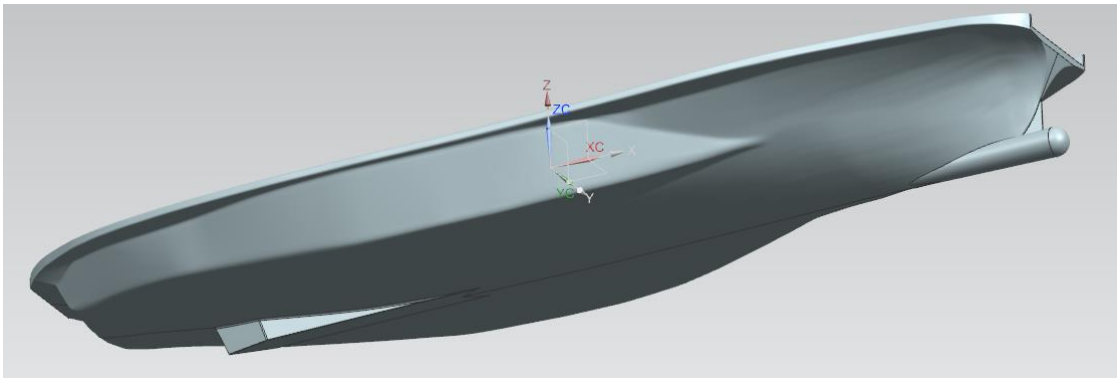

Figure B - 12 Acceptable hull model.

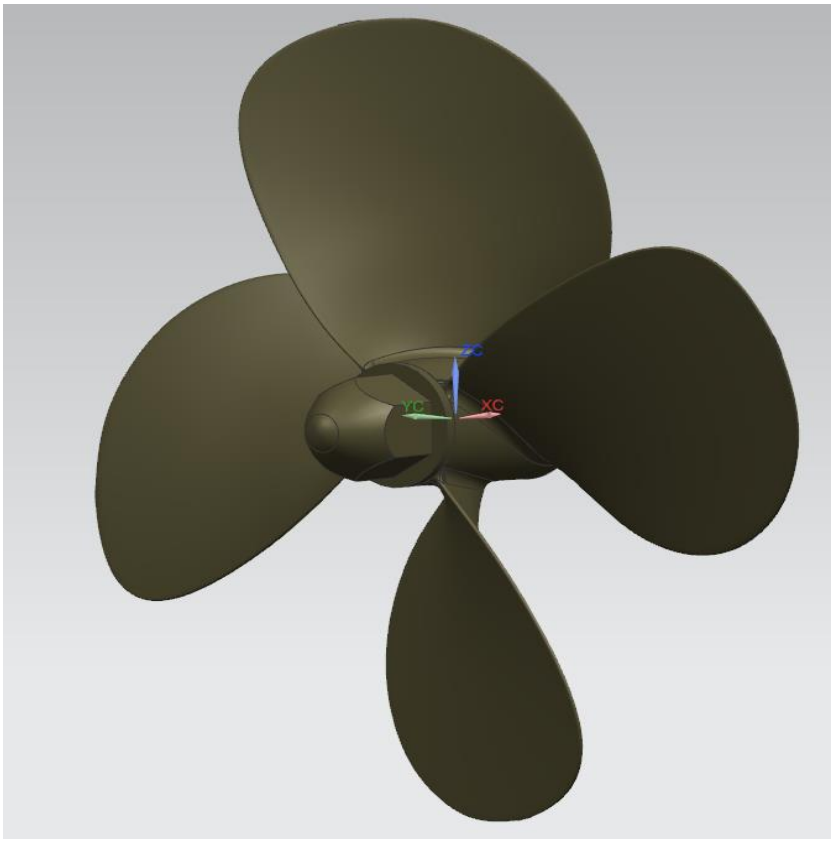

Figure B - 13 Acceptable propeller model.

B1.4 Example of an un-acceptable CAD model:

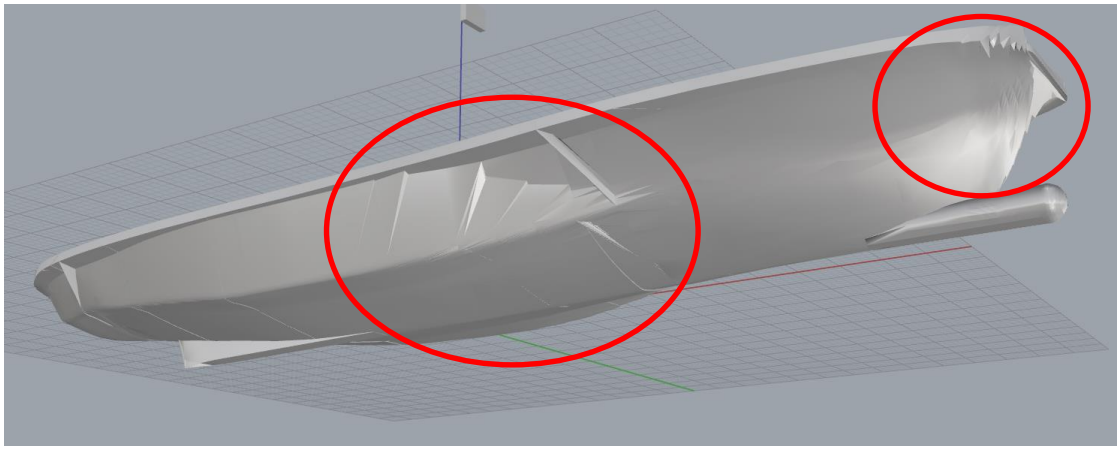

Figure B - 14 Un-acceptable hull model.

B1.5 Process checklist

- ☑ The majority of the hull is created with one surface (appendages were created with additional surfaces)
- ☑ The hull and appendage surfaces form a closed volume
- ☑ The transition between all surfaces is continuous
- ☑ There are no intersecting surfaces
- ☑ The hull model contains a coordinate system located at the ships estimated COG
- ☒ The CAD models contains some relatively sharp edges (In this situation they were concluded to have a negligible effect on the CFD results)
- ☒ Intersecting surfaces
- ☒ Many surfaces with discontinuities at joints
- ☒ Not “water-tight” i.e. surfaces do not form a closed volume

REFERENCES

[1] *https://grabcad.com/questions/how-to-loft-boat-hull*

[2] J. Carlton, Marine propellers and propulsion, Butterworth-Heinemann, 2012.

Appendix C. List of Required Tasks and Preferred Ship Operation Data

This appendix provides the checklists in different areas for the tasks needed to generate the operation profiles of a marine vessel in the completed hybrid electric marine propulsion technology study.

C1 SHIP OPERATION DATA REQUIREMENTS

C1.1 CFD Analysis for Model Parameterization

- CFD analysis of bare hull
- CFD analysis of rear propellers
- CFD analysis of bow thruster
- CFD self-propelled
- Wake fraction and thrust deduction analysis

C1.2 Vessel Dynamics

- ShipMo3D analysis
- Maneuvering model parameterization
- Rudder model
- Surge resistance decomposition

C1.3 CAD Modelling

- Develop 3D CAD model of ship hull for CFD
- Develop 3D CAD model of ship propellers for CFD

C1.4 Vessel Engine and/or Propeller Shaft Speed and Torque Data Collection

- Design, construction, and lab testing of equipment
- Installation planning and equipment procurement
- Installation, commissioning, and monitoring
- Post-collection data analysis and processing
- Decommissioning

C1.5 Plant Modelling

- Powertrain system component information gathering
- Model of diesel and NG engines
- Modelling of Induction Generator
- Model battery energy storage system (ESS) and battery-UC hybrid ESS (HESS)
- Modelling of Variable-Speed Generation Power Electronics
- Model of AC induction motor and PMSM motor
- Modelling of DC/AC and DC/DC bidirectional converters

C1.6 Power System Modelling

- Model of electric power system with a conventional AC power bus
- Model of electric power system with modern DC power bus

C1.7 Powertrain System Modelling

- Model of pure mechanical powertrain system (baseline)
- Model of pure electric powertrain system (short trips with charging opportunity)
- Model of series hybrid electric powertrain system (better for tugs with more dynamic load)
- Model of parallel hybrid electric powertrain system (better for ferries with more static load)
- Model of plug-in hybrid electric powertrain systems (combining pure electric and hybrid)

C1.8 Real-time Control of Power Management

- Analysis of current power management system
- Real-time power management control system and optimization of ship

C1.9 Existing Operational Analysis

- Energy efficiency analysis and actual utilization of existing components
- Study of alternate powertrain architectures for ferry load profile

Appendix D. Model Library of Diesel and Natural Gas Engines

Engine power performance, fuel efficiency and emission models are essential for the design and operation control of vehicle and vessel powertrain systems. Since the theoretical models are too complex and less accurate, empirical engine models are obtained through extensive engine dynamometer tests under various engine operations. Represented as curves and contour maps of output power, fuel consumption, and different emissions at different engine speed and output torque, these models (or simply called engine maps) are the keys to powertrain system design and operation control.

Heavy-duty transportation applications such as marine vessels, mining truck, and locomotive, prefer diesel engine as a primary power source for its higher efficiency and reliability. In recent years, natural gas (NG) engines saw broader applications due to their near-zero soot (particular matter) and lower CO_2 emissions, as well as lower fuel cost.

Up to today, a systematic study and wide collection of the power performance, fuel efficiency and emissions models for heavy-duty diesel and NG engines are not publicly available. To overcome this first obstacle in modelling and design a hybrid electric marine propulsion system, the UVic Clean Transportation team has introduced a fast and relatively straightforward approach to form these models. In particular, the emission models on carbon dioxide (CO_2), nitrogen oxide (NO_x), carbon monoxide (CO), and hydrogen carbon (HC) for NG engines supported the quantitative emission evaluations and development of the new NG engine hybrid electric propulsion system and control technique.

D1 Collection Of Diesel Engine Data

The engine maps, including fuel consumption map and emission map (NOx, CO, HC), need complete engine dynamometer tests under different engine testing cycles. The National Renewable Energy Laboratory (NREL) and Argonne National Laboratory (ARL) under the U.S. Department of Energy (US DOE) have carried out extensive tests, produced some of these maps, and included them in the powertrain system tools, ADVISOR (Advanced Vehicle Simulator) and AUTONOMIE. ADVISOR was originally made available to the public for research and education. These ready-to-use engine maps are listed in Table D - 1.

Table D - 1 AUTONOMIE ready-to-use diesel engine list

Year	Model	Manufacturer	Emission Map	Efficiency Map	Rated Power/kW	Speed Range/rpm
1998	-	-		x	37	1500-5000
1998	-	-		x	54	1000-5000
2001	-	Mercedes	x	x	60	1200-4200
1999	-	Volkswagen	x	x	67	800-4400
1998	-	Audi		x	88	1000-4500
2002	OM611	Mercedes	x	x	92	1250-4250
1998	-	-		x	119	1000-3500
2000	Powerstroke	Navistar T444E	x	x	163	700-2800
1999	-	-		x	171	650-2300
1999	-	-		x	205	650-2100
2002	3126E	Caterpillar	x	x	205	700-2500
1998	-	Cummins		x	246	650-2000
2002	DM4840 02	Caterpillar		x	250	650-2100
2001	DM6006 02	Caterpillar		x	321	650-2100
2002	DM4908 01	Caterpillar		x	324	650-2100
1998	Series 60	Detroit Diesel Corp		x	330	1200-2100

(the year means data created year, which means data should be older than created time. For more detailed source and time, please refer to the appendix.)

D2 General Engine Model Scaling Method

The original engine map models are limited in both types and sizes. Many pieces of research on hybrid electric vehicle components size optimization were carried out using the engine model scale method used in ADVISOR. The scaling method consists of the following three steps:

1) Define the speed scaling factor: tar_speed_range= orig_speed_range*speed_scale_factor;
2) Define the torque scaling factor: tar_torque_range= orig_torque_range*torque_scale_factor;
3) The power scaling factor equals to the speed_scale_factor multiplies torque_scale_factor.

The power scaling factor was always defined first, and the speed range is then scaled to match the required speed. Based on the power and the speed scaling factors, the max torque and torque range are also scaled to match the target. The following example demonstrates the scaling method based on the original Caterpillar 3126E engine to the S12R marine engine.

The CAT 3126E engine is rated at 205 kW with speed range from 700 rpm to 2,400 rpm. The maximum torque is 1,085 Nm at 1,440 rpm. Our targeted engine is rated at 1,190 kW. The power scale factor is then 1,190/205 = 5.8. To match the engine speed range (assuming the engine speed ranges from 600 to 1,800 rpm, since the collected data shows that the engine speed during docking is about 596 rpm and the engine speed can reach up to 1,800 rpm. The speed factor is 1.33. Consequently, the torque scale factor is 4.35. The new engine brake specific fuel consumption can thus be obtained from the scaled index vector, speed range and torque range.

The engine map, file fc_fuel_map_gpkWh, is an 86x55 matrix indexed by the input speed and torque. For the original CAT 205 kW engine, the input speed and torque is a speed vector of

[700:20:2,400], and torque vector of [1:20:1,081], respectively. The maximum torque is an 86x1 vector indexed by the speed vector. The scaled engine speed is calculated by multiplying the speed scale factor with the speed vector, and the scaled engine torque is obtained by multiplying the torque scale factor with the torque vector. The scaled engine maximum torque is also the product of torque scale factor and maximum torque. Since the fuel map is in g/kWh, the matrix remains unchanged, but values are indexed by different inputs.

It is obvious that the speed range cannot match the targeted engine speed range. Another method has been introduced to eliminate the speed mismatch in three steps.

1) Define the idle speed scale factor: tar_idle_speed/orig_idle_speed;
2) Define the maximum speed scale factor: tar_max_speed/orig_max_speed;
3) According to the length of the speed vector, calculate a scale vector between the idle speed scale factor and the maximum speed scale factor, and scale the speed range proportionally.

A matched speed range is obtained. The power scale and torque scale can be matched using the same method.

D3 NG ENGINE SCALING METHOD

The method for NG engine performance and emission map scaling is based upon literature on engine experiments and technical review [1] , [2] . The following rules have been used:

- NG engine speed = scaled diesel engine speed;
- NG engine torque = scaled diesel engine torque * NG engine torque factor;

  The torque factor of the NG engine includes the engine torque loss when fueled by the NG and diesel (pilot fuel) blend (NG accounts 70% of fuel mass and diesel pilot fuel contributes to the rest 30%). Traditionally NG engines have been reported to have 15-30% less peak power. While experimental results on the most recent and most advanced NG engine technology showed a torque loss ranges from 3% to 6%. In this work, this NG engine power loss compensator factor is set to be 5%.

- NG engine BSFC = scaled engine BSFC * NG BSFC factor;

  NG BSFC factor describes the engine efficiency loss in term of thermal efficiency. This value is set as 6.5%.

For the emission map, an emission factor map has been generated first to show how many times that an NG engine emits a specific pollutant over the corresponding diesel engine (shown as emission factor maps). Based on these estimations, the scaled NG engine emission maps are created.

D4 ERROR ANALYSES ON ENGINE SCALING

Using a document that describes the MITSUBISHI S12R-PTA engine data, including the drawings, radiator drawing, emission, noise and fuel consumption data, the engine scaling results are validated. Although the data were from a diesel-electric generator engine, while the engine

under study was a propulsion engine, the comparison can still illustrate the feasibility and usefulness of the presented model scaling method.

The comparison was done for the S12R to operate at 1,500 rpm with the results from several operating points, listed in Table D - 2.

Table D - 2 Errors of engine scaling results

Engine Power		Original	525-1800 (mismatched)		600-1800 (matched)	
PS	kW	BSFC/g/kWh	BSFC/g/kWh	Error%	BSFC/g/kWh	Error%
400	294.2	254.7945	263.3	3.34	260.2	2.12
600	441.3	236.9863	242	2.12	242.7	2.41
800	588.4	226.0274	224.4	-0.72	222.1	-1.74
1,000	735.5	216.4384	220.5	1.88	220.9	2.06
1,200	882.6	212.3288	217.2	2.29	215.8	1.63
1,400	1,029.7	210.9589	215.3	2.06	214.6	1.73
1,600	1,176.8	209.589	209.3	-0.14	207.9	-0.81

Using the absolute error values, the average error and standard deviation are calculated. In the mismatched speed method, the average error is 1.79, with a standard deviation of 0.9791. In the matched method, the average error is 1.79, with a standard deviation 0.4734. Both scaling methods produced reasonably accurate brake specific fuel consumption results, with less than 5% errors. The second scaling method is used in this contract research work to evaluate alternative marine propulsion systems for several reasons: a) the scaled engine speed can match the target engine speed; b) the error on the predicted maximum brake specific fuel consumption rate is about 2.41% that is less than the 3.338% of the mismatched engine speed method; and c) the average error and standard deviation are both better than mismatched engine speed method.

D5 DIESEL ENGINES AND THEIR EMISSION MAPS

37 kW Diesel Engine

Data from [Heywood, John B. Internal combustion engine fundamentals. Vol. 930. New York: McGraw-Hill, 1988.], page 859, Figure 15-22.

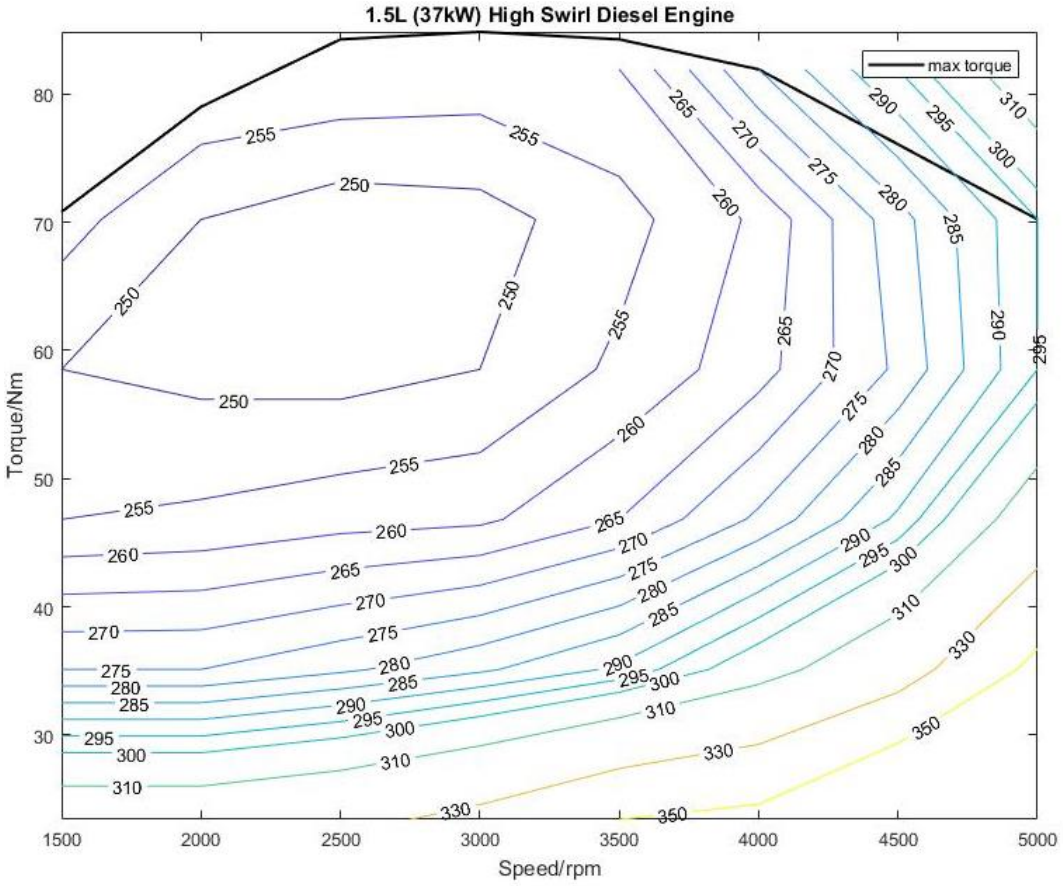

54 kW Diesel Engine

Data from [Heywood, John B. Internal combustion engine fundamentals. Vol. 930. New York: McGraw-Hill, 1988.], page 859, Figure 15-23.

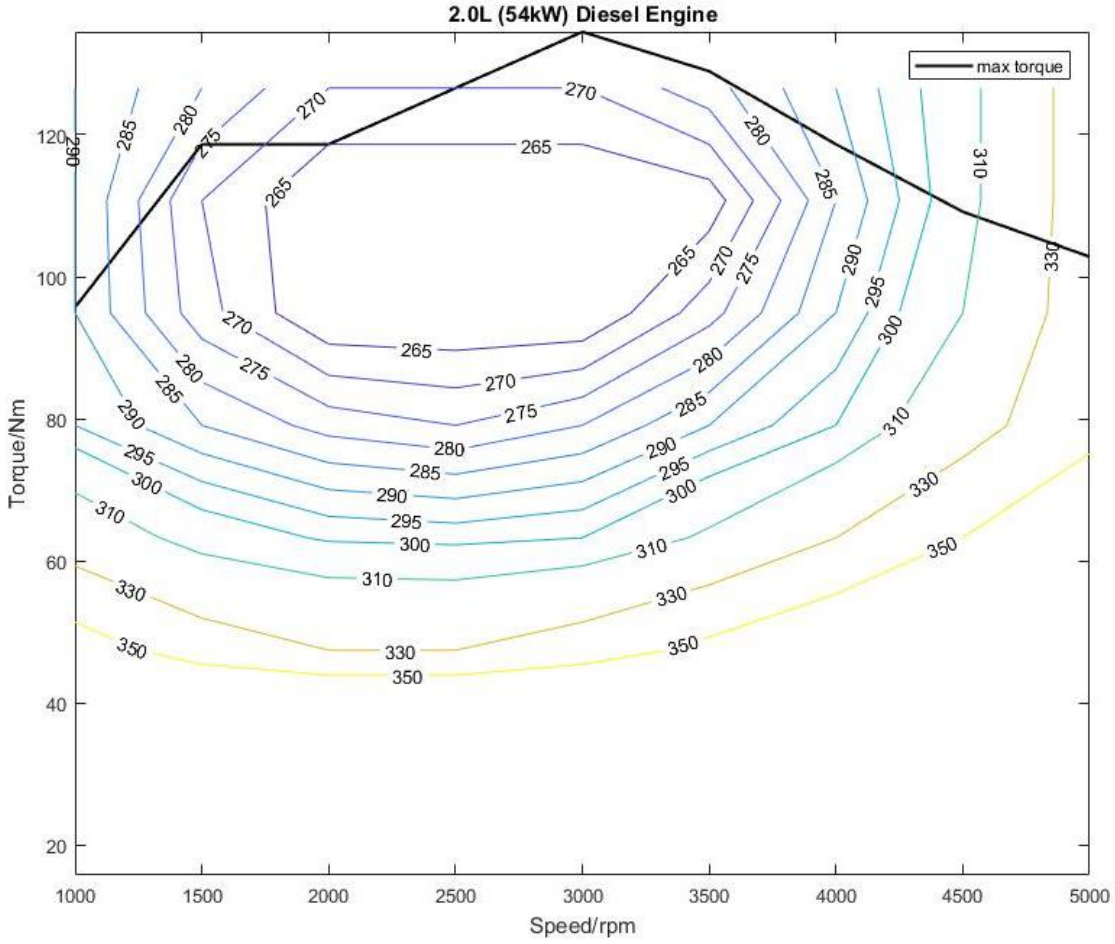

60 kW Diesel Engine

Data came from Scott Sluder of Oak Ridge National Laboratory. Data was gathered by Oak Ridge National Laboratory for the Mercedes 1.7L diesel engine.

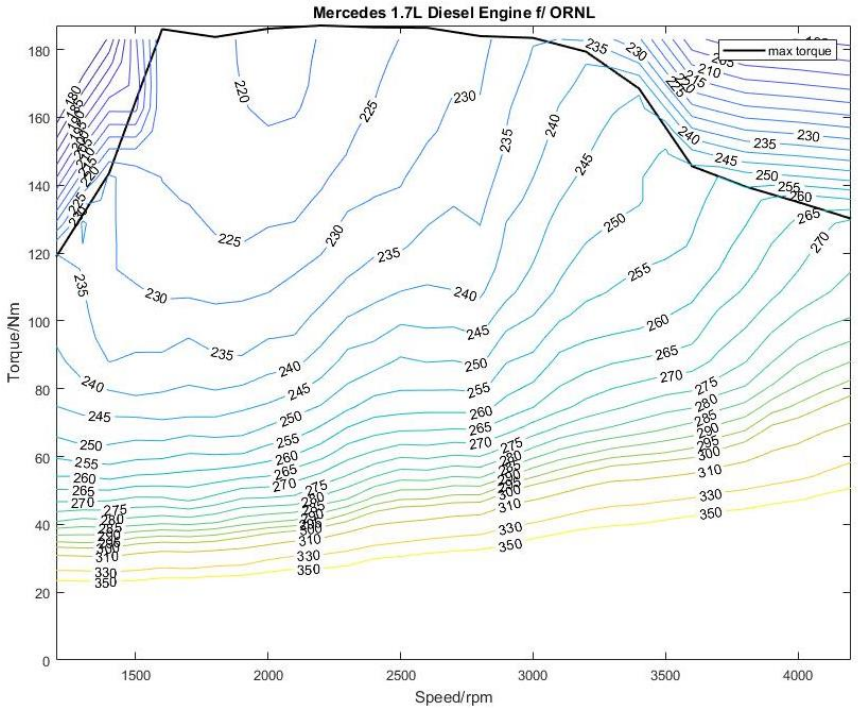

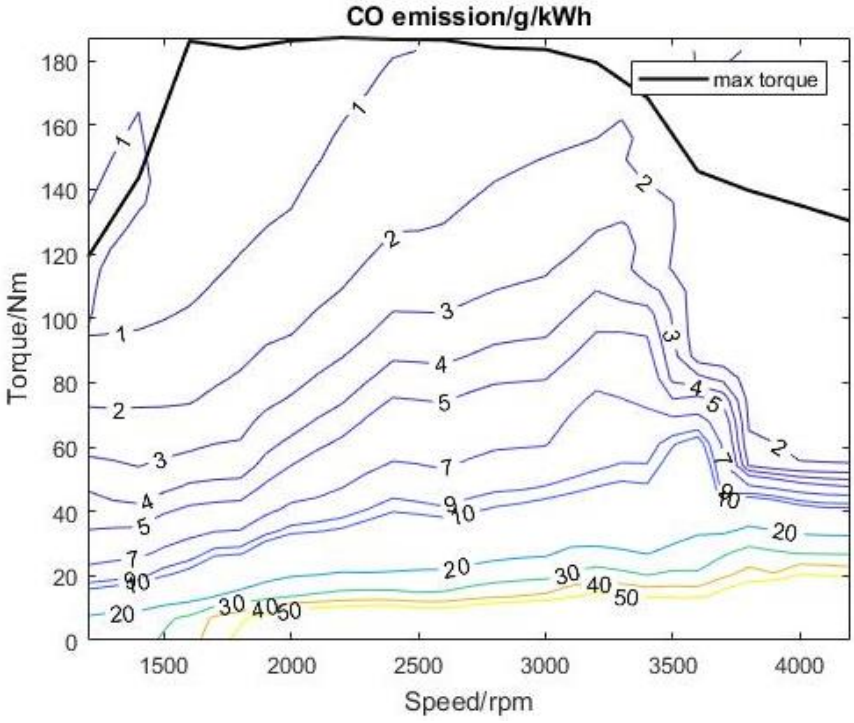

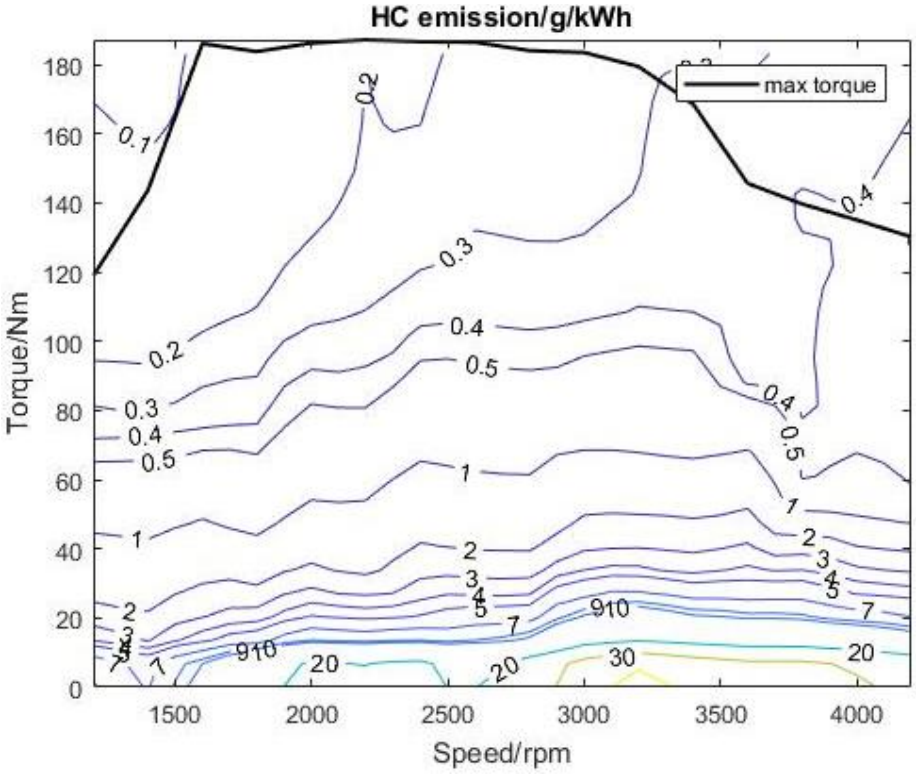
HC emission/g/kWh
max torque
Torque/Nm
Speed/rpm
0
20
40
60
80
100
120
140
160
180
1500
2000
2500
3000
3500
4000

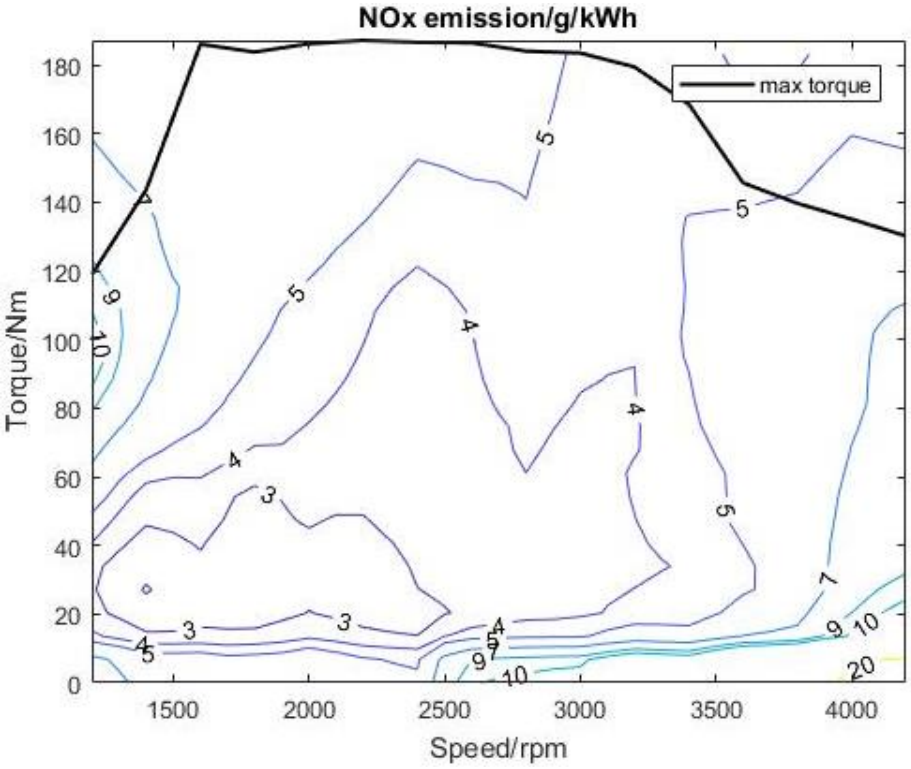
NOx emission/g/kWh
max torque
Torque/Nm
Speed/rpm
0
20
40
60
80
100
120
140
160
180
1500
2000
2500
3000
3500
4000

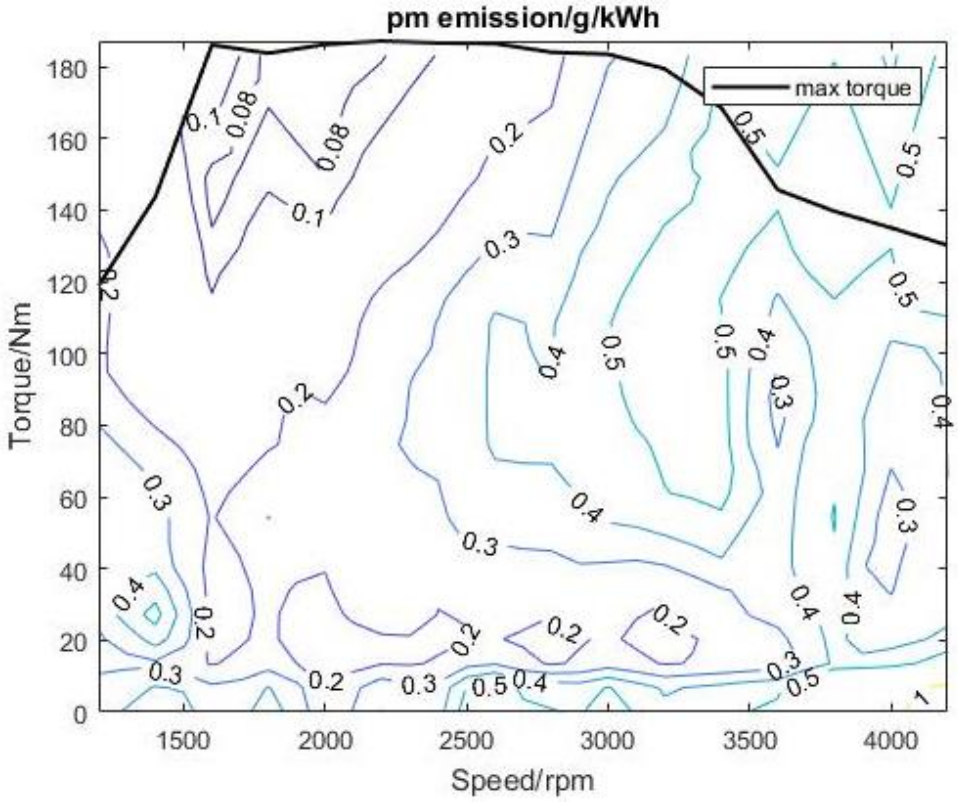
pm emission/g/kWh
max torque
Torque/Nm
Speed/rpm
0
20
40
60
80
100
120
140
160
180
1500
2000
2500
3000
3500
4000

67 kW Diesel Engine

Data came from Scott Sluder of Oak Ridge National Laboratory. Data was gathered by Oak Ridge National Laboratory for the Volkswagen 1.9L diesel engine.

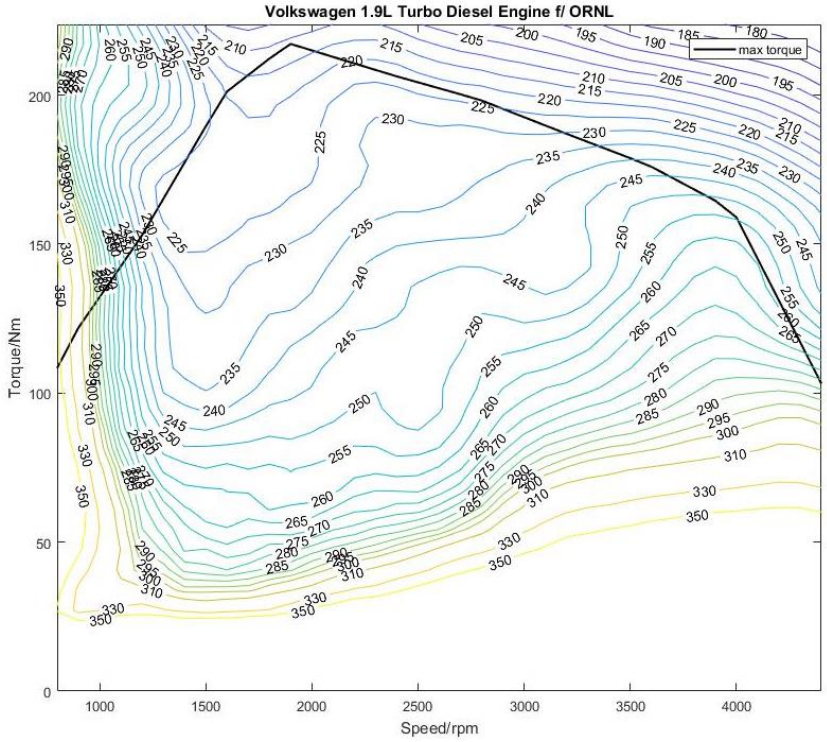

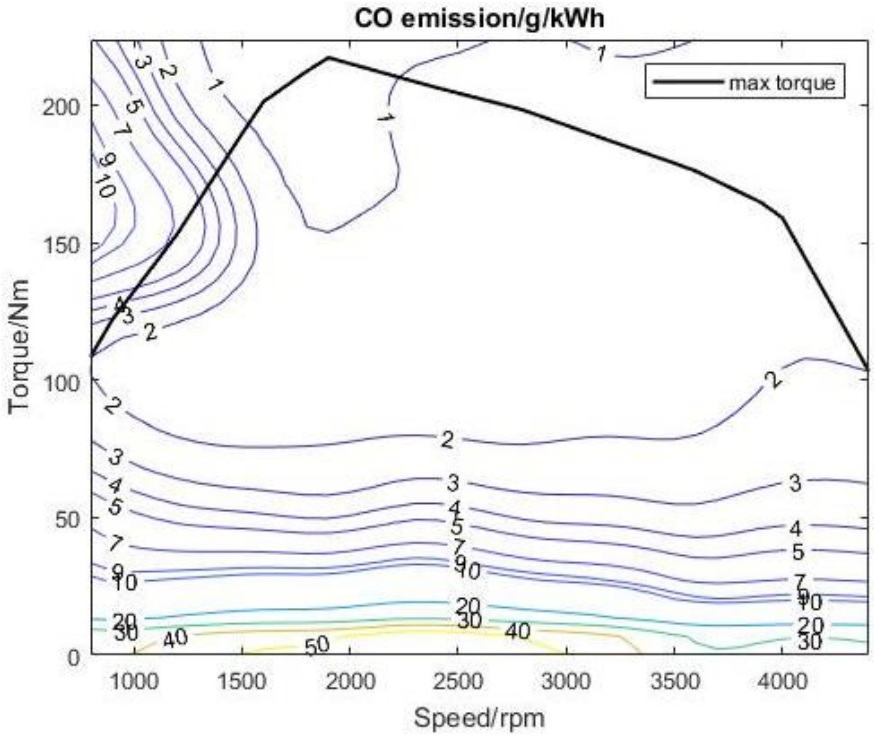

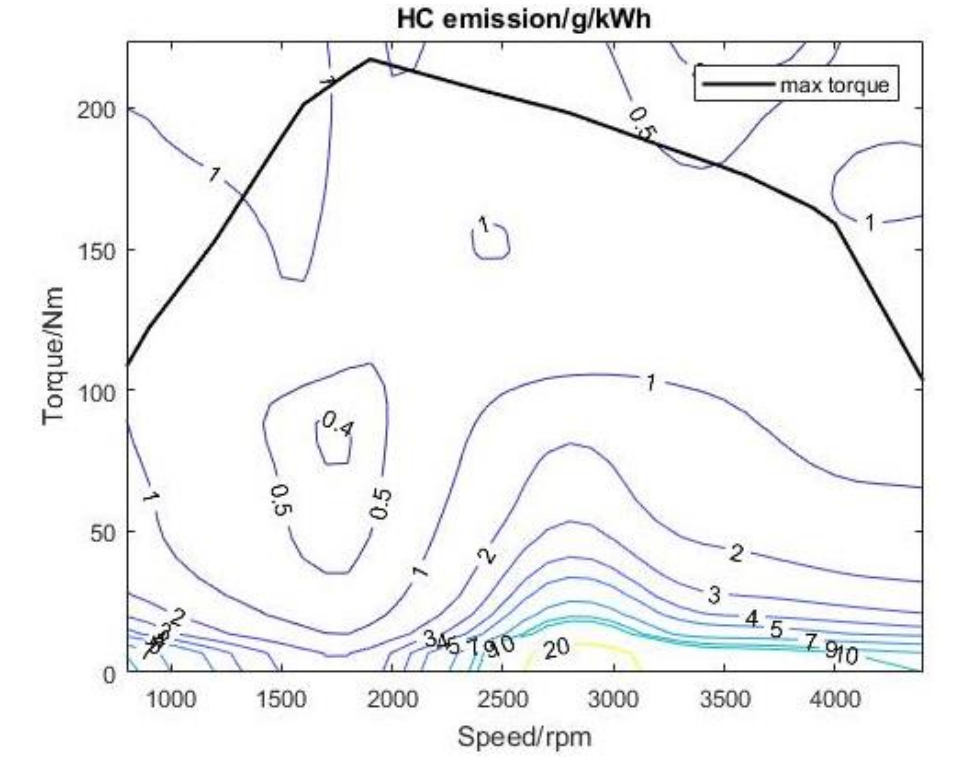
HC emission/g/kWh
max torque
Torque/Nm
Speed/rpm
0
50
100
150
200
1000
1500
2000
2500
3000
3500
4000

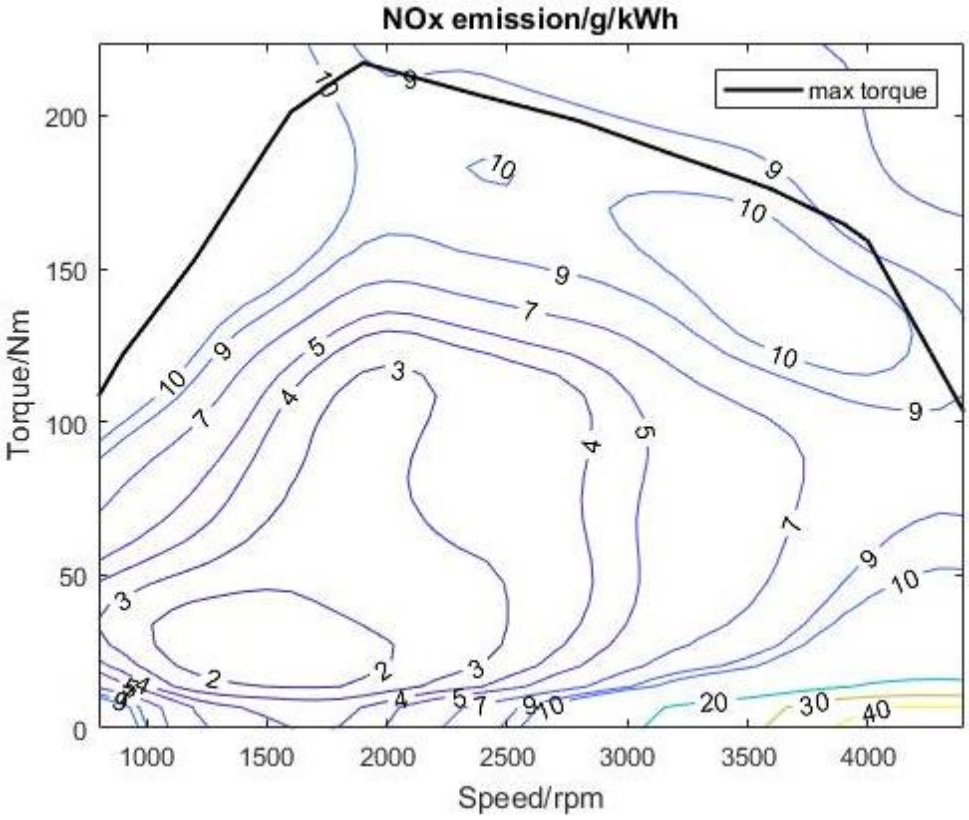
NOx emission/g/kWh
max torque
Torque/Nm
Speed/rpm
0
50
100
150
200
1000
1500
2000
2500
3000
3500
4000

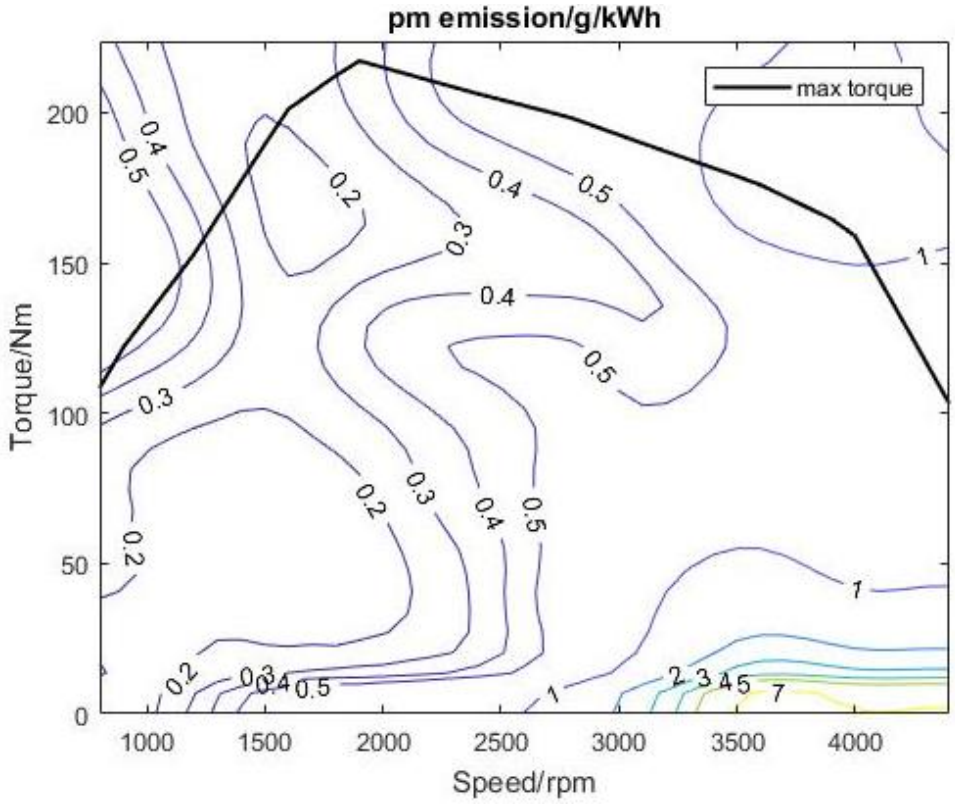
pm emission/g/kWh
max torque
Torque/Nm
Speed/rpm
0
50
100
150
200
1000
1500
2000
2500
3000
3500
4000
0.2
0.3
0.4
0.5
1
2
3
4
5
7

88 kW Diesel Engine

Data came from [Stock, Dieter, and Richard Bauder. The New Audi 5-Cylinder Turbo Diesel Engine: The First Passenger Car Diesel Engine with Second Generation Direct Injection. No. 900648. SAE Technical Paper, 1990.]

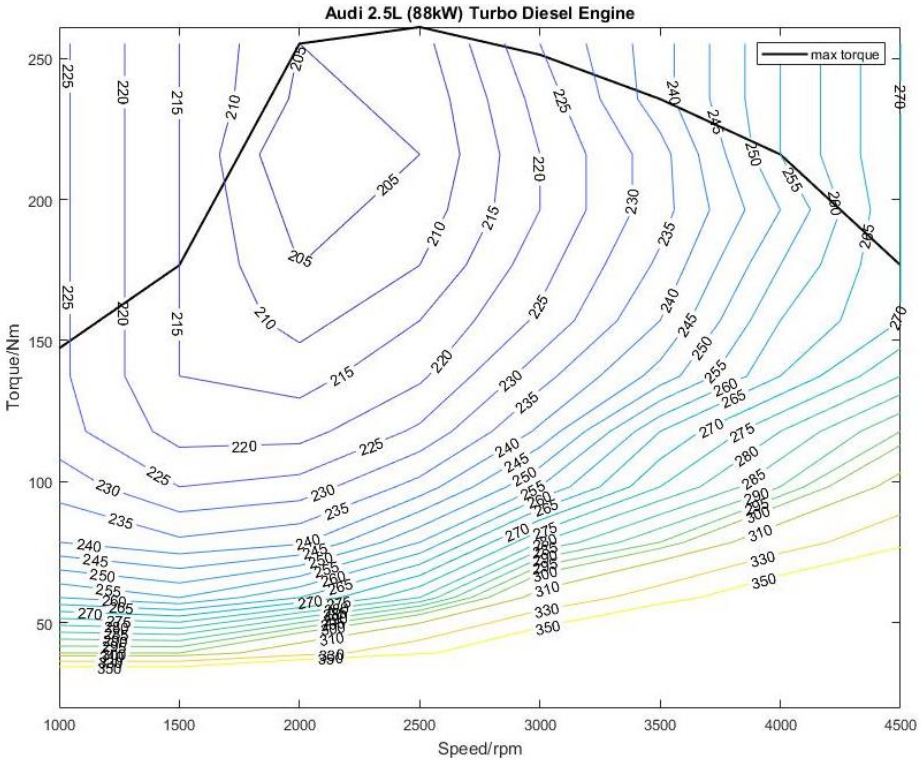

92 kW Diesel Engine

Data came from Southwest Research Institute tests on the Mercedes OM611 engine.

There is no available engine specifications and data collected time in ADVISOR file.

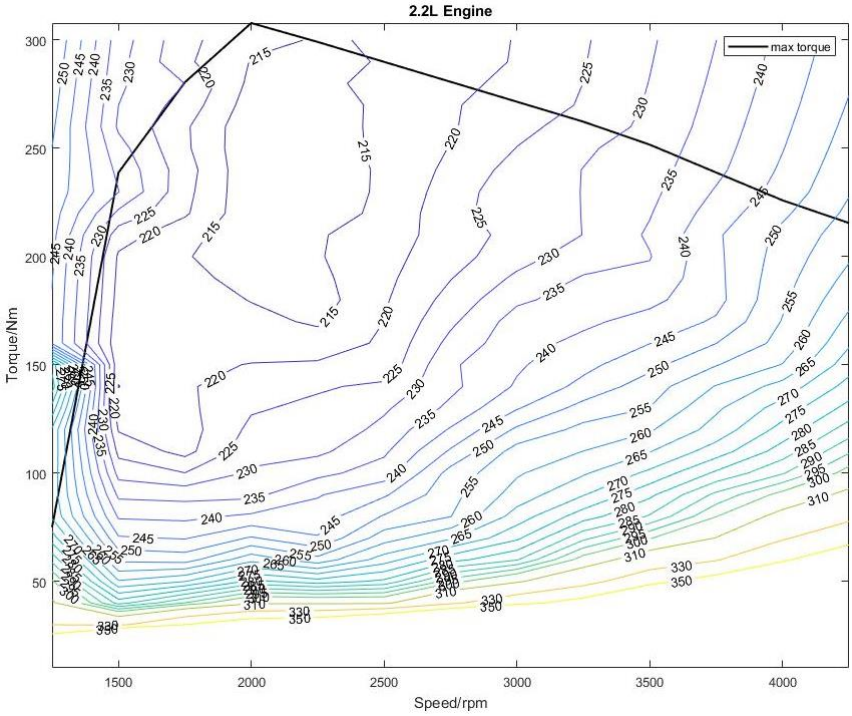

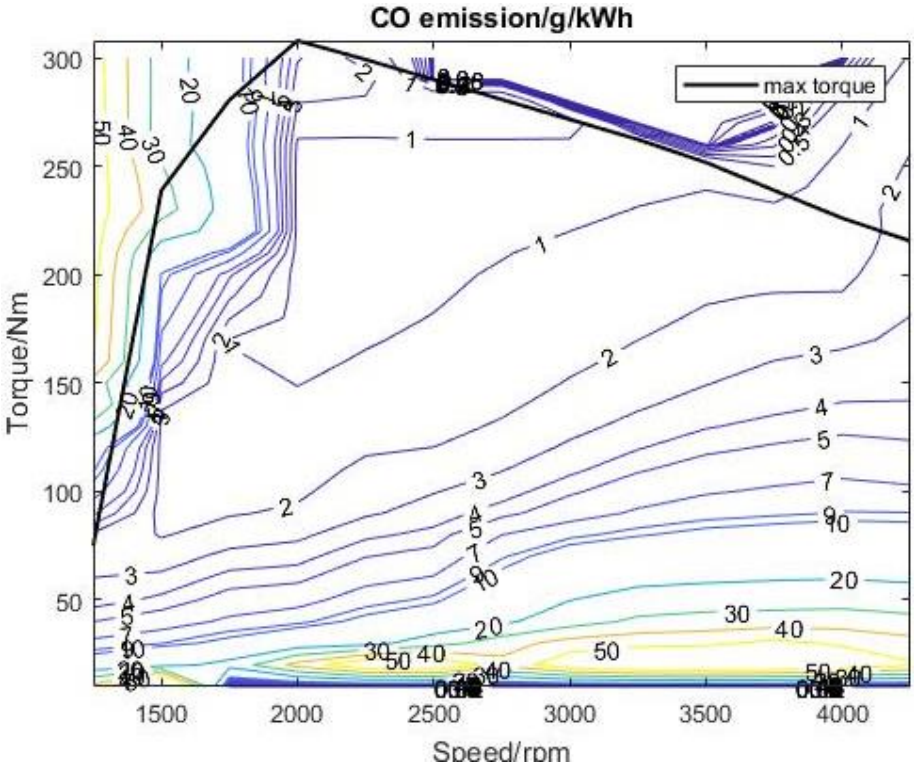

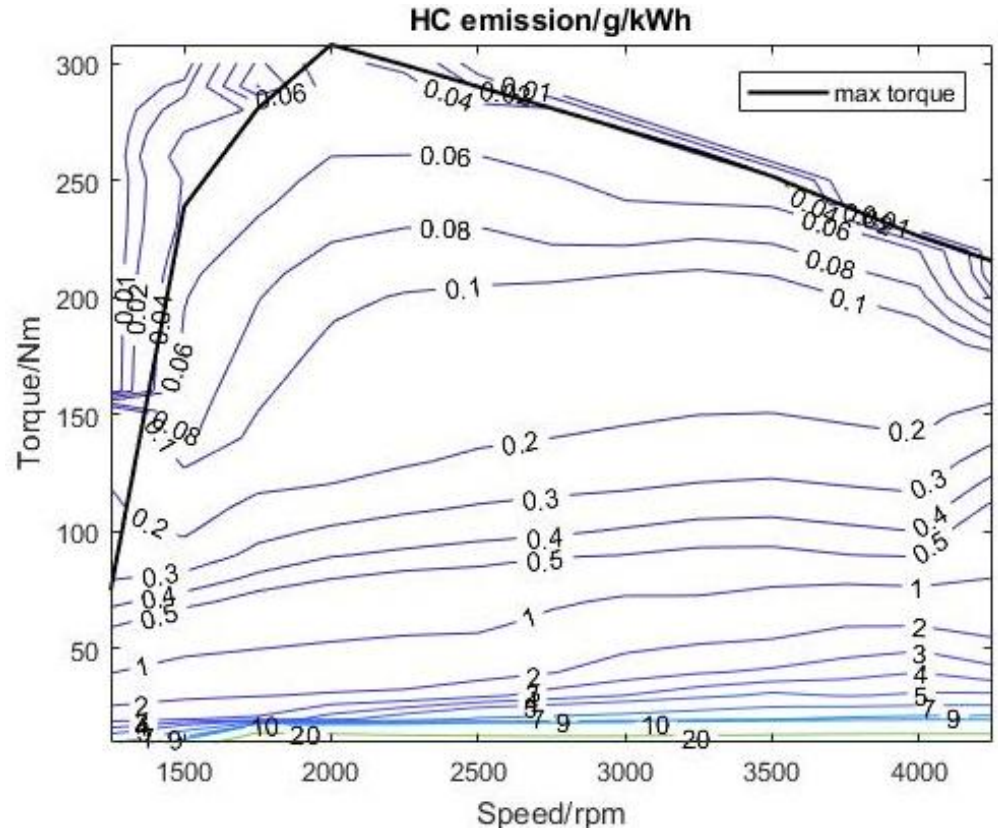
HC emission/g/kWh
max torque
Torque/Nm
Speed/rpm
300
250
200
150
100
50
1500
2000
2500
3000
3500
4000

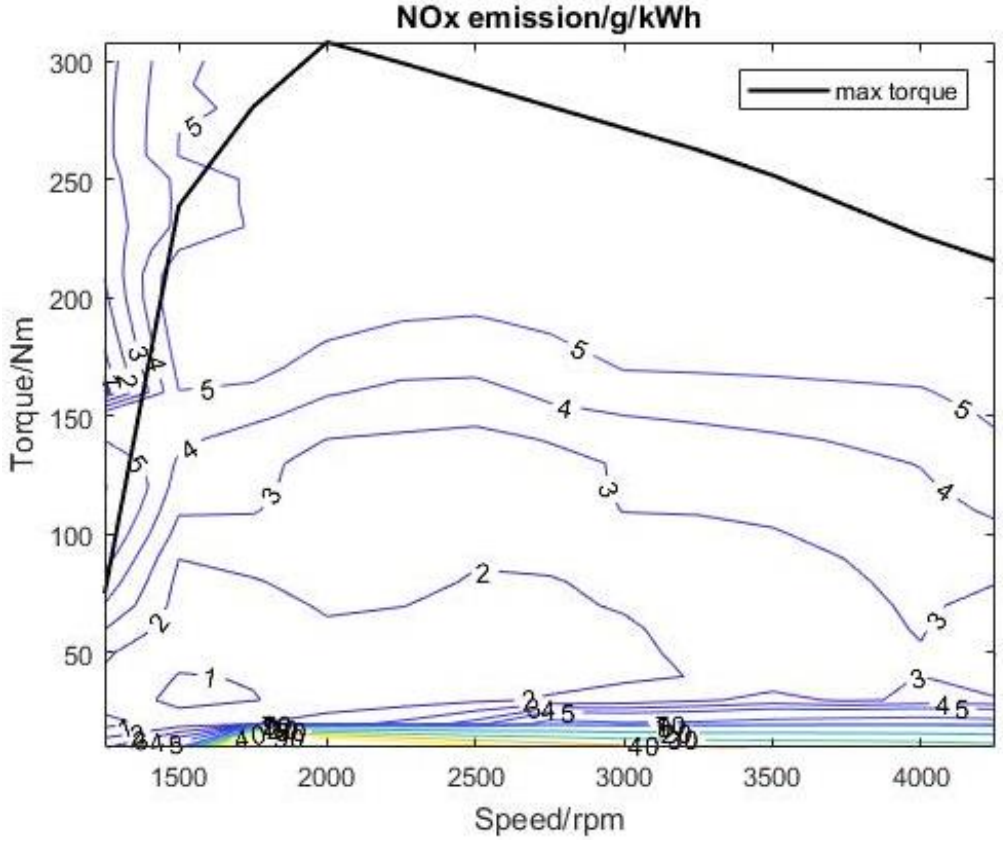
NOx emission/g/kWh
max torque
Torque/Nm
Speed/rpm
300
250
200
150
100
50
1500
2000
2500
3000
3500
4000

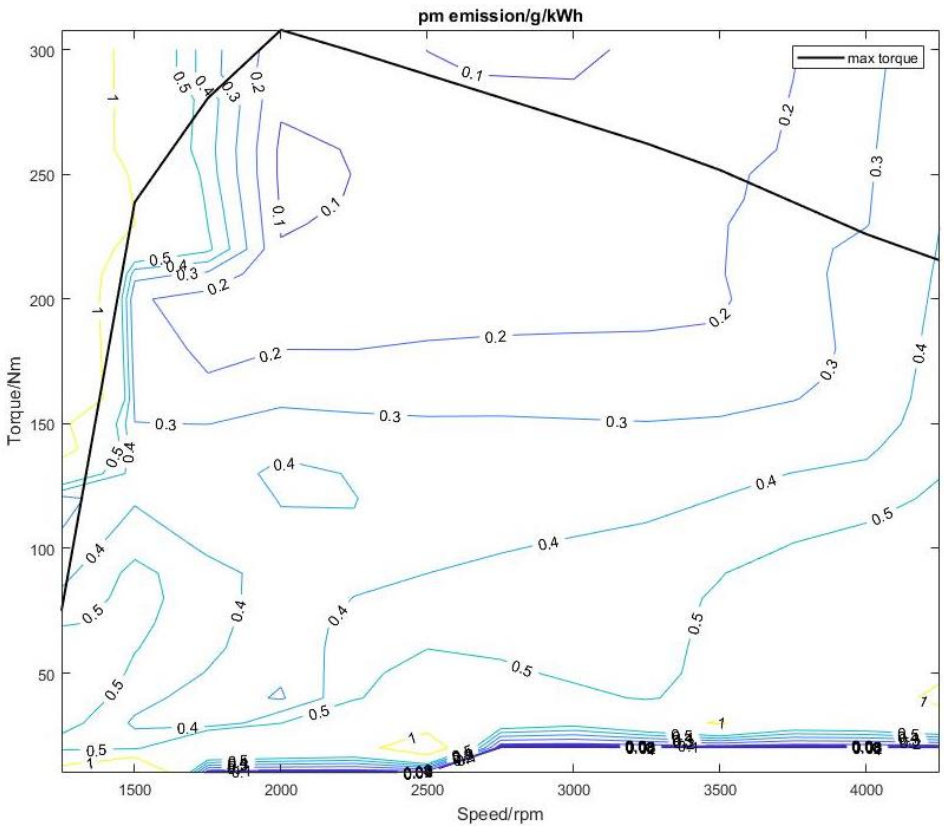
pm emission/g/kWh
max torque
Torque/Nm
Speed/rpm
300
250
200
150
100
50
1500
2000
2500
3000
3500
4000

119 kW Diesel Engine

Data from [Heywood, John B. Internal combustion engine fundamentals. Vol. 930. New York: McGraw-Hill, 1988.], page 859, Figure 15-21.

Engine Specs Table

Bore	102 mm
Stoke	100 mm
Compression Ratio	18
Max rated power	119 kW @ 3200 rpm
Peak Torque	400 Nm @ 2000 rpm

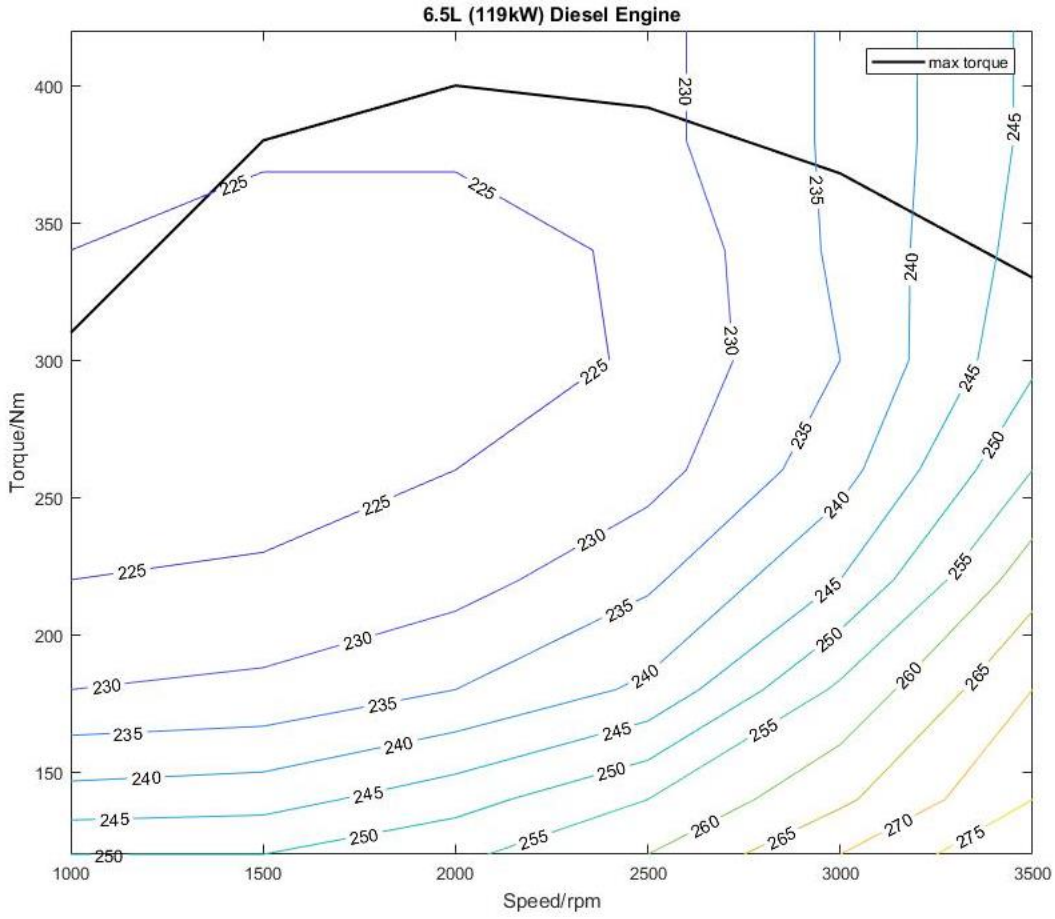

163 kW Diesel Engine

Engine data file for the Navistar T444/ Power stroke 7.3L engines tested on No. 2 Diesel Fuel. Data were collected under the DECSE program and the engines were tested on the OICA test matrix.

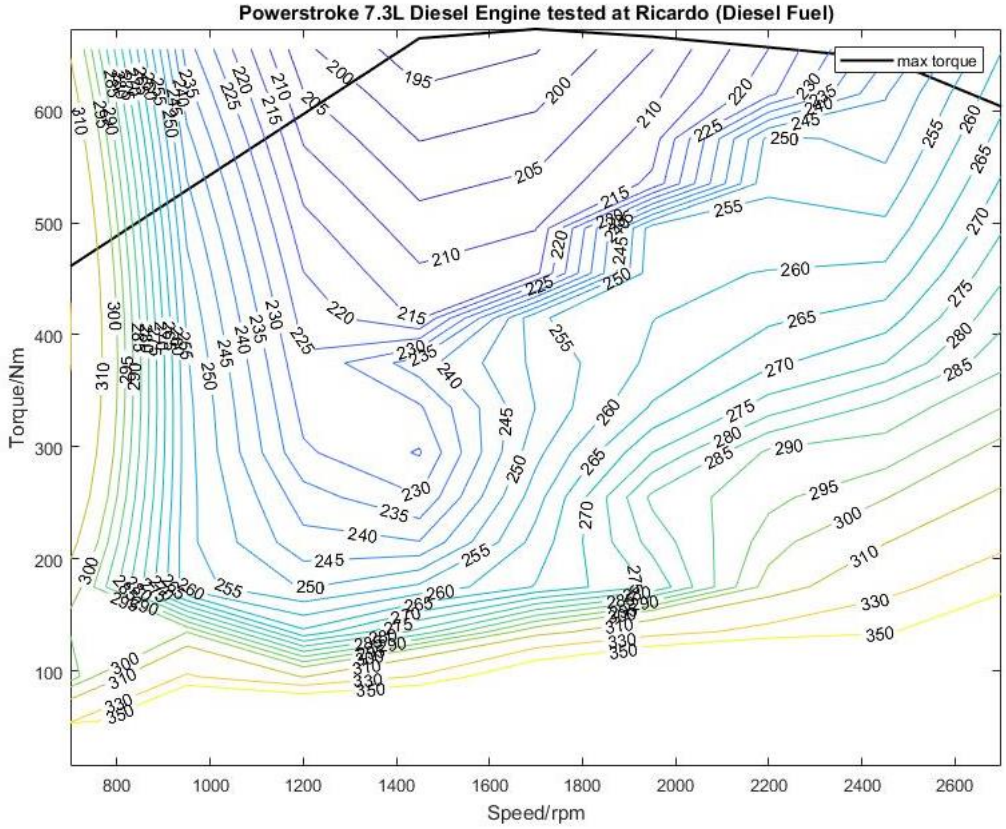

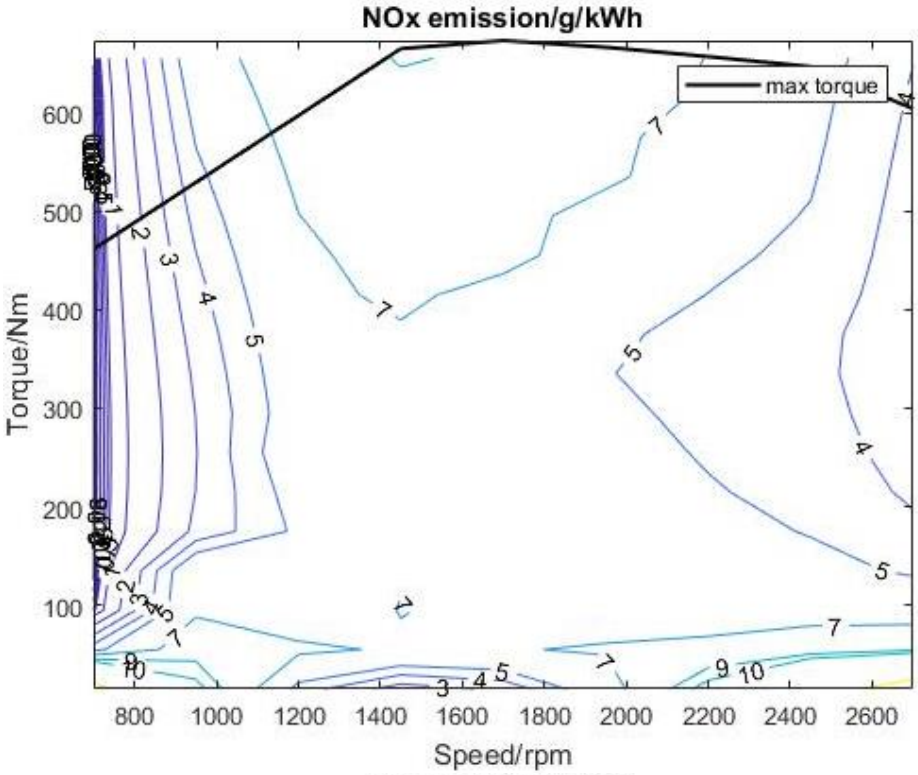
NOx emission/g/kWh
max torque
Torque/Nm
Speed/rpm
100
200
300
400
500
600
800
1000
1200
1400
1600
1800
2000
2200
2400
2600

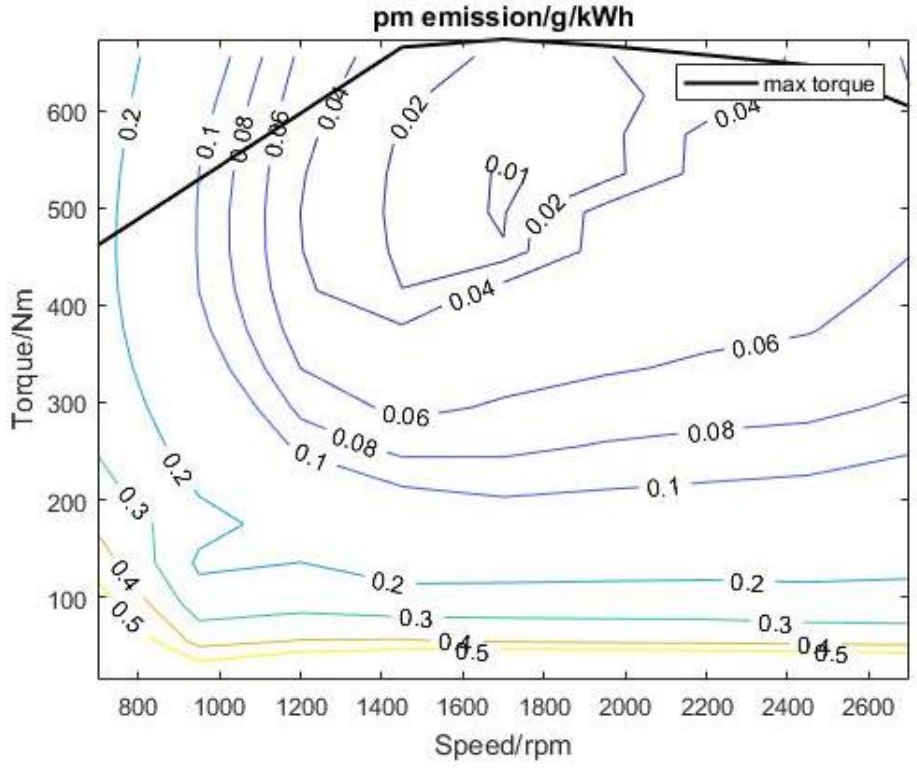
pm emission/g/kWh
max torque
Torque/Nm
Speed/rpm
100
200
300
400
500
600
800
1000
1200
1400
1600
1800
2000
2200
2400
2600

171 kW Diesel Engine

Engine maximum torque and speed range curve are based on data presented at SAE TOPTEC on the Future of Hybrid vehicles (5/99). Efficiency data based on the 330kW diesel engine.

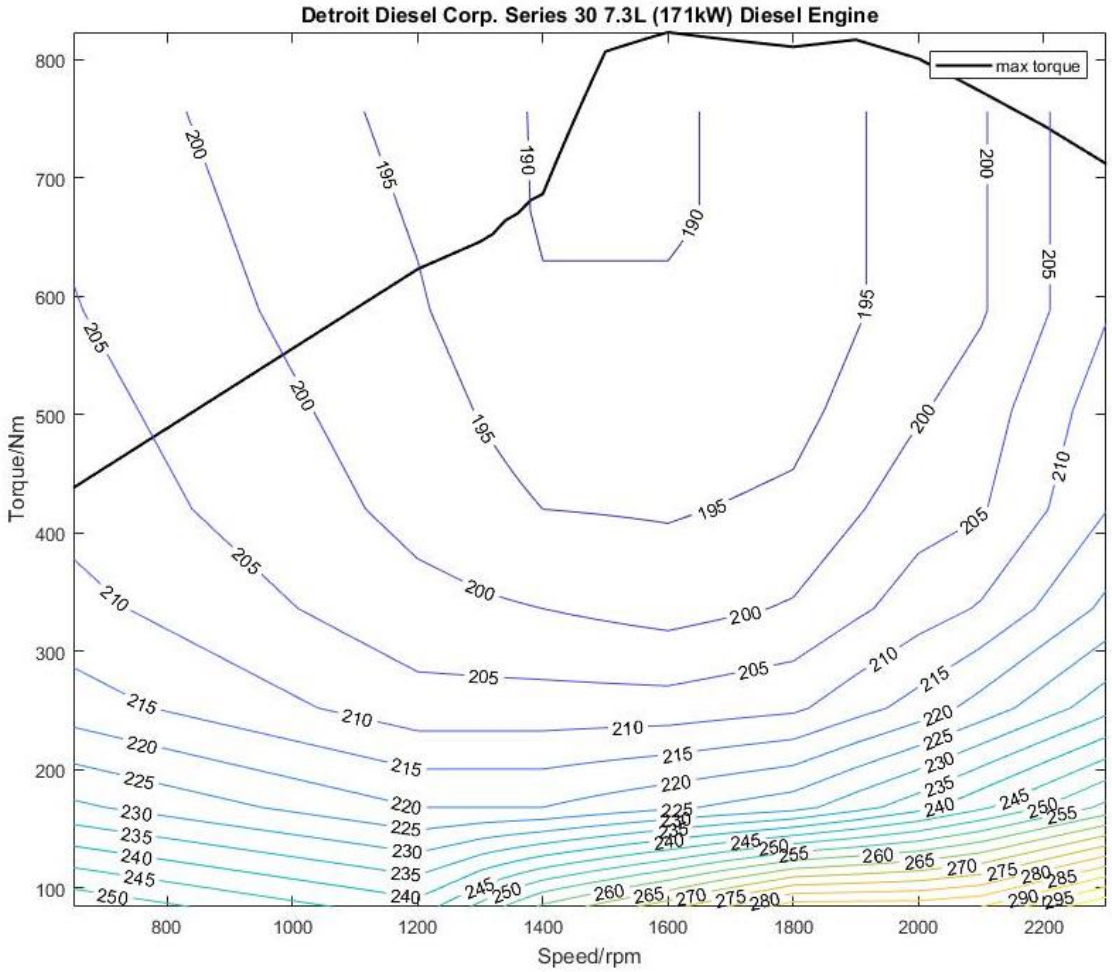

205 kW Diesel Engine

Engine maximum torque and speed range curve are based on data presented at SAE TOPTEC on the Future of Hybrid vehicles (5/99). Efficiency data based on the 330 kW diesel engine.

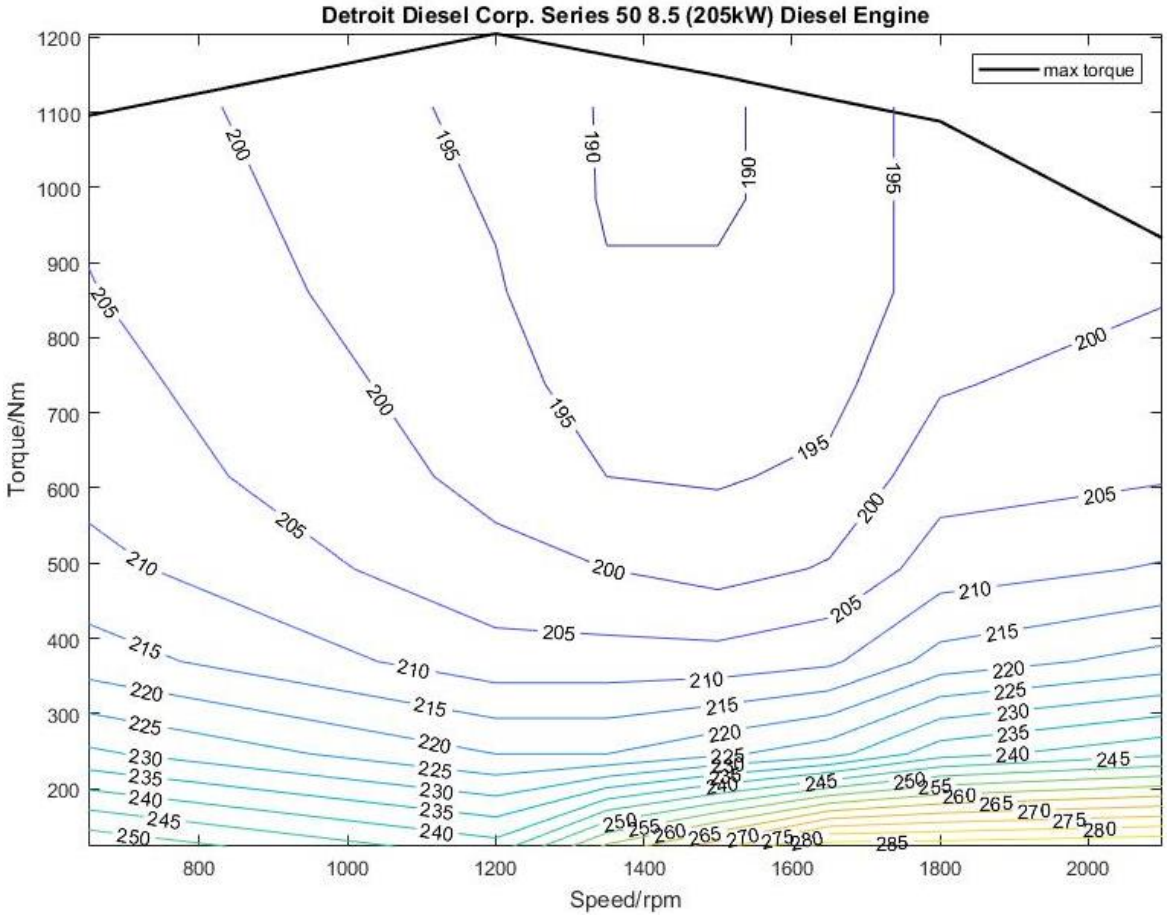

CAT 205 kW Diesel Engine

Engine data based on Caterpillar 3126E diesel engine, including fuel consumption at brake toque and 13 mode test data from Battelle over European Stationary Cycle test.

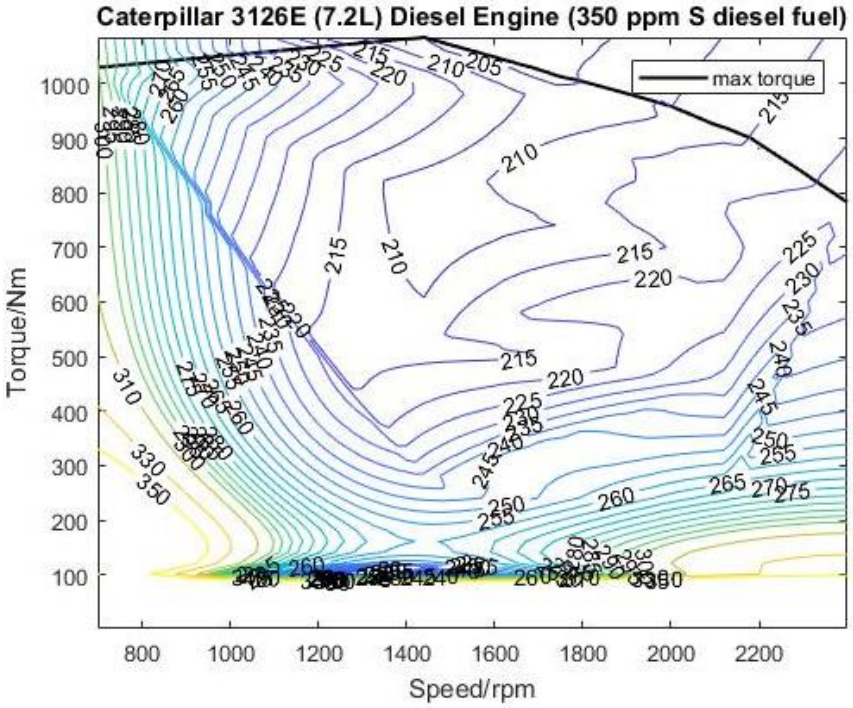

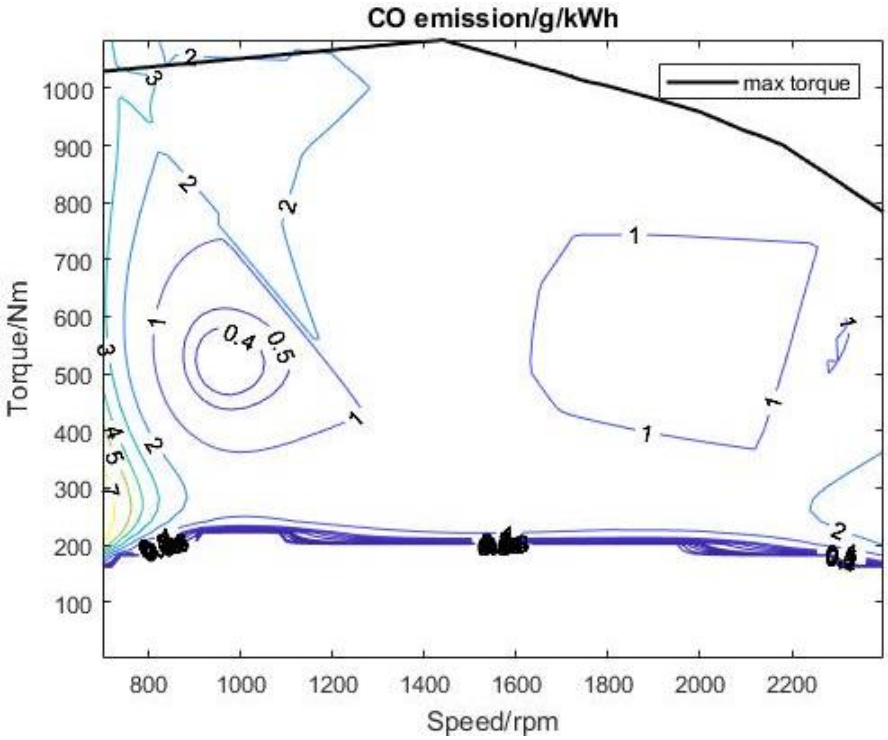

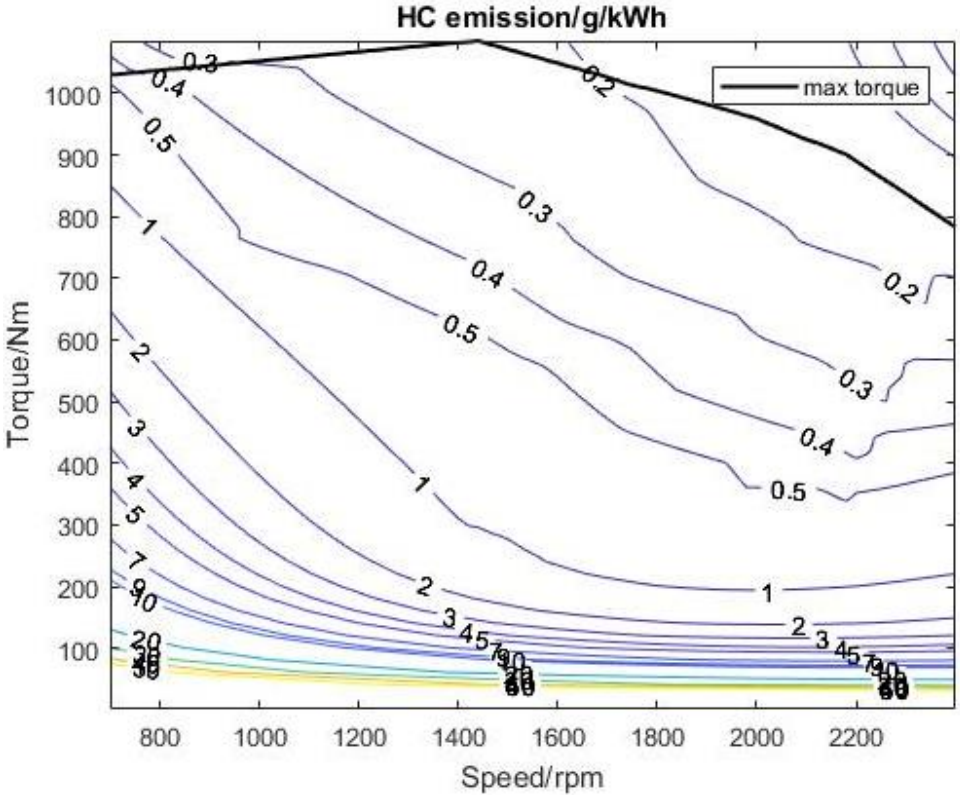
HC emission/g/kWh
max torque
Torque/Nm
Speed/rpm
800
1000
1200
1400
1600
1800
2000
2200
100
200
300
400
500
600
700
800
900
1000

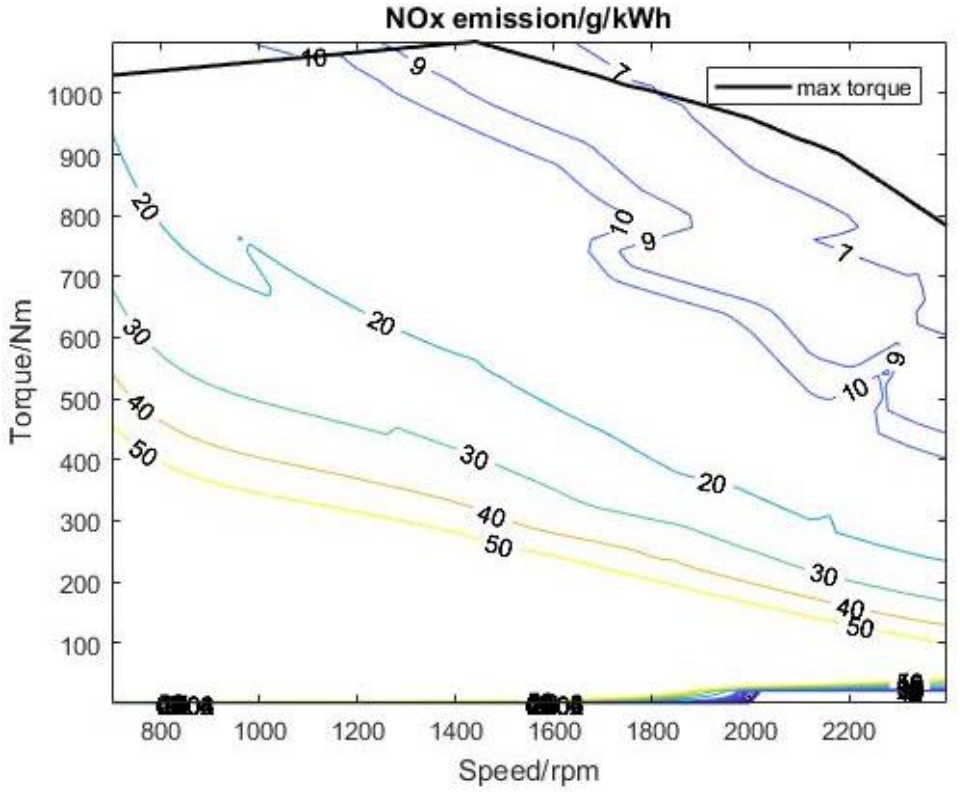
NOx emission/g/kWh
max torque
Torque/Nm
Speed/rpm
800
1000
1200
1400
1600
1800
2000
2200
100
200
300
400
500
600
700
800
900
1000

246 kW Diesel Engine

This engine maximum torque, speed range data and fuel consumption at maximum torque data are from the Cummins engine. Other efficiency points are estimated via other ADVISOR engine maps.

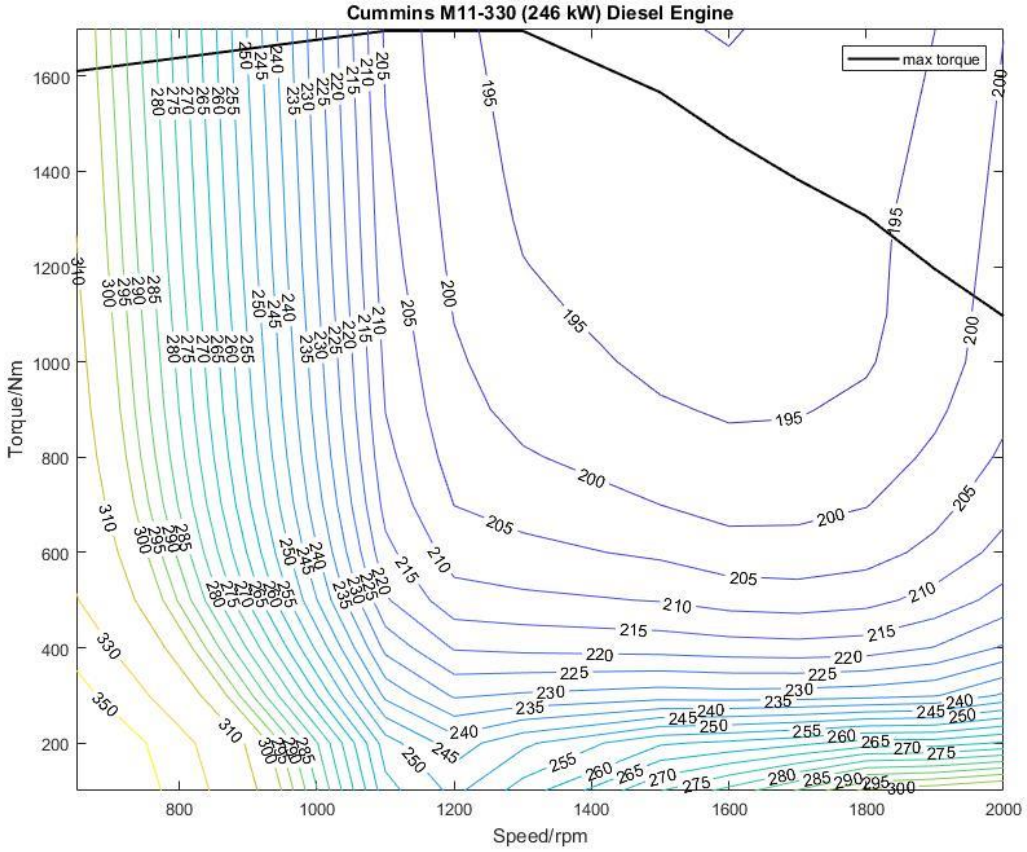

250 kW Diesel Engine

This engine maximum torque, speed range data and fuel consumption at maximum torque data are from Caterpillar engine DM4840 02. Other efficiency points are estimated by a 205kW diesel engine.

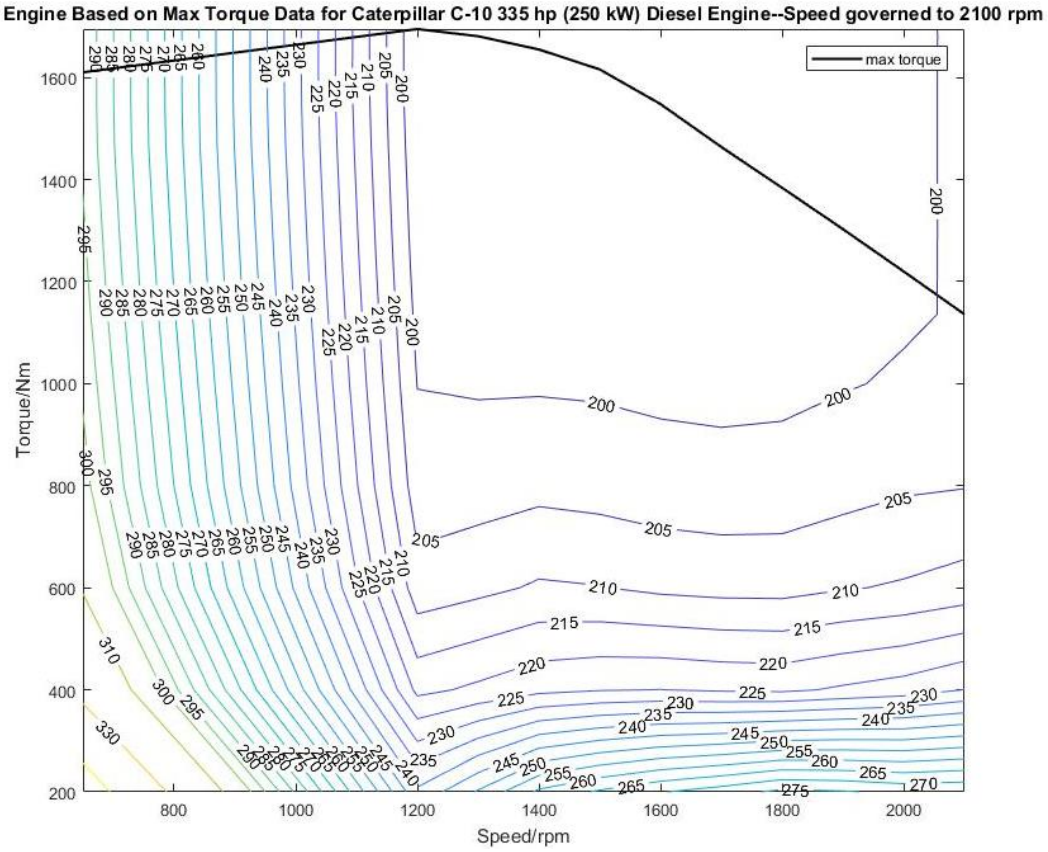

321 kW Diesel Engine

This engine maximum torque, speed range data and fuel consumption at maximum torque data are from Caterpillar engine DM6006 02. Other efficiency points are estimated by scaling a 303 kW diesel engine.

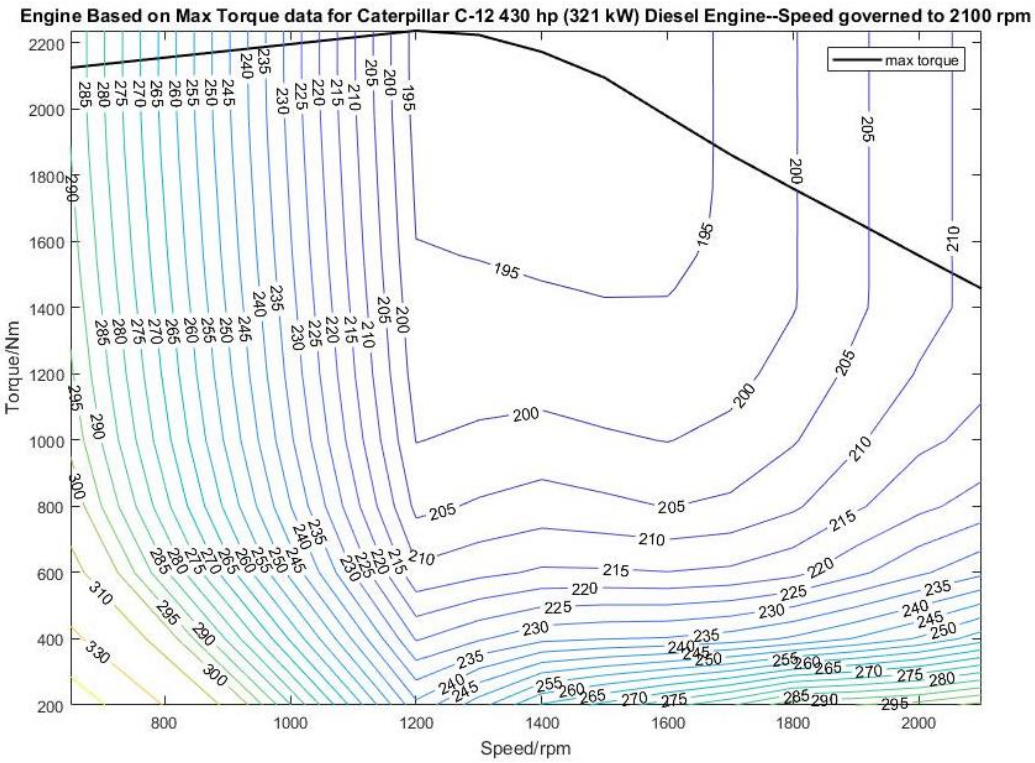

324 kW Diesel Engine

This engine maximum torque, speed range data and fuel consumption at maximum torque data are from Caterpillar engine DM4908 01. Other efficiency points are estimated by a 303 kW diesel engine.

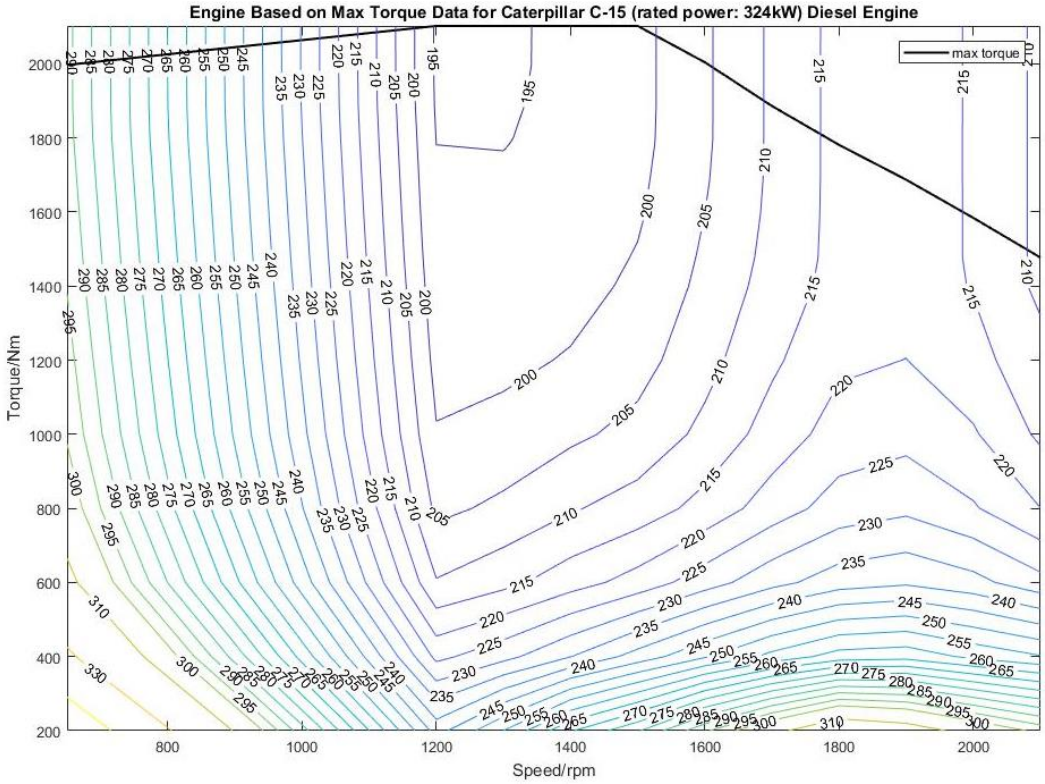

330 kW Diesel Engine

Data was interpreted from [Merrion, David F. Diesel engine design for the 1990s: the fortieth L. Ray Buckendale Lecture. SAE Publication SP-1011, 1994.] Figure 5.1, p.121, Detroit Diesel Corporation.

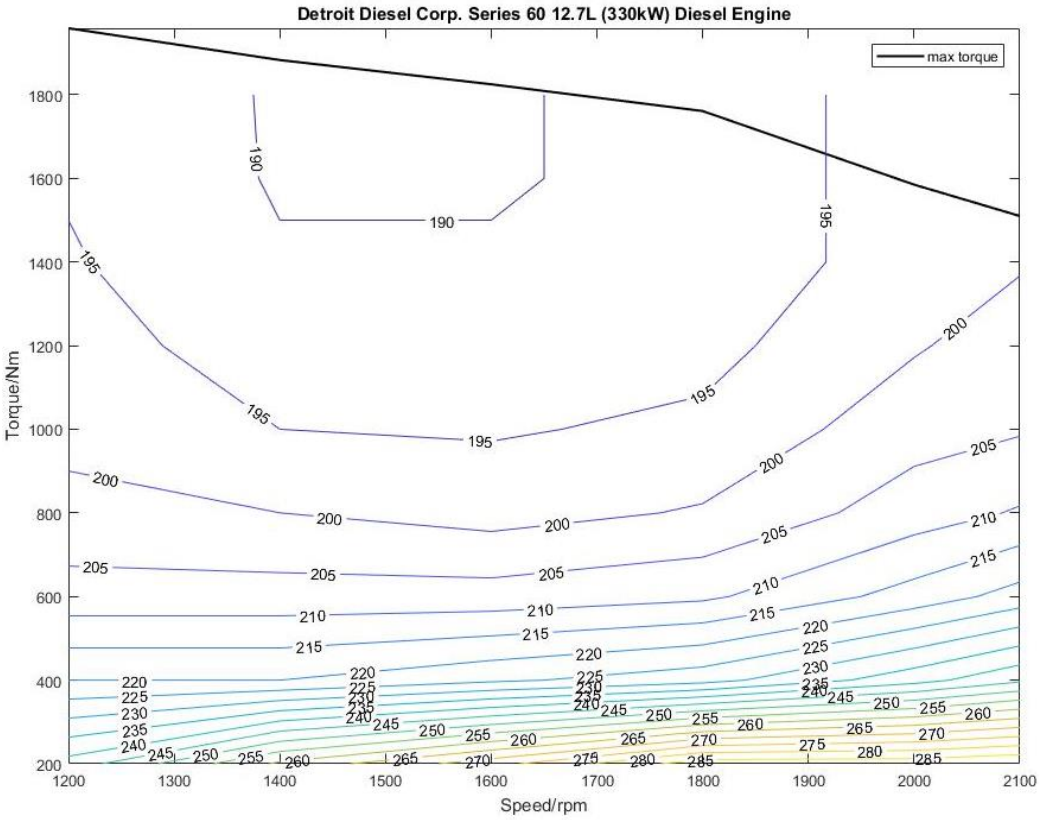

Scaled Diesel Engine for Skeena Queen:

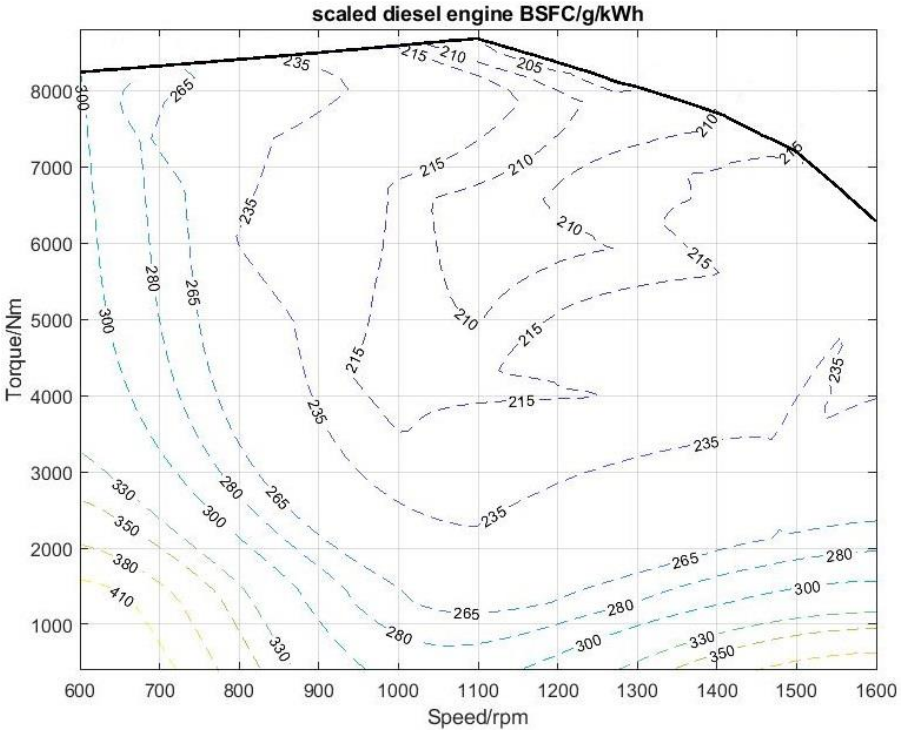

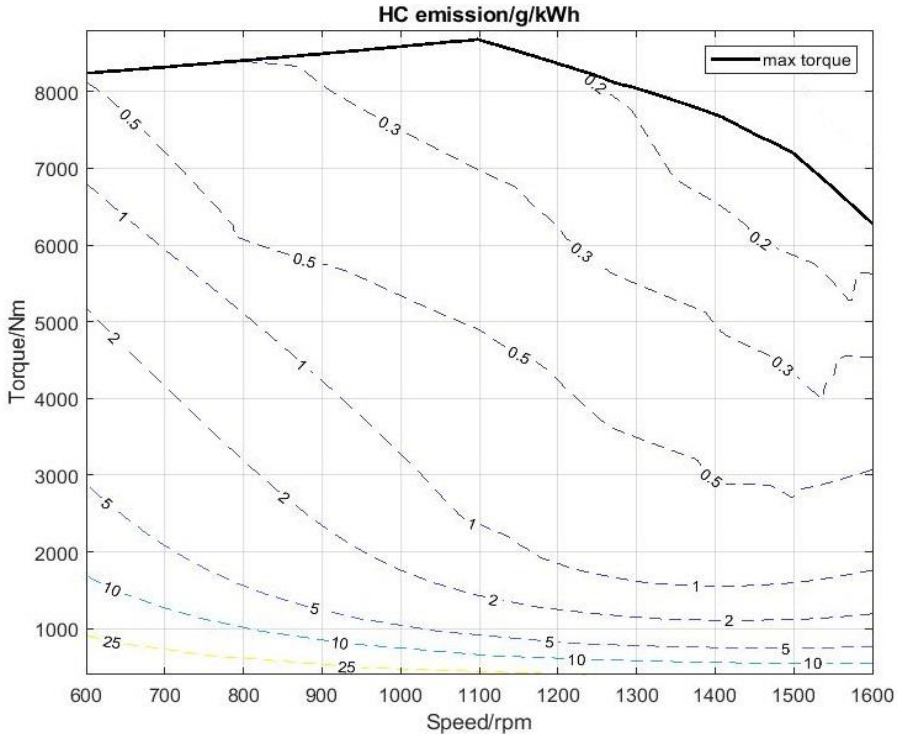

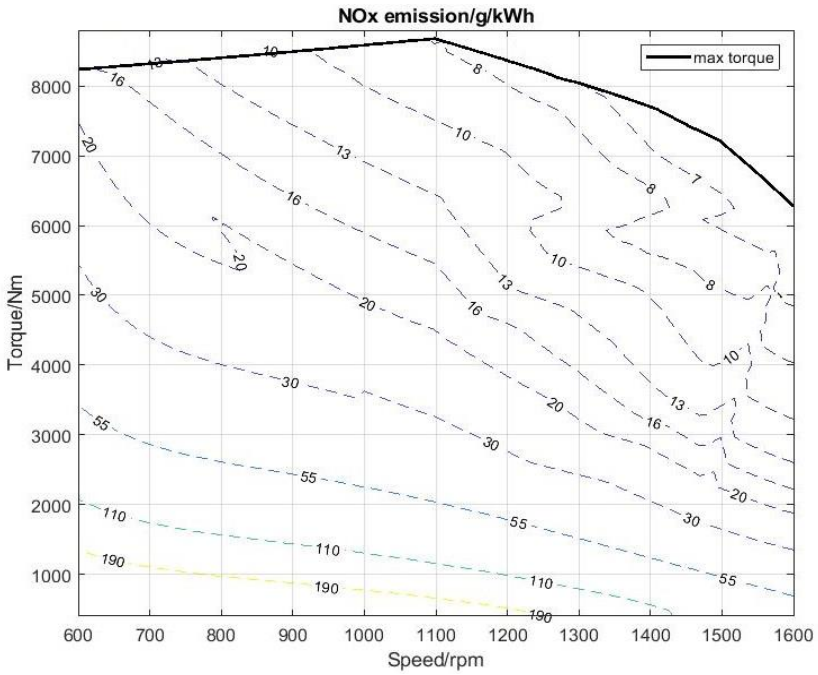

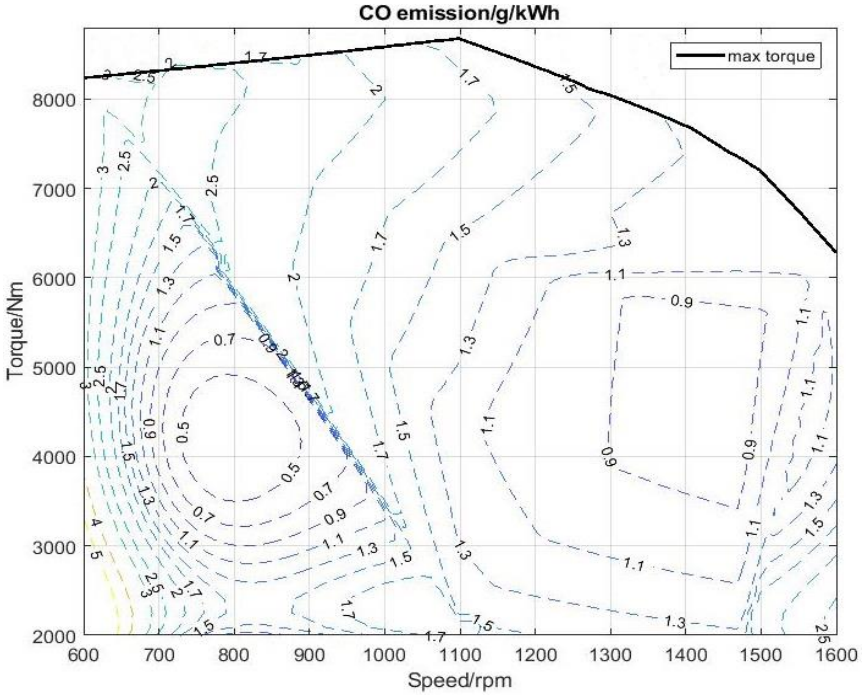

Note:

Since we don't have the efficiency data of the M6U engine, the data of a similar MITSUBISHI S12R diesel engine for marine are used, and the resulting error was estimated. The MITSUBISHI engine data file is attached.

NG Engine Efficiency and Emission Maps

The following NG engine maps are obtained using the methods discussed in Sections D1 and D3.

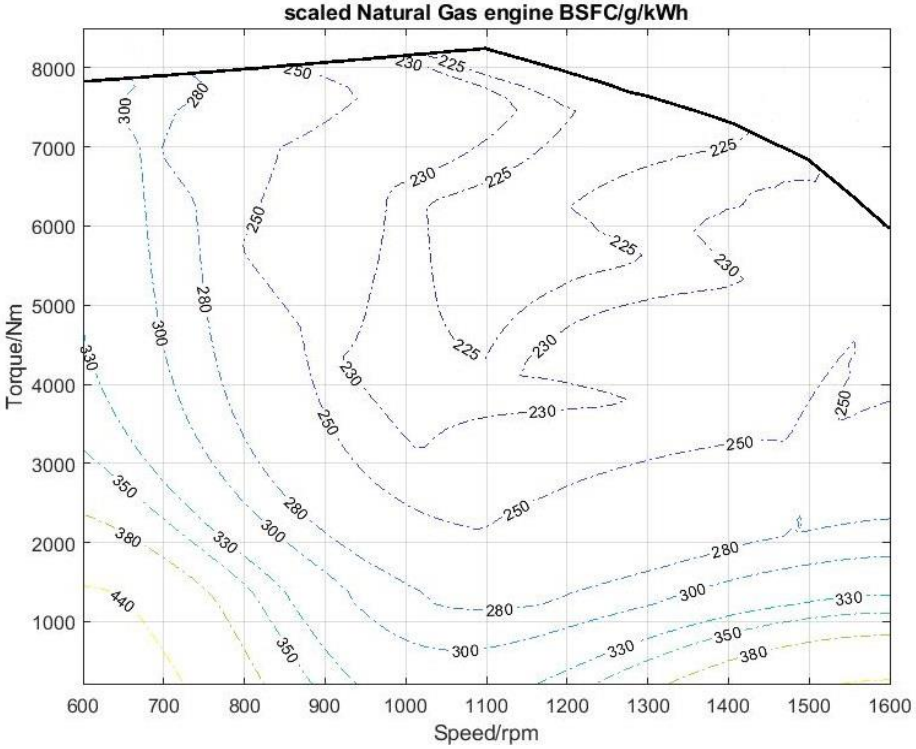

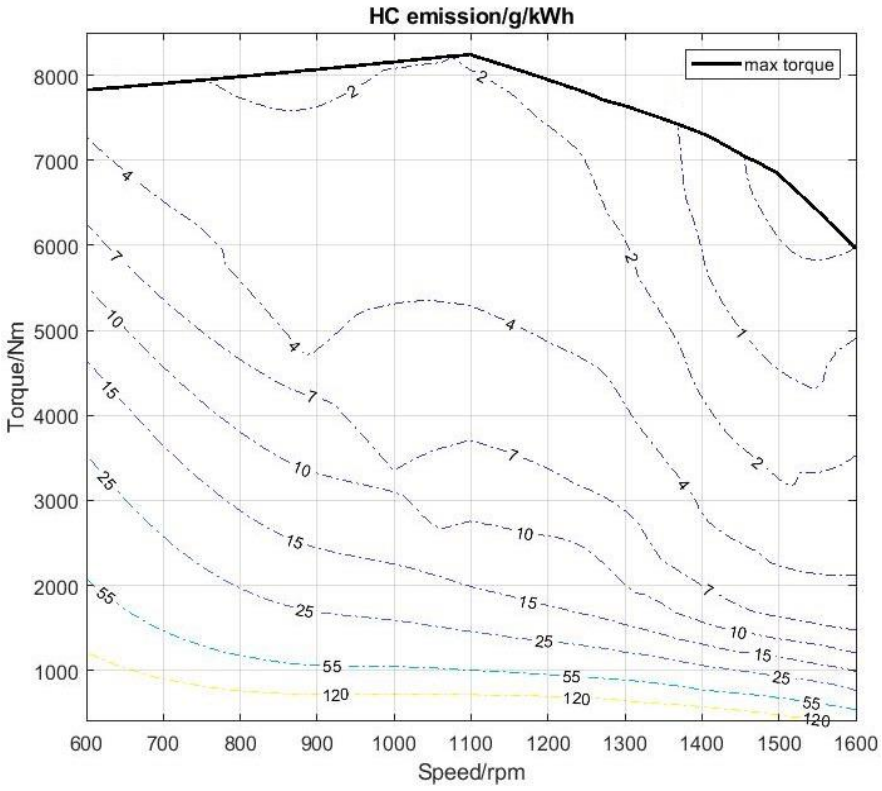

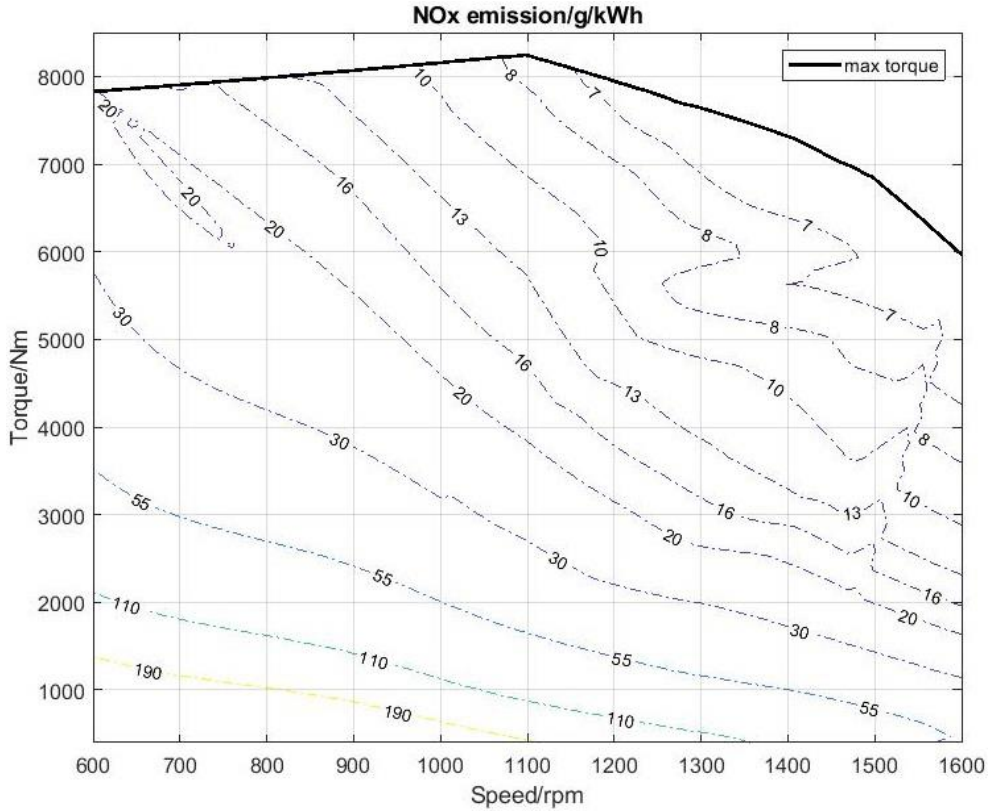
NOx emission/g/kWh
max torque
Torque/Nm
Speed/rpm

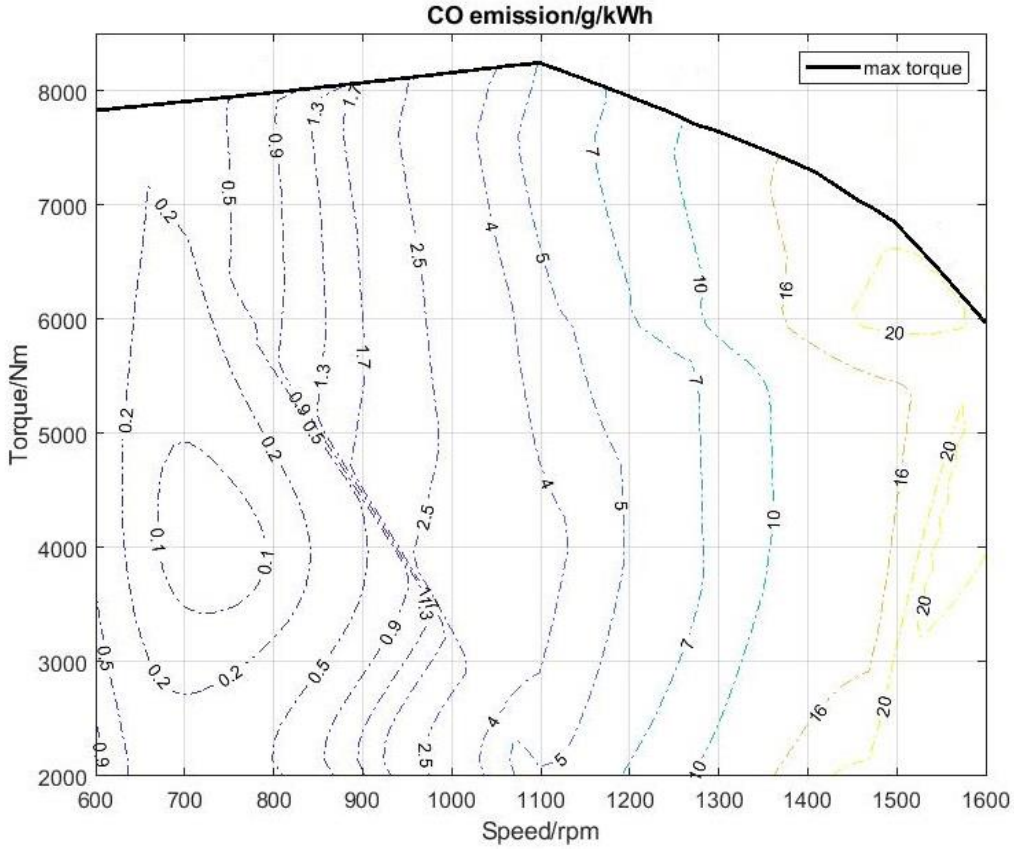
CO emission/g/kWh
max torque
Torque/Nm
Speed/rpm

REFERENCES

[1] Lounici, Mohand Said, Khaled Loubar, Lyes Tarabet, Mourad Balistrou, Dan-Catalin Niculescu, and Mohand Tazerout. (2014) "Towards improvement of natural gas-diesel dual-fuel mode: An experimental investigation on performance and exhaust emissions." Energy 64, 200-211.

[2] Wei, Lijiang, and Peng Geng. (2016) "A review on natural gas/diesel dual-fuel combustion, emissions and performance." Fuel Processing Technology 142, 264-278.

Appendix E. DC-DC Converter Power Loss Data Model Tool

E1 INTRODUCTION

The purpose of developing a generic converter model is to support the calculation of power loss of various DC/DC converters in electrified ships. The hybrid electric powertrain system with a DC power bus uses electrical conversions, besides its mechanical energy conversion, as a key technology for achieving high energy efficiency. In general, power converters can be divided into four types as shown in Table E - 1.

Table E - 1 Types of converter systems

Type of conversion	Converter system	
AC-to-DC	RECTIFIERS (Uncontrolled) (Diodes)	Fixed AC to Fixed DC (Line Commutation)
	RECTIFIERS (Controlled) (SCRs, IGBTs, MOSFETs, GTOs ...)	Fixed ac to Fixed or Variable dc (Line or Forced Commutation)
DC-to-DC		Fixed (or variable) dc to Variable (or fixed) dc
DC-to-AC	Inverters (Uncontrolled)	Fixed voltage dc to Fixed ac
	Inverters (Controlled)	Fixed (or variable) dc to Variable ac
AC-to-AC	AC Voltage Controllers	Fixed to variable ac
	Cycloconverters	Fixed ac to variable voltage & frequency (usually less than input frequency)

The major steps for building a converter model include:

a) Select a suitable converter topology based on a given condition and the state of the art technology.

b) Analyse converter operation and develop a simulation model

c) Identify control variables (from datasheet) and use an appropriate method to estimate the unknown parameters in the model

d) Validate the converter model to evaluate its adequacy

e) Develop an efficiency map of the modelled converter

After the parameters of the model are determined, the model is carefully assessed to see if the underlying assumptions of the analysis are acceptable. If accepted, the converter model will be used to create converter power loss data under different operating conditions and to produce the

converter efficiency map using an appropriate interpolation method. Not all of the converters listed in Table E - 1are needed for modelling the hybrid electric powertrains. The converter systems interested in the marine propulsion applications are discussed in the following section.

E2 DC-DC CONVERTER MODEL

DC-DC converters are required in the ship power system in order to chop DC voltage for other DC loads such as engine and generator controls, instrumentation, navigation equipment, engine room automation and etc. The one-directional DC/DC converter can be divided into two categories: boost and buck converter. In boost converter, the output voltage is higher than the input voltage while in buck converter the output is less than the input voltage.

In this part, a voltage doubler boost converter is selected and simulated in order to develop an accurate power loss model. The developed model must be computationally efficient so that it can be used in different optimization algorithms. For this purpose, according to [1], many high-frequency dynamics related to the converters model can be ignored with little impact on the whole model performance. Table E - 2 shows the variant time constant for different subsystems in IPS.

Table E - 2 Time constants for different subsystems

Source	Time
Semiconductor commutation	~ 1μs
Stator leakage time constant	1-10ms
Rotor time constant	50ms- 1s
PWM period	0.5-2ms
PWM resolution	~ 1μs
DC link ripple period	2.8ms
Propeller run-up time	20-60s
Ship run-up time	60-500s
Wave disturbance interval	10-100s

The power loss model is used to remain computationally efficient. For the simulation using a power loss model, voltage and current across each element of the circuit need to be calculated. The voltage double boost converter circuit diagram illustrated in Figure E - 1 and the result of simulation for 41 voltage input, 1kW output power is shown in Figure E - 2.

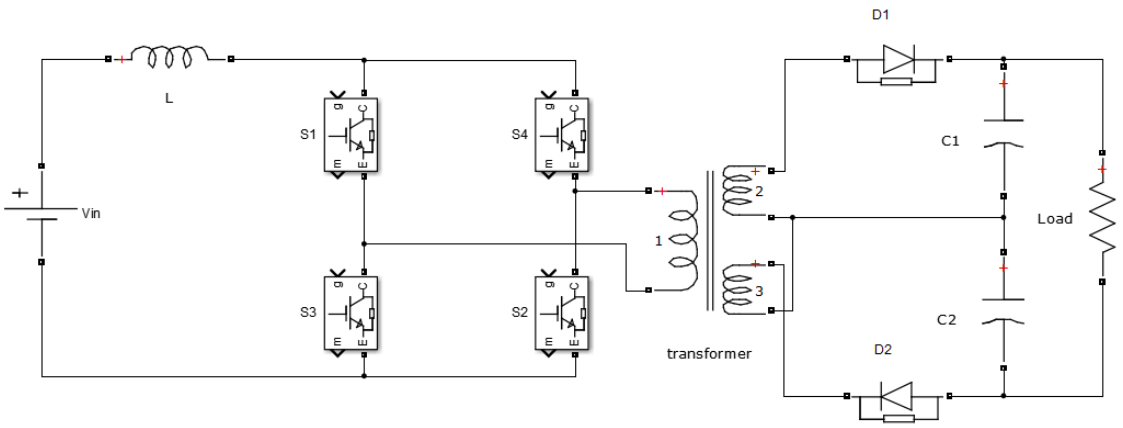

Figure E - 1 Voltage doubler boost converter

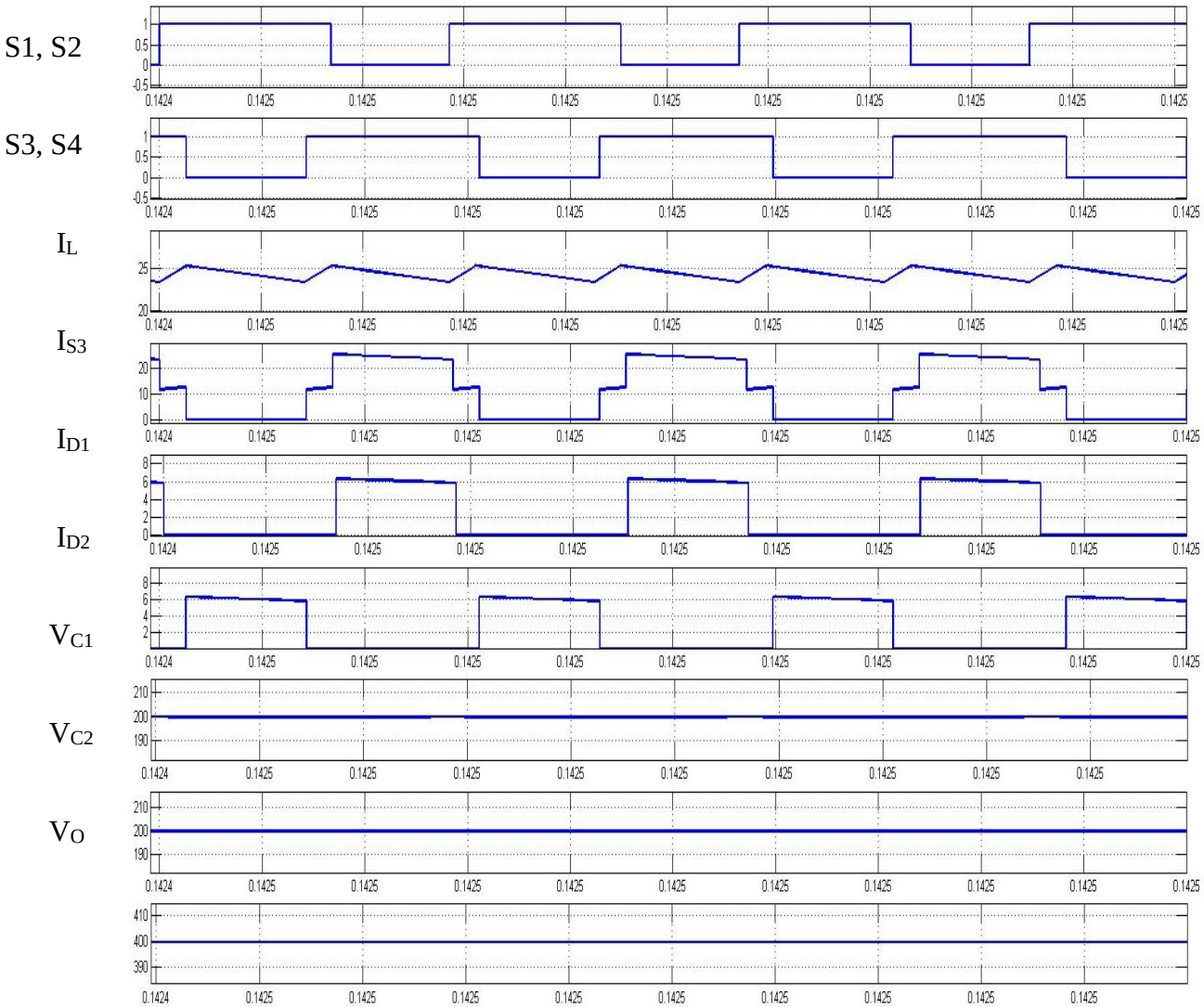

Figure E - 2 Gate signals and chief waveforms

These are five types of power loss in any power converter:

a) Switch turn on loss.
b) Switch turn off loss.
c) Switch conduction loss.
d) Diode conduction loss.
e) Diode recovery loss.

In addition to these losses, there are more losses associated with inverters such as gate loss or snubber loss, and inductor loss, making the calculation more complicated and they are ignored in this work for simplicity. Switches have power loss when they are in on state and conducting. This loss is referred to as switch conduction loss and occurs due to voltage across collector-emitter. In addition to on-state voltage drops and associated power loss, other losses occur when switch turn on and turn off, this loss is known as switching losses. Switching loss happens at each interval when the switch turns on or turns off. Therefore, switching loss is frequency-dependent and the higher switching frequency is associated with higher switching loss.

Figure E - 3Figure E - 3 and Figure E - 4 show the actual switch waveforms at turn on and off stage. In Figure E - 4 when the switch is in on stage, a gate pulse is applied to the switch. There is a delay until the gate signal reaches its maximum level due to the input capacitance of IGBT. At t_1, current starts to rise linearly and voltage across the switch gradually decreases to V_{ces}. The current overshoot ($t_{2(on)} + t_{4\,(on)}$) is due to the reverse recovery current of the freewheeling diode [2]. Similar behaviour happens when the switch is turned off (Figure E - 4). When negative gate voltage at the time $t_{0(off)}$ is applied, the voltage gradually rises to V_{ce0} and collector current decreases linearly.

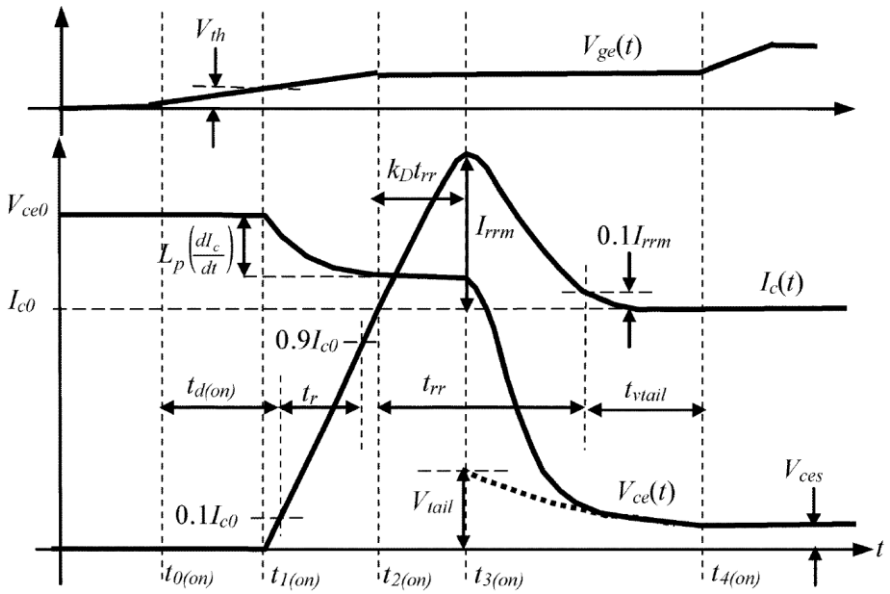

Figure E - 3 Hard-switching turn-on transient waveforms for loss calculation [2].

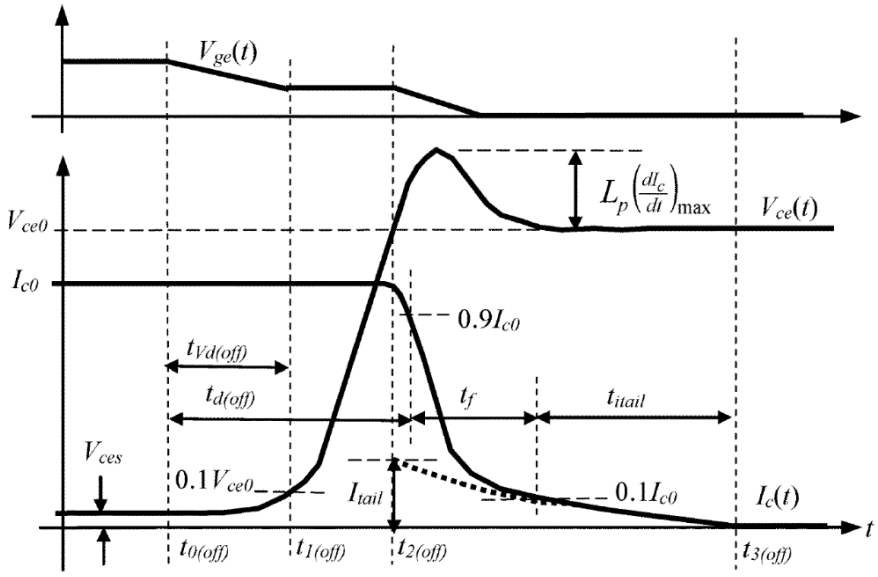

Figure E - 4 Typical hard switching turn-off transient waveforms [2].

Similar current and voltage behaviour exist for the diode in turn on and turn off transients. In modern IGBT switches, a fast recovery diode is used which makes the turn on loss negligible (less than1% of total loss). Therefore, the only turn off process needs to be calculated in this work. The typical diode waveform is depicted in Figure E - 5. As the diode current falls due to reverse voltage across the diode, part of current goes negative until it attains a value of I_{rrm} (maximum reverse current). When the diode current reaches I_{rrm}, voltage starts to go negative and diode stops conducting.

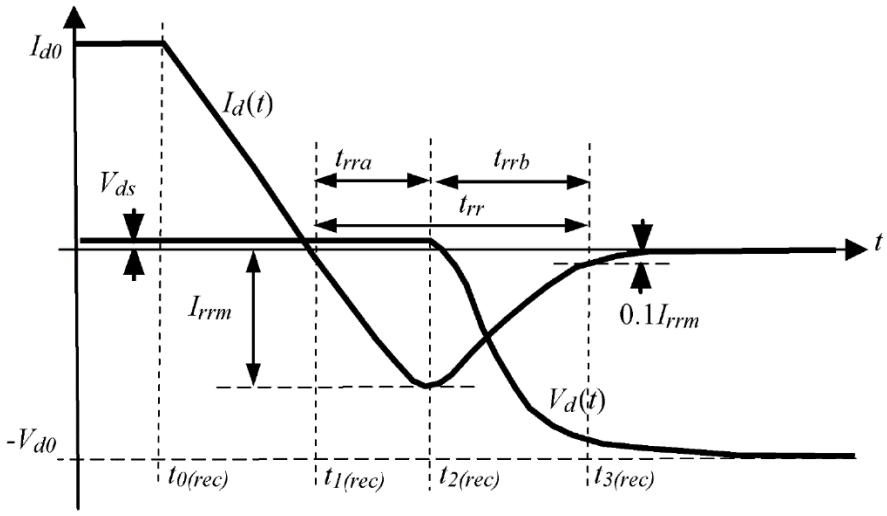

Figure E - 5 Idealized waveforms of diode turn-off transient.

The switching losses of the IGBTs can be calculated by using the fall (t_f) and rise (t_r) time available on the datasheet. For simplicity, it was assumed that voltage and current have linear behaviour (resistive load) shown in Figure E - 6. Based on this assumption, switching losses can be calculated as follow.

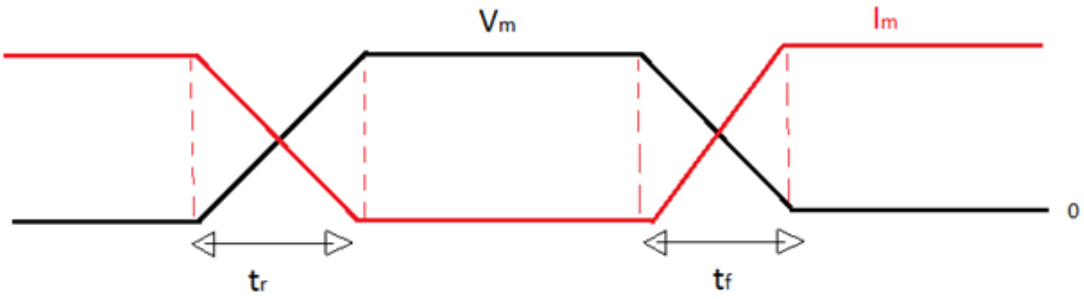

Figure E - 6 Switch voltage and current.

$$P = \frac{1}{T}\int_0^T V(t)\ \ i(t)\ dt \tag{E-1}$$

$$P = \frac{1}{T}\int_0^{t_r} (V_m \frac{t}{t_r})(I_m)(1 - \frac{t}{t_r})\ dt$$

$$P = \frac{1}{T}\frac{V_m I_m}{{t_r}^2}\int_0^{t_r} [t(t_r - t)]\ dt$$

$$P = \frac{V_m I_m}{T\ {t_r}^2}\left[\frac{t_r t^2}{2} - \frac{t^3}{3}\right]_0^{t_r}$$

$$P = \frac{V_m I_m}{T\ {t_r}^2}\left[\frac{{t_r}^3}{2} - \frac{t^3}{3}\right]$$

$$P_{t_r} = \frac{V_m I_m}{T}\frac{t_r}{6} \tag{E-2}$$

With similar calculation for fall time power loss, we have

$$P_{t_f} = \frac{V_m I_m}{T}\frac{t_f}{6} \tag{E-3}$$

The total switching loss is the summation of these two losses.

$$P_{switching\ loss} = P_{t_r} + P_{t_f} = \frac{1}{6} V_m I_m (t_r + t_f) f \tag{E-4}$$

The conduction loss is determined by the on-resistances of the IGBTs and the transistor RMS current.

$$P_{cond} = R_{ds\ ON} \times I^2(rms) \tag{E-5}$$

The antiparallel diode loss is equal to

$$P_{loss}(diode) = V_F I_F(av) + R_F {I_F}^2(rms) \tag{E-6}$$

where I_F and V_F are diode current and voltage; RF is diode resistance and it can be found in data sheet. The power loss model has been developed using Matlab software and result is shown in Figure E - 7. The input voltage has changed from 22 V to 42 V and output power varied from 500W to 1000W. As it is clear from figure, at constant voltage lower power is associated with

higher efficiency. This comes from the fact that less current is passing through circuit elements and Ohmic losses are lower.

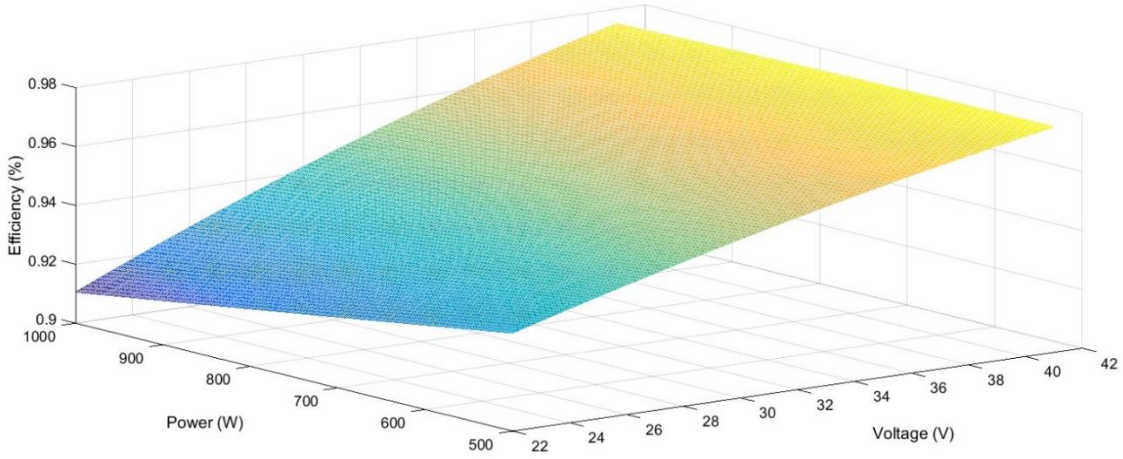

Figure E - 7 Boost DC-DC converter efficiency map.

REFERENCE

[1] J. M. Apsley et al., "Propulsion Drive Models for Full Electric Marine Propulsion Systems," IEEE Transactions on Industry Applications, vol. 45, no. 2. pp. 676–684, 2009.

[2] International IOR Rectifier, "IRF100B202 Product Datasheet," 2014. [Online]. Available: www.irf.com. [Accessed: 22-Feb-2018].

Appendix F. Li-ion Battery and Battery-UC Hybrid ESS Performance Degradation and Lifecycle Cost Models

PART I - LITHIUM-ION BATTERY PERFORMANCE DEGRADATION MODEL

F1 GENERAL INTRODUCTION

Lithium-ion (Li-ion) batteries have been largely used in electrified transportation area as rechargeable energy storage system (ESS). Metallic Li was intuitively chosen as battery electrodes long time ago, due to its low density (0.534 g/cm3 at room temperature), high reduction voltage (-3.04V vs. Standard Hydrogen Electrode) and large theoretical capacity (3860 mAh/g). Li-ion batteries, also described as "rocking-chair" batteries by transferring Li ions between anodes and cathodes, entered the market in 1990s and greatly stimulated the development of electrified transportations. Graphite, Lithium Titanate (LTO), and new materials such as transition-metal oxides or graphene nanosheet (GNS) were invented as negative materials for Li-ion batteries. Positive electrodes include a variety of lithium metal oxide compounds. Lithium-iron phosphate (LFP), lithium-nickel-cobalt-aluminum (NCA), lithium-nickel-manganese-cobalt (NMC) and lithium-manganese oxide (LMO) are most prominent materials in automotive applications. By melting Nickle, Cobalt and Manganese, manufacturers are trying to achieve higher voltage and capacity, as well as maintain a safe working condition.

With the increasing scale of mass production, the price of Li-ion batteries has dropped down dramatically during the last ten years. For instance, the cost of Li-ions batteries dropped from above US $1,000 per kWh in 2007 to about US $250 per kWh in 2014. Moreover, it could fall to about US $200 per kWh by 2020 and about $160 per kWh by 2025 according to an analysis report from Mckinsey [2]. Still, it would be hard to compete with internal combustion engines (ICE) regarding the price if the battery packs could not fall below US$150 per kWh. Giving the common estimation regarding the manufacturing volumes and assembly cost by OEMs, the rough cost of battery pack is among US $300 ~ $500 per kWh for now.

Besides the price and manufacturing barriers, battery performance deterioration may aggravate the total cost of ownership to customers. The ageing phenomena caused by charging and discharging microscopic electrochemical reactions inside each single cell, are increased by cycling numbers and affected by temperature and current. Battery management system (BMS) is very important to manage a good performance during driving. Failure to accurately calculate battery terminal voltage and state-of-charge (SOC) will induce inappropriate usage. A good battery modelling method in BMS can help reduce the pack's volume and capacity while still satisfying required electric range. Since the size of the battery packs greatly influences the total price, a good BMS with accurate modelling method can effectively reduce the total cost for both OEMs and customers.

F2 BATTERY PERFORMANCE MODELLING INTRODUCTION

The equivalent circuit model and electrochemical model are two main methods to model battery performance in BMS. Sometimes empirical models, based on Arrhenius equation, are used to predict batteries' calendar life. However, it is confined to a specific type of cell and needs numerous measurement data. The accuracy and precision of battery models would affect the system control strategy. A highly effective control logic will not only help reduce driving consumption and emission but also prolong the battery lifetime.

F2.1 Equivalent Circuit Model

The electrical equivalent circuit model is a theoretical model that simplifies a physical battery to an electrical source with some passive elements. Empirically, a DC voltage source combines with an internal resistor and two resistor-capacitor parallel elements would be sufficient to simulate a Li-ion battery cell. Most researches [3-9] normally used a one-dimensional equivalent circuit model for rechargeable batteries. Sometimes multi-dimensional equivalent circuit model was built to serve multi-purpose applications, Jung and Kang [10]. In this section, an open circuit voltage V_{oc} with an internal resistor R_i and two RC parallel circuits were adopted for battery performance modelling Figure F - 1. The terminal voltage V_t and SOC were calculated as outputs from this model.

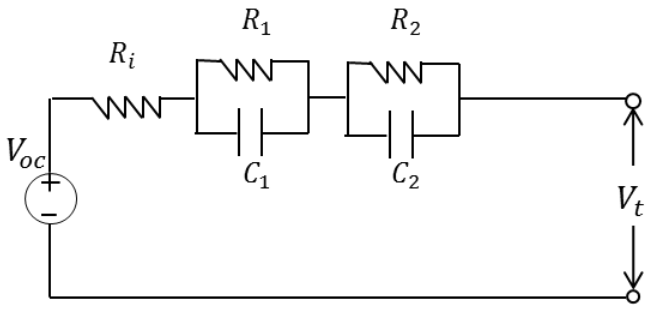

Figure F - 1. Equivalent Circuit Model

The terminal voltage was determined by Kirchhoff laws:

$$V_t = V_{oc} - V_i - V_1 - V_2 \quad \text{(F - 1)}$$

where V_i, V_1, V_2 are voltage drops caused by the resistor and the two RC circuits.

The estimates to V_1 and V_2 are calculated by:

$$\dot{V_1} = \frac{I_{c1}}{C_1} = -\frac{V_1}{R_1 C_1} + \frac{I}{C_1} \quad \text{(F - 2)}$$

$$\dot{V_2} = \frac{I_{c2}}{C_2} = -\frac{V_2}{R_2 C_2} + \frac{I}{C_2} \quad \text{(F - 3)}$$

On the other hand, SOC estimation was based on Coulomb counting which equals to the integral over time of the ration between current and nominal capacity Q (assuming positive current was discharging).

$$\dot{SOC} = -\frac{I}{Q} \quad \text{(F - 4)}$$

The model was implemented in Simulink. A constant current – constant voltage (CC-CV) charging protocol was developed to fulfill its capacity without causing overcharging Figure F - 2.

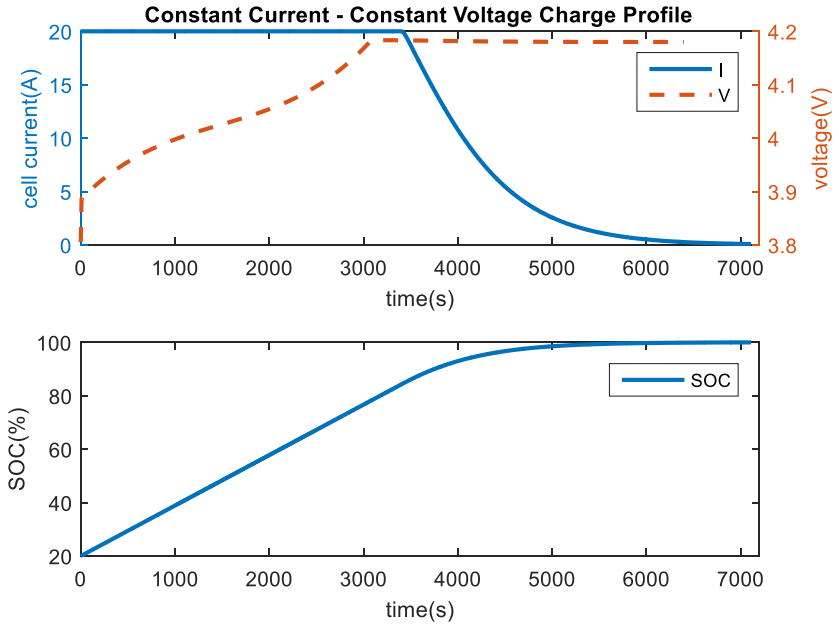

Figure F - 2. CC-CV Charging Profile

Experimental data are needed to adjust parameters in the model. Without enough experiments to get degrade parameters, it cannot be used to evaluate battery life prediction. Errors between simulation results and real performances would be enlarged after a certain time when degradation happens.

F2.2 Electrochemical Model

Many efforts were placed on the electrochemical model lately to seek an accurate simulation result for battery ageing performance. The first electrochemical model was proposed by Doyle, et al. [11] in 1993, so-called 'Doyle-Fuller-Newman' model (or DFN model)[12, 13]. DFN model was trying to capture voltage response based on the lithium-ion concentration variation between cathode and anode, by building a full-order mathematical model. In Figure F - 3, j^{Li} indicates the concentration change of Li-ions along the thickness of battery from negative to positive electrode, where δ_n, δ_p, δ_{sp} are the thickness of negative, positive electrode and separator, respectively.

DFN model is quite complex and computation time consuming due to the spatial and time coupled governing equations. Smith and Wang [14], [15, 16] studied Li-ion's diffusion process inside active solid materials using the finite element method and generated a control-oriented electrochemical model. Ramadass, et al. [17], based on their analysis, built semi-empirical correlations for graphite/LCO 18650 cells, by calculating primary, secondary active material losses, and rate capability losses separately. Wang, et al. [18] built a micro-macroscopic coupled model to study the interfacial properties for batteries and fuel cells. Di Domenico, et al. [19] compared the full order DFN model with a simplified model and applied the extended Kalman filter for the SOC calculation.

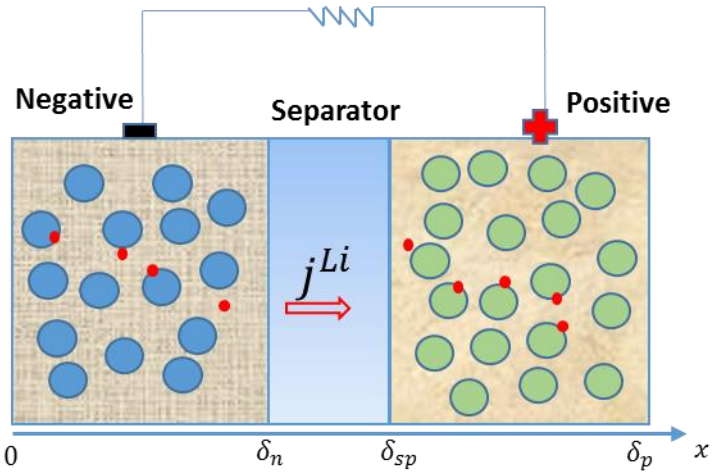

Figure F - 3. Li-ion Battery Discharge Demonstration

In order to improve its computational ability, some assumptions were made to simplify the equations [19, 20]. It is assumed a uniform concentration along both negative and positive electrodes because of the high conductivity of metal current collectors. In addition, the electrolyte concentration can be seen as stable and uniform because of the sufficient supplement of Li-ions. Based on that, a so-called 'Single Particle Model' (or SPM) was developed to use only one carbon particle and one lithium metal oxide particle to represent the responses on the negative and positive electrode. The order was largely reduced hence calculations were much easier in SPM. Figure F - 4 is a demonstration of concentration variation on both anode and cathode solid particles when discharging current.

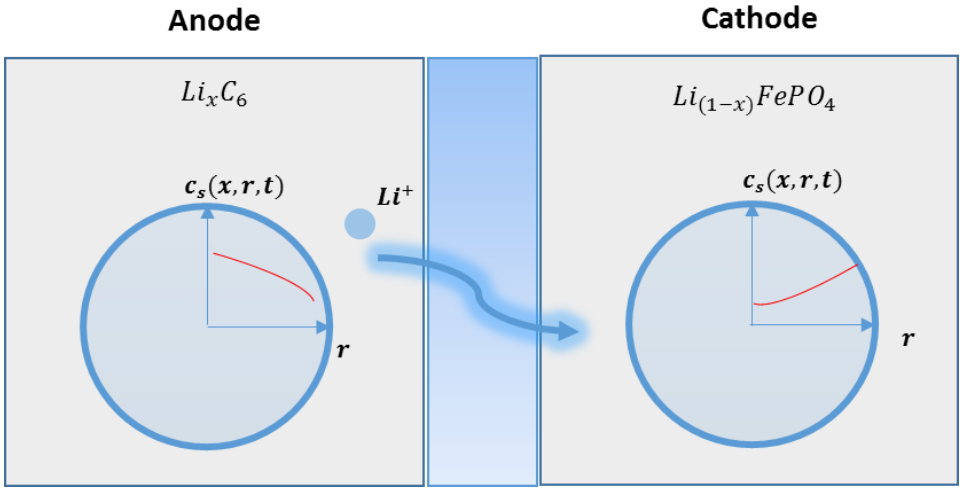

Figure F - 4. Demonstration of Single Particle Model

Here it is assumed that discharging current is positive and charging current is negative. Meanwhile, let j^{Li} be positive when ions leave the particle while negative when ions insert into the particle. During a discharge process, the microscopic current density is determined by the electrode overpotential, which is the net current flow of cathodic and anodic reaction occurring at the same time. The Butler-Volmer kinetic equation was used to describe this phenomenon.

$$j^{Li} = a_s j_0 \left[\exp\left(\frac{\alpha_a F}{RT}\eta\right) - \exp\left(-\frac{\alpha_c F}{RT}\eta\right)\right] \quad \text{(F - 5)}$$

where, α_a, α_c are the anodic and cathodic charge transfer coefficients; a_s is the active surface area per electrode unit volume; η is the overpotential defined by the difference between the solid (ϕ_s) and liquid phase (ϕ_s) potentials minus the open circuit potential of the solid ($U(c_s)$, a function of solid ion concentration).

$$\eta = E - E_{eq} = \phi_s - \phi_e - U(c_s) \quad \text{(F - 6)}$$

j_0 is the exchange current density representing the current flow at equilibrium state, it depends on the electrolyte concentration (c_e) and solid-electrolyte interface concentration (c_{se}):

$$j_0 = k(c_e)^{\alpha_a}\left(c_{s,max} - c_{se}\right)^{\alpha_a}(c_{se})^{\alpha_c} \quad \text{(F - 7)}$$

When there is applied current, I, the macroscopic current can be connected with the microscopic current density by integrating over the electrode length.

$$\frac{I}{A} = \int_0^{\delta_n} j^{Li}(x)dx \quad \text{(F - 8)}$$

where δ_n is the thickness of negative electrode; A is the electrode surface area.

Ions will move instantaneously, along with electrons, under the potential difference between anode and cathode. The concentration of Li-ions varies based on the dynamic diffusion processes inside solid particles and electrolyte solutions.

$$\frac{\partial c_s}{\partial t} = \nabla_r(D_s \nabla_r c_s) \quad \text{(F - 9)}$$

$$\frac{\partial \varepsilon_e c_e}{\partial t} = \nabla_x\left(D_e^{eff}\nabla_x c_e\right) + \frac{1-t^0}{F} j^{Li} \quad \text{(F - 10)}$$

where r and x are length indicators for solid particle radius and cell's thickness. Other symbols can be found in Table F - 1.

Governing equations for potential distribution (ϕ_s and ϕ_e) can be built as below.

$$\nabla_x \sigma^{\text{eff}} \nabla_x \phi_s - j^{Li} = 0 \quad \text{(F - 11)}$$

$$\nabla_x \kappa^{\text{eff}} \nabla_x \phi_e + \nabla_x \kappa_D^{\text{eff}} \nabla_x ln c_e + j^{Li} = 0 \quad \text{(F - 12)}$$

In order to solve these high nonlinear partial differential equations, a discretization method was adopted to divide one particle into several small volumes along its radius. Fick's law related the diffusive flux to the concentration gradient under both steady-state and time-variant conditions. It postulates that the flux goes from regions of high concentration to regions of low concentration, with a magnitude that is proportional to the concentration gradient (spatial derivative).

$$\frac{\partial c}{\partial t} = D\frac{\partial c^2}{\partial x^2} \quad \text{(F - 13)}$$

where c is the concentration in the dimension of x and time t (mol/m^3), D is the diffusion coefficient (m^2/s), x is the space direction, t is the time (s).

By discretizing a physical particle into m slices, the concentration variation in each slice is only connected with its adjacent layers [21]. For the i^{th} layer, the concentration change with time can be described as the molar flux in minus molar flux out according to the conservation of mass,

$$\frac{\delta c_i}{\delta t} = \frac{N_1 - N_2}{A_i \delta r} \quad \text{(F - 14)}$$

where $\delta r = \frac{r}{m}$ is the thickness of each layer, A_i is the surface area of the particle. N_1, N_2 are molar flux in and out of the i^{th} layer. By substituting and rearranging these equations, a generalized form can be deduced as

$$\frac{\partial c_i}{\partial t} = \frac{D}{\delta r^2}\left[\left(\frac{i-1}{i}\right)c_{i-1} - 2c_i + \left(\frac{i+1}{i}\right)c_{i+1}\right] \quad \text{(F - 15)}$$

The concentration boundary conditions are 0 at the particle core and equal to current density at the out shell.

A state space equation can be formed to demonstrate the negative and positive electrodes ions fluxes, where $\dot{c}_i (i = 1, \dots m-1)$ is the concentration changing with time.

Table F - 1. List of Symbols for Electrochemical Model

I	applied current	A
η	overpotential	V
U	open circuit voltage	V
F	Faraday's number	C/mol
R	ideal gas constant	J/mol/K
T	temperature	K
δ_n	thickness _ negative electrode	cm
δ_{sp}	thickness _ separator	cm
δ_p	thickness _ positive electrode	cm
j^{Li}	Butler-Volmer current density	A/cm^3
a_s	active surface area per electrode unit volume	%
j_0	exchange current density	A/cm^3
α_a	charge transfer coefficient	
α_c	charge transfer coefficient	
c_s	concentration of solid particle	mol/cm^3
c_e	concentration of electrolyte	mol/cm^3
c_{se}	concentration of SEI layer	mol/cm^3

c_s^{avg}	average concentration of solid particle	mol/cm^3
ε_e	electrolyte phase volume fraction (i.e., porosity)	%
ϕ_e	electrolyte phase potential	V
ϕ_s	solid-phase potential	V
D_e^{eff}	effective electrolyte phase diffusion coefficient	cm^2/s
D_s	solid phase diffusion coefficient	cm^2/s
κ^{eff}	effective ionic conductivity in electrolyte	1/(Ω.cm)
κ_D^{eff}	effective ionic and diffusion conductivity in electrolyte	1/(Ω.cm))
t^0	transference number	
θ	solid concentration percentage	%
$\theta_{100\%}$	maximum solid concentration at 100% _negative	%
$\theta_{0\%}$	minimum solid concentration at 0% _negative	%
R_f	film resistance	Ω
n	negative electrode	
p	positive electrode	
sp	separator	

$$\begin{bmatrix} \dot{c_1} \\ \dot{c_2} \\ \dot{c_3} \\ \vdots \\ \dot{c_{m-2}} \\ \dot{c_{m-1}} \end{bmatrix} = \frac{D}{\delta r^2} \begin{bmatrix} -2 & -2 & 0 & 0 & \dots & 0 \\ \frac{1}{2} & -2 & \frac{3}{2} & 0 & \dots & 0 \\ 0 & \frac{2}{3} & -2 & 0 & \dots & 0 \\ \vdots & \vdots & \vdots & \ddots & \vdots & \vdots \\ 0 & 0 & 0 & \dots & -2 & \frac{m-1}{m-2} \\ 0 & 0 & 0 & \dots & \frac{m-2}{m-1} & -\frac{m-2}{m-1} \end{bmatrix} \begin{bmatrix} c_1 \\ c_2 \\ c_3 \\ \vdots \\ c_{m-2} \\ c_{m-1} \end{bmatrix} + \frac{1}{\delta r F a_s} \begin{bmatrix} 0 \\ 0 \\ 0 \\ \vdots \\ 0 \\ \frac{m}{m-1} \end{bmatrix} j^{Li} \quad \text{(F - 16)}$$

Well organized ions inside layered or spinel oxide compounds will start to move along the particle radius under a current impulse. Basically, voltage and SOC are determined by the number of ions reacting on the positive side and negative side. If the moving speed could not follow the reacting rate, the output voltage will drop because of lacking ions. The diffusion coefficient varied with the types of material, the physical structure and temperature. For a fresh battery, the ions left negative particles and entered a positive particle when discharged current. When ageing started, compounds' structure was aggregated to make it hard for ions to move. It was shown clearly (in Figure F - 5) that if one particle was sliced into 20 layers, the 20th layer responded quickly to the outermost shell while the first layer next to the core was hardly changed.

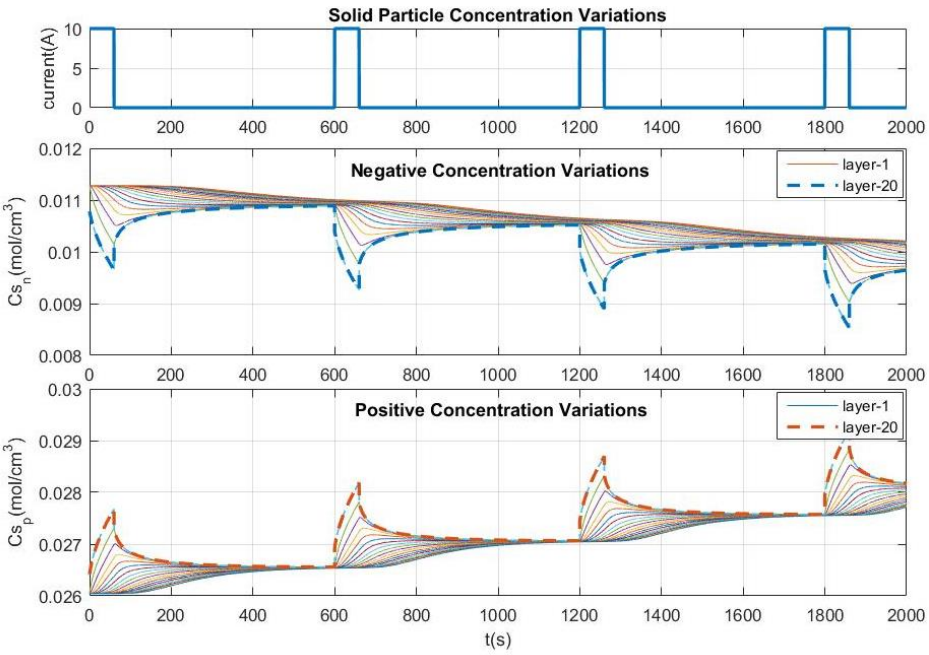

Figure F - 5. Solid Particle Concentration Variation with Pulse Current

The average concentration c_s^{avg} denotes the total energy stored inside the particle, i.e., the SOC state.

$$c_s^{avg} = \frac{1}{V}\int_0^V c_s(r,t)dV \quad \text{(F - 17)}$$

Therefore, an expression for SOC calculation is:

$$SOC = \frac{\theta_n - \theta_{0\%}}{\theta_{100\%} - \theta_{0\%}} \quad \text{(F - 18)}$$

where $\theta_n = \frac{c_s^{avg}}{c_{s,max}}$ is the percentage between the actual and maximum concentrations. $\theta_{100\%}$ and $\theta_{0\%}$ are parameters depending on the materials.

The output voltage is basically the electrode potential differences between the positive and negative electrode, minus the Ohmic resistance losses.

$$V = \phi_{s,p} - \phi_{s,n} - R_f I \quad \text{(F - 19)}$$

where R_f is the film resistance inside the cell; $\phi_{s,p}$, $\phi_{s,\mathrm{n}}$ are the solid potential at the positive electrode and the negative electrode. Since the overpotential between electrode and electrolyte is:

$$\eta = \phi_s - \phi_e - U \quad \text{(F - 20)}$$

Hence, equation (M-19) can be rearranged into four terms:

$$V = (\eta_p - \eta_n) + (U_p - U_n) + (\phi_{e,p} - \phi_{e,n}) - R_f I \quad \text{(F - 21)}$$

The flow chat in Figure F - 6 gives a clear idea on how to use the electrochemical model to calculate SOC and output voltage [11, 12, 18, 19, 22]. Butler-Volmer equation and single-particle model

transferred current to ions' concentration variations and then it can be used to calculate SOC. OCV curve is fitted by experiment data, while electrode and electrolyte overpotential differences are calculated through 1-D ordinary differential equations.

Although it needed lots of physical parameters to run the model, some optimization methods such as Genetic Algorithm ('GA') can be used to identify parameters' value. The discussions about parameters identification and validations are beyond this scope and will be discussed in another papers. In this paper, most parameters value were adopted from published literature [11, 14, 19, 23].

The comparisons between electrochemical model and equivalent circuit model has clearly showed the different dynamic responses (Figure F - 7). Under a pulse discharge current, output voltage varied instantaneously. Based on the dynamic diffusion process inside each solid particle, the voltage of electrochemical model is determined by the electrochemical reactions at the outermost layer. If the diffusion coefficient is decreased because of ageing, there would be not enough ions to supply required current and voltage. Therefore, the voltage will drop immediately to show the effect of ageing phenomena. As for the equivalent circuit model, output voltage is calculated by subtracting resistance voltage drop from open circuit voltage. It is hard to show any physical deterioration of the cell because of the simplification method.

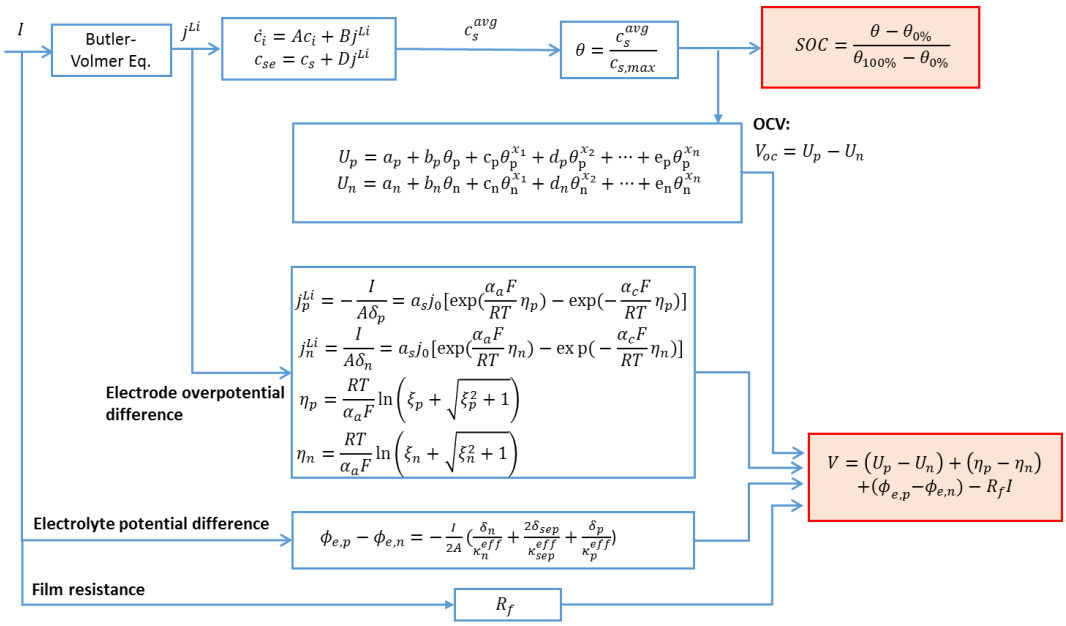

Figure F - 6. MATLAB/Simulink Modelling Flowchart

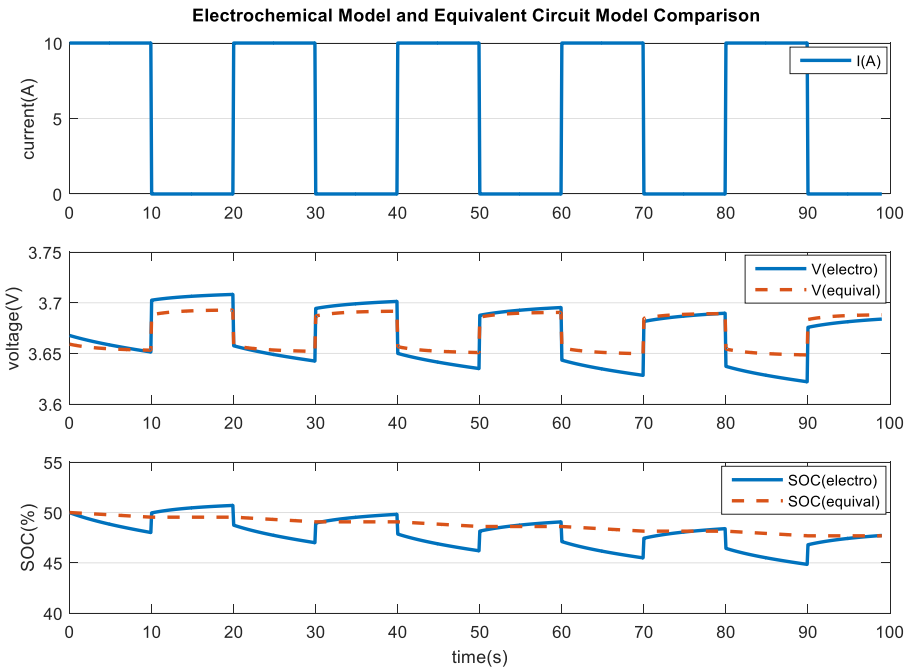

Figure F - 7. Comparisons between Equivalent Circuit Model and Electrochemical Model

The SOC in both models showed the same amount of change. However, in the equivalent circuit model, the Column counting method is hard to indicate the dynamic changing which electrochemical model does. The BMS control logic will make decisions based on the voltage and SOC results. Inaccurate calculations would mislead BMS to give aggressive orders for the battery pack, which might increase its life decay process.

F3 Performance Degradation and Lifetime Estimation Model

Battery degradation is an inevitable phenomenon during its lifetime, no matter whether it is working or in storage. Microscopic electrochemical reactions happen all the time and cause performance decay. The main reasons and key factors that related to the degradation rate were reviewed in this section. A performance degradation model was built based on the electrochemical model to estimate lifetime lasting.

F3.1 Degradation Mechanism Review

Cyclic capacity decay starts right after the first charge/discharge process. A sharp capacity decay can be observed from the negative electrode due to the consumption of Li-ions from electrolyte and graphite anode to build SEI layer [24]. After that, the SEI layer on the negative electrode stayed stable and the positive electrode will contribute to the further capacity losses during cycling. When the cell is on rest, chemical reactions happened only because of the thermodynamic instability between materials. Lithiated graphite has strong reactivity with the organic electrolyte. The reaction intensity is highly related to material properties, storage temperature, and battery

open circuit voltage (or OCV) level. Side reactions, mainly on the negative electrode, were believed to be the main reason of calendar life fading [3, 25, 26].

When temperature rising, SEI starts to dissolve and becomes permeable for solvent. Further reactions between the organic solvent and active LiC_6 cause graphite exfoliation and gas release[27]. Fast charge current can be dangerous and harmful to cycle life. A large amount of Li-ions accumulates in the anode side quickly under high current density, causing metal Li plating along the carbon surface. Dendritic Li might penetrate the separator film. Inner short circuit will induce thermal runaway under some conditions.

Bourlot, et al. [26] compared 1.5 years-aged Li-ion batteries with fresh ones produced by Johnson Controls–Saft, showed clearly that positive electrode limited cycling performance after ageing. Zhang, et al. [28] examined the contributions of positive $LiCoO_2$ and negative graphite to the impedance increment and capacity loss during cycling by using electrochemical impedance spectroscopy (EIS). Some key factors such as temperature, current, and operating voltage would greatly affect the life-fading rate. Ramadass et.al.[29, 30] analyzed Sony 18650 cells at elevated temperature and showed an increase of capacity losses.

Some conclusions for life degradation can be concluded from previous studies [25, 26, 31-34]. The main reasons for carbon-based anodes ageing include SEI formation and growth, loss of available lithium due to side reactions, lithium metal plating at low temperature and high rate current, etc. As for lithium-metal oxide cathodes, wearing of active materials, compound structure changing, and electrolyte dissolving are all relevant to performance decay.

F3.2 Performance Degradation Modelling

The electrochemical modelling method was proved as an effective way to predict performance degradation. Safari, et al. [35] built a multimodal physics-based ageing model that can predict cycling and storage capacity losses by calculating the thickness growth of SEI layer on the negative electrode surface. Arora, et al. [24] incorporated the side reactions into a general electrochemical model for li-ion batteries to explore the capacity fade and failure mechanisms. Santhanagopalan, et al. [36] built a physics-based model to obtain the change of cyclable lithium and active material loss for Li-ion life prediction.

Capacity loss and resistance increment are two main disadvantages after battery aged. Active contact areas will decrease and the thickness of SEI will be increased. An increased layer outside of the particle will make it difficult for the ions to diffuse from the electrolyte into the particle. Available solid-phase concentration on both positive and negative electrodes will be decreased. The capacity losses (Q_{loss}) can be expressed as:

$$Q_{loss} = f(C_{rate}, SOC, \Delta SOC, T, t) \quad \text{(F - 22)}$$

where ΔSOC is the change of SOC; T is temperature; t is time.

Calendar life calculation has been ignored, considering it normally lasts much longer than cycle life under most of the conditions [3, 25, 26]. It also assumed battery temperature can be controlled and well maintained in a certain range by advanced battery system design and liquid cooling technology. Therefore, the cycle lifetime (or cycling numbers) can be expressed as a function of two variables:

$$N = f(C_{rate}, \Delta SOC) \quad \text{(F - 23)}$$

Battery lifetime is predicted based on the Arrhenius model [37-39], the battery capacity loss is a function of C-rate and ΔSOC:

$$Q_{loss} = Ae^{\left(\frac{-E_a+B\cdot C_{rate}}{RT}\right)}(A_h)^z \quad \text{(F - 24)}$$

where A is pre-determined coefficient; B is the coefficient of C-rate; A_h is the total throughput capacity which accounting for ΔSOC influences;

$$A_h = N \cdot \Delta SOC \cdot Q \quad \text{(F - 25)}$$

N is the total cycling numbers when capacity. In this paper, it is considered a dead battery when $Q_{loss} = 20\%$ of original capacity. Therefore, the calculation of the cycling number can be derived based on the previous function:

$$N = \frac{\left(\frac{Q_{loss}}{Ae^{\left(\frac{-E_a+B\cdot C_{rate}}{RT}\right)}}\right)^{\frac{1}{z}}}{Q\cdot\Delta SOC} \quad \text{(F - 26)}$$

For LiFePO4 battery, some measurement data can be obtained from the literature [39, 40], By using the least square method, coefficients in the cycle number equation can be determined. Measurement data of a 20Ah commercial LiFePO4 battery capacity decay has been provided by the manufacturer in Figure F - 8 that was used for parameter calibration.

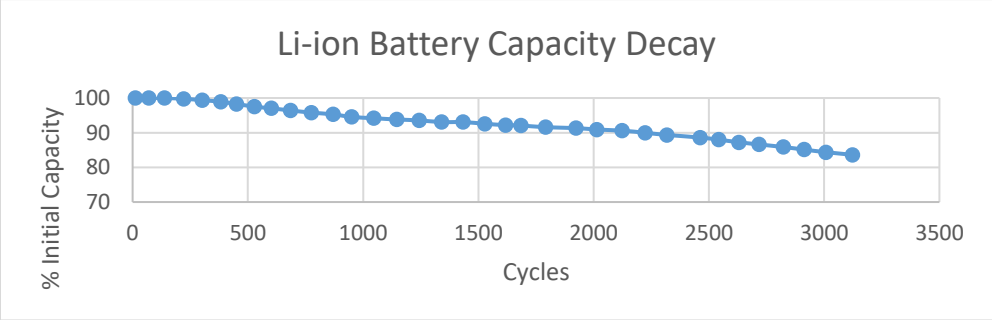

Figure F - 8. Li-ion Battery Capacity Decay (@100% Depth of Discharge (DOD), +1C/-2C, 23°C) [41]

This model was implemented in MATLAB/Simulink. The results of the cycling number for this 20Ah capacity LiFePO4 as a function of C-rate and ΔSOC were plotted in Figure F - 9.

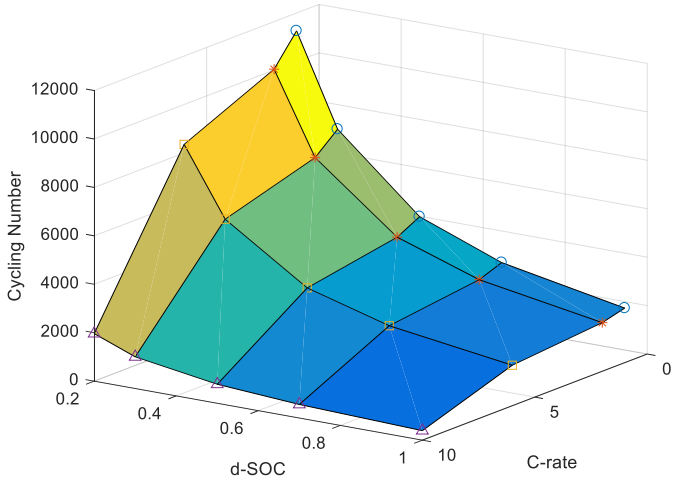

Figure F - 9. Cycling Number Variation with C-rate and ΔSOC

F4 SUMMARY OF PART I

This part of the Appendix focused on building and comparing two different battery modelling methods. The equivalent circuit model is a common method and easy to implement but hard to get accurate results especially when battery ageing happens. On the contrary, the electrochemical model is getting more popular to provide instantaneous voltage response by building dynamically diffusion processes. Physical-chemical reactions were abstracted by mathematic models. Although it is time-consuming to calculate the space and time coupled governing equations, the developed hardware now can handle it more easily than before. The differences between the two models were compared.

A battery performance degradation model was built in this paper to estimate the cycling numbers of LiFePO4 based on the variation of C-rate and ΔSOC. The inputs are SOC and current calculated based on the previous performance model, from either the equivalent circuit model or electrochemical model.

PART II - PERFORMANCE AND LIFECYCLE COST OF BATTERY-UC HYBRID ESS

F5 BATTERY MODEL

F5.1 Equivalent Circuit Model

The internal resistance model, Rint, was implemented in ADVISOR in 1994 [42]. As one of the most widely used battery models, it can represent the battery behaviour as well as reduce the computation time due to its simplicity. The Rint model of a battery cell, shown in Figure F - 10, is adopted without considering the temperature effects. The nominal voltage and capacity of the $LiFePO_4$ cell are 3.3 V and 60 Ah.

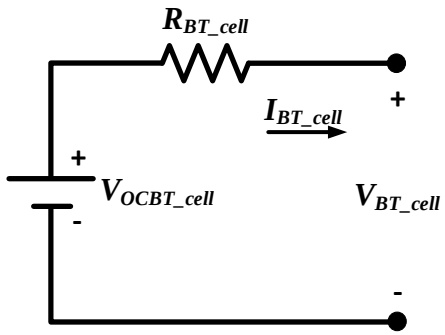

Figure F - 10. ADVISOR's Rint model of a battery cell

The current can be calculated as follows:

$$I_{BT\_cell} = \frac{V_{OCBT\_cell} - (V_{OCBT\_cell}^2 - 4 \cdot R_{BT\_cell} \cdot P_{BT\_cell})^{1/2}}{2 \cdot R_{BT\_cell}} \quad \text{(F - 27)}$$

where V_{OCBT_cell}, P_{BT_cell}, and R_{BT_cell} are the open-circuit voltage, the power, and the internal resistance of the battery cell, respectively. V_{BT_cell} in Figure F - 10 is the output voltage of the battery cell.

The state of charge (SoC) at the discrete step k ($SoC_{BT\_cell}(\mathrm{k})$) is defined as the current capacity (Q(k)) divided by the nominal capacity of the battery cell (Q_{BT_cell}):

$$SoC_{BT\_cell}(\mathrm{k}) = \frac{\mathrm{Q(k)}}{Q_{BT\_cell}} \cdot 100\% \quad \text{(F - 28)}$$

With a time step of Δt, the SoC at the next step is as follows:

$$SoC_{BT\_cell}(\mathrm{k}+1) = SoC_{BT\_cell}(\mathrm{k}) - \frac{I_{BT\_cell}(k) \cdot \Delta t}{Q_{BT\_cell}} \cdot 100\% \quad \text{(F - 29)}$$

In terms of the relationships among the SoC, the V_{OCBT_cell}, and the R_{BT_cell}, Figure F - 11 and Figure F - 12 are shown as follows.

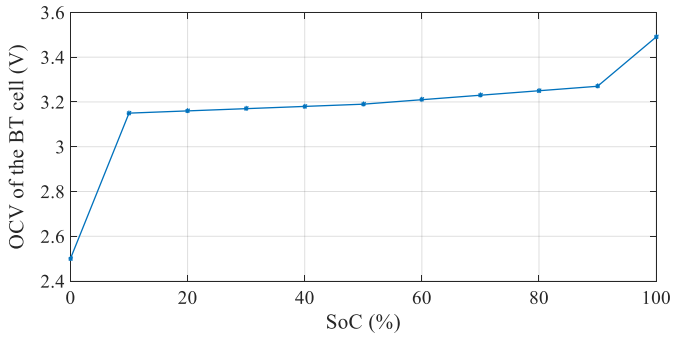

Figure F - 11. V_{OCBT_cell} vs. SoC of a battery cell

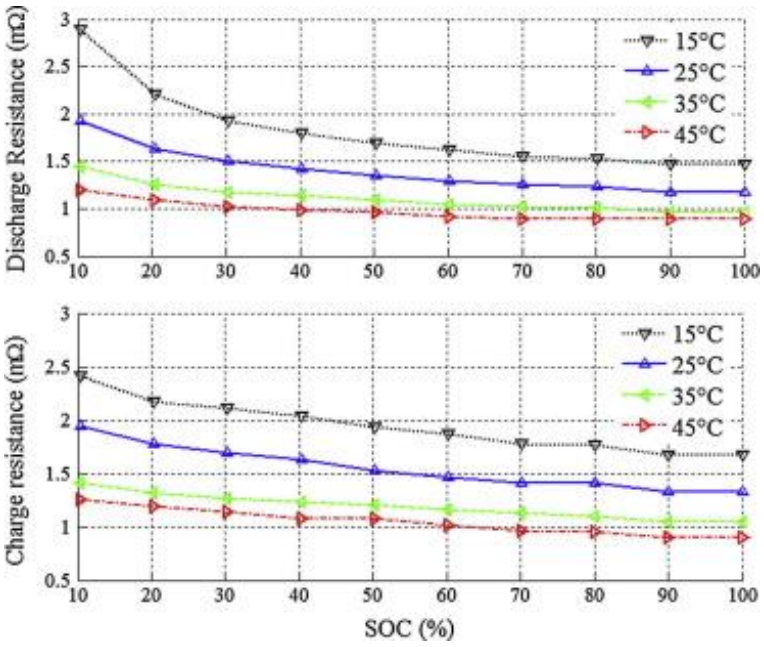

Figure F - 12. Charge and discharge resistances of a battery cell [37]

From the perspective of the battery packs, assume that the packs consist of the battery cells via N_{BT} series and M_{BT} parallel [37].

$$Q_{BT} = M_{BT} \cdot Q_{BT\_cell} \quad \text{(F - 30)}$$

$$R_{BT} = N_{BT} \cdot R_{BT\_cell} \,/\, M_{BT} \quad \text{(F - 31)}$$

$$V_{BT} = N_{BT} \cdot V_{BT\_cell} \quad \text{(F - 32)}$$

where Q_{BT}, R_{BT}, and V_{BT} denote the capacity, the internal resistance, and the voltage of the battery pack, respectively.

F5.2 Performance Degradation Model

In order to analyze the battery capacity loss during the operation, various models have been developed. Wang et al. [39] presented a semi-empirical life model based on the equation described by Bloom et al. [43], including three parameters (Ah-throughput, temperature, and discharge rate) for the purpose of investigating the capacity fade of a LiFePO4 battery (2.2 Ah, 26650 cylindrical cell from A123 Systems). A generalized battery life model is shown in F-33, established using a large cycle test matrix.

$$Q_{loss} = \mathrm{B} \cdot \exp\left[\frac{-31{,}700+370.3 \cdot C\_Rate}{R \cdot T}\right] (A_h)^{0.55} \quad \text{(F - 33)}$$

where Q_{loss} is the percentage of capacity loss, B is the pre-exponential factor, R is the gas constant, T is the absolute temperature in K, A_h is the Ah-throughput, and C_Rate is the discharge rate.

Based on this model, Song et al. [37] performed the battery degradation experiments on the LiFePO4 cell (3.3 V and 60 Ah) to calibrate the parameters indicated in $Q_{loss} = 0.0032 \cdot$

$e^{-\left(\frac{15{,}162-1{,}516\cdot C\_Rate}{R\cdot T}\right)}(A_h)^{0.824}$ (F - 34) and to verify the model accuracy for HESS optimization.

$$Q_{loss} = 0.0032 \cdot e^{-\left(\frac{15{,}162-1{,}516\cdot C\_Rate}{R\cdot T}\right)}(A_h)^{0.824} \quad \text{(F - 34)}$$

Therefore, $Q_{loss} = 0.0032 \cdot e^{-\left(\frac{15{,}162-1{,}516\cdot C\_Rate}{R\cdot T}\right)}(A_h)^{0.824}$ (F - 34) is utilized as the performance degradation model to quantitatively evaluate the capacity loss.

F6UC MODEL

Zhang et al. [44] comparatively studied three equivalent circuit models and concluded that the dynamic model is the best compromise between model precision/robustness and complexity, which is shown in Figure F - 13. The dynamic model of a UC cell and a Maxwell UC cell is tested with its nominal voltage and capacity being 2.7 V and 3000 F, respectively.

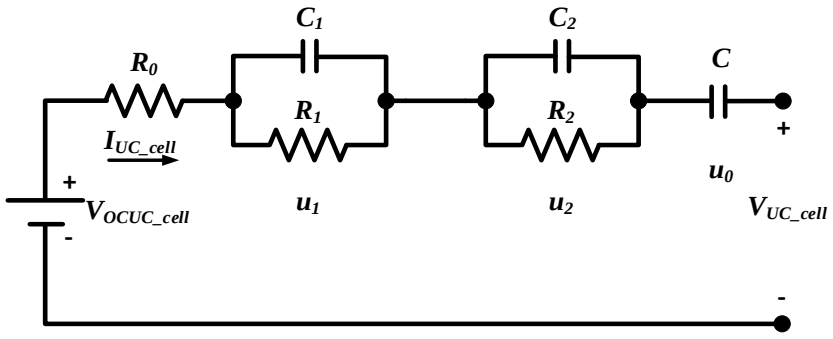

Figure F - 13. The dynamic model of a UC cell

This structure consists of a bulk capacitance, a series resistance, and two RC networks. The continuous-time state-space equations and the output equation are given by

$$\begin{bmatrix} \frac{du_1}{dt} \\ \frac{du_2}{dt} \\ \frac{du_3}{dt} \end{bmatrix} = \begin{bmatrix} 0 & 0 & 0 \\ 0 & -\frac{1}{R_1C_1} & 0 \\ 0 & 0 & -\frac{1}{R_2C_2} \end{bmatrix} \begin{bmatrix} u_1 \\ u_2 \\ u_3 \end{bmatrix} + \begin{bmatrix} \frac{1}{C} \\ \frac{1}{C_1} \\ \frac{1}{C_2} \end{bmatrix} I_{UC\_cell} \quad \text{(F - 35)}$$

$$V_{UC\_cell} = V_{OCUC\_cell} - u_0 - u_1 - u_2 - R_0 I_{UC\_cell} \quad \text{(F - 36)}$$

where u_0, u_1, and u_2 are the voltages of the bulk capacitance and the two RC networks, R_0 is the series resistance, I_{UC_cell} is the current, V_{OCUC_cell} is the open-circuit voltage, and V_{UC_cell} is the output voltage of the UC cell. The parameters of the UC cell are listed in Table F - 2.

Table F - 2. Model parameters of the UC cell

Parameter (Unit)	Value
C (F)	2,712
R_0 (Ω)	8.216×10^{-4}
C_1 (F)	627
C_2 (F)	1,843
R_1 (Ω)	3.146×10^{-4}
R_2 (Ω)	3.883×10^{-4}

Using the same method, suppose that UC packs are composed of the cells via N_{UC} series and M_{UC} parallel [37].

$$C_{UC} = M_{UC} \cdot C_{UC\_cell} \,/\, N_{UC} \quad \text{(F - 37)}$$

$$R_{UC} = N_{UC} \cdot R_{UC\_cell} \,/\, M_{UC} \quad \text{(F - 38)}$$

$$V_{UC} = N_{UC} \cdot V_{UC\_cell} \quad \text{(F - 39)}$$

where C_{UC_cell} and R_{UC_cell} are the capacity and the internal resistance of the UC cell, and C_{UC}, R_{UC}, and V_{UC} denote the corresponding meanings of the UC packs.

Moreover, the relationship between SoC_{UC}, V_{UC}, and the energy of the pack (E_{UC}) are shown in $SoC_{UC} = \frac{V_{UC}}{V_{UC\_max}}$ (F - 40) and $E_{UC} = 0.5 \cdot C_{UC} \cdot V_{UC\_max}^2 \cdot \left(1 - SoC_{UC\_min}^2\right)$ (F - 41).

$$SoC_{UC} = \frac{V_{UC}}{V_{UC\_max}} \quad \text{(F - 40)}$$

$$E_{UC} = 0.5 \cdot C_{UC} \cdot V_{UC\_max}^2 \cdot \left(1 - SoC_{UC\_min}^2\right) \quad \text{(F - 41)}$$

where V_{UC_max} and SoC_{UC_min} are the pack voltage in a fully charged condition and the lower limit of the pack SoC.

F7 DC/DC Efficiency Model

In order to increase the accuracy during the simulation process rather than set the efficiency value of the DC/DC converter as a constant, the efficiency lookup table generated from the DC/DC power loss model by adjusting the ranges of input power and voltage is used. Combining the battery, UC, and DC/DC efficiency models, the performance of the hybrid ESS can be evaluated quantitatively.

F8Lifecycle Cost Model

The lifecycle cost (LCC in $/day) of the hybrid ESS mainly includes the capital costs ($Cost_{cap}$ in $/year) of the battery pack, UC pack, and DC/DC converter, as well as the replacement cost ($Cost_{rep}$ in $/year) of the battery pack due to the performance degradation within a reference time (RT).

$$LCC = Cost_{cap}/360 + Cost_{rep}/360 \quad \text{(F - 42)}$$

$$Cost_{cap} = CRF \cdot \left(C_{kWh\_BT} \cdot N_{BT} \cdot M_{BT} \cdot E_{BT\_cell} + C_{kWh\_UC} \cdot N_{UC} \cdot M_{UC} \cdot E_{UC\_cell} + C_{kW\_DC} \cdot 1.2 \cdot P_{SC\_max}\right) \quad \text{(F - 43)}$$

$$CRF = \frac{i \cdot (1+i)^{RT}}{(1+i)^{RT} - 1} \quad \text{(F - 44)}$$

where C_{kWh_BT} and C_{kWh_UC} are the referential costs of the battery and UC packs in \$/kWh, C_{kW_DC} is the referential cost of the DC/DC converter in \$/kW, E_{BT_cell}, and E_{UC_cell} are the energy of the battery and UC cell that can be acquired from product specifications, P_{SC_max} is the maximum power of the UC pack, and CRF is the capital recovery factor, calculated by the interest rate i and RT.

$$Q_{loss\_LCC} = Q_{loss} \,/\, T \cdot 3600 \cdot 24 \cdot 360 \cdot U \cdot RT \quad \text{(F - 45)}$$

$$Cost_{rep} = \sum_{n=1}^{ceil\left(Q_{loss\_LCC}/0.2-1\right)} (1+i)^{-n \cdot 0.2} \cdot C_{kWh\_BT} \cdot N_{BT} \cdot M_{BT} \cdot E_{BT\_cell} \cdot CRF \quad \text{(F - 46)}$$

where Q_{loss_LCC} is the battery capacity loss within the reference time and the battery pack needs to be replaced when the value exceeds 20%, T represents the duration of the driving cycle in seconds, U is used to show the utilization of the equipment (working mode and time), and the function of $ceil(\,)$ is to obtain the higher integer value of its argument.

REFERENCES

[1] B. Nykvist and M. Nilsson, "Rapidly falling costs of battery packs for electric vehicles," *nature climate change*, 5, (2015): 329.

[2] R. Hensley, J. Newman, M. Rogers, and M. Shahinian, "Battery technology charges ahead," *McKinsey Quarterly*, 3 (2012): 5-50.

[3] L. Gao, S. Liu, and R. Dougal, "Dynamic lithium-ion battery model for system simulation," *IEEE Transactions on Components and Packageing Technologies*, 25 (2002): 495-505.

[4] H. Gu, "Mathematical analysis of a Zn/NiOOH cell," *Journal of The Electrochemical Society*, 130 (1983): 1459-1464.

[5] M. Chen and G. A. Rincon-Mora, "Accurate electrical battery model capable of predicting runtime and IV performance," *IEEE Transactions on Energy Conversion*, 21 2006: (504-511).

[6] H. He, R. Xiong, and J. Fan, "Evaluation of lithium-ion battery equivalent circuit models for state of charge estimation by an experimental approach," *Energies*, 4 (2011): 582-598.

[7] B. Y. Liaw, G. Nagasubramanian, R. G. Jungst, and D. H. Doughty, "Modelling of lithium ion cells—A simple equivalent-circuit model approach," *Solid State Ionics* 175 2004: (835-839).

[8] M. Verbrugge and B. Koch, "Generalized recursive algorithm for adaptive multiparameter regression application to lead acid, nickel metal hydride, and lithium-ion batteries," *Journal of the Electrochemical Society,* 153 (2006): A187-A201.

[9] M. Verbrugge, "Adaptive, multi-parameter battery state estimator with optimized time-weighting factors," *Journal of Applied Electrochemistry*, 37 (2007): 605-616.

[10] S. Jung and D. Kang, "Multi-dimensional modelling of large-scale lithium-ion batteries," *Journal of Power Sources*, 248 (2014): 498-509.

[11] M. Doyle, T. F. Fuller, and J. Newman, "Modelling of galvanostatic charge and discharge of the lithium/polymer/insertion cell," *Journal of the Electrochemical Society*, 140 (1993): 1526-1533.

[12] M. Doyle and Y. Fuentes, "Computer simulations of a lithium-ion polymer battery and implications for higher capacity next-generation battery designs," *Journal of the Electrochemical Society*, 150 (2003): A706-A713.

[13] M. Doyle, T. F. Fuller, and J. Newman, "The importance of the lithium ion transference number in lithium/polymer cells," *Electrochimica Acta*, 39 (1994): 2073-2081.

[14] K. Smith and C.-Y. Wang, "Solid-state diffusion limitations on pulse operation of a lithium ion cell for hybrid electric vehicles," *Journal of Power Sources*, 161 (2006): 628-639.

[15] K. A. Smith, C. D. Rahn, and C.-Y. Wang, "Control oriented 1D electrochemical model of lithium ion battery," *Energy Conversion and Management*, 48 (2007): 2565-2578.

[16] K. A. Smith, C. D. Rahn, and C.-Y. Wang, "Model-Based Electrochemical Estimation and Constraint Management for Pulse Operation of Lithium Ion Batteries," *IEEE Transactions on Control Systems Technology*, 16 (2010): 654-663.

[17] P. Ramadass, B. Haran, R. White, and B. N. Popov, "Mathematical modelling of the capacity fade of Li-ion cells," *Journal of Power Sources*,123 (2003): 230-240.

[18] C. Wang, W. Gu, and B. Liaw, "Micro-Macroscopic Coupled Modelling of Batteries and Fuel Cells I. Model Development," *Journal of the Electrochemical Society*, 145 (1998): 3407-3417.

[19] D. Di Domenico, A. Stefanopoulou, and G. Fiengo, "Lithium-ion battery state of charge and critical surface charge estimation using an electrochemical model-based extended Kalman filter," *Journal of dynamic systems, measurement, and control*, 132 (2010): 061302.

[20] S. Santhanagopalan, Q. Guo, and R. E. White, "Parameter estimation and model discrimination for a lithium-ion cell," *Journal of the Electrochemical Society*, 154 (2007): A198-A206.

[21] D. Britz, "The point method for electrochemical digital simulation," *Analytica Chimica Acta*, 122 (1980): 331-336.

[22] J. C. Forman, S. J. Moura, J. L. Stein, and H. K. Fathy, "Genetic parameter identification of the Doyle-Fuller-Newman model from experimental cycling of a LiFePO 4 battery," in *American Control Conference (ACC) 2011*, (2011): 362-369.

[23] J. Newman, K. E. Thomas, H. Hafezi, and D. R. Wheeler, "Modelling of lithium-ion batteries," *Journal of power sources,* 119 (2003): 838-843.

[24] P. Arora, R. E. White, and M. Doyle, "Capacity fade mechanisms and side reactions in lithium-ion batteries," *Journal of the Electrochemical Society,* 145 (1998): 3647-3667.

[25] P. Liu, J. Wang, J. Hicks-Garner, E. Sherman, S. Soukiazian, M. Verbrugge, *et al.*, "Ageing mechanisms of LiFePO4 batteries deduced by electrochemical and structural analyses," *Journal of the Electrochemical Society,* 157 (2010): A499-A507.

[26] S. Bourlot, P. Blanchard, and S. Robert, "Investigation of ageing mechanisms of high power Li-ion cells used for hybrid electric vehicles," *Journal of Power Sources,* 196 (2011): 6841-6846.

[27] D. Linden, "Handbook of batteries," in *Fuel and Energy Abstracts*, (1995): 265.

[28] D. Zhang, B. Haran, A. Durairajan, R. E. White, Y. Podrazhansky, and B. N. Popov, "Studies on capacity fade of lithium-ion batteries," *Journal of Power Sources,* 91 (2000): 122-129.

[29] P. Ramadass, B. Haran, R. White, and B. N. Popov, "Capacity fade of Sony 18650 cells cycled at elevated temperatures: Part I. Cycling performance," *Journal of power sources,* 112 (2002): 606-613.

[30] P. Ramadass, B. Haran, R. White, and B. N. Popov, "Capacity fade of Sony 18650 cells cycled at elevated temperatures: Part II. Capacity fade analysis," *Journal of power sources,* 112 (2002): 614-620.

[31] A. Barré, B. Deguilhem, S. Grolleau, M. Gérard, F. Suard, and D. Riu, "A review on lithium-ion battery ageing mechanisms and estimations for automotive applications," *Journal of Power Sources,* 241 (2013): 680-689.

[32] M. Broussely, P. Biensan, F. Bonhomme, P. Blanchard, S. Herreyre, K. Nechev, *et al.*, "Main ageing mechanisms in Li ion batteries," *Journal of power sources,* 146 (2005): 90-96.

[33] X. Han, M. Ouyang, L. Lu, J. Li, Y. Zheng, and Z. Li, "A comparative study of commercial lithium ion battery cycle life in electrical vehicle: Ageing mechanism identification," *Journal of Power Sources,* 251 (2014): 38-54.

[34] K. Takei, K. Kumai, Y. Kobayashi, H. Miyashiro, N. Terada, T. Iwahori, *et al.*, "Cycle life estimation of lithium secondary battery by extrapolation method and accelerated ageing test," *Journal of Power Sources,* 97 (2001): 697-701.

[35] M. Safari, M. Morcrette, A. Teyssot, and C. Delacourt, "Multimodal physics-based ageing model for life prediction of Li-ion batteries," *Journal of The Electrochemical Society,* 156 (2009): A145-A153.

[36] S. Santhanagopalan, Q. Zhang, K. Kumaresan, and R. E. White, "Parameter estimation and life modelling of lithium-ion cells," *Journal of The Electrochemical Society,* 155 (2008): A345-A353.

[37] Z. Song, J. Li, X. Han, L. Xu, L. Lu, M. Ouyang, *et al.*, "Multi-objective optimization of a semi-active battery/supercapacitor energy storage system for electric vehicles," *Applied Energy,* 135 (2014): 212-224.

[38] N. Omar, M. A. Monem, Y. Firouz, J. Salminen, J. Smekens, O. Hegazy, *et al.*, "Lithium iron phosphate based battery–assessment of the ageing parameters and development of cycle life model," *Applied Energy,* 113 (2014): 1575-1585.

[39] J. Wang, P. Liu, J. Hicks-Garner, E. Sherman, S. Soukiazian, M. Verbrugge, *et al.*, "Cycle-life model for graphite-LiFePO4 cells," *Journal of Power Sources,* 196 (2011): 3942-3948.

[40] J. Shen, S. Dusmez, and A. Khaligh, "Optimization of sizing and battery cycle life in battery/ultracapacitor hybrid energy storage systems for electric vehicle applications," *IEEE Transactions on industrial informatics,* 10 (2014): 2112-2121.

[41] Product Information Sheet, "Nanophosphate® Lithium Ion Prismatic Pouch Cell AMP20M1HD-A," [On line], Available at: http://liionbms.com/pdf/a123/AMP20M1HD-A.pdf.

[42] V. Johnson, "Battery performance models in ADVISOR," *Journal of power sources,*110 (2002): 321-329.

[43] I. Bloom, B. Cole, J. Sohn, S. Jones, E. Polzin, V. Battaglia, *et al.*, "An accelerated calendar and cycle life study of Li-ion cells," *Journal of Power Sources,* 101 (2001): 238-247.

[44] L. Zhang, Z. Wang, X. Hu, F. Sun, and D. G. Dorrell, "A comparative study of equivalent circuit models of ultracapacitors for electric vehicles," *Journal of Power Sources,* 274 (2015): 899-906.

Appendix G. Improvement of the Reduced-Order Hydrodynamic and Ship Propulsion Model

G1 SUMMARY

In an effort to improve the modelling accuracy of the reduced-order hydrodynamics simulation, the model's parameterization procedures were altered and several of the simulation subsystems were revised. Noteworthy changes to the model include

a) revised formulation of the propeller torque coefficient and thrust coefficient lookup surfaces,
b) a revised process for estimation of the propeller thrust deduction factor,
c) the augmentation of CFD bare hull resistance with appendage resistance,
d) accounting for effects of current and wind loading through ProteusDS simulation.

Simulation results show a noticeable improvement in accuracy when comparing the predicted ship speed with the recorded ship speed. As presented in Figure G - 1, the error between recorded speed and predicted speed was reduced to approximately 5-7% during the transiting portion of the voyage of the studied vessel.

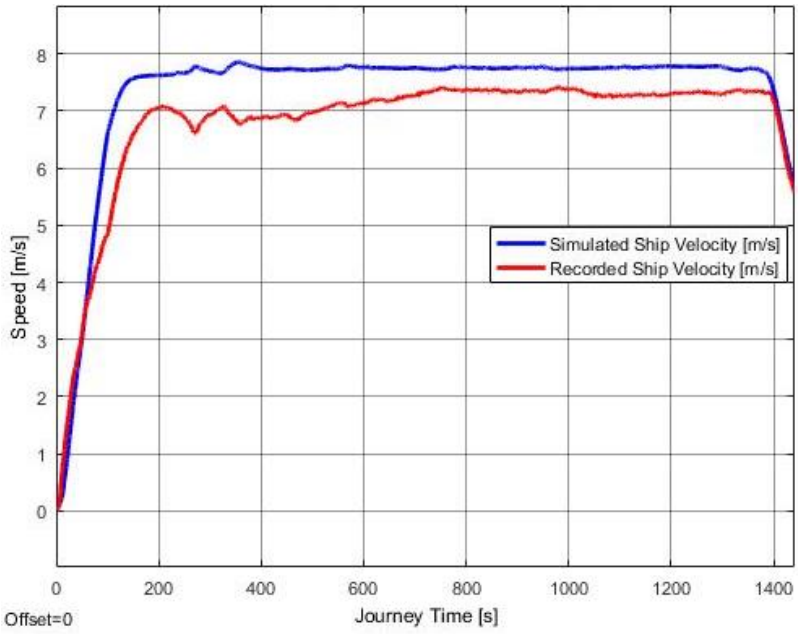

Figure G - 1 – Recorded Ship Speed vs. Simulated Ship Speed

G2 METHODOLOGY

To improve the accuracy of the reduced-order hydrodynamic and propulsion models, and to verify the accuracy improvements of early-developed and newly-added subsystems of the integrated model, the following changes have been made during the model validation.

a) During the voyage of the ferry, the propeller was not operating at a constant speed as assumed previously in the model. The time-varying propeller shaft speed recorded in the collected ship operation data is then used as the actual propeller speed for generating the lookup parameter surface for estimating propeller thrust force using CFD simulations. This led to a more appropriate comparison between the recorded ship speed and the model predicted speed.
b) Since propeller thrust force is influenced by wake fraction, thrust deduction and ship speed, an addition to the model to capture the ship maneuvering was added to better estimate propeller thrust forces during ship-maneuvering to determine the predicted ship speed. Variations of the wake, thrust and ship speed during ship-maneuvering have been considered.
c) In addition to the hydrodynamic calculations parameterized using CFD simulation in calm water, the ship speed influencing wind and current loading was added using a feedback loop in the ship propulsion-modelling module to predict resulting ship speed.
d) The added propulsion-force feedback loop in the ship speed-prediction module affects the estimated thrust force at the next time instance, considering the advance velocity and wake fraction effects, the model predicted ship speed was compared with the experimentally recorded ships speed throughout the voyage, in addition to the straight crossing portion of the voyage, to study the model accuracy.

G2.1 Revised Procedure for Developing Thrust Coefficient and Torque Coefficient Lookup Surfaces

It is well documented in the literature that propeller thrust, T and propeller torque Q can be represented in terms of their respective torque and thrust coefficients K_T and K_Q such that,

$$T = K_T \rho n^2 D^4 \tag{G-1}$$

$$Q = K_Q \rho n^2 D^5 \tag{G-2}$$

Where n is the propeller's angular velocity, ρ is the density of the fluid, D is the diameter of the propeller and the coefficients K_T and K_Q are both functions of advance ratio J and incident flow angle α.

The motivation for the construction of K_T and K_Q lookup surfaces for use in the simulation is to provide a fast and computationally efficient way of solving for thrust force and torque, at every time step, as $\rho, n, D, J \; and \; \alpha$ are known simulation states. The coefficients $K_T = f(\alpha, J)$ and $K_Q = f(\alpha, J)$ are both functions of the incident angle and advance ratio. The advance ratio J is given by

$$J = \frac{Va}{nD} \tag{G-3}$$

where Va is the advance velocity.

Varying the angles of incident flow into a propeller, at an angle of α, results in changes to the advance ratio, as depicted in Figure G - 2.

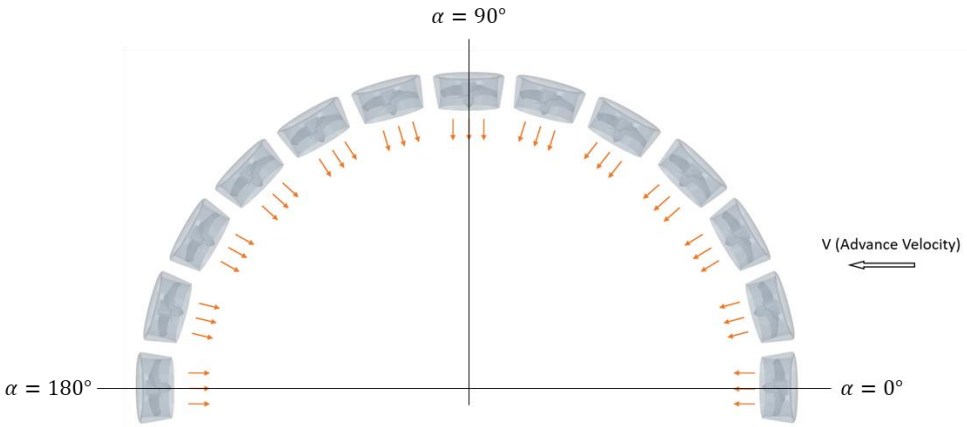

Figure G - 2 – Advance Velocity at Various Incident Angles to Propeller

As J becomes non-finite when $n = 0$, the lookup surfaces for $K_T = f(\alpha, J)$ and $K_Q = f(\alpha, J)$ are remapped to become functions of incident angle α and thrust quadrant angle β, or $K_T = f(\alpha, \beta)$ and $K_Q = f(\alpha, \beta)$ where the thrust quadrant angle β is defined as:

$$\beta = \tan^{-1}\left(\frac{V_a}{0.7\pi n D}\right) \tag{G-4}$$

and β is asymptotically limited to $\frac{\pi}{2}$ when $n = 0$.

To obtain the K_T and K_Q lookup surfaces, CFD experiments (see Figure G - 3) are repeated at incident angles of $\alpha = 0°$ through to $\alpha = 180°$ in 15-degree increments. CFD results for K_T vs β at $\alpha = 0°$ and $\alpha = 180°$ are illustrated in Figure G - 4 and Figure G - 5, respectively.

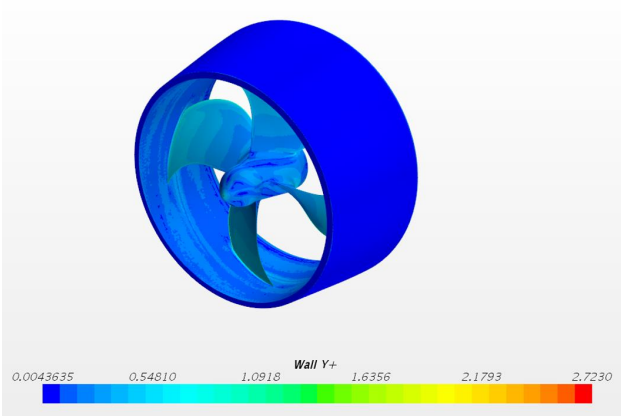

Figure G - 3 – Propeller CFD Study Visualization

These CFD results are fit with polynomial functions, as presented in Figure G - 6 and Figure. Repeating the curve fitting process at all angles of α, the K_T and K_Q lookup surfaces can be constructed as presented in Figure G - 8 and Figure G - 9. These surfaces are then integrated into the propulsion module, providing an efficient method to obtain propeller thrust T and torque Q at each iteration of the simulation.

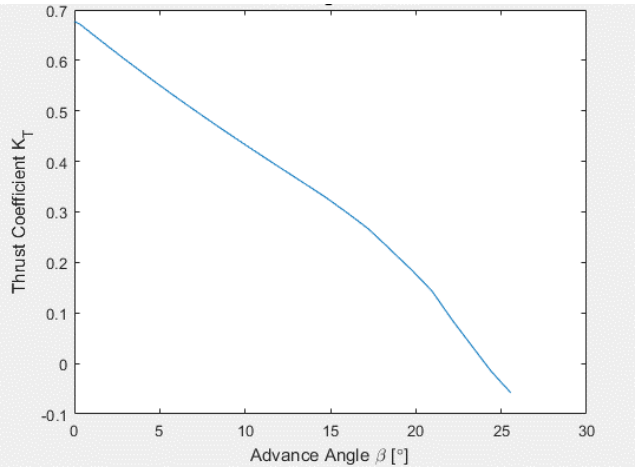

Figure G - 4 CFD Results K_T vs β at $\alpha = 0°$

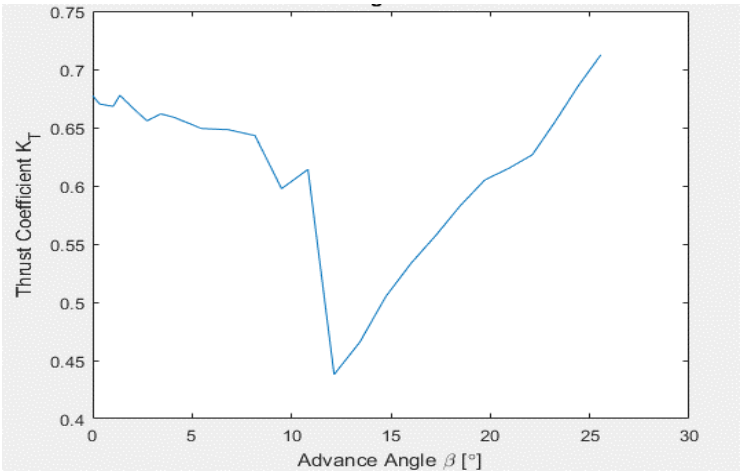

Figure G - 5 CFD Results K_T vs β at $\alpha = 180°$

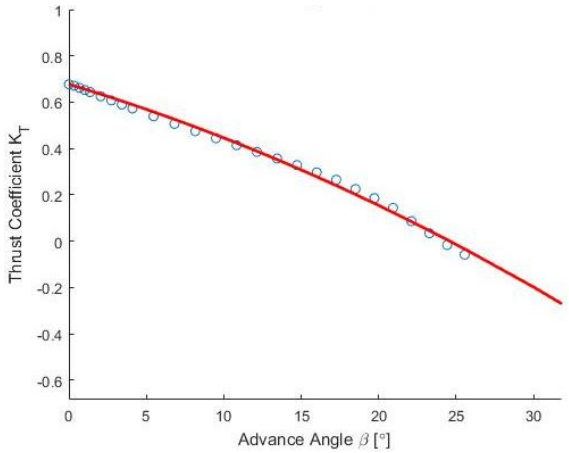

Figure G - 6 Fitted $\boldsymbol{K_T}$ vs $\boldsymbol{\beta}$ at Angle $\boldsymbol{\alpha = 0°}$

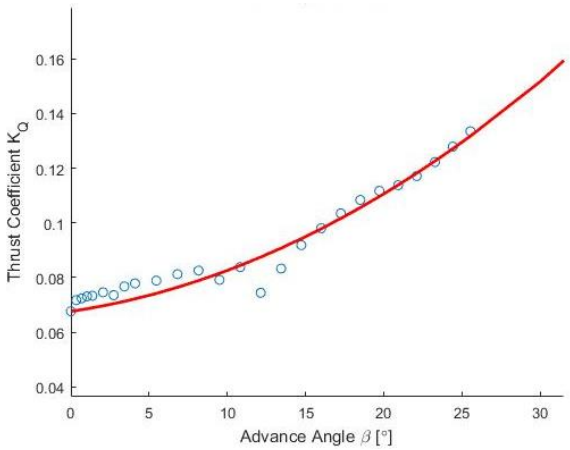

Figure G - 7 Fitted $\boldsymbol{K_T}$ vs $\boldsymbol{\beta}$ at Angle $\boldsymbol{\alpha = 180°}$

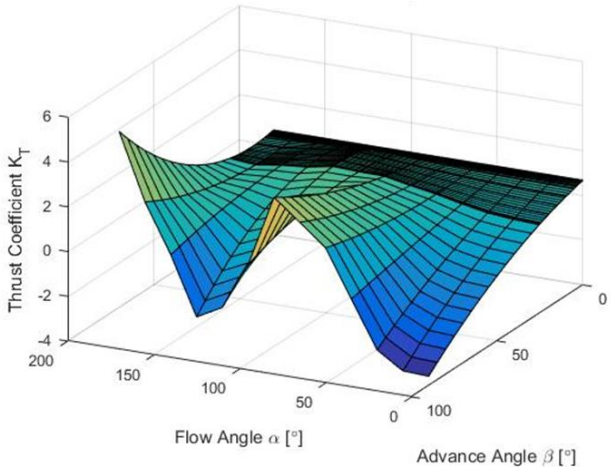

Figure G - 8 Fitted $\boldsymbol{K_T}$ Lookup Surface

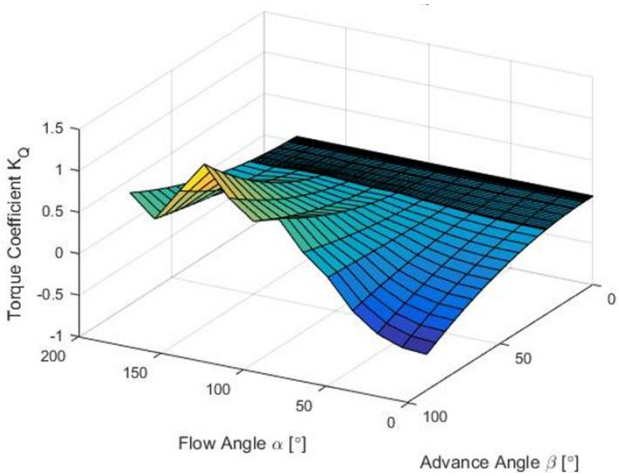

Figure G - 9 Fitted $\boldsymbol{K_Q}$ Lookup Surface

G2.2 Revised Process for Thrust Deduction Factor

Due to numerical instabilities encountered during CFD analysis, the studies of propeller thrust and hull resistance are currently completed independently of each other. Carlton [1] states that the presence of a rotating propeller near the hull causes a propeller-hull interaction that alters the local pressure field around the hull. This interaction has the effect of reducing propeller thrust according to

$$R = T(1 - t) \tag{G-5}$$

Where R is the bare hull towed resistance, T is the required thrust and t is the thrust deduction factor.

Fortunately, as traditional naval architecture relies heavily on tow tank results from bare hulls, empirical relations that quantify the expected thrust deduction effects are available for nearly all hull and propeller combinations. For example, a ship used in one case study used to validate this work employed the use of podded propulsion for which Flikkema et al. [2] proposed the empirical relation of

$$t_P = 0.21593 + 0.099768C_B - 0.56056\frac{D}{\sqrt{BT}} \tag{G-6}$$

Where C_B is the box coefficient, D is the propeller diameter, B is the ship beamwidth, and T is the ship's draft.

G2.3 Revised Process for Hull Resistance Parameterization with Corrections for Appendage Drag and Wake Fraction

To improve accuracy and augment the simulation model with previously unaccounted for sources of resistance, the parameterization process for hull resistance was revised. One such modification was the use of the hull resistance equation proposed by Fossen [3] that was shown to produce more accurate resistance at low speed. This equation calculates drag force in the surge as follows:

$$F_{Drag} = \underbrace{X_u u_r}_{\substack{Linear \\ Force}} - \underbrace{\frac{1}{2}\rho S|u_r|u_r(1+k)\cdot\left[C_F({u_r}^{max}) + \left(\frac{A_x}{S}C_X - C_F({u_r}^{max})\right)e^{-(\alpha\cdot{u_r}^2)}\right]}_{\substack{Non-Linear \\ Force}} \tag{G-7}$$

where A_x is the projected frontal wetted area, S is the wetted surface, u_r is the ship velocity in surge, and $C_F({u_r}^{max})$ is the hull friction coefficient at design speed. X_u, k, C_X, and α are four parameters that can be fitted to CFD bare hull resistance results through regression methods as shown in Figure G - 10.

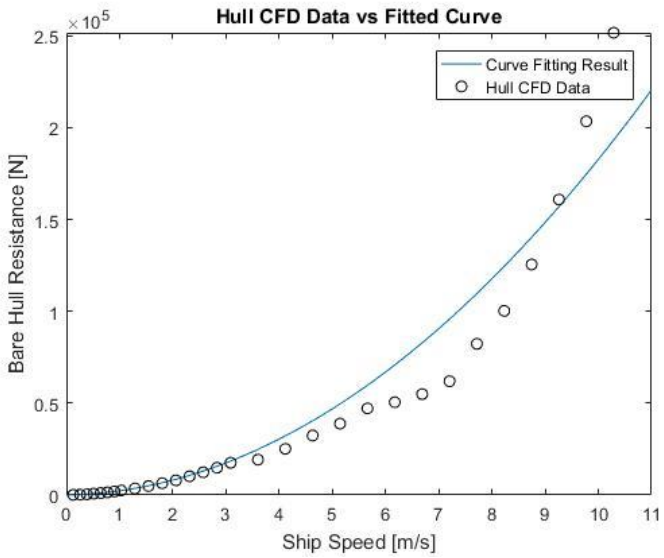

Figure G - 10 – Curve Fitting of CFD Bare Hull Resistance

Once the equation for hull resistance has been parameterized from bare hull CFD results, the bare hull resistance is then augmented with appendage drag resistance using available empirical relations according to the ship geometry being studied. Examples of appendage drag include the study of a ship in Abdul Ghani *et al.* [4], where it was concluded that a podded propulsion module increased the total hull resistance by 20% when compared with experimental bare hull results obtained for the same ship.

In this study, appendage resistance has been conservatively estimated to increase total hull resistance by 15% over results obtained from bare hull CFD studies. At the time of writing, a bare hull ship model used in this work has been modified with four podded propulsion modules as presented in Figure G - 11.

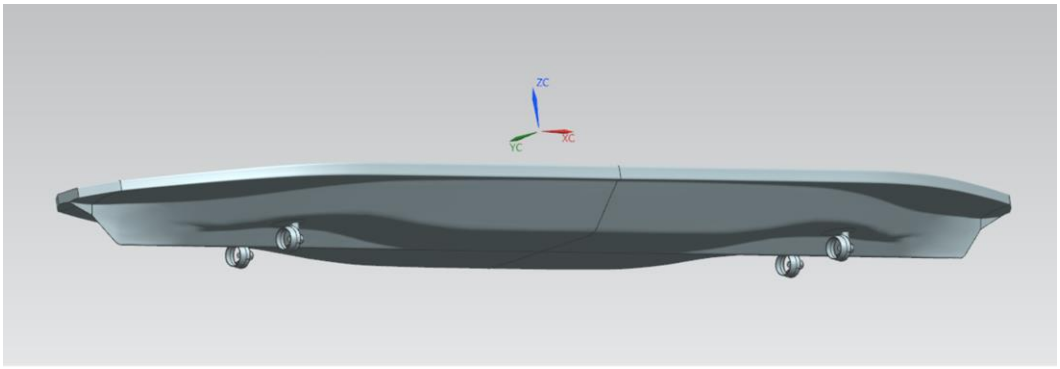

Figure G - 11 – Hull Model with Thrusters Included

In addition to appendage drag, surface roughness and hull fouling can have significant effects on hull resistance. Molland *et al* show that these generally account for a minimum of 10-15% of the total hull resistance [5], as illustrated in Figure G - 12.

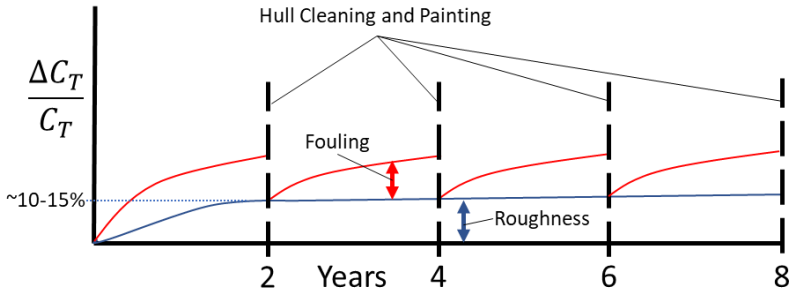

Figure G - 12 The Effects of Roughness and Fouling on Overall Resistance. Reproduced from [5]

Proceedings from ITTC 2017 [6] discuss recent developments and attempts to account for the increased drag caused by hull surface roughness and fouling effects. Although several groups have studied these effects, there is no generally agreed-upon method that can be universally applied to all ships in all scenarios. The ITTC recommended procedures and guidelines document *7.5-03-02-03* remarks that "Surface roughness is still an active field of research, and no general guidelines can yet be given" [7].

In many CFD applications, the common assumption of hydraulically smooth surfaces will produce adequate results. In the case of ships, however, this assumption breaks down at typical cruising velocities and can lead to erroneous results. This is due to a decrease in the height of the viscous sublayer that forms over the ship hull as Reynolds number increases. When Reynolds number has surpassed the critical Reynolds number, the surface roughness of the ship hull protrudes through the viscous sublayer and the surface can no longer be considered hydraulically smooth as illustrated in Figure G - 13 and Figure G - 14.

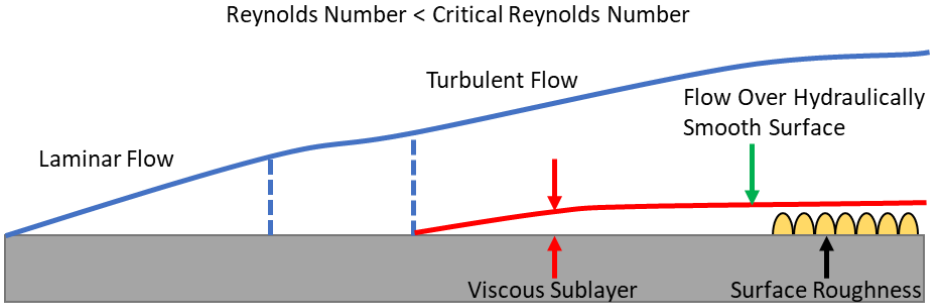

Figure G - 13 Flow Over Smooth Surface at Low Reynolds Number [1]

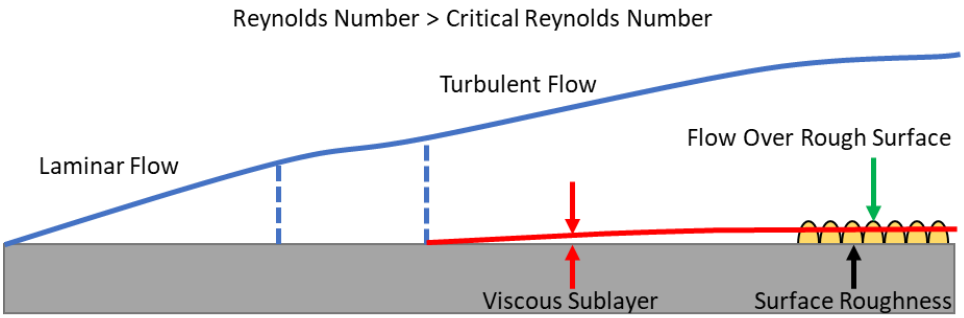

Figure G - 14 Flow Over Rough Surface at High Reynolds Number [1]

One promising method to account for surface roughness through CFD is proposed by Demirel *et al.* [8] which describes the modification of the wall function from within the CFD software StarCCM+ and produced results within 2% of experimental data. This method is particularly attractive as StarCCM+ is the CFD software currently relied upon in this work. Until modifications to the wall function have been implemented as in [8], this work has conservatively estimated that surface roughness increases the total hull resistance by 10% over results obtained from bare hull CFD studies.

In addition to accurately capturing hull surge resistance, it is essential to account for the hull propeller interaction known as wake fraction. Due to the geometry of the hull and its effect on the flow field, the advance velocity of the fluid into the propeller is not always equal to the ships forward velocity. Advance velocity is provided by

$$V_a = (1 - w)u_r \tag{G-8}$$

where w is the wake fraction parameter and u_r is the ship velocity in surge.

To obtain estimates for wake fraction, velocity probes were inserted into the bare hull CFD studies and placed at locations where a ship's propeller(s) would have been. Advance velocities were measured and values for wake fraction were obtained for a range of forwarding ship speeds as presented in Figure G - 15. The wake fraction curves and augmented bare hull resistance were then integrated into the model to account for these effects.

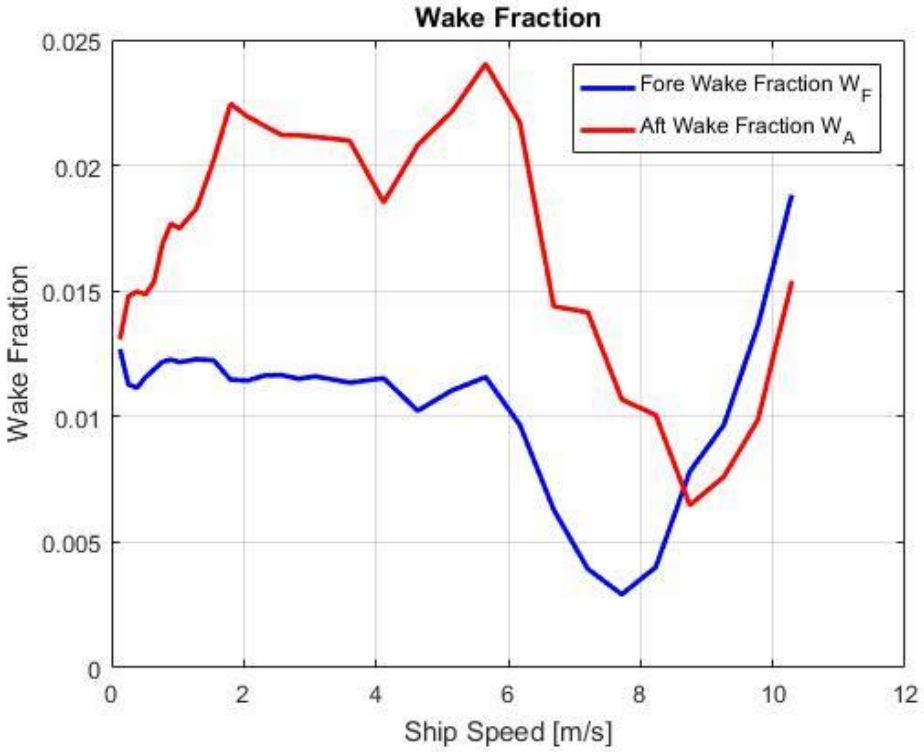

Figure G - 15 Wake Fraction

G2.4 Ocean Current and Wind Loading Estimates through ProteusDS Simulations

To account for ocean current and wind forces on the hull and superstructure, simulations in ProteusDS software were conducted. For this process, both current and wind velocity data were harvested from weather buoys near the route being studied.

A 3D mesh representing the hull and superstructure is loaded into ProteusDS (see Figure G - 16) and the software calculates the total loading forces through the summation of the force from each panel of the mesh using

$$F = \frac{1}{2}\rho C_d A v_{rel}^2 \tag{G-9}$$

where ρ is the density of the fluid (seawater for current forces, or air for wind forces).

Figure G - 16 Wind Loading Study above Waterline View

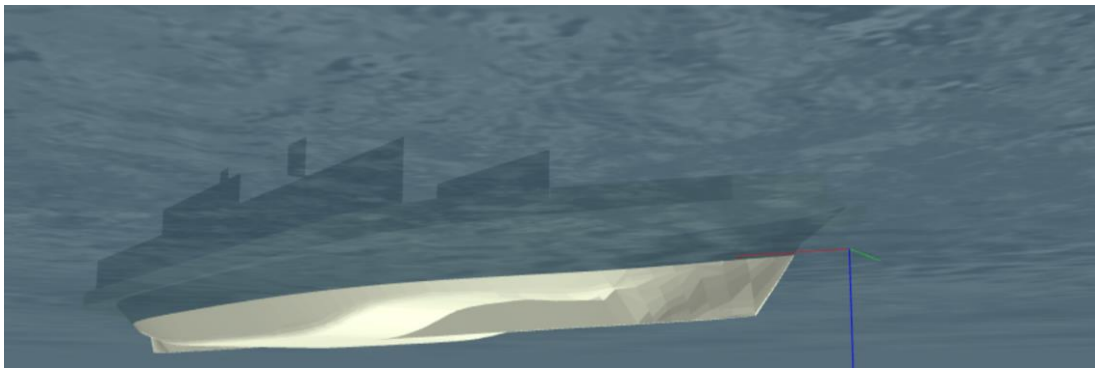

Figure G - 17 – Ocean Current Loading Study below Waterline View

Simulation parameters and the resulting current and wind loads are presented in Table G - 1.

Table G - 1 Ocean Current and Wind Loading Study

Ship Speed (m/s)	7.0
Ship heading (deg)	13
Current Direction	80
Current speed (m/s)	1.03
Wind Direction	100
Wind Speed (m/s)	2.78
Wind loading - x Direction (N)	1.46E+02
Wind loading - y Direction (N)	4.30E+02
Current loading - x direction (N)	1.20E+04
Current loading - y direction (N)	1.10E+05

While current and wind loading is presently approximated as constant for the duration of short voyages, the capability to vary wind and current velocities over the course of a voyage is presently being implemented.

REFERENCES

[1] J. S. Carlton, Marine Propellers and Propulsion, Waltham: Elsevier, 2012.

[2] M. B. Flikkema, J. Holtrop and T. J. C. Van Terwisga, "Aparametric power prediction model for tractor pods," in *Proceedings of Second International Conference on Advances in Podded Propulsion*, Brest, 2006.

[3] T. I. Fossen, Handbook of Marine Craft Hydrodynamics and Motion Control, Chichester: John Wiley & Sons Ltd., 2011.

[4] M. P. Abdul Ghani, O. Yaakob, N. Ismail, A. S. A. Kader and A. F. Ahmad Sabki, "Experimental Analysis of Podded Propulsor on Naval," *TransNav*, vol. 8, no. 1, pp. 153-156, 2014.

[5] A. F. Molland, S. R. Turnock and D. A. Hudson, Ship Resistance and Propulsion: Practical Estimation of Ship Propulsive Power, New York: Cambridge University Press, 2011.

[6] ITTC, "The Resistance Committee Final Report and Recommendations to the 28th ITTC," in *Proceedings of 28th ITTC*, Wuxi, 2017.

[7] ITTC, "7.5-03-02-03 Practical Guidelines for Ship CFD Application," in *ITTC Recommended Procedures and Guidelines*, 2011.

[8] Y. K. Demirel, M. Khorasanchi, O. Turan, A. Incecik and M. P. Shultz, "A CFD model for the frictional resistance prediction of antifouling coatings," *Ocean Engineering,* no. 89, pp. 21-31, 2014.

[9] K. Andersen, Development of a Time-Domain Modelling Platform for Hybrid, Victoria: University of Victoria, 2009.

Appendix H. Experimental Investigation of Cavitation-induced Propeller Noise

ABSTRACT

Ship-induced acoustic noise can be treated as a measure of the environmental impact of the marine transportation industry, where, if present, cavitation is often the dominant noise source. Quantitative prediction of emitted noise levels requires detailed characterization of cavitation regimes associated with the operation of marine propellers. Appendix H outlines an experimental campaign conducted in a pressurized cavitation tunnel, following the experimental standards set by the International Towing Tank Conference (ITTC). Using stroboscopic photographic images of cavitation events, measurements of propeller loads, and high-resolution acoustic pressure level measurements across a broad frequency spectrum, the acoustic emissions of four distinct cavitation regimes were examined in various combinations.

The results of this experimental investigation provide fundamental insights into modelling techniques for acoustic noise from propeller cavitation:

- A small number of high-level parameters, such as cavitation number, thrust coefficient, advance ratio, and pitch angle, could be sufficient in defining appropriate, reduced-order noise estimation tools.
- Logarithmic decay models can be effective for predicting acoustic noise spectra from tip vortex, sheet, and pressure side cavitation, but may be ineffective for the case of bubble cavitation.
- Linear ship speed-noise models are insufficient for predicting propeller cavitation noise in off-design conditions.

This experimental campaign will also be used as a benchmark to validate the numerical methods being used in an ongoing computational campaign studying the prediction of cavitation noise from ship propellers.

The results of these experiments were originally presented at the *9th International Symposium on Fluid-Structure Interactions, Flow-Sound Interactions, Flow-Induced Vibration & Noise* in Toronto, Canada on July 10, 2018 [13].

H1. CONTEXT

Acoustic noise is a critical component of the overall pollution emitted from marine vessels, where the dominant noise source is often cavitation induced by the ship propellers [1], [2]. Attention to this anthropogenic noise source has grown following a recent understanding of its chronic impacts on marine fauna [3], [4], and ship noise emission regulations are expected to become widespread in the near future. The ability to predict noise production from marine vessels is of primary importance for developing intelligent mitigation approaches, including operational strategies and propeller designs. While semi-empirical noise prediction models relying primarily on vessel velocity have existed since the WWII era, these models neglect the significant influence of varied propeller cavitation types, limiting their applicability and validity. It is, therefore, necessary to

investigate the influence of cavitation characteristics on propeller noise, as well as the predictive value of related high-level hydrodynamic parameters.

An experimental campaign was conducted on a scale model propeller in a cavitation tunnel. The present results intend to serve as a validating benchmark for numerical simulations. Measurements were conducted under steady inflow conditions, which eliminated the effects of the hull wake and shaft inclination in order to provide a set of simplified cases for the validation of numerical methodologies before moving to more complex conditions.

A range of operating parameters was examined to produce a representative range of cavitation phenomena. The cavitation types observed in the current study are tip vortex cavitation, sheet cavitation, pressure-side cavitation, and bubble cavitation. The corresponding cavitation patterns are shown schematically in Figure H - 1. Control of the cavitation number and thrust coefficient allowed noise contributions from these individual types of cavitation to be studied both in isolation and in various combinations. Relations between the observed cavitation structures and the corresponding acoustic spectra were analyzed in order to develop semi-empirical models of cavitation induced noise.

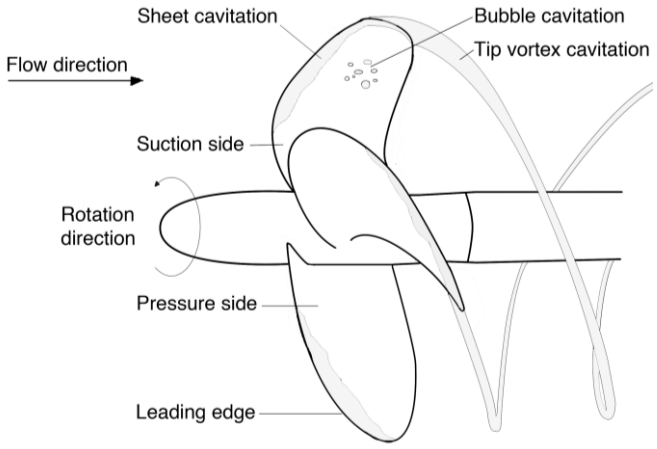

Figure H - 1 Schematic of Propeller Cavitation Regimes

H2. GLOSSARY

CPP	Controllable pitch propeller
D	Propeller diameter [m]
J	Advance ratio ($J = \frac{V_A}{nD}$)
K_Q	Torque coefficient ($K_Q = \frac{Q}{\rho n^2 D^5}$)
G	Average power spectral density [Pa^2/Hz]
K_T	Thrust coefficient ($K_T = \frac{T}{\rho n^2 D^4}$)
K_P	Non-dimensional pressure coefficient ($K_P = \frac{P}{\rho n^2 D^2}$)
L_{KP}	Non-dim. Sound pressure level ($L_{KP} = 20log_{10}\left(\frac{K_p}{10^{-6}}\right)$) [dB re 10^{-6}]

L_P	Sound pressure level ($L_P = 10log_{10}\left(\frac{G}{P_{ref}^2}\right)$) [dB re 1 μPa^2/Hz]
N	Shaft revolution rate [RPS]
P	Pressure [Pa]
P_∞	Undisturbed pressure [Pa]
P_{ref}	Acoustic reference pressure (1 μPa)
Q	Propeller torque [Nm]
T	Propeller thrust [Nm]
σ_N	Cavitation index ($\sigma_N = \frac{P_\infty - P_v}{1/2 \rho n^2 D^2}$)
ρ	Water density [kg/m^3]

H3. EXPERIMENTAL SYSTEMS AND TECHNIQUES

Cavitation tunnel tests were carried out at the University of Genoa cavitation tunnel. The closed-circuit water tunnel had a square test section of 0.57 m x 0.57m cross-section with a length of 2 m, as shown in Figure H - 2. Water quality was monitored by routine measurements of the amount of dissolved oxygen. A dissolved oxygen content level of approximately 4.5 ppm was maintained in order to correctly simulate cavitation while avoiding possible noise absorption by free bubbles.

The propeller thrust, torque, and rotation speed were measured with a dynamometer. The corrections of Wood and Harris [5] were used to correct the measurements to account for tunnel effects. Stroboscopic images of the propeller cavitation were captured by three Allied Vision Tech Marlin F145B2 Firewire cameras, with a resolution of 1392 x 1040 pixels. Lighting was provided by two Movistrob type 900 lamps driven by a stroboscope Movistrob type 900-s.

Noise measurements were recorded by means of two miniaturized hydrophones, namely one Bruel & Kjaer type 8103 and one Reson TC4013, both driven by individual Bruel & Kjaer type 2635 charge amplifiers. Each acoustic acquisition consisted of 2^{21} samples, acquired with a sampling frequency of 200 kHz. Hydrophone positions within the cavitation tunnel are shown in Figure H - 3. One hydrophone, referred to here as ‘H1’, was a Bruel & Kjaer type 8103 and was positioned outside the tunnel test section in a plexiglass tank below the propeller. This tank is completely filled with water and separated from the flow. The second hydrophone, referred to here as ‘H2’, is placed inside the tunnel, protruding from a fin. Acoustics measurements of hydrophone H2 only are presented hereafter for brevity.

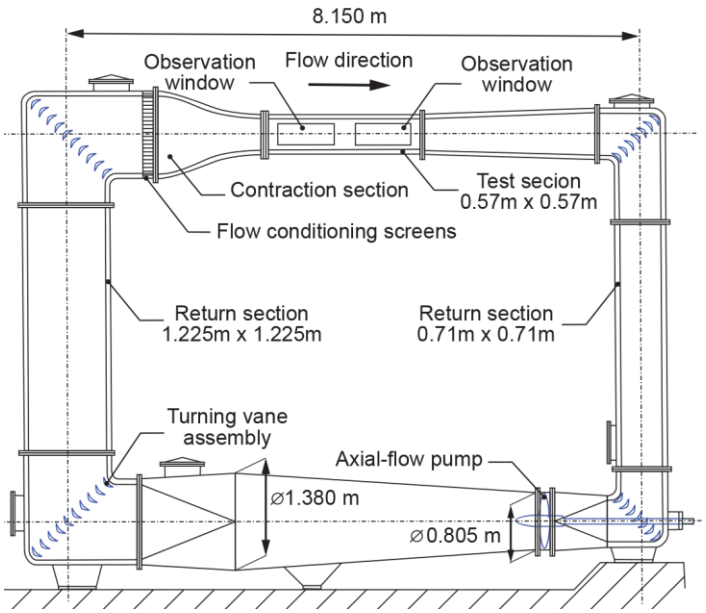

Figure H - 2 Schematic of the Cavitation Tunnel

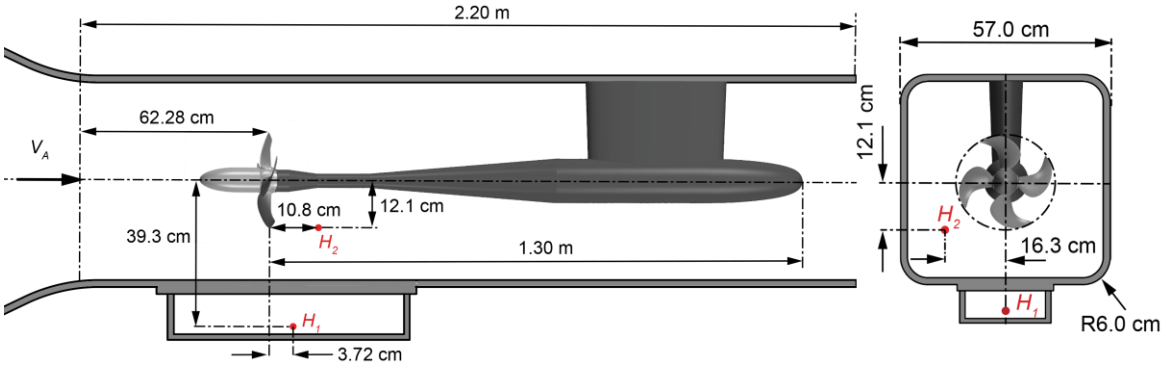

Figure H - 3 Left: Longitudinal View of The Test Section. Right: Transversal View. H1, H2 – Hydrophone Locations

The experiments were performed on a controllable pitch propeller (CPP) at two pitch settings, referred to hereafter as the design pitch and the reduced pitch. The main propeller characteristics are reported in Table H - 1. Uniform inflow conditions were implemented for all present cases.

Table H - 1 Propeller Characteristics.

Type	CPP
Number of blades	4
Direction of rotation	Left
Model diameter (m)	0.24
Design pitch $(P/D)_{0.7R}$	0.876
Reduced pitch $(P/D)_{0.7R}$	0.521

The advance ratio and the cavitation index were varied to achieve a range of cavitation phenomena as listed in Table H - 2. Definitions of the parameters used are provided in the nomenclature. Several noise measurements were carried out for each operation condition after stopping and restarting the cavitation tunnel to check the repeatability of the results. Further, a sensitivity study was performed by inducing small percentage variations to functioning parameters to check measurement uncertainty.

The propeller cavitation patterns that developed for each operating condition are broadly categorized in Table H - 2. Further descriptions and visual observations of the cavitation phenomena are provided in the following section.

Table H - 2 Experimental Conditions.

Name	$(P/D)_{0.7R}$	J	σ_N	N (rps)	K_T	$10K_Q$	Observed Cavitation Type(s)
C1	0.87	0.516	2.9	25	0.205	0.293	Tip vortex
C2	0.87	0.516	2.3	25	0.205	0.293	Tip vortex
C3	0.87	0.516	1.4	25	0.205	0.293	Bubble, streak, tip vortex, suction side sheet
C4	0.87	0.769	2.3	25	0.090	0.172	Pressure side leading edge
C5	0.87	0.345	2.3	25	0.270	0.350	Tip vortex, suction side sheet
C1b	0.521	0.404	2.6	30	0.095	0.125	Pressure side leading edge
C2b	0.521	0.404	2.3	30	0.095	0.125	Pressure side leading edge
C3b	0.521	0.404	1.4	30	0.095	0.125	Pressure side leading edge
C4b	0.521	0.500	2.3	30	0.050	0.095	Pressure side leading edge
C5b	0.521	0.345	2.3	30	0.120	0.140	None

Post-processing procedures for the radiated noise primarily followed the ITTC guidelines for model scale noise measurements [6]. In addition, the average power spectral density, G(f) in Pa^2/Hz, was computed from each sound pressure signal P(t) using Welch's method [7] of averageing modified spectrograms. The sound pressure power spectral density level L_P is then given by:

$$L_P(f) = 10log_{10}\left(\frac{G(f)}{P_{ref}^2}\right)\left(dB\ re\frac{1\mu Pa^2}{Hz}\right) \quad \text{(H-1)}$$

Results are presented in terms of the non-dimensional pressure coefficient K_p:

$$L_{KP} = 20log_{10}\frac{K_p}{10^{-6}} \quad \text{(H-2)}$$

The net sound pressure levels were computed by subtracting background noise from total noise as:

$$L_{PN} = 10log_{10}\left(10^{\left(\frac{L_{Ptot}}{10}\right)} - 10^{\left(\frac{L_{Pbg}}{10}\right)}\right) \quad \text{(H-3)}$$

Further definitions and methodologies were unvaried from the ITTC guidelines.

H4. RESULTS

H4.1. Cavitation Imaging

Stroboscopic images of selected operating conditions with the design pitch are provided in Figure H - 4 and Figure H - 5, showing the suction side and pressure side of a single blade, respectively, at the 90° and 270° positions. Periodic unsteadiness in cavitation patterns throughout a rotation cycle was not visualized.

Stable tip vortex cavitation occurred in isolation in cases C1 (not shown) and C2. Condition C2, with a lesser cavitation number, showed a thicker vortex cavity. Condition C3, with a further decrease in cavitation number, exhibited small bubble-type cavitation and in some cases, narrow streak cavitation, in addition to a further thickened tip vortex.

The advance ratio for condition C4 was increased to induce sheet cavitation on the pressure side, which developed on the leading edge from r/R~0.5 outward to the tip. A tip vortex cavitation was not present. In contrast, the advance ratio for condition C5 was reduced to an extent that a suction side sheet cavitation and a developed tip vortex were present.

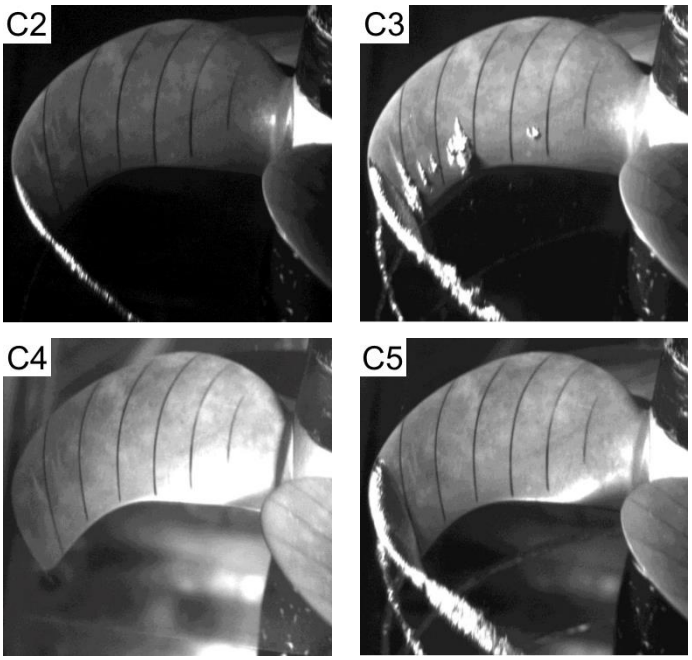

Figure H - 4 Stroboscopic Images of Cavitation Events During Conditions C2, C3, C4, C5. The Suction Side of The Blade Is Shown At 90°, Viewed from Above.

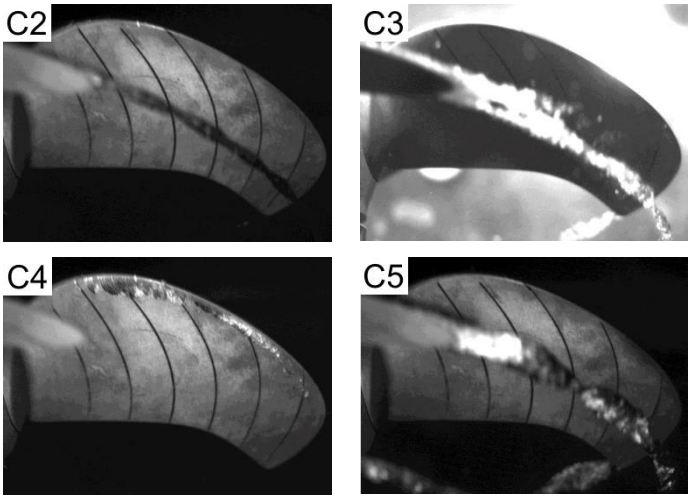

Figure H - 5 Stroboscopic Images of Cavitation Events During Conditions C2, C3, C4, C5. The Pressure Side of The Blade Is Shown At 270°, Viewed from Above.

Not shown in the single blade views are the equivalent operating cases at the reduced pitch, as labelled C1b through C5b in Table H - 2. This off-design condition corresponded to lower effective angles of attack than the design pitch cases. As a result, conditions C1b, C2b, C3b, and C4b developed leading-edge vortex cavitation on the pressure side of the blade, from r/R~0.6 outward to the tip. The views of the pressure side of the blade corresponding to cases C2 and C2b are shown in Figure H - 6, highlighting the presence of pressure side cavitation in the reduced pitch condition. Conditions C3b and C4b are the ones in which pressure side cavitation was more developed, showing a rather large vortex from sheet face; the extension of this cavity, anyway, is still smaller in dimension than many of the vortices observed at the design pitch cases (in this case, on the suction side). Condition C5b had no visible cavitation. Its noise signature, which was slightly above the baseline non-cavitating condition, indicates it was near cavitation inception.

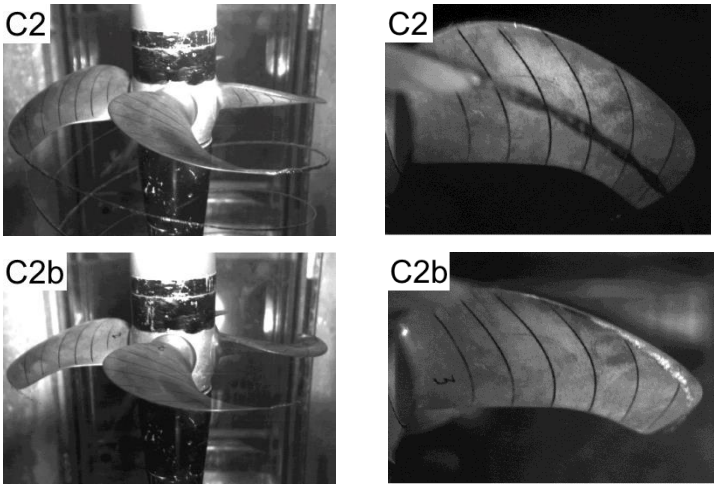

Figure H - 6: Comparison of Stroboscopic Images from Comparable Design Pitch (C2) and Reduced Pitch (C2b) Cases, Showing Full Propeller (Left) and Pressure Side Single Blade (Right) Views.

Trailing tip vortices were observed in the design pitch cases, excepting C4, and they persisted for several propeller diameters downstream before collapsing. The pressure side leading edge vortex cavities of the reduced pitch cases and case C4 collapsed on the propeller blades or shortly downstream.

H4.2. Acoustic Measurements

Acoustic measurements corresponding to representative conditions C1, C2, and C3 tested in non-cavitating regimes are provided in Figure H - 7, and compared against background tunnel noise. The noise emitted by the non-cavitating propeller was primarily background noise, with exceptions at the tone of the blade rate and, occasionally, its first multiple.

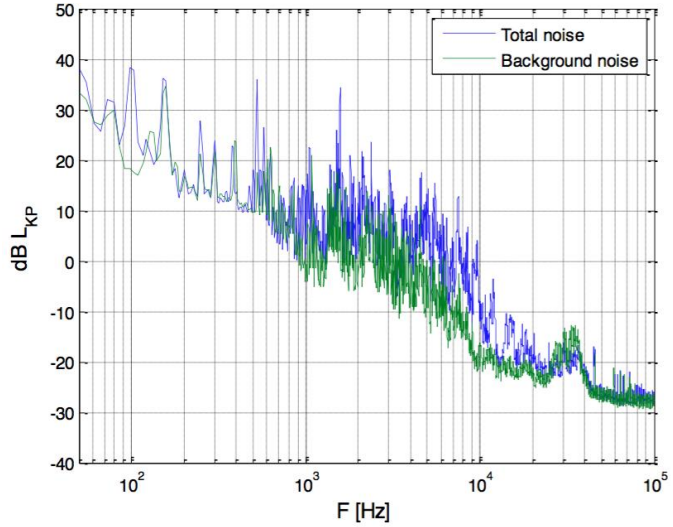

Figure H - 7 Non-Cavitating Propeller Noise for Conditions C1, C2, C3; and Background Tunnel Noise

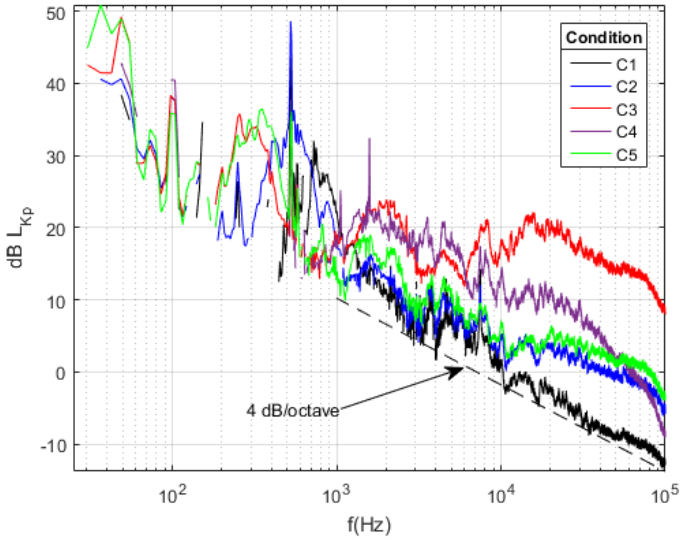

Figure H - 8 Net Power Spectrum Levels from Cavitating Experiments Operating at the Design Pitch, as Measured by Hydrophone H2. A 4db/Octave Decay is Shown for Reference Only.

Acoustic spectra for cavitating propeller cases with the design pitch are provided in Figure H - 8. Total noise spectra have been corrected for background noise, according to ITTC guidelines, in order to isolate propeller noise. Portions of the dataset that have a signal-to-background noise ratio of less than 3 dB have been omitted. In some cases, primarily those corresponding only to tip vortex cavitation, this omission included a significant portion of the low-frequency range, indicating minimal noise generation by the propeller sources in this range.

The conditions that experienced tip and sheet cavitation showed an approximate 4 – 4.5 dB/octave decay at frequencies above ~250 Hz. The results lay within the range predicted more recently by [10] and suggest that sound pressures in this range can be modelled by a simple equation fit. The bubble cavitation observed at condition C3 represented an exception, where the sound pressure at high frequencies decayed at a lower rate and with no clear trend.

Acoustic spectra for the propeller operating under the reduced pitch are provided in Figure H - 9. Qualitatively similar acoustic patterns were seen for each case, particularly in the frequency range above 1000 Hz. This result is expected, considering that pressure side cavitation was characteristic of each case C1b through C4b. The amplitude of each spectrum differed between cases, roughly corresponding to the net cavity size observed in the stroboscopic images.

Large portions of the data in the low-frequency range were omitted due to low signal-to-noise ratio, indicating that the noise in this range was primarily the background noise.

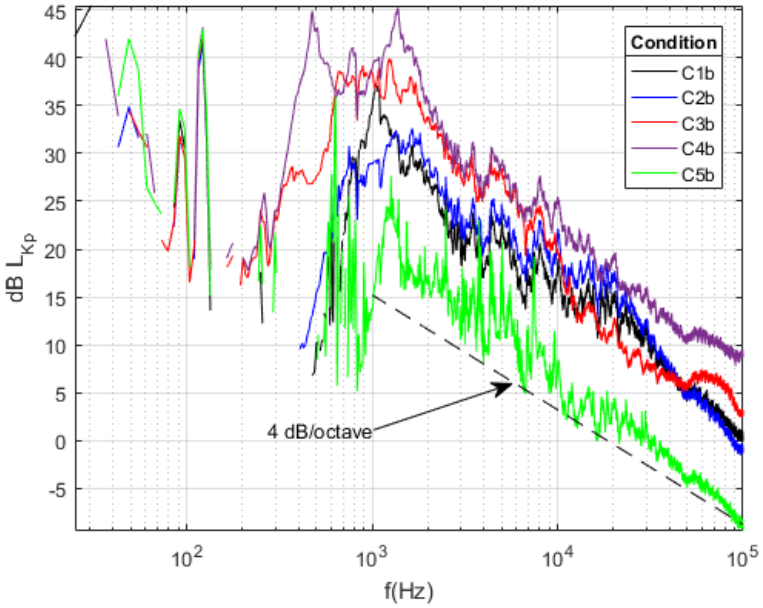

Figure H - 9 Net Power Spectrum Levels from Cavitating Experiments Operating at the Reduced Pitch, as Measured by Hydrophone H2. A 4db/Octave Decay is Shown for Reference Only.

Figure H - 10 presents a comparison between the design pitch and reduced pitch cases. Similar patterns are seen between all cases in the tonal frequency range. However, in the design pitch cases, a notable hump was present in the spectra between 200 Hz and 800 Hz. This increased noise level is characteristic of tip vortex cavitation and it was absent in the reduced pitch cases [11]. At frequencies above 1000 Hz, the general trend of logarithmic decay was observed for each case,

excepting condition C3. While the acoustic data trends were preserved between the design and reduced pitch cases, the reduced pitch experiments showed increases in sound pressure levels up to 20 dB greater than their comparable design pitch conditions. This result is counterintuitive, considering that the reduced pitch tests were performed at lower freestream velocities, thrust coefficients, and torque coefficients. However, pressure side cavitation is expected to result in significantly higher levels of noise than comparable suction side cavitation and is less likely to occur during design operating conditions [10]. Indeed, the higher noise levels measured for the reduced pitch cases were accompanied by pressure side cavitation in the stroboscopic images.

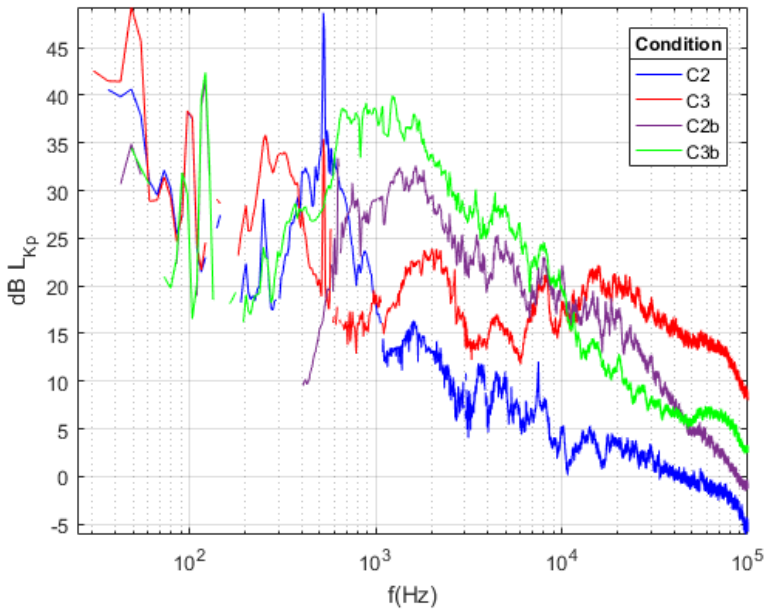

Figure H - 10 Net Power Spectrum Levels from Cavitating Experiments with Design Pitch (C2, C3) and Reduced Pitch (C2b, C3b)

This study revealed the need for intelligent operating strategies to reduce anthropogenic marine noise. Rudimentary control strategies that assume linear ship velocity-to-noise relations should be avoided. For example, in the case of a decelerating ship with a controllable pitch propeller, keeping the engine speed fixed while adjusting the propeller pitch would result in excessive noise levels [12]. Rather, a more appropriate speed-reduction strategy would be to maintain the effective angle of attack of the propeller blades close to the design values in order to reduce cavitation, especially on the pressure side of the blades.

H5. CONCLUSIONS

Scaled cavitating propeller experiments were performed, providing insight into underlying relations between cavitation events and their noise signatures. The observed data trends suggest that only a few high-level parameters, such as cavitation number, thrust coefficient, advance ratio, and pitch angle, could be sufficient in defining appropriate, reduced-order noise estimation tools. The present results suggest that logarithmic decay models can be effective for predicting acoustic noise spectra from tip vortex, sheet, and pressure side cavitation, but may be ineffective for the case of bubble cavitation.

In the case of reduced-pitch propeller operation, the acoustic effects of pressure-side cavitation were observed to dominate the effects of the reduction of cavitation number and thrust coefficient, resulting in higher levels of noise. This finding confirms the assertion that linear ship speed-noise models are insufficient for predicting propeller cavitation noise.

The stroboscopic images of the cavitation events and the concurrent acoustic measurements provide a benchmark for the development of numerical and semi-empirical models of cavitation-induced noise. These models will allow cavitation noise, the primary source of ship-induced noise, to be effectively considered in designing marine propulsion systems, choosing propellers, and operating marine vessels.

REFERENCES

[1] Ross, D., 2013. *Mechanics of underwater noise*. Elsevier.

[2] Blake, W., 2012. Mechanics of flow-induced sound and vibration: Complex flow-structure interactions, Volume 2. Elsevier

[3] Clark, C.W., Ellison, W.T., Southall, B.L., Hatch, L., Van Parijs, S.M., Frankel, A. and Ponirakis, D., 2009. "Acoustic masking in marine ecosystems: intuitions, analysis, and implication". *Marine Ecology Progress Series*, ***395***, pp.201-222.

[4] Ellison, W.T., Southall, B.L., Clark, C.W. and Frankel, A.S., 2012. "A new context-based approach to assess marine mammal behavioral responses to anthropogenic sounds". *Conservation Biology*, ***26(1)***, pp.21-28.

[5] Wood, R.M. and Harris, R.G., 1921. Some notes on the theory of an airscrew working in a wind channel. HM Stationery Office.

[6] Specialist Committee on Hydrodynamic Noise of the 27th ITTC, 2014. "Model scale noise measurements". *Recommended Procedures and Guidelines.* International Towing Tank Conference.

[7] Welch, P.D., 1967. "The use of fast Fourier transform for the estimation of power spectra: A method based on tie averageing over short, modified periodograms". *IEEE Transactions on Audio and Electroacoustics.* ***15(2)***, pp. 70-73.

[8] Lurton, X., 2002. An introduction to underwater acoustics: principles and applications. Springer Science & Business Media.

[9] Brown, N.A., 1976. "Cavitation noise problems and solutions". *Proceedings International Symposium on Shipboard Acoustics*, pp. 21-38. Elsevier, Amsterdam.

[10] Traverso, F., Gaggero, T., Tani, G., Rizzuto, E., Trucco, A. and Viviani, M., 2017. "Parametric Analysis of Ship Noise Spectra". *IEEE Journal of Oceanic Engineering*, ***42(2)***, pp.424-438.

[11] Bosschers, J., 2009, June. Investigation of hull pressure fluctuations generated by cavitating vortices. In Proc. First Symposium on Marine Propulsors.

[12] Gaggero, T., Rizzuto, E., Traverso, F. and Trucco, A., 2014. "Comparing ship underwater noise measured at sea with predictions by empirical models". *Proc. 21st Int. Congr. Sound Vib*, pp. 1510-1516.

[13] Iverson, D., D. W. McIntyre, M. Rahimpour, G. Tani, F. Miglianti, M. Viviani, Z. Dong, and P. Oshkai, "Experimental Investigation of Cavitation-Induced Acoustic Noise from Marine Propellers," *Proceedings of the 9th International Symposium on Fluid-Structure Interactions, Flow-Sound Interactions, Flow-Induced Vibration & Noise*, July 8-11, 2018, Toronto, Ontario, Canada.

Appendix I. Improvements of Propeller Cavitation Noise Model

Propeller cavitation is the dominant source of induced underwater noise from marine vessels, particularly in abnormal, or off-design, operating conditions, including speed reduction and docking maneuvers. This portion of our project is aimed at developing the capability to predict the level of noise for given ship operation profiles and propulsion system designs to guide the design and conversion of electric or hybrid propulsion systems and to find solutions in propulsion controls.

I1. MODELLING PROCESS

Propeller cavitation noise has a low-frequency spectrum that peaks at around 50 Hz, and it comes with almost all vessels independent of their type. The level of the noise is found to be heavily speed dependent. Our study has thus focused on the propeller in-flow speed that is a result of the speed and direction of the vessel, ocean current, Z-drive/rudder angle, and the propeller (rotation) speed. The study has proceeded in three related areas:

a) Introducing the process and model for cavitation noise prediction through full-scale CFD simulations for a specific propeller under different water in-flow and propeller rotation speeds; and validating the modelling method using experimental data;
b) Conducting water-tank experiments and collecting data of cavitation noise measurements for a specific propeller under different water in-flow and propeller rotation speeds;
c) Developing an effective method to calculate the propeller in-flow speed
    - Collecting vessel speed (and rudder/Z-drive angle) data for representative vessels
    - Accurately predicting vessel speed using the integrated propulsion system modelling tools
    - Getting ocean current speed and velocity on different sailing routes as part of the Marine Weather State (MWS) model

These tasks have been completed, except the newly added MWS model that requires a considerable amount of collaborative efforts, and the present work is limited to a feasibility study.

In this work, our team has also made an effort to go beyond the scope of the contract to predict propeller cavitation noise through a simplified, semi-empirical numerical model to avoid the extensive computation needed using the current approach. The new approach extends the panel method for the cavitation modelling function, which is used in the propeller design tool to be discussed later. The MWS and propeller data to be collected include the contents shown as Table I-1. These data are used to predict the propeller cavitation and cavitation noise level.

Table I-1 Vessel Operation Data and Noise Prediction for Design/Control Use

Data Points (sec)	GPS Data		Ship Speed (m/s)	Propeller		Ocean Current		Wake Fraction	Cavitation Level (%)	Cavitation Noise (dB)
	latitude	longitude		Speed (rpm)	Angle	Speed (m/s)	Direction			

Here, the level of cavitation noise is calculated based on the level of cavitation on the propeller, which is determined by the water in-flow speed and propeller rotation speed, and the water in-flow speed is determined by ship speed, z-drive angle, ocean current speed, wake fraction, and thrust deduction in our model. Wake fraction and thrust deduction are calculated from CFD simulation. An example datasheet of the vessel operation, ocean current and wind data is shown in the attached Excel file Appendix J-2 Example Skeena Queen operation and MWS data. In this file, the ferry ship has no "off-design" operation, thus no propeller cavitation and unacceptable cavitation noise. In our future work, we will change vessel speed to create "off-design" operation, record the actual ship noise and verify the cavitation noise model using real ferry operation data.

For a better global picture, we can divide the research and development on ship-induced ocean noise and mitigation technologies into three stages, as described in the following sections.

Stage I - General awareness and a basic understanding of the problem and its causes:

a) Monitoring and measurement of ship-induced ocean noise
b) Finding the threshold of harmful noise level to marine life
c) Introducing regulations prohibiting severe ship noise
d) Finding the major cause of ship noise: cavitation noise of marine propellers
e) Propeller cavitation noise occurs at the abnormal working conditions of the bad combination of propeller in-flow (water) speed and propeller (rotation) speed.
f) Building a generic model that links ship-induced noise to propeller cavitation

Stage II - Linking of ship-induced noise to the specific source and finding the causes of the noise:

For a given propeller (design), identify the "abnormal" propeller operation conditions that cause cavitation and the degree of cavitation, and connect the degree of cavitation to the level of generated noise

a) Numerically using full-scale Computational Fluid Dynamics (CFD) simulations on a supercomputer supporting parallel computation (numerical modelling)
b) Experimentally using Experimental Fluid Dynamics (EFD) in a water tank equipped with cavitation and noise detection apparatus (experiment validation)
c) Vessel sea trial and noise measurement using underwater acoustics-hydrophones arrays (on-site data acquisition and validation) (Planned)

Stage III - Introducing noise mitigation technology:

a) Propeller, hull, and vessel propulsion system design
   - A standalone full-scale CFD model
   - Simplified, semi-empirical model integrated into the propulsion system model (Ongoing)

b) Vessel operation control constraints
   - Adding ocean noise as an additional attribute of ship pollutions, similar to GHG emissions
   - Mapping the severe cavitation noise to abnormal propeller in-flow speed, and associating it to ship speed and Z-drive/rudder angle under known ocean current speed and direction

c) Semi-autonomous steering and control of marine vessel
   - Optimize route and speed during sailing for giving destination and ocean current state docking
   - Plan better departing and docking operations

During this contract work, we continued on our Stage I) work; completed the research tasks on Stage II) and part of Stage III), as scheduled in the milestones; and initiated studies on the other Stage III) tasks. Specifically, we have completed the underlined tasks, as defined in the present contract. These include tasks of Stage I (f), Stage II (a) and (b), and Stage III (a), (b) and (c). The team is also preparing more practical design/operation tools and applications of the learning through joint work with industrial partners. The detailed outcomes are summarized in the following sections.

I2. INTRODUCTION OF SIMPLIFIED, SEMI-EMPIRICAL CAVITATION NOISE MODEL BY EXTENDING PROPELLER MODELLING AND DESIGN TOOL - ROTORYSICS

At the core of propulsion system design and analysis lay hydrodynamic modelling of propellers themselves. Accurate knowledge of propeller operation physics is fundamental to both propulsion system design and acoustic noise generation; both of which are core aspects of our research. Many tools exist to model propeller performance, of varying complexity and accuracy, from rudimentary actuator disk theory to high-resolution computational fluid dynamics (CFD) simulations. A satisfactory balance of accuracy and computational expense is provided by a panel method approach, as found in the software package used by Green Ship researchers, ROTORYSICS (formally PROPELLA, 1999-2015). Specifically, ROTORYSICS is a low order source-doublet, steady/unsteady time domain panel method code developed to predict the hydrodynamic performance of screw propellers, and has been extensively validated against experimental data.

ROTORYSICS is being used by our project team to quantify propeller performance under the influence of many parameters. The code capably models the flow physics of a ship's propeller under the influence of pods, nozzles, rudders, ice-blockage, non-uniform hull-wake profiles, blade surface cavitation, and any combination of these parameters. Importantly, unlike fully resolved CFD approaches, ROTORYSICS does not require supercomputing resources but rather can be run on common computing devices. The low computational expense of the panel method allows a

large number of numerical tests to be completed in a reasonable time frame. ROTORYSICS, therefore, facilitates batch execution, covering a large parametric space for database development and performance optimization. As an example, the range of operating conditions that represent a vessel's operating route can be calculated in an automated manner. Alternatively, propeller geometries can be optimized provided a set of constraints to minimize acoustic emissions or maximize propulsive efficiency.

ROTORYSICS is capable of predicting sheet cavitation occurring on the propeller blades. The size of the cavitation sheet can be related to the net noise emissions of the propeller. The cavitation event is modelled within the software by means of a sophisticated semi-empirical scheme that models "chop-off and fill-in" of pressure in the vicinity of cavitating regions. Time-varying cavity volume changes can also be calculated, which are responsible for a large portion of the generated acoustic noise spectrum. The panel method approach is limited to computing sheet cavitation only. Other forms of cavitation, such as tip vortex cavitation and bubble cavitation, are not accurately estimated by these approaches but occur less commonly.

An example use of ROTORYSICS is provided in Table I-2. The software has been used to model propulsion performance and cavitation dynamics of the propeller of the BC Ferries' Skeena Queen throughout a typical route operation. An accurate relation between propulsion metrics and propeller cavitation is integral to developing an efficient design strategy, and the goal of which is to reduce cavitation-induced noise while maintaining acceptable propulsion efficiencies.

In Table I-2, field data was acquired through direct measurements of the vessel, and values were averaged over one-minute intervals to yield discrete data points.

ROTORYSICS was then used to numerically reproduce these conditions that occurred at the propeller in order to calculate the propulsion metrics (thrust, torque, and efficiency) and cavitation occurring on the propeller blades surface. The numerical results are provided in bold headed columns.

ROTORSYICS predicted torque and thrust to reasonable accuracy (given the current simplifications) for the portions of the voyage near the vessel's cruising speed. Larger errors are seen during acceleration and deceleration near the ends of the voyages, indicating further refinements in the model are needed to accurately capture all possible operating conditions. It is noted here that the present suite of numerical results is subject to some simplifications that are expected to have an influence on the accuracy of results. These include neglecting wake fractions and propeller pods. The application of the software is being further developed and refined to include such factors.

The component of ship noise due to cavitation may be related to the area of the blade exposed to a sheet cavity by means of semi-empirical equations. The accuracy and robustness of the cavitation prediction models, and the equations that relate cavitation to noise, are currently being validated against an experimental campaign conducted in a scale cavitation tunnel, as outlined in Appendix H. Of the current cases studied, none exhibited sheet cavitation occurring on the surface of the propeller's blades, and thus negligible contributions from cavitation to the overall noise levels is expected. This is expected for a ship operating under its normal operation conditions.

Table I-2 Typical discrete operating conditions for the vessel Skeena Queen. Measured field data is compared against results simulated from the software ROTORYSICS.

Data Interval (Minute)	Ship Speed through water (m/s)	Propeller		Torque			**Cavitation Level (%)**	**Cav. Noise (dB)**
		Speed (rpm)	Angle (deg)	Measured (Nm)	**Numerical (Nm)**	**% Dif.**		
1	0.596	83.9	-3.5	4836	1337	72.4	0	-
2	3.600	225.4	-15.0	12991	9903	23	0	-
3	5.749	279.4	-0.5	15163	14777	2.5	0	-
…								
5	6.904	280.9	-4.0	14190	14182	0.06	0	-
…								
11	7.148	281.1	5.9	13075	14042	7.4	0	-
…								
15	7.361	281.0	5.9	12714	13794	8.5	0	-
…								
25	5.438	179.8	13.5	5099	5129	0.6	0	-
26	3.140	179.7	78.6	9999	6254	37.5	0	-
27	0.886	196.6	156.9	10860	7145	34.2	0	-
28	0.159	58.2	8.9	1988	613	69.1	0	-

I3. LINKING OF SHIP-INDUCED NOISE TO THE SPECIFIC SOURCE AND FINDING THE CAUSES OF THE NOISE

I3.1 Experimentally using Experimental Fluid Dynamics (EFD) in a water tank equipped with cavitation and noise detection apparatus (experiment validation)

The detailed work in this part is documented in detail in Appendix H Experimental Investigation of Cavitation-induced Propeller Noise.

We conducted an experimental campaign in a pressurized cavitation tunnel, following the experimental standards of the International Towing Tank Conference (ITTC). The experiments were designed to reproduce various cavitation regimes that are expected to occur during the operation of a typical four-bladed propeller of a tanker ship. The measurements were conducted under steady inflow conditions, which eliminated the effects of the hull wake and shaft inclination in order to provide the first set of simplified cases for validation of numerical methodologies, before moving to more complex conditions. We obtained stroboscopic photographic images of the cavitation event, measurements of propeller loads, and high-resolution acoustic pressure levels across a broad frequency spectrum. The distinct regimes of bubble cavitation, sheet cavitation, and tip vortex cavitation were created experimentally in varying combinations, along with a reference

case of cavitation suppression. For each considered cavitation regime, we identified the corresponding dominant frequencies and levels of the acoustic noise. The experiments will validate the propeller cavitation noise model that is used to guide ship hybrid electric propulsion system design and operation control to reduce ship induced ocean noise.

I3.2 Numerically using full scale Computational Fluid Dynamics (CFD) simulations on a super computer supporting parallel computation (numerical modelling)

We have conducted comprehensive CFD modelling and simulation and developed the numerical procedure to accurately predict cavitation noise for vessel and propeller working at abnormal conditions. Results from this full-scale CFD simulation using the introduced model well match the acquired data from the experimental study conducted at University of Genova [1]. The study employed unsteady Reynolds-averaged Naiver-Stokes (uRANS) simulations in combination with Sauer and Schnerr mass transfer and volume-of-fluid (VOF) multiphase models to predict the cavitation patterns for a marine propeller in different operating conditions. The considered operating regimes, indicated by combinations of the thrust coefficient and the cavitation index, resulted in different types of cavitation, e.g. tip vortex and sheet cavitation as well as a case of cavitation suppression. The simulated cavitation patterns and performance characteristics of the propeller were compared with those obtained through a series of model-scale experiments in a cavitation water tunnel.

As the first step of the validation of the numerical simulations, the performance characteristics of the propeller were compared with those of the experiments, which showed that the average error in calculation of the thrust and torque coefficients for all tested operation conditions were respectively 4.25 and 2.3%.

The experiments were designed to isolate various cavitation regimes, allowing the identification of noise spectra for each type of cavitation. The patterns of cavitation, obtained by numerical simulations, showed good agreement with those of the experiments, as shown in Figure I-1 (a)-(d).

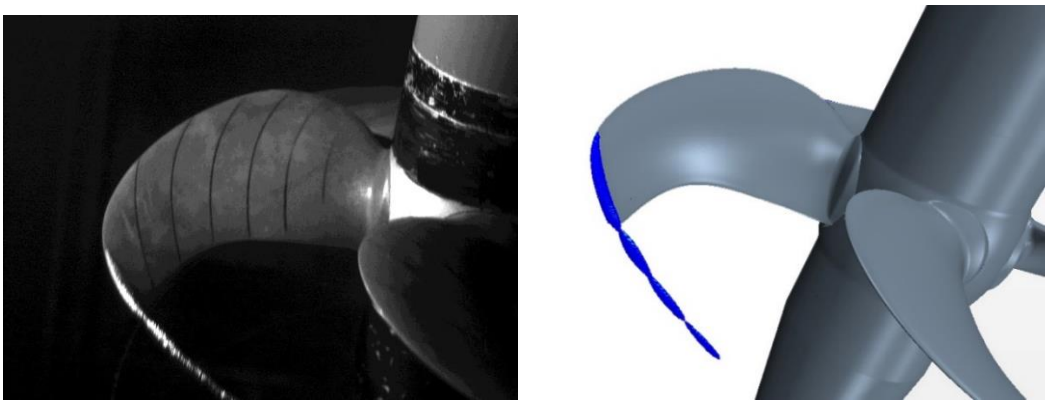

(a) Design pitch, thrust coefficient and cavitation index of 0.205 and 2.3 respectively.

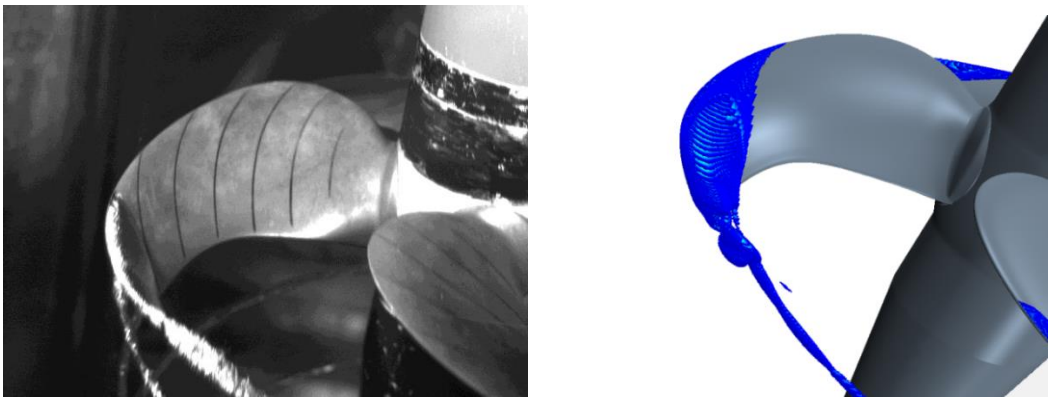

(b) Design pitch, thrust coefficient and cavitation index of 0.09 and 2.3 respectively.

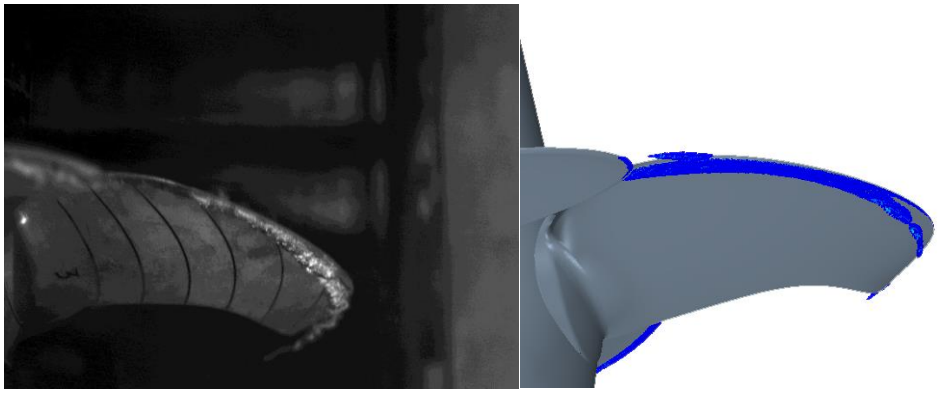

(c) Design pitch, thrust coefficient and cavitation index of 0.05 and 2.3 respectively.

Figure I-1 Results from water tank experiments vs. results from numerical simulations.

A semi-empirical relation for broadband noise was used to relate the simulated cavitation patterns to acoustic spectrum levels, which were directly compared to the experimental measurements. The resulting propeller cavitation noise model can be used to guide ship hybrid electric propulsion system design and operation control to reduce ship induced ocean noise.

REFERENCE

[1] Iverson, D., D. W. McIntyre, M. Rahimpour, G. Tani, F. Miglianti, M. Viviani, Z. Dong, and P. Oshkai, "Experimental Investigation of Cavitation-Induced Acoustic Noise from Marine Propellers," *Proceedings of the 9th International Symposium on Fluid-Structure Interactions, Flow-Sound Interactions, Flow-Induced Vibration & Noise*, July 8-11, 2018, Toronto, Ontario, Canada.

Appendix J. Marine Weather State (MWS) or Metocean Loads

J1. INTRODUCTION OF MARINE WEATHER STATE LOAD

Traditionally, the sea state is used to describe the general condition of the ocean considering wind, waves and swell at a given location and time. Sea states of calm, smooth, moderate, rough, high, etc. grades present different levels of challenge to the marine operation and are recorded as statistical data in oceanography. However, the sea state does not directly translate to vessel propulsion loads. The ocean science community also uses the term Metocean to describe ocean wind, wave, etc. Metocean data are considered as an important and highly useful category of oceanographic and marine data which comprises observed measurements of the current, wave, sea level and meteorological data. We have not yet decided whether to use Metocean Conditions to replace Marine Weather State (MWS) due to its less direct connection to ocean current that is not caused by wind.

The vessel propulsion resistance is directly related to current, wind, and waves, in this work, we re-name the load to Marine Weather State (MWS) load from Sea State (SS) load used previously. Specifically, the major influences on marine vessel propulsion resistance are divided into two major components: Marine Weather State (MWS) Load and Cargo Load. The MWS load adds to the propulsion resistance of the vessel from the pure hydrodynamic load during its travelling in calm wind and calm water. While the cargo load changes the actual displacement and submerged hull volume and mass of the vessel and change of hull drag force from its norm.

The relative contribution of viscous, wave-making and air resistance is shown in Figure J - 1, published by the USNA.

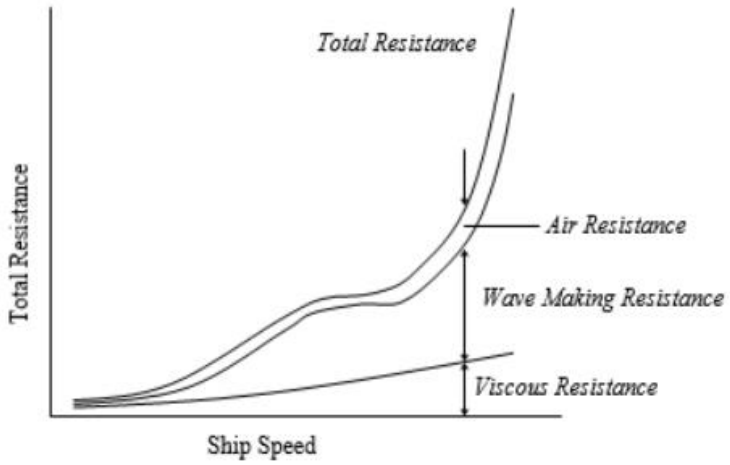

Figure J - 1 Ship Resistance Components

J1.1 Reasons for MWS Consideration

Propulsion load variation consideration based on the proposed Marine Weather State modelling is critical due to the following three key reasons:

- Accuracy improvement of vessel operation pattern modelling

  In our work, we have acquired vessel operation data, including the recorded propulsion power of the representative vessels. According to the marine operators, the actually needed power varies about 10-20% in different seasons and weather conditions. It will be ideal if we can collect the vessel power data, remove the seasonal effect at the time of data collection, and add the statistical variations of all seasons to reflect the actual needed propulsion power of the vessel at any time of the year, as well as the best- and worst-case scenarios.

- Reduction of energy consumption and emissions through semi-autonomous sailing

  The current and wind maps often show different magnitudes and directions due to the shore and landscape features, while marine navigation allows more freedom in sailing route variation due to the nonexistence of "narrow road" constraints for road vehicles. Semi-autonomous or semi-auto piloting of the vessel adapted to the current and wind (strength and direction) variations will lead to reducing energy consumption and emissions [5]. This would be a more beneficial and feasible application technique that gained popularity in smart vehicle research and development. Our preliminary research supported this approach.

- More effective control of ship-induced noise

  The primary source (70-80%) of broadband, ship-induced ocean noise is due to propeller cavitation. While propeller cavitation only occurs when the propeller operates beyond its designed operation conditions with a dramatic change to the propeller in-flow stream. This only occurs when the propeller in-flow stream dramatically slows down, speeds up, or turns. In addition to ship maneuvers, these changes were often introduced by the varying ocean current. Introductions of current flow condition from the MWS load model and semi-autonomous sailing can avoid these situations by modest adjustments on vessel speed and sailing route, reducing propeller cavitation and the consequent propeller wear and noise.

J1.2 Wave Making and Viscous Resistance or Hull Resistance

Drag on surface vessel comes from wave-making resistance and viscous resistance due to the energy required to push the water out of the way of the hull and the effect of surface friction between the hull and the water as the vessel moves through the water. We model these two sources of drag force using the hull hydrodynamic models (full or reduced-order). This calculation is made for calm water.

J1.3 Air Resistance or Wind

"Air resistance is the resistance caused by the flow of air over the ship with no wind present. This component of resistance is affected by the shape of the ship above the waterline, the area of the ship exposed to the air, and the ship's speed through the water. Ships with low hulls and small "sail area" or the projected area above the waterline will naturally have less air resistance than ships with high hulls and large amounts of sail area. Resistance due to air is typically 4-8% of the

total ship resistance, but maybe as much as 10% in high-sided ships such as aircraft carriers. Attempts have been made to reduce air resistance by streamlining hulls and superstructures, however; the power benefits and fuel savings associated with constructing a streamlined ship tend to be overshadowed by construction costs" [6].

This analysis is for calm seas and calm winds (i.e., classical naval architecture). The presence of a wind and the sea state will present as a scalar of Figure J-1 (with the scalar depending on magnitude and incidence angle of the wind, current, and waves). With the air resistance on a vessel moving through calm seas and calm winds at a given speed can be determined. We might handle the wind forces (and similarly current forces) acting on a vessel underway by means of a superposition of these two cases (underway in calm seas plus station keeping in a sea state).

J1.4 **Sources of MWS Data**

Since all marine vessels operate at different ocean current (or wave) and wind conditions under real-world conditions. Based on this preliminary study, optimization of ship operating control of the ferry under variable wind and ocean current conditions is viable. It is expected that the propulsion system design and operation control optimization according to the wind and ocean current load variations can produce efficiency, emission, fuel cost and noise-reduction benefits.

To investigate the wind and current influence on ferry operation, data acquisition and analysis are important. Thanks to the historical data on weather, climate and hazard collected by the Government of Canada [2] [3] , it is convenient to get the wind historical data. In this research, we use 2017 all year data. Additional data from the West Coast Wave Initiative (WCWI) and Ocean Canada teams on ocean energy data [4] and further collaboration with these teams may lead to more relevant and improved results. Optimization on the sailing route and ship control under different current and wind resistance and direction will be further investigated.

J2. OCEAN CURRENT DATA

Unlike the seasonal characteristics in wind data, the presently collected ocean current is almost entirely related to the tide current influenced by the moon. Thus, the current speed should be related to the moon phase. At present, we did not find any data on the exact Skeena Queen operation route. To investigate the current influence on ferry operation, we decide to pick up a nearby current data to look into this, thus use the current data from NOAA website at "Turn Point, Boundary Pass", whose latitude/longitude is 48.6953° N 123.2355° W. From Google Maps, that site is very close to the Skeena Queen route, as Figure J - 2 shows. We can believe that point current data should be much closer to, but a little higher than, the route current speed and direction. It is sufficient to investigate the current influence on ferry operation via that current data.

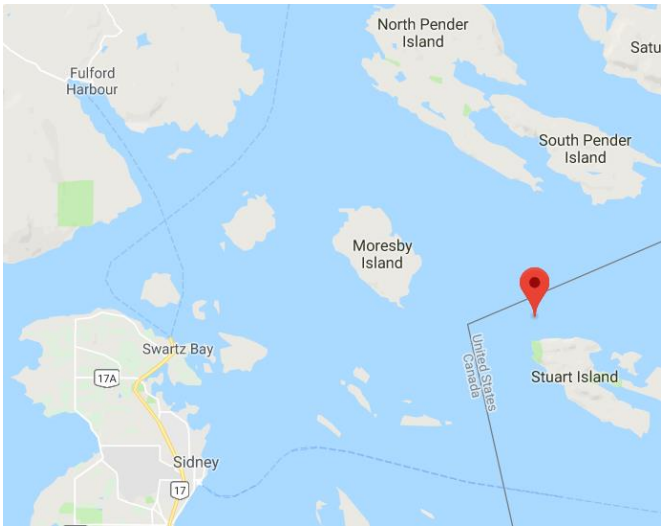

Figure J - 2 Ocean current data point and Skeena Queen sailing route

Figure J - 3 shows the current speed variations in January 2017, where the red rectangle is where the full moon phase occurred. In the tide current, the positive speed means flood, whose direction is about 80 degrees; the negative speed means ebb, whose direction is about 260 degrees.

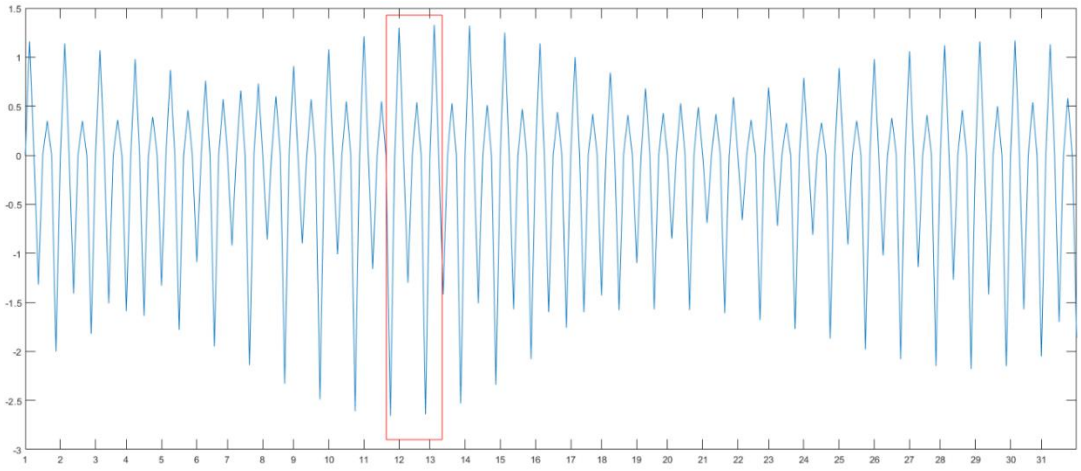

Figure J - 3 January 2017 current speed (unit in knots)

Since the moon phase varies in a monthly period, the current varies monthly. During daylight at each day, the current speed is much less than midnight. The maximum flood value occurs around mid-day.

J3. WIND DATA ANALYSIS

We attempted to identify wind data around the sailing route of the BCFS' Skeena Queen. The data came from the Canadian government's website on Historical Data - Climate - Environment and Climate Change Canada [7]. The site contains year around wind data, including wind speed, direction, air temperature, visibility, press, etc. Redundancy information, such as air temperature, visibility, has little influence on ferry operating control, can be neglected. Furthermore, the ferry only operated from around 6:00 AM to 9:00 PM each day. Data beyond this period are also

neglected. For each day, the collected data have 16 rows. For the 5840 rows of data, each column represents a specific wind feature. Figure J - 4 shows the all year around data statistics, where the y-axis represents the number of times.

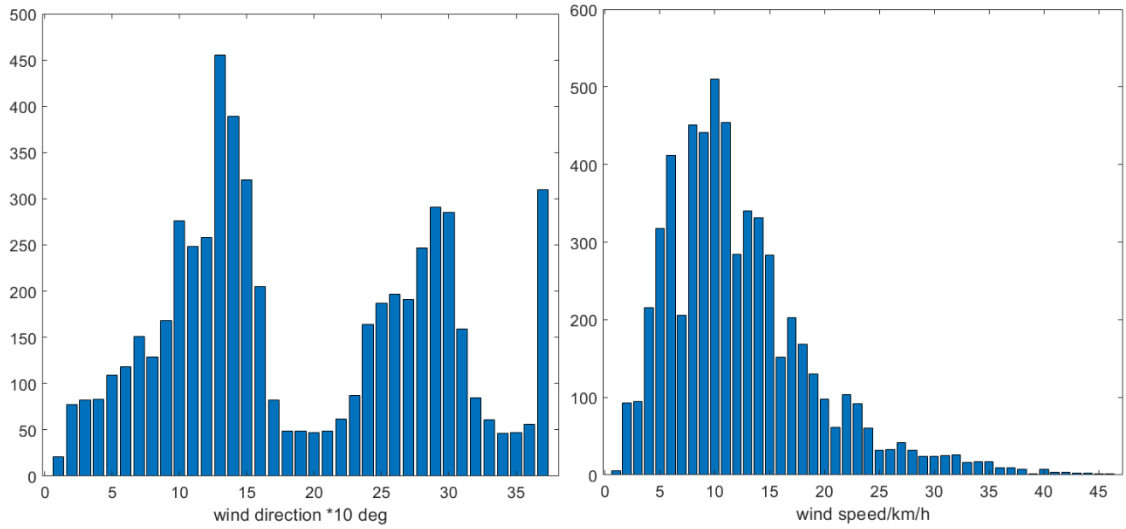

Figure J - 4 All year around wind statistics

From wind direction point, it is obvious that wind in nearby Victoria is divided into two main categories: one is about 130 degrees, direction is southeast; the other is about 260 degrees, direction is west or west-northwest. The wind speed is centralized from 5km/h to 15km/h.

To look into the two different wind direction information, Figure J - 5 shows the wind speed at the two main wind directions.

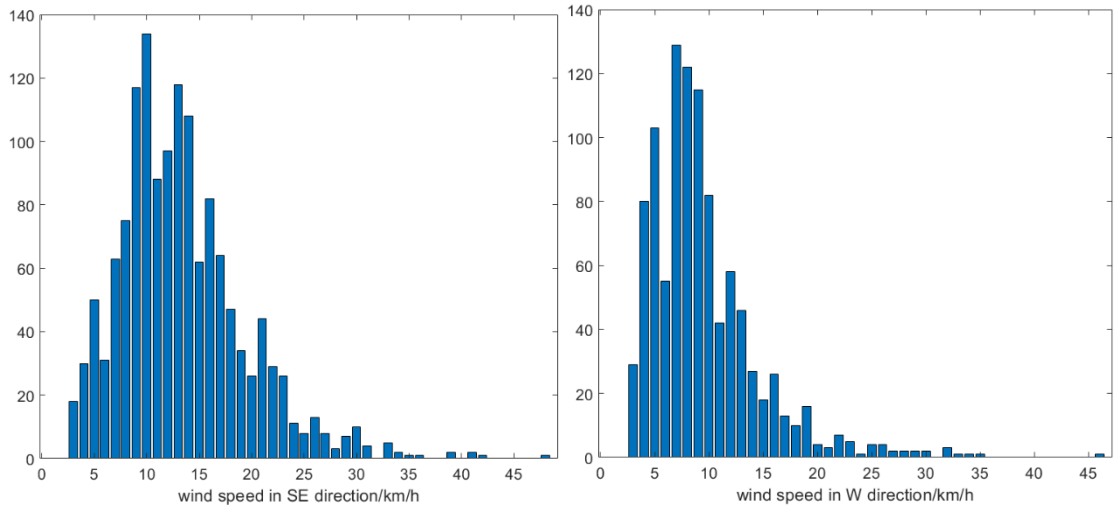

Figure J - 5 wind speed distribution in two directions

The wind from southeast direction gathered around 10 to 15 km/h, while the wind from the west direction gathered around 5 to 10km/h. It is obvious that different wind direction results in wind speed variation. To further look into this wind variation in direction and speed, we analyzed the wind information in each of the 12 months, as shown in Figure J - 6 (a) – (l).

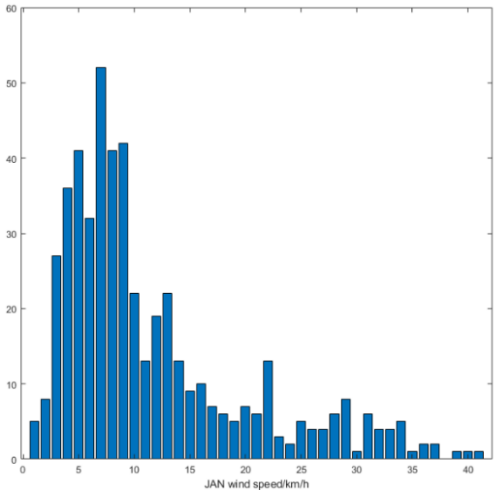

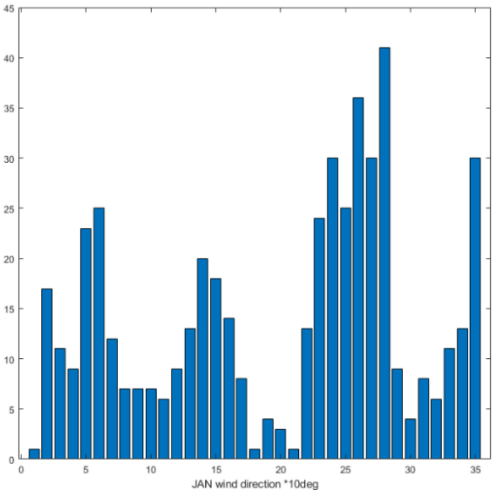

(a) January wind statistics

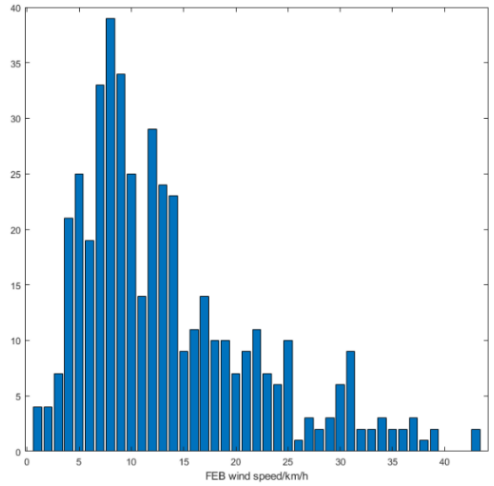

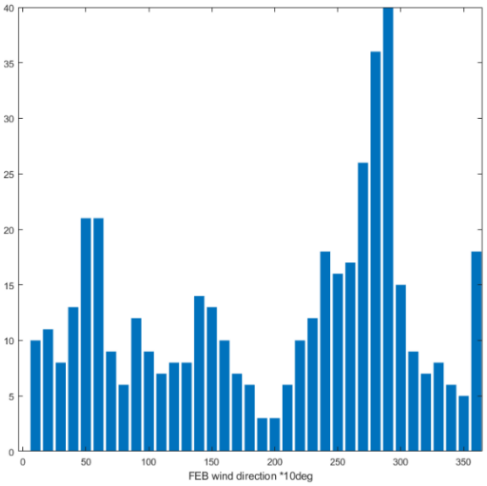

(b) February wind statistics

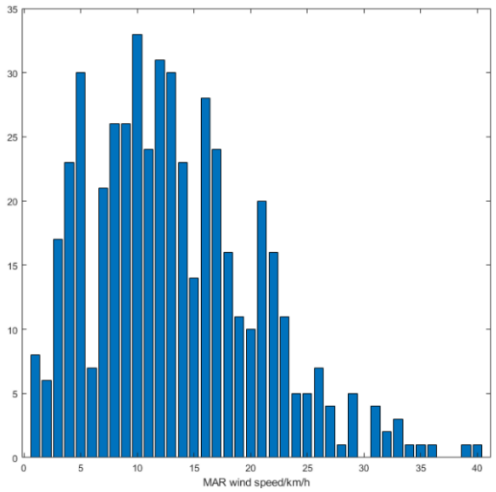

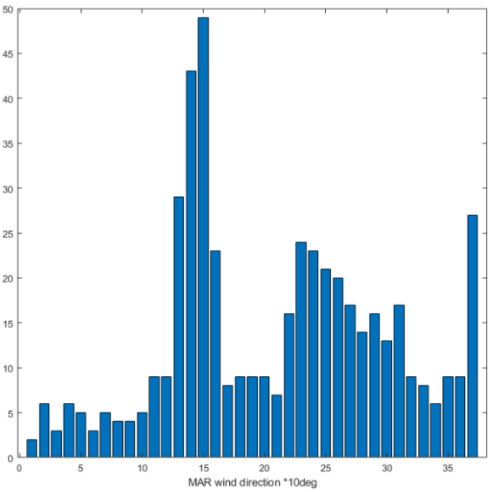

(c) March wind statistics

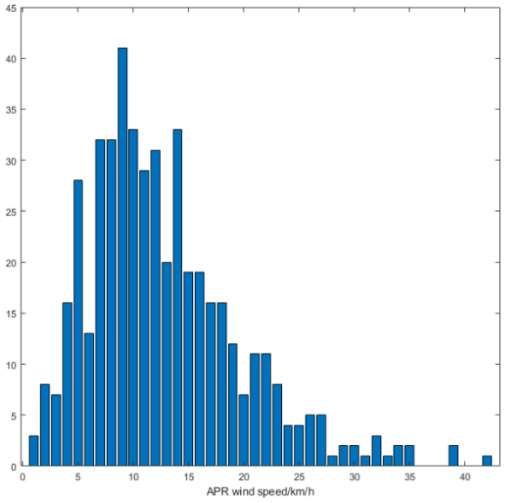

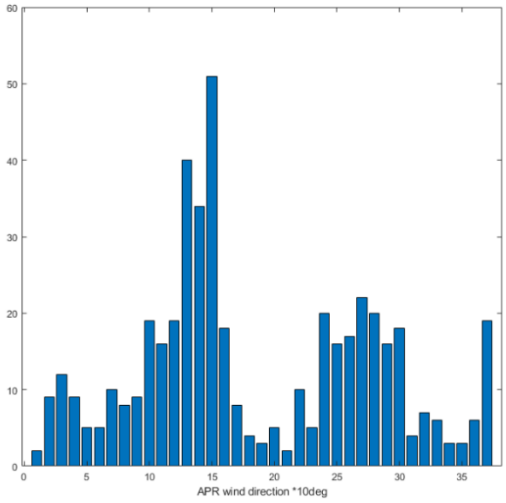

(d) April wind statistics

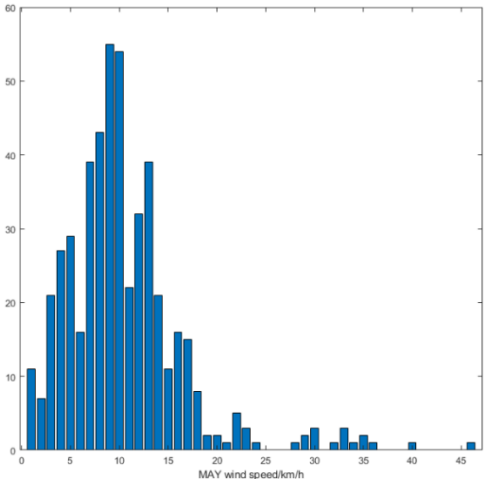

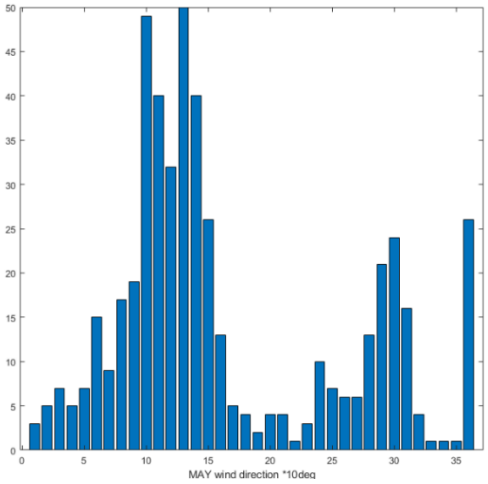

(e) May wind statistics

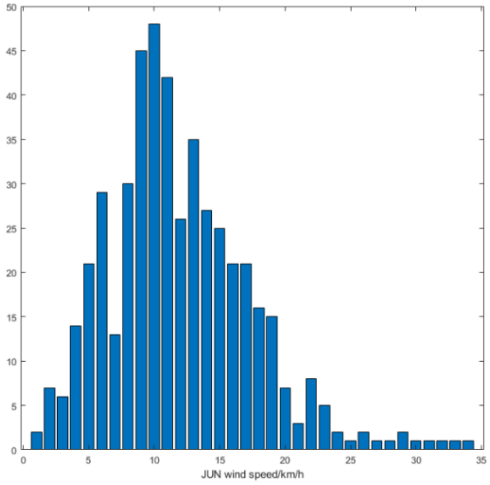

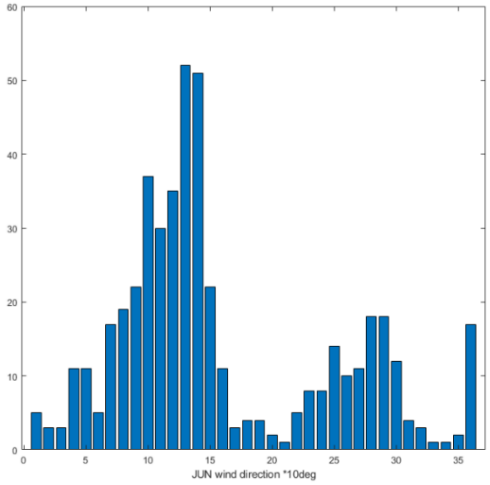

(f) June wind statistics

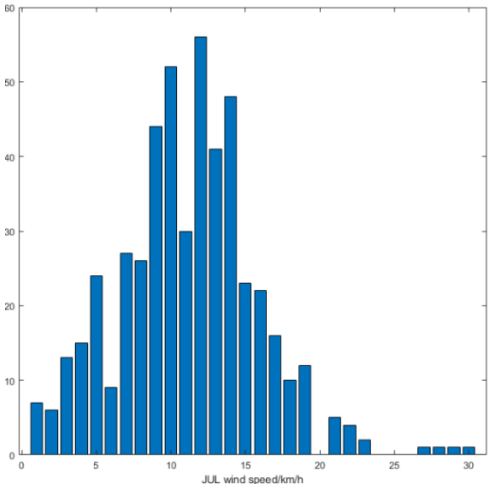

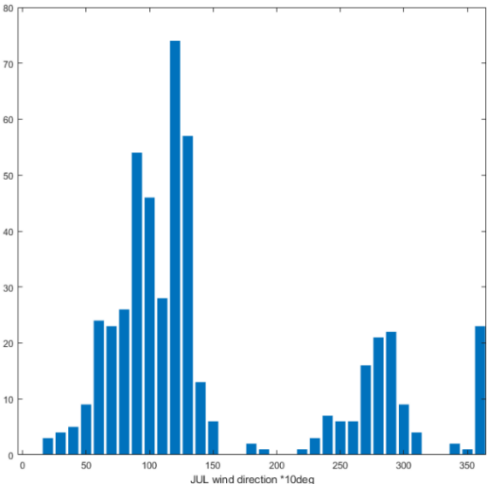

(g) July wind statistics

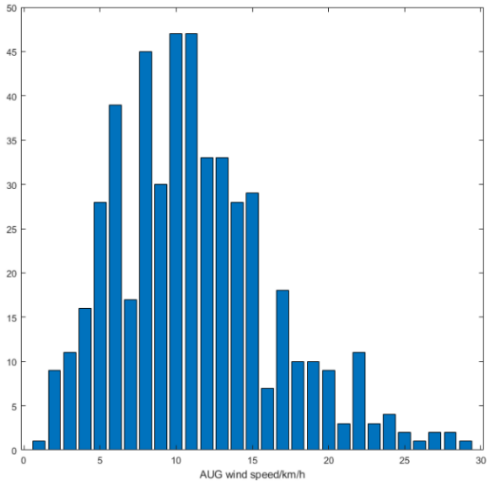

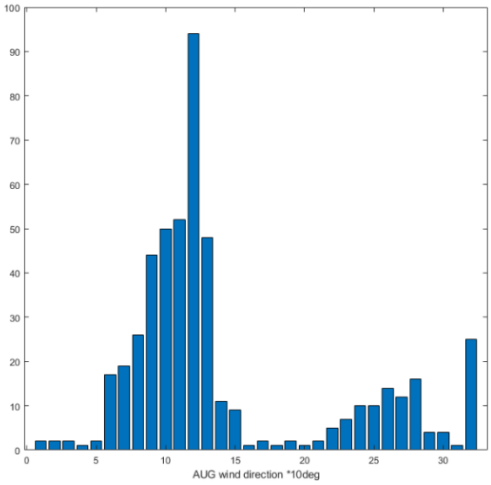

(h) August wind statistics

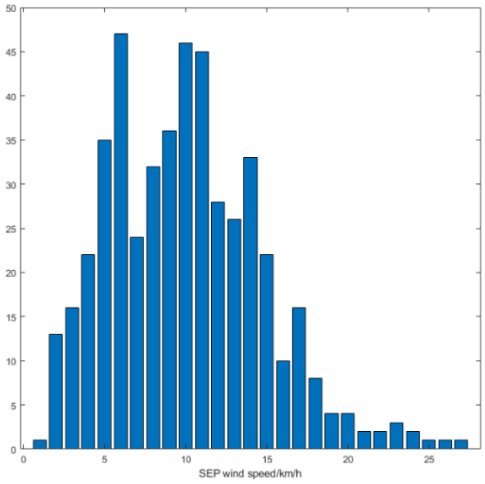

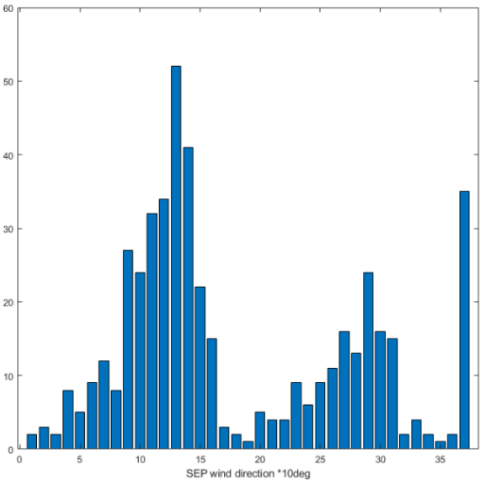

(i) September wind statistics

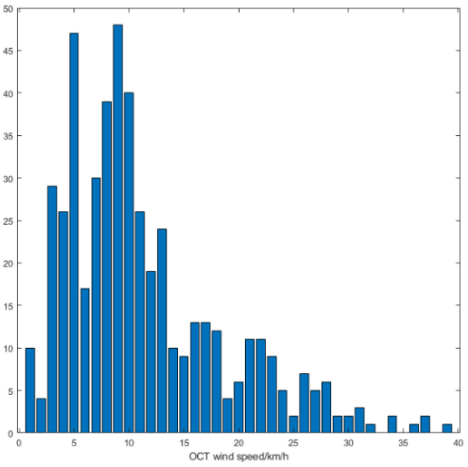

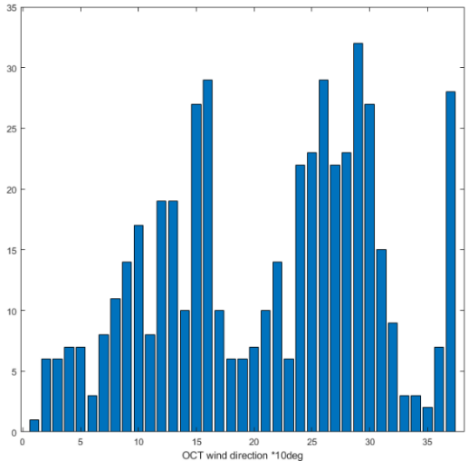

(j) October wind statistics

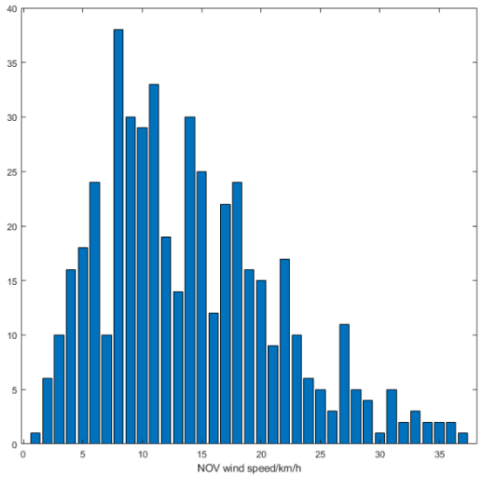

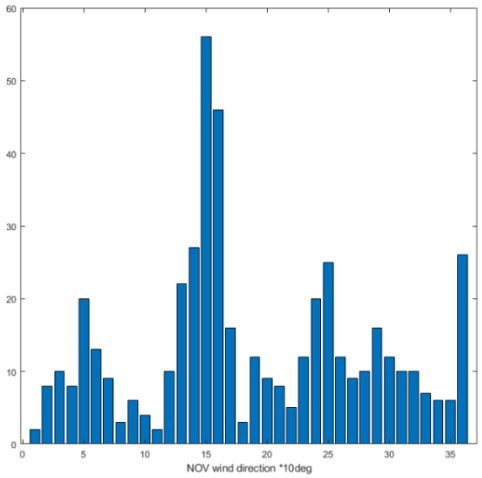

(k) November wind statistics

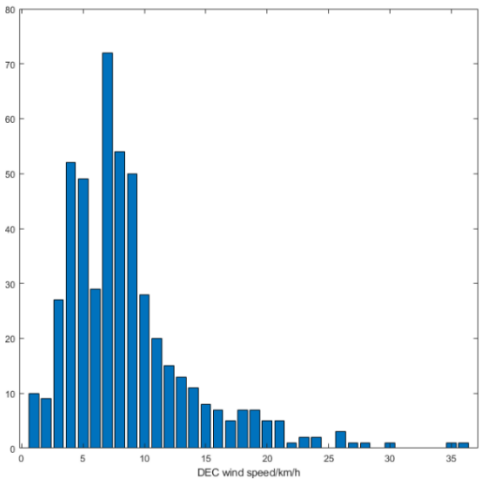

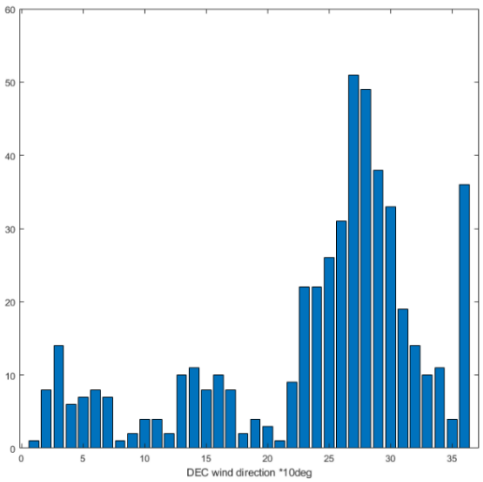

(l) December wind statistics

Figure J - 6 Wind statistics over each of the twelve months

The wind direction varies along with season variation. In the winter months, mainly the December, January and February, wind mostly come from west or west-northwest. While in summer months, May, June, July, August and September, wind mostly come from the southeast.

The variation of wind direction does have impact on ferry operation with different air resistance force.

REFERENCES

[1] US Navy Lecture Notes on Resistance and Powering of Ships, [Online]. Available at: https://www.usna.edu/NAOE/_files/documents/Courses/EN400/02.07%20Chapter%207.pdf)

[2] Climate.weather.gc.ca. (2018). Historical Data - Climate - Environment and Climate Change Canada. [online] Available at: http://climate.weather.gc.ca/historical_data/search_historic_data_e.html

[3] Tidesandcurrents.noaa.gov. (2018). NOAA Current Predictions - Current Predictions. [online] Available at: https://tidesandcurrents.noaa.gov/noaacurrents/Predictions?id=PCT2256_1

[4] B. Buckingham's Research Group, "Ocean Energy Data Collection and Analyses," West Coast Wave Initiative (WCWI) and Ocean Canada Internal Report, University of Victoria, 2016.

[5] A. Elings, B. A. Wolst, J. Man, and K. Petersen, "Autonomous Sailing – Interconnectivity," Rotterdam Mainport University of Applied Science, July 6th 2016, [Online]. Available: http://www.maritimesymposium-rotterdam.nl/uploads/Route/Autonomous%20sailing%20INTERCONNECTIVITY.pdf.

[6] W. Blendermann (1994). Parameter identification of wind loads on ships. Journal of Wind Engineering and Industrial Aerodynamics, 51:339, 351. DOI: 10.1016/0167-6105(94)90067-1.

[7] Historical Data - Climate - Environment and Climate Change Canada. [On line] Available: http://climate.weather.gc.ca/historical_data/search_historic_data_e.html

Appendix K. Case Study for Skeena Queen: Integrating Natural Gas Engine and Hybrid Electric Powertrain with Special Controls for Fuel Cost and Emission Reductions

ABSTRACT

Ferries are essential transportation tools for the west coast residents of Canada, as well as for about 10% of people of the world's population, who live on islands. However, the ferry fleet with a large amount of marine diesel fuel consumption bears high fuel costs and produces heavy Green House Gas (GHG) emissions, including particulate matter (PM), NO_x, SO_2, CO_2 and hydrocarbon (HC), emitted from the old cumbersome marine diesel engines. BC Ferries, one of the industrial partners of this project, has been providing transportation services for passengers and vehicles between various islands and the mainland in British Columbia since 1960. As the largest passenger ferry company in North America, it owns 47 operation lines, which has consumed 115.4 million litres of marine diesel at a cost of CAD$103.3 million in fiscal 2016. To reduce fuel cost and GHG emissions, BC Ferries has been seeking new technologies for its future ships. This work focuses on the new propulsion system designs of Skeena Queen - one of the typical middle size ferries, running between Salt Spring Island and Vancouver Island, a category of vessels for clean energy propulsion technology adoption.

The use of natural gas (NG), often in the form of liquefied natural gas (LNG), to replace diesel fuel presents a feasible and attractive fuel cost and emission reduction solution for heavy-duty transportation applications, particularly for large marine vessels. The present NG engines have some shortcomings in comparison to its diesel counterpart, including less peak power, slower response, the complexity of different NG-diesel pilot fuel ratios under varying load, and surge of hydrocarbon (HC) emissions at low and high loads. To overcome these drawbacks, an NG engine hybrid electric powertrain with specialized controls has been introduced in this work. The model of a specially designed hybrid electric powertrain system has been introduced with important new developments on its three key powertrain components. First, the NG engine model contains detailed fuel economy and emissions maps, including HC, to support the consideration of engine carbon dioxide equivalent (CO_{2e}) emissions to effectively control and reduce the overall emissions of the NG engine. Secondly, the use-caused degradation and life-cycle cost consideration have been added to the battery ESS performance degradation model to support its size optimization and optimal energy management. Thirdly, special control strategies for the series hybrid electric powertrain system have been introduced to address the shortcomings associated with present NG engine to ensure it operates in the ideal torque and speed region identified in this work.

The work uses the acquired operation and power load patterns of the BC Ferries Skeena Queen as a case study to demonstrate the fuel cost and emission reduction potentials of the newly proposed technology by comparing results from three powertrain alternatives: traditional diesel engine, NG (or NG-diesel dual fuel) engine, and series hybrid electric with NG engine and dedicated controls. The results showed that the combination and optimization of NG engine, hybrid electric powertrain, and special controls could significantly reduce both fuel cost and harmful emissions.

The series hybrid electric powertrain design has been focused in this work, due to its architectural similarity and relatively ease of retrofitting work from the traditional diesel-electric powertrain system.

K1. INTRODUCTION

According to the US EPA (Environmental Protection Agency) prediction, marine NOx and particulate matter (PM) emissions may reach 2.1M tons and 170K tons a year by 2030, respectively [1]. To reduce the health and environmental effects, the IMO (International Maritime Organization) launched MARPOL (the International Convention for the Prevention of Pollution from Ships), and introduced prevention measures of air pollution, mainly the nitrogen oxides (NOx), particular matter (PM) and sulphur oxides (SOx), from ship engines in 2005 [2]. Furthermore, the European Commission's white paper "Roadmap to a Single European Transport Area" in 2011 states that the carbon dioxide (CO2) emissions from maritime transport should be reduced by 40% in 2050 compared to 2005 levels [3]. An as much stricter convention is foreseeable in the near future, it is necessary to implement clean energy into the marine application. Recently, the photovoltaic (PV) system and wind turbine integrated hybrid electric technology has been introduced to the marine propulsion system for their clean and sustainable characteristics. Hai Lan [4] presented a sizing optimization problem in a series diesel hybrid electric ship integrated with a PV system. In the PV system modelling, this research considered the season and solar angle influence. Due to the introduction of PV and energy storage systems (ESS), both total cost, mainly the diesel fuel cost, and emission have a significant reduction. In terms of hybrid system stability and robustness, Li Wang [5] analyzed the hybrid electric marine power system with a high-voltage direct-current link. In two different operation cases (case 1 differs from case 2 in whether the fuel cell system works or not), the hybrid system can maintain system stability under different conditions including sudden load drop/rise (influence the diesel generator operating), sudden wind speed drop (influence the wind turbine operating). The highly integrated hybrid system and similar hybrid technology application can also be found in references [6]-[12].

The previously mentioned researchers still use the diesel-fueled engine as a prime power. In terms of alternative fuel types in marine primary power sources, many researchers have already reported the benefit of adopting natural gas as fuel for the ship propulsion system [13], [14]. Fabio Burel [15] analyzed the applicability of natural gas utilization in ships. Then, a specific ship equipped with an NG engine was studied. Beyond the liquefied natural gas (LNG), Selma Brynolf [16] also investigated the liquefied biogas, methanol, and bio-methanol impact on the environment. Their study concluded that the LNG had the same magnitude of impacts to global warming as heavy fuel oil due to the unburned and slip methane since the global warming potential of methane is 25 times greater than CO_2.

Despite the emerging hybrid and natural gas fueled technology in marine, our study case still uses the diesel engine to propel the ferry directly. The diesel engine output shaft drives the thruster via a reducer and a z-drive. Four diesel engines drive four thrusters around the ferry. The propulsion system is over-designed, resulting in low efficiency and high fuel cost. This case study looks into the combination of dual-fuel engine and series hybrid technology, to further utilize the potential of both technologies. This paper is organized as follows: Section 2 gives an overall view of ferry electrification and hybridization; Section 3 models the ferry propulsion system; simulation results are presented and discussed in Section 4; followed by the conclusion in Section 5.

K2. ELECTRIFICATION, HYBRIDIZATION AND APPLICATION OF LNG

The ferry ship, Skeena Queen with four diesel engines capable of producing 6,000 *hp*, operates between Fulford Harbour and Swartz Bay in BC and is able to carry 92 cars and 450 passengers. Its operation profile is given in Table K - 1.

Table K - 1 Operation profile of the studied ferry

Navigation condition	Time [min]
Leaving Swartz Bay and Sailing full load	28
Unloading/Loading in Fulford Harbor	15
Leaving Fulford Harbour and sailing	29
Unloading/Loading in Swartz Bay	15

To look into the ferry configuration, our research group conducted an experiment on the Skeena Queen ferry. Torque and speed sensors location is illustrated in Figure K - 1.

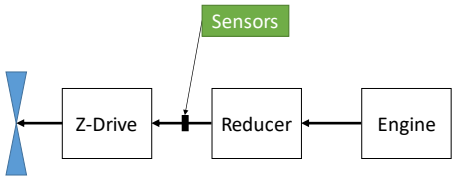

(a) Z-drive

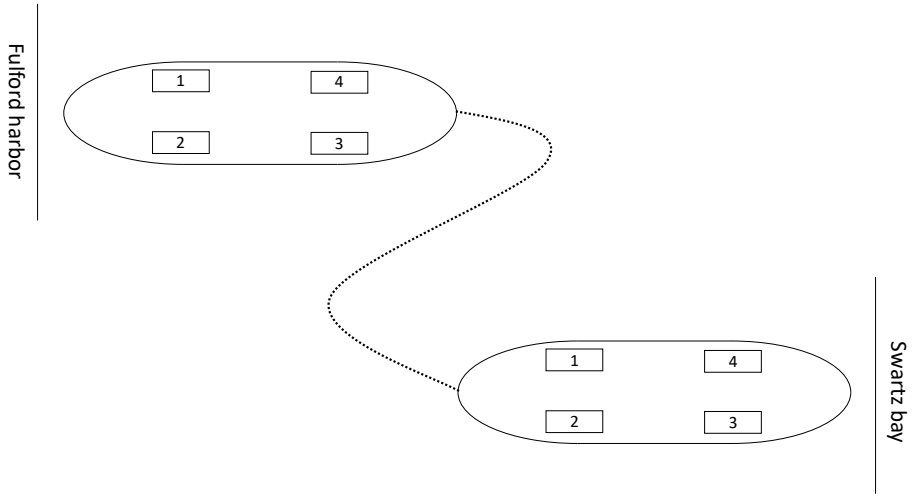

(b) Engine Layout

Figure K - 1 Ship Propulsion System Configuration

In Figure K - 1(a), rectangles represent the propulsion components, including engine, reducer, z-drive reducer, and the thruster. Those components connect via shaft, which is represented by the black line in Figure K - 1, where the arrow demonstrates the power flow direction. The speed and torque sensors mount on the shaft between reducer and z-drive. In the ferry propulsion system,

there are four separate engine-thruster systems, marked as 1, 2, 3, and 4 in Figure K - 1(b). In the sailing period, all four engines drive four thrusters, propelling the ferry. During docking, two engines continuously work to generate forces to keep the ferry tightly attached to the dock. Those operating characteristics can be seen from the acquired ferry torque and speed data shown in Figure K - 2.

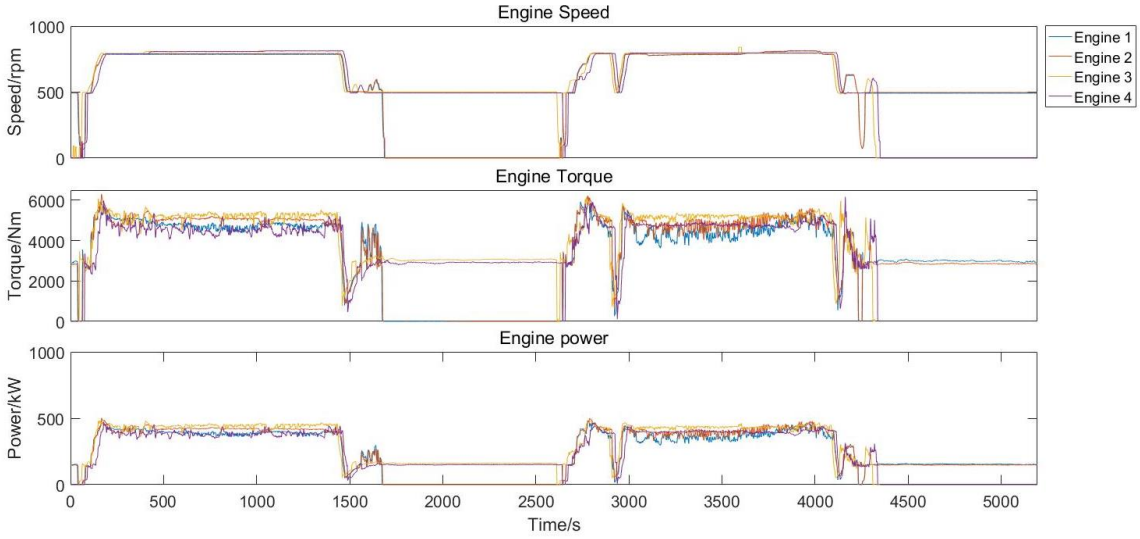

Figure K - 2 Engine Operating Cycle

In the sailing period, the engine speed increases to match the ferry velocity, and its output torque to overcome the hull resistance. In our chosen operation cycle, the ship sails at about 14 knots. Engine speed keeps constant: two engines operate at about 960rpm, 970rpm; the other two engines in the front of the ferry (so the rear during the other direction) have two-speed steps. Due to the current influence, engine output torque varies in each sailing period. Furthermore, the tide has a significant impact on the morning sailing and near-dusk sailing.

To give a feasibility study on ferry hybridization, this section introduces a series hybrid electric propulsion architecture. An electric drive system is needed to build a series hybrid electric propulsion system. Architectures of the two electrified propulsion systems are shown in Figure K - 3.

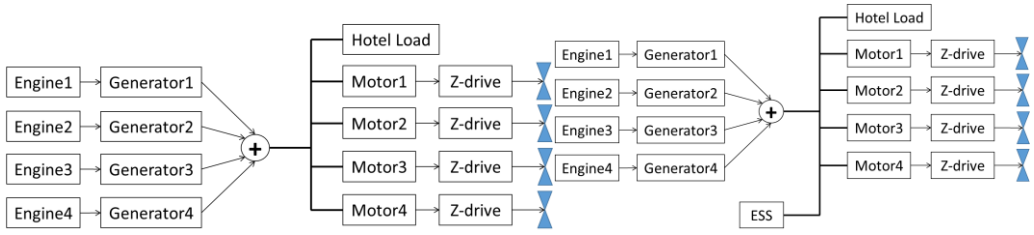

(a) ICE-electric drive (b) Series hybrid electric drive

Figure K - 3 Electrified Marine Propulsion

By choosing the suitable synchronous generators and high torque motors in the marine application area, we modify the traditional distributed-engine mechanical drive system into an integrated electrified system. To look into the benefits of electrification and hybridization, the following assumptions are made:

- The rated speed of the motor is 800 *rpm*, following the measured shaft speed of 790 *rpm*. The motor produces at the measured speeds and torques, modelled by the ferry's operation cycle, for repeated ferry operations.
- The engine-generator's dynamic characteristics are neglected.
- The power electronics, including rectifier and inverter, dynamic models are ignored, which are replaced by the look-up table and fuel efficiency map.
- The hotel load is not accounted for the total power demand since the experimental data did not include it either.

To generate a proper battery package, this study applies the battery parameters from AUTONOMIE software, where the battery cell resistance, discharge/charge power versus battery State of Charge (SOC) are available. The battery cell/pack information is given in Table K - 2.

Table K - 2 Battery Information

	Battery Cell	Battery Pack
Nominal capacity/Ah	41	615
Nominal voltage/V	3.6	720
Number of series	-	200
Number of parallel	-	15

The NG-diesel dual-fuel technology allows a heavy-duty diesel engine to be modified into a compression ignited (CI) NG engine that is mainly fueled by NG, using diesel as the pilot fuel to lower the engine's ignition temperature.

This case study evaluates the heavy-duty engine fuel conversion from diesel-only fuel to LNG fuel with 25% mass portion pilot diesel fuel. The engine performance and emission conversion are based on the published literature [17].

K3. SYSTEM EFFICIENCY ANALYSIS, MODELLING AND CONTROL

Figure K - 3 depicts the system architecture of the electrified marine propulsion, including (a) traditional diesel-electric powertrain, and (b) hybrid electric powertrain systems. The propulsion systems consist of four engine-generator sets, four motors drives, and four thrusters as in the original ship. A battery ESS and more complex hybrid electric powertrain system control are added to form the hybrid electric propulsion system in Figure K - 3 (b). In each engine-generator set, the prime mover is coupled to a synchronous generator. The AC power produced by the engine-generators is converted to DC power on the ship's power bus. The generated electric power then drives the motors to propel the thruster. For the hybrid electric powertrain, the generated electric power is supplemented by the power from the ESS, or is used to both drive the motors and to charge the battery ESS.

In the traditional mechanical propulsion system, the power loss comes from the reducer shaft and z-drive. For the electrified propulsion systems shown in Figure K - 3, however, additional energy conversion losses are introduced, mechanical to electrical, electrical back to mechanical, electrical

to electrochemical and electrochemical back to electrical. The diesel-electric and hybrid electric powertrain systems need to ensure the engines operate at higher energy efficiency to offset the additional energy conversion losses. Effective power control and energy management methods are needed to accomplish the benefits of powertrain electrification and hybridization.

K3.1. ICE-Generator Set Model and Power Distribution Control

The main power source of our study case is the four internal combustion engines (ICEs), fueled with the marine diesel oil (MDO). The ICE specific fuel consumption is modelled as a function of speed and torque. In this work, we found that the trailer truck diesel engines from Detroit Diesel are used as the propulsion engines in a slightly smaller ferry, Klitsa. The data of the Skeena Queen's diesel engines were then obtained by scaling the data of a heavy-duty diesel truck engine. Scaling is a common practice used for modelling powertrain system components in powertrain system modelling tools. From the diesel engine data to the dual-fuel NG engine data, a transfer matrix is generated based on the published literature.

In an AC power system, all generator sets must be synchronized to one fixed frequency, and the speed of an AC propulsion motor is adjusted by controlling the variable frequency. The DC power system maintains a stable power bus voltage, a fix engine frequency of 50Hz was used in this modelling study. By combining the generator efficiency and the ICE fuel consumption, the electric power versus the specific fuel consumption curves are given in Figure K - 4, in which the LNG engine fuel consumption rate includes the total mass of pilot diesel fuel and the primary NG fuel.

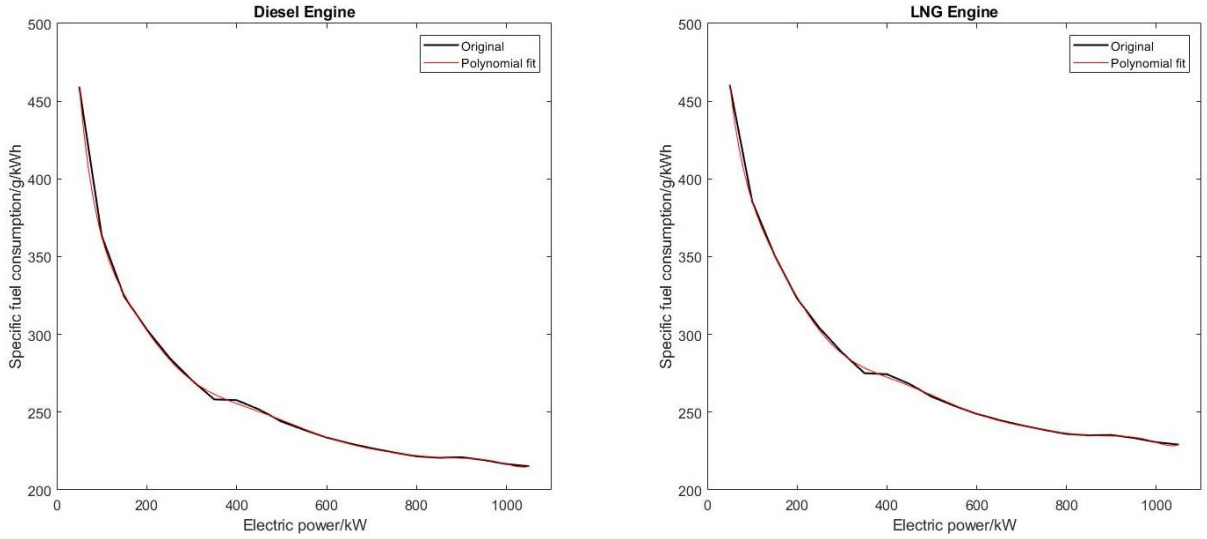

Figure K - 4 Fuel Consumption of an ICE-Generator Set

In a heuristics power distribution system in multi ICE-generator sets (IGSs) on board, the IGS activation can be described as follows: the power distributor receives the power demand from power bus and activates the first set; along with the power demand increases, the first IGS reaches its rated power or the pre-set power, then the second set starts to power the system, while the first engine still outputs its rated or pre-set power; and then the third set is activated, until all four sets are activated. Due to the nonlinear characteristics of ICE specific fuel consumption, this method cannot achieve the optimal ICE-generator power distribution. This study provides an optimization-based power distribution of multi IGSs.

The equivalent specific fuel consumption (SFC) of multi IGSs is the average of each set fuel consumption weighted by the power output.

$$SFCe = \frac{\sum P_i * SFC_i}{\sum P_i} \quad \text{(Eq K - 1)}$$

where, *SFCe* is the equivalent fuel consumption, g/kWh; *P*, *SFC* is the *i*th IGS output power and specific fuel consumption.

At each power bus demand power, the optimization objective is to minimize the equivalent specific fuel consumption. Hence, the power distribution is an optimization problem.

$$\text{Minimize } SFCe = \frac{\sum P_i * SFC_i}{\sum P_i} \quad \text{(Eq K - 2)}$$

$$\text{Subject to: } \sum P_i = P_{dmd} \quad \text{(Eq K - 3)}$$

where P_{dmd} is the exact power demand at power bus.

For each power demand, from zero power to the maximum power, there is an exact optimal power distribution among all ICE-generator sets. When the power demand less than the one IGS rated power, it is optimal to activate one IGS. Beyond the one IGS rated power, the optimization method is implemented to find the optimal distribution.

Evolution algorithms can provide good approximate solution of problems, especially the equality constrained problems, which cannot be easily solved by other optimization methods. Based on the genetic algorithm, the power distribution among all IGSs is optimized.

For power demand less than the one IGS rated power, the optimal result shares the same power distribution with the heuristic result. After the power demand exceeds the one IGS rated power, the first IGS starts to decrease a little output power, which can hardly be seen in Figure K - 5. After the optimization, it is reasonable to consider the multiple engines as one integrated engine with a power distribution controller. Those optimization results, including the diesel and LNG engine power distribution, are suitable for ICE-electric and series hybrid electric propulsion systems.

K3.2. Motor and Load Model

The electric motor provides power for the thruster in the electric propulsion and series hybrid electric propulsion system. Those electric motors cannot function as a generator. The electric motor is mechanically connected to the z-drive, propelling the thruster.

The efficiency of the motor was modelled, as a function of motor speed and torque, and the power of the motor was modelled using collected data. Since the speed and torque sensors were mounted onto the input shaft to the z-drive, the acquired speed and torque data are not exact motor outputs. By the summation of all four electric motors electric power demand, Figure K - 6 gives the total electric power demand for propulsion.

According to the ferry operating file, the hotel load in ferry varies along with the weather: about 200kW in summer, while more than 300kW in winter. Since this hotel load does not change from the mechanical propulsion system to the electrified propulsion system, it is reasonable to ignore it during the comparison of different propulsion systems. The electric power demand can also be treated as the total power demand or the total load.

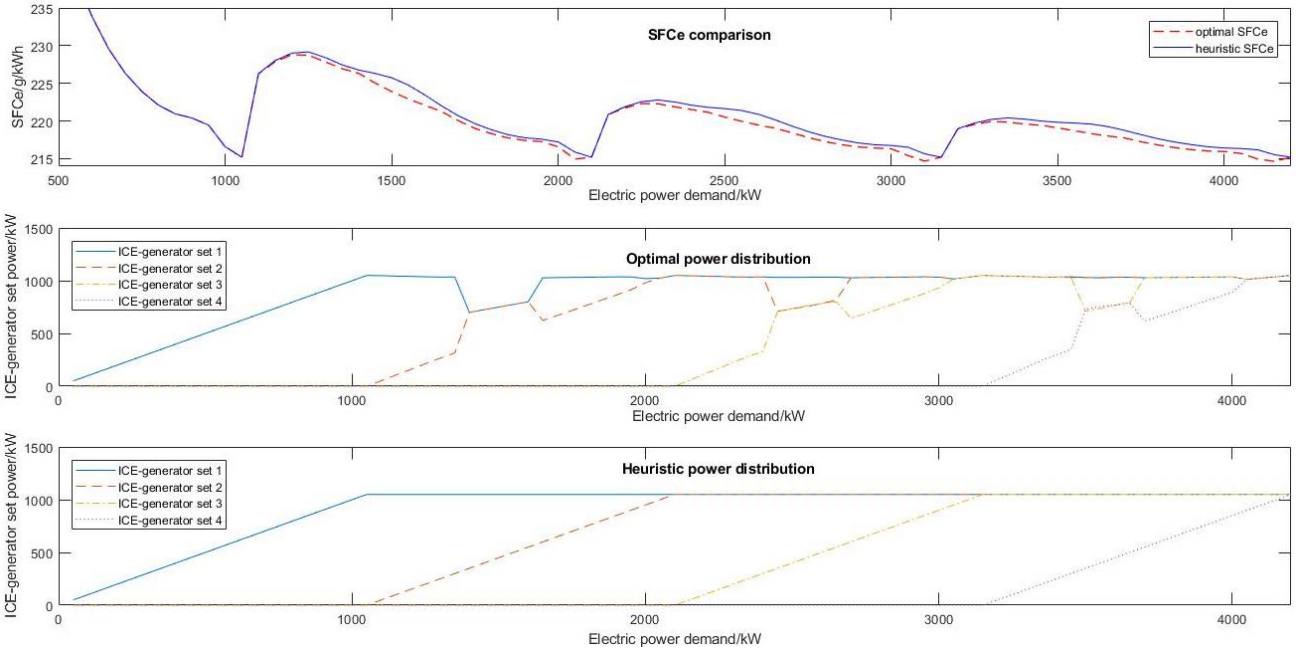

(a) Diesel-generator Set Power Distribution

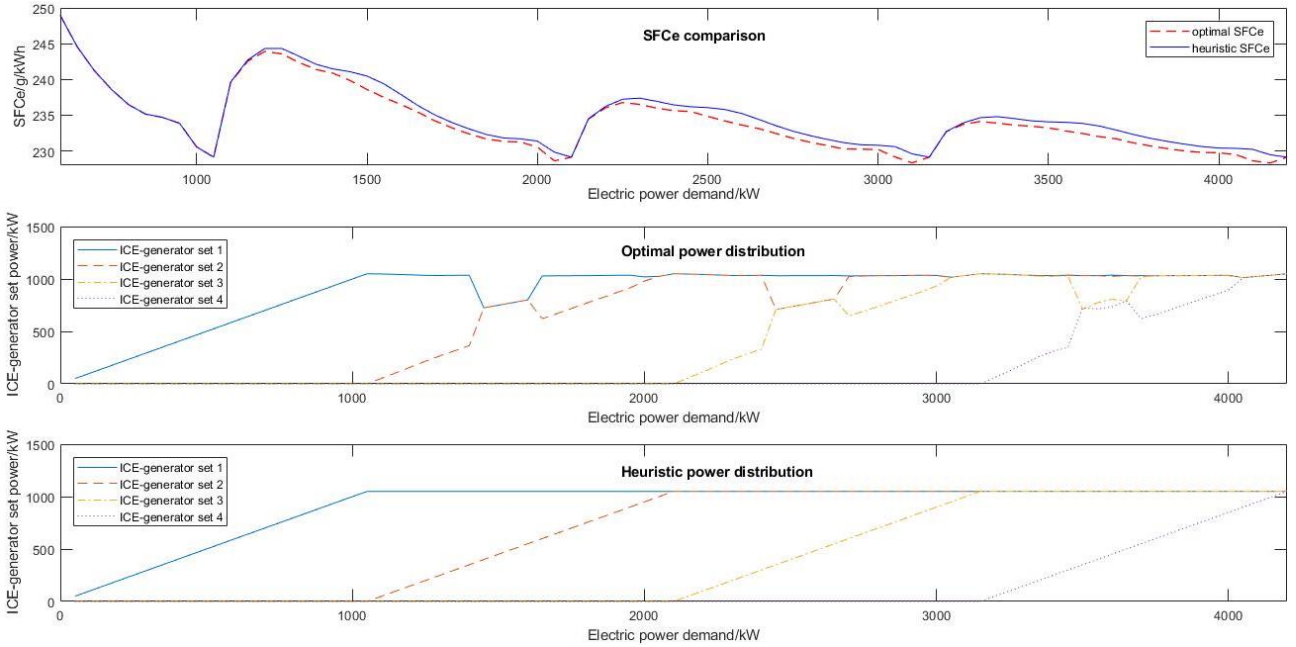

(b) LNG-generator Set Power Distribution

Figure K - 5 IGS Power Distributions

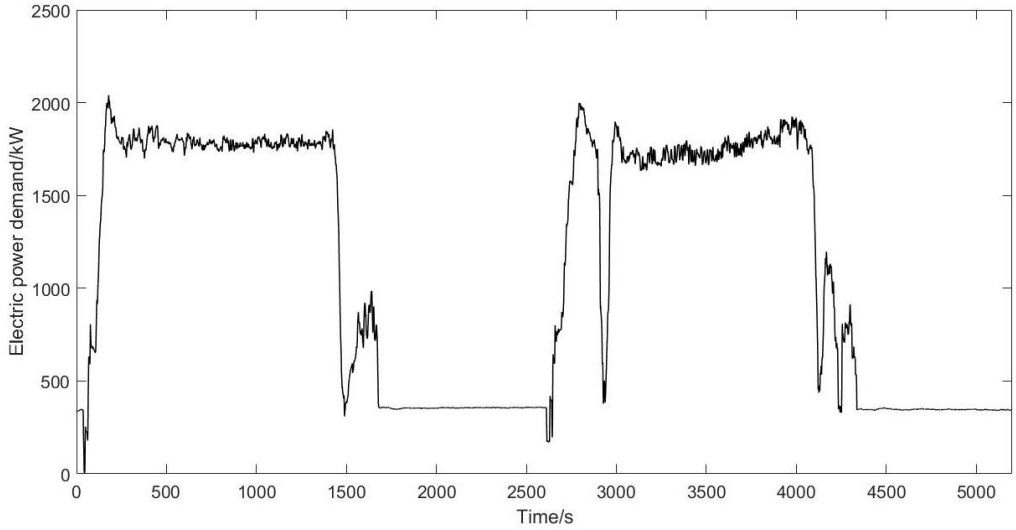

Figure K - 6 Electric Power Demand

K3.3. Battery Model

A battery (ESS) is one of the costly, key components of a hybrid electric propulsion system. Its cost becomes dominant for full hybrid and plug-in hybrid powertrains. For the energy management of the battery ESS, the equivalent circuit model of the battery serves as an appropriate tool with the best balance of model accuracy and complexity and finds wide applications. In this work the form of the equivalent circuit model and model parameters from the hybrid electric powertrain modelling tool, AUTONOMIE, are used:

$$U = U_{ocv} - I * R_{eq} - \sum I_{pc\_i} * R_{pr\_i} \qquad \text{(Eq K - 4)}$$

where, U and I are battery voltage and current; R_{eq} and U_{ocv} are battery resistance and open circuit voltage; R_{pr} and I_{pc}, are polarization resistance and polarization current; and i is the ith polarization current. The variations of R_{eq} and U_{ocv} under varying battery SOC are shown in Figure K - 7. The polarization current can be calculated by:

$$I = \int \frac{I - I_{pc}}{T_{soc}} \qquad \text{(Eq K - 5)}$$

where, T_{SOC} is a SOC-dependent constant.

All the polarization parameters can be obtained in the AUTONOMIE software as well.

To properly size the battery ESS and to develop the optimal energy management strategies, the performance degradation model of the battery ESS under different use patterns is essential. The more complex electrochemical models for battery ESS can provide higher modelling accuracy and capability, including life degradation prediction [18][19][20]. However, the complex model could not be used directly for online energy management due to many difficult to determine model parameters.

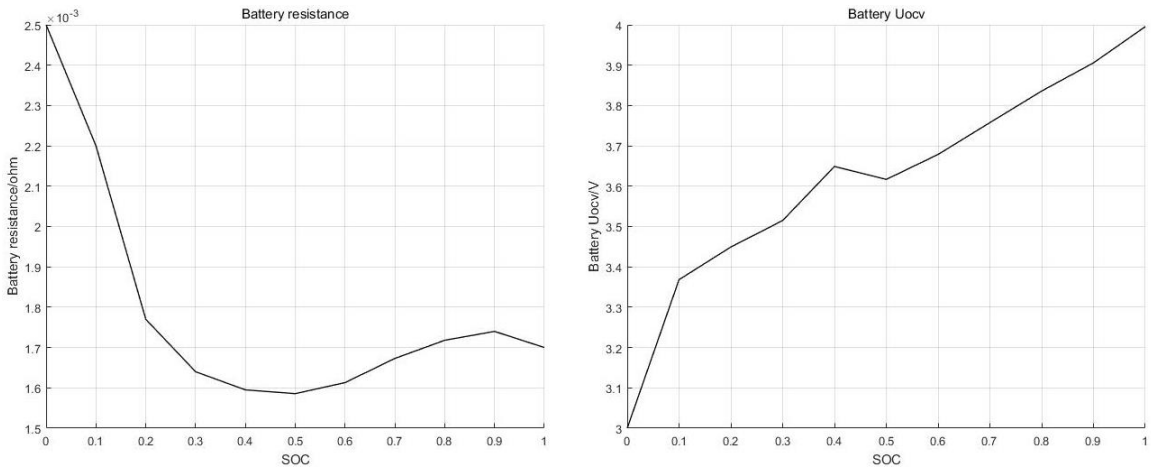

Figure K - 7 Battery Resistance and U_{ocv}

K3.4. Online Control Strategy for Hybrid Propulsion System

In Figure K - 6, the maximum power demand during the whole cycle is about 2060kW. There are two typical operating patterns during a cycle: one is the sailing pattern, and another is the docking pattern. In this section, developments of the control strategies for the series hybrid electric propulsion system are demonstrated.

The hybrid electric system for the ferry differs from the hybrid propulsion and power systems for road vehicles and stationary power. The electric energy in the ESS comes only from the IGS, and no regenerative braking or other sustainable energy sources, including PV systems or wind turbine, are involved. The energy available from the battery is directly related to the amount of fuel consumed and the battery charge/discharge efficiencies. The power loss of the ESS occurs on the equivalent resistor and polarization resistor during charge and discharge. The battery model indicates that the power loss of the battery is time-variant and SOC-dependent. Since the polarization current and resistance are two orders of magnitude smaller than the equivalent resistance, it is thus feasible to evaluate battery efficiency by only considering its internal resistance. Assuming the battery operates at its maximum continuous charge and discharge power, the battery efficiency is obtained as shown in Figure K - 8.

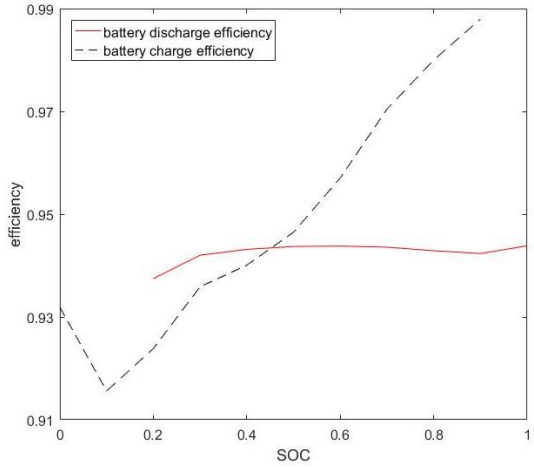

Figure K - 8 Battery Charge/Discharge Efficiency

In the battery discharge process, from SOC 0.5 to 0.9, the efficiency is near-constant, about 94.5%. Because the charge power decreases along with the SOC increasing, the battery charge efficiency increases from 94.5% to 98.9% along with the SOC increases from 0.5 to 0.9. In the range 0.5 to 0.9, even if the worst situation, the energy efficiency via a battery, (from electrical energy to chemical energy, then to electricity energy), is about 89.4%. The battery power is converted to an equivalence of 89% of IGS power considering energy conversion losses.

During docking, the thrusters push the ferry steadily against the ship dock at the wharf. For thruster control at this moment, the thruster speed should be minimum when the relative velocity of the ship against water becomes zero. In the traditional mechanical propulsion system, the engine operates at the idle speed, and the two engines generate about 300 kW power during docking, as shown in Figure K - 2. At this moment, both engines operate outside their efficient speed and torque zone, resulting in fuel consumption at about 357g/kWh. In the series hybrid electric propulsion system, as shown in Figure K - 7, the average electric power demand from the power bus is about 360 kW during docking. This is slightly higher than the mechanical propulsion system due to energy conversion losses. Based on optimal power control strategies, only one engine is running to produce about 360 kW to power the two motor-driven propellers, and the specific fuel consumption is about 260 g/kWh at the diesel engine. The change of engine operating conditions to a more efficient speed and torque zone led to reduced fuel consumption.

The ferry sails at about 14 knots during crossing. To match the ferry relative velocity against water, the thruster should operate at an optimal thruster rotation speed, which is directly coupled to the measured shaft speed. In the series hybrid electric propulsion system, that speed and torque match process is applied to the motor, while the engine is totally decoupled from the thruster shaft. The motor can operate at its near rated speed, resulting in 94% efficiency. The IGSs output the demand power (average 1,800 kW) according to the optimal power distribution. From the optimal power distribution, the specific fuel consumption is about 220 g/kWh.

From the above analyses, the fuel consumption rate for the crossing is 220 g/kWh, while the battery output at 360kW during docking with a fuel consumption rate at 247 g/kWh and a battery operation efficiency of 0.89. The rule-based control strategies for the entire cycle is described as following:

- During docking, the battery ESS supplies the needed power;
- During sailing, the IGSs increase the output power up to the rated power of the two engines to propel the vessel and to charge the battery;
- Switching from docking to sailing, the ferry operates at the IGS only mode;
- The lower and upper bounds of the battery SOC are 0.5 and 0.9, with its initial SOC in between at an average of 0.7 at the beginning of each crossing;
- Battery charge and discharge power should not exceed the available continuous power at different SOC of the ESS.

K4. SIMULATION RESULTS AND DISCUSSION

The modelling and simulations conducted in this work considered three alternative ferry propulsion systems: a) the traditional ICE-mechanical propulsion system, b) the ICE-electric propulsion system, and c) the series ICE hybrid electric propulsion system. For each propulsion system configuration, a regular diesel engine and an NG-diesel dual-fuel engine are considered for comparison. In evaluating the carbon dioxide emission, complete combustions at the ICE, 1 kg

diesel for 3.2262 kg CO_2, and 1kg LNG for 2.2815 kg CO_2 are assumed [21]. For evaluating the CO_{2e} emissions, the used equivalent factors are based on the 100-year global warming potential for each emission component [22][23][24]. The simulation results are shown in Table K - 3.

Table K - 3 Fuel consumption, cost and emission comparison

Powertrain Type	Engine Type	Fuel (kg)	Fuel Cost (US$)	Emissions (kg)				
				CO_2	NO_x	CO	HC	CO_{2e}
ICE Mechanical	Diesel	398.8	509	1286.5	55.28	3.6153	5.1738	1931.3
	LNG	106.2(D) 318.6	216	1069.44	57.73	3.12	43.32	1930.5
ICE Electric	Diesel	400.3	511.2	1291.6	14.84	1.89	0.59	1463.5
	LNG	106.5(D) 319.6	216.4	1073	14	32	3.77	1342
Hybrid Electric	Diesel	389.8	497.7	1257.4	11.4	1.9	0.41	1390.9
	LNG	103.7(D) 311.2	132.5	1044.7	10.8	32.34	2.26	1271.8

where, (D) denotes the pilot diesel fuel consumption in LNG engine, and Hybrid Electric presents the series hybrid electric propulsion system.

K4.1. The traditional mechanical propulsion system

In the original direct drive propulsion system with four diesel engines, the engines are coupled with the four thrusters directly, operating at the same speed as the four thrusters after gear reduction. At normal cruising speed, all four engines are on, but two engines are enough to cover the maximum power demand of the vessel. The superfluous engine power made them to operate at the speed and torque far from their optimal and most efficient speed and torque zone, as shown in Figure K – 9. Each engine only produces about 460 kW of power during sailing, while their rated power is about 1,100 kW.

During docking, two engines operate at their idle speed to generate the docking force and to maintain marine docking stability from ocean current disturbance, using 180 kW power, as shown in Figure K - 9. The traditional mechanical propulsion system provides ample power and capacity to vessel cruising and docking, while the powertrain architecture limits its energy efficiency.

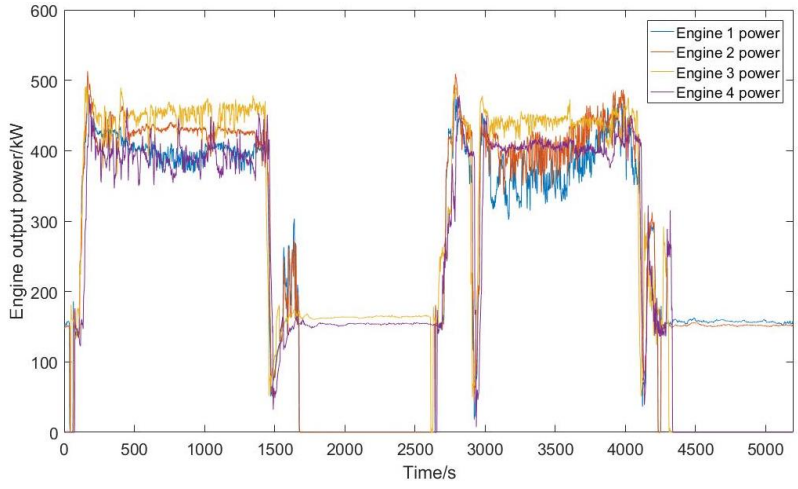

Figure K - 9 Engine Power in Mechanical Propulsion

As shown in Table K - 3, the model projected that the diesel-mechanical propulsion system would consume about 398.8 kg of diesel fuel and produce 1,931.3 kg CO_{2e} emissions. The ferry fuel logbook showed that the average fuel usage for each round trip is about 640 L or 530 kg of diesel. The simulation prediction is about 25% less than the measured fuel consumption for each round trip of the vessel. The following reasons led to the difference.

(a) The hotel load of the ferry has not been counted. Based upon the experience from the ferry operator, ferry hotel load in summer is about 200 kW and over 300kW in the winter due to heater operation. Adding the 200 kW fuel use to cover the summer hotel loads, the total fuel consumption would be about 472 kg, about 10.9% less than the measured diesel use.
(b) The power consumptions from engine accessories, including cooling pumps and fuel feeding pumps, has not been considered;
(c) During docking, the engines are idling while the shaft speeds are zero with disengaged clutches, and this amount of fuel consumption has not been considered;
(d) Fuel consumption results are based on the scaled diesel engine performance data.

The fuel conversion from diesel to LNG led to significant fuel cost reduction due to the lower cost of the NG fuel. Both of the diesel and NG engines are assumed to have the same output power as shown in Figure K - 9. With less carbon content in the NG fuel, the NG fueled engine produced less CO_2. However, an NG-diesel dual-fuel compression ignited engines still has a number of drawbacks, including the surge of hydrogen carbon (HC) and CO emissions at low speed and low load, due to incomplete combustion of the NG fuel, the so-called “methane slip”. Because of the large increase of HC and CO emissions, the equivalent carbon dioxide emissions, CO_{2e}, almost show no improvement at all. The distributed engine-thruster layout in the mechanical propulsion system contributed to these problems.

K4.2. ICE-Electric Propulsion System

With the powertrain electrification using an ICE-electric powertrain system, each thruster is propelled by an electric motor. The energy flow efficiency from the engine to thruster for a traditional mechanical propulsion system is about 0.94, with 0.98 shaft efficiency and 0.98*0.98 reducer/z-drive efficiency. The powertrain electrification spared the reducer and added a generator and a propulsion motor in the power flow pipeline. Assuming the efficiencies of the generator and the motor are both 0.94, the overall energy flow efficiency in the electrified system would be 0.85. The electrified propulsion system is less efficient than the pure mechanical counterpart. However, the optimal power distribution in the electric system could make up part of this loss, as illustrated by the simulation results in Table K - 3.

Based on the discussions on electric power demand and distribution in Section K3, the electric propulsion system can turn off two engine generators to supply enough propulsion power. Figure K - 10 showed that the power outputs from engines 3 and 4 are zero. The two engines in operation can now operate at their close to optimal speed and torque zone, with a considerably lower specific fuel consumption rate. Although the total amount of energy needed for propelling the vessel has increased by 0.4%, from 398.8 kg to 400.3 kg of diesel fuel, due to the additional energy conversion loss, the efficiency gain from improved engine operation efficiency is about 9.5%, presenting a net fuel efficiency improvement. This is different from the vehicle powertrain system, in which only one ICE is involved.

Besides the engine specific fuel consumption rate, the engine sub-optimal operating zone can benefit the total emission result. As Table K - 3 shows, the CO_2 emission has little increase because of the fuel consumption increase. However, the diesel engine in higher torque output area results in the air/fuel ratio reduction, leading to the NO_x emission reduction. Combining the other emission reduction, the total CO_{2e} in diesel-electric architecture decrease by about 24.2%.

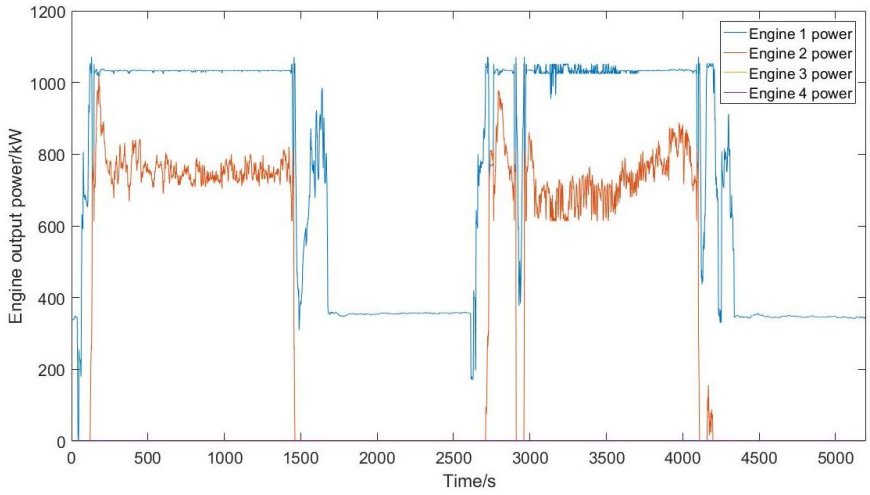

Figure K - 10 Engine Output Power in the Electric System

The modified LNG engine shares the same engine power output with a diesel-electric system. For the cleaner characteristics of natural gas, total CO_2 emission in the LNG-electric system decreases against diesel-electric, while CO_2 emission increases over the mechanical propulsion system equipped with an LNG engine. That is because the energy flow efficiency deteriorates in an electric propulsion system. Thanks to the lower price of LNG, the LNG-electric has a lower operation fuel cost than diesel-electric, while comparable to the LNG mechanical propulsion system.

The four NG-generator electric propulsion system has improved fuel efficiency and reduced CO_2 emission. Even with the increased HC and CO emissions from the NG engines, the total CO_2 emissions are still lower than the pure mechanical powertrain, or the diesel-electric powertrain.

K4.3. Series Hybrid Electric Propulsion System

As Figure K - 3 showed that the ICE-electric propulsion system is turned into an ICE series hybrid electric propulsion system by adding an ESS and advanced controls. The energy management strategies discussed in Section K3 and the system controls illustrated in Figure K - 11 are needed.

During sailing, the SFC value is relatively low, indicating that engines are operating within or close to their maximum fuel efficiency zone. The higher SFC readings during docking indicate that the engines are operating inefficiently, resulting in a higher fuel consumption rate. The function of the hybrid electric system is to make sure that the operating engines work at their peak fuel efficiency during docking. This is accomplished by using the electric energy from the ESS to drive the propellers with light loads and only turn on the engine(s) to run at full speed/load when the stored energy is not enough.

The battery and engine power management strategies in a hybrid propulsion system are shown in Figure K - 12. During the complete operation cycle, the battery ESS functions as an energy reservoir, absorbing the surplus energy during sailing and using the stored energy to replace the

engine(s) when they only need to run at partial load and low efficiency. At around the 1,300th and 3,700th seconds during the cycle, the engines adjust their output power to match the needed battery charge power. The initial SOC of the battery was assumed to be at its average value of 0.7, and the final SOC recorded was 0.7187. The difference in SOC implies that actual fuel consumption may be slightly less after SOC level correction.

The results of the modelling and simulation showed the benefits of the series hybrid electric propulsion system. With the diesel engine, the diesel fuel consumption decreased from 400.3 kg of the diesel-mechanical system to 389.8 kg, and the CO_{2e} emissions reduced by 5% compared to the diesel-electric propulsion system. With the NG-diesel compression ignition engine, the NG fuel cost is only 26% of diesel fuel cost of the diesel-mechanical propulsion system. The NG hybrid electric propulsion system also led to reduced total CO_{2e} emissions, from 1,931.3kg in the diesel-mechanical system to 1,271.8 kg in the NG hybrid electric system. These improvements are predicted using the same modelling method with no relative modelling errors, and the improvements were over the best fuel efficiency and emission capabilities of traditional propulsion systems, ICE-mechanical and ICE-electric powertrains.

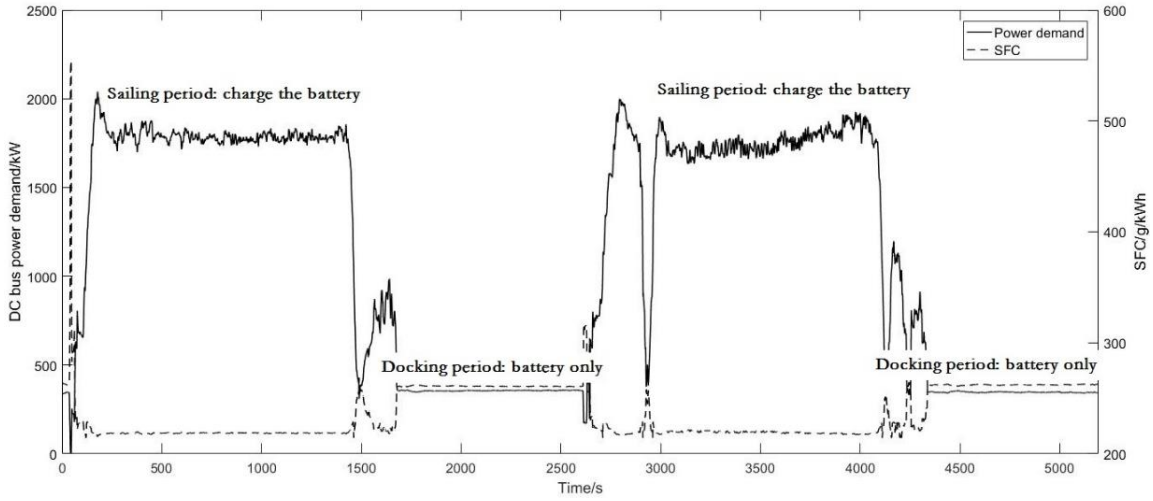

Figure K - 11 Power Demand and Control

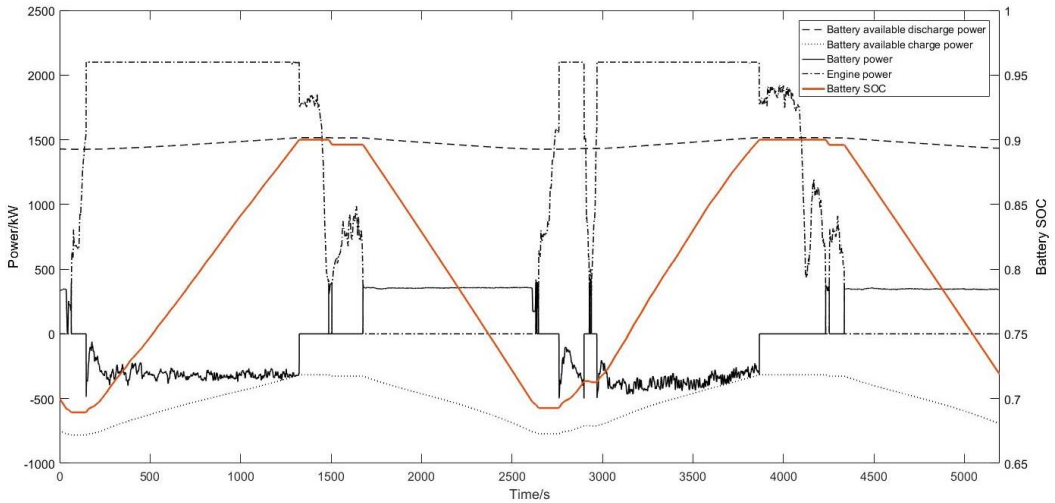

Figure K - 12 Energy Management and ESS SOC

K5. CONCLUSIONS

This study modelled and simulated the fuel efficiency and emissions of six different propulsion system options on Skeena Queen, considering the hybridization of the powertrain and the use of NG engines to replace the conventional diesel-mechanical propulsion system. The powertrain system models were introduced using model parameters matching those obtained from acquired ferry operation data. The optimal power distribution among multi-IGSs and the rule-based control strategy were developed. The study led to the following conclusions:

- The use of LNG fueled engines can significantly reduce the fuel cost due to the lower cost of NG fuel. In the three different powertrain architectures, the introduction of the LNG fueled engine brings 57.6% (mechanical propulsion system), 57.7% (electric propulsion system), and 73.4% (series hybrid electric propulsion system) fuel cost reduction over the systems using diesel engines. However, the emission improvements with the LNG engine replacement would be limited. For the mechanical propulsion system in particular, there was almost no improvement in CO_{2e}, despite the significant reduction of CO_2.

- Due to the relatively constant power load during the crossings and the additional energy conversion losses, the electrification and hybridization of the ferry's powertrain system had no and minimum energy efficiency improvements. The diesel-electric powertrain led to lower overall energy efficiency, since the gain on improved engine operation efficiency during the entire operation is not enough to offset the mechanical-electric-mechanical energy conversion losses of the system. The series hybrid electric propulsion system with added peak-cut and valley-fill power adjusting ability using the added battery ESS led to about 2.26% and 2.55%, fuel consumption improvements over the diesel-electric and mechanical propulsion systems, respectively.

- Electrification and hybridization could reduce the total emissions effectively by constraining the engine operating speed and torque to the low emission zone. The engines are operating at or close to their rated power, and ideal speed and torque zone, leading to more efficient combustion. This resulted in lower NO_x, CO, and HC emissions for the diesel-fueled engines, and lower NO_x, and HC emissions for the NG fueled engines. The hybrid propulsion systems reduced the total CO_{2e} emissions by 28% and 34% for the diesel-fueled and NG fueled engine, separately.

- The adoption of the NG-diesel dual-fuel engine can reduce the fuel cost significantly. The NG engine series hybrid electric powertrain system has effectively improved the total CO_{2e} emissions. The combination of the two cleaner propulsion technologies, NG engine and hybrid electric powertrain with dedicated controls, led to 26 % fuel cost and 34% CO_{2e} emission reductions over the traditional diesel-fueled mechanical propulsion systems.

- AN NG engine tends to have much higher HC and CO emissions at low speed and load, special attention are needed to introduce the dedicated control logics, as done in this work, to avoid the NG engine to operate within these speed and torque regions to control the overall GHG or CO_{2e} emissions. Our further research will seek the development of globally optimized control strategies to find a balanced solution for fuel efficiency and CO_{2e} emission reduction improvements.

K6. ACKNOWLEDGEMENTS

The authors would like to thank Michael Grant, Haijia Alex Zhu and Xiaofei Wen for their work on operation data collection from Skeena Queen, and the extensive support from Bruce Paterson, William Russell, Bob Kearney and François Cambron at BC Ferries. Financial supports and guidance from the Clean Transportation Initiative of Transport Canada are gratefully acknowledged.

REFERENCES

[1]. US Environmental Protection Agency, 2009, US Environmental Protection Agency, Proposal of Emission Control Area Designation for Geographic Control of Emissions from Ships, US EPA, Washington (2009)

[2]. Eyring, V., et al. "Emissions from international shipping: 2. Impact of future technologies on scenarios until 2050." Journal of Geophysical Research: Atmospheres 110.D17 (2005).

[3]. European Commission. Directorate-General for Mobility and Transport. White Paper on Transport: Roadmap to a Single European Transport Area: Towards a Competitive and Resource-efficient Transport System. Publications Office of the European Union, 2011.

[4]. Lan, Hai, et al. "Optimal sizing of hybrid PV/diesel/battery in ship power system." Applied Energy 158 (2015): 26-34.

[5]. Wang, Li, et al. "Analysis of a novel autonomous marine hybrid power generation/energy storage system with a high-voltage direct current link." Journal of Power Sources 185.2 (2008): 1284-1292.

[6]. Zahedi, Bijan, Lars E. Norum, and Kristine B. Ludvigsen. "Optimized efficiency of all-electric ships by dc hybrid power systems." Journal of power sources 255 (2014): 341-354.

[7]. Diab, Fahd, Hai Lan, and Salwa Ali. "Novel comparison study between the hybrid renewable energy systems on land and on ship." Renewable and Sustainable Energy Reviews 63 (2016): 452-463.

[8]. Wen, Shuli, et al. "Allocation of ESS by interval optimization method considering impact of ship swinging on hybrid PV/diesel ship power system." Applied Energy 175 (2016): 158-167.

[9]. Chen, Wenjie, et al. "Super-capacitors based hybrid converter in marine electric propulsion system." Electrical Machines (ICEM), 2010 XIX International Conference on. IEEE, 2010.

[10]. Lee, Dong-Jing, and Li Wang. "Small-signal stability analysis of an autonomous hybrid renewable energy power generation/energy storage system part I: Time-domain simulations." IEEE Transactions on Energy Conversion 23.1 (2008): 311-320.

[11]. Bianucci, Marco, et al. "The optimal hybrid/electric ferry for the Liguria Natural Parks." OCEANS 2015-Genova. IEEE, 2015.

[12]. Rozine, Vassili, and John Ockerman. "Plug-In Hybrid Direct Current Distribution for Ferry Systems, Escort Tugs, and Harbour Vessels." Journal of Ship Production and Design 28.2 (2012): 82-86.

[13]. Cofala, Janusz, et al. "Analysis of policy measures to reduce ship emissions in the context of the revision of the national emissions ceilings directive." (2007).

[14]. Haack, Tobias. "Energy efficient gas propulsion system with hybrid shaft generator." Ship Efficiency 2011 3rd International Conference, Hamburg, Germany. 2011.

[15]. Burel, Fabio, Rodolfo Taccani, and Nicola Zuliani. "Improving sustainability of maritime transport through utilization of Liquefied Natural Gas (LNG) for propulsion." Energy 57 (2013): 412-420.
[16]. Brynolf, Selma, Erik Fridell, and Karin Anderson. "Environmental assessment of marine fuels: liquefied natural gas, liquefied biogas, methanol and bio-methanol." Journal of cleaner production 74 (2014): 86-95.
[17]. Cheenkachorn, Kraipat, Chedthawut Poompipatpong, and Choi Gyeung Ho. "Performance and emissions of a heavy-duty diesel engine fuelled with diesel and LNG (liquid natural gas)." Energy 53 (2013): 52-57.
[18]. Schmidt, Alexander P., et al. "Experiment-driven electrochemical modelling and systematic parameterization for a lithium-ion battery cell." Journal of Power Sources 195.15 (2010): 5071-5080.
[19]. Subramanian, Venkat R., et al. "Mathematical model reformulation for lithium-ion battery simulations: Galvanostatic boundary conditions." Journal of the Electrochemical Society 156.4 (2009): A260-A271.
[20]. Mu, Hao, and Rui Xiong. "Modelling, Evaluation, and State Estimation for Batteries." Modelling, Dynamics and Control of Electrified Vehicles. 2018. 1-38.
[21]. US Energy Information Administration, available at https://www.eia.gov/tools/faqs/faq.php?id=307&t=11
[22]. Turner, Louise K., and Frank G. Collins. "Carbon dioxide equivalent (CO 2-e) emissions: a comparison between geopolymer and OPC cement concrete." Construction and Building Materials 43 (2013): 125-130.
[23]. Pandey, Divya, Madhoolika Agrawal, and Jai Shanker Pandey. "Carbon footprint: current methods of estimation." Environmental monitoring and assessment 178.1 (2011): 135-160.
[24]. Myhre, Gunnar, et al. "Anthropogenic and natural radiative forcing." Climate change 423 (2013): 658-740.

Appendix L. Case Study for Skeena Queen - Optimal Design of Series Hybrid Marine Propulsion System with Li-ion Battery Performance Degradation and Life Cycle Cost Model

ABSTRACT

Ferries are essential transportation tools for the west coast residents of Canada, as well as for about 10% of people of the world's population, who live on islands. However, the ferry fleet with a large amount of marine diesel fuel consumption bears high fuel costs and produces heavy GHG emissions, including PM, NO_x, SO_2, CO_2 and HC, emitted from the old marine diesel engines. BC Ferries, one of the industrial partners of this project, has been providing transportation services for passengers and vehicles between various islands and the mainland in British Columbia since 1960. As the largest passenger ferry company in North America, BC Ferries owns 47 operation lines, which has consumed 115.4 million litres of marine diesel at a cost of CAD$103.3 million in fiscal 2016. To reduce fuel cost and GHG emissions, BC Ferries has been seeking new technologies for its future ships. This work focuses on the new propulsion system designs of Skeena Queen. The ship is one of the typical middle size ferries, running between Salt Spring Island and Vancouver Island, and it represents a category of vessels for clean-energy propulsion technology adoption.

This study focuses on the performance degradation of the battery energy storage system (ESS) of electrified ferries, using Skeena Queen as the testbed. Besides the traditional mechanical propulsion architecture, hybrid and pure electric propulsion systems were proposed and compared with the original design. Liquefied Natural Gas (LNG)-diesel dual-fuel engines and rechargeable Lithium-ion (Li-ion) batteries have been adopted in the new designs. The Li-ion battery ESS can provide extra energy to allow the engines to operate at their most efficient speed and torque to reduce emissions. However, depending upon the designed capacity and the use pattern of the battery ESS, the Li-ion batteries may reach their end of operation life quickly, causing frequent replacements and interruption of service. In this work, a semi-empirical battery life-prediction model under a different use pattern has been introduced to predict the life degradation of the battery ESS. The modelling considered the impacts of battery state of charge variation (ΔSOC) and discharge current rate (C-rate), which are determined by the operation pattern of the ferry, the size of the battery and the energy management system (BMS).

The new model made optimization of battery ESS size and BMS possible, as demonstrated in this case study.

L1. LI-ION BATTERY SEMI-EMPIRICAL LIFE DEGRADATION MODEL

Li-ion battery has been largely used in the transportation area in recent years. With the increment of its production, the cost has been dropped from about $1000 /kWh in 2010 to about $200/kWh in 2016 in vehicle application [2]. However, a more realistic problem of using Li-ion battery is the difficulties to evaluate its lifetime. It is normally considered a dead battery in the industry after

20% of original capacity losses. Moreover, it is hard to quantify the degradation process due to complicated electrochemical reactions.

L1.1. General Review of Li-ion Battery Life Degradation

Battery degradation is an inevitable phenomenon that happens right after the first charge/discharge process. A sharp capacity decay can be observed after the first few charging cycles due to the consumption of Li ions to build a Solid Electrolyte Layer (SEI) on the negative electrode [3]. After that, microscopic electrochemical reactions happen all the time and cause capacity fading, regardless of its use. Battery ageing rate can be affected by many factors, such as the charge and discharge C-rate, the state of charge (SOC), the change of SOC (ΔSOC) in usage, temperature, operating time and so on.

Bloom, et al. [4] presented the calendar life and power fade of Li-ion battery follow the Arrhenius kinetics model through accelerated lifetime study, which can be expressed as

$$P = Ae^{\left(-\frac{E_a}{RT}\right)}t^{0.5} \qquad \text{(L - 15)}$$

where P is power, t is time. A is a pre-exponential factor, E_a is the activation energy, R is the ideal gas constant, T is the temperature in K.

However, the power of the time drops to below ½ for cycle life fading when ΔSOC goes from 3% to 6%, which means the degradation has been accelerated when the SOC range increased [4]. Ashwin, et al. [5] showed that battery cyclic capacity fade has a direct link with the thickness of the SEI layer. Many factors are interlinked together to affect the performance and battery life, such as cycling C-rate, operating temperature, SOC range etc. Ramadass, et al. [6] showed the relationship of battery film resistance increment with the cycle number, as well as the negative electrode capacity fading with the cycle number. Broussely, et al. [7] thoroughly studied the ageing mechanisms and showed the importance of temperature for battery life prediction. Obviously, high temperatures will reduce calendar life.

The capacity losses (Q_{loss}) can be expressed as

$$Q_{loss} = f(C_{rate}, SOC, \Delta SOC, T, t) \qquad \text{(L - 16)}$$

where, ΔSOC is the change of SOC; T is temperature; t is time.

As for battery lifetime prediction, Omar, et al. [8] presented a cycle life model and considered the effects of temperature and depth of discharge (DOD). However, the discharge current rates were treated unchangeable in each case. Song, et al. [9] employed a semi-empirical life model based on the Arrhenius equation in the evaluation of life for a hybrid energy storage system. It showed the relationship of battery capacity losses with the C-rate and throughput capacity. However, the influence of ΔSOC was not considered in the experiments. Wang, et al. [10] listed a testing data for a LiPePO4 type battery under different temperature, DOD and C-rate. Most of the measurement data were not yet finished when they provide a generalized battery life model. Therefore, the model parameters might need to be adjusted for future use.

L1.2. Semi-empirical Battery Life Model

Battery cycle life prediction is a key research topic. The calendar life of the battery has been ignored, as it is negligible when compared to the cycle life of the battery in most cases [11-13]. It

also assumed battery temperature could be controlled and well maintained in a certain range by an advanced battery system design and liquid cooling technology. Therefore, the cycle lifetime (or cycling numbers) can be expressed as a function of two variables:

$$N = f(C_{rate}, \Delta SOC) \qquad \text{(L - 17)}$$

There are three main types of battery models reported in the literature. The empirical model provides a mathematical equation based on experiments [4]. However, it is hard to perform so many tests and difficult to validate its accuracy. The equivalent circuit model uses a DC voltage source with some resistor/capacitor elements to represent the physical battery [14]. It is more accurate and easy to implement. The electrochemical model has the highest accuracy regarding the calculations in describing the ions' movement between anode and cathode during the charge/discharge process. It is very popular these days to capture battery dynamic response based on the lithium ions' concentration variation by building a full-order mathematical model [15, 16]. However, the calculation is quite sophisticated and hard to implement.

Based on the literature, a new modelling method was proposed in this work. A second-order equivalent circuit model was used first to calculate battery voltage and SOC. The results was then used for lifetime estimation in the BMS. The lifetime was expressed as is a function of discharge C-rate and ΔSOC (as shown in Figure L - 1). The performance degradation model has been fitted and validated using 2,000 sets of battery test data.

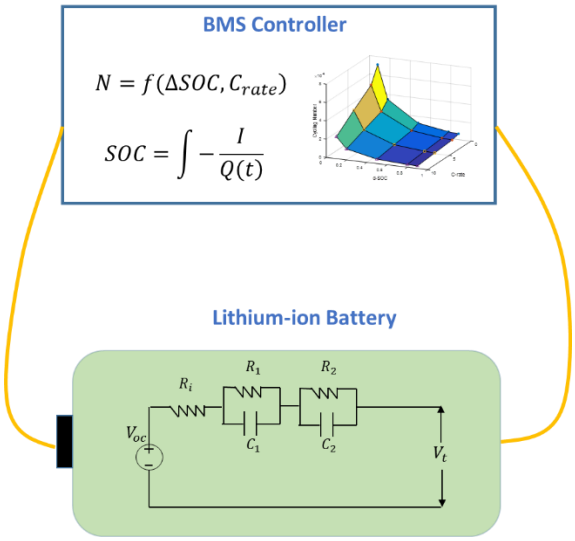

Figure L - 1 Demonstration of Semi-empirical Lifetime Prediction Model

The battery terminal voltage is determined by Kirchhoff laws:

$$V_t = V_{oc} - V_i - V_1 - V_2 \qquad \text{(L - 18)}$$

where V_i, V_1, V_2 are voltage drops caused by the resistor and two RC circuits.

$$\dot{V_1} = -\frac{V_1}{R_1 C_1} + \frac{I}{C_1} \qquad \text{(L - 19)}$$

$$\dot{V_2} = -\frac{V_2}{R_2 C_2} + \frac{I}{C_2} \qquad \text{(L - 20)}$$

Battery SOC is based on Coulomb counting which equals the integral over time of the ration between current and nominal capacity Q (assuming positive current is discharging).

$$\dot{SOC} = -\frac{I}{Q} \qquad \text{(L - 21)}$$

C-rate is then calculated as a comparison between requested current and nominal capacity:

$$C_{rate} = \frac{I}{Q} \qquad \text{(L - 22)}$$

ΔSOC is the maximum SOC variation in a cycle:

$$\Delta SOC = SOC_{max} - SOC_{min} \qquad \text{(L - 23)}$$

Battery lifetime is predicted based on the Arrhenius model [8-10], the battery capacity loss is a function of C-rate and ΔSOC:

$$Q_{loss} = Ae^{\left(\frac{-E_a + B \cdot C_{rate}}{RT}\right)} (A_h)^z \qquad \text{(L - 24)}$$

where, A is pre-determined coefficient; B is the coefficient of C-rate; A_h is the total throughput capacity which accounting for ΔSOC influences;

$$A_h = N \cdot \Delta SOC \cdot Q \qquad \text{(L - 25)}$$

N is the total cycling numbers when capacity. In this paper, it is considered a dead battery when $Q_{loss} = 20\%$ of original capacity. Therefore, the calculation of the cycling number can be derived based on the previous function:

$$N = \frac{\left(\frac{Q_{loss}}{Ae^{\left(\frac{-E_a + B \cdot C_{rate}}{RT}\right)}}\right)^{\frac{1}{z}}}{Q \cdot \Delta SOC} \qquad \text{(L - 26)}$$

For $LiFePO_4$ battery, some measurement data can be obtained from the literature [10, 17], By using the least square method, coefficients in the cycle number equation can be determined. Measurement data of a 20Ah commercial LiFePO4 battery capacity decay has been provided by the manufacturer in Figure L - 2 that was used for parameter calibration.

This model was implemented in MATLAB/Simulink. The resulting cycling number for this 20Ah capacity $LiFePO_4$ as a function of C-rate and ΔSOC was plotted in Figure L - 3.

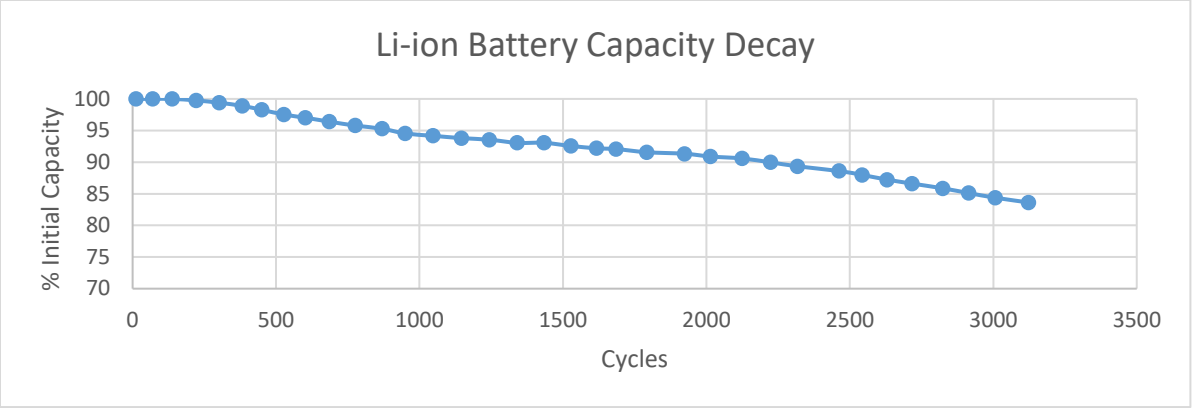

Figure L - 2 Li-ion Battery Capacity Decay (Test @100% Depth of Discharge (DOD), +1C/-2C, 23°C) [18]

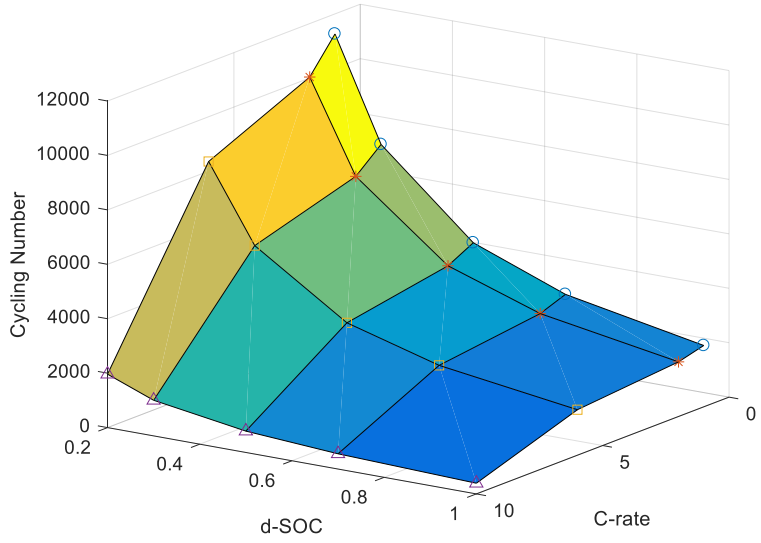

Figure L - 3 Cycling Number Variation with C-rate and ΔSOC

L2. Optimal Design of Series Hybrid Marine Propulsion System

L2.1. Case Introduction

As part of the collaboration project between BC Ferries and the University of Victoria, Skeena Queen has been chosen for a study case to analyze fuel consumption and emissions with new propulsion systems. Some general information of Skeena Queen can be found in Figure L - 4.

Skeena Queen	
Overall Length:	110 metres
Maximum Displacement:	2,942 tonnes
Car Capacity:	92
Passenger & Crew Capacity:	450
Maximum Speed:	17.3 knots
Horsepower:	6,000
Route:	Fulford Harbour-Swartz Bay
Corssing Time:	35 mins
Distance:	5 nautical miles

Figure L - 4 General Information about Skeena Queen

With a total maximum of 6,000 *hp* propulsion power from four marine diesel engines, the ferry has the capacity for carrying 92 vehicles and 450 passengers, and its voyage is about 35 minutes or 2,100 seconds. The data acquisition system recorded 11 trips (or 5.5 crossings) of the ferry during a working day. The speed of the ferry has been measured and recorded as shown in Figure L - 5. The recorder propulsion power at engine shafts is shown in Figure L - 6.

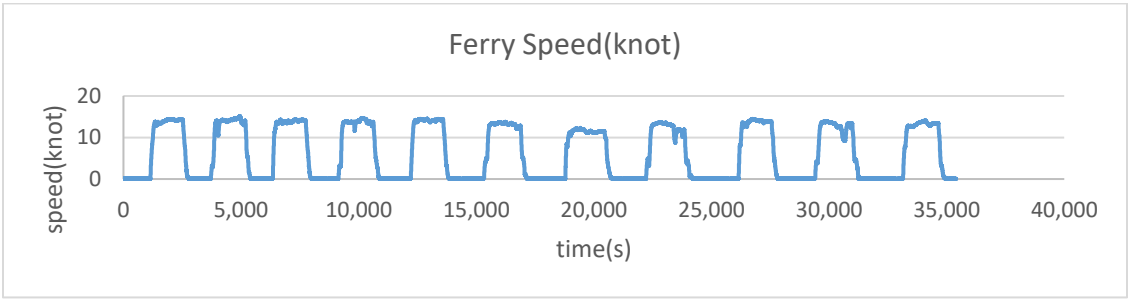

Figure L - 5 Ferry Speed Measurement

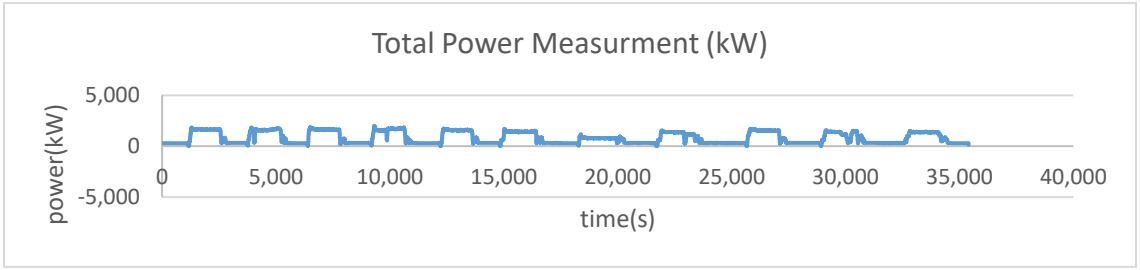

Figure L - 6 Total Power Measurement from Engine Shaft

The original propulsion system in Skeena Queen has a conventional mechanical propulsion system. Four diesel engines were paired with four thrusters. In between, there are gearboxes connecting to the four Z-drive azimuth thrusters. To carry out fuel consumption analysis, the fuel efficiency and emissions maps of the marine diesel and a dual-fuel diesel/NG engines (with a maximum power of 1,132 *kW*) were obtained by scaling up the fuel efficiency and emissions maps

of a smaller diesel engine. The brake specific fuel consumption map and emissions map of this 205 *kW* maximum power rated diesel engine are available from powertrain modelling tool, ADVISOR, developed by the US National Renewable Energy Laboratory [19]. This scaling method is commonly used powertrain system modelling. In our recent study, the scaling error was found to be acceptable at around 5 percent.

In comparison, pure electric propulsion and hybrid electric propulsion were proposed for fuel saving and emission reduction. These powertrain architectures are able to use clean energy sources and cleaner drive technologies to reduce emissions and to allow a versatile powertrain system design with multiple power supplies. The fast advancing power electronics technology also enables a more flexible propulsion architecture for marine system design.

The pure electric propulsion architecture adopted large Li-ion battery ESS to satisfy the power requirement during operation. The ESS package is designed by using single battery cells in series and parallel to reach the high power and energy density.

Hybrid propulsion architecture can combine a large battery ESS and an electric motor to the mechanical system to achieve higher efficiency. The advantages of hybrid propulsion include high operating flexibility as well as being more environment friendly. Depending on the structure, series, parallel or series-parallel combined system are all available. In this paper, a series hybrid system was adopted for the ferry Skeena Queen.

A series hybrid electric ship (HES) transforms the power from an internal combustion engine (ICE) into electrical energy through a generator (Figure L - 7). ESS works as a buffer to store the energy and supply power to an electric motor, driving the propeller. The motors are driven by electric energy from the ESS, the generator or both. By de-coupling the mechanical connection, engine design becomes more flexible. If the ESS is sufficiently large, the powertrain can work in a pure electric mode without running the engine. The hybrid propulsion system allows the engine to work more efficiently with ideal speed and torque outputs and eliminates engine idle time. The hybrid electric powertrain can also respond quickly to overcome the slower response of an NG engine, as well as adding to the peak power using the stored electric energy.

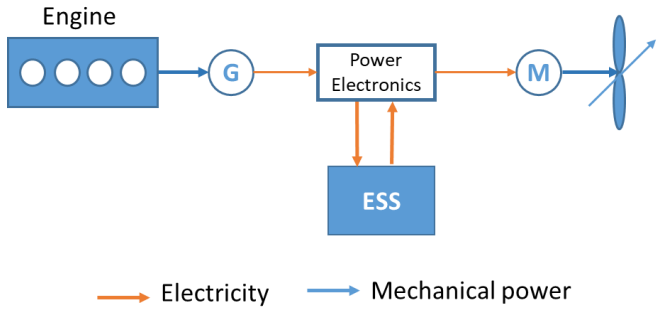

Figure L - 7 Series Hybrid Propulsion System

The plug-in series hybrid electric ship (PHES) is similar to HES but equipped with a much larger ESS that is also charged using grid power. PHES requires charge facilities from the power grid to charge the ship at berth. The dedicated charging infrastructure may cost more than the PHES itself, but PHES overcomes the range limitation of a pure electric ship and uses lower-cost electric energy that may be derived from renewable energy sources. Pure electric powertrain better suits lighter ships with relatively short range, due to the higher battery cost and limited range at present.

In total, this paper will compare three different architectures: pure mechanical, pure electrical and hybrid architecture (Table L - 1). With the multiple selections from diesel engines, natural gas (NG) engine and Li-ion battery ESS, this paper provided versatile solutions for the ferry in terms of fuel-saving and emission control.

Table L - 1 Different Propulsion Systems for Ferry Study

Architecture	Case	Power Source(s)
Pure Mechanical	1	Diesel engine
	2	Natural gas engine
HES	3	Diesel engine + ESS
	4	Natural gas engine + ESS
PHES	5	Diesel engine + ESS + Grid Power
	6	Natural gas engine + ESS + Grid Power
Pure Electrical	7	ESS + Grid Power

The main difficulty of HES and PHES system design is the sizing of engine and ESS. Engine power and battery capacity must be carefully optimized.

L2.2. Optimal Design of a Series Hybrid System

The size of battery ESS is very important in a hybrid propulsion system. It will not only affect the total system cost but also influence system performance. From pure mechanical to a pure electric system, the capacity of ESS increases gradually, between them, a hybrid architecture can choose a different capacity of ESS in cooperating with engines (Figure L - 8).

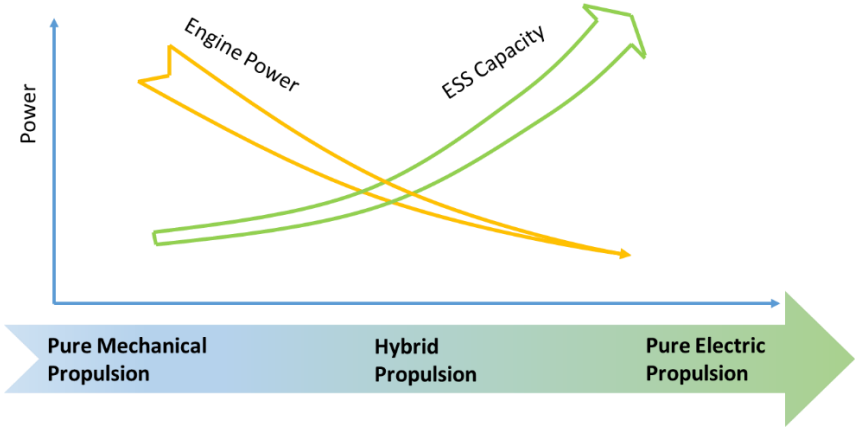

Figure L - 8 Variation of ESS Capacity in Different Architecture

The design optimization of the hybrid electric powertrain involves the selection of major powertrain components, such as the engine, motor/generator and ESS, and the development of powertrain controls. To minimize the fuel consumption and operation costs optimal control is needed to coordinate the operations of all powertrain components. The Skeena Queen normally

operates at calm ocean conditions with constant crossing speed, requiring almost constant power during the voyage. A straightforward rule-based control algorithm is then used, rather than more complex optimal control methods for dynamically changing power demands.

The main control idea is to use battery power when the ferry is in berth to reduce emission by shutting down idled engines while letting engines work at its most efficient point during travelling. The battery can be charged when engine is working. However, battery SOC should be maintained in certain range between the beginning and end of the trip.

Based on previous discussion, it has design variables as:

$$x = [x1, x2]' \tag{L - 27}$$

where, x1 is ESS energy in kWh, and x2 is the optimal engine operating power in kW.

The objective of this optimization problem is to maintain battery SOC in a certain range during ferry operation, minimize engine fuel consumption, and extend battery life. The objective function can be expressed as:

$$\begin{gathered} \min_x f = w1 \times f1 + w2 \times f2 + w3 \times f3 \\ f1 = |SOC_0 - SOC_{end}| \\ f2 = C_{fuel} \\ f3 = L_{ess} \\ \text{subject to: } E_{min} \le x1 \le E_{max} \\ P_{min} \le x2 \le P_{max} \end{gathered} \tag{L - 28}$$

where $w1, w2, w3$ are weighted factors; f1 is the cost function of SOC variation at the beginning and end of a one-day operation; f2 is the cost function of total fuel consumption; f3 is the cost function of battery life with each designed ESS energy; E_{min}, E_{max} are minimum and maximum values for the designed ESS energy; and P_{min}, P_{max} are minimum and maximum values for the engine power;

For HES, the initial SOC of ESS should be the same after a one-day operation, i.e. the end of SOC in the trip equals the initial SOC at the beginning. Meanwhile, the SOC variation in each voyage was constrained within certain range for the consideration of prolonging its lifetime.

As for PHES, the main idea is to take advantage of low price electricity from the power grid to charge the battery during the night. Therefore the initial SOC is always 1 and at the end of the day, it should reach its constrained low SOC to maximize electricity usage. The size of ESS energy may vary largely for the total cost of the whole system. But the main idea of the optimal design of PHES is similar to the previous HES.

With the increment of total ESS energy, battery SOC varied dramatically among different cases during the ferry's operation (Figure L - 9). Under the same driving profile, battery SOC variation or ΔSOC is greater in small ESS, so does the charging/discharging C-rate. Higher current flow and

larger SOC variation result in a shorter life. The variation of SOC, as well as the discharge current rate, would both affect battery cycling numbers.

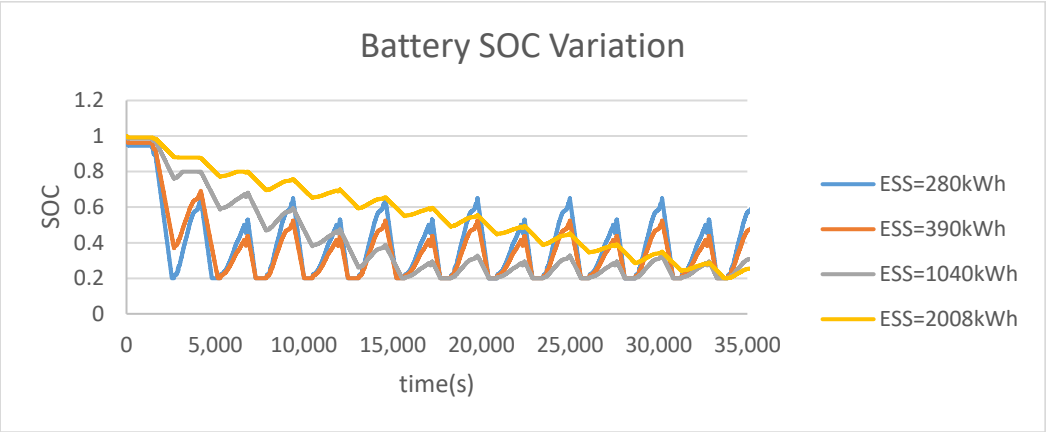

Figure L - 9 Battery SOC Variation under Different ESS Energy

Based on the semi-empirical battery lifetime estimation model introduced in the previous section, ESS cycling numbers can be calculated for each different design cases. Battery life estimation can be evaluated from the model.

Genetic Algorithm (GA) has been used to solve this constrained optimization problem. It selects the best result among the current population at each step and generates the next population through crossover and mutation to approach the optimal solution. After a certain amount of generations, it can converge to the best result. The simulation model was built in MATLAB/Simulink. The GA searching results for HES were presented in Figure L - 10. The highest, middle and lowest objective function value at each generation was shown as the upper, average and lower value in the figure.

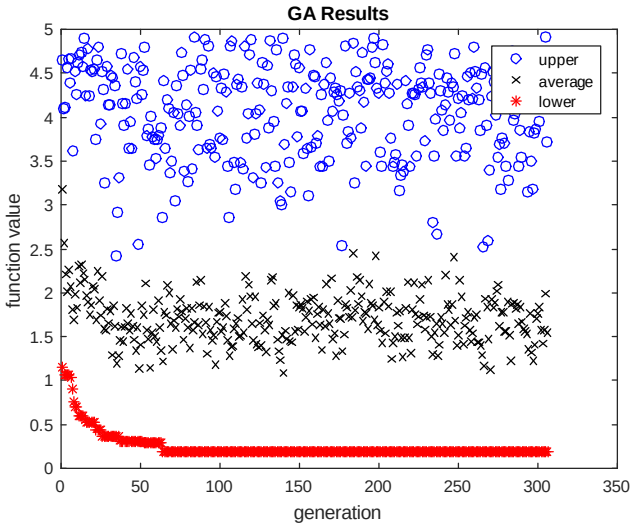

Figure L - 10 GA Searching Results for the Design Optimization of HES

The best result found for HES is x1=600 and x2=1600, which indicates a combination of 1600kW engine power with 600kWh Li-ion battery ESS. The best result for PHES is 940 *kWh* ESS and 1,350 *kWh* engine. The increased ESS energy can support a small engine for power peak shaving

in the PHES. The battery lifetime in HES and PHES is about 7.18 years and 8.53 years, respectively.

L3. RESULTS DISCUSSION AND COMPARISON

The fuel consumption of different powertrain system configurations listed in Table L - 1 were evaluated. Following the powertrain system component model scaling method used in ADVISOR, the fuel efficiency and emissions maps of the diesel and NG engines used for the Skeena Queen at the rated power of 1,132 *kW* have been obtained. In original mechanical propulsion, four engines are needed due to the ferry's original configuration, and fuel consumption was calculated as the baseline of comparison. For HES and PHES propulsions, the sizes of the engine and ESS were based on the optimization results acquired from the global optimization discussed in the previous section. The optimized engine power was assumed from one single large engine. ESS in PHES and pure electrical propulsion requires a charging facility to charge the battery with electricity from the power grid. The total fuel consumption for each different case is shown in Figure L - 11.

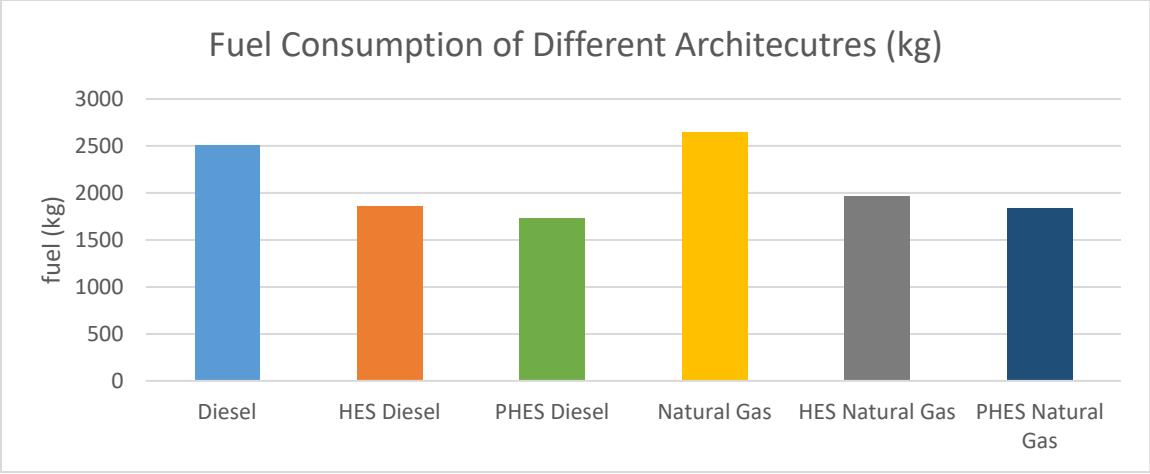

Figure L - 11 Fuel Consumption of Different Architectures

It is clear to see that by using hybrid technology, the HES fuel consumption can save about 25.68% compared to the pure mechanical configuration, while the PHES can save 30.75%. The advantage of PHES is not so obvious compare to the HES. With the requirement of almost doubled ESS capacity as well as charging facilities, PHES only has about 5% increment compared to HES. The reason may lie in the special operation mode of the ferry. In hybrid propulsion, the engine always runs at its maximum operating point during transportation and shut down when it is in the berth. Therefore the fuel-saving for PHES with a small engine may not acquire too many advantages. In addition, PHES requires a larger ESS than HES, which may drive to the conclusion that HES is more suitable for this case of the Skeena Queen.

The natural gas engine consumes about 5.61% more fuels than a diesel engine, as shown in Figure L - 11. It is normal to see this conclusion because of the lower specific power natural gas can provide compared to diesel. However, the fuel cost of natural gas is only about a quarter of marine diesel in BC, which gives a great potential for fuel cost saving by using an NG engine [20]. The fuel consumption improvement for the natural gas engine in HES and PHES is similar to the diesel engine.

Emissions such as NOx, HC and CO were calculated using an engine emission map. CO_2 emission has a direct correlation with the consumed fuel. Based on the US DOE guidelines for the voluntary reporting of GHG emissions, the CO_2 emission coefficients of different types of fossil fuel were adopted here[21]. As for the electricity used in this case, CO_2 releasing has been considered in the process of electricity generation for the pure electric architecture. BC Canada has 92% hydropower according to the report from BC Hydro [22]. The CO_2 emissions in this situation is about 11 tonne per *GWh*.

To compare the environmental impacts with different types of GHG emissions, the global warming potential (GWP) was adopted in this work. Developed by the International Panel on Climate Change (IPCC), GWP gives a relative measurement of the amount of heat trapped by a certain type of gas in the way of equivalent CO_2 (CO_{2e}) over a specified time horizon [23], presenting an easy way to measure the total carbon footprints. The U.S. Environmental Protection Agency (EPA) provided a calculation method to acquire greenhouse gas equivalencies expressed in CO_{2e} [24]. The CO_{2e} under five different scenarios was calculated and compared in Figure L - 12.

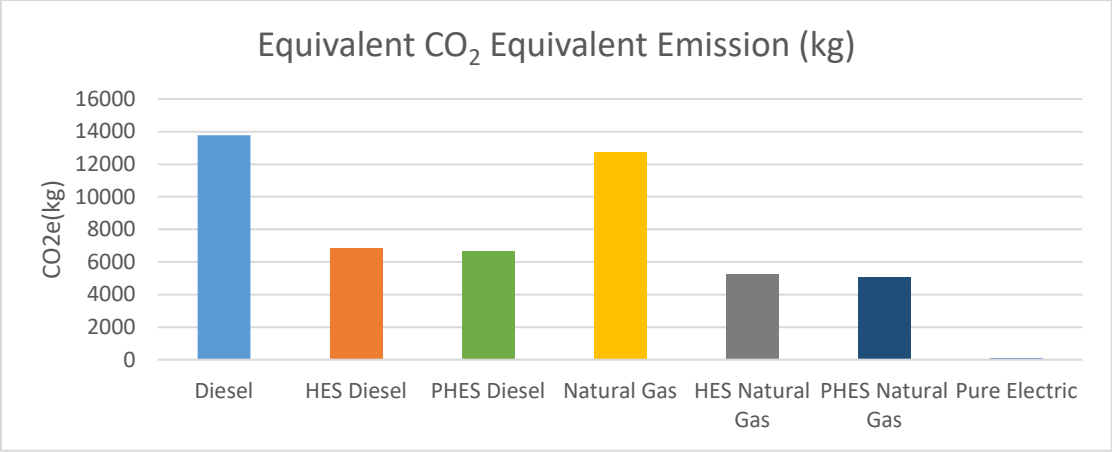

Figure L - 12 CO_{2e} Comparison for Different Cases

Pure electric propulsion presents as the most environment-friendly solution, as its CO_{2e} can be ignored comparing to others. Among the other scenarios, an NG engine produces lower CO_{2e} comparing to a diesel engine with the same powertrain architecture.

L4. CONCLUSION

The possibility of using a hybrid electric and electric propulsion system for Skeena Queen has been studied in this work. The sizes of engine and battery ESS were optimized using global optimization method. A semi-empirical battery model was used and the lifetime evaluation of Li-ion battery was performed under the effects of discharge C-rate and SOC variation. Among different possible propulsion solutions, the series hybrid electric propulsion system with advanced NG engine and Li-ion battery ESS was considered as the best design solution based on the comparisons of fuel costs and emissions from several alternative powertrain systems. The hybridization of the powertrain led to considerably improved energy efficiency, smaller engine and short engine operation time. The NG fuel presents a low cost and cleaner fuel option. The relatively simple series hybrid powertrain system also allows a diesel-electric propulsion system to be upgraded by adding an electric ESS and advanced powertrain system controls.

Future work will be focused on improving the accuracy of battery life evaluation by using the electrochemical model instead of the equivalent circuit model. The microscopic influences of the Li-ion movement under different discharge current certainly will affect the response voltage and lifetime evaluation. It will be examined and reflected in the controlling system to have better energy management for a hybrid powertrain system.

ACKNOWLEDGEMENT

The authors would like to thank Michael Grant, Haijia Alex Zhu and Xiaofei Wen for the collection of ship operation data, Anthony Truelove for the discussions and comments from a marine engineering perspective, and the extensive support from Bruce Paterson, William Russell, Bob Kearney and François Cambron at BC Ferries. Financial supports and guidance from the Clean Transportation Initiative of Transport Canada are gratefully acknowledged.

REFERENCES

[1] B. C. F. S. Inc., "British Columbia Ferry Services Inc. Fuel Strategies-Update Report," http://www.bcferries.com/files/AboutBCF/2016_06_24_FY16_Fuel_Strategies_Update_Report.pdf2016.

[2] P. A. Nelson, K. G. Gallagher, I. D. Bloom, and D. W. Dees, "Modelling the performance and cost of lithium-ion batteries for electric-drive vehicles," Argonne National Laboratory (ANL)2012.

[3] P. Arora, R. E. White, and M. Doyle, "Capacity fade mechanisms and side reactions in lithium ‐ ion batteries," *Journal of the Electrochemical Society,* vol. 145, pp. 3647-3667, 1998.

[4] I. Bloom, B. Cole, J. Sohn, S. Jones, E. Polzin, V. Battaglia, *et al.*, "An accelerated calendar and cycle life study of Li-ion cells," *Journal of Power Sources,* vol. 101, pp. 238-247, 2001.

[5] T. Ashwin, Y. M. Chung, and J. Wang, "Capacity fade modelling of lithium-ion battery under cyclic loading conditions," *Journal of Power Sources,* vol. 328, pp. 586-598, 2016.

[6] P. Ramadass, B. Haran, R. White, and B. N. Popov, "Mathematical modelling of the capacity fade of Li-ion cells," *Journal of Power Sources,* vol. 123, pp. 230-240, 2003.

[7] M. Broussely, S. Herreyre, P. Biensan, P. Kasztejna, K. Nechev, and R. Staniewicz, "Ageing mechanism in Li ion cells and calendar life predictions," *Journal of Power Sources,* vol. 97, pp. 13-21, 2001.

[8] N. Omar, M. A. Monem, Y. Firouz, J. Salminen, J. Smekens, O. Hegazy, *et al.*, "Lithium iron phosphate based battery–assessment of the ageing parameters and development of cycle life model," *Applied Energy,* vol. 113, pp. 1575-1585, 2014.

[9] Z. Song, J. Li, X. Han, L. Xu, L. Lu, M. Ouyang, *et al.*, "Multi-objective optimization of a semi-active battery/supercapacitor energy storage system for electric vehicles," *Applied Energy,* vol. 135, pp. 212-224, 2014.

[10] J. Wang, P. Liu, J. Hicks-Garner, E. Sherman, S. Soukiazian, M. Verbrugge, *et al.*, "Cycle-life model for graphite-LiFePO 4 cells," *Journal of Power Sources,* vol. 196, pp. 3942-3948, 2011.

[11] L. Gao, S. Liu, and R. Dougal, "Dynamic lithium-ion battery model for system simulation," *Components and Packageing Technologies, IEEE Transactions on,* vol. 25, pp. 495-505, 2002.

[12] P. Liu, J. Wang, J. Hicks-Garner, E. Sherman, S. Soukiazian, M. Verbrugge, *et al.*, "Ageing mechanisms of LiFePO4 batteries deduced by electrochemical and structural analyses," *Journal of the Electrochemical Society,* vol. 157, pp. A499-A507, 2010.

[13] S. Bourlot, P. Blanchard, and S. Robert, "Investigation of ageing mechanisms of high power Li-ion cells used for hybrid electric vehicles," *Journal of Power Sources,* vol. 196, pp. 6841-6846, 2011.

[14] B. Y. Liaw, G. Nagasubramanian, R. G. Jungst, and D. H. Doughty, "Modelling of lithium ion cells—A simple equivalent-circuit model approach," *Solid state ionics,* vol. 175, pp. 835-839, 2004.

[15] M. Doyle and Y. Fuentes, "Computer simulations of a lithium-ion polymer battery and implications for higher capacity next-generation battery designs," *Journal of the Electrochemical Society,* vol. 150, pp. A706-A713, 2003.

[16] M. Doyle, T. F. Fuller, and J. Newman, "The importance of the lithium ion transference number in lithium/polymer cells," *Electrochimica Acta,* vol. 39, pp. 2073-2081, 1994.

[17] J. Shen, S. Dusmez, and A. Khaligh, "Optimization of sizing and battery cycle life in battery/ultracapacitor hybrid energy storage systems for electric vehicle applications," *IEEE Transactions on industrial informatics,* vol. 10, pp. 2112-2121, 2014.

[18] http://liionbms.com/pdf/a123/AMP20M1HD-A.pdf.

[19] K. B. Wipke and M. R. Cuddy, "Using an advanced vehicle simulator (ADVISOR) to guide hybrid vehicle propulsion system development," National Renewable Energy Lab., Golden, CO (United States)1996.

[20] FortisBC. *Natural Gas Rates 2006-2018*. Available: www.fortisbc.com

[21] E. I. A. E. U.S. Department of Energy (DOE), "Voluntary Reporting of Greenhouse Gases Program," 2014.

[22] www.bchydro.com.

[23] T. F. Stocker, D. Qin, G.-K. Plattner, etc, "Technical Summary. In: Climate Change 2013: The Physical Science Basis. ," 2013.

[24] https://www.epa.gov/energy/greenhouse-gas-equivalencies-calculator.

Appendix M. Case Study for Skeena Queen - Design of Parallel Hybrid Marine Propulsion System

ABSTRACT

Ferries are essential transportation tools for the west coast residents of Canada, as well as for about 10 percent of the world's population. However, the ferry fleets with a large amount of marine diesel fuel consumption bear high fuel costs and produce heavy GHG emissions, including PM, NO_x, SO_X, CO_2 and HC, emitted from old marine diesel engines. BC Ferries, one of the industrial partners of this project, has been providing transportation services for passengers and vehicles between various islands and the mainland in British Columbia since 1960. As the largest passenger ferry company in North America, the company owns 47 operation lines, which has consumed 115.4 million litres of marine diesel at a cost of CAD$103.3 million in fiscal 2016. To reduce fuel cost and GHG emissions, BC Ferries has been seeking new technologies for its future ships. This work focuses on the new propulsion system designs of Skeena Queen - one of the typical middle size ferries, running between Salt Spring Island and Vancouver Island. This is a category of vessels considered for clean-energy propulsion adoption by the BC Ferries.

Due to the similarity in powertrain structure, conversion from a traditional diesel-electric powertrain system to a series hybrid electric powertrain is more straightforward. The retrofitting cost is lower and the needed control development is less extensive. However, many passenger and car ferries, such as Skeena Queen, travel on calm water with relatively steady power loads, except the short docking operations at berths. The operation resembles more as vehicles travelling on highways, rather than stop and go vehicles driving in city centers. The advantage of a series hybrid electric powertrain to use the electric drive to handle dynamics loads while keeping the engine operate at a constant speed and torque outputs are thus less useful. In addition, the constant energy conversions from mechanical to electrical to mechanical and to/from battery ESS, from the engine to generator/battery, from the generator/battery to electric motor, and from the electric motor to propeller shaft present unavoidable and unnecessary energy and efficiency loss. This study adds to the research outlined previously in Appendixes K and L, to focuses on the adoption of a parallel hybrid electric powertrain system and the resulting benefits.

The advance of marine propulsion systems went from diesel-mechanical drive to diesel-hydraulic drive, and to diesel-electric drive with electric propulsion. Natural development is to add a battery-electric ESS and powertrain system control to make it a hybrid electric system with a series architecture. This series hybrid electric powertrain system will allow the diesel (or gasoline or NG) generator to operate at its ideal speed and torque zone with top efficiency, regardless of the speed change of the ship, thus increasing the energy efficiency and reducing emissions. As proved in-ground vehicle applications, this series hybrid electric powertrain architecture is superior for heavy-traffic city driving with constant decelerations and accelerations. For vehicles driving on highways at static speed, the inherent mechanical to electrical and electric to mechanical energy conversion loss of the series hybrid electric powertrain is recognized to be less energy efficient than the parallel hybrid electric powertrain in which mechanical power from the engine can directly flow to the propulsion wheels. Recognition on this fact led to the wide adoption of parallel and

series/parallel powertrain designs for modern hybrid electric vehicles today. The acquired operation and propulsion power patterns of the ferry ships have confirmed that a large portion of the ferry's power demand and travelling speed remain constant during the crossing. It is thus worthwhile to examine the feasibility and benefits of a parallel hybrid electric propulsion system, although the design, retrofitting, and control of the parallel hybrid powertrain system is more complex. These considerations form the motivation of the study reported in this document.

Specifically, two cases are used to illustrate the concept of parallel hybrid electric ship modelling and improvement compared to a mechanically propelled ship: NG parallel hybrid and diesel parallel hybrid propulsion systems. A mechanically propelled ship is also modelled and simulated based on Skeen Queen's powertrain configuration to serve as the baseline for this study.

M1. INTRODUCTION

The powertrain architecture of Skeen Queen (as shown in Figure M - 1) is composed of four diesel engines and three diesel generators at present. The detailed ship configuration and information are documented in Appendix A - All Studied Marine Vessels, thus are not further discussed in this section. Details on the parallel hybrid electric powertrain system modelling, model implementation, as well as the control problem and its solutions are discussed.

Figure M - 1 Skeena Queen

M1.1. Parallel Hybrid

The thrusters are driven through gearboxes and Z-drives. All the propulsion power is produced by diesel engines. The diesel generator is used to provide the electric load in real-time. Obviously, there is a direct link between the power used at the thrusters and the power produced by engines. The hybrid electric ship, on the other hand, contains more power sources in the system. The thruster may be propelled by the electric machine, engine or the combination of both. The electric machine may operate as a generator or an electric motor.

In this study, mechanical and electric parallel propulsion is realized by coupling the engine and the electric machines (or electric motor/generator) through a speed reduction gearbox. The combined power is then passed to the thruster to propel the vessel. An engine on-off system is

added so that the engine can be completely turned off in the pure electric propulsion mode. The architecture of the parallel hybrid electric ship is shown below. In the Skeen Queen, four identical shaft lines with parallel engine-motor connections, as shown in Figure M - 2, are used.

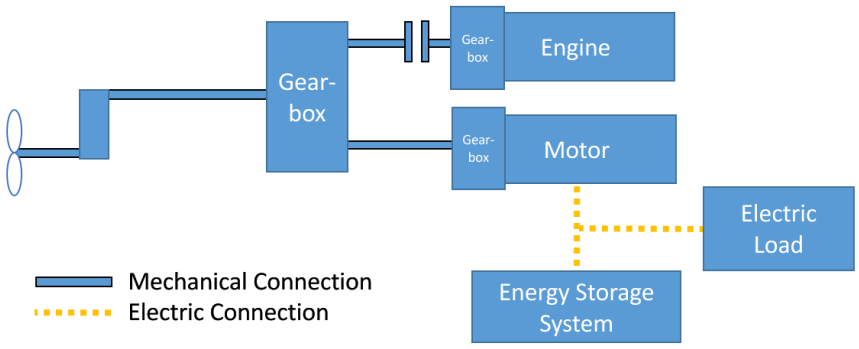

Figure M - 2 Simplified diagram of a parallel configuration

M1.2. Powertrain Model

The parallel hybrid electric powertrain can have either a co-shaft or a parallel-shaft arrangement for the engine and motor/generator. In this work, a more flexible parallel shaft configuration that allows the use of different speed reduction gearboxes and engine clutch, as shown in Figure M - 2, have been studied.

The energy flow of the parallel hybrid powertrain is presented in Figure M - 3. The engine and the electric machine are connected in parallel through a gearbox so that the output power is combined. A clutch is used to disconnect the engine from the driveline in the ship's pure electric and engine-off mode, reducing emissions and improving fuel efficiency. The motor can operate as a peak shaving device to provide extra propulsion power when needed so that the engines can operate at the preferred speed and torque zone with peak energy efficiency, rather than being pushed for higher speed and torque outputs with lower efficiency and more emissions. A set of speed reduction gearboxes are added to allow the engine and electric motor to operate at their different preferred or maximum speeds independently. The electric machine is connected to the energy storage system (ESS) through a bi-directional DC/DC converter. The ESS acts as a buffer. The electric power for the electric load can be provided by a generator, ESS or a combination of both.

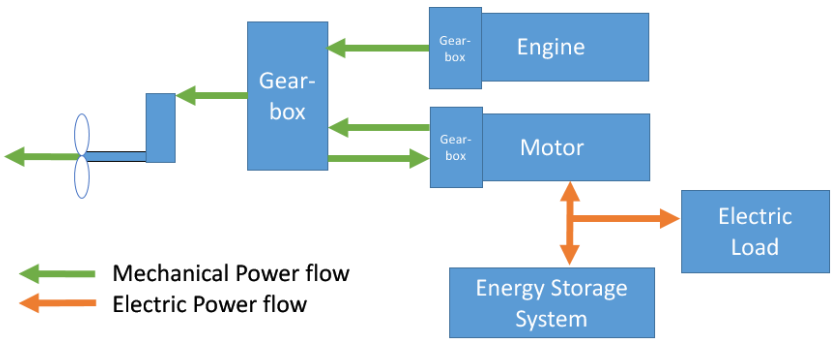

Figure M - 3 Power flow in a hybrid electric ship

Four different configurations are discussed in this report. The main parameters are presented in Table M - 1. NG and diesel represent the conventional mechanically propelled ship while hybrid NG and hybrid diesel represent the parallel hybrid ship. The total power that the hybrid system can provide is 5136kW and is close to a conventional mechanical propulsion system. It should be noted that the generator is included in this comparison. The emergency generator is added to provide redundancy but is not used in this study. The main parameter is given in Table 1.

The engine and electric machine are modelled using lookup tables. A set of data in terms of speed, torque and corresponded BSFC/motor efficiency at each operation point are shown in Figure M - 4 and Figure M - 5, respectively. The electric machine has a continuous power of 338.26 kW, and its model is scaled up from a 75kW induction motor. The rated power for the NG and diesel engines has been scaled up to 1119kW. The engine emission is also modelled using the same method.

Table M - 1 Main parameter

	Diesel	NG	Hybrid Diesel	Hybrid NG
Engine	1119kW*4	1119kW*4	1119kW*4	1119kW*4
Engine Gearbox	NA	NA	1.2	1.2
Electric Machine	NA	NA	338.26kW*4	338.26kuW*4
ESS	NA	NA	266.4kWh	266.4kWh
Gearbox Ratio	1.226	1.226	1.226	1.226
Generator	330kW*2	330kW*2	330kW*2	330kW*2
Emergency Generator	209kW*1	209kW*1	209kW*1	209kW*1

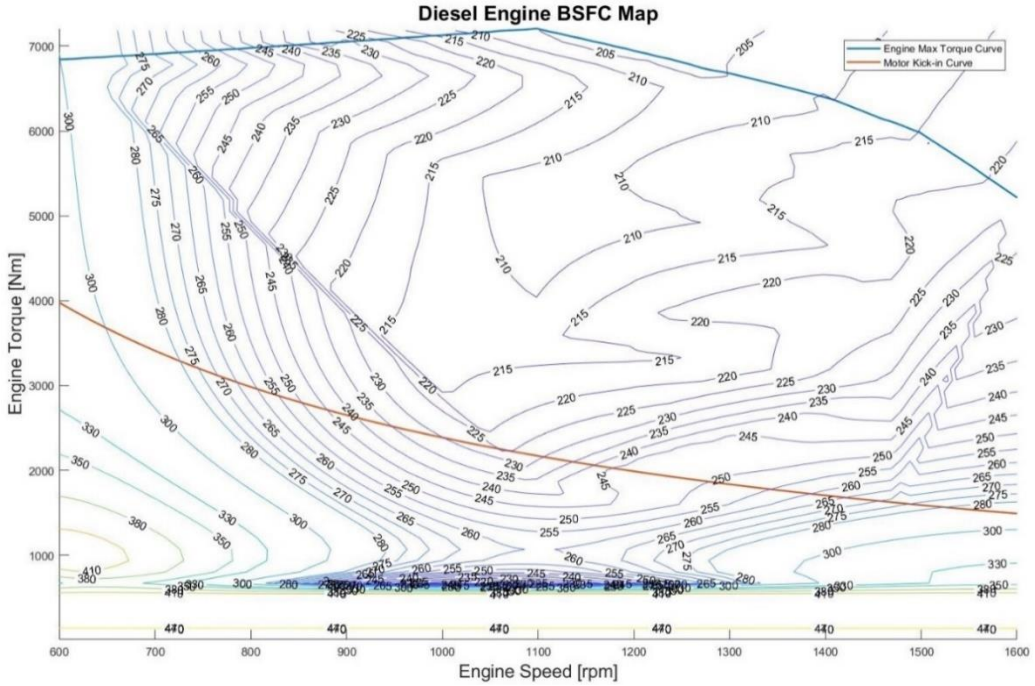

Figure M - 4 Diesel engine BSFC map

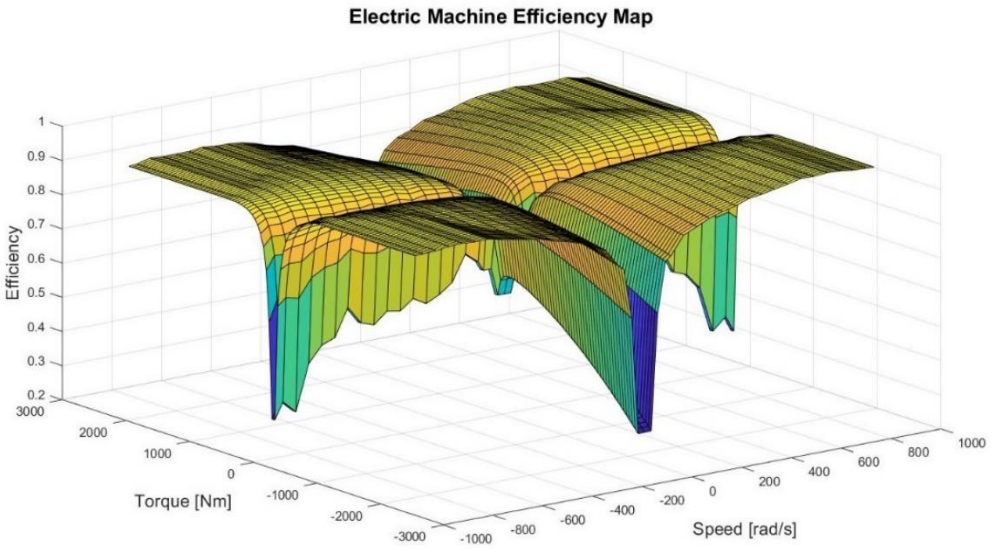

Figure M - 5 Motor efficiency map

The engine power P_{eng} on the hybrid system can be represented:

$$P_{eng} = P_{propel} + P_{electric} + P_{EM} \qquad \text{(M - 1)}$$

where P_{propel} represents the propulsion power, P_{elec} represents the electric load on the ship and P_{EM} represents the power provided by or taken from the electric machine. In a hybrid electric propulsion system, a portion of the power produced from the engine will be used to charge the ESS or to serve the electric load, keeping the engine operating at its highly efficient speed and torque output. In the original diesel-electric powertrain system, the power output from the engine is between 430 and 800 *kW*, and the engine mainly operates at low speed, since the engine power is directly linked to the needed propulsion power at each instance of time. To allow the engine to operate at more fuel-efficient speed and torque, a speed reduction gearbox is added.

The ESS is modelled using the PNGV model. The cell parameters are provided by A123 during the UVic EcoCAR2 development. The main battery ESS parameters include:

Table M - 2 ESS parameters

ESS Nominal Voltage (V)	297
ESS Capacity (kWh)	266.4
Battery Cells (A123 3p15s Li-ion Module)	4860 (6 in series and 18 in parallel)
Maximum Power (Charge and discharge)	2,718 kW peak and 918 kW continuous

Different from the traditional marine propulsion system, the power flow in a hybrid system is more flexible. The ship can operate in different modes and thus the energy flow will need to be managed. A rule-based energy distribution rule is developed in this study. The control rules can be summarized as below and in Figure M - 4:

- When power demand is lower than the red line (engine kick-in curve), then use pure electric drive unless the SOC is low.
- When power demand is higher than the blue line (engine max torque curve), then the electric motor will kick in to provide extra power unless the SOC is low.
- When power demand is in the middle,
  - If the SOC is low, force the engine to be the only power source and the electric machines are forced to operate as generators.
  - If the SOC is high, the electric machine will provide extra power to propel the ship and the ESS will be used to support service load.
  - If the SOC is in the middle, the electric machine will operate as a generator.
    - When torque demand is lower than the orange line in Figure M - 4, then use the pure electric drive and turn off the engine.
    - When torque demand is higher than the blue line (engine maximum torque curve), then the electric motor will kick in to provide extra power.
    - When torque demand is in the middle, force the engine to operate at its efficiency zone and use the electric machine to assist or absorb extra power.

With this rule-based controller, the ship will automatically choose the mode to operate and maintain the SOC at a predetermined range.

The vessel's power demand cycle is obtained by measuring the consumed propulsion power on propeller shafts. A wireless strain gauge Data Acquisition (DA) system was installed on the Skeena Queen. An example of measured torque on the Z drive and the shaft speed during a ferry trip is shown in Figure M - 6. An eleven trip (5.5 crossings) cycle was used in this study. The vessel's hotel electric load is considered as a constant. During the summer, the load is at 110 *kW*. The diesel generators provide electric power on Skeena Queen at present.

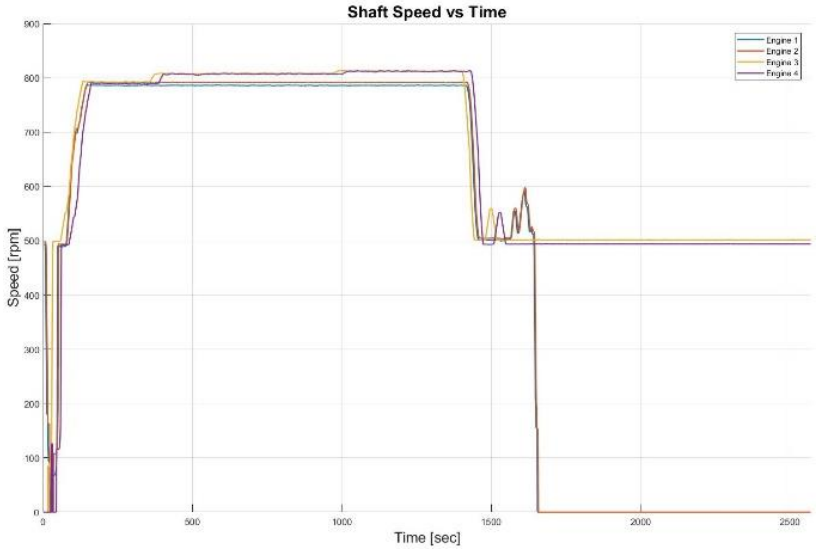

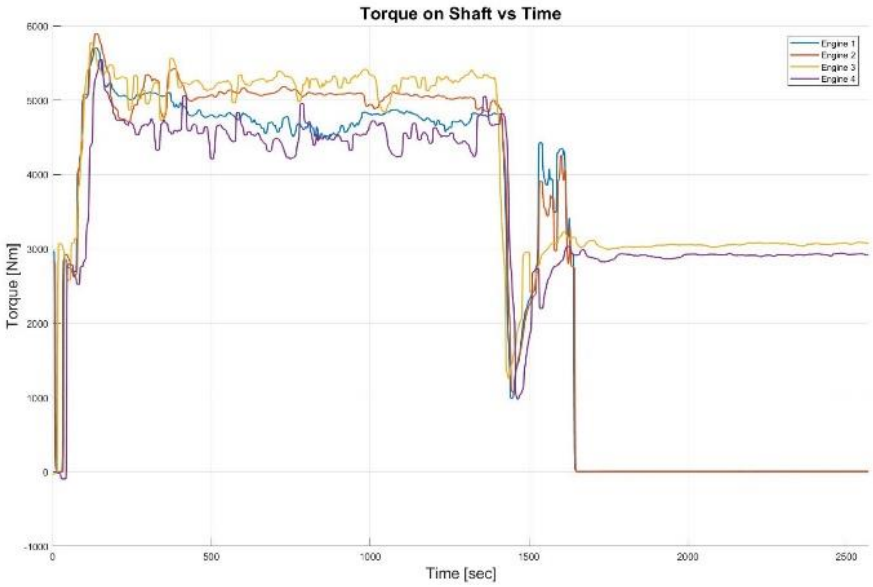

Figure M - 6 Shaft speed and torque (during a single sailing trip)

M2. MODEL IMPLEMENTATION

Implementation of the powertrain system modelling and simulation results are discussed in this section. The structure of the powertrain system simulator is shown in Figure M - 7. A less computation-intensive, backward simulation method that is suitable for control strategy development and for component size optimization is used. Flowing back through the drivetrain, the ship speed acts as input and the power request from the end of the shaft line goes backward to determine the needed torque and propulsion power.

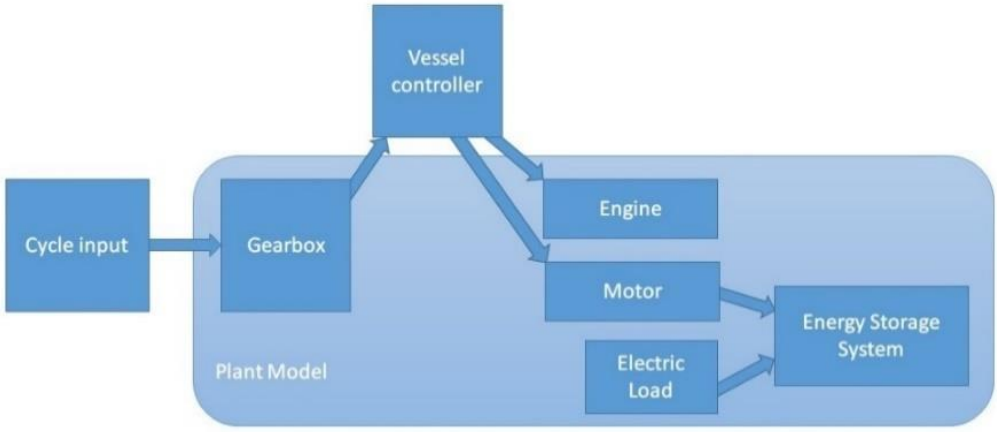

Figure M - 7 Backward Powertrain System Simulation

- Load cycle input: The collected power demand data from Skeena Queen is used as the vessel's power demand at the propeller shaft. A sequence of data points of recorded torque and speed were used as system inputs. Load impacts from ocean current, wind and wave can be added to this load cycle model in the future.

- Vessel controller: A rule-based controller was developed. This control block generates a sequence of step points for each actuator, including the electric machines and the diesel engines. The inputs to this block include the input torques and speeds to the gearbox, the electric load, and the SOC of the ESS (Figure M - 8). The information is used to decide the torque distribution and operation mode of the powertrain.

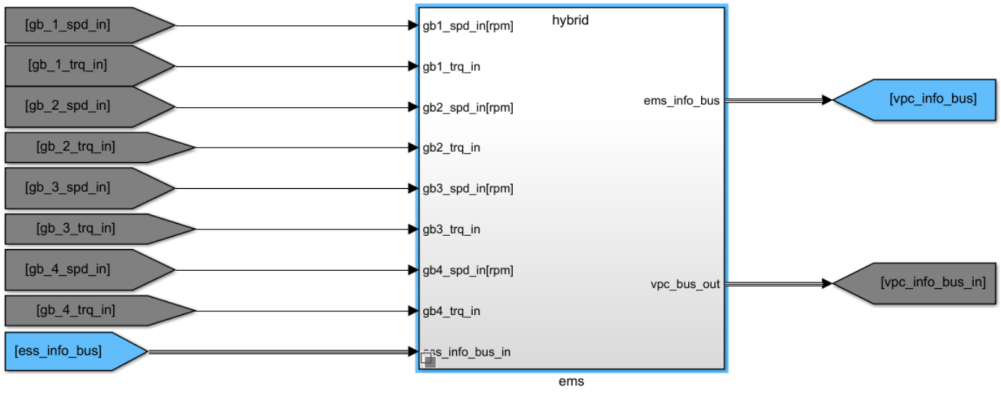

Figure M - 8 Energy management

- Vessel plant model: This model contains all the physical powertrain system components onboard, including engines, electric machines, gearbox, Bi-DC/DC convertor, ESS, electric load, etc. as shown in Figure M - 9.

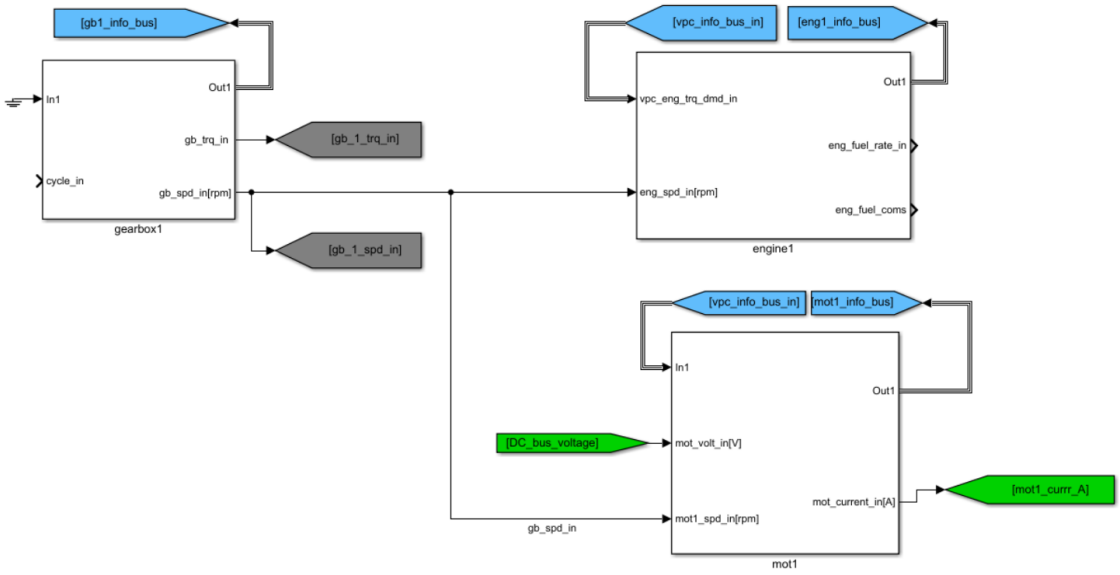

(a) Engine, Motor and Gearbox Models

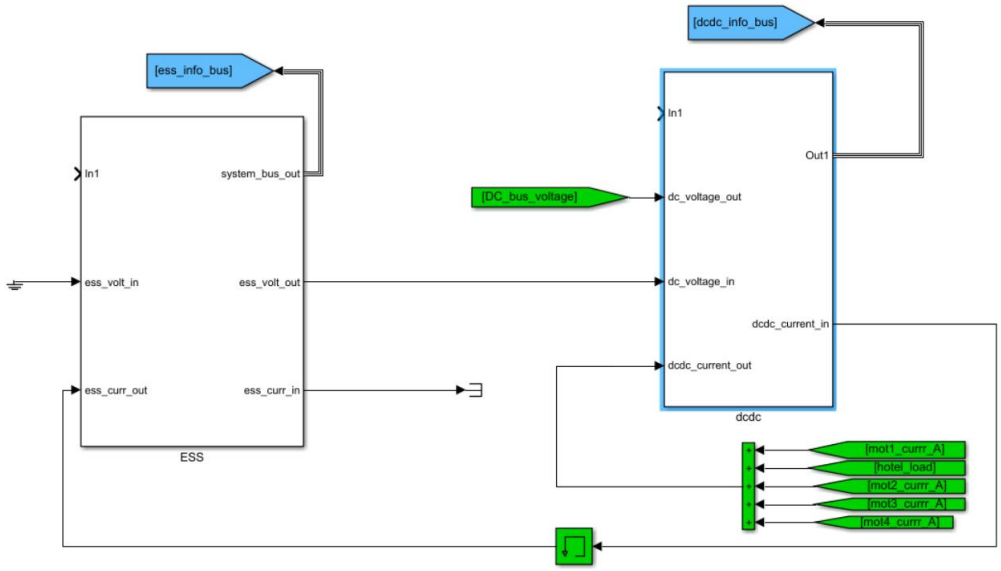

(b) ESS and DC/DC Converter Models

Figure M - 9 Plant Model

M3. NG-DIESEL DUAL-FUEL COMPRESSION ENGINE

With higher efficiency and potentially lower emissions over gasoline counterpart, the diesel engine is widely used in mining equipment, covering about 46% of total energy use in mine operations [1]. On the other hand, the cost of diesel fuel remains high, and the wide use of diesel fuel in mining produces a negative impact on miners' health [2]. Diesel exhausts have recently been added as a human carcinogen by the World Health Organization (WHO) in 2012 [3]. The reduction of harmful emissions from diesel-fueled engines is an important driving factor for green mining transportation research. Heavy-duty diesel engines produce a considerable amount of NO_x, HC, PM, CO and CO_2 that are the primary constituent of the greenhouse gas (GHG) emissions [4]-[5]. For instance, a 175hp diesel engine bulldozer emits the amount of smog and haze forming PM as much as 500 new automobiles [8], and a considerable amount of other stated emissions that contribute to global warming and human health problems.

NG fuel presents as an attractive alternative to diesel due to its much-reduced emissions under ideal operation conditions, its considerably lower costs [9], and its increasing availability in many parts of the world. Previously, NG could only be directly used in spark ignition (SI) engine due to its long ignition delay [11]. More recently, the use of NG and pilot diesel fuel in a CI engine led to improved emissions and power characteristics. The broader applications of large NG-diesel dual-fuel CI (or simply NG) engine can significantly lower NO_x and CO_2 emissions, and produce almost zero smoke and PM [12].

While NG has been recognized as a good alternative of diesel for heavy-duty transportation applications, it does have a number of inherent drawbacks that must first be addressed. These include:

1) With higher auto-ignition temperature and lower flame velocity, NG fuel normally has to be used in an NG-diesel dual-fuel CI engine for large vehicles and ships. A small amount of diesel is used acts as the pilot fuel with varying NG to diesel mix ratio, and complex control

to maintain good fuel efficiency and low emissions at different engine speed and load, causing fuel management and control complexity.

2) Although the NG-diesel dual-fuel CI engines have significantly lower NO_x and CO_2 emissions and produce almost zero smoke and PM consistently, the HC and CO emissions could be orders of magnitude higher than the neat diesel engine at very low and high speed/load operations due to incomplete combustion of NG. The surge of HC emission is due to methane slip as a small proportion of the NG injected into the engine combustion chambers fails to burn and escapes through the exhaust system to the atmosphere at low and high engine speed. These NG engines only operate efficiently and remain very clean within a narrow low to intermediate speed range.
3) An NG-diesel dual-fuel CI engine usually produces lower peak power than a diesel counterpart. Although the pre-mixture system and high-pressure direct-injected (HPDI) system have made considerable progress in recent years, a 5% peak power gap still exists [12]. The power output of the NG engine could not match its diesel counterpart at high speeds (>1000 *rpm*) [18][19].
4) AN NG engine normally shows a slower dynamic response in power surge comparing to its diesel counterpart [20].

Efforts have been made by the UVic Clean Transportation Research Team to introduce new methods that integrate NG engine, hybrid electric powertrain system, and global optimal powertrain system control to overcome the inherent drawbacks of the NG engines. The additions of electric ESS, dedicated global optimal controls, and motors/generators to the pure mechanical powertrain will decouple the NG-diesel dual-fuel CI engine and the propulsion wheels, add flexible power boost and absorption capabilities, and ensure the NG engine operate efficiently at the operating states with no significant HC and CO emission increases. The new powertrain system approach presents an alternative and more viable method than improving the NG engine alone. Specifically, the hybrid electric propulsion system and associated optimal control will:

1) enable the NG engine to operate at its ideal, relatively narrow torque and speed range, to allow a fixed NG-diesel fuel ratio using simple engine control with excellent fuel efficiency and reduced CO_2 emission, and also achieve low HC and CO emissions;
2) fill in the peak power gap of the NG-diesel engine, and respond to the need for power surge quickly using the energy in the ESS and electric drive of the hybrid powertrain.

Developments of these detailed techniques are beyond the scope of this contract. Nevertheless, the energy efficiency, emission reduction and fuel cost results from diesel and NG engine hybrid electric propulsion systems for Skeena Queen are presented and explained in the following section.

M4. SIMULATION RESULTS

In this study, four different powertrain configurations are compared. The simulation result is present in Table M - 3. To better explain the obtained results, several engine fuel efficiency and emission maps of the first of the four engines (Engine I) are included in this section. These include

a) The map of fuel efficiency, as well as the maps of CO, NO_x and HC emissions of the used diesel engine with a pure mechanical drive, are given in Figures M - 10. In this figure, the traces of the engine operating points during the ferry operation are illustrated, and the engine torque variation is plotted in Figure M - 11.

b) The map of fuel efficiency, as well as the maps of CO, NO_x and HC emissions of the used diesel engine within the proposed hybrid electric powertrain, are given in Figures M - 12. In this figure, the traces of the engine operating points during the ferry operation are illustrated.
c) The torque variation of the engine and the EM (motor/generator) is plotted in Figure M - 13.
d) The output torques of the diesel engine and the EM for the whole day of operation are shown in Figure M - 14.
e) Similarly, the map of fuel efficiency, as well as the maps of CO, NO_x and HC emissions of the used NG engine, are given in Figure M - 15. In this figure, the traces of the NG engine operating points during the ferry operation are illustrated.
f) Following the same pattern, the map of fuel efficiency as well the maps of CO, NOx and HC emissions of the used NG engine within the proposed hybrid electric powertrain are given in Figures M - 16. In this figure, the traces of the engine operating points during the ferry operation are illustrated
g) The output torques of the diesel engine and the EM for the whole day of operation are shown in Figure M - 14.
h) The State of Charge of the battery ESS is shown in Figure M - 10.

Table M - 3 Simulation result

Ship Type	Fuel (Kg)	CO (Kg)	NO_x (Kg)	HC (Kg)	Initial SOC	Final SOC
Diesel	2638.02	19.52	356.52	442.34	NA	NA
Diesel Hybrid	2037.86	11.48	145.72	4.12	0.7	0.5625
Improvement	22.75%	41.19%	59.13%	99.07%	NA	NA
NG	2700.32	65.06	10.842	13163.00	NA	NA
NG Hybrid	2161.01	32.29	5.88	441.20	0.7	0.5669
Improvement	19.97%	50.37%	45.77%	96.65%	NA	NA

The simulation results showed that the hybrid powertrain system could significantly reduce fuel consumption and emissions. The NG and diesel ships have a similar amount of fuel consumption, but the cost of NG is much lower than diesel, leading to lower fuel costs. On the other hand, the hydrocarbon emission from the NG engine increases significantly compared to a diesel engine, due to the incomplete combustion at low engine speed during ship manoeuvring and docking. At these low-speed operating points, the HC emission of the NG engine (Figure M - 16) is much higher than the diesel engine (Figure M - 16.

For mechanically propelled ships, the engine operation points are directly linked to the ship operation speed. Comparing the HC emission of the diesel engine at low speed, as shown in Figure M - 11 and the HC emission of the NG engine at low speed, as shown in Figure M - 15, the NG engine HC emission surge is more than 100 times. It is impossible to avoid the propulsion engine to operate under the low-speed regime; the hydrocarbon emission produced by the NG ship is thus increased significantly.

For the hybrid electric ships with the assist of the engine on-off system and pure electric propulsion, this HC emission surge problem can be solved. Figure M - 13 and Figure M - 17 showed the operation points of the diesel and NG engines in the hybrid electric powertrains. With the assist of the added electric propulsion element, the majority of the diesel and NG engine operation points have to be moved to the ideal speed and torque zone with higher fuel efficiency and lower CO, NOx and HC emissions. Due to the high sensitivity of NG engine HC emission to the engine operating speed, the HC emission reduction is more significant. The smaller number of undesired low-speed engine operation points occurred only during engine starts in engine on-off mode.

The engine operating in the hybrid electric powertrain system, as shown in Figures M13, M14 and M17, is smoother and more stable compared to the engine in the pure mechanical propulsion system, as shown in Figure M11. This would reduce the thermal load on engine components and improve system reliability [21].

Figure M - 19 showed that the hybrid powertrain system could maintain a stable battery state of charge (SOC). The final SOC did not meet the initial SOC due to the ship final operating condition. In this study, the cycle ends at ship docking, in which the ship usually operates in pure electric mode and all engines are turned off (considering only energy efficiency, not present marine safety regulations), as shown in Figure M - 15 and Figure M - 18. The ESS is the only power source in this pure electric mode. After operating in this mode for a short period, once the SOC is low, the engine will kick in to charge the battery. The SOC curve of eleven trips, illustrated in Figure M - 19, showed that the battery SOC has been maintained within an acceptable range.

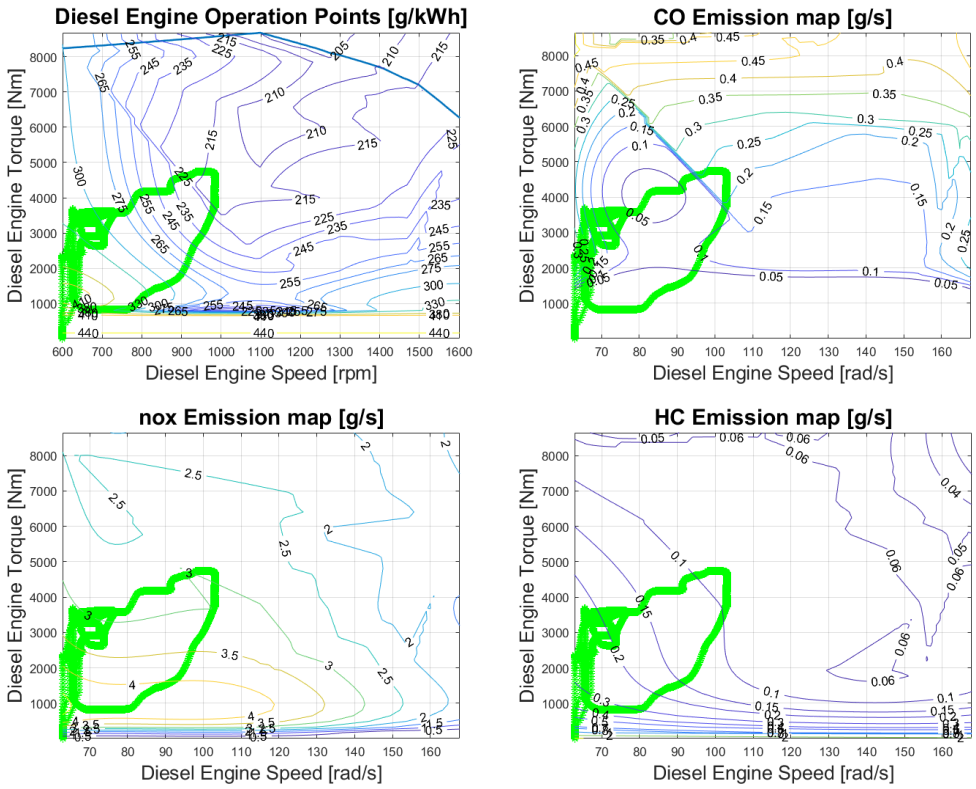

Figure M - 11 Diesel engine I operation points

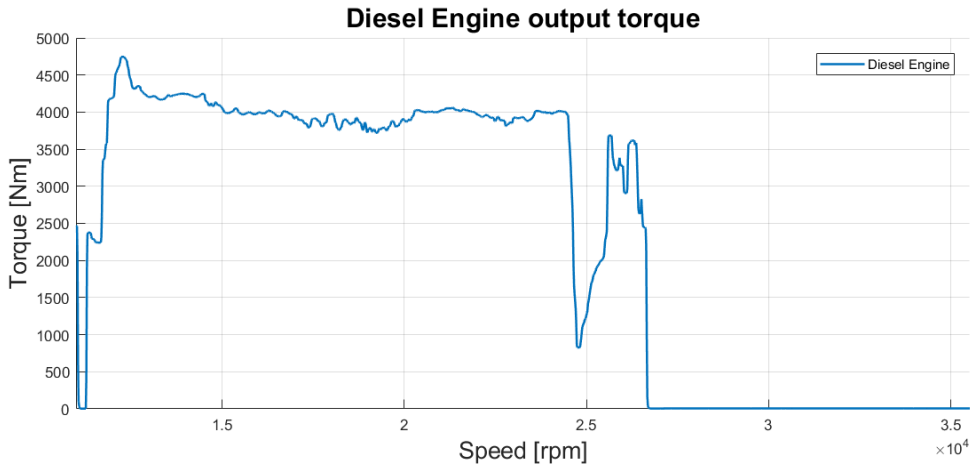

Figure M - 12 Diesel engine torque

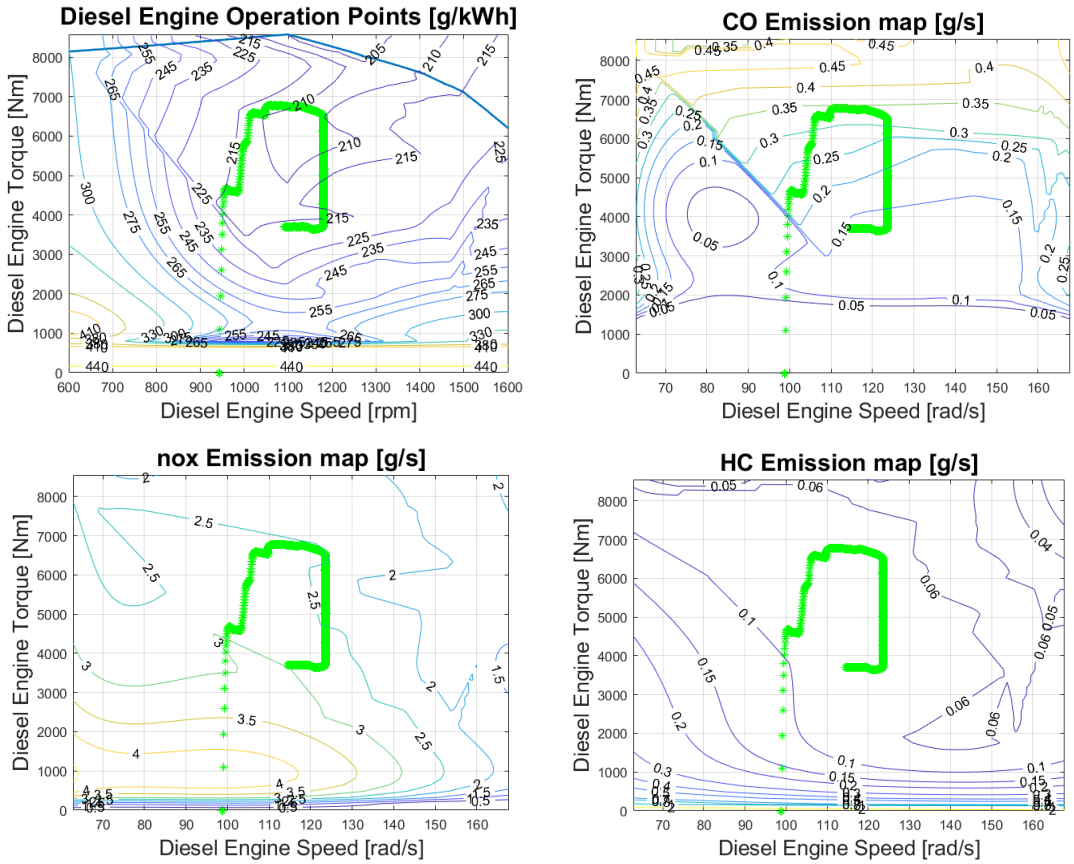

Figure M - 13 Diesel Hybrid Engine I operation points

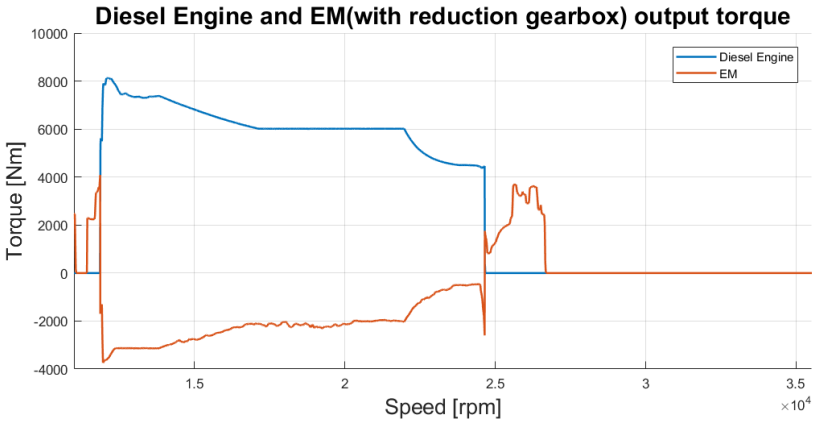

Figure M - 14 Diesel hybrid engine I and electric machine torque for one trip

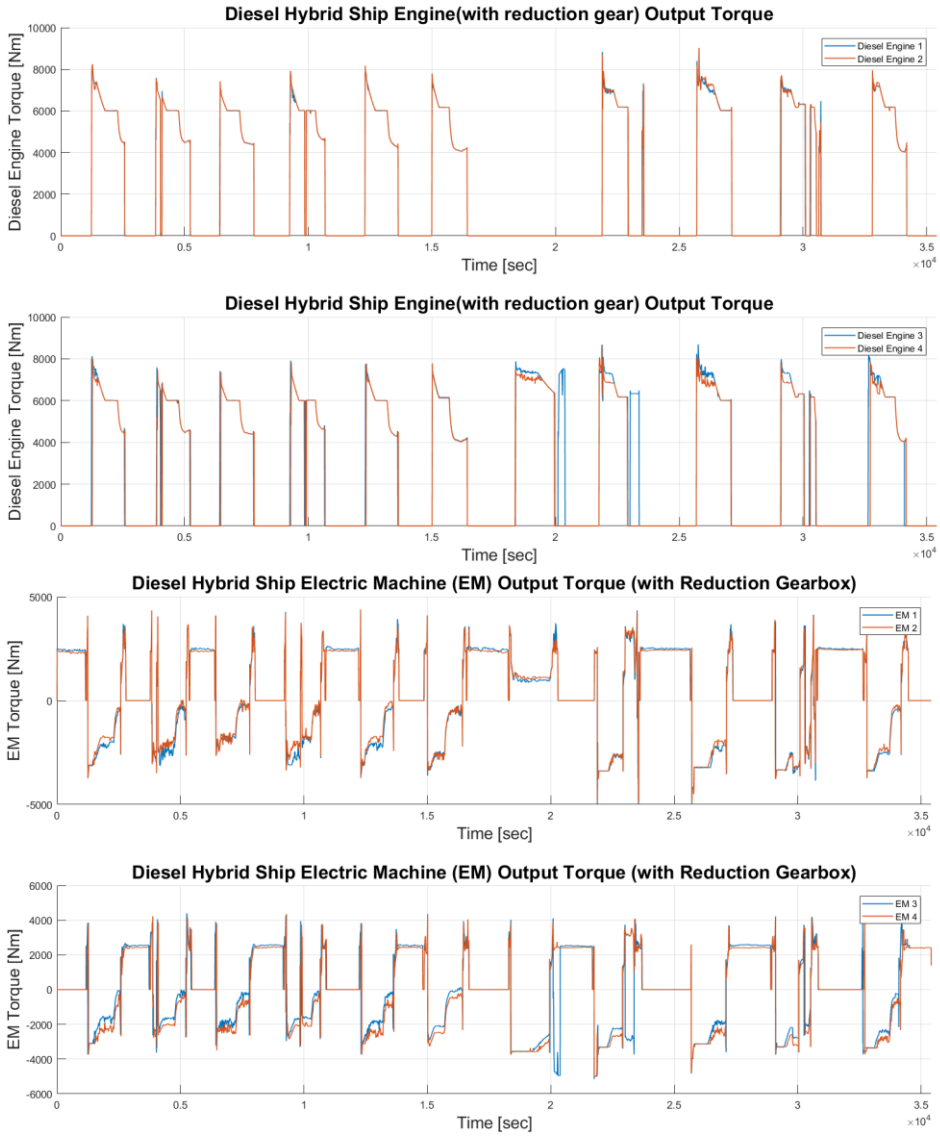

Figure M - 15 Diesel Hybrid Engine and EM operating condition

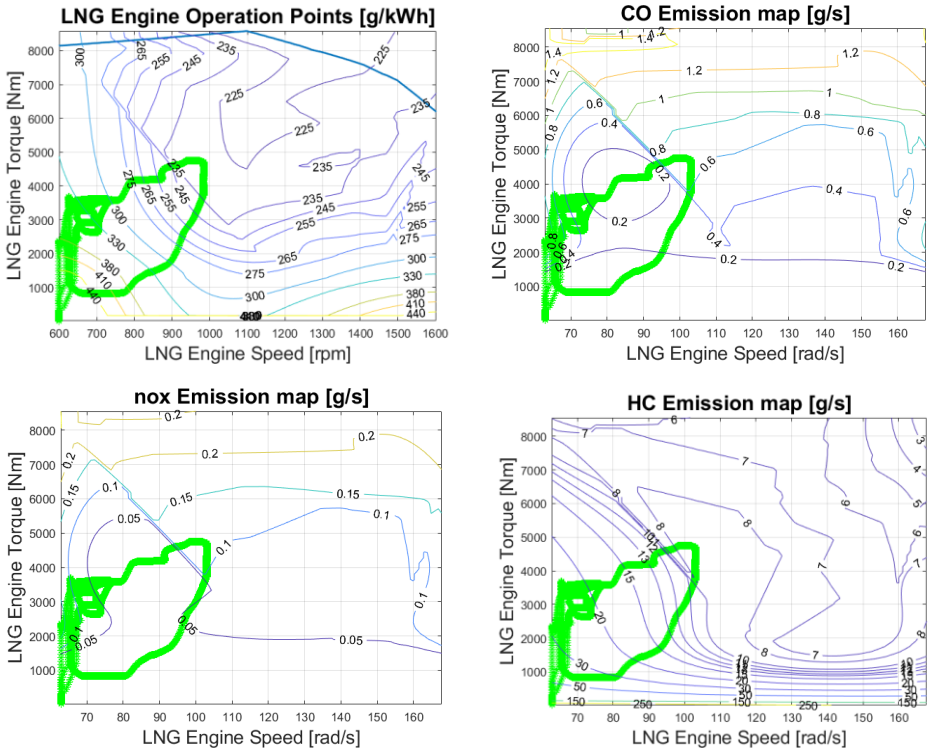

Figure M - 16 NG ship engine I operation points

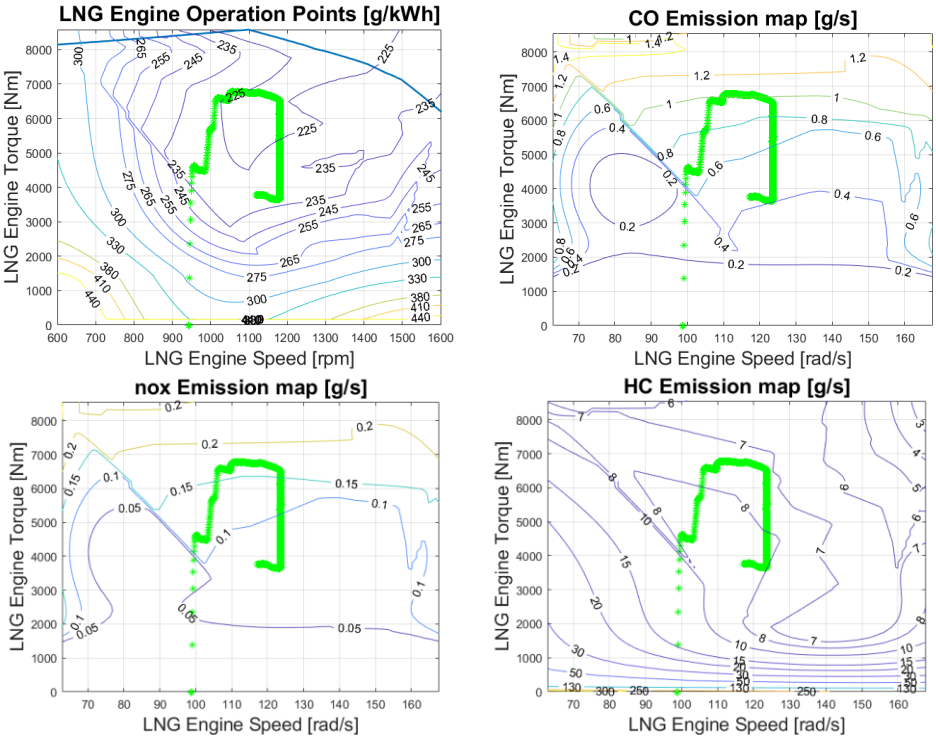

Figure M - 17 NG hybrid engine I operation points

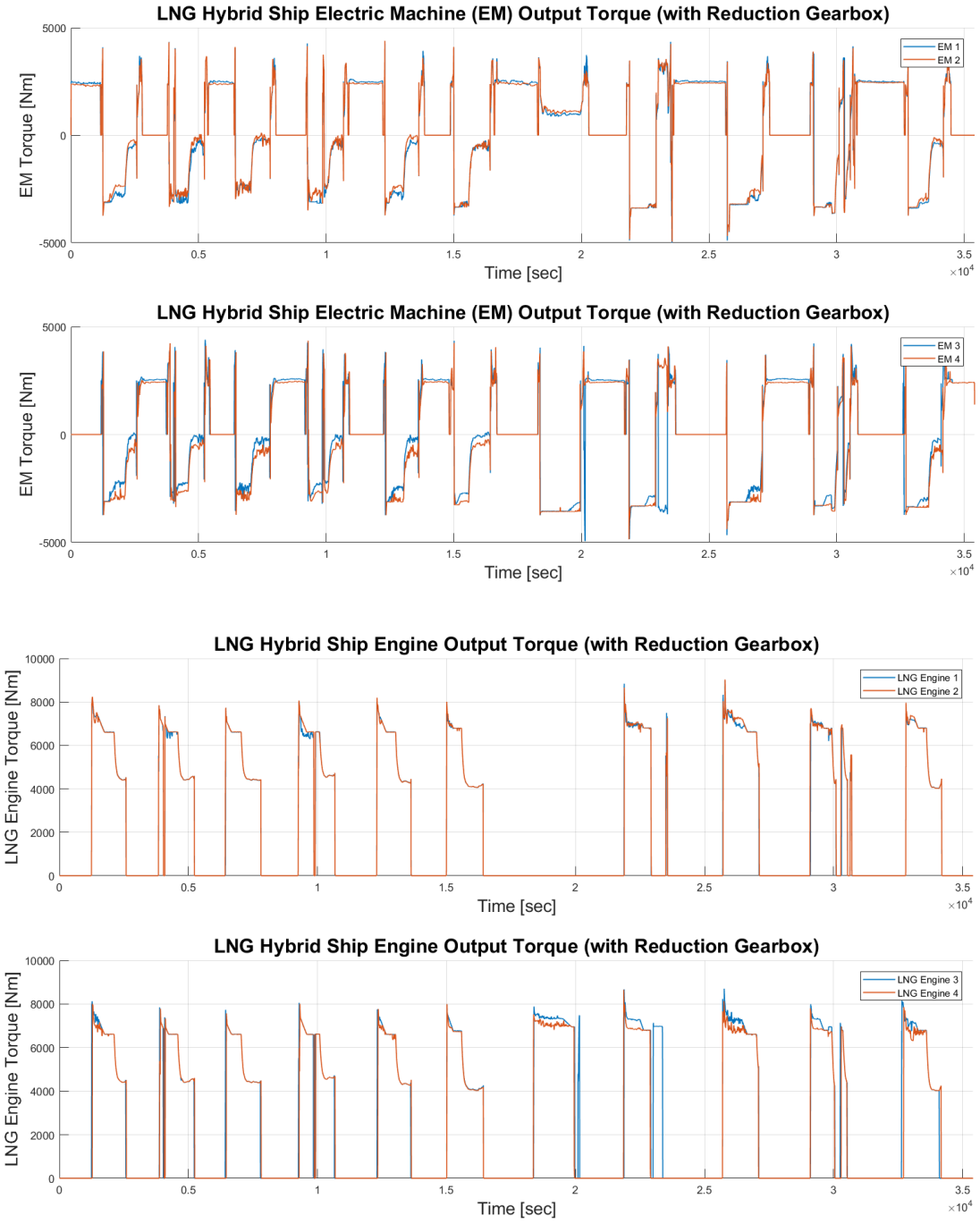

Figure M - 18 NG Hybrid: Engine and EM operating condition

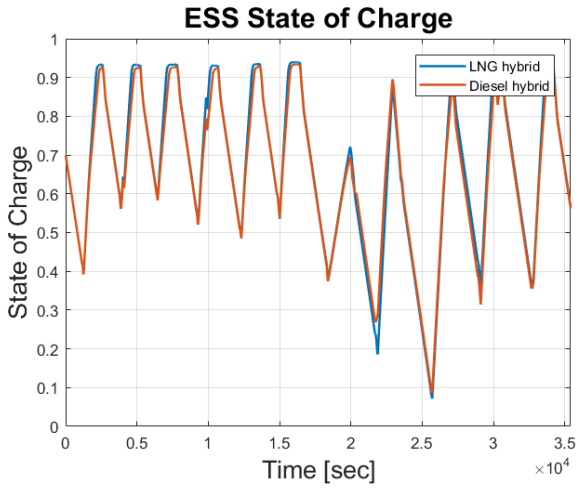

Figure M - 19 Battery State of Charge

M5. FUTURE WORK

Accomplishing the full energy efficiency and emission reduction potential for a hybrid electric propulsion system largely relies on the real-time optimal control of an optimal design system. This appendix documented the preliminary case study aimed at identifying the benefits and potentials of a parallel hybrid electric powertrain system for propelling a vehicle and passenger ferry with dominant static propulsion load. Due to the limited time, system energy management has not been optimized. A forward powertrain system simulator, dynamic programming (DP) based optimization benchmark study, and real-time optimal control methods will be investigated in the future to reveal the full potential of the and to support the full application of the technology.

ACKNOWLEDGEMENT

We would like to thank the extensive support from Bruce Paterson, William Russell and Bob Kearney at BC Ferries. Financial supports and guidance from the Clean Transportation Initiative of Transport Canada are gratefully acknowledged.

REFERENCES

[1] Carvalho, Monica, and Dean L. Millar. "Concept development of optimal mine site energy supply." Energies 5.11 (2012): 4726-4745.

[2] Silverman, Debra T., et al. "The diesel exhaust in miners study: a nested case–control study of lung cancer and diesel exhaust." Journal of the National Cancer Institute (2012).

[3] International Agency for Research on Cancer. "IARC: Diesel engine exhaust carcinogenic." Press release 213 (2012).

[4] Dreher, David B., and Robert A. Harley. "A fuel-based inventory for heavy-duty diesel truck emissions." Journal of the Air & Waste Management Association 48.4 (1998): 352-358.

[5] Clark, Nigel N., et al. "Factors affecting heavy-duty diesel vehicle emissions." Journal of the Air & Waste Management Association 52.1 (2002): 84-94.

[6] Abolhasani, Saeed, et al. "Real-world in-use activity, fuel use, and emissions for nonroad construction vehicles: a case study for excavators." Journal of the Air & Waste Management Association 58.8 (2008): 1033-1046.
[7] Zhu, Dongzi, et al. "Real-world PM, NO x, CO, and ultrafine particle emission factors for military non-road heavy duty diesel vehicles." Atmospheric Environment 45.15 (2011): 2603-2609.
[8] Lewis, Phil, et al. "Requirements and incentives for reducing construction vehicle emissions and comparison of non-road diesel engine emissions data sources." Journal of Construction Engineering and management 135.5 (2009): 341-351.
[9] Wei, Lijiang, and Peng Geng. "A review on natural gas/diesel dual-fuel combustion, emissions and performance." Fuel Processing Technology 142 (2016): 264-278.
[10] Cheenkachorn, Kraipat, Chedthawut Poompipatpong, and Choi Gyeung Ho. "Performance and emissions of a heavy-duty diesel engine fueled with diesel and LNG (liquid natural gas)." Energy 53 (2013): 52-57.
[11] Bhandari, Kirti, et al. "Performance and emissions of natural gas fueled internal combustion engine: A review." (2005).
[12] Wei, Lijiang, and Peng Geng. "A review on natural gas/diesel dual-fuel combustion, emissions and performance." Fuel Processing Technology 142 (2016): 264-278.
[13] Namasivayam, A. M., et al. "Biodiesel, emulsified biodiesel and dimethyl ether as pilot fuels for natural gas fueled engines." Applied Energy 87.3 (2010): 769-778.
[14] Azimov, U., et al. "Premixed mixture ignition in the end-gas region (PREMIER) combustion in a natural gas dual-fuel engine: operating range and exhaust emissions." International Journal of Engine Research (2011): 1468087411409664.
[15] Korakianitis, T., A. M. Namasivayam, and R. J. Crookes. "Diesel and rapeseed methyl ester (RME) pilot fuels for hydrogen and natural gas dual-fuel combustion in compression–ignition engines." Fuel 90.7 (2011): 2384-2395.
[16] Sun, Lu, et al. "Combustion performance and stability of a dual-fuel diesel–natural-gas engine." Proceedings of the Institution of Mechanical Engineers, Part D: Journal of Automobile Engineering 229.2 (2015): 235-246.
[17] Park, Cheolwoong, et al. "Operating strategy for exhaust gas reduction and performance improvement in a heavy-duty hydrogen-natural gas blend engine." Energy 50 (2013): 262-269.
[18] Selim, Mohamed YE, M. S. Radwan, and H. E. Saleh. "Improving the performance of dual-fuel engines running on natural gas/LPG by using pilot fuel derived from jojoba seeds." Renewable energy 33.6 (2008): 1173-1185.
[19] Cheenkachorn, Kraipat, Chedthawut Poompipatpong, and Choi Gyeung Ho. "Performance and emissions of a heavy-duty diesel engine fueled with diesel and LNG (liquid natural gas)." Energy 53 (2013): 52-57.
[20] Roecker, Ryan C., et al. "State-based diesel fueling for improved transient response in dual-fuel engine." U.S. Patent No. 9,518,516. 13 Dec. 2016.
[21] T. Harald, Z. Piero and H. Nico, "Hybrid propulsion is part of the future for RoPax ferries," [Online]. Available: http://www.wartsila.com.

Appendix N. Case Study on BC Ferries' Tachek - Hybrid Electric Propulsion System Designs for Fuel Economy and Emission Improvements

ABSTRACT

Ferries are essential transportation tools for the west coast residents of Canada, as well as for about 10% of people of the world's population, who live on islands. However, the ferry fleet with a large amount of marine diesel fuel consumption bears high fuel costs and produces heavy GHG emissions, including PM, NO_x, SO_2, CO_2 and HC, emitted from the marine diesel engines. BC Ferries, one of the industrial partners of this project, has been providing transportation services for passengers and vehicles between various islands and the mainland in British Columbia since 1960. As the largest passenger ferry company in North America, it owns 47 operation lines, which has consumed 115.4 million litres of marine diesel at a cost of CAD$103.3 million in fiscal 2016. To reduce fuel cost and GHG emissions, BC Ferries has been seeking new technologies for its future ships.

Tachek is an open deck passenger and car ferry that is operated on the Quadra Island – Cortes Island route with dynamically changing ocean conditions. The ferry has been retrofitted with a hybrid electric propulsion assist system with a modern data acquisition and control system. The vessel was built in 1969 in Vancouver. In 2013, a life extension project was applied on this ship to add a part-time hybrid electric propulsion system. At present, the benefits and room for improvement of the hybrid electric propulsion system of MV Tachek have not yet been systematically investigated. The ease of operation data acquisition and the motivation to improve its hybrid electric propulsion controls make the ship a good candidate for a full hybridization study. This work focuses on the new full hybrid electric propulsion system design for Tachek. Three different types of ship propulsion systems are modelled and simulated in this work to illustrate to different levels of fuel economy and emission improvements, including a) a diesel engine and mechanical propelled benchmark powertrain system; b) the present part-time hybrid electric powertrain system; and, c) a redesigned hybrid electric powertrain with more capable operations.

N1.

INTRODUCTION

The vehicle and passenger ferry, MV Tachek, operated by BC Ferries (Figure 1), was built in 1969 in Vancouver. Tachek went through various refits and upgrades. In 2013, a life extension project was applied on this ship to add a part-time hybrid electric propulsion system with which the ferry only operates in its electric mode during docking operations. Tachek was the first ferry that has a hybrid electric powertrain with a battery energy storage system (ESS) on board (Figure N - 1). The ship operates on the Quadra Island – Cortes Island route as shown in Figure N - 2.

Figure N - 1 MV Tachek, approaching the dock

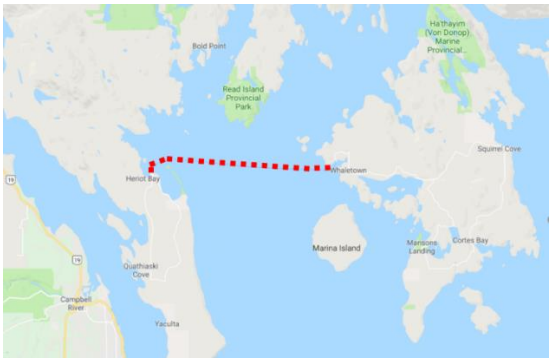

Figure N - 2 Route

At present, the benefits and room for improvement of the hybrid electric propulsion system of MV Tachek have not yet been systematically investigated. In this work, three different types of ship propulsion systems are modelled and simulated to illustrate different levels of fuel economy and emission improvements, including

- a diesel engine and mechanical powertrain that represents conventional ship propulsion technology to serve as the benchmark technology in this study;
- the present part-time hybrid electric powertrain of the MV Tachek; and
- a redesigned hybrid electric powertrain with a more capable operation.

The key ship parameters are given in Table 1. Detailed technical information of the ship is documented in Appendix A - All Studied Marine Vessels.

Table N - 1 Ship parameters

Built:	1969, Vancouver
Overall Length:	49.53 m
Maximum Displacement	807 tonnes
Passenger & Crew Capacity:	150
Car Capacity:	30
Service Speed:	12.5 knots
Route:	Quadra Island – Cortes Island

Extensive operation data of MV Tachek have been collected during this research through various means. Among them, the subtracted operation pattern is shown in Figure N - 3. Only one round trip operation data are shown here, which are collected directly from Tachek's propeller shaft. The engine is idling when the ship is at the dock. Other collected ship operation data, such as the rudder angle, are not used in this study.

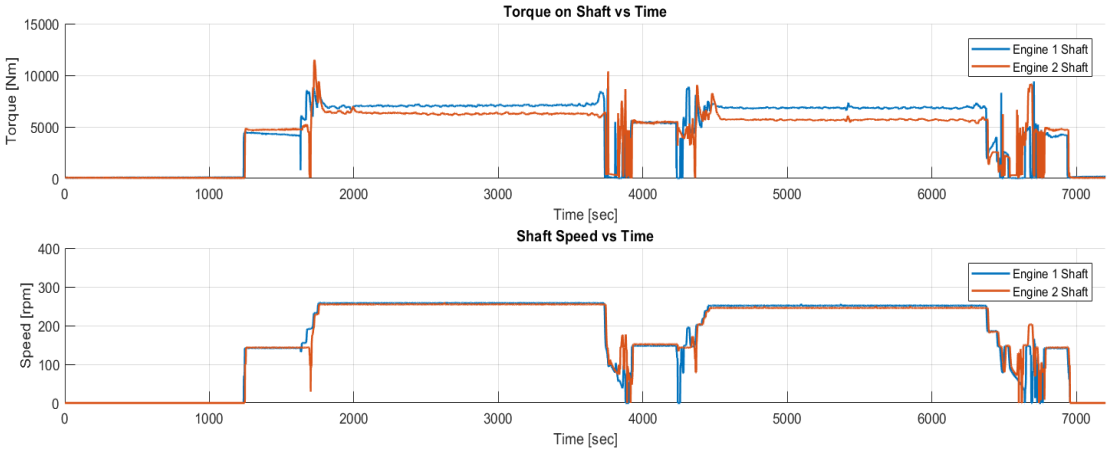

Figure N - 3 MV Tachek operation profile

N2. DEGREE OF HYBRIDIZATION

The degree of hybridization (DOH), which specifies the portion of the power provided by electric machine and engine, is defined as below:

$$DOH = P_{EM}/P_{total} \quad \text{(O - 1)}$$

where P_{total} represents the total power on board; P_{EM} represents the total power of the electric machine. The DOH that is linked to the cost of the ship hybridization has a significant impact on fuel economy and emissions. In this work, hybrid ship designs with three different DOH are used to illustrate how DOH affects fuel consumption. Component size optimization of the hybrid electric powertrain was not covered in this work, and it needs to be done in the future.

N3. MODEL IMPLEMENTATION

The modelling platform for the propulsion systems of the ferry ship has been discussed in detail in Appendix M Case Study for Skeena Queen - Design of Parallel Hybrid Marine Propulsion System, thus will not be further discussed in this appendix. The ferry has the same hull, propeller, and power load demands for the same crossing. The same diesel engines and generators were used. These allowed the use of the same model implementations in MATLAB/Simulink for the competing powertrain system designs.

MECHANICAL PROPELLED SHIP

N4. The conventional propulsion system design of the ferry uses two diesel engines and mechanical drives for propulsion, and an electric bow tunnel thruster for turning. The diesel engines are connected to the propellers through speed reduction gearboxes. Diesel generators supply electric power to meet the hotel power load and to power the small bow thruster. This type of conventional ship propulsion system design is considered as the baseline for the comparative study documented here.

The MV Tachek's main engines had an upgrade in 2013 to serve as the Power Take-Off (PTO) generator that supplies electric power. With the additional propulsion power from the added battery ESS and electric drive, and the ability of the hybrid electric propulsion system to provide the power reserve for marine safety, a smaller engine is used in the new hybrid powertrain.

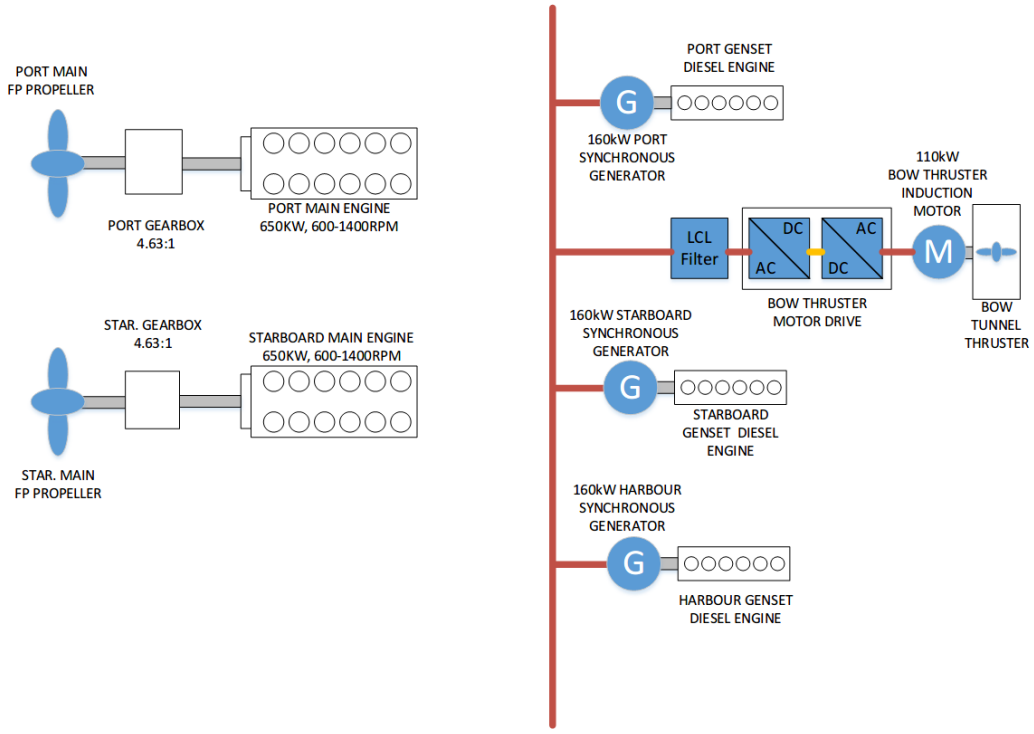

Figure N - 4 Conventional mechanical propelled ship diagram

The main powertrain parameters as presented in Table 2.

Table N - 2 Mechanical propelled ship powertrain parameters

Diesel Engine:	650 kW * 2
Generator:	160 kW * 2
Gearbox Ratio:	4.63:1
Emergency Generator:	160 kW
Bow Thruster:	110 kW

MV TACHEK

Some ships operate with *Power Take* Off (PTO) and *Power Take In (PTI***)** modes when equipped with both mechanical and electric drives. The main engines are used to provide propulsion power through mechanical links to the propellers and gear reductions, while the gensets are used to supply auxiliary electric power to the vessel. For diesel-electric propulsion, the main engines are connected to shaft generators to generate electric power. The main engines and the gensets for auxiliary electric power often share the same power bus using different power converters.

N5.

In the PTO mode, the gensets for auxiliary power are stopped, and the electrical power is supplied by the main engine through the shaft generator. In the PTI mode, the main engines-generators provide additional electric power (possibly through a variable-frequency drive (VFD)) to supplement the electric power produced by the gensets.

MV Tachek went through a life extension project in 2013. It was an innovative effort to bring advanced hybrid electric propulsion technology to a marine vessel. The modifications to the powertrain system was conservative, covering the following two major changes:

a) Two larger diesel engines (985 kW each) with 45% power increase replaced the old engines (640 kW each). The change was made to address the engine overheating issue of the ferry under some extreme operating conditions, and to support the new PTO operation; and
b) Upgrade of the vessel into a PTO hybrid ship was done to allow the main engines-generators and the battery ESS to replace the old gensets to supply hotel loads and to drive the tunnel thruster of the vessel during ducking operations.

The propulsion system of MV Tachek is shown in Figure N - 5, and powertrain parameters of MV Tachek is given in Table N - 3. The shaft generators were connected to the main engines through PTO gearboxes, allowing the main engines to drive the shaft generators to supply electric power. Normally the old diesel generators no longer need to operate. A battery ESS connected to the electric bus through a bi-direction DC/AC convertor was added. This ESS worked as a buffer to store extra energy produced by the main generators to meet the electric power demands from the tunnel thruster and hotel loads. The PTO operation and the ESS had been over engineered, and the State of Charge (SOC) variation of the ESS was normally less than 5%. Since the shaft generators had no propulsion (or electric motor) function, the part-time hybrid electric propulsion system had not realized the full potential of the hybrid electric propulsion technology.

N6.

NEWLY PROPOSED HYBRID ELECTRIC DRIVE

In this work, efforts are made to explore the full energy efficiency and emission reduction potentials of hybrid electric propulsion system for MV Tachek. The new and revised hybrid electric powertrain system of the vessel has both PTI and PTO ability, and the Electric Machines (EM), or Motor/Generator (M/G), connected to the main engines can as both motors and generators, to support the full hybrid electric propulsion function. The revised powertrain system with full electric drive capability is illustrated in Figure N - 6, and powertrain parameters of the newly proposed, full-hybrid MV Tachek is given in Table N - 4. The minor powertrain system change required different powertrain system components and system control strategies.

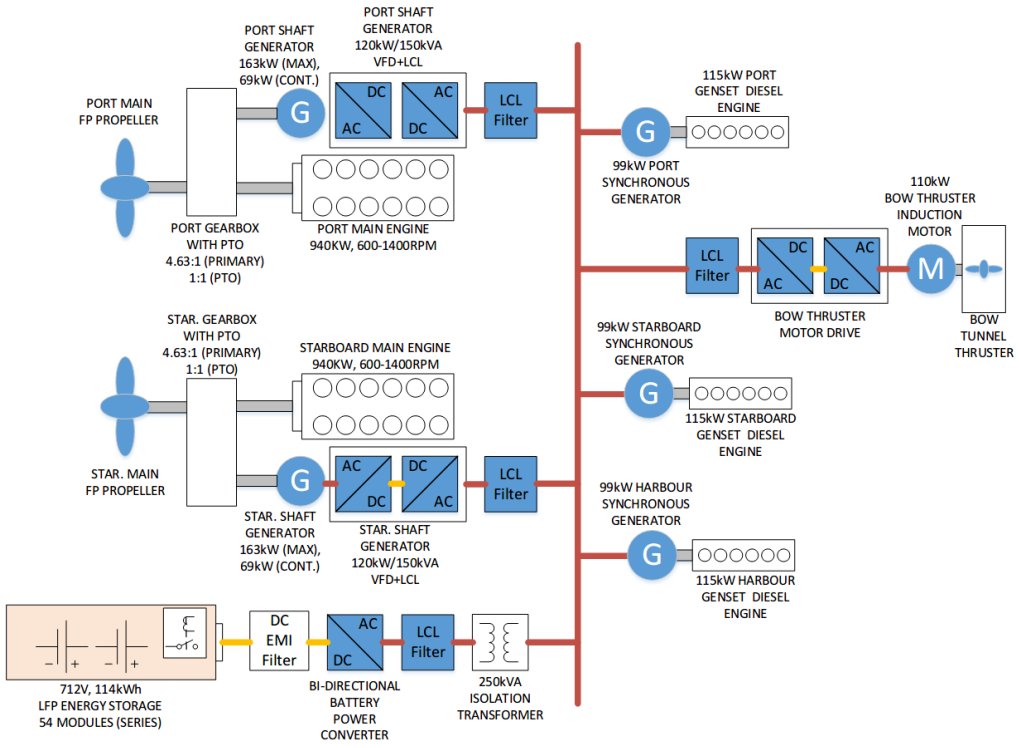

Figure N - 5 MV Tachek powertrain system

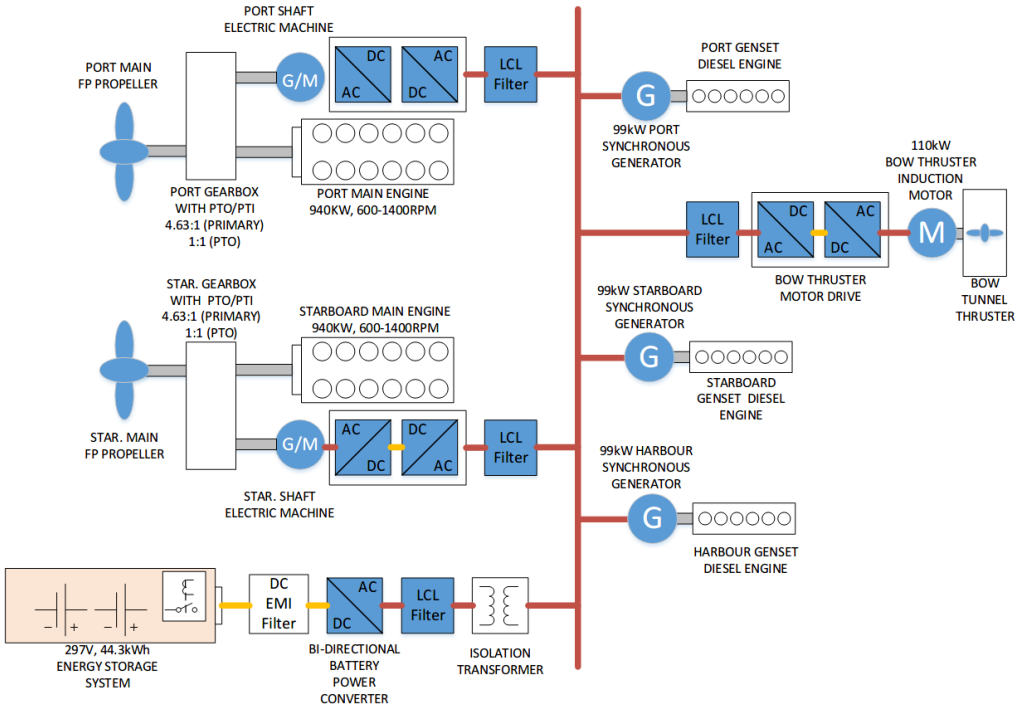

Figure N - 6 Proposed hybrid electric drive for MV Tachek

Table N - 3 MV Tachek powertrain parameters

Diesel engine	940 kW * 2
Gearbox Ratio:	4.63:1
Shaft Generator:	160 kW (MAX) and 69 kW (CONT.) * 2
PTO Gearbox:	1:1
Diesel Generator	99 kW * 2
Emergency Generator:	99 kW
Battery Capacity:	114 kWh
Bow Thruster:	110 kW

Table N - 4 Hybrid ship powertrain parameters

Diesel engine	940 kW * 2
Gearbox Ratio:	4.63:1
Shaft Electric Machine:	160kW/ 402kW/ 940kW (CONT.) *2
PTO Gearbox:	1:1
Diesel Generator	99 kW * 2
Emergency Generator:	99 kW
Battery Capacity:	44.3 kWh/ 44.3 kWh/132.9 kWh
Bow Thruster:	110 kW

The engine is now coupled with an on-off system. When the ship is propelled by the electric machines, the engine shafts will disengage from the gearbox and the main engines will be completely turned off to save fuel and reduce emissions.

A new rule-based controller has been introduced to manage the energy flow in the hybrid powertrain system. The essence of the rule-based controller is to force the engine to operate at its high efficiency zone while maintaining the battery state of charge (SOC) within a given range.

For the newly proposed hybrid powertrain, system designs with different levels of DOH have been investigated. The variations on the level of hybridization led to shaft EM with different power capabilities of 160 kW, 402 kW and 940 kW, and different types. Three types of EM are used in the vessel's propulsion and power systems, electric generator (G), propulsion motor (M), and generator and motor (G/M).

N7.

RESULT AND ANALYSIS

The fuel efficiency and emissions of the present MV Tachek's part-time hybrid electric propulsion system and three newly proposed full hybrid electric propulsion systems (I, II and III) with different degrees of hybridization are modelled, and the results are shown in Table N - 5. The conventional mechanically propelled ship was used as the baseline in the comparative study.

Table N - 5 Simulation result and improvement

	Mech. Propelled	MV Tachek	Improve-ment (%)	Hybrid electric I	Improve-ment (%)	Hybrid electric II	Improve-ment (%)	Hybrid electric III	Improve-ment (%)
EM Power (kW)	NA	NA	NA	160	NA	402	NA	940	NA
Fuel Used (Kg)	146.03	158.29	-8.40	145.91	0.08	140.64	3.69	144.2	1.25
CO Emiss. (Kg)	0.76	0.80	-5.26	0.79	-3.95	0.70	7.89	0.92	-21.05
NO_x Emiss. (Kg)	23.56	43.85	-86.12	22.65	3.86	8.92	62.14	7.76	67.06
HC Emiss. (Kg)	6.27	2.49	60.29	0.55	91.23	0.26	95.85	0.24	96.17
ESS Initial SOC	NA	0.7	NA	0.7	NA	0.7	NA	0.7	NA
ESS Final SOC	NA	0.6366	NA	0.6753	NA	0.5523	NA	0.6069	NA

The simulation result showed that the MV Tachek with part-time hybridization does not save fuel compared to the mechanically propelled vessel. The engine operation points are shown in Figure N - 6, Figure N - 7, Figure N - 8 and Figure N - 9, are largely located in the low-load zone, which presents high emissions and low fuel efficiency for both of the baseline mechanically propelled ship and MV Tachek.

During the life-extension overhaul, two larger engines were installed on Tachek, which led to worse fuel efficiency. To meet the ship's service speed, a total propulsion power of 600 kW is enough; however, the MV Tachek has a total engine power of 1,840 kW at 1200 rpm. The two larger engines now operate at even lower fuel efficiency bands than the original mechanically propelled ship with smaller engines. The engine-overheating problem has been effectively addressed, and the marine safety power reserve has been accomplished through the increase of engine size, not the available additional electric propulsion capability of the hybrid electric propulsion system.

The new, full hybrid electric propulsion system designs with three different levels of hybridizations, on the other hand, are more fuel-efficient. The engine operation points are shown in Figure N - 10, Figure N - 11, Figure N - 12, Figure N - 13, Figure N - 14 and Figure N - 15 operate at higher engine loads (or speeds and torques outputs) with higher fuel efficiency and lower emissions. These figures showed that the engines are forced to operate in a narrow and limited speed and torque region. The significant improvement in HC emission is largely due to two factors, the better engine operating points and the engine on-off system with reduced operation time. The hybrid powertrain system turns off the engine when the engine is idling.

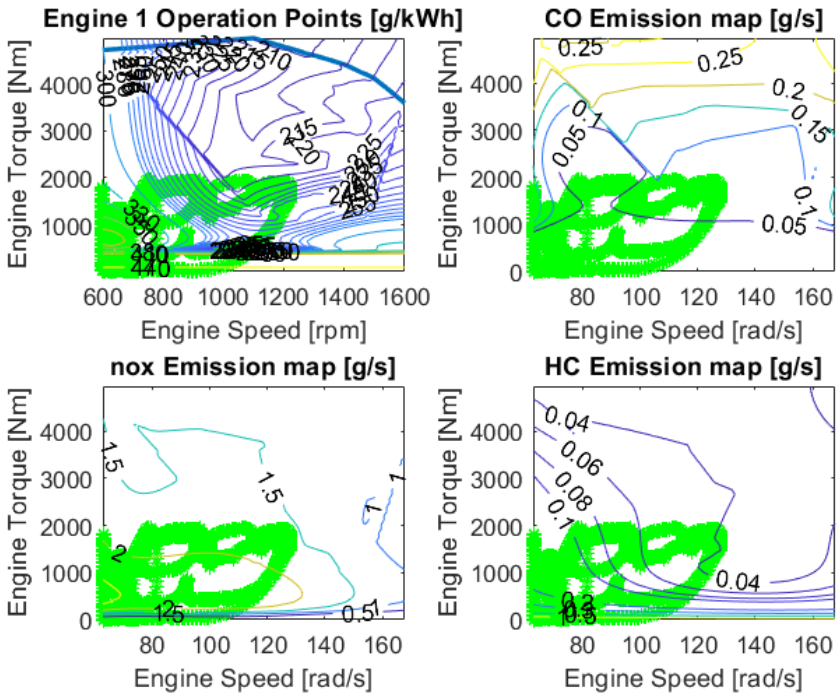

Figure N - 6 Operation points of Engine 1 in the mechanically propelled ship

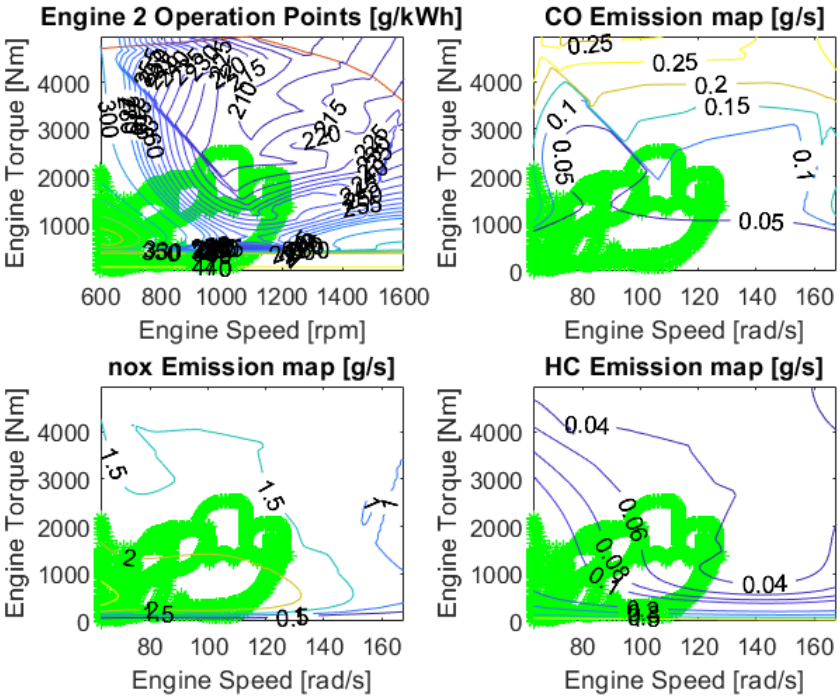

Figure N - 7 Operation points of Engine 2 in the mechanically propelled ship

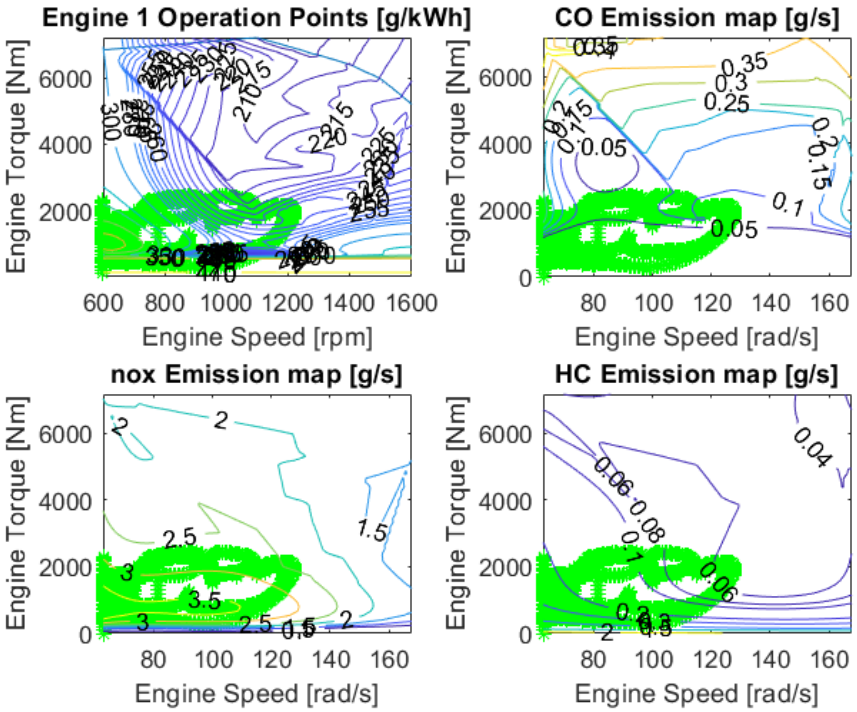

Figure N - 8 Operation points of Engine 1 in MV Tachek

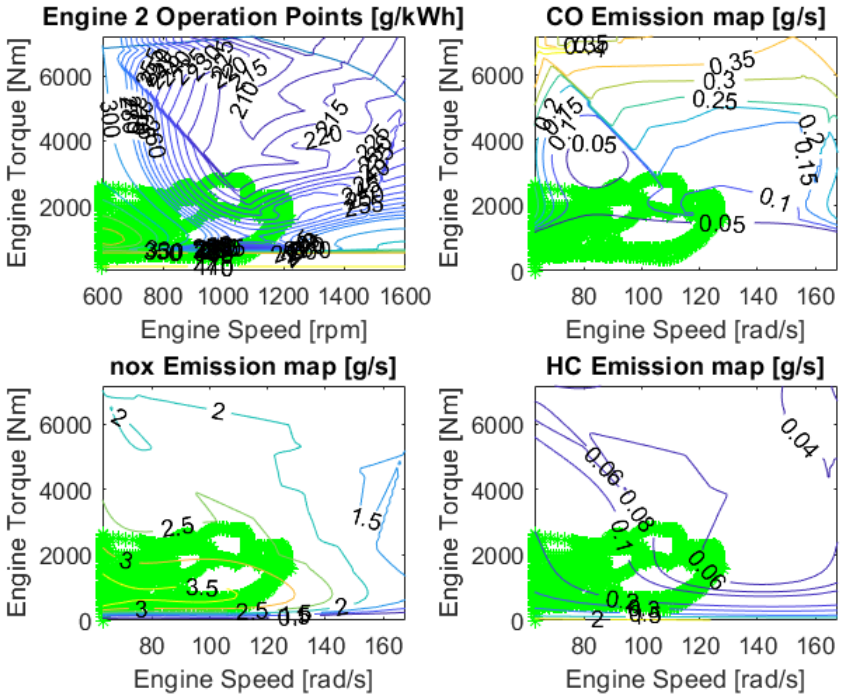

Figure N - 9 Operation points of Engine 2 in MV Tachek

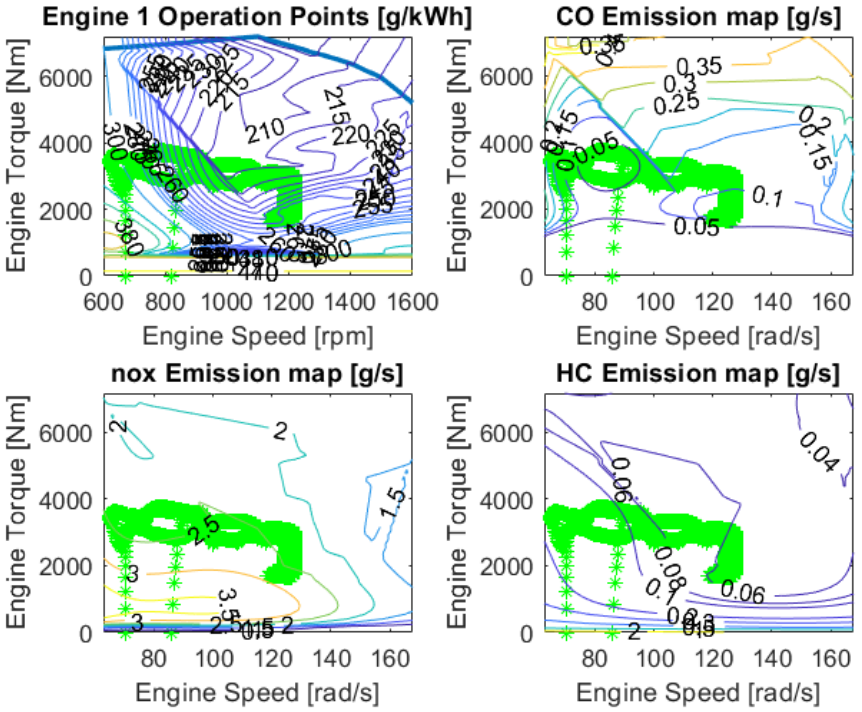

Figure N - 10 Operation points of Engine 1 in the hybrid ship with 160 kW EM

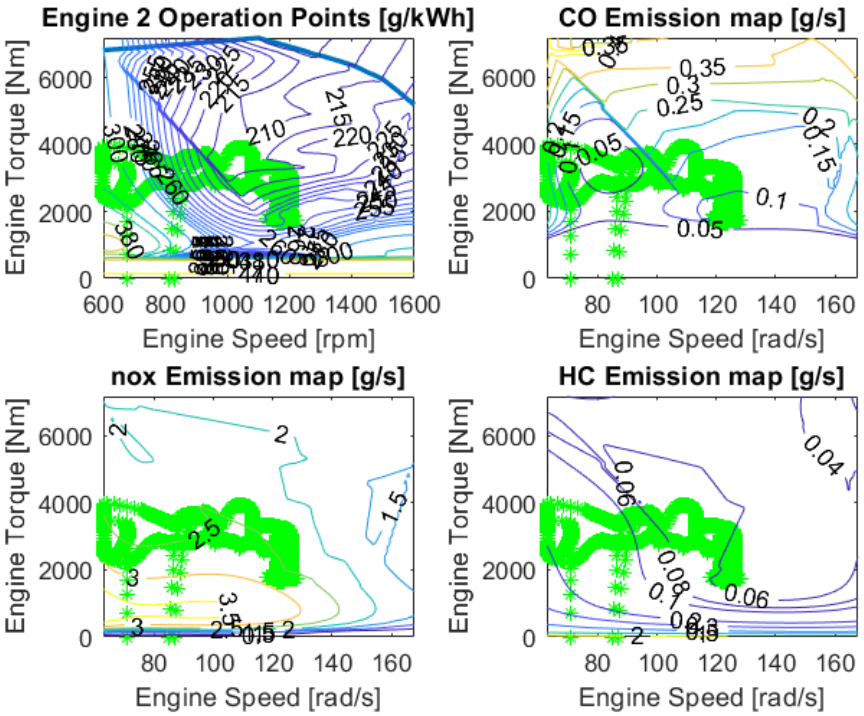

Figure N - 11 Operation points of Engine 2 in the hybrid ship with 160 kW EM

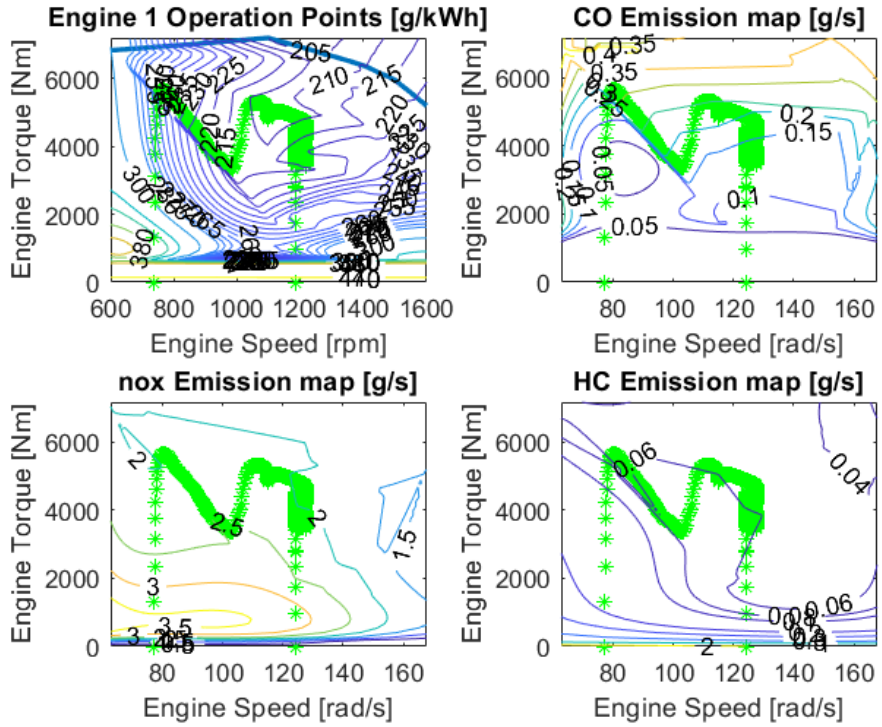

Figure N - 12 Operation points of Engine 1 in the hybrid ship with 402 kW EM

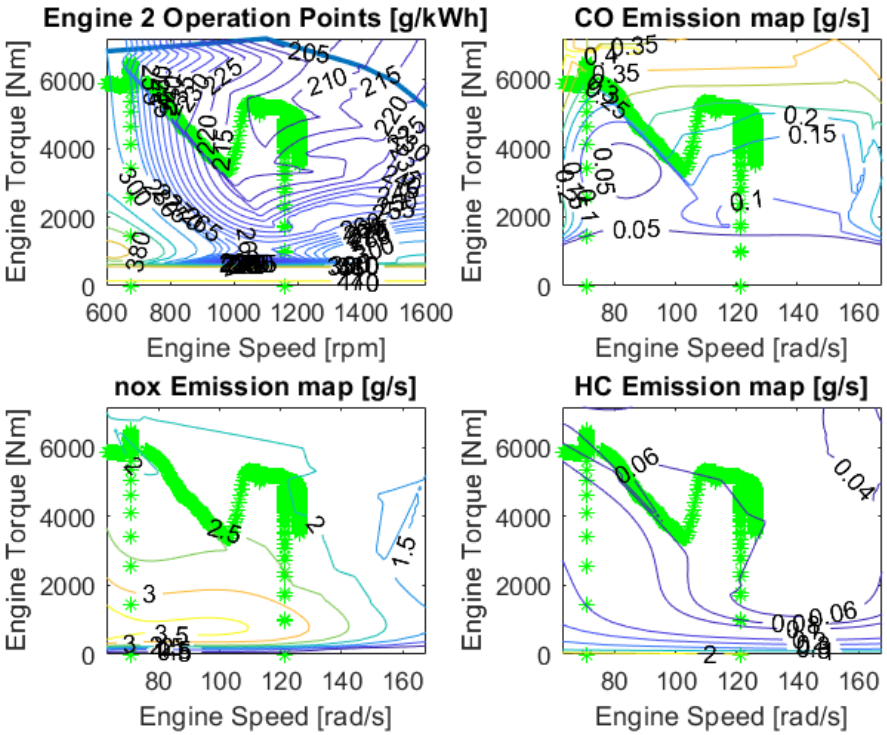

Figure N - 13 Operation points of Engine 2 in the hybrid ship with 402 kW EM

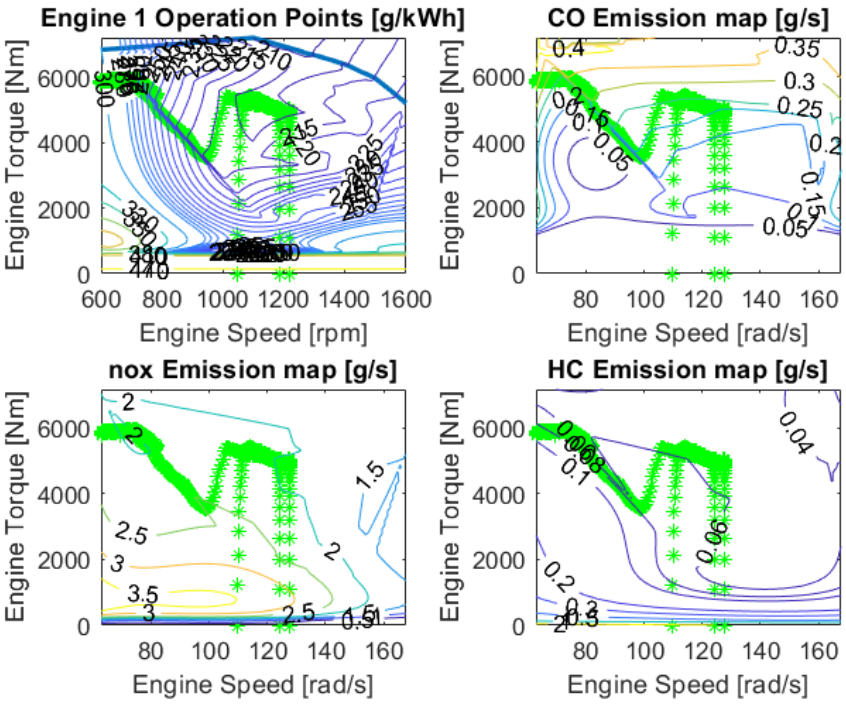

Figure N - 14 Operation points of Engine 1 in the hybrid ship with 940 kW EM

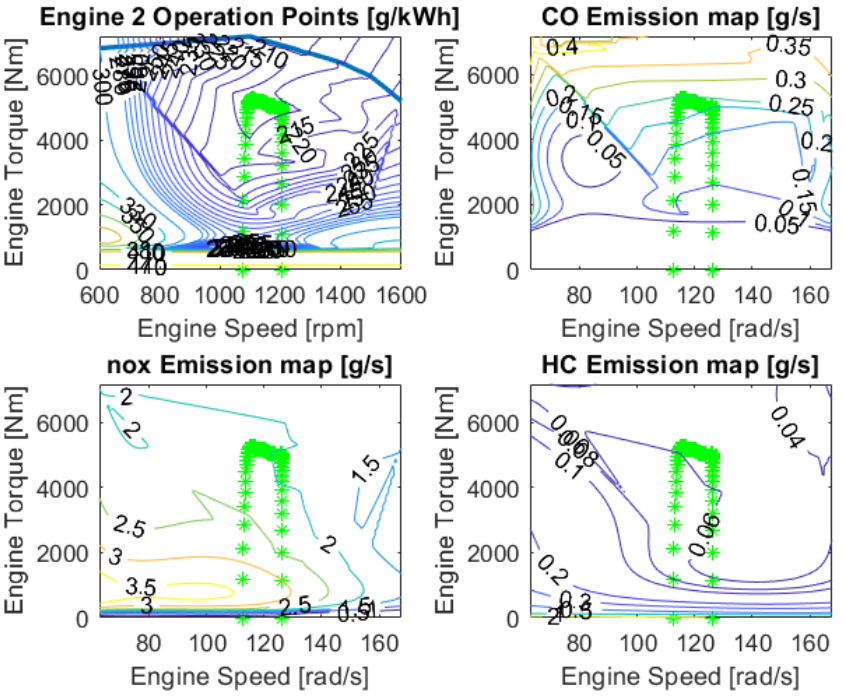

Figure N - 15 Operation points of Engine 2 in the hybrid ship with 940 kW EM

Figure N - 16, Figure N - 17 and Figure N - 18 present the SOC and voltage variations of the ESS. Those figures illustrate that the rule-based controller can manage power flow in the system and maintain the SOC within a specific range so that the battery ESS is not overcharged or completely drained.

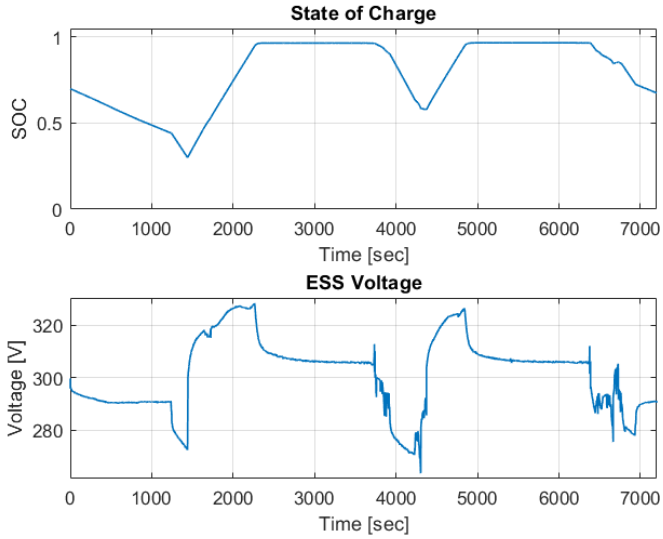

Figure N - 16 Proposed hybrid ship with 160kW EM: ESS State of charge and voltage

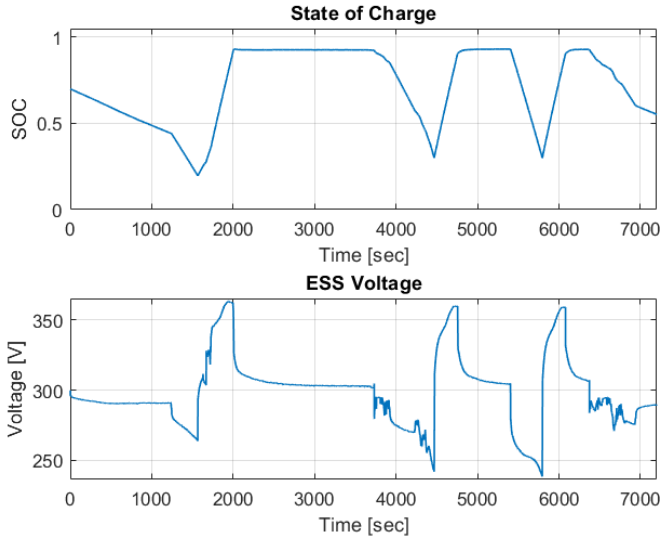

Figure N - 17 Proposed hybrid ship with 402kW EM: ESS State of charge and voltage

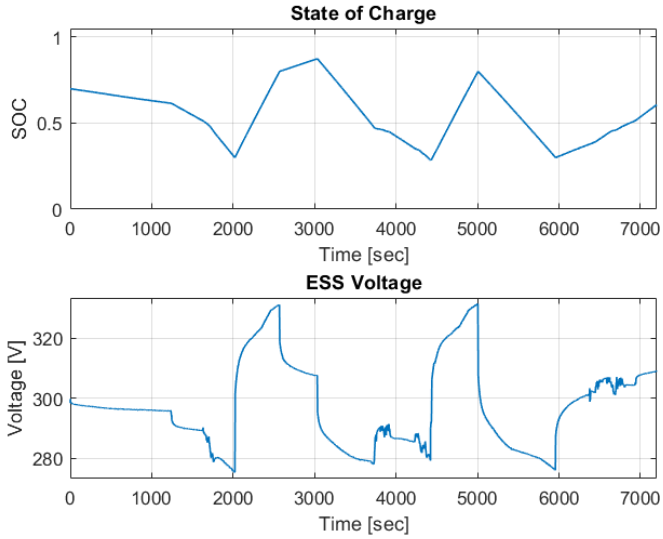

Figure N - 18 Proposed hybrid ship with 940kW EM: ESS State of charge and voltage

Figure N - 19, Figure N - 20 and Figure N - 21 presented are the output torques from the engines and motors. For low DOH powertrain shown in Figure N - 19, the EM operates as an engine peak shaving and assistant device. The main propulsion power comes from the engine. With the increase of the DOH, the EM becomes more and more important in propulsion. The vessel operates similar to a pure electric ship as long as the stored energy in the ESS is sufficient. The EM also charges the ESS more aggressively than the low DOH vessel, which may affect the life of the battery ESS.

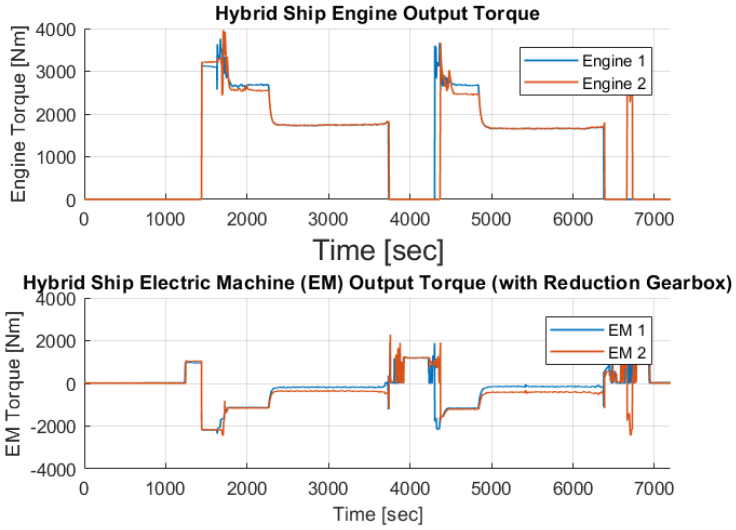

Figure N - 19 Proposed hybrid ship with 160 kW EM: engine and EM output torque

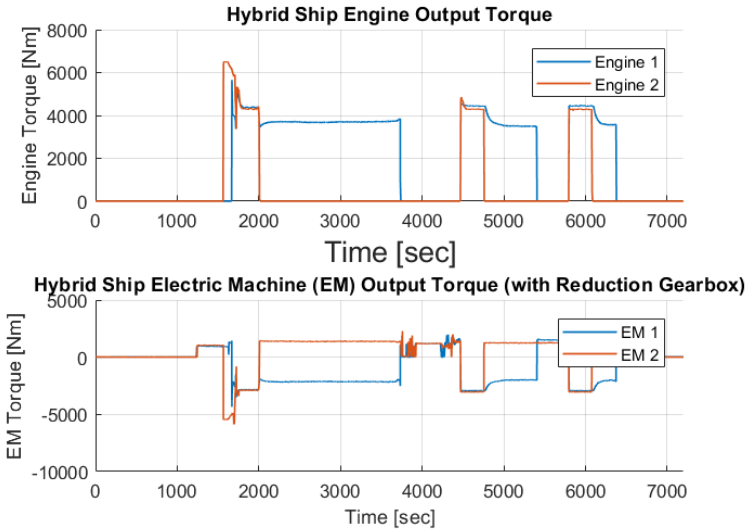

Figure N - 20 Proposed hybrid ship with 402 kW EM: engine and EM output torque

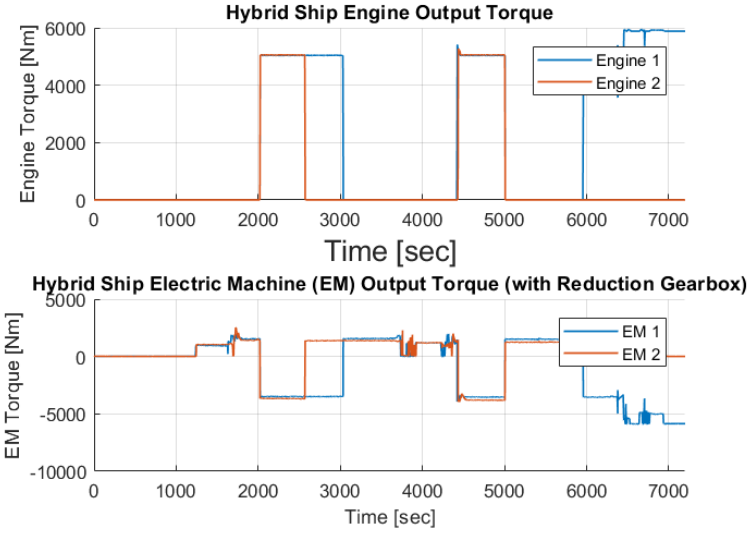

N8.

Figure N - 21 Proposed hybrid ship with 940 kW EM: engine and EM output torque

CONTINUING WORK

The additions of the battery ESS and the parallel hybrid electric powertrain system add considerable freedom and flexibility to the control of the full hybrid electric propulsion system. The true globally optimal operation of the hybrid electric powertrain system can only be accomplished through the "exhaustive" dynamic programming (DP) operation optimization over the ferry's operation cycle or a full back-forth crossing. The DP-based best operation benchmark can reveal the full potential of the technology to allow the optimal control strategies for the hybrid electric powertrain system to be derived. This will be the next step of our study.

Different degree of hybridization leads to different GHG emissions and lifecycle cost results, which warrant further study and optimization. Subsequently, optimization on powertrain component sizes and impact of the optimization on fuel economy and lifecycle cost of the ship will be investigated, to form solid guidelines for future hybrid electric ferry design and development.

The hybrid electric propulsion system that has been proposed in this study has the ability to operate in series, parallel, and series-parallel hybrid modes. In real-time operation, the ship's power demands will vary to some degree from the acquired operation pattern used in this work. A real-time intelligent controller that can switch between different operation modes and dynamically control the powertrain system to maximize fuel economy and minimize emissions will be developed. Other hybrid electric powertrain configurations, such as the straightforward series hybrid is not discussed in this report. The economic benefits of the simple and more advanced powertrain system designs will be investigated.

ACKNOWLEDGEMENT

We would like to thank the extensive support from Bruce Paterson, François Cambron, Andre Bosveld, Cliff Provost, Igor Bagmet, Hugh Stainsby, and Dan Scott at BC Ferries. Financial supports and guidance from the Clean Transportation Initiative of Transport Canada are gratefully acknowledged.

REFERENCE

[1] Holtrop, J and Mennen, G.G, "An approximate power prediction method," *International Shipbuilding Progress*, pp. 166-170, 1982.

[2] J. Carlton, Marine propellers and propulsion, Butterworth-Heinemann, 2012.

Appendix O. Case Study for Klitsa - Modelling and Simulation of Hybrid Electric Ships with AC Power Bus

ABSTRACT

Ferries are essential transportation tools for the west coast residents of Canada, as well as for about 10% of people of the world's population, who live on islands. However, the ferry fleet with a large amount of marine diesel fuel consumption bears high fuel costs and produces heavy GHG emissions, including PM, NO_x, SO_2, CO_2 and HC, emitted from the old cumbersome marine diesel engines. BC Ferries, one of the industrial partners of this project, has been providing transportation services for passengers and vehicles between various islands and the mainland in British Columbia since 1960. As the largest passenger ferry company in North America, it owns 47 operation lines, which has consumed 115.4 million litres of marine diesel at a cost of CAD$103.3 million in fiscal 2016. BC Ferries has been seeking new technologies for its future ships to reduce fuel costs and GHG emissions. This work focuses on the new propulsion system designs of Klitsa – one of the smaller ferries with short crossing time, a good candidate for pure electric or plug-in hybrid electric propulsion system.

Today many electrified ships operate on an AC power bus. As a well-proven technology that has been extensively adopted, the AC distribution will be still dominant for the shipboard power system in the near future. Combined with a battery ESS through a bi-directional DC/AC power converter, diesel generator sets of hybrid AC power systems can also operate at their maximum efficiency point at different load levels. Compared with conventional diesel-electric ship power systems, hybrid electric power systems with an AC power bus offer higher fuel economy, reliability, responsiveness, as well as reduced emission and maintenance cost. In addition, these systems do not have the notable fault protection challenge inherent in a hybrid DC power system. The fault of a DC power system could cause a surge of electric power in the circuit, damaging powertrain components. This work focuses on a dynamic model of shipboard AC hybrid power system, which is composed of six major components: three diesel-generator sets, a battery Energy Storage System (ESS), an AC power sources synchronizer and a bi-directional DC/AC power converter, using a ferry ship as the modelling platform. Due to the complexity of the system, effective modelling and simulation tools are essential for the design, analysis, optimization and evaluation of the hybrid electric propulsion system.

The power converter is modelled as a nonlinear dynamic average-value model to suit system-level studies. Each component model is parameterized using datasheet information from the manufacturers. The PID controllers are implemented for diesel engine speed governors, synchronous generators, Automatic Voltage Regulators (AVR), and the power converter controller. A rule-based supervisory controller is proposed to coordinate power-sharing among diesel-generator sets and the ESS. The research used a load profile acquired from M.V. Klitsa as the representative power cycle of the ferry. With the new models and control methods introduced in this work, power-sharing solutions among four power sources for four operation modes and voltage and frequency stabilization of the system AC bus have been generated. The simulation

results demonstrated the benefits of hybrid electric propulsion using conventional AC power bus and powertrain components.

O1. INTRODUCTION

The benefits of electrification and hybridization of the ship propulsion systems are intensifying the interest in All-electric ship technologies. By replacing direct mechanical couplings between the prime mover and propeller with an electrical network and integrating a large-scale battery ESS (BESS), all-electric ships with hybrid power systems can provide a significant reduction in fuel consumption, maintenance, and emissions as well as improved reliability, responsiveness and flexibility in ship layout [1]–[4].

From the view of the power distribution, an AC distribution or a DC distribution can be adopted for the shipboard hybrid power system [3]. Though the hybrid DC power systems are a promising technology for the long-run goal of maximizing energy efficiency, reliability and minimizing size & weight [4], their immature protection technology may hinder their wide application in large-scale shipboard power systems [5]–[7].

Today many electrified ships operate on an AC power bus. As a well-proven technology and extensively adopted in the shipboard, the AC distribution will be still dominant for the shipboard power system in the near future [6]. Combined with a battery ESS through a bi-directional DC/AC power converter, diesel generator sets of hybrid AC power systems can also operate at their maximum efficiency point at different load levels. A dynamic model of shipboard AC hybrid electric power system, consisting of three diesel-generator sets, a battery Energy Storage System (ESS), an AC power source synchronizer and a bi-directional DC/AC power converter, has been introduced.

Despite the advantages provided by shipboard hybrid AC power systems, the multidisciplinary nature and complex dynamic interactions among various components make it difficult to analyze new systems. Modelling and simulation are indispensable for their design, analysis, optimization and virtual evaluation. Specifically, being a virtual platform of a complex system, the system-level dynamic model of the shipboard hybrid AC power system should support:

- Energy consumption evaluation and design optimization. To take full advantage of fuel-saving prospects, each power source must be carefully chosen and an advanced energy management strategy should be designed to coordinate the power-sharing (and reactive power) among each power source.
- Power system stability analysis and control. The shipboard hybrid AC power system is a non-stiff power system with significant power electronic contents (like an isolated AC microgrid). A sophisticated control strategy is required to balance and keep the bus frequency and voltage stable in the presence of varying loads or mode transition.

This work focused on the dynamic modelling and simulation of shipboard hybrid AC power systems. Well-known dynamic models of each powertrain component are used and put together including three diesel-generator sets, a bi-directional DC/AC converter, a BESS, an AC power source synchronizer. The power converter is modelled as a nonlinear dynamic average-value model to suit system-level studies. Each component model is parameterized using datasheet information from the manufacturers. The PID controllers are implemented for diesel engine speed governors, synchronous generators, Automatic Voltage Regulators (AVR), and the power

converter controller. A rule-based supervisory controller is proposed to coordinate power-sharing among diesel-generator sets and the BESS. The research used load profile acquired from a local ferry ship, M.V. Klitsa, operated by the British Columbian Ferry Services Inc. (BCFS) in Canada as the vessel's power load cycle. With the new models and control methods introduced in this work, power-sharing solutions among four power sources for four operation modes and voltage and frequency stabilization of the system AC bus have been generated. The simulation results demonstrated the benefits of hybrid electric propulsion using conventional AC power bus and powertrain components.

O2. SYSTEM CHARACTERISTICS AND OVERVIEW

A shipboard hybrid AC power system concept is proposed for BCFS ferry ship Klitsa (as shown in Figure O - 1), which is a double-ended ferry that shuttles between two terminals with a sailing distance of about three nautical miles. The ferry is currently driven by two fixed pitch propellers, which are driven directly by two 250 kW diesel engines. Another 250 kW diesel engine-generator is on board to produce electric power for the vessel's hotel loads. Based on the total power produced by the presently installed propulsion engines, the proposed shipboard hybrid AC power system will have three 250 kW diesel generator sets, a 185 kWh BESS, a bi-directional DC/AC converter, an AC power source synchronizer and a supervisory controller. The single-line diagram of this system as shown in Figure O - 1. This hybrid electric power system architecture provides seven models of operation, as shown in Table O - 1. To maximize the performance of the hybrid power system, the optimal selection of operation modes depends upon various conditions, e.g. the battery SOC, speed profile and driving conditions. To reconnect power sources to the AC bus, the synchronizer model was used to measure the frequency, voltage and phase angle difference across the breakers being synchronized and close the breakers when these three variables on both sides are matched. Each component is dynamically modelled using the MATLAB SimPowerSystems and Simulink tools from MathWorks. In order to simplify the analysis, all models and variables are normalized to a per-unit basis.

Table O - 1: Hybrid AC power system operation modes

No.	Mode	Description
1	BES	Use electric energy from the battery, and no diesel generator is connected to the power system
2	HES1DG	Use electric energy from one diesel generator set. The battery can be charged or discharged
3	HES2DG	Use electric energy from two diesel generator sets. The battery can be charged or discharged.
4	HES3DG	Use electric energy from three diesel generator sets. The battery can be charged or discharged
5	DES1DG	Use electric energy from one diesel generator set without battery involved.
6	DES2DG	Use electric energy from two diesel generator sets without battery involved.
7	DES3DG	Use electric energy from three diesel generator sets without battery involved.

Here, BES represents Battery Electric ship mode; HES1DG represents Hybrid electric ship mode with one diesel generator connected to the power system, and DES1DG represents Diesel-electric ship mode with one diesel generator connected to the power system.

O3. COMPONENTS DYNAMIC MODELLING

O3.1. Model of Diesel Generator Sets

The diesel-generator set consists of a diesel engine and a synchronous generator coupled to the same shaft, an automatic voltage regulator (AVR) and a speed governor.

O3.2.1.Diesel Engines

In the hybrid power system, the response of the diesel engine set is slower compared with the battery power source with a power converter. The two key features of the diesel engine model are the time delay τ for a fuel command to the result in torque applied to the shaft and the dynamic time constant τ_c [2].

$$T_m(s) = e^{-\tau s}\frac{K_y}{1+\tau_c}Y(s) \quad \text{(O - 2)}$$

where T_m is the output torque of the engine, Y is the fuel-pump index (0-100%) and K_y is the torque constant. The value of time delay depends on the shaft speed n_m in [rps] and the number of active cylinders in the engine N.

$$\tau \approx \frac{1}{2n_m N} \quad \text{(O - 3)}$$

Table O - 2: Parameters of the diesel engine

Engine speed	1800 rpm
Engine standby power	255 kW
Engine prime power	233 kW
Nominal frequency	60 Hz
Stator reactance	2.55 (p.u.)
Engine inertial	1.54 kg·m^2

(a)

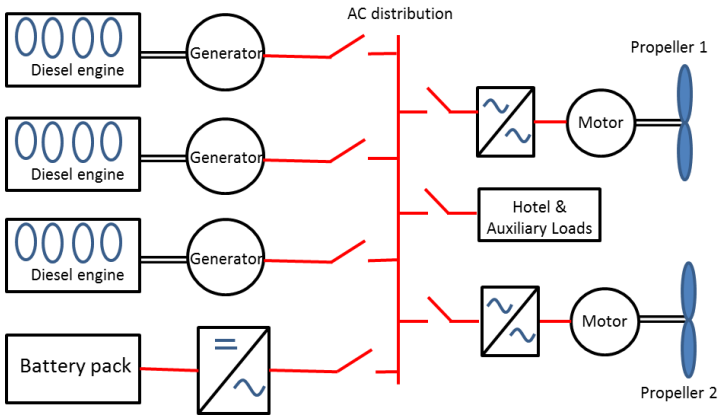

(b)

Figure O - 1: BCFS M.V. Klitsa and proposed shipboard hybrid AC power system

The dynamic constant can be evaluated by

$$\tau\_c \approx 0.9/(2\ 〚\ \pi\ n〛\_m\ ) \qquad \text{(O - 3)}$$

In addition, the brake specific fuel consumption (BSFC) map given by the manufacturer was used to calculate the fuel consumption of the diesel engine, as shown in Figure O - 2. The most efficient point is at about 80% of the rated power.

O3.2.2. Synchronous Generator

The third-order synchronous generator model is commonly used in the dynamic analysis of power systems, which can model the dynamics of the rotor and the excitation system. Magnetic saturation, hysteresis, eddy current, damping windings, the leakage reactance of armature winding, three-phase voltage asymmetry and higher harmonics are neglected [8], [9].

SimPowerSystems library contains a built-in simplified synchronous generator model, which represents the equations of the third-order synchronous generator model [10]. The parameters of the used generator are listed in Table O - 3.

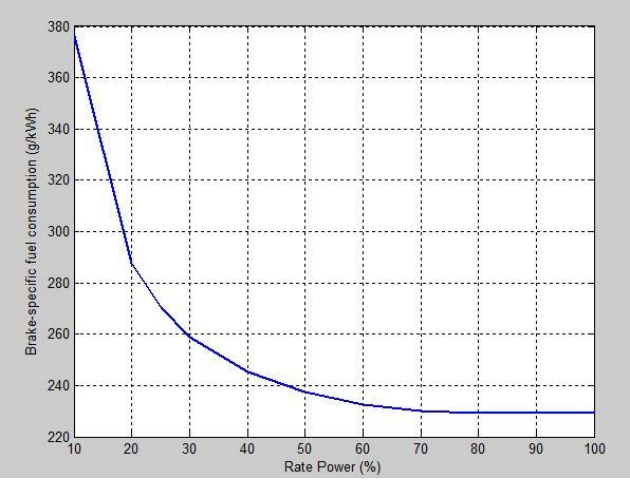

Figure O - 2: The diesel engine BSFC map

Table O - 3: Parameters of the synchronous generator

Parameter	Value
Nominal apparent power	250 kVA
Nominal active power	200 kW
Nominal line voltage	480 v
Nominal frequency	60 Hz
Nominal rotor speed	1800 rpm
Stator resistance	0.5 (p.u.)
Stator reactance	2.55 (p.u.)
Rotor inertia	3.65 kg·m^2

O3.2.3.Diesel Engine Governor and Automatic Voltage Regulator

The governor and AVR were designed to control the frequency and voltage of the bus bar respectively and were modelled as classic PID controllers in [11]. The parameters of PID controllers were tuned such that a reasonable frequency and voltage response for a step in active and reactive power demand were obtained. Due to the parallel operation of the three diesel generator sets, PID controllers with droop were used to achieve equal load sharing. The diagram of the diesel engine governor is shown in Figure O - 3.

O3.2. Model of Bi-directional DC/AC Converter

A bi-directional DC/AC converter is used to incorporate the BESS into the three-phase AC power system. Several methods have been developed to derive the models of this power converter including detailed switching models and average-value models. These models are prominent for optimal energy management of the AC power system. Detailed switching models are more complicated and require very small sample time, thus, they are extremely time-consuming for large

power system simulation. Average models can be used to make the system-level simulation faster while preserving the average voltage dynamics [12].

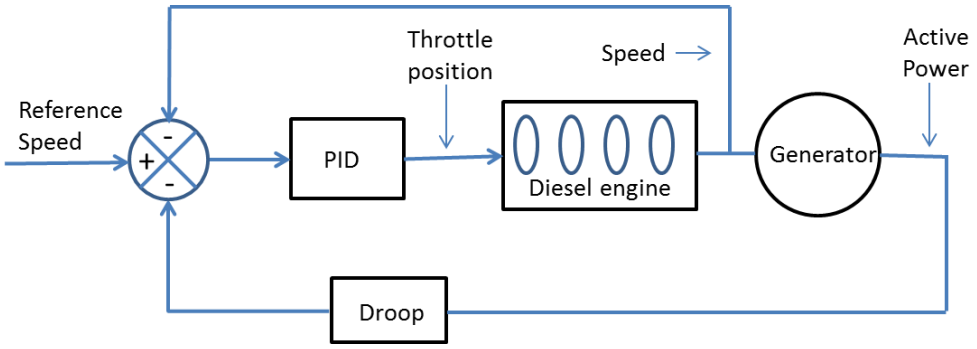

(a)

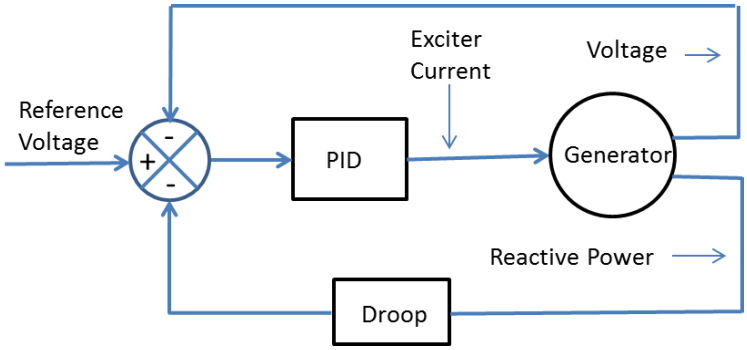

(b)

Figure O - 3: (a) the model of the diesel engine governor (b) the model of the automatic voltage regulator

Depending on the operation mode of the hybrid AC power system, the power converter should operate in different control modes. In BES operation mode, only the BESS powers the whole system. The voltage and frequency of the AC bus should be formed by the power converter, which works in voltage and frequency (V-F) control mode [13]. For the other operation modes of the hybrid AC power system, the frequency and voltage of the AC bus are formed through the diesel generator sets and the power converter should operate in active and reactive power (P-Q) control mode. Thus, the BESS can absorb or inject real and reactive power into the AC bus through the power converter.

O3.2.1. V-F control mode

In the V-F control mode, the Voltage Source Converters (VSC) works as an ideal AC voltage source with a given amplitude v^* frequency ω^* and initial phase angle θ^0. The V-F control structure of the VSC is shown in Figure O - 4. The regulation of the VSC output voltage is achieved via two closed PI control loop on the variation of the reactive power. The outer loop is for voltage control ensuring steady-state reference voltage tracking performance while the inner loop is for current control providing fast dynamic compensation for system disturbances and improving stability.

O3.2.2. P-Q control mode

The VSC was used to feed active power and reactive power to the AC bus when it works in parallel with diesel generator sets, which form the three-phase AC voltage. The reference active power and reactive power setpoints are provided by the supervisory controller. The output active power and reactive power of the VSC can be determined by its voltage amplitude and phase angle [14], as stated in the following equations:

$$P = \frac{VE}{\omega L}\sin\delta i_q \qquad \text{(O - 4)}$$

$$Q = \frac{V^2}{\omega L} - \frac{VE}{\omega L}\cos\delta i_q \qquad \text{(O - 5)}$$

where V is the VSC output voltage amplitude, E is the AC bus voltage, L is the coupling inductance and δ is the phase angle between these two voltages. As δ is very small, the control of active power and reactive power flows are decoupled. The active power depends mainly on the phase angle and the reactive power depends mainly on the VSC output voltage amplitude.

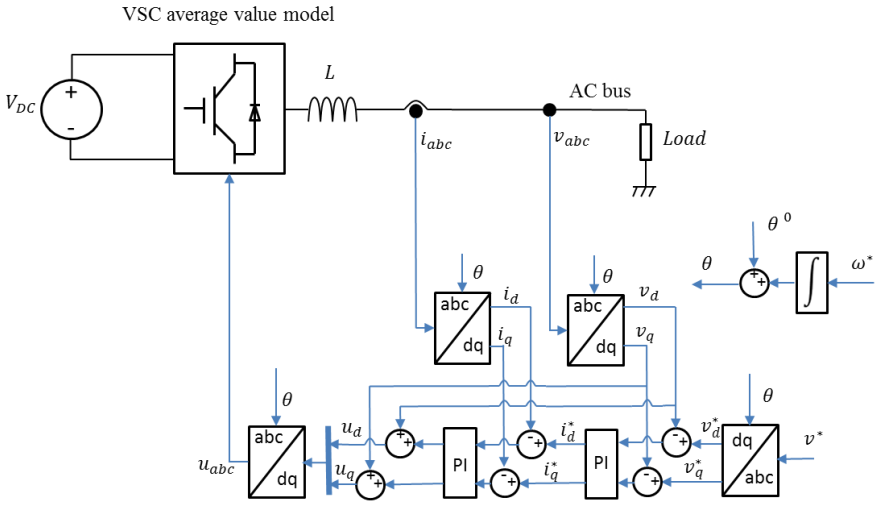

Figure O - 4: V-F control structure of the three-phase VSC in dq reference frame

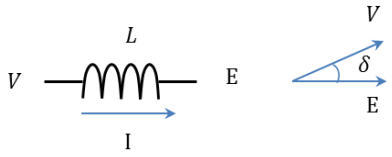

Figure O - 5: Active and reactive power flows

A two PI control loop was used to achieve the active power and reactive power regulation, as shown in Figure O - 6. Similar to the V-F controller, the outer of the P-Q controller is ensuring steady-state reference power tracking performance and the inner loop is improving the transit performance and stability.

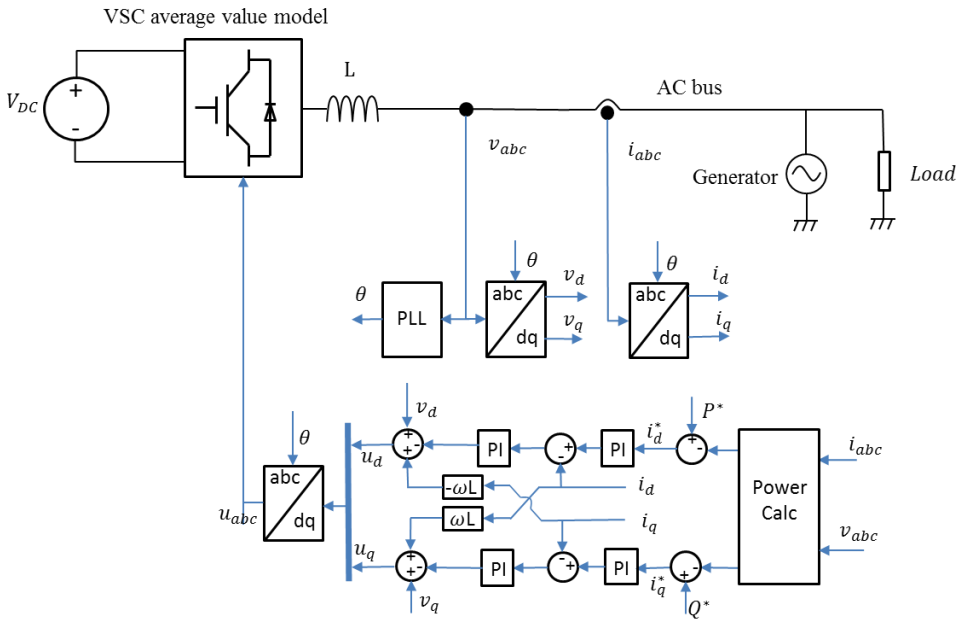

Figure O - 6: P-Q control structure of the three-phase VSC

O3.2.3. Simulation results

The three-phase VSC average value model with V-F and P-Q controller shown in Figure O - 4 and Figure O - 6 is simulated in MATLAB Simulink and SimPowerSystems. The parameters of the studied converter are given in Table O - 4. The operation mode and active power request of the power converter are shown in Figure O - 7. The converter operation mode changes from P-Q mode to V-F mode at T = 4 s and back to P-Q mode at T = 8 s. The direction of the converter active power request changes at T = t. Figure O - 8(a) shows the power output of the converter can follow the power request very well. The AC bus phase voltage RMS and frequency are both maintained stable when operation mode of the converter are changed and direction of power flow is altered, as illustrated in Figure O - 8(b) and Figure O - 8(c).

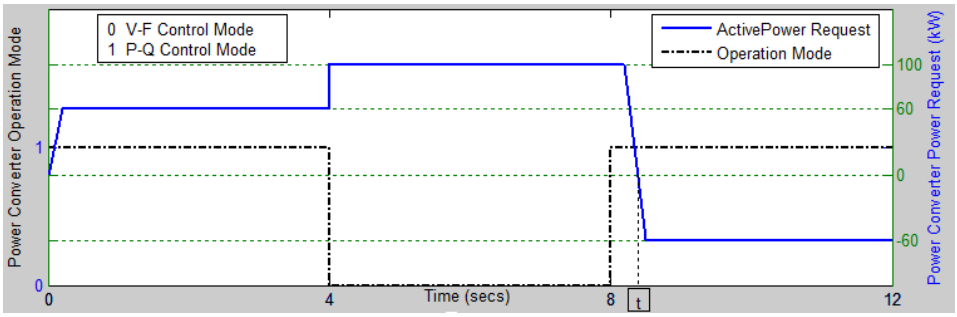

Figure O - 7: Operation mode & power request of the power converter

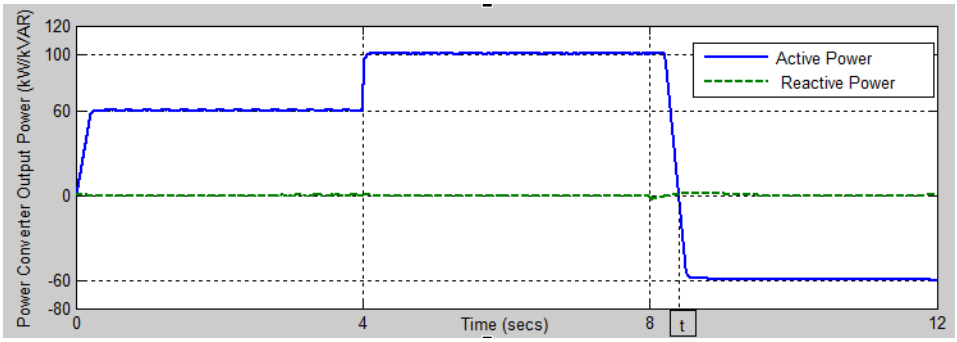

(a)

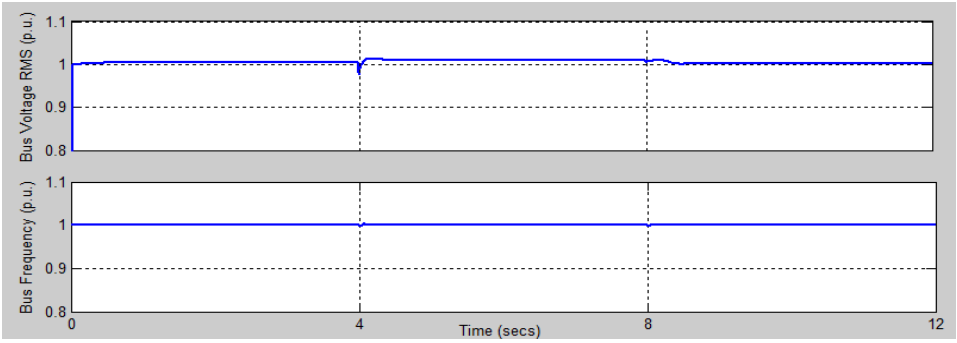

(b)

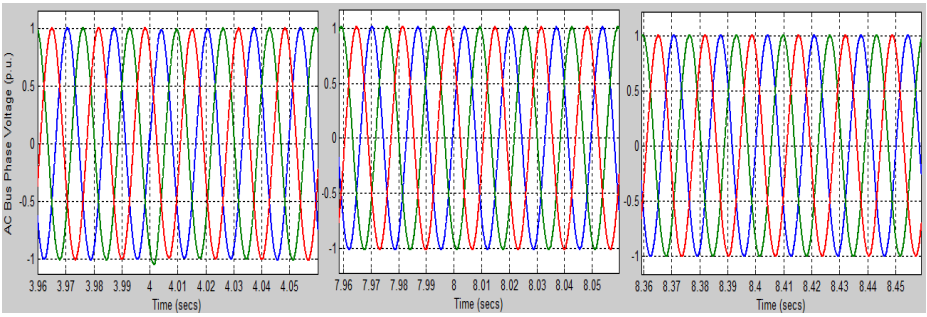

(c)

Figure O - 8: (a) The output active and reactive power of the power sources, (b) AC bus phase voltage RMS and frequency, (c) AC bus three-phase voltages waveform at T = 4s, 8s and t.

Table O - 4: Parameters of the power converter under study

Parameter	Value
Coupling inductance L	900 µH
Three-phase AC load	100 kW
DC voltage	805 v
AC generator Nominal frequency	60 Hz
AC generator Nominal line voltage	480 v

O3.3. Battery Model

For using within the dynamic simulation of the hybrid power system, the battery model should accurately represent the I-V performance and state-of-charge (SOC) without excessive simulation times. The electrical battery model is the best choice to satisfy this requirement compared with the electrochemical and mathematical battery model. There are six types of electrical battery models, specifically: simple models, Thevenin-based models, impedance-based models, runtime-based models, combined electrical circuit-base models and generic models [15]. The generic model is used widely in many applications and was chosen in this work.

The generic model, shown in Figure O - 7, uses a controlled voltage source in series with a constant resistance. The charge and discharge cycle have different characteristics and their controlled voltage source are described by the following equations [15]:

$$E_{discharge} = E_0 - K \cdot \frac{Q}{Q-it} \cdot i^* - K \cdot \frac{Q}{Q-it} \cdot it + A \cdot \exp(-B \cdot it) \qquad (O - 6)$$

$$E_{charge} = E_0 - K \cdot \frac{Q}{0.1 \cdot Q-it} \cdot i^* - K \cdot \frac{Q}{Q-it} \cdot it + A \cdot \exp(-B \cdot it) \qquad (O - 7)$$

where, E_{batt} is the open circuit voltage (V), E_0 is constant voltage (V), K is the polarization resistance (Ohms), i^* is the low frequency current dynamics (A), Q is the maximum battery capacity (Ah), A is the exponential voltage (V), and B is the exponential capacity (Ah^{-1}).

The parameters of this model can be extracted the form manufacturer's data sheet. The parameters of the BESS and the cell model are shown in Table O - 5 and Table O - 6 respectively. Without considering the cell imbalance, the parameters of the BESS can be easily calculated using this table. The generic battery model is shown in Figure O - 9.

Table O - 5: The BESS characteristics

Parameter	Value
Nominal voltage	805 V
Rated capacity	322 Ah
Internal resistance	17.86 mΩ
Fully charged voltage	925 v
Continuous discharge current	3 C
Continuous charge current	1 C
Continuous discharge power	744 kW
Continuous charge power	257 kW
Cells in parallel	140
Cells in series	250

Table O - 6: Parameters of a cell model

Parameter	Value
Nominal voltage	3.22 V
Rated capacity	2.3 Ah
Internal resistance	10 mΩ
Fully charged voltage	3.7 V
Maximum capacity	2.3 Ah
Continuous charge current	1C
Nominal discharge power	2.3 A
Exponential zone	[3.4 V, 0.23 Ah]
Capacity at nominal voltage	2.07 Ah
Nominal ambient temperature	25 °C
Second ambient temperature	0 °C
Maximum capacity at 0°C	2.208 Ah
Initial discharge voltage at 0°C	3.45 V
Exponential zone at 0°C	[3.224 V, 0.23 Ah]

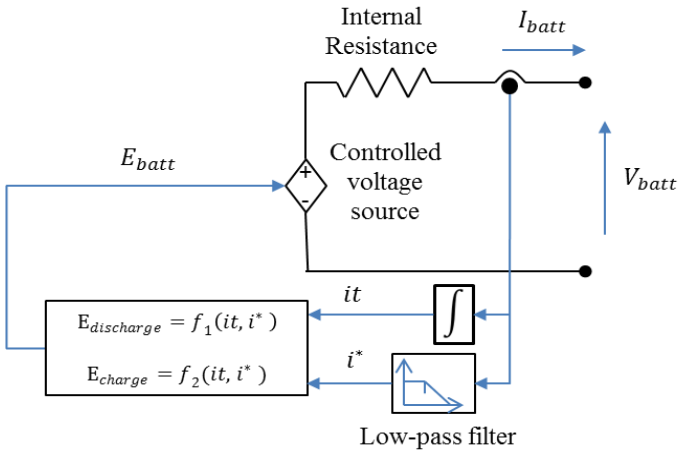

Figure O - 9: Generic battery model

O4. SYSTEM SIMULATION

The complete diagram of the shipboard AC hybrid power system is shown in Figure O - 8. A thermostatic control strategy, widely used in series HEVs energy management system, was applied to coordinate the power-sharing among diesel-generator sets and the BESS. The diesel generator sets will be turned on and power the system when the SOC reaches the lower threshold until the SOC reaches its upper threshold, as shown in Figure O - 7. The key tunable parameters of the thermostatic control strategy are the SOC bounds as shown in Figure O - 7. The SOC range for charge sustain mode (25%-28%) was applied. Without considering the failure of the BESS, only four operation modes are implemented in the supervisory controller. Considering the synchronization of power sources, three transition modes were constructed to achieve smooth transitions. The supervisory control strategy was implemented in Stateflow. The mode selection

command based on meeting the request of system load power, the SOC of the BESS and the synchronization signals, as illustrated in Figure O - 8.

To illustrate the capability of the hybrid AC power system model, the load profile of a local ferry was used to analyze the fuel consumption, power-sharing among power sources and frequency and voltage stabilization in different operation modes. The ferry sails between Mill Bay and Brentwood Bay terminals 16 times a day. The distance is about three nautical miles. The speed profile and power profile of a typical trip, as shown in Figure O - 9, were obtained by an onboard data acquisition system. The power profile is composed of four zones: ramping up, cruising, ramping down and harbour.

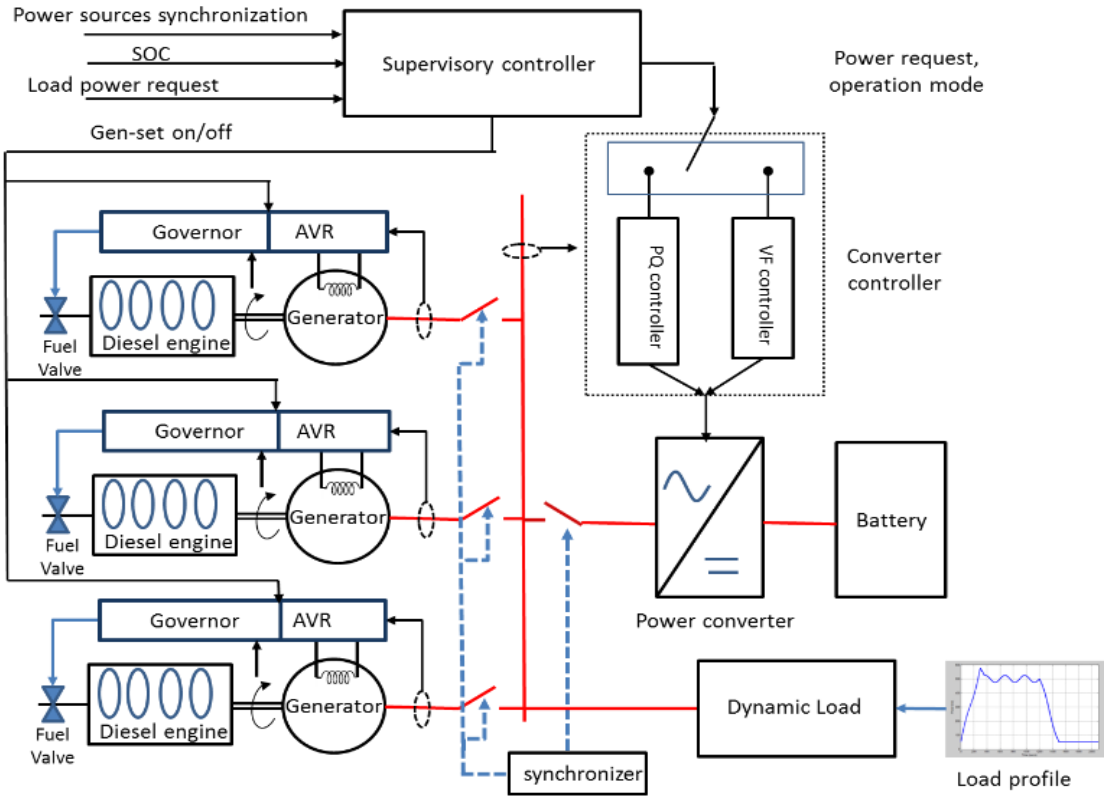

Figure O - 10: Diagram of the shipboard AC hybrid power system

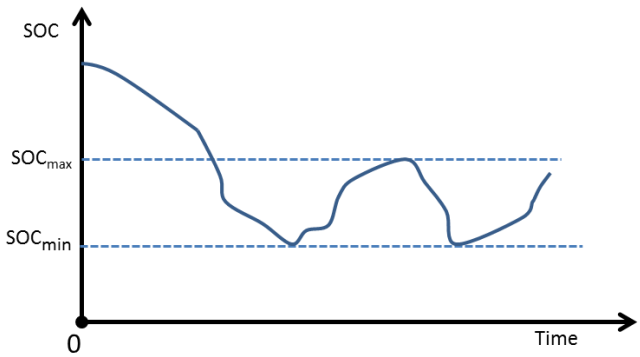

Figure O - 11: Thermostatic control

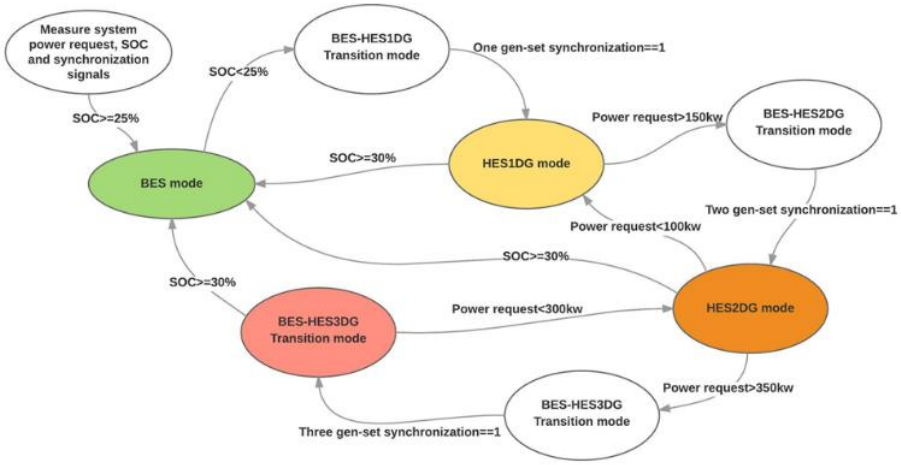

Figure O - 12: State transition diagram of the supervisory controller

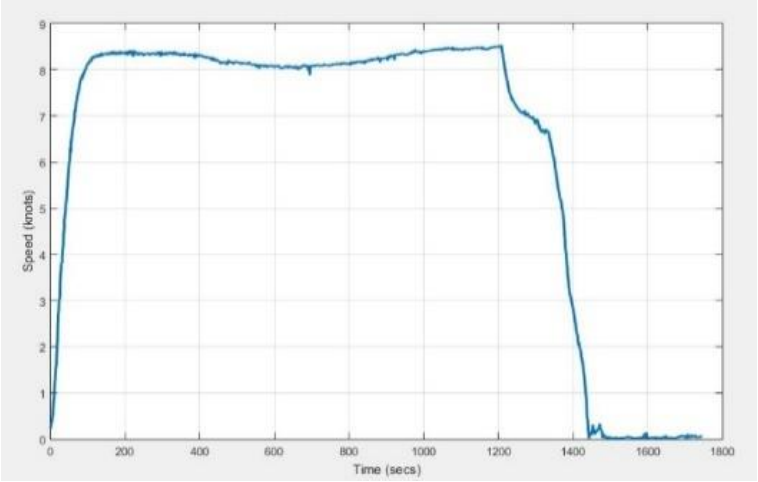

(a)

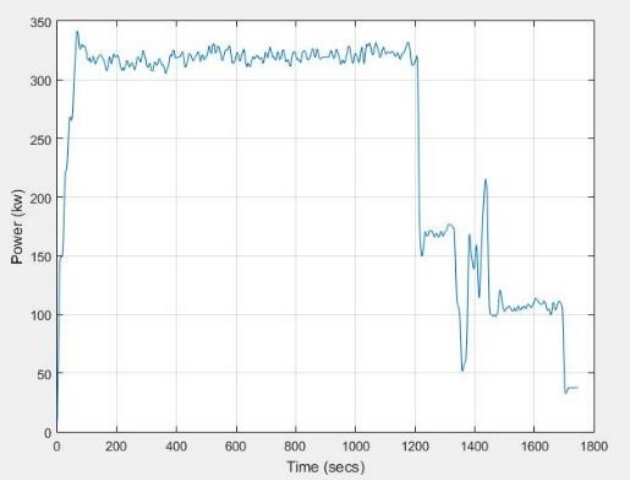

(b)

Figure O - 13: (a) Speed profile, (b) power profile

O4.1. AC Bus Voltage Stability

The influence on the AC bus voltage stability from the transition of system operation mode and the load power fluctuation was evaluated. In the ramping up zone, the increasing of the load power and changing of the system operation mode pose a challenge to the stabilization of the AC bus voltage when the initial battery SOC is near the low threshold.

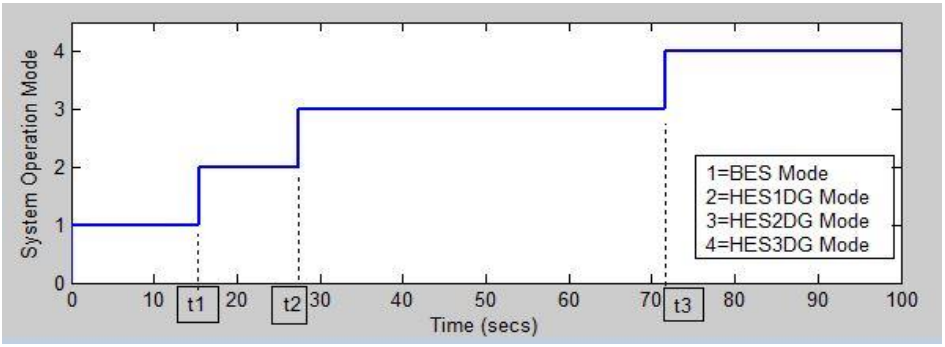

(a)

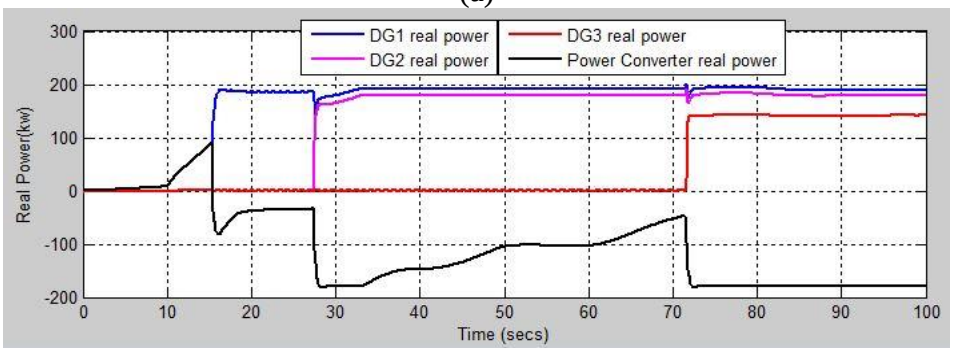

(b)

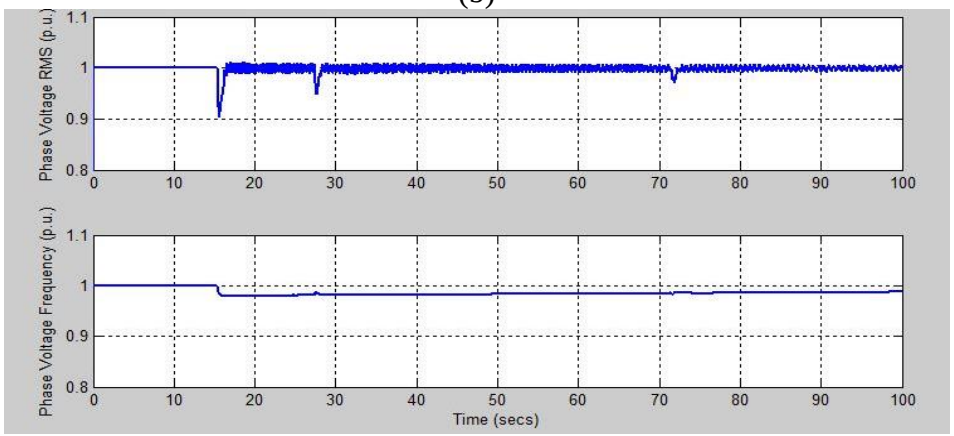

(c)

Figure O - 14: (a) System operation mode, (b) real power-sharing in power sources, (c) AC bus phase voltage RMS & frequency for the simulation of ramping up

The simulation results for ramping up are shown in Figure O - 14(a). At the start of the trip, the ferry operated in BES mode and the BESS is the only power source to supply AC power to the bus voltage. At T=t1, as the battery SOC decreased to the low threshold, a diesel generator set started to power the whole system and to charge the BESS. With the further increase of the load, the

available power of the active diesel generator set decreased to a predefined threshold at T= t2, then the second diesel generator set was turned on. Normally, two diesel generator sets can satisfy the given load profile. To evaluate the AC bus voltage behaviour in HES3DG mode, the third engine was connected to the bus at T=t3 intentionally. The system mode transition and the real power-sharing among power sources are shown in Figure O - 14 (a) and (b), respectively. The AC bus phase voltage RMS and frequency are both maintained stable with a droop characteristic as expected, as shown in Figure O - 10(c). The three-phase voltage waveform of the AC bus for three-mode transitions are shown in Figure O - 15.

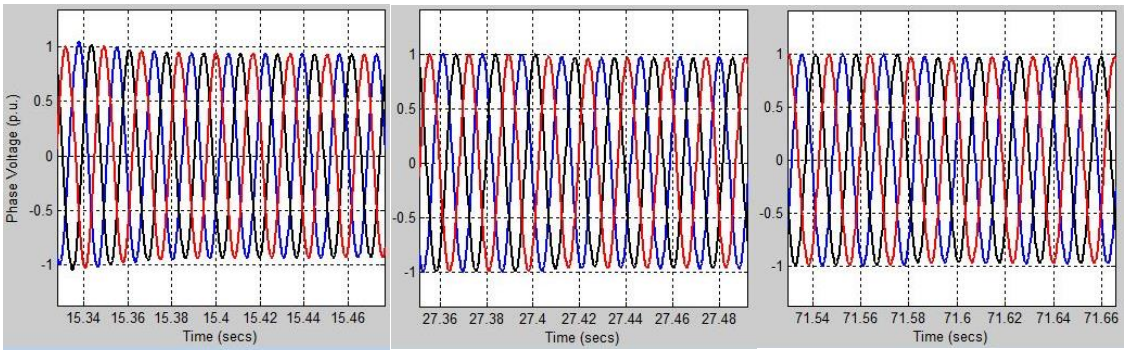

Figure O - 15: AC bus three-phase voltages waveform at T=T1, T2 and T3

O4.2. Load Sharing and Energy Consumption

To assess the fuel consumption of the shipboard hybrid power system, a simulation was executed over the given power load cycle. First, the initial battery SOC was set to 25.1%. Three operation modes were involved in this trip, as shown in Figure O - 16 (a). In the BES mode, only the BESS powers the whole system. Hence, the battery was discharged in this mode. In the HES2DG mode, two diesel generator sets are connected to the AC bus and both operate at the most efficient point. As the output power of these two generator sets is greater than the load power request, the rest of the energy can be fed to the BESS. When the load power decreases to a predefined threshold and the battery SOC is still under the upper threshold, the system will operate in HES1DG mode, which happens when the ferry arrived at the terminal. The power-sharing among the power sources and battery SOC over the trip are shown in Figure O - 16 (b) and (c), respectively. The fuel and net electric energy consumption of the hybrid power system for different initial battery SOC are shown in the table below. To better illustrate the fuel-saving benefit of the hybrid power system, the system was forced to operate as a conventional diesel-electric ship and the corresponding fuel consumption was presented in the table as well. Additionally, the cost of energy consumption was calculated by using the current local marine diesel fuel price ($91.9 per 100 litres) and electricity rate ($0.35 per kWh). The shipboard hybrid power system decreased the energy consumption cost by about 10%. The small difference in battery SOC is caused by the continuously functional ESS energy management system. The battery ESS maintained charge between the maximum and minimum allowed SOC during the ferry's continuous operations.

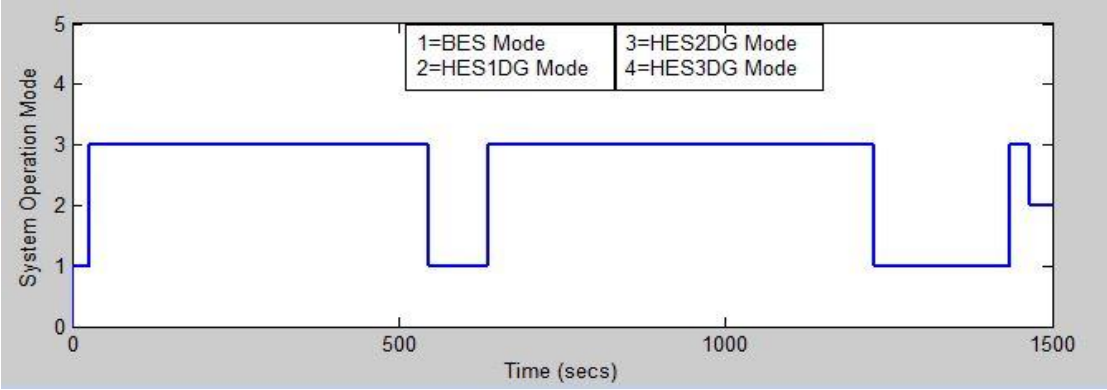

(a)

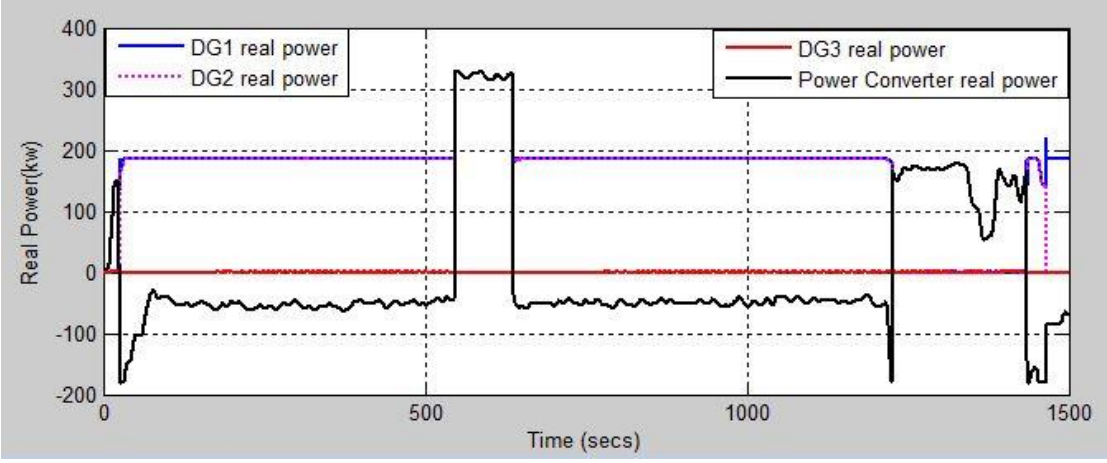

(b)

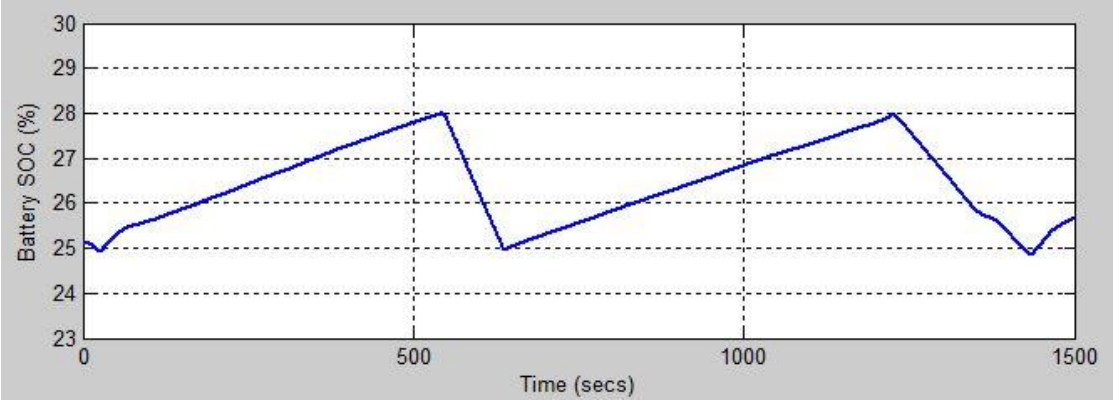

(c)

Figure O - 16: (a) System operation mode, (b) real power-sharing in power sources, (c) battery SOC for the simulation of full given load profile

Table O - 7: Energy consumption and cost comparison for the given load profile

	Fuel consumption (Liter)	Electricity consumption (kwh)	Energy consumption Cost ($)
Conventional diesel-electric ship	34.09	0	31.33
Hybrid ele. ship Initial SOC=25.1%	30.66	-1.05	27.84
Hybrid elec. ship Initial SOC=26%	29.63	1.77	27.85
Hybrid elec. ship Initial SOC=28%	28.31	5.36	27.89

O5. CONCLUSION

To study the benefits of fuel consumption, maintenance, and emission reduction, as well as improved reliability and responsiveness of an all-electric ship with a hybrid electric propulsion system and AC power bus, modelling and simulation of a dynamic shipboard three-phase AC hybrid power system, were carried out. The nonlinear dynamic average-value method was used to model the bi-directional DC/AC power converter by neglecting high-frequency switching behaviour to increase computational efficiency. Each component model was parameterized using the datasheet information from the manufacturers. A rule-based supervisory controller was proposed to coordinate the power-sharing among diesel-generator sets and the BESS. The study used the acquired load profile of a local ferry operated by BCFS as a testing platform, to carry out modelling and simulations of the ship with a proposed hybrid electric propulsion system. Results produced by the newly introduced modelling tool presented power-sharing solutions among four power sources in four operation modes with voltage and frequency stabilization of the system AC bus with improved energy efficiency and reduced emissions.

ACKNOWLEDGEMENT

The authors would like to thank Kevin Andersen for Klitsa ship operation data acquisition and acknowledge the support from Bruce Paterson, Bob Kearney, Bambino Da Silva at BC Ferries. Financial supports and guidance from the Clean Transportation Initiative of Transport Canada are gratefully acknowledged.

REFERENCES

[1] G. Seenumani, “Real-time Power Management of Hybrid Power Systems in All Electric Ship Applications,” p. 150.

[2] B. Zahedi and L. E. Norum, “Modelling and Simulation of All-Electric Ships With Low-Voltage DC Hybrid Power Systems,” *IEEE Trans. Power Electron.*, vol. 28, no. 10, pp. 4525–4537, Oct. 2013.

[3] R. Nilsen and I. Sørfonn, “Hybrid Power Generation Systems,” p. 9.

[4] J. F. Hansen, J. O. Lindtjørn, and K. Vanska, “Onboard DC Grid for enhanced DP operation in ships,” p. 8, 2011.

[5] L. Qi and J. Liang, “Design issues and practical application challenges of DC shipboard distribuiton system protection,” 2015, pp. 403–408.

[6] U. Javaid, D. Dujic, and W. van der Merwe, “MVDC marine electrical distribution: Are we ready?,” 2015, pp. 000823–000828.

[7] P. Cairoli and R. A. Dougal, “New Horizons in DC Shipboard Power Systems: New fault protection strategies are essential to the adoption of dc power systems.,” *IEEE Electrification Mag.*, vol. 1, no. 2, pp. 38–45, Dec. 2013.

[8] Zhijun Li, Yu Yang, and Xiujuan Bao, “Simulation and analysis of the third-order model of synchronous generator based on MFC,” 2009, pp. 4252–4256.

[9] E. Ghahremani, M. Karrari, and O. P. Malik, “Synchronous generator third-order model parameter estimation using online experimental data,” *IET Gener. Transm. Distrib.*, vol. 2, no. 5, p. 708, 2008.

[10] Z. Spoljaric and Miklosevic, “Synchronous Generator Modelling Using Matlab,” 2010.

[11] J. F. Hansen, “Modelling and control of marine power systems,” Norwegian University of Science and Technology, Trondheim, Norway, 2000.

[12] Z. Jankovic, B. Novakovic, V. Bhavaraju, and A. Nasiri, “Average modelling of a three-phase inverter for integration in a microgrid,” 2014, pp. 793–799.

[13] C. Chandorkar and R. Adapa, “Control of Parallel Connected Inverters in Standalone ac Supply Systems,” p. 8.

[14] T. Kalitjuka, “Control of Voltage Source Converters for Power System Applications,” p. 69.

[15] S. M. Mousavi G. and M. Nikdel, “Various battery models for various simulation studies and applications,” *Renew. Sustain. Energy Rev.*, vol. 32, pp. 477–485, Apr. 2014.

Appendix P. Case Study for Klitsa - Modelling and Simulation of Hybrid Electric Ships with DC Power Bus

ABSTRACT

Ferries are essential transportation tools for the west coast residents of Canada, as well as for about 10% of people of the world's population, who live on islands. However, the ferry fleet with a large amount of marine diesel fuel consumption bears high fuel costs and produces heavy GHG emissions, including PM, NO_x, SO_2, CO_2 and HC, emitted from the marine diesel engines. BC Ferries, one of the industrial partners of this project, has been providing transportation services for passengers and vehicles between various islands and the mainland in British Columbia since 1960. As the largest passenger ferry company in North America, BC Ferries owns 47 operation lines, which has consumed 115.4 million litres of marine diesel at a cost of CAD$103.3 million in fiscal 2016. To reduce fuel cost and GHG emissions, BC Ferries has been seeking new technologies for its future ships. This work focuses on the new propulsion system designs of Klitsa – one of the smaller ferries with short crossing time, a good candidate for pure electric or plug-in hybrid electric propulsion system.

Recently, research has increased in the area of ship electrification. Shipowners are now keen to deploy energy storage system (ESS) and electric propulsion in order to increase the overall efficiency and availability of their vessels. In this work, hybrid series and battery-electric power architectures are developed and investigated for short-range car deck ferries. Due to a lack of standardized drive cycles for marine vessels, real data was collected from BC Ferries' MV Klitsa and compared with the simulation results. An actual diesel engine fuel consumption map (FCM) was implemented in the model, and the optimal engine and battery size were obtained using the hybrid adaptive meta-modelling (HAM) optimization algorithm.

The proposed ship propulsion system is based on a DC power bus due to the extensive knowledge and experiences of DC bus based HEV/EV research, the more straightforward interface between DC power bus to larger battery ESS, and the availability of power electronic devices for this relatively smaller vessel. The cost-benefit and GHG emission analyses showed the benefits of the electrified ship proportion technologies.

Nomenclature

k_D, k_N, k_H	Emission factor in kg/litre where *D*, *N* and *H* subscripts denoting Diesel, Natural gas and Heavy fuel oil gas respectively	N_g	Number of diesel generators
FC	Fuel consumption function	P_{ij}	Power produced by the ith thermal unit in the jth time interval
$Fuel\ Cost$	Cost of the fuel consumed per litre	SOC	State of charge of a battery in percentage
$Electricty\ Cost$	Cost of the electricity in kWh	FCM	Fuel consumption map
i	ith diesel generator	SFC	Specific fuel consumption
j	jth time interval	T	Optimization time period
L_{Hotel}	Ship electric hotel load in the jth time interval	OE	Total maintenance, operation and investment cost function
L_j	Ship electric propulsion load in the jth time interval	TFC	Total fuel cost function
R	Overall ship resistance	V	Ship speed in knots
E_{BESS}	Stored electric energy in a battery energy storage system	ΔT_j	The jth time interval of the optimization time period
LF	Ship loading factor	$TC_{Hybrid\ series}$	Total cost associated with the hybrid series architecture
n	Number of years	$TC_{Battery\ powered}$	Total cost associated with the battery-powered architecture
n_t	Time in seconds	$Trips$	Number of voyages per day
n_G	Number of generators	k_{et}	Emission factor for fuel types
P_{ss}	Steady-state power	k_{BC}	Emission factor for BC Hydro Co

P1. INTRODUCTION

Maritime transport accounts for about 80% of world global trade by volume and 70% of global trade by value [1]. In addition, this mode of transportation is generally considered environmentally friendly when compared to alternative modes such as air, road and rail [2]. However, the shipping industry is continuously seeking new ways to increase its overall efficiency. Recently, this has been accomplished by introducing an integrated power system (IPS) and electric propulsion systems in commercial ships to replace conventional mechanical propulsion. The potential reduction in greenhouse gas (GHG) emissions due to the IPS architecture will aid the commercial shipping industry in meeting the strict and ever-evolving environmental regulations enforced by regional and national governments as well as the International Maritime Organization (IMO) [3].

Despite the relative environmental friendliness, ship emissions contribute a significant portion of global GHG emissions [4]. For example, it has been reported that the shipping industry contributes to 15% of global NOx emissions [5]. In response to this, IMO Tier 1 and 2 regulations have been introduced to limit on the allowable NOx emissions of diesel engines fitted in ships constructed after January 2011. This has prompted new research focused on the reduction of NOx emissions. In addition, many marine manufacturers have implemented new technologies such as exhaust gas recirculation (EGR) and selective catalytic reduction [6],[7],[8].

Electric propulsion is not a new concept and it has been applied for more than 100 years in ship design (albeit in few vessels). The river tanker Vandal is an example of an electrically propelled ship. Vandal was also the first vessel to be powered by a diesel generator, whereas up to that point most vessels had been powered by steam turbine generators [9]. In the 1980s, a revolution in solid-state and semiconductor switching devices occurred which made speed control of large electrical motors possible and, as a result, electric propulsion became a more feasible choice for ship designers. Initially, speed control of DC motors was introduced and later replaced by precise control of AC motors using sophisticated control mechanisms such as vector control. Synchronous and asynchronous motors were the most common choices for propulsion and they dominated propulsion and thruster applications for a long time. In general, asynchronous motors are used for applications below 5 MW and synchronous motors are used for higher power ratings along with voltage source inverters (VSIs).

A particular advantage of electric propulsion is its high efficiency of the electric propulsion motor at all speeds (85% to 95%). In contrast, diesel engines are designed to operate at rated power and rated speed that makes them inefficient in off-design conditions. In addition to the high efficiency at all speeds, maneuverability can dramatically increase due to the capability of electric machines to respond rapidly to abrupt changes in power demand. Without the diesel engine operating on a steady load and no speed reduction gears, electric propulsion also has lower acoustic noise emissions when compared to traditional mechanical propulsion, which makes them more environmentally friendly. For these reasons, electric propulsion has recently been implemented in many vessels, especially those that require high dynamic maneuverability, i.e. ice breakers [10]. Figure P - 1 illustrates the recent trend in the number of vessels worldwide, which are fitted with electric propulsion.

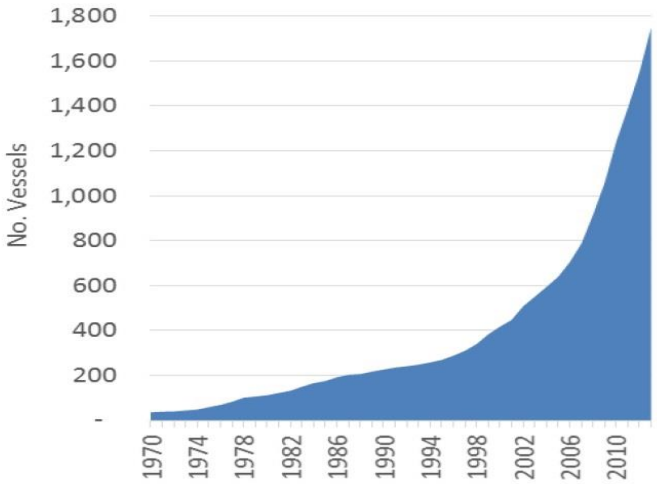

Figure P - 1 Trend in the number of electrically-propelled ships [9].

The broad electrification of ship power has resulted in the all-electric ship (AES) concept. In an AES, all shiploads, i.e. propulsion, steering, navigation systems and hotel loads, are satisfied with electric power. The power plants in these vessels are very similar to commercial land-based power plants consisting of AC power generation at a fixed frequency. However, the combination of the power plant and electric propulsion in an AES must satisfy many performance criteria such as fuel consumption, maneuverability, redundancy, GHG emissions, acoustic noise, capital and maintenance costs.

While there has been significant research on the simulation, optimization, and analysis of different hybrid electric terrestrial vehicle architectures [11]–[13], similar research for marine vessels is lacking. Moreover, relevant studies in this area either focus on overall system optimization and ignore component interactions or offer detailed (albeit isolated) analyses of different subsystems. This paper introduces a system-level model of sufficient detail to capture all component dynamics, facilitate design optimization, and support cost analyses. Moreover, due to a lack of standardized drive cycles for marine vessels, real data has been collected for small car-deck ferries. In the next section, a description of BC Ferries MV Klitsa, including its mechanical propulsion architecture, is given. In Section P4, hybrid-series powertrain and battery-electric powertrain architectures are proposed as replacements for the traditional mechanical architecture. These new architectures are modelled using MATLAB/Simulink and the results are validated using the data collected from the MV Klitsa. In Section P5, overall cost, GHG emissions, and architecture efficiency are compared with current mechanical systems and optimum battery and diesel generator sizes are selected. A discussion of the results is presented in Section P6.

P2. System Description And Data Collection

Ferries, unlike other marine vessels such as tug boats, have a very predictable load profile. They usually have a routine schedule and this makes them an attractive case study for modelling and investigation. In addition to having a predictable load profile, the MV Klitsa has other advantages such as available space for battery installation and the fact that it operates in sheltered waters. Lower environmental variability also makes the Klitsa an ideal choice for research on ship

hydrodynamics. The Klitsa is a car-deck ferry that was built in 1972 and operates between Brentwood Bay and Mill Bay on southern Vancouver Island [14]. It has a total installed power of 700 hp with a maximum speed of 10 knots. The passenger capacity of the ferry is about 150 people and it can carry 19 cars per voyage.

In terms of daily routine, the vessel makes 18 crossings of 5.7 km each, 8 in the forenoon and 10 in the afternoon. In addition, between the forenoon and afternoon crossings, there is a one-hour mid-day layover during which the vessel is secured in Brentwood Bay. More information about the ship is given in Table P - 1.

Table P - 1 MV Klitsa information [14].

Built:	1972, Vancouver
Overall Length:	47.55 metres (156')
Maximum Displacement:	450 tonnes
Car Capacity:	19
Passenger & Crew Capacity:	150
Maximum Speed:	10.0 knots
Horsepower:	700
Amenities:	Accessible car deck lounge

The Klitsa is currently equipped with two 14 litres Detroit Series 60 diesel engines, each coupled to an azimuthing thruster system. A separate 50 kW diesel generator provides electrical power for all other shiploads. After finishing its daily routine the ship is secured in Brentwood Bay, connected to shore power (cold ironing), and all engines are shut down [15].

The current powertrain architecture of the Klitsa is illustrated in Figure P - 2. This architecture is an example of a conventional propulsion system consisting of the prime mover(s), reduction gears, medium length shafts, and propeller(s). The prime mover rotates the shaft with medium speed and transfers the torque through the shaft via reduction gears in order to drive the propeller. The propeller converts torque to thrust at rotational speeds on the order of a few hundred RPM [16]. The 50 kW diesel generator is designed to operate at a constant speed and supplies electrical power at 60 Hz to the remaining shiploads.

A data acquisition system has been installed onboard the Klitsa in order to obtain the data required for simulation and model validation. The input torque, power, and speed of each propeller, ship velocity during transit, angle of the azimuthing thrusters, and output power of the 50 kW diesel generator have all been collected. These measurements enable a direct comparison between the current mechanical powertrain and the proposed powertrain architectures.

The data was collected over a two-month period and three representative mission profiles were identified as a good representation of the ship's operational variability. Figure P - 3 shows the low, medium and high load profile for the vessel engine. The engine maximum power varies between 170kW to 90kW for steady-state conditions. In the case of MV Klitsa, the engine power variation is mainly due to the time schedule and less impacted by environmental factors due to its operation

in sheltered water. Figure P - 5 illustrates the velocity of the ship corresponded to ship power shown in Figure P - 3. As expected, higher engine power corresponds to higher vessel speed and lower travel time.

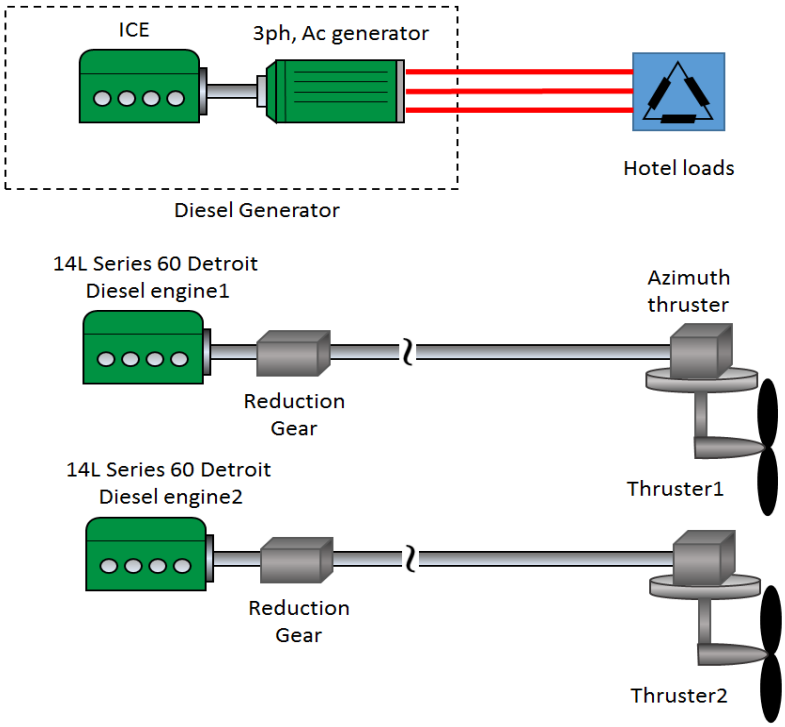

Figure P - 2 Current powertrain architecture for MV Klitsa.

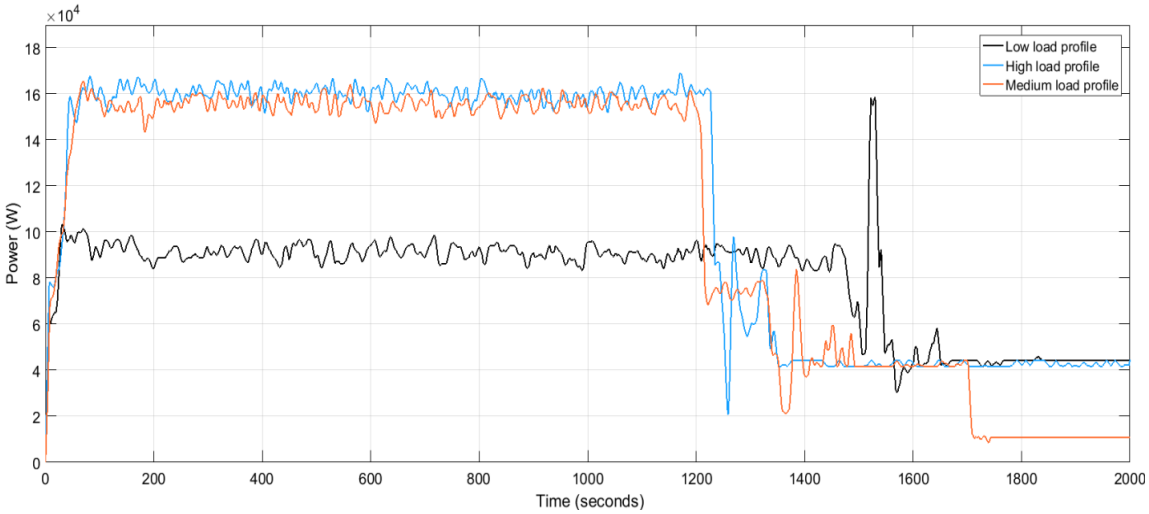

Figure P - 3 Diesel engine output power for low, medium and high load profile.

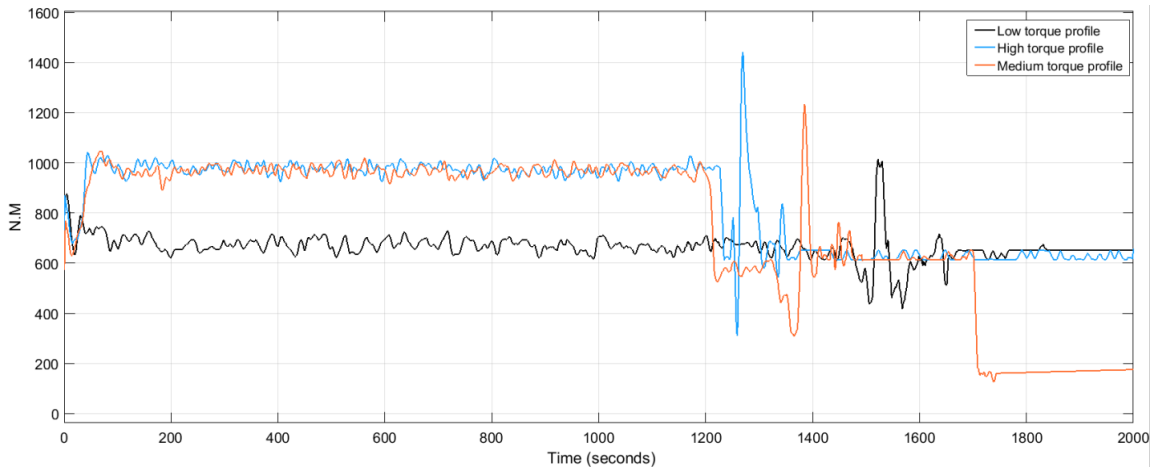

Figure P - 4 Diesel engine output torque for low, medium and high torque profile.

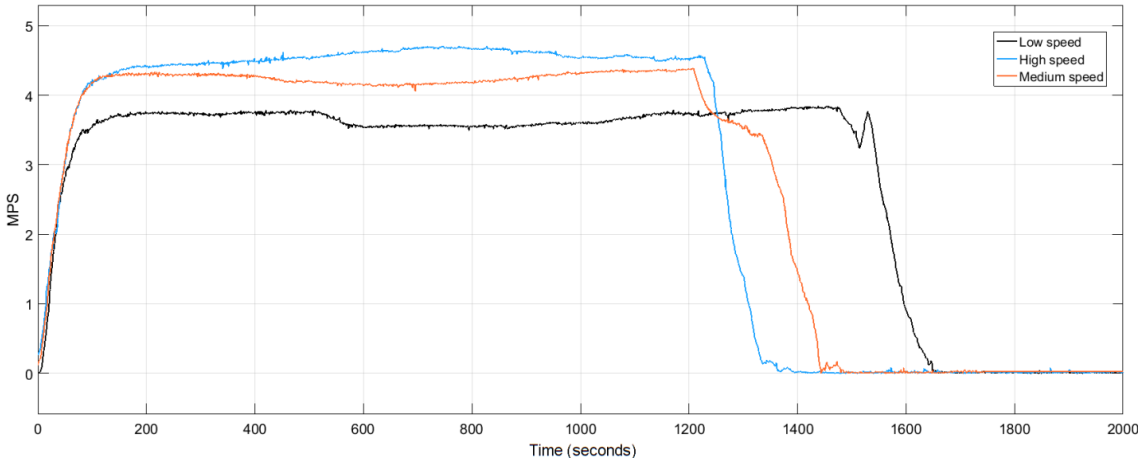

Figure P - 5 Ship velocity for low, medium and high speeds.

Engine torque pulses can be observed in Figure P - 4 when Klitsa nears either Mill Bay or Brentwood Bay. These pulses represent the short bursts of power required to maneuver the ship into alignment with the jetty at either terminal. While the Klitsa is pushing into the jetty (during loading and unloading), the engines are working at slightly more than their idle speed. The torque pulses that are characteristic of a vessel maneuvering into a jetty are of major significance since they often require oversizing the engines to accommodate for this transient load. This is one of the major advantages of hybrid electric propulsion since the plant can better tolerate transient loads.

P3. PROPOSED POWERTRAIN ARCHITECTURES

When designing a ship, the choice of a powertrain architectures *t* depends on the operational profile of the vessel. Finding the optimal architecture for a particular vessel, however, is generally not an easy task. Designers must take into account many factors like the availability of technologies at the time of construction and design flexibility. In this paper, hybrid-series and battery-electric architectures are investigated for application onboard the MV Klitsa while keeping the existing hull and propeller system.

P3.1 Series Hybrid Electric Powertrain Architecture

In this study, the two Detroit diesel engines and the 50 kW generator are replaced by a pair of 270 kW Caterpillar diesel generators [17]. These diesel generators are electrically connected to a common 1 kV DC bus by means of AC/DC converters. A DC distribution system was selected in order to facilitate the use of a battery energy storage system (BESS) and to be consistent with the approach of leading companies in advanced marine vessel propulsion like ABB and Siemens. A BESS is connected to the DC bus by means of an islanding bidirectional DC-DC converter. There are two common ways of incorporating a BESS into the power system, connected directly to the DC bus or connected indirectly by means of a DC/DC converter. In this paper, the BESS is connected indirectly using a bidirectional DC/DC converter. Two high-performance permanent magnet synchronous motors (PMSM) drive the Klitsa's azimuthing thrusters at reference (i.e. data) speeds and torques. The PMSM output torque and power illustrated in Figure P - 6 shows a close approximation between PMSM and diesel shaft torque and power. This ensures that the PMSM can provide enough power and torque for MV Klitsa to reach its desired speed.

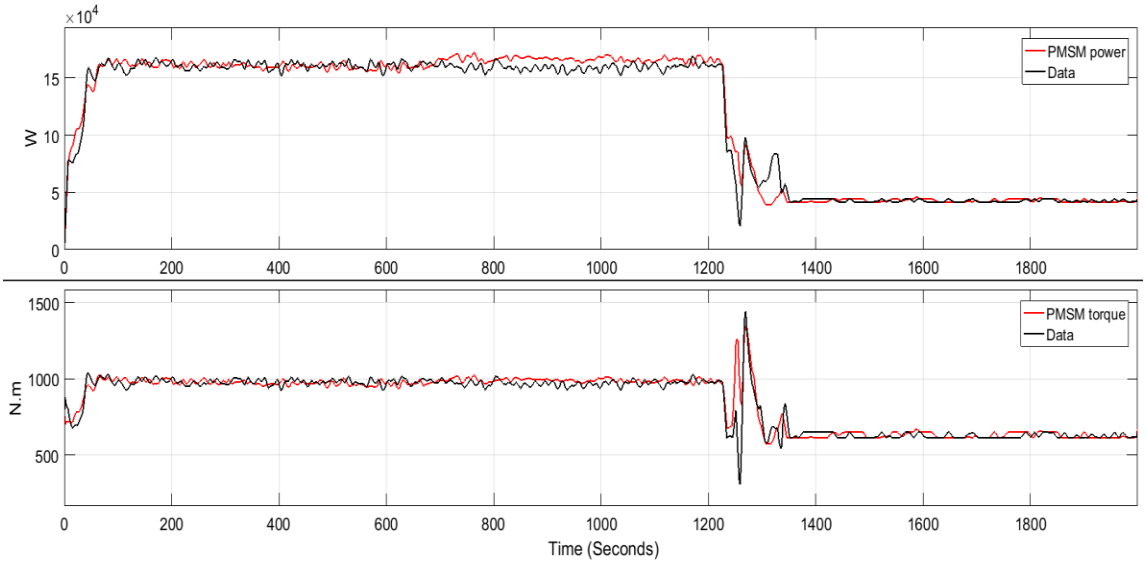

Figure P - 6 PMSM output power and torque.

The proposed hybrid-series architecture is depicted in Figure P - 7Figure P - 7. A great advantage of hybrid-series architectures, besides the relatively high efficiency, is flexibility in the location of equipment (for example, the lack of need for a shaft line allows the diesel generators to be placed wherever is ideal). The common DC electrical grid would provide several advantages for the Klitsa such as servicing shiploads with a smaller number of prime movers; this would result in noticeably improved fuel efficiencies over the low and medium speed ranges. Moreover, this design can reduce capital investment while maintaining a level of redundancy, which is an important design factor, especially in passenger vessels which are required to always have a redundancy of 50% of the total propulsion demand [18].

The hybrid-series architecture has higher efficiency at the low-speed range when compared to traditional mechanical propulsion; however, it introduces 5-15% [19] extra electrical losses due to electrical components such as electric motors, converters, generators, and transformers. Depending on the operating profile being considered, these losses at full power can outweigh the benefits of

switching to a hybrid-series architecture. Therefore, extra care must be taken before selecting a hybrid-series architecture for given ship design. This simple fact makes hybrid-series architectures unfavourable for applications with relatively constant operating profiles. However, there are still several other arguments one can make in favour of a hybrid-series architecture (lower noise level, better dynamic response).

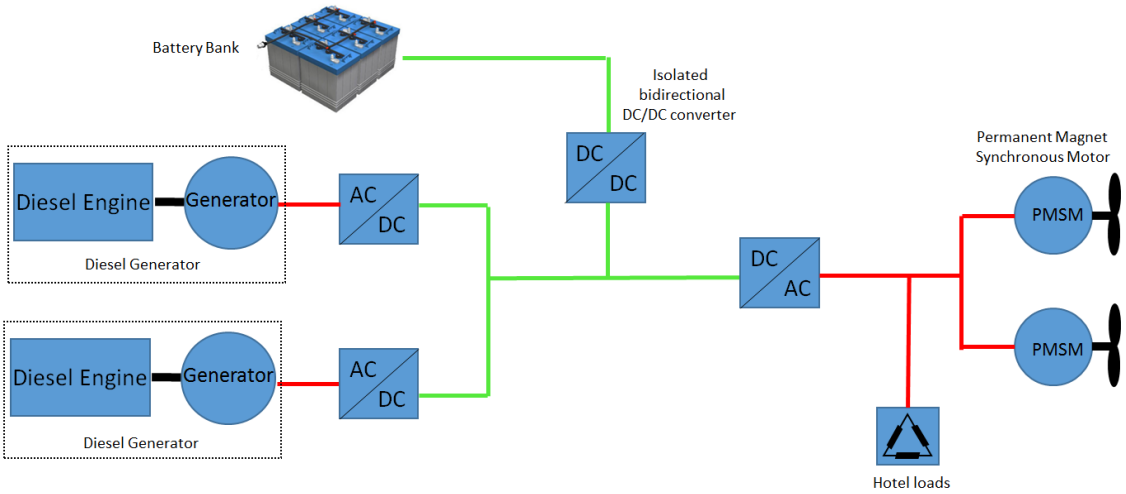

Figure P - 7 the proposed hybrid-series architecture.

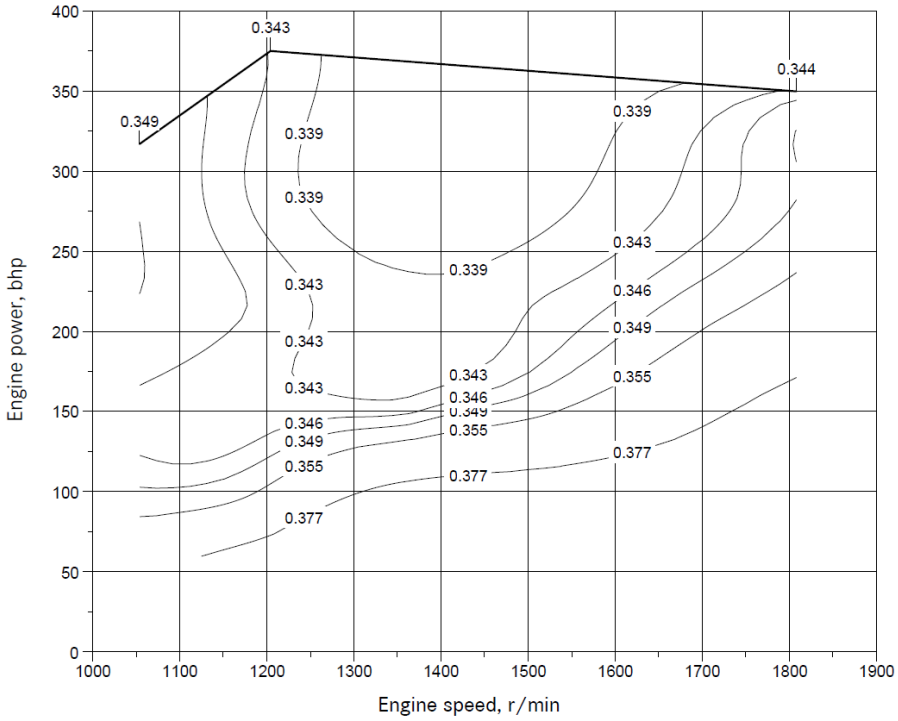

Figure P - 8 Fuel consumption map, [lbm/bhp-h] [20]

The real diesel engine FCM [20] shown in Figure P - 8 was implemented in the series hybrid electric model. Before implementation, the FCM was scaled up and checked in order to match with

the fuel consumption reported by BC ferries. Moreover, a 20% electrical and mechanical loss has been introduced in the model to represent the losses associated with electric propulsion systems.

The vessel speed was calculated to follow the reference speed using (7)

$$P_{prop} = P_s \times \eta_s = R_{ship} \times V \quad \text{(P - 1)}$$

where P_{prop} is actual propeller power, P_s is the shaft power, η_s is shaft efficiency, V is vessel velocity and R_{ship} is the total resistance of the vessel [21]. The total resistance of a vessel in calm waters can be expressed as the summation of four main resistance components: fractional resistance, wave-making resistance, eddy resistance, and air resistance. The wave-making and eddy components can then be combined into a single component called residuary resistance. A simple way to express the total resistance is given in ITTC-78 and [21]

$$R_s = C_{TS} \frac{1}{2} \rho V^2 S_s \quad \text{(P - 2)}$$

where C_{TS} is the total Klitsa resistance coefficient, ρ is the water density, and S_s is the wetted surface. C_{TS} was calculated using vessel data provided by the manufacturer and computational fluid dynamics (CFD) software [22].

P3.2 Battery Electric Powertrain Architecture

Battery-electric architectures have become quite popular in recent years. They offer significant advantages over other architectures such as higher energy efficiency, lower noise levels, and greater reliability. However, factors such as high capital cost, the need for proper cooling mechanisms, bulky and expensive fast-charging stations, and (in some cases) the cost of expanding the existing electrical grid have limited the implementation of this design. Despite this, the first battery-electric car ferry, the Norled AS MF Ampere, entered service in Sognefjord, Norway, in 2015 [20]. It has been estimated that it offsets the use of one million litres of diesel annually, which translates to emissions of 570 tonnes of carbon dioxide and 15 tonnes of nitrogen oxide when compared to conventional ferries in service on the same route [23].

In a battery-electric architecture, the BESS is the only primary source of energy and it services all shiploads (although a back-up diesel generator is usually installed to satisfy redundancy requirements). This makes the battery-electric architecture very similar to the architecture of the extended-range electric vehicles (EREV) that are currently available on the market. The BESS is the main source of energy like a diesel generator in hybrid-series architecture. However, a BESS has a very high efficiency over its entire operating range when compared to a diesel generator.

The proposed battery-electric architecture is illustrated in Figure P - 9. The BESS is coupled to a bidirectional DC/DC converter in order to charge the battery and step up the voltage. Similar to the series hybrid electric architecture, the distribution system can be either AC or DC. In the case of a DC distribution grid, electrical power is transferred to a DC/AC converter to provide power for big loads like propulsion. Smaller loads are connected to the grid by means of individual islanding converters. The current trend in the shipping industry is moving towards DC distribution systems because of the flexibility they offer in introducing energy storage, fuel cell, and solar technologies [10].

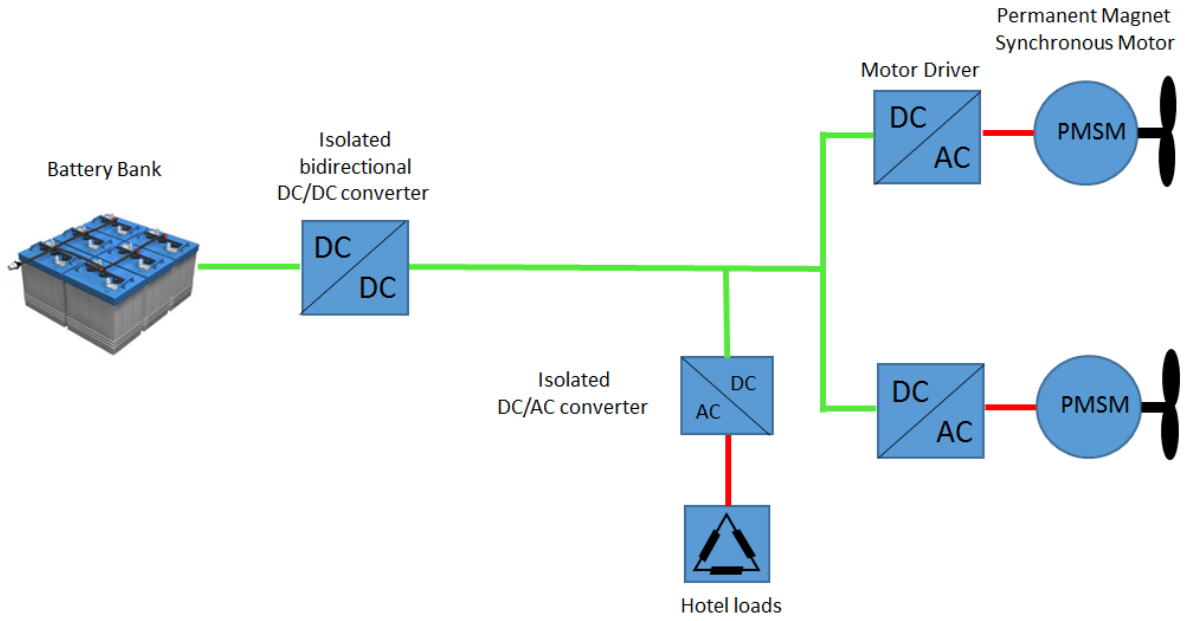

Figure P - 9 The proposed battery-electric architecture.

Nanophosphate lithium-ion battery cell was selected for the battery-electric architecture. This decision was made because Nanophosphate lithium-ion batteries have desirable features such as a long life, low per-cycle cost, the ability to operate over a wide temperature range, and the ability to support rapid charging. Table P - 2 shows the properties for a single AMP20 high power Nanophosphate lithium ion cell. In designing a BESS for the Klitsa, 130 kWh of energy must be cycled, for each transit, within the minimum and maximum state of charge (SOC) limits for the BESS, which are here assumed to be 40% and 90%, respectively.

The SOC defined as follows [24]

$$SOC\%(t) = \frac{Q_0 - \int_{t0}^{t} I_b(\tau)\, d\tau}{Q_0} \times 100 \qquad \text{(P - 3)}$$

where Q_0 is the battery charge capacity, $I_b(t)$ is the battery current, and $\int_{t0}^{t} I_b(\tau)\, d\tau$ is the battery charge delivered over the time interval $[t_0, t]$ with the battery assumed to be at full charge at the time t_0.

From the assumed 50% minimum SOC limitation, A total capacity of 2,340 kWh is required for nine consecutive transits at a cost of $600 per kWh [25]. This cost does not include additional expenses such as installation and inverter costs. These costs will be calculated separately in the next chapter. As detailed in Table P - 2, the life cycle for a lithium-ion battery at 50% depth of discharge (DOD) is estimated to be about 6,000 cycles. This means that the BESS lifetime with only two charges per day is about eight years before the battery capacity degrades to 80% of the original installed capacity.

Table P - 2: AMP20 Lithium Ion Prismatic Pouch Cell specifications[26].

Performance Characteristics	**Typical**
Capacity (minimum)	19.5 Ah
Voltage (Nominal)	3.3 V
Energy density	247 Wh/L
Weight	496 g
Specific Energy	131 Wh/kg
Cycle Life	
90% DOD Cycles @ 1C charge-discharge	>2,300 cycles
80% DOD Cycles @ 1C charge-discharge	>3,500 cycles
Operational Range	
Operating Temperature	-30°C to 55°C
Storage Temperature	-40°C to 60°C
Cell Dimensions (Millimeters)	**LxWxT 7.25 x 160 x 227**

In the case of a battery-electric architecture, all of the demand power is provided by the BESS. The BESS is charged using a fast charger facility installed onshore which is assumed to be located in Brentwood Bay. The battery size in this architecture should provide power for nine consecutive transits without the BESS dropping below 50% SOC. During the one-hour noon layover, the batteries have a chance to fully charge by the fast charger station.

P4. DIESEL GENERATOR AND BATTERY OPTIMAL SIZING

P4.1 Optimization problem

The general problem of optimizing component sizes can be expressed as a minimization problem in which cost (both capital and operational) and equivalent CO2 emissions are the objectives. The constraints on this problem are

$$\sum_{i=1}^{n_G} P_{Gi} + \sum_{j=1}^{n_{BESS}} P_{BESSj} = P_{ss} \quad \text{(P - 4)}$$

$$0 \leq P_{Gi} \leq P_{Gi_{max}} \quad \text{(P - 5)}$$

$$0 \leq P_{BESSj} \leq P_{BESSj_{max}}$$

where P_{Gi} is the power generated by the ith generator, P_{BESSj} is the power generated by the jth, and P_{ss} is the total, steady-state power demand of the vessel (which must be satisfied by the installed generators (n_G) and BESS (n_{BESS}). In the case of the Klitsa, the steady-state total generated power is about 370 kW and maximum output generator power is set to $P_{Gi_{max}} = 270$kW based on the available Caterpillar diesel generators. Constraints and formulation of the optimization problem are explained next.

P4.2 Constraints for MV Klitsa

The simulation model and optimization problem for MV Klitsa requires the following additional limitations to satisfy physical laws and safe operating requirements.

- Electrical power balance: The instantaneous generated power should be equal to the vessel power demand and losses so that

$$\sum_{j=1}^{T}\left(\sum_{i=1}^{k} P_{G_{ij}} + P_{BESS_j} - P_{Losses_j}\right) = \sum_{j=1}^{T}\left(\sum_{i=1}^{Ng} L_{p_{ij}} + L_{Hotel_j}\right) \quad \text{(P - 6)}$$

- Mechanical power balance: The motor output torque and speed must follow the reference (i.e., data) propeller torque and speed.
- Ship velocity: Using (P - 1), the variation in vessel speed during steady-state operation should not exceed 3 km/h. This ensures that the Klitsa can complete a given transit in the prescribed time.
- Generator capacity: The diesel generator output power should not exceed its maximum rating power.
- GHG emissions: The CO_{2e} emission should not exceed the CO_{2e} emissions of the current mechanical system.
- BESS power rating: The battery power rating must be sufficient to provide power for the worst-case scenario.

$$\sum_{j=1}^{n_{BESS}} P_{BESSj} = \sum_{i=1}^{n_G} P_{Gi} - \underbrace{\max}_{t}[P_{ss}] \quad \text{(P - 7)}$$

- State of charge: The BESS state of charge should not exceed its minimum and maximum limits of 50% and 100%, respectively.

P4.3 Total Cost Function Formulation

The total hybrid series architecture cost is the sum of the fuel costs of all generators and other expenses

$$TC_{Hybrid\ series} = n \times trips \times \sum_{j=1}^{n_t} \sum_{i=1}^{n_G} FC_{ij} \times Fuel\ Cost \times \Delta t_j + OE \quad \text{(P - 8)}$$

Information about the symbols can be found in the nomenclature. The fuel cost, component cost and other expenses (OE) are presented in Table P - 3. The total battery powered architecture cost is

$$TC_{Battery\ powered} = n \times Electricity\ Cost \times \sum_{d=1}^{365} \text{BESS}_{kWh-consumed_d} + OE \quad \text{(P - 9)}$$

Table P - 3 System costs.

Variable	Value
Inverter cost	0.21 $/Wdc [27]
Battery cost	600 $/kWh (Lithium Ion) [25]
Battery Installation labor	0.15 $/W [27]
Battery operation and maintenance	20 $/kW-yr [27]
300kW PMDC motor	$50000
Transformer	$5000
Fast charger station	$20000
Diesel fuel cost	1.121 $/L [28]
Diesel generator unit cost	Varies depend on size [29]
Diesel generator operation and maintenance	30 $/kW
Diesel generator Installation labor	50 $/kW
Electricity cost	Varies [30]

P4.4 Thermal Efficiency

The thermal efficiency of a heat engine is:

$$\eta = \frac{W_{out}}{Q_{in}} \quad \text{(P – 10)}$$

where W_{out} is the work done by the engine on its surroundings, and Q_{in} is the heat put into the engine. W_{out} is given by

$$W_{out} = \sum_{i=1}^{n} P_i \, \Delta t_i \qquad \text{(P - 10)}$$

and Q_{in} is:

$$Q_{in} = q_{\text{comb}} \sum_{i=1}^{n} m_i \qquad \text{(P - 11)}$$

where P_i is the engine power output during time step i, m_i is the mass of fuel consumed during time step i, and q_{comb} is the specific heat of combustion for a particular fuel which for marine diesel oil is about 41003.2 kJ/kg [31].

P4.5 Equivalent CO_2 Emission

GHG emissions can be calculated directly from the mass of fuel consumed by each engine. However, GHGs have different radiative forcing, which means that they have a different ability to absorb heat in the atmosphere; therefore, a different metric is required to take this effect into account. The global warming potential (GWP) measures the ability of these gases and is expressed as the ratio of each gas heat-trapping capacity relative to that for CO_2. Based on the United Nations Framework Convention on Climate Change (UNFCCC) [32] and the Intergovernmental Panel on Climate Change (IPCC) 4th Assessment Report [33] the GWP of three main gases are given in Table P - 4.

Table P - 4 Global warning potential for thee gases.

GHG emissions	CO_2	CH_4	NO_2
GWP	1	25	298

The equivalent CO2 (CO2e) emissions for marine diesel fuel is then calculated based on the emission factors given in [34]. In the case of a battery-electric architecture, the emission factor is calculated as follows. Since more than 90% of the electricity generated in BC is produced by hydroelectric generation, the emission factor for a battery-electric architecture is considerably lower than for hybrid-series architecture. Based on the information provided in [35] [36], the emission factor for BC Hydro and North American powerplants is, on average, about 15 g/kWh and 1031 g/kWh [30], respectively.

P5. Results And Analysis

P5.1 Component Interactions

One of the reasons for conducting a study on the MV Klitsa was to create a system-level model to explore the component interactions and interdependencies. Then, the behaviour of each component

can be cross-checked against real system results. Figure P - 10 illustrates the battery usage during transit as determined by a rule-based energy management strategy shown in Figure P - 13. Initially, the battery is charged at 100% of its capacity and then gradually discharged until the diesel generator provides all power required by Klitsa. When the generated power exceeds the demand power, the excess power flows back into the BESS and charges the battery. This follows from the formulation of the objective function that tries to minimize the SFC of the diesel engine during its operation by running the diesel generator at its rating power. The power profiles for different powertrain components are illustrated in Figure P - 11Figure P - 11 where demand power consists of the two propulsion loads and the hotel load. The summation of the BESS power, total losses and diesel generator power are equal to the total demand power and satisfy (P - 6). Figure P - 12 illustrates Klitsa velocity during steady-state conditions calculated by (P - 1). The accuracy of ship velocity significantly depends on the calculated resistance coefficient (C_{TS}) value of the ship. In case of Klitsa, this coefficient was calculated using CFD software.

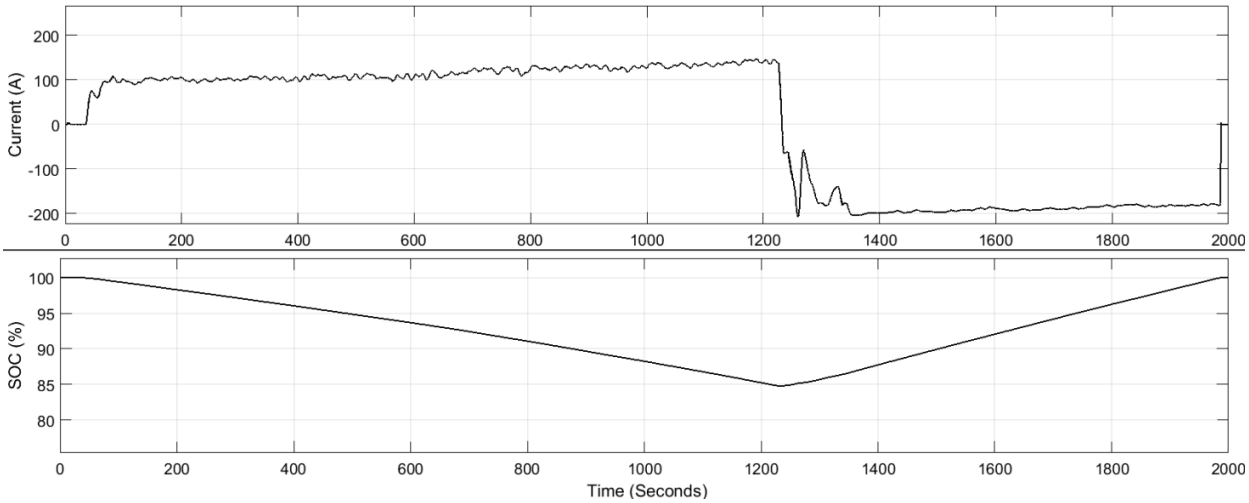

Figure P - 10 BESS SOC and current during a voyage.

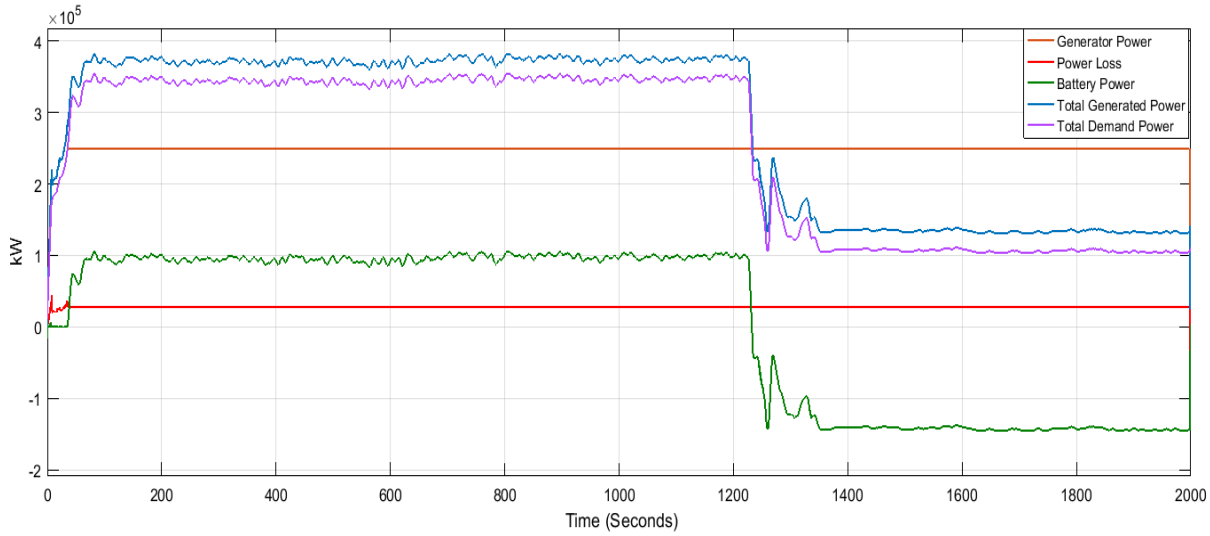

Figure P - 11 Different simulated component powers during a transit.

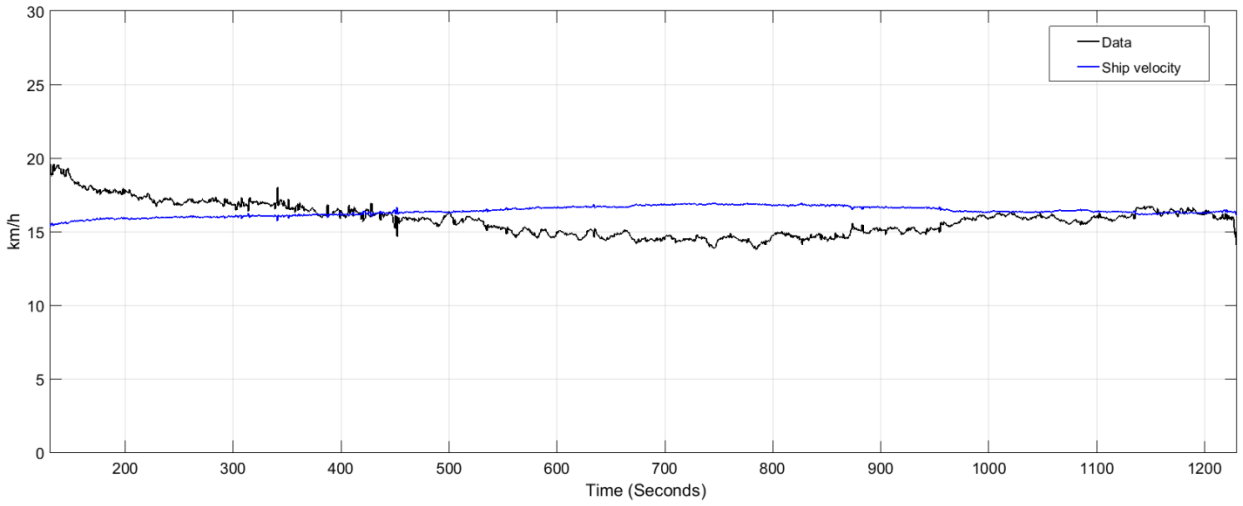

Figure P - 12 Simulated ship velocity during a transit.

P5.2 Optimal Battery and Engine Size

The HAM algorithm [37] was used to find the optimal size of the battery and diesel generators with respect to the cost and GHG emissions. HAM algorithm was selected due to expensive and time-consuming simulation calls. The HAM algorithm seeks to generate a cheap surrogate model (i.e., a metamodel) for the expensive objective and then proceeds to optimize over the surrogate. However, rather than choosing a single surrogate model, the HAM algorithm fits three distinct surrogates: a response surface model, a radial basis functions model, and a Kriging model. As the algorithm proceeds, the performance of these surrogates is dynamically assessed and the algorithm gradually begins to favour the best surrogate. The algorithm also alternates between performing a global search and a local search over-promising regions (in order to better resist getting caught in local optima). The HAM algorithm cost and GHG analysis for a 10-year period are now examined.

Table P - 5 Result of global optimization.

Generator 1 capacity (kW)	**Generator 2 capacity (kW)**	**ESS capacity (kWh)**	**Associated costs**
2.4261e+02	1.2447e+02	0	$4,780,386

Table P - 6 CO_{2e} emission analysis.

Different Powertrains	**Various Fuels**	**CO_{2e} Emissions (Tonnes)**			**CO_{2e} Reduction**
		Gen1+Gen2	BESS	Total	
Mechanical system	Diesel fuel	103,452	0	103,452	0
Series hybrid system	Diesel fuel	95,974.4	0	95,974.4	-7.23%
Pure electric system	Various fuels	0.0	142.8	142.8	-99.86%

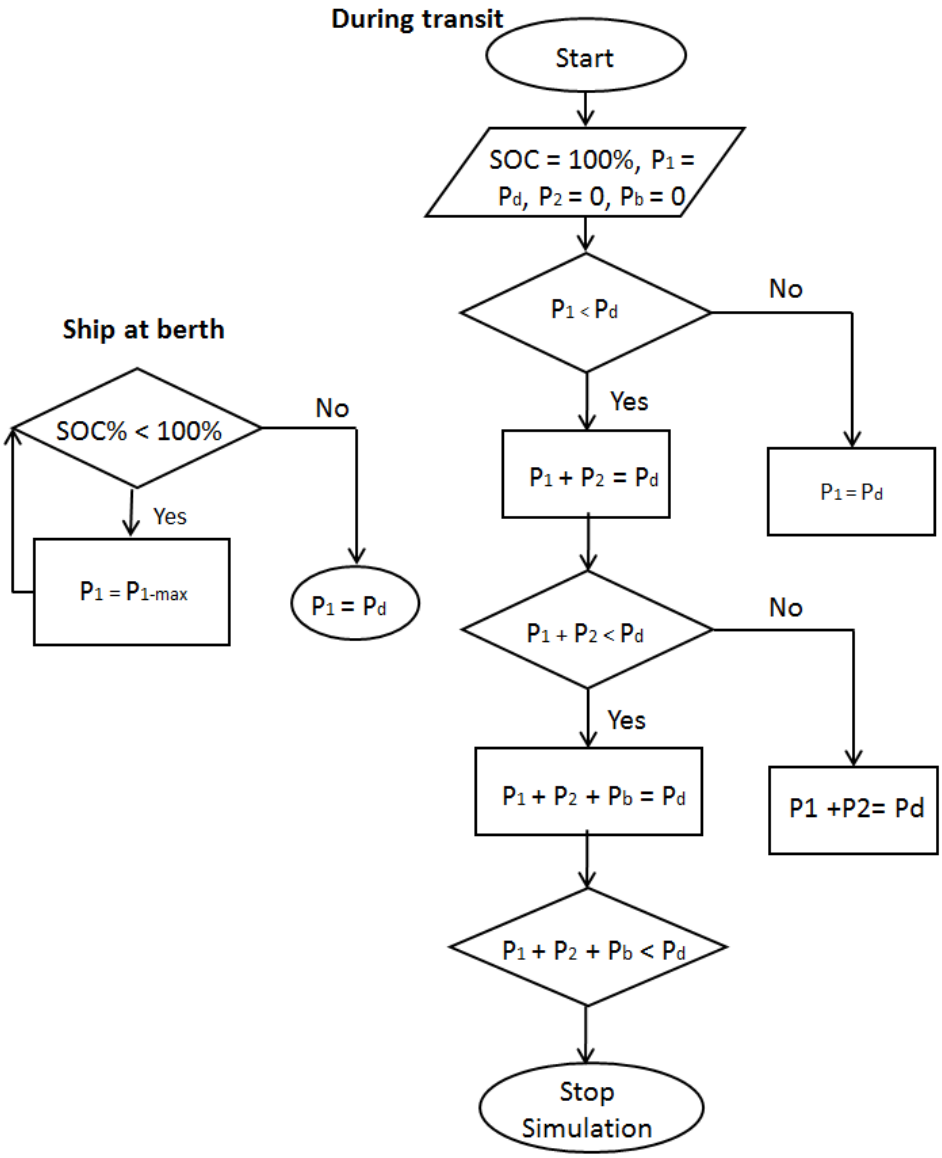

Figure P - 13 Rule-based energy management strategy.

As shown in Table P - 5, the minimum overall cost for the hybrid-series architecture is associated with one diesel generator and a BESS at capacities of 215 kW and 101kWh, respectively. In this combination, one diesel generator works at its maximum rating power and extra required power is provided by the BESS instead of another diesel generator. This combination of diesel generator and BESS is also able to provide enough power for power pulses required to maneuver the ship into alignment with the jetty. These pulses often require oversizing the engines to accommodate for this transient load. However, these pulses are better tolerated in this configuration.

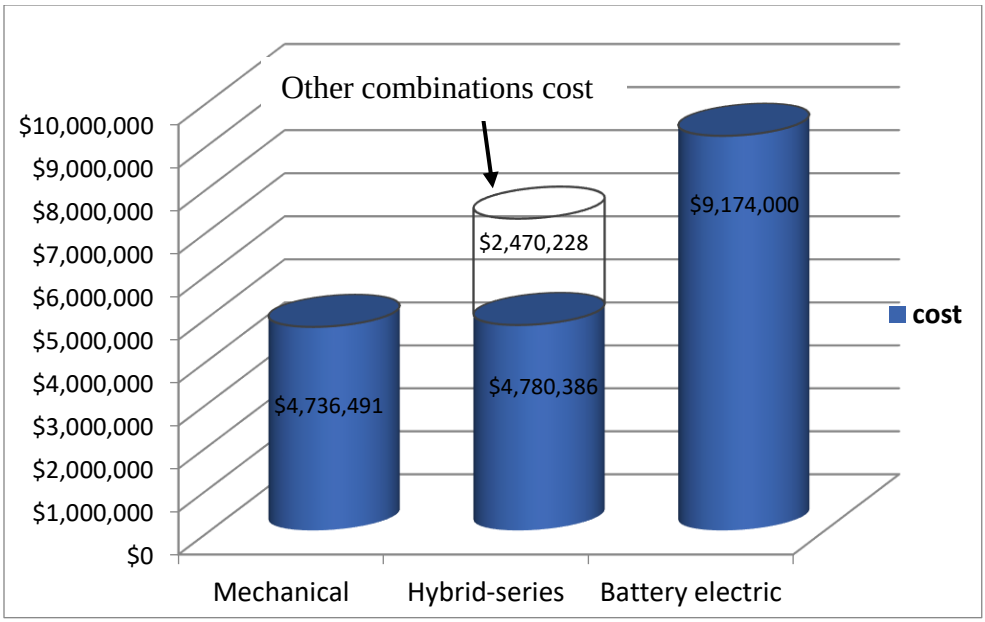

Figure P - 14 Cost analysis for various architectures over 10 years period.

Figure P - 14 shows the result of the cost analysis for the candidate point selected by the HAM algorithm. It is clear that mechanical architecture has a slightly lower cost over the 10 years period. However, this architecture is associated with the highest CO_{2e} emission as shown in Table P - 6. Hybrid series architecture cost is slightly higher than the mechanical architecture but it produces 7.5% lower CO2e emission. The battery-electric architecture has a 91% higher cost compared to the mechanical architecture but produces the lowest CO2e emissions between all architectures.

Selecting proper powertrain architecture for MV Klitsa is a multi-objective problem (MOP) since more than one objective function, such as cost and CO2e, are of interest. In these problems, the objectives are in conflict with each other. Therefore, reaching a solution that optimizes each objective function without deteriorating the other one is impossible. The answer to such problems is a set of solutions, referred to as the Pareto optimum [38]. As shown in Figure P - 15, cases M, H, and B are Pareto optimal points for MV Klitsa since none of them has superior over other points.

The three Pareto design points are shown in Figure P - 15 represent the mechanical (M), hybrid-series (H) and battery electric (B) architectures. Since the power plant emission factors are region-dependent, the B point can be divided into two points representing the British Colombia (B-BC) and North America (B-NA) CO2e. The point H is the most cost-efficient hybridization combination of battery and diesel engine for hybrid series architecture determined by the HAM algorithm. The path from point H toward B represents a series of Pareto points, which are all optimal solutions. By moving from point H toward point B, hybridization level increases and the cost of hybrid-series architecture increases while, CO2e decreases due to higher battery capacity and diesel engine rating. Point B-BC, has lower CO2e than North America due to the vast use of hydroelectric power plants and cleaner electricity.

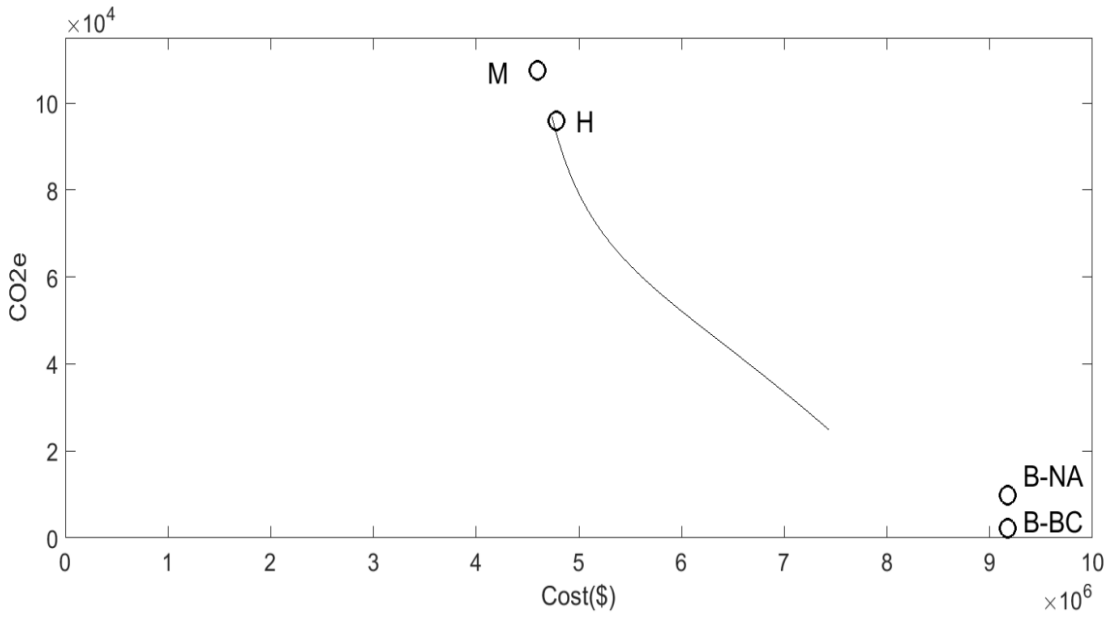

Figure P - 15 Pareto design points for three architectures.

P6. CONCLUSION

This paper presented various propulsion architectures for a car-deck ferry. BC Ferries MV Klitsa was selected for this case study and real vessel performance data was collected for comparison purposes. Hybrid series and battery-electric architecture models were developed and the results were compared with current mechanical architecture. The HAM optimization algorithm elucidated the optimal size and combination of generators and battery systems in hybrid-series architecture. The HAM results indicated that the most cost-effective combination happens when two diesel generators with 240kW and 125kWh power ratings provide all power. This combination also reduces the CO2e emission by 7% compared to mechanical architecture. Although the cost analysis results indicated that mechanical architecture is the most cost-efficient architecture for Klitsa, this architecture is associated with the highest amount of CO2e emission. The battery-electric architecture has remarkable CO_{2e} emission reduction; however, 92% higher costs, when compared to mechanical systems mainly due to battery replacement, have limited the implementation of this design. Based on Pareto optimal theory, hybrid-series architecture has the widest balance in terms of cost and environmental footprint.

P7. ACKNOWLEDGEMENT

The authors would like to thank Kevin Andersen for Klitsa ship operation data acquisition and acknowledge the support from Bruce Paterson, Bob Kearney, Bambino Da Silva at BC Ferries. Financial supports and guidance from the Clean Transportation Initiative of Transport Canada are gratefully acknowledged.

REFERENCES

[1] Unctad, Review of Maritime Transport 2013, no. October. 2015.

[2] R. Weisbrod, "The Geography of Transport Systems," J. Urban Technol., vol. 18, no. 2, pp. 99–101, 2011.

[3] I. M. O. (IMO), "International Convention for the Prevention of Pollution from Ships (MARPOL)." [Online]. Available: http://www.imo.org/en/About/conventions/listofconventions/pages/international-convention-for-the-prevention-of-pollution-from-ships-(marpol).aspx.

[4] V. Eyring, H. W. Kohler, J. van Aardenne, and Lauer, "Emissions from international shipping: 1. The last 50 years," J. Geophys. Res., vol. 110, no. D17305, pp. 1–12, 2005.

[5] I. M. O. (IMO), "Third IMO greenhouse gas study 2014, executive summary and final report.," London (UK), 2015.

[6] S. I. Raptotasios, N. F. Sakellaridis, R. G. Papagiannakis, and D. T. Hountalas, "Application of a multi-zone combustion model to investigate the NOx reduction potential of two-stroke marine diesel engines using EGR," Appl. Energy, vol. 157, pp. 814–823, 2015.

[7] R. Verschaeren, W. Schaepdryver, T. Serruys, M. Bastiaen, L. Vervaeke, and S. Verhelst, "Experimental study of NOx reduction on a medium speed heavy duty diesel engine by the application of EGR (exhaust gas recirculation) and Miller timing," Energy, vol. 76, pp. 614–621, Nov. 2014.

[8] MAN Diesel & Turbo, "Exhaust Gas Emission Control Today and Tomorrow. Application on MAN B&W Two-stroke Marine Diesel Engines.," Denmark.

[9] H. Pestana, "Future trends of electrical propulsion and implications to ship design," 2014.

[10] J. F. Hansen and F. Wendt, "History and State of the Art in Commercial Electric Ship Propulsion, Integrated Power Systems, and Future Trends," Proceedings of the IEEE, vol. PP, no. 99. pp. 1–14, 2015.

[11] E. Silvas, T. Hofman, N. Murgovski, P. Etman, and M. Steinbuch, "Review of Optimization Strategies for System-Level Design in Hybrid Electric Vehicles," IEEE Trans. Veh. Technol., pp. 1–1, 2016.

[12] H. Kim and D. Kum, "Comprehensive Design Methodology of Input- and Output-Split Hybrid Electric Vehicles: In Search of Optimal Configuration," IEEE/ASME Trans. Mechatronics, vol. 21, no. 6, pp. 2912–2923, Dec. 2016.

[13] H. S. Ramadan, M. Becherif, and F. Claude, "Energy Management Improvement of Hybrid Electric Vehicles via Combined GPS/Rule-Based Methodology," IEEE Trans. Autom. Sci. Eng., vol. 14, no. 2, pp. 586–597, Apr. 2017.

[14] BC Ferries, "BC Ferries, Klitsa." [Online]. Available: http://www.bcferries.com/onboard-experiences/fleet/profile-klitsa.html. [Accessed: 26-Jul-2017].

[15] K. Andersen, "Development of a time-domain modelling platform for hybrid marine propulsion systems," 2016.

[16] J. V. A. J. Timothy J. McCoy, "McCoy_Amy," IEEE, vol. 978-1–4244, 2009.

[17] CaterpillarCo, “Marine Generator Sets.” [Online]. Available: http://www.finning.com/en_CA/products/new/power-systems/marine-power-systems/marine-generator-sets.html. [Accessed: 26-Jul-2017].

[18] S. Kim, S. Choe, S. Ko, and S. Sul, “Power System with a Battery Energy Storage System,” IEEE Electrif. Mag., no. May, pp. 22–33, 2015.

[19] R. D. Geertsma, R. R. Negenborn, K. Visser, and J. J. Hopman, “Design and control of hybrid power and propulsion systems for smart ships: A review of developments,” Appl. Energy, vol. 194, pp. 30–54, 2017.

[20] Siemens, “Setting a Course for Carbon-Free Shipping,” 2016. [Online]. Available: https://www.siemens.com/innovation/en/home/pictures-of-the-future/mobility-and-motors/electromobility-electric-ferries.html. [Accessed: 31-Jul-2017].

[21] L. Larsson, H. C. Raven, and J. R. Paulling, Ship resistance and flow. Society of Naval Architects and Marine Engineers, 2010.

[22] ANSYS, “Computational fluid dynamics software.” [Online]. Available: http://www.ansys.com/products/fluids. [Accessed: 12-Sep-2017].

[23] Siemens Drilling & Marine, “Ship – A Smarter Journey,” 2015.

[24] J. Chiasson and B. Vairamohan, “Estimating the state of charge of a battery,” IEEE Trans. Control Syst. Technol., vol. 13, no. 3, pp. 465–470, May 2005.

[25] “Corvus Energy. Co.” [Online]. Available: http://corvusenergy.com/. [Accessed: 02-Aug-2017].

[26] A123, “A123 battery manufacturer.” [Online]. Available: http://www.a123systems.com/. [Accessed: 15-Sep-2017].

[27] and S. J. Nicholas DiOrio, Aron Dobos, “Economic Analysis Case Studies of Battery Energy Storage with SAM,” 2015.

[28] G. of Canada, “Natural Resources Canada,” 2017. [Online]. Available: http://www.nrcan.gc.ca/home. [Accessed: 24-Aug-2017].

[29] “Caterpillar dealer: Fining.” [Online]. Available: http://www.finning.com/en_CA.html.

[30] Commission for Environmental Cooperation, “North American power plant air emissions,” Québec, 2011.

[31] T. R. ROMANA, “MARINE FUEL OIL type DMB Commercial denomination: Marine Diesel Oil – MDO.”

[32] “United Nations Framework Convention on Climate Change.” [Online]. Available: http://www.omnimpex.ro/texte/petroliere/engleza_07/MARINE DIESEL OIL (MDO).pdf. [Accessed: 10-Aug-2017].

[33] A. Pachauri, R.K and Reisinger, “A REPORT OF THE INTERGOVERNMENTAL PANEL ON CLIMATE CHANGE,” Geneva, Switzerland, 2007.

[34] Ministry of Environment, “BEST PRACTICES METHODOLOGY FOR QUANTIFYING GREENHOUSE GAS EMISSIONS,” Victoria, BC, 2016.

[35] Bchydro.com, “British Columbia Hydro and Power Authority, ANNUAL SERVICE PLAN REPORT.”

[36] N. Doe, “Proposal for the calculation of the EF for BC Canada in GHG audits.”

[37] J. Gu, G. Y. Li, and Z. Dong, “Hybrid and adaptive meta-model-based global optimization,” Eng. Optim., vol. 44, no. 1, pp. 87–104, Jan. 2012.

[38] K. Deb, Multi-objective optimization using evolutionary algorithms. John Wiley & Sons, 2001.

Appendix Q. Case Study on Tugboats - Operation Profile Modelling and Benefits of Hybrid Electric Propulsion

ABSTRACT

Tugboats (or Tugs) are important tools in harbours to assist large ships to and from their berths. Today multi-purpose tugboats are designed to perform various jobs such as offshore support, salvage, icebreaking, etc. Some key parameters that define the performance of a tugboat include the bollard pull capacity, maximum free-running speed, time taken to achieve maximum free-running speed from rest, distance covered to crash stop, time taken to complete a 360 turn in its own axis, soundproofing of machinery spaces, etc. According to the type of work they perform, tugs can be categorized into three major groups: harbour tugs, escort tugs and ocean-going tugs. Tugs form a different type of marine vessel, for which the forces needed to propel itself is often just a small portion of its operation loads, while the primary loads come from its ship handling duty cycles. Robert Allan Ltd. (RAL) of British Columbia, another industrial partner of this project, is a leading tug design company with extensive experience developing different types of tugboats and is a pioneer in adopting new, clean energy propulsion technology.

In this work, the critical load profiles of various tugboats are first introduced. These statistical load profiles, rather than the hull resistance, determine the actual power demands of these tugboats. The unique energy demand time-shift characteristics of a hybrid electric propulsion system with onboard ESS has fundamentally changed the type of load profiles to be used to guide the propulsion system design. Traditionally the fuel efficiency and emission of tugboats have been evaluated based on the generic load profiles of the tugboats working at different function modes. In this work, we have chosen a representative tugboat load profile (or a very similar version) that has been used by multiple organizations in tugboat power analysis and design to carry out the fuel efficiency and emission simulations using our marine propulsion system model. Considering different tugboats may have different load profiles unique to their routine duties, a timescale load profile has been generated based on collected data from the literature for a typical harbour tugboat as an alternative power demand input in analyzing tugboat energy efficiency and emissions. This timescale load profile can be obtained by recording the actual power load data of a tugboat, serving as the statistical driving and load cycles. The higher resolution of power demand records and the time history provide a better load profile for the modelling, design optimization and optimal operation control of a tugboat with a hybrid electric propulsion system. The addition of the battery ESS for the hybrid electric or plug-in hybrid electric tugboats allows peak power shift in the time domain, a timescale load profile that shows the vessel's power demand at a different time becomes essential in designing the hybrid propulsion system. In this work, fuel consumption and emission simulations using both traditional duty-divided and our new time-scale load profiles have been carried out in alternative propulsion system analyses and designs. To ensure consistency, the newly proposed, standard time-scale load profile expressing power demand at each specific instance of tug operation and the commonly used duty-divided load profile indicating the overall power demand of the tug operation have the same amount of energy consumption.

The preliminary study showed that the proposed hybrid electric propulsion system can lead to 18% fuel saving and significant emission reductions. Results from duty-divided and time-scale load profiles are presented and compared, showing the need and benefit of acquiring statistical time-scale power load data for a specific tugboat. As the next step, the lifecycle cost of the hybridized tugboat will be studied to consider both the additional investment costs of the added battery ESS and power electronics, and the fuel cost saving gained by improved fuel economy. This is supported by our new battery performance degradation/lifecycle cost model under different ESS use patterns and by the newly proposed time-scale load profile model. The study will produce an accurate prediction on the payback time of the vessel electrification and hybridization, facilitate the selection of propulsion system architecture and optimization of hybrid electric powertrain components and support accurate cost estimation for a specific application. Additional hybrid powertrain architectures, including plug-in hybrid, best suited for different tugboat load profiles will also be investigated.

The battery performance degradation model will be used in system design to evaluate battery lifecycle cost and optimize the size of the battery ESS and engine. The use of the LNG-diesel dual-fuel engine will be investigated with different propulsion system architectures in comparison to traditional diesel-mechanical and diesel-electric drivetrains for fuel cost and emission reductions. Further research will also incorporate our propeller cavitation model to predict and prevent tugboat induced ocean noise with needed design and operation changes. The study will lead to improved modelling and design optimization tools for tug electrification and hybridization.

Q1. TYPES OF TUGBOATS

Tugboats (or tugs) are important tools in harbours to assist large ships to and from their berths. Today multi-purpose tugboats are designed to perform various jobs such as offshore support, salvage, icebreaking, etc. Some key parameters that define the performance of a tugboat include the bollard pull capacity, maximum free-running speed, time taken to achieve maximum free-running speed from rest, distance covered to crash stop, time taken to complete a 360 turn in its own axis, soundproofing of machinery spaces, etc.[1]. According to the type of work they perform, tugs can be categorized into the following three major groups [2].

(1) Harbour tugs

Harbour tugs are required to assist large ships onto and off a berth by pushing and pulling.

The maneuverability of large ships is insufficient in restricted waters, therefore tugs are used in harbours to safely handle the ships while entering or leaving a port. Some special applications of harbour tugs with the more rigid construction of hull and fender are for inland sea transportation and coastal shipping.

(2) Escort tugs

Escort towing tugs are designed to provide emergency steering and braking functions to tankers in critical or confined coastal areas. Due to the past accidents that caused oil leakage from tankers, it is required by some jurisdictions that tankers within specific waters must be ‘escorted’ by a tugboat.

Escorting is more challenging than regular ship-handling because it takes place at a higher speed [3]. A towrope will be connected to the vessel being assisted from the tug’s towing

winch. Tugs need to generate the required ship control forces for steering and braking by carefully balancing all force from their propulsion drive units and ship hull hydrodynamic forces.

(3) Ocean-going tugs

Seagoing tugs are generally larger and capable of performing good sea keeping characteristics to ensure that vessels can provide required power in any rough sea weather. They can perform various operations including assisting ships in ports as well as at sea.

- Terminal support tug: Terminal support tugs are typically larger and more sea-capable to work at large oil or gas terminals. They frequently include capacity for fire fighting and spill response. These tugs are normally equipped with a dynamic positioning system to prevent drift off from position due to waves, wind and currents.
- Offshore support tug: This type of tugs is typically larger and more powerful to perform anchor-handling, cargo transfer, tailback duties etc.
- Offshore rescue / Salvage: These tugs are designed for fast response speed, long-distance towing capability and the best possible seakeeping for crew safety in rough sea conditions.
- Coastal towage tug: Coastal towing tugs are used to provide sustainable pulling power to barges between coastal ports. It is specially designed to handle more severe ocean weather.
- Deep-sea towage: This kind of tugs helps tow ships in any sea area and any period of the year without restrictions.
- Integrated tug barges (ITB) or articulated tug barges (ATB), the barge stern of the vessel is notched to accept a special tug that can be rigidly connected to the barge forming a single vessel.

In this work, the load profile of tugboats was first introduced and then used in the study on fuel efficiency and emission improvements potentials of the hybrid electric powertrain with added Li-ion battery energy storage system (ESS). This study formed the foundation for tug electrification and hybridization modelling and design optimization tool development.

Q2. REPRESENTATIVE TUGBOATS FROM ROBERT ALLAN LTD.

Robert Allan Ltd is a world-leading tugboat design firm based in Canada. The company is an independent, privately-owned firm of Consulting Naval Architects and Marine Engineers, established since 1930 in Vancouver, Canada. Over the past many years, the company has designed and developed many of tugboats of different types for a variety of tasks in the categories listed below. However, the most common and representative tugboats are the Escort, Ship-Handling and Terminal Support tugs, such as the Vancouver Harbour Tugboats operated by Seaspan Marine. Robert Allan Ltd. has designed the world's first hybrid-powered tug, the RApport-2400-Carolyn-Dorothy-1440x960, and many tugs with LNG or diesel-LNG dual-fuel systems, such as the ART-80-32-RT-Evolution-1440x960. The company has also developed a powerful analytical tool, the ***Raptures*** **program** to enable a thorough analysis of the relative merits and efficiency of a variety of hybrid or conventional powering options, whether diesel-mechanical, diesel-electric or any combination thereof.

Figure Q - 1 RApport 2400 MkII (Courtesy of RAL)

Figure Q - 2 RT Evolution – Advanced Rotortug (Courtesy of RAL)

The *RANGLer* series of LNG (or dual fuel) powered escort and ship-handling tugs (introduced in 2014) were conceived to take maximum advantage of the very limited space available for LNG fueled systems in tugs. The unique *RANGLer* design places the gas tank forward and oriented vertically to best utilize space.

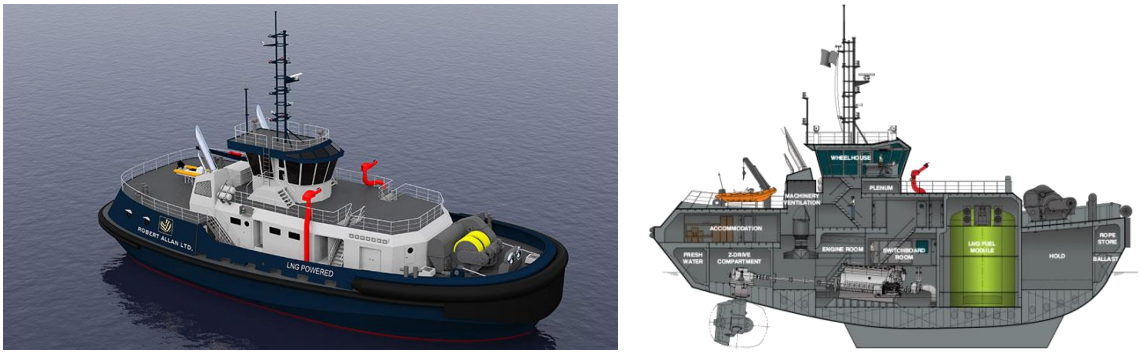

Figure Q - 3 RANGLer Figure (Courtesy of RAL)

Working closely with both Bureau Veritas (BV) and the American Bureau of Shipping (ABS) on the LNG safety aspects of the design, Robert Allan Ltd has announced that the *RANGLer 3600* Class concept has received Approval in Principle from both classification societies for either single gas fuel or dual-fuel engines. The particulars of this new LNG tug design are as follows (Table Q - 1):

Table Q - 1 General Information of LNG Tugboat from RAL

Length, Overall	36.5 m
Beam, Moulded	15.4 m
Depth, Least Moulded	7.1 m
Draft, Navigational	5.8 m (above the bottom of drives)
Installed Power	2 x 2430 kW
Complement	up to 10 crew
LNG Capacity	80 m^3 (gross)
Vessel Speed, ahead	14 knots, approx.
Bollard Pull, ahead	80 tonnes, approx.

Q3. REVIEW OF ALTERNATIVE PROPULSIONS FOR TUGBOAT

Today, tugs are mostly powered by marine diesel engines coupled to propellers, azimuthing propulsors (Z-drives), or Voith Schneider Propellers (VSP drives)[4]. Electric power for hotel and auxiliary requirements is typically supplied by one or more small generator sets (Genset). The heavy fuel cost and greenhouse gas (GHG) emissions from tugs have laid great stress on operators. Tugboat operators are looking for alternative ways to make their vessels more efficient and clean to the environment. However, the direct connection between engine and propulsor makes emission control difficult. Alternative propulsion configurations have gained more interest recently for potential fuel-saving and emission-reducing.

The world's first hybrid harbour tug, the *Carolyn Dorothy*, was built by Foss Maritime Company and started to operate in 2009 to reduce emissions and fuel consumption. A sister tug, the *Campbell Foss*, joined the operation in 2012 by converting a conventionally powered tug to a hybrid at the Foss shipyard in Rainier, Oregon, USA. The Foss hybrid tugboat used a combination of smaller main diesel engines and larger diesel-generator sets (as compared to a conventional *Dolphin* tug), main shaft-driven motor/generators, batteries and state-of-the-art power conversion and control technology [5]. The boat can operate in direct-diesel, diesel-electric, and electric configurations. The benefits of this hybrid tugboat include reductions of emissions, fuel use, engine maintenance, noise, and power loss risk. The emissions reduction was about 73% for particulate matter, 51% for nitrogen oxides and 27% for fuel-related pollutants such as sulphur oxide and carbon emissions. The fuel consumption was reduced by 20-30%. The main engine maintenance costs were reduced by about 50% through decreased operating hours. The noise pollution was lowered by using batteries and generators. Safety had been improved by effectively removing any chance of power loss with multiple system redundancies [6].

Inspired by Foss hybrid tug, Europe's first hybrid ship handling tug *E-KOTUG* was converted from a traditional tug named *RT Adriaan* and entered into service in 2012 by the KOTUG fleet in Rotterdam, Netherlands [7]. It was retrofitted with a 78 kWh lithium-polymer battery pack to provide pure electric drive at low speed. The main engines only start when demands are made for high bollard pull situations. It showed a 50% reduction in harmful emissions of CO_2, NOx, and PM2.5.

The world's first hybrid offshore platform supporting vessel, *Viking Princess*, was designed by Finland's Company - Wärtsilä. It also is the world's first hybrid ship with a dynamic positioning system. This vessel has completed sea trials and handed over to the customer - Ediesvik Offshore

in Norway in October 2017. The vessel was originally built in 2003 with four LNG engine generator sets as the world's first offshore supply vessel powered by LNG fuel. Now, by replacing one LNG gen-set with a 533 kWh Li-ion based energy storage system (ESS) provided by Corvus Energy, it can reduce fuel consumption by up to 30% in various operations. CO_2 emissions can also be reduced.

Robert Allan Ltd. has developed a tool named *Raptures* (as the abbreviation of "Robert Allan Ltd: Powering Tugs for Real Energy Savings") to analyze a wide range of hybrid or conventional powering options for typical harbour tug propulsion systems, including diesel-mechanical, diesel-electric or any combinations[4]. With inputs of basic tug power and an operating profile, the fuel consumption, emissions and installed costs can be calculated. Cost comparisons included equipment capital costs, fuel operation cost and equipment maintenance cost. A net present cost method was used in this paper for a 20 years evaluation. Four powering configurations: diesel-mechanical, series diesel-mechanical/electrical, diesel electric-running standby, diesel electric-cold standby, were compared for a tugboat *Ramparts 2800* designed by Robert Allan Ltd. for both harbour duty and ship assist duty. The series diesel-mechanical/electrical configuration showed more attractive after comparing the fuel consumption, emission and cost.

Researchers in Nanyang Technological University published several papers for a new design of electric tugboat [8-10]. In [8]and [9], the author presented optimal power management to split the power supply from engines and batteries in response to the load demand, while minimizing the engine fuel consumption and maintaining the battery life. The cost function includes power load demand tracking, engine fuel consumption, and change of battery SOC. A load prediction method was introduced to anticipate the load demand based on a typical tugboat operation profile provided by ABB Singapore. In [10] equivalent consumption minimization strategy (ECMS) control method was adopted in a hybrid all-electric tugboat for power management and showed 17.6% of fuel-saving compared to the conventional rule-based control strategy.

MacPherson and Boyd [11] presented an optimal design approach for a tugboat through computational analysis of alternative propulsions. Instead of using a traditional single design point such as bollard pull or cruising speed, this paper optimizes the propulsion system components by using the all-inclusive duty cycle profile of multi-role service (as a harbour tug and in long haul ocean barge towing). Variables include main engines and gearboxes (gearbox reduction ratio), propellers (type, blade count, and blade area ratio), speed (mode operational speed). The cost function is to minimize propulsion fuel consumption over a representative transit voyage or operational duration. Key performance indicators (KPI) were used for qualitative comparisons of different design options. Three different consumption index forms were used for analyses: fuel, energy and power. By replacing original open propellers with high-efficiency ducted propellers and increasing the gear reduction ratio, the tugboat can achieve a 29% overall fuel reduction in harbour duty profile and 19% in ocean towing duty profile.

Researchers at the Tokyo University of Marine Science and Technology have published several papers to study fuel consumption of a new proposed hybrid propulsion system without a large capacity battery for a tugboat[12, 13]. A hybrid propulsion powertrain with two motor/generators (M/G) and three electric power converters (EPC) added to the conventional two main diesel engine propulsion system was introduced in [13]. A DC bus was built with one EPC connected to auxiliary diesel generator and tow EPCs connected to M/G and main engines respectively. A changeover gear is installed to one of the main engines to adjust load torque so that the main engine can mechanically drive and electrically drive. The fuel consumption is calculated with consideration

of all the efficiencies of apparatus for different energy flow paths. It concluded that the hybrid system has 20% less fuel consumption than the conventional system when the tugboat is in waiting mode and out of service mode. However, the consumption is higher of the hybrid system when demanded power is high in service mode due to the efficiency losses.

Moreover, [12] compared different control strategies for this hybrid tugboat energy management when it is not in service. It also employed a number of efficiency data banks of main components to evaluate different control strategies. Three control patterns were evaluated from the view of controllability, redundancy and efficiency. However, the threshold in each control pattern to shift EPA1 and EPA3 was arbitrarily chosen. In their work, a more efficient control strategy was introduced for the non-service operations of the tug, not covering the complete tugboat operations.

Völker [14] presented hybrid propulsion designs for two cases: a harbour tugboat and a vehicle. For harbour tug, a DC-bus with two main engine-generators and a large battery pack was designed to support two thrusters. For the ferry with a 20-minute crossing, the structures of AC and DC power buses were proposed.

Lindstad and Sandaas [15] provided hybrid propulsion design for offshore support vessels with 10,000 kW installed engine power and compared the emissions from the hybrid system with the traditional four diesel-generator diesel-electric propulsion. Two battery packages of 500 kWh each were used in the hybrid propulsion system. The vessel operates at its full installed engine power for 5 mins in the rough ocean, and then 20 mins at calm water. Three alternative fossil fuels were used: marine diesel oil (MDO) with a sulphur content up to 0.5%, marine gas oil (MGO) with a sulphur content up to 0.1% and LNG in dual-fuel engines with high-pressure and low-pressure systems. Region-specific global warming potentials (GWPs) were used to evaluate each emission species with a time length of 20 and 100 years. In their work, the global warming impact (GWI) has been developed for each of the four regions for non-Arctic areas, including East Asia, Europe and North Africa, North America, and South Asia, as well as for the Arctic (activities in the Barents Sea) operations. Considering the only CO_2, the hybrid propulsion options reduce emissions by 5% for all technologies. The hybrid system reduces 10-25% of all emissions using the CO_2 equivalents measure for operations in non-Arctic regions and 25-40% in Arctic regions with GWI 20 years. In the non-Arctic region, the MDO fueled hybrid electric propulsion produces the least climate impact. In the Arctic region, the high-pressure LNG engine hybrid electric system produces 25-60% fewer emissions compared to others.

In conclusion, the main methods that can be adopted to improve the tugboat fuel economy and reduce emission include using LNG dual-fuel engines, using a large battery package for peak power shaving, and using a hybrid electric propulsion system to improve engine operation efficiency.

Q4. GENERIC TUGBOAT OPERATION DATA

The collection of tugboat operation data is the first step for designing a new electrified propulsion system. From a leading Canadian tugboat designer, Robert Allan Ltd (RAL), four generic tug operational profiles based on statistical data have been established and confirmed. Combining with information from open literature, in total seven different tugboat operation data sets have been identified as showed in Figure Q - 4 to Figure Q - 10.

These profiles reflected the typical operating missions of harbour tugs, such as ship-handling, escorting or other harbour duties. The individual modes in the duty profiles are similar with respect to the percentage of main engine rated power. However, the operating time percentages are quite different varying with the actual working conditions in different harbours around the world.

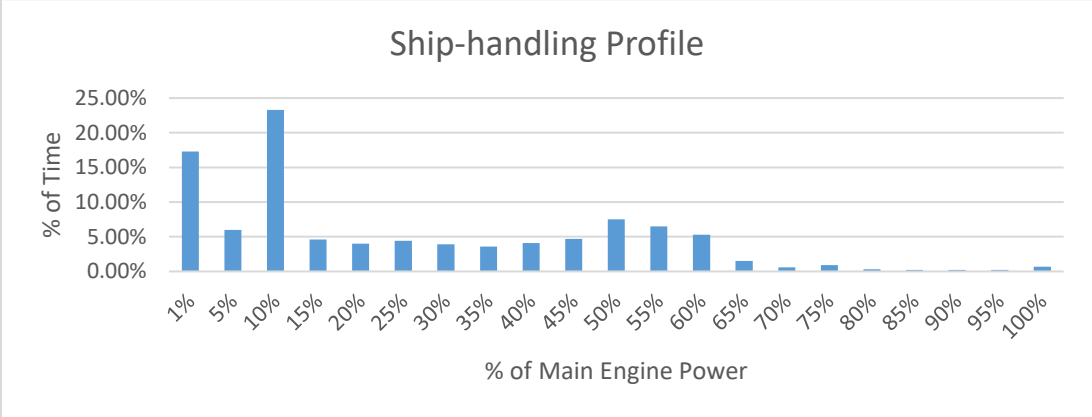

Figure Q - 4 Load Profile of a Ship-handing Tugboat

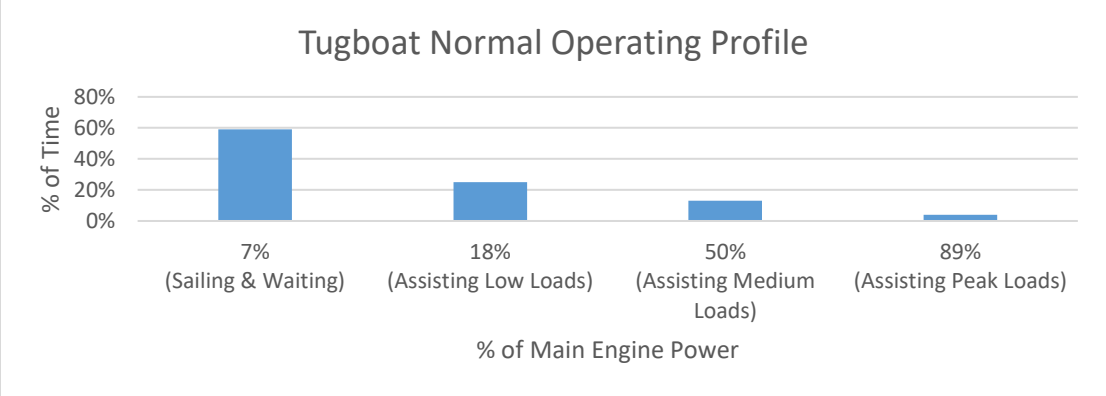

Figure Q - 5 Normal Operation Profile of a Tugboat

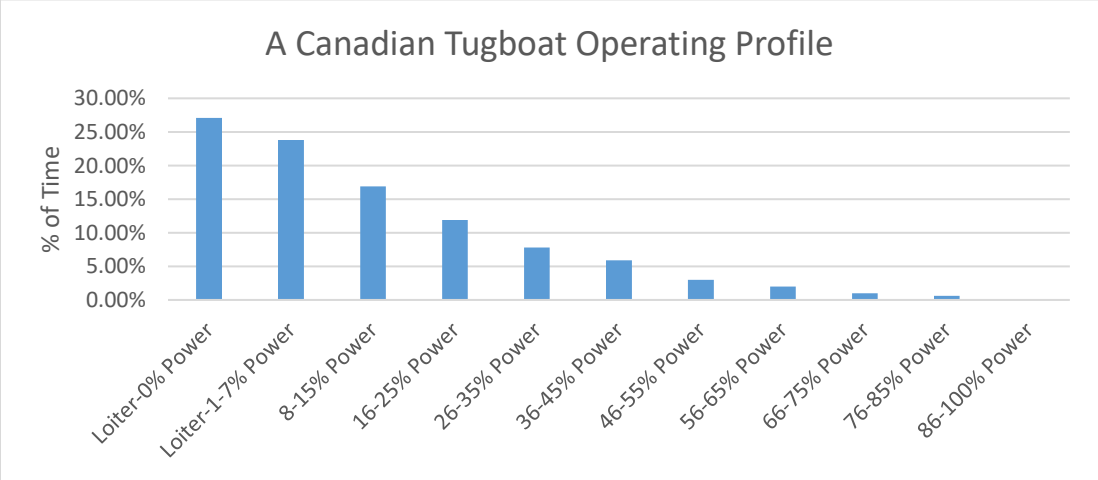

Figure Q - 6 Operating Profile of a Canadian Tugboat

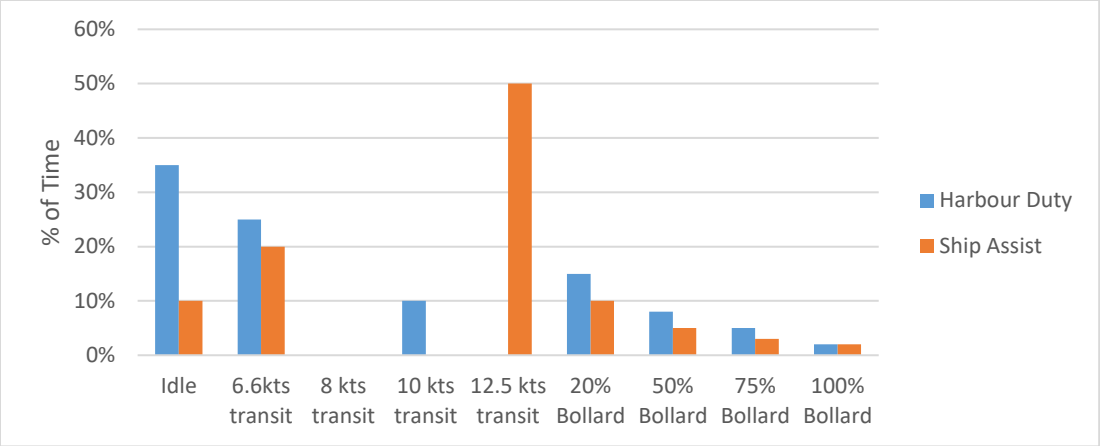

Figure Q - 7 Tug Operational Profiles [4]

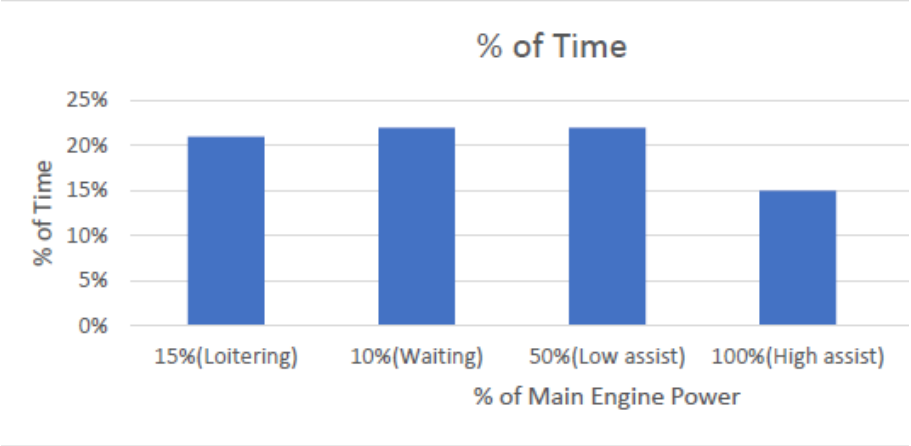

Figure Q - 8 Tugboat Power Requirements [8]

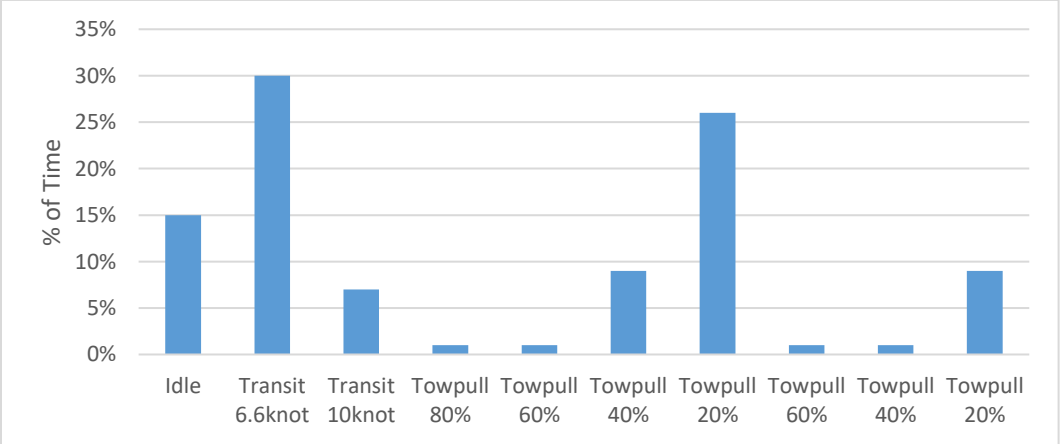

Figure Q - 9 Harbour Duty Profile [11]

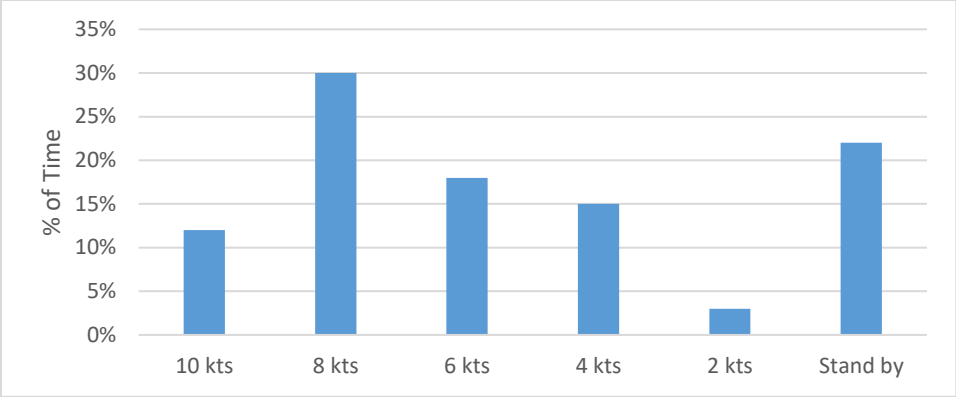

Figure Q - 10 Ocean Towing Profile [11]

Q5. HYBRID ELECTRIC PROPULSION SYSTEM DESIGN AND MODELLING FOR A HARBOUR TUG

A typical tugboat with two main engines and two auxiliary gensets was chosen as the case study for the hybrid electric propulsion system application. Its maximum continuous rating power (MCR) of the main engine is 2,240 kW. The auxiliary genset is about 75 kW to support hotel loads and deck machinery loads. The auxiliary loads are about 60kW requirement. Extra deck machinery loads are required when the tug is performing ship-assisting jobs (about 70kW).

The generic operation data of this harbour tug is shown in Figure Q - 11. The annual operation time is about 2500 hours. During each operation cycle, it has 20% of the time sailing out from the harbour, spends 25% of the time waiting until it gets the order, then takes 42% of the time assisting large ships, at the end takes 13% of the time sailing back. During the ship-handling process, the assisting loads were separated into low, medium and high that took about 25%, 13% and 4% of the total time respectively.

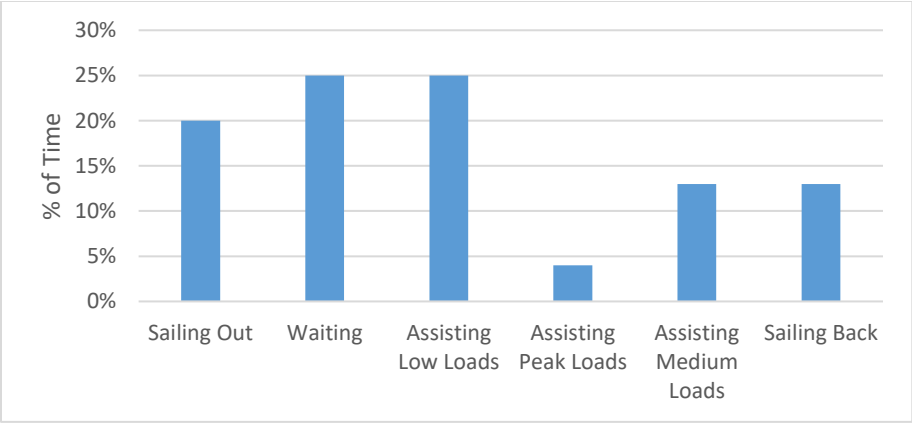

Figure Q - 11 Tugboat Generic Operating Data

Q5.1. Original Mechanical Propulsion Calculation

The tugboat originally has a mechanical propulsion system as shown in Figure Q - 12. Since the tug spends 58% of the total time at 7% of MCR, its main engines operate inefficiently with high fuel consumption and harmful emissions.

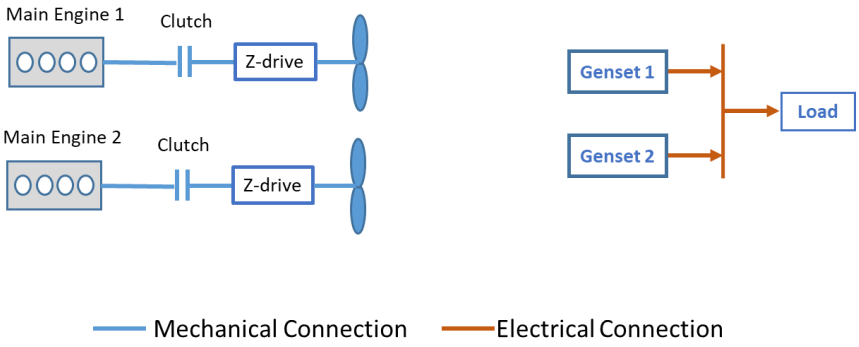

Figure Q - 12 Powertrain Architecture of Mechanical Propulsion System

In order to calculate the fuel consumption and exhaust emissions, the engine's specific fuel consumption and emission data were collected. The specific fuel consumption of the main engine and genset, illustrated in Figure Q - 13, was obtained from [4].

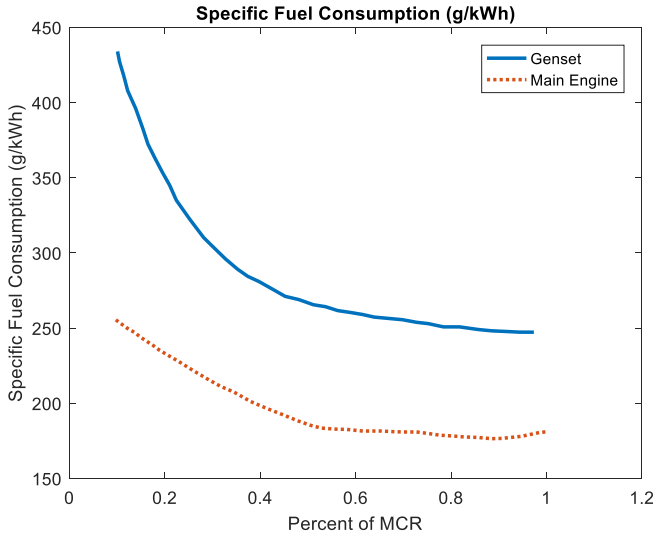

Figure Q - 13 Specific Fuel Consumption for Main Engine and Genset [4]

The US EPA has presented the methodologies and best practices for calculating vessel emissions at ports [16]. Marine emissions can be categorized as greenhouse gas (GHG) emission and Criteria Air Contaminants (CACs). Carbon dioxide (CO_2), as the main GHG emissions from the tugboat, was evaluated for this tugboat. In addition, NO_x, PM, CO and HC, as main CACs, were also calculated and compared.

The vessel emission was determined using Equation (Q - 1).

$$E = P \times LF \times A \times EE \qquad \text{(Q - 1)}$$

where, *E* is emission (g), *P* is maximum continuous rating power (kW), *LF* is load factor (percent of vessel's total power), *A* is activity time (hours), and *EF* is emission factor (g/kWh).

The important part of the emission calculation is to decide the emission factor, which is given in terms of emissions per unit of energy from the engine. Entec UK Limited [17] analyzed emissions data from 142 propulsion engines, including the most recent results from Lloyd's Register Engineering Services and IVL Swedish Environmental Research Institute. Entec has listed individual emission factors for different diesel engines. The results for a medium-speed diesel engine using marine diesel oil (MDO) with a sulphur content of 0.1% were used in this work.

Table Q - 2 Emission Factors of Diesel Engine [16]

	Emission Factor (g/kWh)
NOx	13.2
CO	1.1
HC	0.5
PM	0.72

Emission factors were considered constant for engine working above 20% of MCR. Below 20% load, adjustment factors emissions tend to increase when the load decreases. The adjustment factors were demonstrated by Energy and Environmental Analysis Inc. (EEA) in a study prepared for the EPA and are shown below [16].

Table Q - 3 Emission Factor Adjustment at Low Engine Loads

Load	**NO_x**	**CO**	**HC**	**PM**	**SO_2**
1%	11.47	20	89.44	19.17	1
2%	4.63	10	31.62	7.29	1
3%	2.92	6.67	17.21	4.33	1
4%	2.21	5	11.18	3.09	1
5%	1.83	4	8	2.44	1
6%	1.6	3.33	6.09	2.04	1
7%	1.45	2.86	4.83	1.79	1
8%	1.35	2.5	3.95	1.61	1
9%	1.27	2.22	3.31	1.48	1
10%	1.22	2	2.83	1.38	1
11%	1.17	1.82	2.45	1.3	1
12%	1.14	1.67	2.15	1.24	1
13%	1.11	1.54	1.91	1.19	1
14%	1.08	1.43	1.71	1.15	1
15%	1.06	1.33	1.54	1.11	1
16%	1.05	1.25	1.4	1.08	1
17%	1.03	1.18	1.28	1.06	1
18%	1.02	1.11	1.17	1.04	1
19%	1.01	1.05	1.08	1.02	1
20%	1	1	1	1	1

Based on this collected information, the calculated fuel consumption and emissions of the tugboat with its original mechanical propulsion system for a one-year operation are shown in Table Q - 4.

Table Q - 4 Yearly Fuel Consumption and Emissions for the Mechanical Propulsion System

Fuel Consumption (ton)	NOx (ton)	PM (ton)	SOx(ton)	CO (ton)	HC (ton)	CO_2 (ton)
500.37	33.47	1.93	2.69	3.53	2.05	1571.2

Q5.2. Hybrid Electrical Propulsion System

To improve the main engines' operating efficiency and reduce emissions, an integrated electrical propulsion system, or series hybrid electric powertrain in automotive terminology, was proposed as shown in Figure Q - 14.

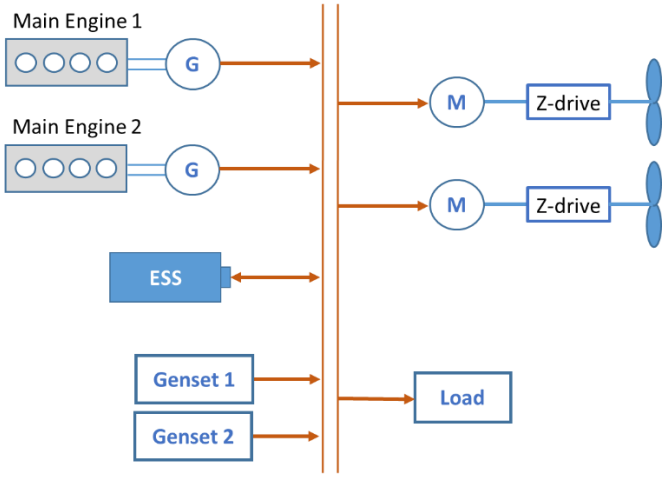

Figure Q - 14 Architecture of the Integrated Electrical Propulsion System

In this electrical propulsion system, two motors were used for the Z-drive propellers. The two main engines were coupled with electric generators to work as large gensets. A large Li-ion battery energy storage system (ESS) was added to store and release electrical energy. The ESS works as an energy buffer to spare the engine from working in inefficient areas. The design has a great potential for fuel saving and emission reduction.

With the addition of a Li-ion battery ESS, the original diesel-electric propulsion system of the tugboat was turned into a series hybrid electric propulsion system with the ability to cut off the main engines when the tug is loitering, using battery power to meet the hotel loads and basic propeller movements. To take advantage of low-cost electricity from the power grid, the ESS can be fully charged during the night with a "plug-in" hybrid design.

In this paper, the hybrid system was designed without the plug-in capability for the preliminary study. The main advantage of using a Li-ion battery is to increase the capability of having the engines run within their most efficient torque and speed zone. However with the generic operation data (shown in Figure Q - 11Figure Q - 11), it is not sufficient for the system design. The control

logic cannot be implemented on the statistical data. Without power changing in time scale, it is hard to decide when and how to use ESS energy. Therefore, system design and ESS sizing are impossible.

Based on the statistical operating data, it can only be sure that engines will not work at 7% of its maximum power during sailing and waiting periods since ESS can cover this job. As the sweet spot is located around 80% of maximum engine load, it was assumed all the energy requirements at low load would be produced by the engine at 80% of maximum load to have less fuel per kWh. Based on this analysis, the total fuel consumption and emissions can be estimated.

Table Q - 5 Results of Hybrid Electric Tugboat based on Statistical Data

	Fuel Consumption	NO_x	PM	SO_x	CO	HC	CO_2
Yearly Mass(ton)	462.37	30.76	1.675	2.49	2.61	1.17	1451.85
Improvement (%)	7.59	8.07	13.38	7.59	26.35	42.57	7.59

By raising engine output from 7% to 80% of maximum power in a series hybrid propulsion system, it can achieve 8% improvements of total fuel consumption based on the calculation from statistical data. Annual emissions also gained reductions compared to the original mechanically driven system (showed in Table Q - 5).

However, these results only show an estimation of the benefits of adopting a hybrid electric propulsion system. The exact benefits can only be verified using power demand data collected during tug operations.

Q5.3. Tugboat Load Profile with Timescale

Traditional tugboat design takes generic operation data as an input. The choice of engine capacity mainly depends on the maximum bollard pull required by the harbour customer. However, the tugboats spend almost half of their time working at less than 20% of engine rated power as shown by Figure Q - 4 to Figure Q - 10, indicating that the engines often work on its off-design area. This tugboat design practice and the nature of tugboat power demand led to the use of over-capacity engines. For a significant portion of time, the engine works on its off-design, inefficient speed and torque outputs, and produces severe air pollutants.

The hybrid architecture of the tugboat created more control variables to achieve better efficiency for engines. Batteries can kick in when the power requirement is low. Meanwhile, the engine can either shut off or operate at high speed to charge the battery. The control logic is determined by the battery SOC and tug operating conditions at different times.

Seldom were tugboat engine operating data with timescale presented in literature due to the difficulty of data logging from engines. Without the power variation profile, it is difficult to develop control logic for the hybrid system. Therefore, system design and evaluation cannot be achieved. To overcome this obstacle, an artificial engine load profile for the previous tugboat statistical data was created.

The total operating hours of this tugboat per year is about 2500 hours. It assumes each time of operation it takes 2.5 hours. To generate main engine load profile changing with time, it was assumed the tug first sails out of the harbour and waits when accepted operating order, performs ship-assisting jobs with different power outputs, then sails back when finished the job. During the ship-assisting process, the load transition among low, medium, and high were changed with different time scales in accordance with the statistic data. The created main engines' load profile for this harbour tugboat is presented in Figure Q - 15.

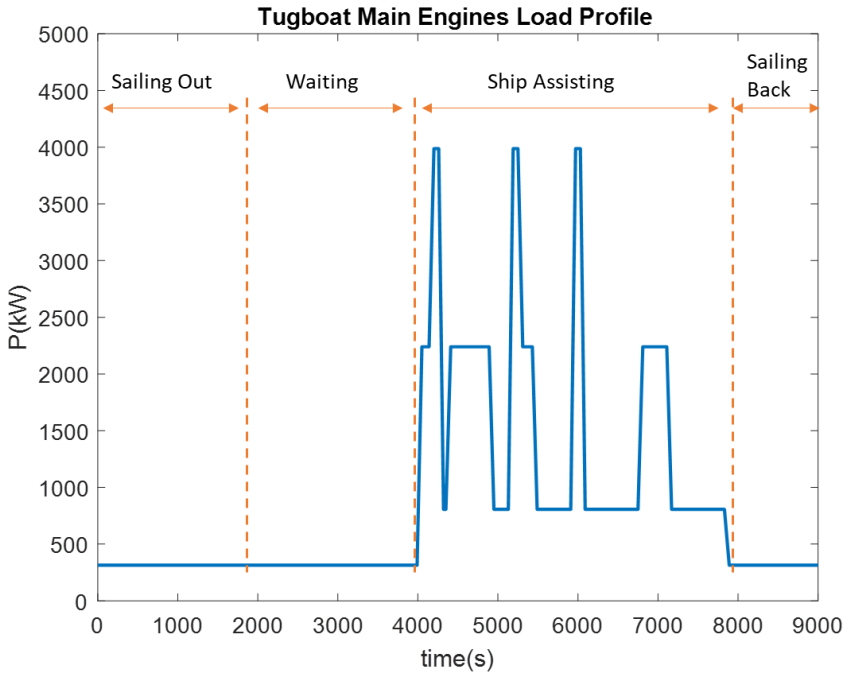

Figure Q - 15 Proposed Time Scale Load Profile for Tugboat's Main Engines

With this created load profile, the original diesel-mechanical and the newly proposed hybrid electric propulsion system have been modelled using our generic hybrid electric marine propulsion system modelling tools implemented in MATLAB/Simulink. During each working cycle, it must keep the battery State of Charge (SOC) constant, which means the end of SOC after one trip should be equal to the initial SOC at the beginning. When the battery SOC is too low, the engine will start and work at 80% of its maximum power. This simple rule-based control algorithm is suitable for the tugboat operation.

In order to choose the right size of battery ESS, an optimization problem was formed to achieve minimum fuel efficiency as well as longest battery lifetime. A Genetic Algorithm (GA) was used to solve this constrained non-linear optimization problem.

The objective of this optimization problem is to maintain battery SOC during operation, minimize engine fuel consumption, and extend battery life. The objective function can be expressed as:

$$\min_x f = w1 \times f1 + w2 \times f2 + w3 \times f3$$
$$f1 = |SOC_0 - SOC_{end}| \quad \text{(Q - 2)}$$
$$f2 = C_{fuel}$$

$$f3 = L_{ess}$$

$$subject\ to: E_{min} \leq x1 \leq E_{max}$$

where x is unknown variable, battery size in kWh; $w1, w2, w3$ are weighted factors; $f1$ is the cost function of SOC variation at the beginning and end of one operating cycle; $f2$ is the cost function of total fuel consumption; $f3$ is the cost function of battery life with each designed ESS energy; and $\mathrm{E_{min}}, \mathrm{E_{max}}$ are the minimum and maximum values for the designed ESS energy.

The searching results of the GA were presented in Figure Q - 16. The best option of ESS size is 703 *kWh* for this special case.

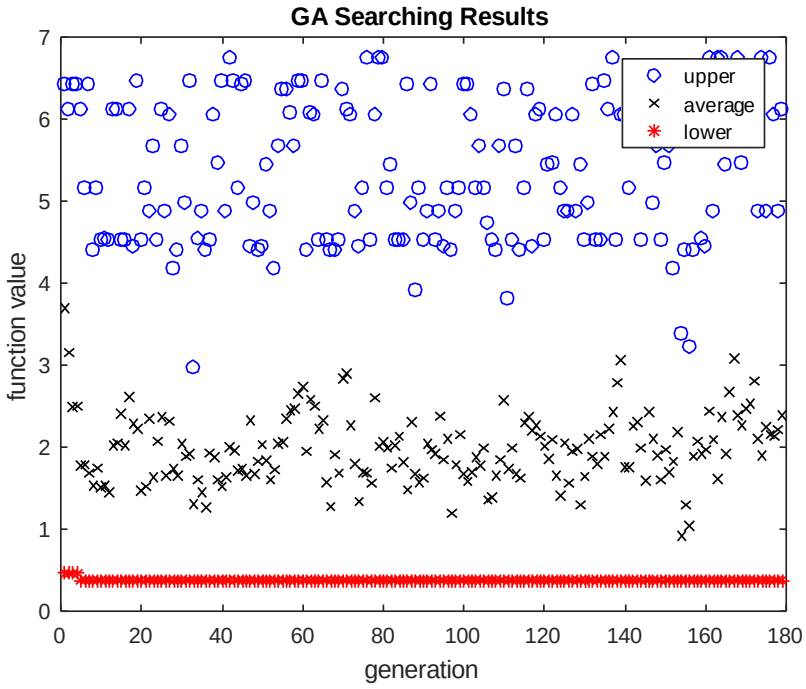

Figure Q - 16 Quick Convergence of ESS Size Optimization

Based on the optimized battery size, the hybrid system can work more efficiently. The battery SOC variation in one working cycle during 2.5hours was presented in Figure Q - 17. The beginning and end of SOC during the trip were both 0.5. Therefore, it can always perform the same job constantly during each working cycle. The variation of SOC was limited from 0.2 to 0.8, which can help maintain a long lifetime for the battery with only 60% of the depth of discharge. By adopting a 20Ah $LiFePO_4$ type of battery cell, the ESS package needs 224 series and 50 parallel cells to reach 700 V operating voltage for the electric motor. The discharge current rate (C-rate) will only be 0.47 during tug sailing and loitering operations, leading to a long-lasting lifetime. Using our newly introduced Li-ion battery performance degradation model presented in Appendix L, the battery lifetime was estimated to be about 6.4 years.

The power distribution between the main engines and ESS in the series hybrid system was presented in Figure Q - 18. It can be seen that engine always works at 80% of its maximum power. Battery ESS covers most of the power requirements during tug sailing and waiting, while engines only started when battery SOC is low. The negative value in Figure Q - 18 means the battery was

charged during that time. The total operating time of the main engines was significantly decreased in such circumstance.

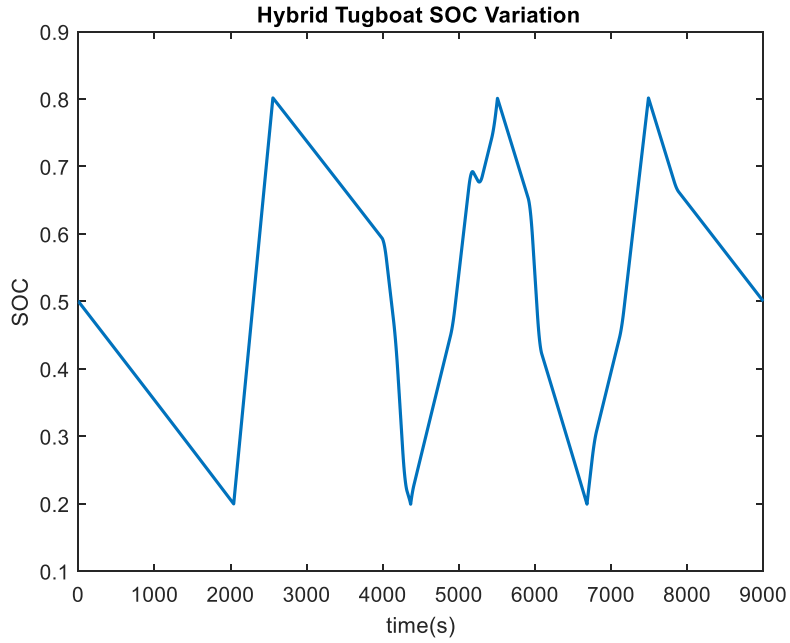

Figure Q - 17 Battery SOC Variation in One Working Cycle

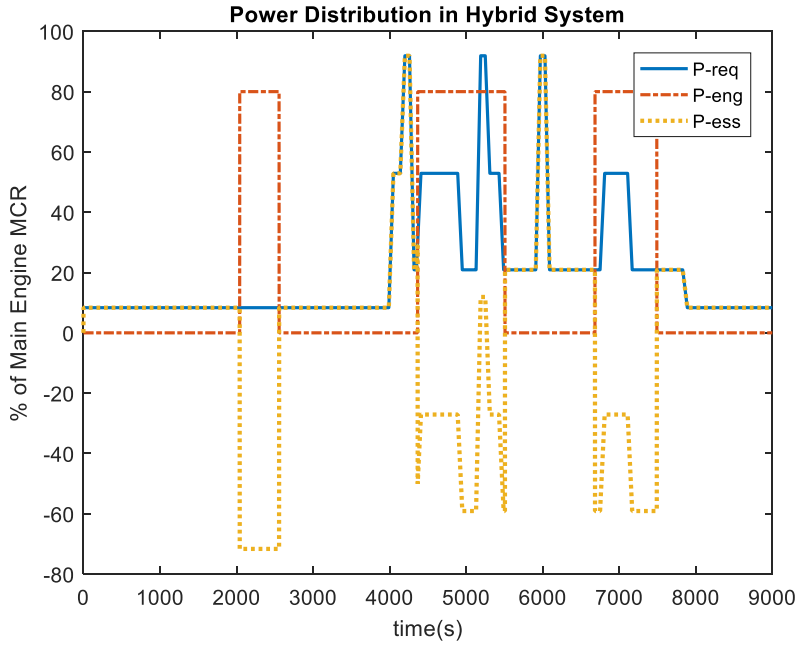

Figure Q - 18 Power Demand and Distribution between Engine and ESS

Conversion to the series hybrid electric propulsion system with the 700 kWh battery ESS allows the fuel consumption and emissions from the two main engines to be significantly reduced. First,

these main engines will not operate in idle. Secondly, the small auxiliary gensets will not be started most of the time. Hotel load and deck machinery load will be provided from either the ESS or the main engines. Thirdly, when the total power requirement is less than 2,000 kW, only one main engine will be started to allow it to operate at the most efficient zone. The second engine only kicks in when a large power requirement occurs. Fuel consumption and emissions were calculated and presented in Table Q - 6.

Table Q - 6 Hybrid Propulsion Calculation Results based on Timescale Data

	Fuel Consumption	NO_x	PM	SO_x	CO	HC	CO_2
Yearly Mass (ton)	411.58	30.48	1.66	1.45	2.54	1.15	1292.4
Improvement (%)	17.75	8.94	14.01	45.94	28.07	43.57	17.75

Table Q - 6 showed that the series hybrid electrical propulsion tugboat without plug-in function led to 18% fuel economy improvement, as well as significant emission reduction compared to its original diesel-mechanical counterpart. The detailed emission reductions include 9% for NOx, 14% for PM, 46% for SOx, 28% for CO, and 44% for HC. Since CO_2 emission is directly tied with fuel consumption, it is also reduced by 18%.

Moreover, the system redundancy was greatly improved. The main engine operation time can be significantly reduced by 73%. The comparison between the original and hybrid propulsion systems was presented in Figure Q - 19. Auxiliary gensets were hardly used since all electricity can come from the ESS. The whole system was more reliable and flexible. Reduced operation time of the main engine means less wear of machinery, which can save maintenance costs.

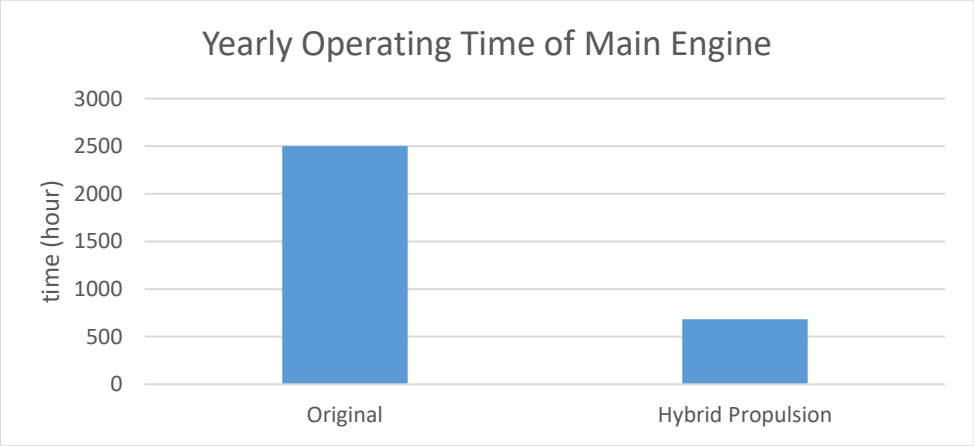

Figure Q - 19 Comparison of Main Engine Operation Time per Year

The comparison of simulation results was shown in Figure Q - 20, with different input data: statistical vs. generated timescale data. For the same hybrid architecture, the timescale load profile enables control logic to balance power from the engine and battery, which gives 10% more potentials of fuel efficiency improvement. Emissions were also reduced due to the less engine operation time.

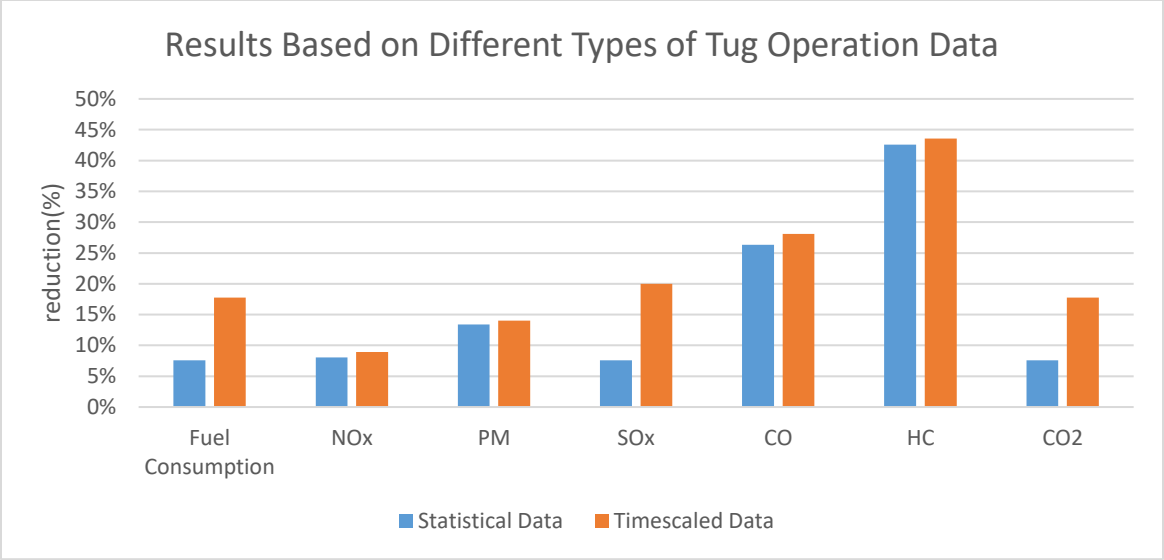

Figure Q - 20 Fuel Consumption and Emission Reduction of Hybrid Electric Tugboat

In the future, it is recommended to acquire real operating data from tugboats. With the implementation of measuring sensors, detailed information such as engine speed, torque, power, tugboat speed etc. can be recorded. The measured data then can be analyzed and used for further system design.

Q6. SUMMARY AND CONTINUING RESEARCH

In this work, we first modelled the load profile of various tugboats and then used the obtained load profile and our generic hybrid electric propulsion modelling tools to study the fuel efficiency and emission improvements potentials of a hybrid electric powertrain with added Li-ion battery ESS.

Traditionally the fuel efficiency and emission of tugboats have been evaluated based on the generic load profiles of the tugboats working at different function modes. In this work, we have chosen a representative tugboat load profile (or a very similar version) that has been used by multiple organizations in tugboat power analysis and design to carry out the fuel efficiency and emission simulations using our marine propulsion system model.

Considering different tugboats may have different load profiles unique to their routine duties, a timescale load profile has been generated based on collected data from the literature for a typical harbour tugboat as an alternative power demand input in analyzing tugboat energy efficiency and emissions. This timescale load profile can be obtained by recording the actual power load data of a tugboat, similar to the statistical driving and load cycles for ground vehicles. The higher resolution of power demand records and the time history provide a better load profile for the modelling, design optimization and optimal operation control of a tugboat with a hybrid electric propulsion system. The addition of the battery ESS for the hybrid electric or plug-in hybrid electric tugboats allows peak power shift in the time domain, a timescale load, or power demand, profile thus becomes essential in designing the hybrid propulsion system. In this work, fuel consumption and emission simulations using both traditional duty-divided and our new time-scale load profiles have been carried out in alternative propulsion system analyses and designs. To ensure

consistency, the newly proposed, standard time-scale load profile produces an identical duty-divided load profile used in the study.

The preliminary study showed that the proposed hybrid electric propulsion system can lead to 18% fuel saving and significant emission reductions. Results from duty-divided and time-scale load profiles are presented and compared, showing the need and benefit of acquiring statistical time-scale power load data for a specific tugboat. As the next step, the lifecycle cost of the hybridized tugboat will be studied to consider both the additional investment costs of the added battery ESS and power electronics, and the fuel cost saving gained from improved fuel economy. This is supported by our new battery performance degradation/lifecycle cost model under different ESS use patterns and by the newly proposed time-scale load profile model. The study will produce an accurate prediction on the payback period of the vessel electrification and hybridization, facilitate the selection of propulsion system architecture and optimization of hybrid electric powertrain components, and support accurate cost estimation for a specific application. Additional hybrid powertrain architectures, including plug-in hybrid, best suited for different tugboat load profiles will also be investigated.

The battery performance degradation model will be used in system design to evaluate battery lifecycle cost and optimize the size of the battery ESS and engine. The use of the LNG-diesel dual-fuel engine will be investigated with different propulsion system architectures in comparison to traditional diesel-mechanical and diesel-electric drivetrains for fuel cost and emission reductions. Further research will also incorporate our propeller cavitation model to predict and prevent tugboat induced ocean noise with needed design and operation changes. The study will lead to improved modelling and design optimization tools for tug electrification and hybridization.

ACKNOWLEDGEMENT

The authors would like to thank the support from Vince den Hertog, Brendan Smoker and Robin Stapleton at Robert Allan Ltd, and the discussions and comments from our group member Anthony Truelove. Financial supports and guidance from the Clean Transportation Initiative of Transport Canada are gratefully acknowledged.

REFERENCE

[1] P. K. Balakrishnan and S. Sasi, "Technological and Economic Advancement of Tugboats," in *International Conference on Emerging Trends in Engineering & Management (ICETEM)*, 2016.

[2] R. A. Ltd. *Tugboat Introduction*. Available: http://ral.ca/

[3] (2016) TUG AND WORKBOAT DESIGN GUIDE. *BC Shipping News*.

[4] V. d. Hertog, K. Harford, and R. Stapleton, "Raptures: Resolving the Tugboat Energy Equation," presented at the TUGNOLOGY, Amsterdam, The Netherlands, 2009.

[5] G. Faber and J. Aspin, "The foss hybrid tug: From innovation to implementation," in *Proc. of The 20th International Tug & Salvage convention and exhibition*, 2008, pp. 149-156.

[6] *The Hybrid Tug*. Available: www.foss.com

[7] C. Energy. Case Study: E-Kotug, RT Adriaan [Online]. Available: corvus-energy.com

[8] T. L. Vu, J. S. Dhupia, A. A. Ayu, L. Kennedy, and A. K. Adnanes, "Optimal power management for electric tugboats with unknown load demand," in *American Control Conference (ACC), 2014*, 2014, pp. 1578-1583.

[9] T. L. Vu, A. A. Ayu, J. S. Dhupia, L. Kennedy, and A. K. Adnanes, "Power management for electric tugboats through operating load estimation," *IEEE Transactions on Control Systems Technology*, vol. 23, pp. 2375-2382, 2015.

[10] L. C. W. Yuan, T. Tjahjowidodo, G. S. G. Lee, R. Chan, and A. K. Ådnanes, "Equivalent consumption minimization strategy for hybrid all-electric tugboats to optimize fuel savings," in *American Control Conference (ACC), 2016*, 2016, pp. 6803-6808.

[11] D. MacPherson and E. Boyd, "Understanding and Optimizing Vessel Propulsive Power and Fuel Use Using Duty Cycle Analysis Computations," *Journal of Ship Production and Design*, vol. 32, pp. 174-185, 2016.

[12] H. Kifune and T. Nishio, "Fuel Saving Effect of Hybrid Propulsion System-Case: Tugboat is not in Service," *Marine Engineering*, vol. 52, pp. 811-817, 2017.

[13] T. Nishio and H. Kifune, "A Study on Fuel Saving Effect in Hybrid Propulsion System for Tugboat," *Proceedings of 7th PAAMES and AMEC2016*, vol. 13, p. 14, 2016.

[14] T. Völker, "Hybrid propulsion concepts on ships," 2015.

[15] H. E. Lindstad and I. Sandaas, "Emission and fuel reduction for offshore support vessels through hybrid technology," *Journal of Ship Production and Design*, vol. 32, pp. 195-205, 2016.

[16] L. Browning and K. Bailey, "Current methodologies and best practices for preparing port emission inventories," *ICF Consulting report to Environmental Protection Agency*, 2006.

[17] C. Whall, D. Cooper, K. Archer, L. Twigger, N. Thurston, D. Ockwell, *et al.*, "Quantification of emissions from ships associated with ship movements between ports in the European Community," *Report for the European Commission. Entec UK Limited, Northwich, Great Britain*, 2002.

Appendix R. Case Study on Fishing Boats - Emission and Life-Cycle Cost Analysis of Hybrid and Pure Electric Propulsion Systems

Abstract

Commercial fishing is an important part of the Canadian economy, playing a vital role in the economic well-being of the coastal communities along the east and west coasts of Canada. Traditionally, these smaller fishing boats and commercial boats use less-efficient engines and produce considerable amounts of pollution collectively. Commercial fishing boats are capable of hauling thousands of kilograms of fish per voyage. Larger fishing boats that operate in greater depth have advanced equipment and facilities where the fish can be prepared and stored for sale. These vessels are also equipped with some amenities for workers for long stay in the ocean and they can do the job of several smaller boats. Fishing boats have a dynamic load profile. The location of fishing, method of capture and duration of the trip can also vary significantly each trip. Glas Ocean Electric of Halifax, NS, the subcontracting team of this project, has collected the operation data from a number of representative fishing and commercial boats. The company has been working with the east coast fishing communities in seeking clean energy fishing-boat propulsion solutions to reduce fuel cost and GHG emissions for the industry. In this work, the operations of lobster fishing boats have been selected for detailed study, including data acquisition, modelling, and simulations on various alternative propulsion system designs.

In recent years, progress on electrification of marine vessels has been made; however, the pace has been impacted by the different operational requirements of each type of vessel, relatively small batch of production, longer or varied lifetime, and complex design optimizations of the vessels' electric propulsion system and energy storage system (ESS). In this work, the hybrid electric and pure electric propulsion system designs for lobster fishing boats are studied based on in-field acquired operation data. A new integrated marine propulsion system modelling and simulation method and software tools, and a dedicated mobile data acquisition system have been introduced to support the quantitative analyses of energy efficiency, emission reductions, and life-cycle costs of a new or retrofitted fishing boat with hybrid electric and pure electric powertrains, compared with the traditional ICE-powered benchmark. Following the automotive industry's model based design (MBD) approach, modelling and simulation of electrified fishing ships under the acquired operation profile in MATLAB/Simulink have been carried out. Series hybrid electric and pure electric powertrain system designs with powertrain component models and rule-based system control, including properly sized electric ESS with SC or battery, have been studied. The total GHG emissions and life-cycle costs of various new, electrified boat propulsion system designs have been quantitatively evaluated against conventional ICE-powered boats with both gasoline and diesel engines. The life-cycle costs of the competing powertrain systems include the investment costs, operation/energy-consumption costs, and the replacement costs of key powertrain components over a projected ten-year operation life. Both of the new hybrid electric and battery-powered pure electric boat designs showed considerable GHG emissions reduction and favourable life-cycle cost saving. The study presents superior clean propulsion system solutions for lobster fishing boats with quantitative justification and detailed powertrain system and control system designs, forming the foundation for further research and development.

Nomenclature

AC	Alternative current	MBD	Model based design
BESS	Battery energy storage system	MOO	Multi-objective optimization
BEV	Battery electric vehicle	Ni-MH	Nickel metal hydride
CO_{2e}	Carbon dioxide equivalent	n	Number of years
DC	Direct current	n_t	Time in seconds
DOD	Depth of discharge	OE	Total operation and investment cost
ESS	Energy storage system	PEVs	Pure electric vehicles
e_a	Input voltage	P_{ESS}	Generated power by energy storage system
e_b	Back electromotive force	P_{DG}	Power generated by the diesel generator
FC	Fuel consumption	P_{demand}	Vessel's power demand
GDP	Gross domestic product	RPM	Revolutions per minute
GHG	Greenhouse gas	R_F	Diode resistance
HEVs	Hybrid electric vehicles	R_a	Motor armature resistance
hp	Hours power	$R_{ds\ ON}$	Drain-to-source on-state resistance
ICE	Internal combustion engine	SC	Supercapacitor
IMO	International Maritime Organization	SOC	State of charge
I_F	Diode average current	$TC_{Hybrid\ series}$	Total cost of hybrid series architecture
I_m	Maximum switch current	t_f	Switch fall time
i_a	Armature current	t_r	Switch rise time
j	Motor's moment of inertia	V_F	Diode average voltage
K	Machine constant	V_m	Maximum current
K_b	EMF constant	v	Applied voltage
K_t	Torque constant	B	Friction constant
kt	Knot	$\theta(t)$	Motor's angular position
Li-ion	Lithium-ion	ΔT_j	The jth time interval
L_a	Armature inductance		

R1. INTRODUCTION

Maritime transportation emits about 961 million tonnes of CO2 equivalent (CO2e), accounting for 2.8% of global GHG emissions [Smith et al., 2015]. This is more than the total emissions produced by Canada in 2013 [EC, 2014] and this number is expected to increase to 5% by 2050 [EMSA, 2018]. Depending upon the future gross domestic product (GDP) and socio-economic and energy efficiency, the growth rate could be higher than this predicted value. To address this issue, the International Maritime Organization (IMO) standards, referred to as Tier I, Tier II and Tier III, were introduced to set limits on NOx and SOx emissions from marine vessels.

The strict and evolving environmental regulations enforced by regional and national governments as well as the IMO have forced ship owners to seek alternative solutions to meet these standards while trying to lower associated operational expenses at the same time. Electric and hybrid-electric propulsions have been proven in a range of vessel types over the last few decades as one of the most efficient powertrain architectures. The fuel-saving potential of electric propulsion in comparison with mechanical propulsion is a strong driver for the adoption of electric propulsion for many of these vessels. The fuel-saving is largely due to the fact that many vessels usually have a very dynamic load profile and seldom operate at the most efficient rpm of the vessel's Internal Combustion Engines (ICE). The hybrid electric propulsion systems can use its ESS to store surplus energy from the ICE when it is not needed and return it to the system when required. In these systems, the size of the ICE can be reduced, and the ICE can operate at its maximum power and efficiency. The maritime industry is also moving fast to maintain pace with current hybridization and electrification demand.

Although hybridization and electrification of vessels is an appealing solution for different vessel types, it may not be the best option for many vessels that spend most of their time at a constant speed with a constant power load and long sailing distance. The optimum powertrain architecture for vessels should be selected based on their specific designs and operational load profiles. This means that naval architects need to consider a different vessel classification type from the recognized classification societies like the International Association of Classification Societies (IACS). For electrification, naval architects need to classify the ships and boats based on their load profiles and select a proper powertrain architecture that best suits the power demand.

Unlike the other publications that prescribe a powertrain for all vessels, the focus of this paper and the produced results are based on a specific type of fishing boats. These boats have a very dynamic load profile and this makes them an excellent candidate for hybrid and electric propulsion systems [Capasso et al., 2017; Martelli et al., 2017]. In this work, a specific load profile of two lobster fishing boats has been introduced using their statistical operation data. Series hybrid electric and battery electric powertrain architectures are modelled, and performance of these design variations are examined based upon the obtained load profiles. The MBD methodology employed in this work, however, is generically applicable to all different types of marine vessels as long as their operation profiles are established.

R1.1 Modelling of Fishing Boat Operation Patterns

R1.1.1. Fishing Boats and Their Operation

Fishing boats have a dynamic load profile. Commercial fishing boats are capable of hauling a catch of thousands of kilograms of fish per voyage. Larger fishing boats that operate in higher depth

have advanced equipment and facilities where the fish can be prepared and stored for sale. These vessels are also equipped with some amenities for workers for longer trips in the ocean and they can do the job of several smaller boats. The location of fishing, method of capture and duration of the trip can also vary significantly each trip. For this purpose, two different lobster fishing boats, similar to the vessel shown in Figure R - 1, have been selected for this study. These boats typically have a single diesel engine that provides all power used aboard. The power is distributed via a direct mechanical link, as well as hydraulic and electrical systems from the main engine to various appliances aboard the vessel. These typically include propulsion, trap-haulers (winches), power steering, water pumps, navigation electronics, and heaters.

Figure R - 1 A typical Canadian east coast lobster fishing boat [6].

Each boat operates approximately 6 hours per day. The total operational hours of each boat is estimated around

$$6\ \frac{hours}{day} \times 30\ \frac{days}{month} \times 6\ \frac{months}{year} = 1080\ \frac{hours}{year}$$

Detailed information about the two fishing boats is given in Table R - 1.

Table R - 1 Detail information of the studied boats.

	Boat 1	**Boat 2**
Length:	12.2 m	13.7 m
Beam:	5.2 m	3.66 m
Displacement:	15 tonnes	15 tonnes
Engine:	300 kW	242 kW
Max speed:	14 kt	16 kt
Cruise Speed:	10 kt	13 kt
Engine RPM at cruise:	1,600 RPM	1,200 RPM
Propeller:	5 blades, 0.76mx0.66m	4 blades, 0.6 m/0.66 m
Daily operation time:	6 hrs	6 hrs
Yearly operation time:	1,080 hrs	1,080 hrs

R1.1.2. Current Fishing Boats Powertrain Configuration

At present, smaller fishing boats have a conventional mechanical powertrain with a gasoline or diesel engine connected with the mechanical drivetrain. Some larger vessels may have a hydraulic drive system to improve the torque characteristics over mechanical drive and use an additional generator for hotel loads. The current mechanical powertrain of small fishing boats is illustrated in Figure R - 2, and used as the benchmark in this study. This powertrain architecture represents a conventional propulsion system, consisting of the prime mover(s), reduction gears, medium length shafts, and propeller(s). The prime mover drives the shaft at medium speed and connects to the propeller through reduction gears to obtain appropriate speed and higher torque. The propeller works at several hundred revolutions per minute (RPM) and produces thrust. Meanwhile, the hydraulic pump attached to the diesel engine provides power for the trap hauler and power steering. A representative trap-hauler consumes an average of 8.7 kilowatts power based on the manufacturer's specifications. A small alternator attached to the engine meets the remaining electrical loads in the boat.

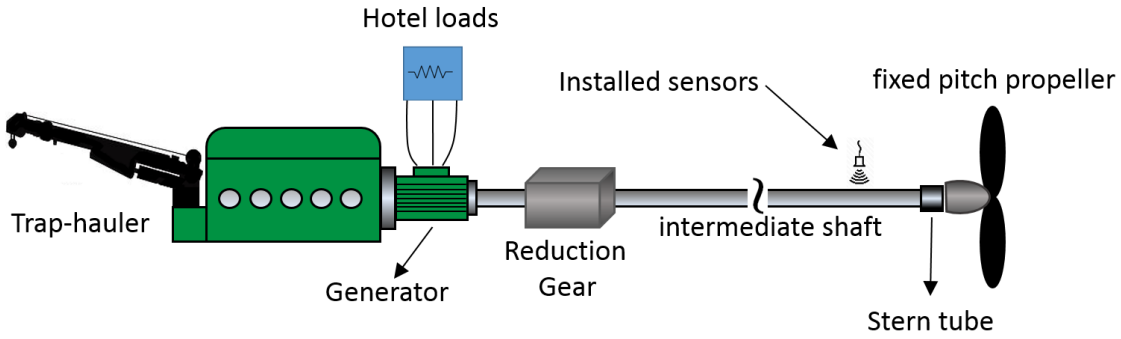

Figure R - 2 Pure mechanical propulsion system.

R1.1.3. Acquisition System Description and data collection

Evaluation of energy efficiency, GHG emissions, and operation costs of a marine vessel needs to be based upon their actual operations. To accurately assess the engine performance, speed and torque sensors have been mounted onto the propeller shaft of the vessel understudy for representative operation days, as shown in Figure R - 3.

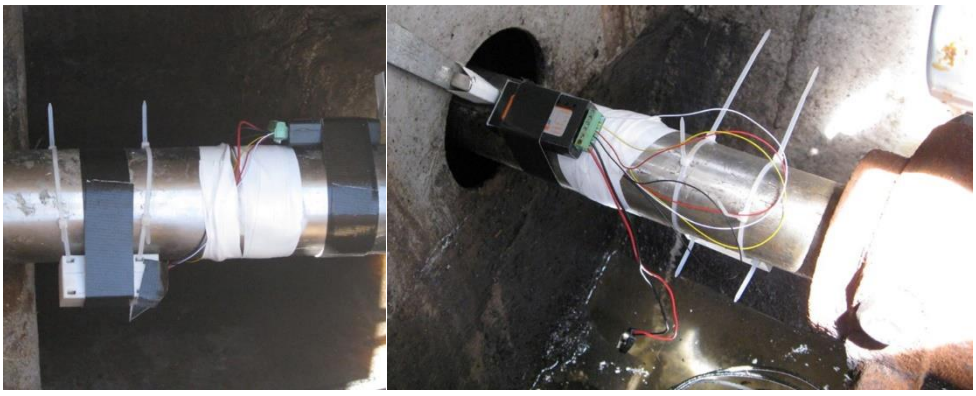

Figure R - 3 Strain gauge installations.

Figure R - 4 through Figure R - 9 illustrate the collected data from two fishing boats. The data acquisition system was installed on both vessels and shaft torque and speed data were collected for simulation and model validation. The collected data enable a direct comparison between the current mechanical powertrain and the two proposed powertrain architectures. Operational data was collected over the summer of 2017 and one representative mission profile was identified as a good representation of the boat's daily operational variability.

Given that both boats are under operation as lobster fishing vessels, the similarity in the load profile is expected. Figure R - 6 and Figure R - 9 illustrate the required vessel's engine power. Travelling to the fishing zone from the wharf accounts for the sustained peaks at the beginning of the collected torque and rpm data. Upon arriving at the fishing zone the Captain brings the boat to a stop at each trap to work on the trap and moves to the next afterward (as illustrated by Figure R - 6 and Figure R - 9). This process accounts for the intermittent peaks and negative torques before each stop. After all traps have been serviced, the vessel returns to the wharf. This process accounts for the sustained peak near the end of the collected torque and rpm data. Finally, the vessel motors around the wharf unloading catch, traps and gear before docking. This process accounts for the smaller peaks at the end of the collected torque and rpm data.

In designing a traditional, mechanical marine propulsion system, the "power spectrum" approach is commonly used for accessing the propulsion power and determining the engine size of marine vessels. However, the addition of sizable battery ESS and the optimal energy management in a hybrid electric powertrain system have changed the needed design approach and demand consideration on the "time series" of power consumption. This is due to the fact that energy produced by the ICE can be stored in the ESS and used at a different time. The time-series data of power and energy demands allow optimal energy management and power control to be developed through global optimization of energy use during the complete trip using Dynamics Programming (DP). This is the foundation and one of the principal advantages of hybrid electric propulsion technology, and the approach is commonly used in the automotive industry for the development of hybrid and plug-in hybrid electric vehicles. Using this approach, the power and torque pulses of a vessel over a very short duration can be satisfied by borrowing the stored energy and power from the ESS without oversizing the engine to accommodate these transient loads. The hybrid electric powertrain system handles transient loads without oversizing the engine(s), and ensuring the properly sized engine(s) to operate mostly at its preferred speed and torque with peak fuel efficiency. This is particularly the case for smaller vessels, such as the fishing boats included in this study.

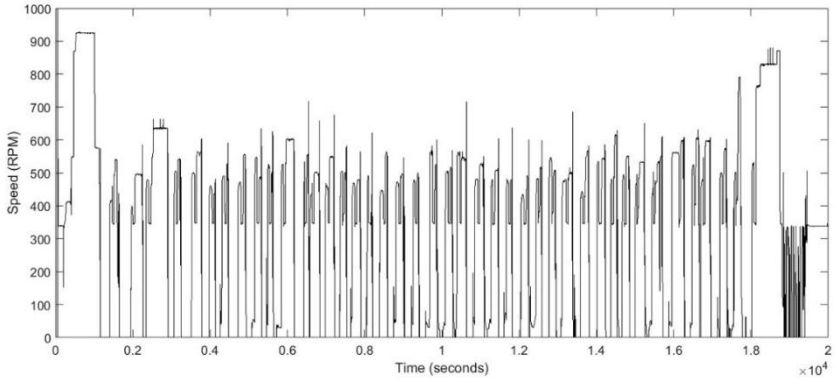

Figure R - 4: Propeller speed for boat1.

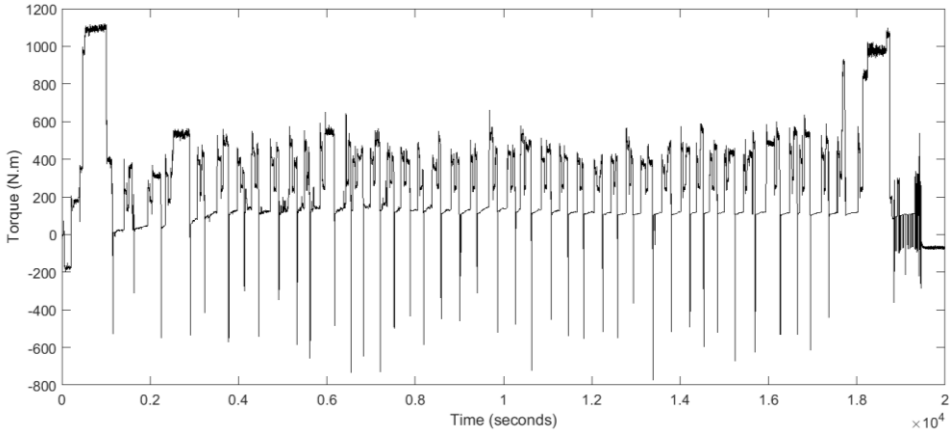

Figure R - 5 Shaft torque for boat1.

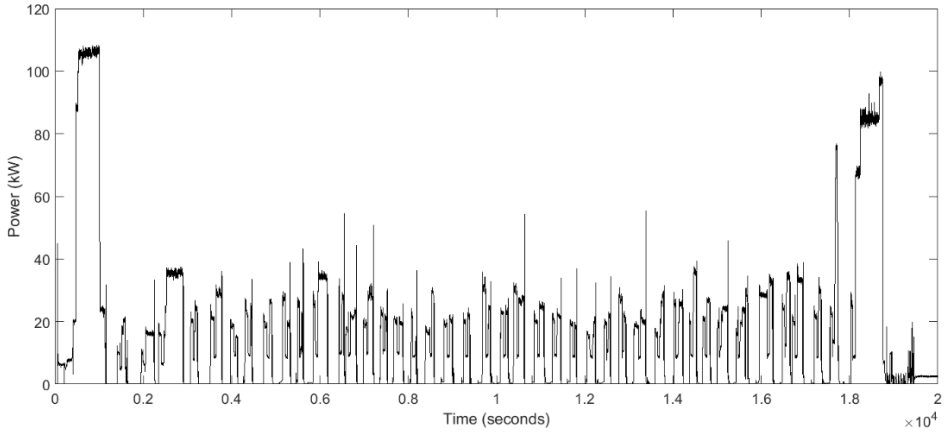

Figure R - 6 Engine power for boat1.

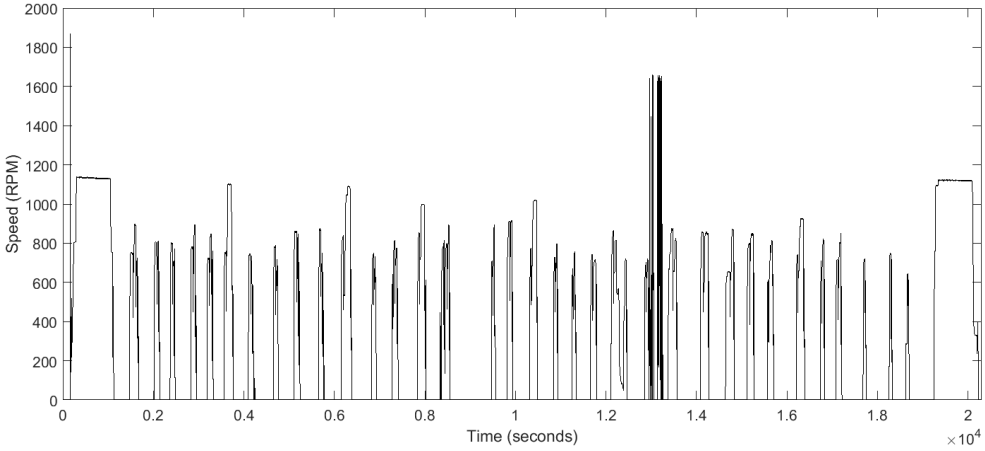

Figure R - 7 Propeller speed for boat2.

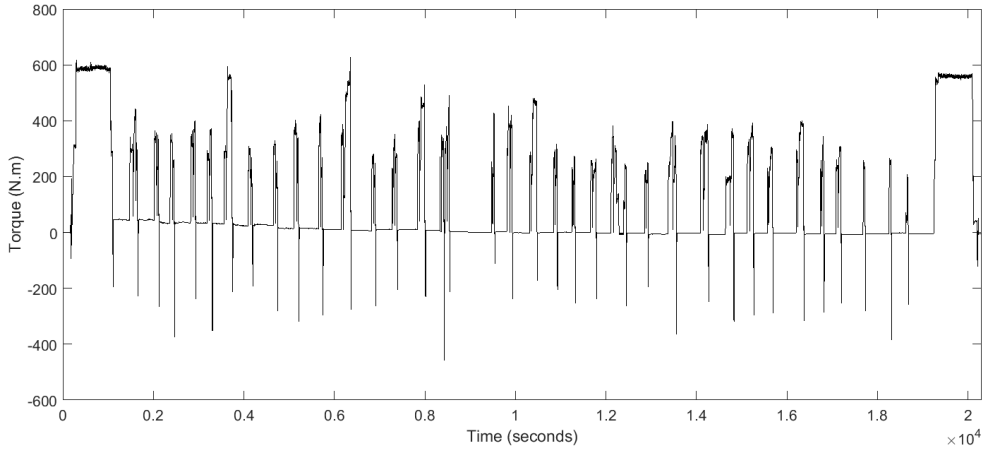

Figure R - 8 Shaft torque for boat2.

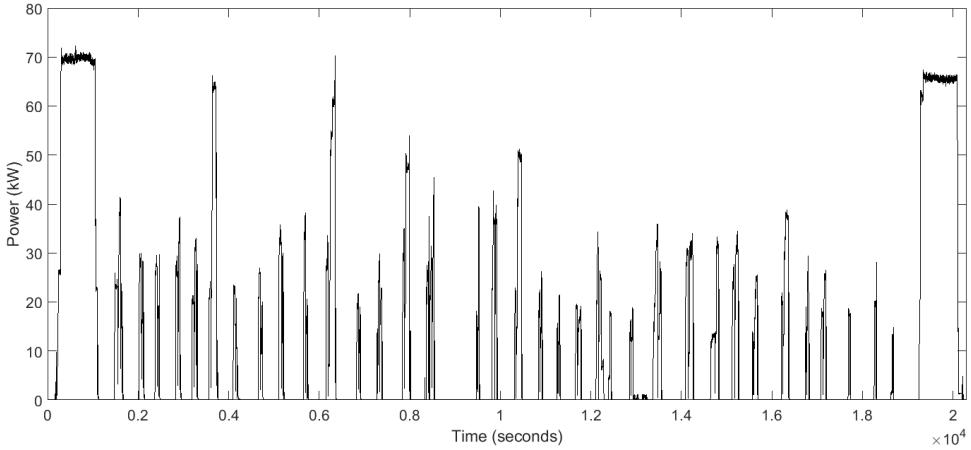

Figure R - 9 Engine power for boat2.

R2. POWERTRAIN HYBRIDIZATION

R2.1 Advantages of Advance Hybrid Electric Propulsion System with DC Power Bus

The proposed series hybrid electric powertrain system design is depicted in Figure R - 10. The advantages of this powertrain system design include longer life-time of diesel engine, flexibility in powertrain component layout, higher system energy efficiency, and the possibility of using a smaller ICE. These would result in noticeably improved fuel consumption over the low/medium speed ranges. The hybridization also increases the dynamic response of the boat and reduces engine noise.

The DC power system used in this powertrain has some obvious advantages over a traditional AC system. The DC power system uses the same well-proven AC electrical machine as a generator and motor while increasing the overall system efficiency. The DC power system improves the

diesel engine's efficiency and reduces its fuel consumption due to variable speed generation. The ICE can operate at optimal fuel consumption, as the ICE and rotor are not mechanically coupled. More weight and space is saved in the DC power system and the connection of generators in parallel is simpler in comparison to the AC power system. The current trend in the shipping industry is moving towards DC distribution systems because of the flexibility they offer in introducing energy storage, fuel cell, and solar technologies [7].

R2.2 Proposed Hybrid Series Architecture

Figure R - 10 illustrates a schematic of the series hybrid powertrain system with a DC bus. The power from the synchronous generator is rectified to DC voltage. Other loads, including hydraulic pumps and auxiliary (hotel) loads, are connected to the DC bus via DC/AC inverters. The ESS is also connected to the DC bus by an internal DC/DC converter. A three-phase electrical motor is fed through the DC bus via an electric driver and rotates the propeller at the desired speed. The battery and supercapacitor have been selected to be used in the ESS. The supercapacitor was studied because a supercapacitor ESS, unlike a battery system, has none or very little degradation over a high rate of charge and discharge with dynamic load changes of the type of boats studied in this work. More discussion on supercapacitor ESS is given in the following section.

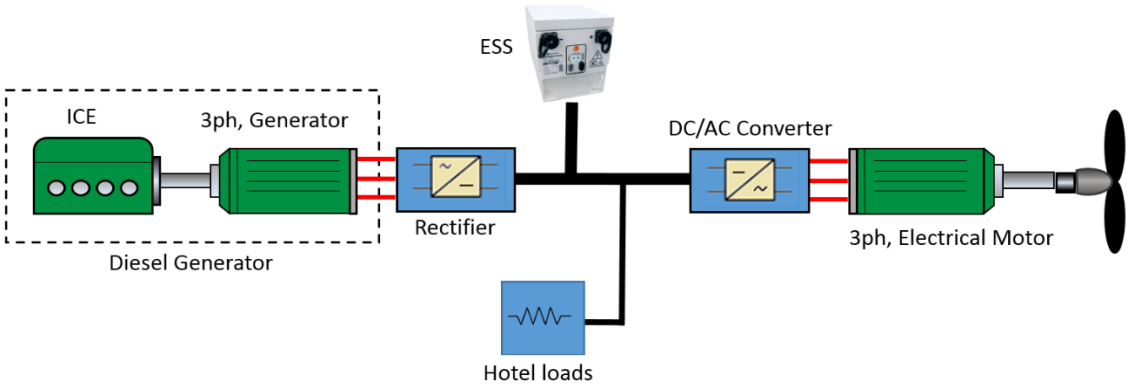

Figure R - 10 Series hybrid electric propulsion system.

R3. BATTERY ELECTRIC POWERTRAIN

R3.1 Advantages of Battery Electric Fishing Boats

Pure battery-electric powertrain systems offer unique advantages over other architectures such as higher energy efficiency, lower noise levels, and greater reliability. Factors such as high capital cost, the need for proper battery cooling mechanisms, bulky and expensive fast-charging stations, and the high cost of expanding existing electrical grid infrastructure in some cases have limited the widespread adoption of this design. The number of battery electric vessels is increasing rapidly. The first battery-electric car ferry, the Norled AS MF Ampere, entered service in Sognefjord, Norway, in 2015 [8]. It has been estimated that it annually offsets the use of one million litres of diesel which translates to the emissions of 2,680 tonnes of carbon dioxide and 37 tonnes of nitrogen oxide [9].

R3.2 Pure Battery Powered Powertrain System

The proposed battery-powered powertrain architecture is illustrated in Figure R - 11. The Battery Energy Storage System (BESS) is coupled to a DC/AC converter to step up the voltage and provide power for the rest of the system. Similar to the series hybrid electric powertrain architecture, the power distribution system can be either AC or DC. In the case of a DC distribution grid, electrical power is transferred to a DC/AC converter to provide power for propulsion. Auxiliary loads can also be connected to the AC or DC bus. In the case of the DC bus, extra DC/AC inverter(s) is needed to provide power for the AC loads aboard.

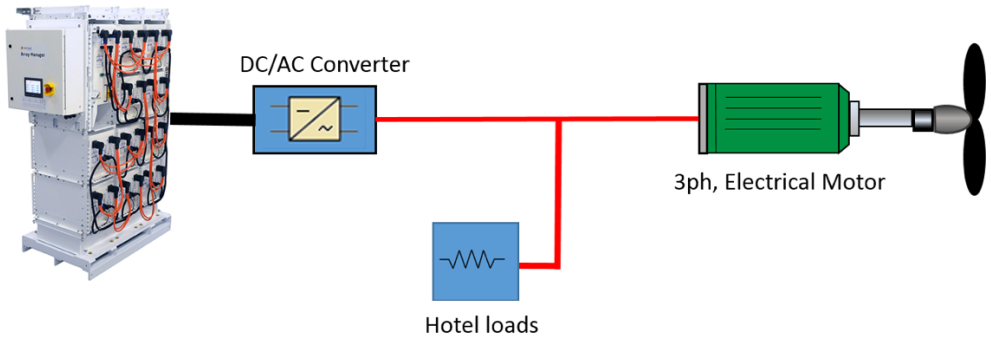

Figure R - 11 Pure battery electric propulsion system.

R4. MODELLING OF POWERTRAIN SYSTEM

The core of this study is to develop a powertrain system model with sufficient resolution to capture the dynamic behaviour of all critical powertrain components to optimize the size of the ICE and ESS. The developed model must be computationally efficient so that it can be used in the system design optimization. For this purpose, according to [10], many high-frequency dynamics related to converter models can be replaced with a more straightforward power loss model with little impact on modelling and simulation results. The Model Based Design (MBD) approach that is widely used in the automotive industry has been using in this work to form the powertrain system model of the marine propulsion system, and implemented in MATLAB/Simulink. The complete powertrain system model consists of blocks of powertrain system component models as illustrated in Figure R - 12. These components are connected to form the complete powertrain system of different powertrain system architectures, such as the hybrid electric powertrain system architecture detailed in Figure R - 12 to capture power flow or power loss of the system. Methods for constructing MATLAB/Simulink models are explained in various reference books.

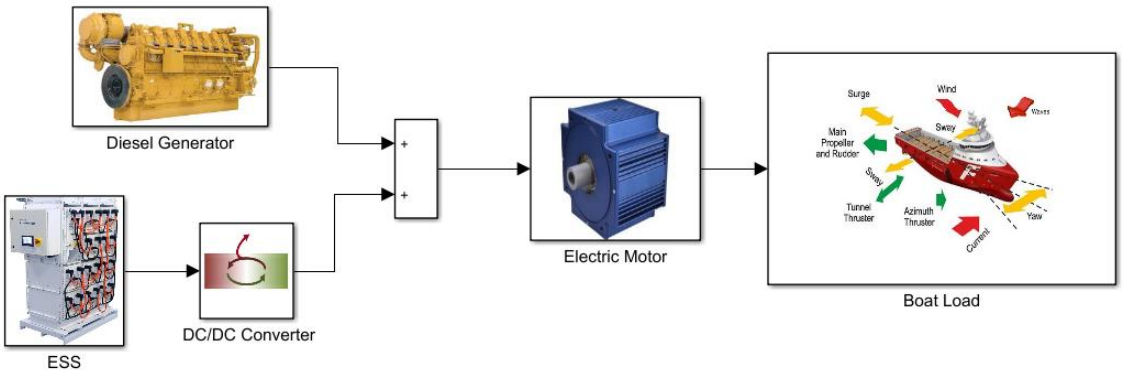

Figure R - 12 Different components of the hybrid electric powertrain

R4.1 ICE Model

In this work, the gasoline and diesel engine performance and emission models are based on the models in the Advanced Vehicle Simulator (ADVISOR), developed by the US DOE National Renewable Energy Laboratory [32]. As a MATLAB/Simulink based simulation program for rapid analysis of the performance and fuel economy of light and heavy-duty vehicles, the engine powertrain component models in ADVISOR fit the engine specifications of the fishing boats well. The engine Fuel Consumption (FC) was calculated for every step of the simulation for given power and torque demands from the powertrain control system. To capture the dynamics of the engine model, a linear first-order transfer function was employed [11]–[15]. Similarly, an engine actuator and controller transfer function along with a feedback loop were implemented and parameters tuned up within the range given in [12]. The simulated engine model in MATLAB/Simulink is shown in Figure R - 13.

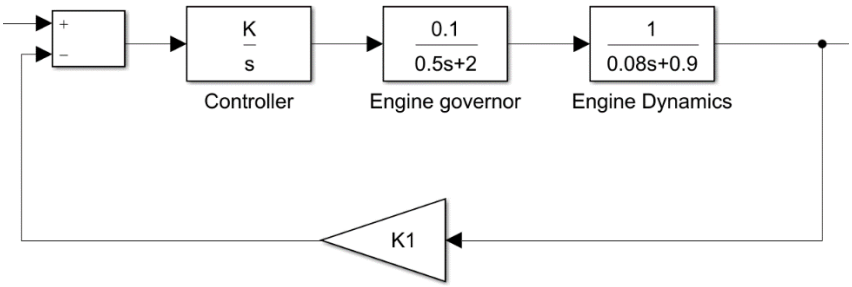

Figure R - 13 Engine model transfer functions

R4.2 DC/DC Converter Power Loss Map

DC/DC converters have taken much attention in recent years, mostly because of their applications in hybrid electric vehicles and renewable energy systems. In these systems, power constantly flows between the ESS (usually battery) and the rest of the systems. This converter is an essential component for power management in an electrified boat. A hybrid electric powertrain uses DC/DC converters to transfer the excessive power from the genset to the ESS or reverse.

A voltage doubler boost converter was modelled and simulated to produce an accurate power loss model for the DC/DC converter, to account for its power use and to remain computationally efficient. In simulating its power loss, the voltage and current across each element of the circuit are calculated. The voltage double boost converter circuit diagram is illustrated in Figure R - 14.

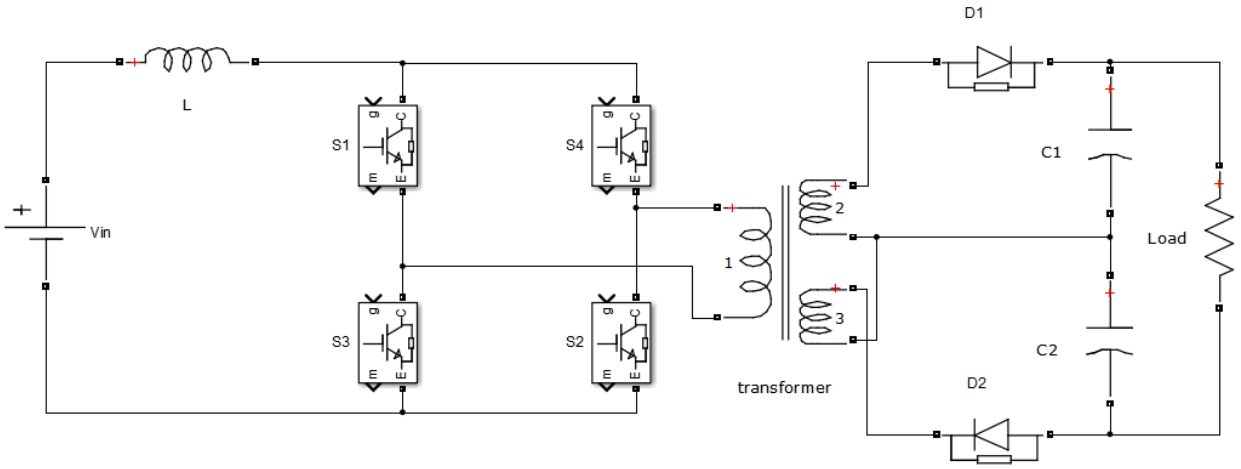

Figure R - 14 A generic voltage doubler boost converter.

The total switching loss of the converter can be calculated by using the fall (t_f) and rise (t_r) time available on the datasheet [16].

$$P_{switching\ loss} = P_{t_r} + P_{t_f} = \frac{1}{6} V_m I_m (t_r + t_f) f \qquad \text{(R - 1)}$$

where V_m and I_m are the maximum voltage and current across the switch and f is the switching frequency. The conduction loss is determined by the on-resistances of the switch ($R_{ds\ ON}$) and the transistor RMS current (I).

$$P_{cond} = R_{ds\ ON} \times I^2(rms) \qquad \text{(R - 2)}$$

The antiparallel diode loss is equal to

$$P_{loss}(diode) = V_F I_F(av) + R_F {I_F}^2(rms) \qquad \text{(R - 3)}$$

where I_F and V_F are diode current and voltage; R_F is the diode resistance which can be found in the datasheet. The converter efficiency map is shown in Figure R - 15. The input voltage has changed from 22 V to 42 V and the output power varied from 500W to 1000W. Converter power loss calculated using three components:

$$P_{converter\ loss} = P_{loss} + P_{cond} + P_{switching\ loss} \qquad \text{(R – 4)}$$

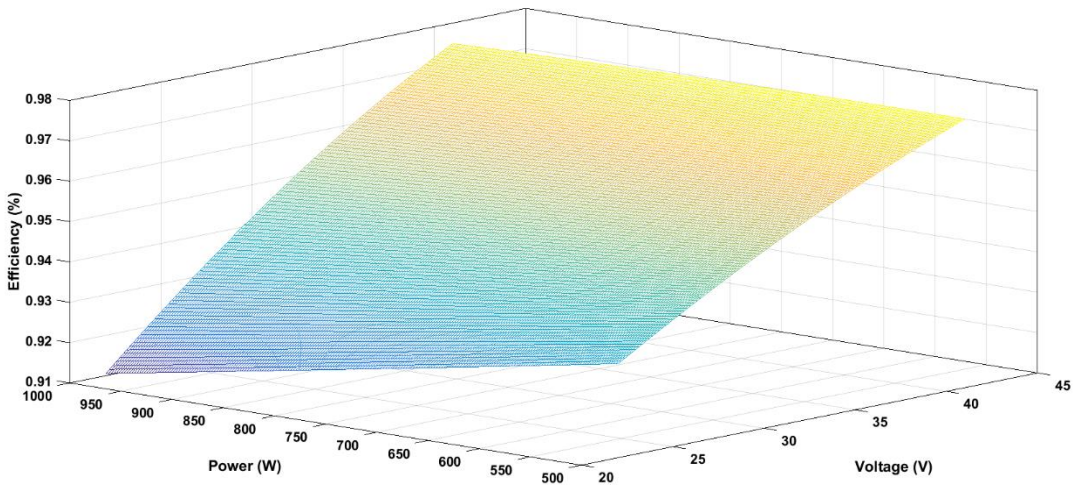

Figure R - 15 Efficiency map of the DC/DC converter.

R4.3 Battery ESS Model

A battery energy storage system (ESS) is an essential part of the hybrid electric and pure electric powertrains. A lithium-ion (Li-ion) battery was selected as a suitable candidate due to high energy density, low self-discharge rates, and successful applications in the maritime industry [9]. The battery performance model has been extensively discussed in the literature and a comprehensive review of the battery system is given in [17]. A more simplified model, which is required for system modelling is given in [18] and the model parameters of an equivalent circuit battery model as shown in Figure R - 16 are determined using experimental data [19]. This Thevenin equivalent circuit model is selected due to its capability of approximating the dynamic behaviour of different types of batteries, including valve-regulated lead-acid [20], nickel-metal hydride (Ni-MH) [21], and LiB [22]. The battery Thevenin equivalent circuit is shown in Figure R - 16.

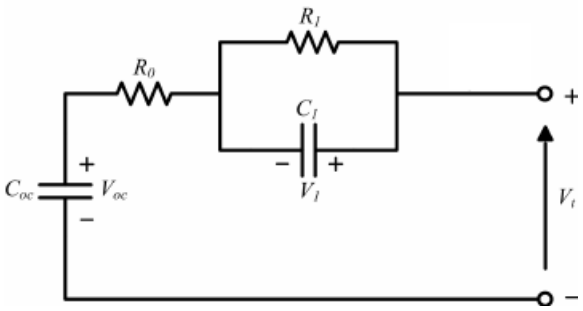

Figure R - 16 Thevenin equivalent circuit for the battery system.

Since the introduction of Li-ion battery in the 1990s, the performance, life cycle and cost have improved significantly. A comprehensive cost analysis of Li-ion battery technology for a battery electric vehicle (BEV) is given in [23]. The cost of Li-ion battery has dropped from CDN$655 per kWh in 2008 to about CDN$394 per kWh in 2014. It is also predicted that battery cost may drop to CDN$262 per kWh in 2020 and CDN$197 per kWh in 2025 [23]. In this paper, CDN$700/kWh

is used for battery pack cost based on harsh marine conditions and the data from a leading marine battery ESS manufacturer.

The life-cycle costs of the hybridized and electrified propulsion system consist of various costs of all powertrain components, including their investment costs, the costs of fuel and/or electric energy, and the replacement costs of key powertrain components within the projected lifetime. Among those, the batteries have a shorter life and need to be replaced within the life-cycle of the system. The hybrid electric boat has a smaller BESS and a shallow depth of discharge (DOD), thus last for a longer time. For shallow DOD, a lithium-ion phosphate battery can last for about ten years, before its charging capacity drops by 20%. With proper battery sizing at 30 kWh to work with a 40kW diesel engine, the battery pack in this study is expected to cover the ten-year lifetime of the hybrid electric powertrain. The proper use of the BESS is controlled by the energy management system of the hybrid electric powertrain. The battery pack of representative HEV, Toyota Prius, has been reported to have an average of thirteen years of operation life [J. Goreham, 2017].

The BESS of the pure electric powertrain provides all propulsion energy that can be calculated from the measured power load of the boat, leading to a much larger battery and a deep DOD. During the six hours of boat operation under the obtained load profile and the total amount of energy consumption, the state of charge (SOC) of the BESS is controlled between 15% and 95% between each deep charge at night. For six hours of operation, the BESS needs to have a capability of 97 kWh. At 80% deep DOD of each operation day, the battery will last about 1,000 cycles [S. G. Chalk and J. F. Miller, 2006], equal to five years under the more demanding working condition. In this work, the battery life of pure electric boat was based upon similar studies on pure electric vehicle (PEV) [S. G. Chalk and J. F. Miller, 2006], and more accurate battery life and life-cycle cost predictions can be made using the accurate battery performance degradation model and given load profiles, forming our future work.

R4.4 Supercapacitor ESS Model

In-depth reviews on supercapacitors and their modelling can be found in [25][26]. Conventional capacitors have features similar to supercapacitors, but their volumetric energy density is about two orders of magnitude lower and cycle life is only half of the supercapacitors [27]–[29]. The cycle life of a supercapacitor is also slightly affected by its operating temperature and voltage [30]. In this work, the operating temperature and voltage of the supercapacitor is assumed to be constant. This is a reasonable approximation as the cooling seawater at about 12°C can be used for the thermal management of ESS and a controller can keep the voltage constant. Supercapacitors have low internal resistance, long cycle life, and high power density, and these advantages make supercapacitors an excellent candidate for the fishing vessels with dynamically changing power loads. A supercapacitor block [30] in MATLAB/Simulink was implemented to capture the dynamic behaviours of the supercapacitor and its interaction with other powertrain components. The computation efficient model can depict the dynamics of the supercapacitor with acceptable accuracy.

R4.5 Transfer Function of Electric Motor

Using motors governing differential equations, the transfer function of the electric motor can be derived [31]. The motor torque equation can be written as

$$T_m(t) = j\frac{d^2}{\mathrm{dt}}\theta(t) + B\frac{d}{dt}\theta(t) \quad \text{(R - 5)}$$

where j is the moment of inertia, B is the friction constant, and $\theta(t)$ is the motors angular position. The motors back Electromotive Force (EMF) voltage equations is given by

$$e_b(t) = K_b\frac{d}{dt}\theta(t) \quad \text{(R - 6)}$$

where K_b is the EMF constant. Motor input voltage can be written as

$$e_a(t) = R_a\, i_a(\mathrm{t}) + L_a\frac{d}{dt}i_a(t) + e_b(t) \quad \text{(R - 7)}$$

where K_b is the EMF constant and R_a is the armature resistance, L_a is the armature inductance and i_a is the armature current. By assuming a zero initial condition and then using a Laplace transform we have:

$$\frac{w(s)}{E_a(s)} = \frac{K_t}{(L_a s + R_a)(Js + \mathrm{B}) + K_b K_t} \quad \text{(R - 8)}$$

The electric motor parameters are given in Table R - 2.

Table R - 2 Motor parameters

Armature resistance ($\boldsymbol{R_a}$)	Armature inductance $\boldsymbol{L_a}$	Moment of inertia ($\boldsymbol{J}$)	Friction constant ($\mathbf{B}$)	Torque constant ($\boldsymbol{K_t}$)	EMF constant ($\boldsymbol{K_b}$)
2 Ω	0.5 H	0.02 Kgm^2	0.2 Nms	0.015 Nm/A	0.01 Vs/rad

R5. OPTIMAL SIZING OF GENERATOR AND BATTERY ESS

The aim of powertrain component optimization is to find the optimal sizes of the genset and the battery ESS to form a proper powertrain system design. The optimization of any maritime vessel's powertrain system should provide a design that meets all vessel performance and regulatory requirements while minimizing the cost and fuel consumption of the vessel. The fishing boat powertrain system optimization problem is formulated as a Multi-Objective Optimization (MOO) problem with conflicting design objectives of minimizing the overall life-cycle costs (both capital and operational) and minimizing GHG emissions at the same time. The design constraints of the formulated MOO problem include:

$$P_{DG} + P_{ESS} = P_{demand} \quad \text{(R - 9)}$$
$$0 \le P_{DG} \le P_{DG_{max}}$$
$$P_{ESS_{Min}} \le P_{ESS} \le P_{ESS_{max}}$$

where P_{DG} is the power generated by the diesel generator, P_{ESS} is the power provided by the ESS, and P_{demand} is the given vessel's power demand.

R5.1 Formulation of Emission Reduction Objective

The Global Warming Potential (GWP) method that is established for calculating the impact of all released gases at a future time (e.g. 100 years) has been used to calculate the total equivalent CO2 emissions of the vessel. The total equivalent CO2 formulated as:

$$CO_{2_{e\ TOTAL}} = FC \times y \times trips \times K_f \times n \quad \text{(R - 10)}$$

where n is the number of vessel's operation days, FC is the engine fuel consumption per trip, y is the number of years, $trips$ is the number of vessel trip per day and K_f is the emission factor for marine diesel given in [32]. The total CO2e is calculated based on the GWP values of different gases given in the fourth assessment report of the Intergovernmental Panel on Climate Change (IPCC) [33]. The GWP values of CO2 and two other related gases are given in Table R - 3.

Table R - 3 Global warming potential of three gasses.

GHG emissions	CO_2	CH_4	NO_2
GWP	1	25	298

R5.2 Formulation of Overall Lifecycle Cost Objective

The total cost of hybrid electric and battery electric powertrain are given as:

$$TC_{Hybrid\ Electric} = n \times trips \times \sum_{j=1}^{n_t} \sum_{i=1}^{n_G} FC_{ij} \times Fuel\ Cost \times \Delta t_j + OE \quad \text{(R - 11)}$$

$$TC_{Battery\ Electric} = n \times Electricity\ Cost \times \sum_{d=1}^{180} \text{BESS}_{kWh-consumed_d} + OE \quad \text{(R - 12)}$$

where Δt is the simulation's time step, and OE represents other expenses listed in Table R - 4.

R6. RESULTS AND ANALYSIS

R6.1 Component Interactions

The introduced hybrid electric propulsion system model is computationally efficient for predicting the energy efficiency and emissions of different design options, thus supporting the propulsion system design optimization. The model could capture the component interactions and interdependencies with a sufficient level of detail. The powers derived from the generator and the ESS for the hybrid electric system are shown in Figure R - 17. Initially, the ESS and genset provide power for travelling to the fishing zone from the wharf at full power of about 60 kW. When the vessel reaches a lobster trap, the propulsion power drops to zero but the genset continuously works at its maximum power (13 kW) to charge the ESS. When the ESS reaches its maximum State of Charge (SOC), the charging stops and the genset follows the power demand (black solid curve). The supercapacitor SOC, current and voltages are shown in Figure R - 18. At present, the duration of the simulation spans more than six hours of operation, due to the need for the genset to fully charge the ESS at the start or end of the trip. A better and more preferred alternative is to obtain this full charge using the "plug-in" charge capability from the electric power grid at the shore. The present setting is used to facilitate a fair energy use comparison.

Figure R - 19 illustrates the response of the engine and supercapacitor to abrupt changes in the vessel's power requirements. As the vessel's power increases, the engine tends to increase power output, however, due to engine inertia and engine time lag, this response is slow. The ESS responds first and provides power until the engine power catches up.

Table R - 4 System costs.

Variables		Conventional ICE powertrain	Series hybrid with SC ESS	Pure battery powered
Investment Costs	Inverter cost	-	0.21 $/W-DC [34]	0.21 $/W-DC [34]
	ESS cost	-	5,500 $/kWh[35]	700 $/kWh [36]
	ESS Installation labor	-	0.15 $/W [34]	0.15 $/W [34]
	Electric motor	-	$8,000	$8,000
	Charger station	-	-	$20,000
	Charger station Transformer	-	-	$5,000
	Diesel generator unit cost	121,000$ @238kW [37]	11,000$ @ 15kW [37]	-
	Diesel generator Installation labor cost	50 $/kW	50 $/kW	-
Total		132,900$	226,150$	56,250$
Operational costs	ESS operation and maintenance	-	20 $/kW/ year [34]	20 $/kW/ year [34]
	Fuel cost	1.121 $/L [38]	1.121 $/L [38]	-
	Diesel generator operation and maintenance	30 $/kW/year	30 $/kW/year	-
	Electricity cost	-	-	Varies [39]

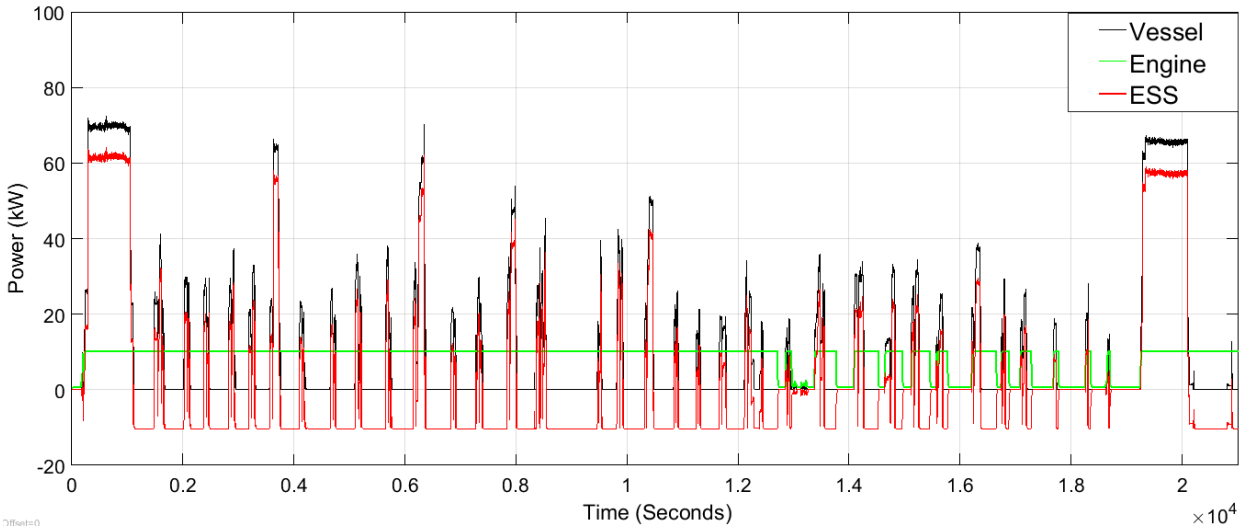

Figure R - 17 Generator power, ESS power and vessel demand power.

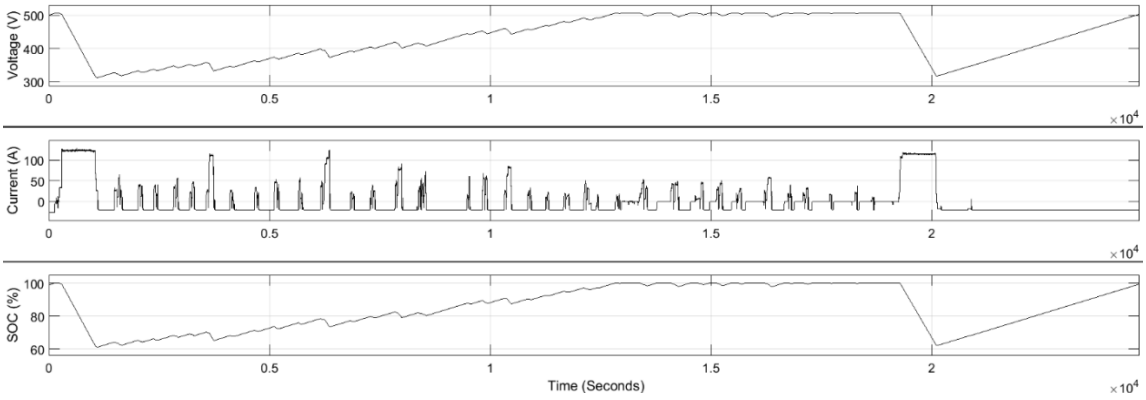

Figure R - 18 Supercapacitor voltage, current and SOC (%) during a trip.

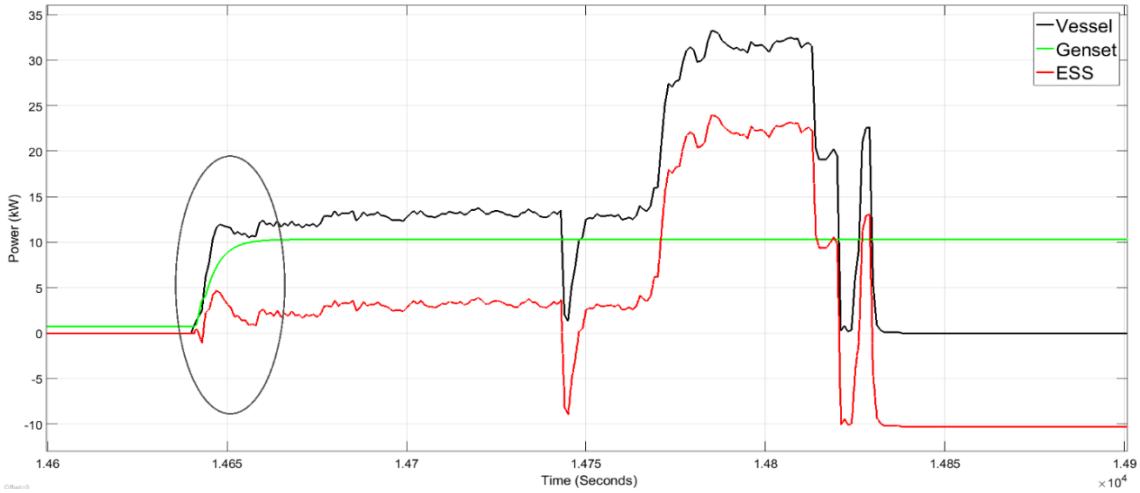

Figure R - 19 Response of the diesel generator and ESS to abrupt changes in the vessel's power requirements

R6.2 Optimal Engine and ESS Size

The Pareto optimal solutions of the multi-objective optimization can provide various optimized engine sizes under different design trade-offs on the overall lifecycle costs (investment and operation) and the equivalent CO2 emissions over a ten-year period. For a given design preference with a proper weight on the lifecycle costs and equivalent CO2 emissions, the optimized engine and ESS sizes can be determined. The proposed approach provides a set of solutions for the series hybrid electric powertrain system design, referred to as the Pareto optimum [40], as shown in Figure R - 20. Pareto optimization was performed to maximize the CO2e reduction and minimize the system cost. As the size of the ESS increases, the cost of the system increases. A larger ESS results in a smaller engine and lower CO2e emissions. Different levels of hybridization are possible, and each Pareto optimum point presents an optimal solution of the hybrid powertrain system for a given design trade-off decision.

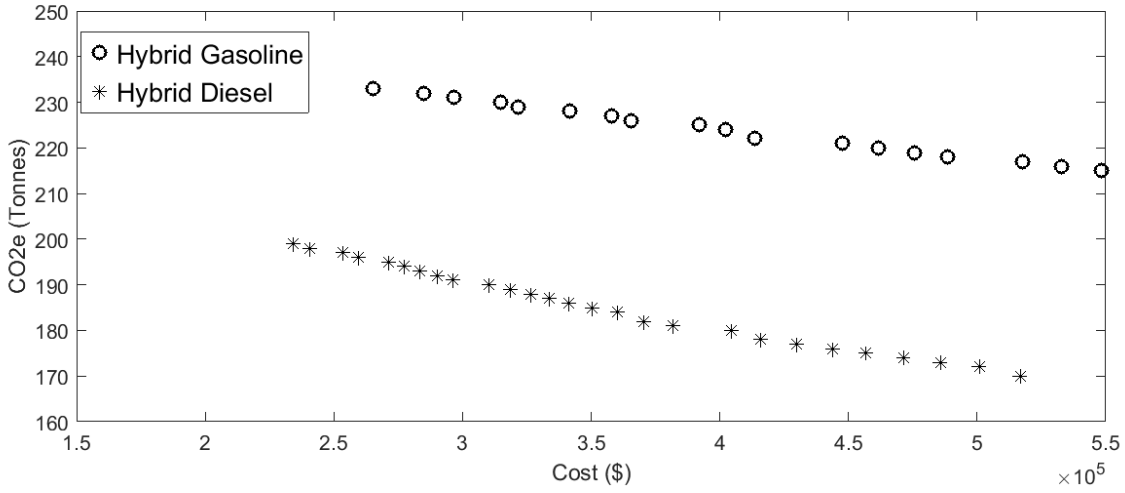

Figure R - 20 Pareto optimum solutions for systems.

The total CO_2 equivalent emissions and the life-cycle costs of the conventional ICE-powered boat with gasoline and diesel engines, the series hybrid electric boat with gasoline and diesel engines and battery/SC ESS, and the pure electric boat with battery ESS have been projected, using the collected vessel operation data and the newly-developed powertrain system models. Figure R - 21 illustrates the simulation results of life-cycle costs and emissions under different powertrain systems.

The new hybrid electric boat design and the battery-powered pure electric boat design showed considerable GHG emissions reduction and favourable life-cycle cost saving. The pure battery-powered powertrain has the lowest CO2e emissions and higher overall costs in comparison to the hybrid electric powertrain system with a diesel engine and a battery ESS. The hybrid electric powertrain system with supercapacitor ESS emits the same amount of CO_{2e} as hybrid powertrain with battery ESS and diesel engine and has higher overall cost due to the higher cost of the supercapacitors.

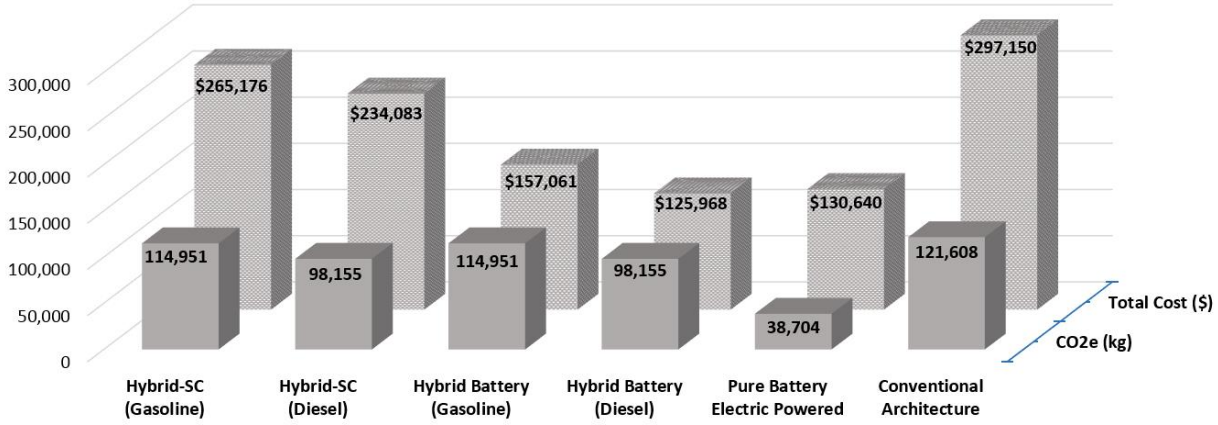

Figure R - 21 Cost and emission comparison of different architectures over a ten-year period.

Similarly, the gasoline engine hybrid electric powertrain system with a battery ESS is less expensive than the same system with a supercapacitor ESS. The life-cycle cost of the hybrid electric powertrain system with a gasoline engine is slightly higher than the same system with a diesel engine due to the higher efficiency of diesel engines. Diesel engines normally have higher efficiency and potentially lower emissions over gasoline counterparts. On the other hand, diesel exhausts have recently been added as a human carcinogen by the World Health Organization (WHO) in 2012 [42]. Heavy-duty diesel engines produce a considerable amount of NO_x, HC, PM, CO and CO_2, and more smoke and PM than gasoline engines [43][44]. The pure-electric powertrain system with a battery ESS presents the lowest CO_{2e} emissions among all alternative powertrain systems due to the low emissions of the North American electric power generation at about 0.3794 Kg/kWh [40][41]. In contrast, the conventional powertrain system of the fishing boat has the highest life-cycle cost and CO2e among all powertrain architectures.

R7. CONCLUSIONS

In this paper, the hybrid electric and pure electric powertrain system designs for a specific class of fishing boats are proposed, and their performance, energy efficiency and life-cycle cost are modelled and quantitatively analyzed. Dedicated data acquisition systems have been installed on two representative fishing boats to collect their daily operational data for accurate powertrain system performance, energy efficiency and life-cycle cost prediction and comparison, against the conventional fishing boat powertrain system to reveal the benefits of fishing boat powertrain system hybridization and electrification. The life-cycle cost and GHG emissions of hybrid electric, pure electric and conventional mechanical powertrain systems are quantitatively compared using the simulation results.

Moreover, the engine and ESS size are optimized for different powertrain architectures under existing technical and operational constraints of the fishing vessels. Simulation results indicated that the hybrid electric powertrain architecture with BESS can ensure lower life-cycle cost and reduced GHG emissions in comparison with conventional mechanical powertrain. Simulation results also showed that significant reduction in GHG emissions can be achieved using the pure electric powertrain with a battery ESS, although the life-cycle cost of this system was higher than the hybrid electric powertrain system with a battery ESS due to battery performance degradation under heavy use and large depth of charge/discharge.

ACKNOWLEDGEMENT

The authors would like to thank members of the project team at the University of Victoria and Glas Ocean Electric for valuable discussions and assistance in boat operation data acquisition, particularly John Porter, Haijia Alex Zhu, and Yanbiao Feng. The financial supports from the Clean Transportation Initiative of Transport Canada are gratefully acknowledged.

REFERENCES

[1] A. Smith, TWP; Jalkanen, JP; Anderson, BA; Corbett, JJ; Faber, J; Hanayama, S; O'Keeffe, E; Parker, S; Johanasson, L; Aldous, L; Raucci, C; Traut, M; Ettinger, S; Nelissen, D; Lee, DS; Ng, S;

Agrawal, A; Winebrake, JJ; Hoen, M; Chesworth, S; Pandey, “Third IMO Greenhouse Gas Study 2014,” London,UK, 2015.

[2] Environment Canada, “Canada’s Emissions Trends,” Quebec, 2014.

[3] “EMSA - European Maritime Safety Agency.” [Online]. Available: http://emsa.europa.eu/main/air-pollution/greenhouse-gases.html. [Accessed: 05-Feb-2018].

[4] C. Capasso, O. Veneri, E. Notti, A. Sala, M. Figari, and M. Martelli, “Preliminary design of the hybrid propulsion architecture for the research vessel ‘G. Dallaporta,’” in *2016 International Conference on Electrical Systems for Aircraft, Railway, Ship Propulsion and Road Vehicles and International Transportation Electrification Conference, ESARS-ITEC 2016*, 2017, pp. 1–6.

[5] M. Martelli, G. Vernengo, D. Bruzzone, and E. Notti, “Holistic Modelling of the Global Propulsion Energy Index in Waves for Small Craft,” *Int. J. Offshore Polar Eng.*, vol. 27, no. 04, p. 6, Dec. 2017.

[6] “Stock Photography Images Royalty Free at Can Stock Photo,” 2013. [Online]. Available: https://www.canstockphoto.ca/. [Accessed: 19-Mar-2018].

[7] J. F. Hansen and F. Wendt, “History and State of the Art in Commercial Electric Ship Propulsion, Integrated Power Systems, and Future Trends,” *Proceedings of the IEEE*, vol. PP, no. 99. pp. 1–14, 2015.

[8] Siemens, “Setting a Course for Carbon-Free Shipping,” 2016. [Online]. Available: https://www.siemens.com/innovation/en/home/pictures-of-the-future/mobility-and-motors/electromobility-electric-ferries.html. [Accessed: 31-Jul-2017].

[9] C. Energy, “WORLD’S FIRST ALL-ELECTRIC CAR FERRY.” [Online]. Available: http://corvusenergy.com/marine-project/mf-ampere-ferry/. [Accessed: 18-Mar-2018].

[10] J. M. Apsley *et al.*, “Propulsion drive models for full electric marine propulsion systems,” *IEEE Transactions on Industry Applications*, vol. 45, no. 2. pp. 676–684, 2009.

[11] G. S. Stavrakakis and G. N. Kariniotakis, “A general simulation algorithm for the accurate assessment of ISOLATED Diesel - Wind Turbines Systems Interaction. Part I: A General Multimachine Power System Model.,” *IEEE Trans. Energy Convers.*, vol. 10, no. 3, pp. 577–583, 1995.

[12] S. Roy, O. P. Malik, and G. S. Hope, “An Adaptive Control Scheme for Speed Control of Diesel Driven Power-Plants,” *IEEE Trans. Energy Convers.*, vol. 6, no. 4, pp. 605–611, 1991.

[13] T. Theubou, R. Wamkeue, and I. Kamwa, “Dynamic model of diesel generator set for hybrid wind-diesel small grids applications,” in *2012 25th IEEE Canadian Conference on Electrical and Computer Engineering: Vision for a Greener Future, CCECE 2012*, 2012, pp. 1–4.

[14] T. Senjyu, T. Nakaji, K. Uezato, and T. Funabashi, “A Hybrid Power System Using Alternative Energy Facilities in Isolated Island,” *IEEE Trans. Energy Convers.*, vol. 20, no. 2, pp. 406–414, Jun. 2005.

[15] C. D. Rakopoulos and E. G. Giakoumis, *Diesel engine transient operation: Principles of operation and simulation analysis*. Springer, 2009.

[16] International IOR Rectifier, “IRF100B202 Product Datasheet,” 2014. [Online]. Available: www.irf.com. [Accessed: 22-Feb-2018].

[17] C. C. D. Rahn and C.-Y. C. Wang, *Battery systems engineering*, 1st Editio. Oxford, UK: John Wiley & Sons Ltd, 2012.

[18] M. Chen and G. A. Rincon-Mora, “Accurate Electrical Battery Model Capable of Predicting Runtime and I–V Performance,” *IEEE Trans. Energy Convers.*, vol. 21, no. 2, pp. 504–511, Jun. 2006.

[19] T. Huria, M. Ceraolo, J. Gazzarri, and R. Jackey, “High fidelity electrical model with thermal

dependence for characterization and simulation of high power lithium battery cells," in *2012 IEEE International Electric Vehicle Conference, IEVC 2012*, 2012, pp. 1–8.

[20] B. Yann Liaw, R. G. Jungst, A. Urbina, and T. L. Paez, "Modelling of Battery Life I. The Equivalent Circuit Model (ECM) Approach."

[21] M. W. Verbrugge and R. S. Conell, "Electrochemical and Thermal Characterization of Battery Modules Commensurate with Electric Vehicle Integration," *J. Electrochem. Soc.*, vol. 149, no. 1, pp. A45–A53, Jan. 2002.

[22] E. Barsoukov, J. H. Kim, D. H. Kim, and K. S. Hwang, "Parametric analysis using impedance spectroscopy: relationship between material properties and battery performance," *J. New Mater. Electrochem. Syst. 3*, vol. 310, p. 303–310 (2000), 2000.

[23] B. Nykvist and M. Nilsson, "Rapidly falling costs of battery packs for electric vehicles," *Nat. Clim. Chang.*, vol. 5, no. 4, pp. 329–332, Apr. 2015.

[24] A. H. Zimmerman, "Failure Threshold Prediction from Li-Ion Battery Life Tests," Huntsville, AL, 2014.

[25] L. Zhang, Z. Wang, X. Hu, F. Sun, and D. G. Dorrell, "A comparative study of equivalent circuit models of ultracapacitors for electric vehicles," *J. Power Sources*, vol. 274, pp. 899–906, Jan. 2015.

[26] A. González, E. Goikolea, J. A. Barrena, and R. Mysyk, "Review on supercapacitors: Technologies and materials," *Renew. Sustain. Energy Rev.*, vol. 58, pp. 1189–1206, May 2016.

[27] H. Chen, T. N. Cong, W. Yang, C. Tan, Y. Li, and Y. Ding, "Progress in electrical energy storage system: A critical review," *Prog. Nat. Sci.*, vol. 19, no. 3, pp. 291–312, Mar. 2009.

[28] L. P. Lima, F. A. Farret, J. G. Trapp, F. Z. Ferrigolo, D. B. Ramos, and F. T. Fernandes, "Integration of alternative sources of energy as current sources," in *XI Brazilian Power Electronics Conference*, 2011, pp. 589–594.

[29] S. M. Schoenung and W. V Hassenzahl, "Long-vs. Short-Term Energy Storage Technologies Analysis A Life-Cycle Cost Study A Study for the DOE Energy Storage Systems Program," 2003.

[30] C. J. Kaiser, "The capacitor handbook," 1995. [Online]. Available: https://books.google.ca/books/about/The_Capacitor_Handbook.html?id=wlD1PQAACAAJ&redir_esc=y. [Accessed: 20-Feb-2018].

[31] P. M. M. and R. G. Kanojiya, "Tuning of PID controller using Ziegler-Nichols method for speed control of DC motor," in *IEEE-International Conference On Advances In Engineering, Science And Management (ICAESM -2012)*, 2012.

[32] M. of Environment, "2016/17 B.C. BEST PRACTICES METHODOLOGY FOR QUANTIFYING GREENHOUSE GAS EMISSIONS," Victoria,BC, 2016.

[33] M. T. and H. L. M. (eds. . Solomon, S., D. Qin, M. Manning, Z. Chen, M. Marquis, K.B. Averyt, "Contribution of Working Group I to the Fourth Assessment Report of the Intergovernmental Panel on Climate Change," 2007.

[34] NREL, "Economic Analysis Case Studies of Battery Energy Storage with SAM," 2015.

[35] J. Liu, T. Jin, L. Liu, Y. Chen, and K. Yuan, "Multi-Objective Optimization of a Hybrid ESS Based on Optimal Energy Management Strategy for LHDs," *Sustainability*, vol. 9, no. 10, p. 1874, 2017.

[36] Http://corvusenergy.com/, "Corvus Energy. Co."

[37] "Caterpillar dealer: Fining." [Online]. Available: http://www.finning.com/en_CA.html.

[38] G. of Canada, "Natural Resources Canada," 2017. [Online]. Available: http://www.nrcan.gc.ca/home. [Accessed: 24-Aug-2017].

[39] Commission for Environmental Cooperation, "North American power plant air emissions," Québec,

2011.

[40] K. Deb, *Multi-objective optimization using evolutionary algorithms*. John Wiley & Sons, 2001.

[41] J. L. Matthew, Brander, Aman Sood, Charlotte Wylie, and Amy Haughton, “Electricity-specific emission factors for grid electricity,” *Ecometrica*, UK, p. 22, 2011.

[42] International Agency for Research on Cancer. "IARC: Diesel engine exhaust carcinogenic." Press release 213 (2012).

[43] Dreher, David B., and Robert A. Harley. "A fuel-based inventory for heavy-duty diesel truck emissions." Journal of the Air & Waste Management Association 48.4 (1998): 352-358.

[44] Zhu, Dongzi, et al. "Real-world PM, NO x, CO, and ultrafine particle emission factors for military non-road heavy duty diesel vehicles." Atmospheric Environment 45.15 (2011): 2603-2609.

Appendix S. Generating Representative Drive and Load Cycles for Arbitrary Surface Vessels

S1. CONTEXT

In marine engineering, problems having the general form "given a drive cycle, optimize ( )" or "given a load cycle, optimize ( )" are common and of practical interest. However, the drive cycle and load cycle data for marine vessels is sparse, and so the engineer trying to solve such problems must be able to first generate the required drive and load cycles for their particular case. This work, therefore, focuses on developing a general process by which an engineer can obtain the requisite drive and load cycles.

S1.1. Stating the Problem

Suppose one is given a mission, a surface vessel, and forecasted weather conditions, and then asked to design an optimal (by whatever metric) propulsion architecture capable of accomplishing the given mission.

S1.1.1. Definition – Mission

A mission is defined by where a vessel needs to be and when it needs to be there. As such, one can define a mission as a time series of latitude (μ), longitude (l), and heading (ψ) values that define the position and orientation of the vessel at key points.

S1.1.2. Definition – Surface Vessel

A surface vessel is a vessel designed to ride on the surface of the water by means of buoyancy. This is different from vessels that depend on a dynamic lift, such as hydrofoils, hovercraft, or ground effect vehicles. A surface vessel can be roughly defined by its length (L), beam (B), draft (T), and displacement (M).

S1.1.3. Definition – Weather Conditions

Weather conditions at sea are comprised of three main components: (1) current conditions, (2) wave conditions, and (3) wind conditions:

1) Current conditions are defined by a fluid velocity and heading, (U_c, ψ_c), at a given position, (μ, l), at a given time.
2) Wave conditions are defined by significant wave height, peak period, and dominant heading, (H_s, T_p, ψ_d), at a given position, (μ, l), at a given time.
3) Wind conditions are defined by a fluid velocity and heading, (U_w, ψ_w), at a given position, (μ, l), at a given time.

S.1.1.4. Definition – Propulsion Architecture

A propulsion architecture is the vessel's plant, along with the controls that govern its operation.

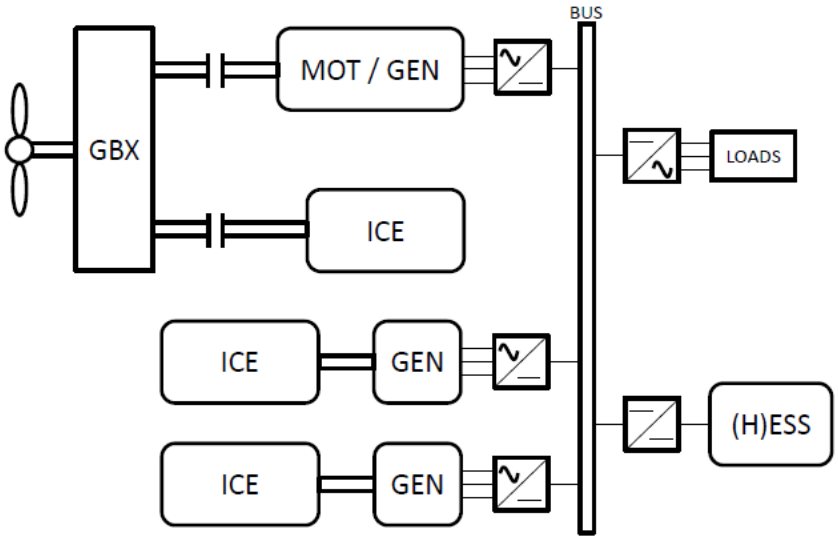

Figure S - 1 Example Plant

For example, the plant illustrated in Figure S - 1 is a hybrid electric plant consisting of two generator sets, a parallel drive, and a hybrid energy storage system (HESS). This plant operating under, say, the equivalent consumption minimization strategy would constitute a particular propulsion architecture.

S2. METHOD

This section summarizes the current state of the general process being developed for the purpose of generating drive and load cycles for arbitrary surface vessels.

S2.1. Generating Drive Cycles

S2.1.1. Definition – Drive Cycle

For the purpose of this work, a drive cycle is taken to be a time series of the surge, sway, and yaw velocities (i.e., $\nu = [u \quad v \quad r]^{\mathrm{T}}$) that satisfy the given mission. That is, a drive cycle defines how the vessel must move in order to achieve the required positions and headings, (μ, l) and ψ, at the required times.

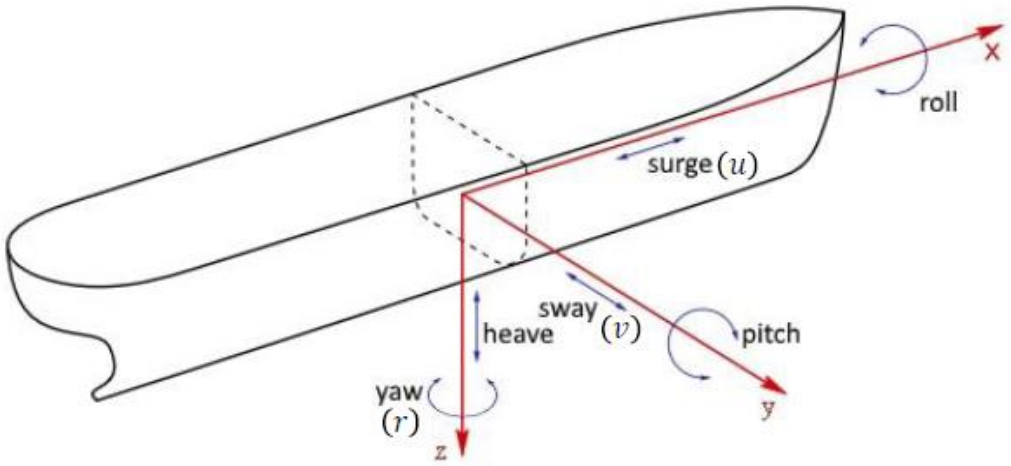

Figure S - 2 Surge, Sway, and Yaw (set in the body-fixed frame)

S2.1.2. From Mission to Drive Cycle

Given the definition of the drive cycle presented above, mapping from a mission to a drive cycle is fairly straightforward. First, consider an earth-centred, earth-fixed frame of reference illustrated as follows

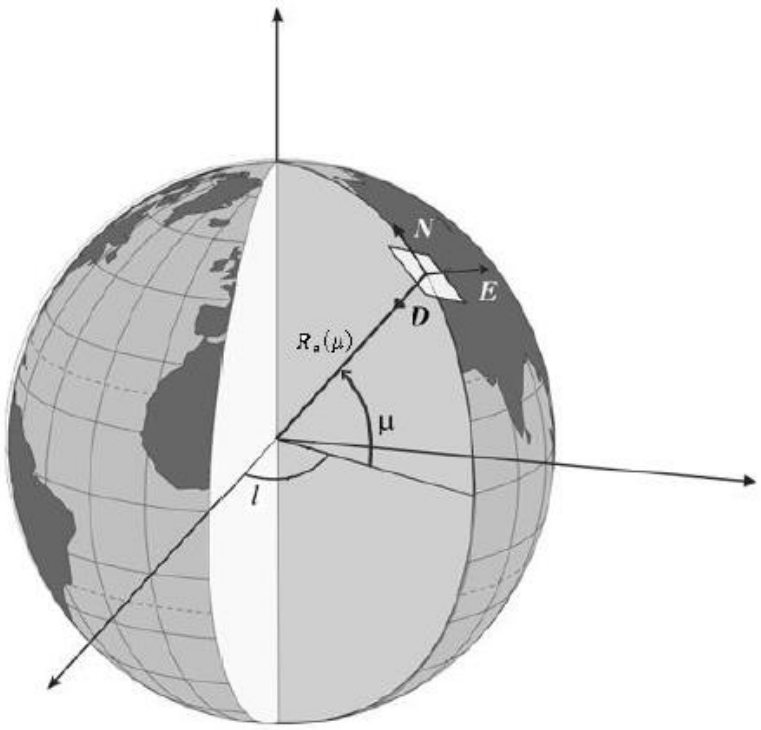

Figure S - 3 Earth-Centered, Earth-Fixed Frame (adapted from [1])

In the plane tangent to the vessel's position, (μ, l), the vessel's velocity in a North-East-Down frame can be described by

$$\nu_{\{n\}} = \begin{bmatrix} R_e(\mu)\dfrac{d\mu}{dt} \\ R_e(\mu)\cos(\mu)\dfrac{dl}{dt} \\ \dfrac{d\psi}{dt} \end{bmatrix} \tag{S-29}$$

where $R_e(\mu)$ is the radius of the earth, defined as

$$R_e(\mu) = \frac{r_e^2}{\sqrt{r_e^2\cos^2(\mu) + r_p^2\sin^2(\mu)}} \tag{S-2}$$

with r_e and r_p being the equatorial and polar radii respectively. Given functions $\mu(t)$, $l(t)$, and $\psi(t)$, which would follow from the mission, one can define all elements needed to construct the function $\nu_{\{n\}}(t)$. If one then defines the rotation matrix $\mathbf{R}_{\{n\}}^{\{b\}}$, mapping from the North-East-Down frame to the body-fixed frame (illustrated in Figure S - 2) as follows

$$\mathbf{R}_{\{n\}}^{\{b\}} = \begin{bmatrix} \cos(\psi) & \sin(\psi) & 0 \\ -\sin(\psi) & \cos(\psi) & 0 \\ 0 & 0 & 1 \end{bmatrix} \tag{S-3}$$

then the drive cycle is given by

$$\nu = \mathbf{R}_{\{n\}}^{\{b\}}\nu_{\{n\}} \tag{S-4}$$

S2.2. Generating Load Cycles

S2.2.1. Definition – Load Cycle

For the purpose of this work, a load cycle is taken to be a time series of power demands, where the power demands are given by the summation of the demand at the propellers and the demand at the steering gear.

S2.2.2. Governing Equations

The actuator, or control, forces/moments that must be acting upon the vessel given a prescribed motion can be determined via the following equation [1]

$$\mathbf{M}_{RB}\dot{\nu} + \mathbf{C}_{RB}(\nu)\nu + \mathbf{M}_A\dot{\nu}_r + \mathbf{C}_A(\nu_r)\nu_r + \mathbf{D}(\nu_r)\nu_r = \tau_{\text{control}} + \tau_{\text{wind}} + \tau_{\text{waves}} \tag{S-5}$$

The details are exhaustive and hence omitted here, but suffice it to say that ν_r is vessel velocity relative to the ocean (whereas ν is vessel velocity relative to the earth), the $\mathbf{M}$ are rigid-body and added mass/inertia matrices, the $\mathbf{C}$ are rigid-body and hydrodynamic Coriolis matrices, $\mathbf{D}$ is a drag matrix, τ_{control} is a vector of actuator forces/moments (in the surge, sway, and yaw respectively), τ_{wind} is a vector of external forces/moments due to wind conditions, and τ_{waves} is a vector of external forces/moments due to wave conditions. If one defines all components of equation S-5

other than τ_{control}, then one can determine the necessary actuator forces/moments at any instant during the vessel's mission.

S2.2.3. Generalized Hull Dynamics

In order to achieve the desired level of generality, a surrogate hull geometry is used to rapidly approximate the elements of $\mathbf{M}_{RB}$, $\mathbf{M}_{A}$, and $\mathbf{D}$. This work employs the Wigley N43 geometry as it has a closed-form expression, making it simple to implement and easy to generalize, while at the same time having form coefficients typical for merchant vessels [2]. Ultimately, however, the choice of surrogate hull geometry is immaterial to the general process presented here; one can replace the N43 with any geometry they wish.

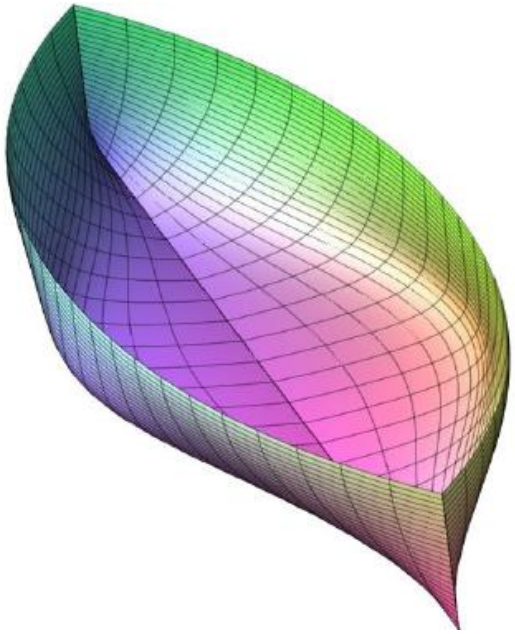

Figure S - 4 Wigley N43 Hull Geometry

Table S - 1 Wigley N43 Form Coefficients

C_b	Block Coefficient	0.5607
C_{wp}	Waterplane Coefficient	0.6933
C_m	Midship Section Coefficient	0.9091
C_p	Prismatic Coefficient	0.6168

Having defined $\mathbf{M}_{RB}$ and $\mathbf{M}_{A}$, one can generate the elements of $\mathbf{C}_{RB}$ and $\mathbf{C}_{A}$ as per the methodology presented in [1].

S2.2.4. Generalized Propeller Dynamics

In order to achieve the desired level of generality, a surrogate geometry is again employed, albeit this time for the propellers. This work employs the Wageningen B-series geometry as this propeller geometry has already been well studied and empirical formulas for thrust coefficient (K_T) and torque coefficient (K_Q) have been published in [3]. Again, this choice of surrogate propeller geometry is ultimately immaterial and one can replace it with any geometry they wish without affecting the general process presented here.

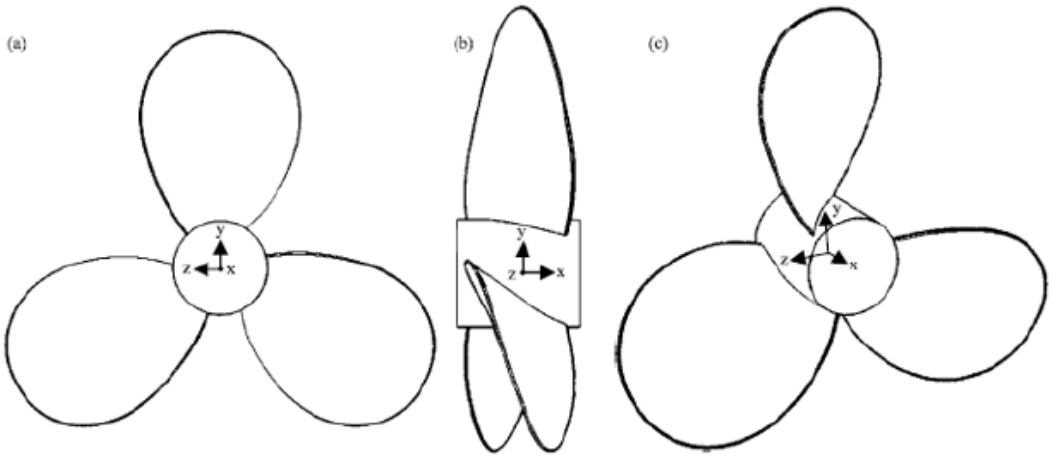

Figure S - 5 Wageningen B-Series Geometry, Example Three-Bladed Variant [4]

Given formulas for K_T and K_Q, one can then determine propeller dynamics via the following

$$T = \rho K_T (\text{rps})^2 D^4 \tag{S-6}$$

$$Q = \rho K_Q (\text{rps})^2 D^5 \tag{S-7}$$

where T is propeller thrust, Q is propeller shaft torque, ρ is fluid density, rps is propeller shaft speed (in revs/sec), and D is propeller diameter.

S2.2.5. From Drive Cycle to Load Cycle

Given the necessary governing equations, surrogate geometries, and relevant weather data, one can map from drive cycle to load cycle via the following algorithm

1) Populate the elements of equation S-5, generate values for τ_{control} throughout the vessel's mission.
2) Given defined placements, (x_i, y_i), of propellers $i = 1,2,\cdots,n$ in the body-fixed frame (see Figure S - 2), seek propeller thrust components, $\left(F_{ix}, F_{iy}\right)$, that both satisfy the following equality

$$\underbrace{\begin{bmatrix} 1 & 1 & \cdots & 1 & 0 & 0 & \cdots & 0 \\ 0 & 0 & \cdots & 0 & 1 & 1 & \cdots & 1 \\ -y_1 & -y_2 & \cdots & -y_n & x_1 & x_2 & \cdots & x_n \end{bmatrix}}_{\mathbf{P}} \underbrace{\begin{bmatrix} F_{1x} \\ F_{2x} \\ \vdots \\ F_{nx} \\ F_{1y} \\ F_{2y} \\ \vdots \\ F_{ny} \end{bmatrix}}_{\vec{F}} = \tau_{\text{control}} \tag{S-8}$$

and minimize the value of $\left\|\vec{F}\right\|_2$.

3) Given thrust components (F_{ix}, F_{iy}), generate values for propeller thrust, T_i, and propeller angle, θ_i, as follows

$$T_i = \sqrt{F_{ix}^2 + F_{iy}^2} \tag{S-9}$$

$$\theta_i = \arctan\left(\frac{F_{iy}}{F_{ix}}\right) \tag{S-10}$$

4) Given T_i, seek propeller shaft speeds, rps_i, via equation S-6.
5) Given rps_i, seek propeller shaft torques, Q_i, via equation S-7.
6) Given Q_i and rps_i, generate propeller shaft power values, P_{shaft_i}, as follows

$$P_{\text{shaft}_i} = 2\pi Q_i(\text{rps}_i) \tag{S-11}$$

7) Given θ_i, generate steering gear power values, P_{steer_i}, via some function of the form $f(\theta_i, \dot{\theta}_i, \ddot{\theta}_i)$ (the details of this step have yet to be investigated).
8) Generate load cycle values as follows

$$P = \sum_i \left(P_{\text{shaft}_i} + P_{\text{steer}_i}\right) \tag{S-12}$$

S3. FUTURE WORK

While the mapping from mission to drive cycle to load cycle appears to be well defined, the intricacies of implementing it programmatically remain to be completed. At present, a particular case study is underway, using MATLAB, which is intended to guide the implementation of the general process. Future work also includes developing a means of completing step 7 of the drive to load algorithm (i.e., generating steering gear powers in general), as well as determining a means of incorporating weather data into the population of equation S-5.

REFERENCES

[1] Fossen, T. (2011). *Handbook of Marine Craft Hydrodynamics and Motion Control*. John Wiley & Sons, Ltd. ISBN: 978-1-119-99149-6

[2] Avallone, E. (2017). *Mark's Standard Handbook for Mechanical Engineers*. McGraw-Hill, 11th edition. ISBN: 978-0-07-142867-5

[3] Bernitsas, M. *et al*. (1981). *K_T, K_Q and Efficiency Curves for the Wageningen B-Series Propellers*. University of Michigan: Department of Naval Architecture and Marine Engineering.

[4] Yeo, K. *et al.* (2014). *Prediction of Propeller Blade Stress Distribution through FEA*. Journal of Applied Sciences, 14: 3046 – 3054. DOI: 10.3923/jas.2014.3046.3054

Appendix T. UVic Global Optimization Program Toolbox

T1. About This Collection

This Global Optimization (GO) Program Toolbox (GO-Tools) is compiled, built, maintained and improved by Dr. Zuomin Dong's Research Group at the University of Victoria (zdong@uvic.ca). The global optimization programs contained in this library, nature-inspired or surrogate-based, have been implemented in MathWorks' MATLAB.

The Toolbox consists of three major components:

- Global optimization programs developed by our research team over the past years with a brief overview on the characteristics and unique capability of each of these programs and the research publications that present the algorithms behind and test results.
- Well-known and representative global optimization programs developed by other researchers, made available to us through open sources. Most of these programs have been tested and used as benchmarks in our previous research. We would like to acknowledge their contributions and willingness to share the codes.
- Special benchmark test cases and optimization application examples, which can be used to evaluate and compare the capability, performance and limitations of various global optimization algorithms and implementations.

Drs. Gary Wang, Adel Younis, Jichao Gu, Huachao Dong, Abdulbaset Saad, and Pengcheng Ye have contributed to this global optimization library through their Ph.D. research at the University of Victoria (UVic) with innovative search algorithms and extensive testing. Many others have also contributed to this special collection of optimization programs in MATLAB (independent to the MATLAB Optimization Toolbox), including Professor Gary Wang of Simon Fraser University (e.g. PDOL) and Professor Guoqiang Wang of Jilin University (GA & SA). The Linear and Quadratic MATLAB programs from Professors A. Antoniou and W.-S. Lu's book are also included.

We have also included several well-known and mature GO programs from other researchers, as acknowledged in each of the related sections. The aim of this collection is to allow its users to carry out and to integrate local and global optimization search programs into their MATLAB based analysis and simulations more easily to solve various complex engineering analysis and design problems.

For global optimization problems in which the objective and/or constraints involve computationally expensive simulations, the surrogate-based global optimization algorithms, introduced in Chapter 2, would be better choices since they use fewer function evaluations in locating the global optimum. On the other hand, if the simulations of the objective and constraint functions only require a modest amount of computation, it would be better to choose the nature-inspired global optimization algorithms (for large scale problems) discussed in Chapter 1, or the gradient-based local optimization algorithms (for small scale problems) in Chapter 3. Moreover,

you can refer to the details of each algorithm and the associated technical paper provided in the folder of References.

We are grateful to all contributors to this special collection, and we welcome any suggestions (to the collection, rating, etc.) and any additions to these programs and studies. Dr. Huachao Dong has reorganized the library in 2018.

T2. NATURE-INSPIRED GLOBAL OPTIMIZATION ALGORITHMS

All algorithms in this category are independent MATLAB code. No requirements to use the Optimization Library. The ability of the algorithm is roughed rated by three numerical measures (accuracy, robustness, search efficiency), based upon our best knowledge and the tests using commonly used benchmark problems. The value of the measures is an integer between 1 and 10.

T2.1. Genetic Algorithms (GA)

Description:

- Global optimization method
- Following the evolutionary control strategy.
- Solves both constrained and unconstrained problems

Developer: *John Holland* (1975) [1].

Pros:

- Can be used for optimization in continuous multi-dimensional space.
- Useful for multimodal functions
- Capable of exploring and exploiting promising regions of the search space.
- Always operate on a whole population of points or strings, leading to the robustness of the algorithm, improving the chance of reaching the global optimum and reducing the risk of being trapped within a local stationary point.
- Can be applied to any continuous or discrete optimization problem

Cons:

- Slow convergence
- Different optimum solutions in different simulation runs

Mechanism:

GAs work with a population of individuals, each of these individuals could be a possible solution to a given problem. Each individual is assigned a fitness score to judge how good it is as a solution to the problem. Those highly-fit individuals are “selected” to reproduce, by cross-breeding or “crossover” with other individuals in the population. The production creates new individuals as offspring, which carry some features taken from each parent. The least fit members of the population are less likely to get selected for reproduction and

are forced out. A completely new population of possible solutions is thus produced by selecting the best individuals from the current "generation", and mating them to produce a new set of individuals with a higher proportion of the characteristics possessed by the good members of the previous generation. By favouring the more fit individuals, the most promising areas of the search space are explored. Eventually, the population might converge to an optimal solution to the problem. Finally, the *mutation* is realized as a random deformation of the strings with a certain probability. This allows the search to preserve genetic diversity, thus avoiding local maxima.

Benchmark Tests:

Application Tests: Hybrid vehicles, machining processes, networks, robotics, aerospace applications

Code: In the library

T2.2. Simulated Annealing (SA)

Description:

- Global Robust probabilistic optimization method
- Combinatorial
- Solves both constrained and unconstrained problems

Developer: *S. Kirkpatrick, C. Gelatt, and M. Vecchi* (1983) [2]

Pros:

- Deal with optimization problems with highly nonlinear, chaotic and noisy data in its objective with a large number of constraints;
- Capability to allow parameter tuning for enhanced performance;
- Can be used for optimization in continuous multi-dimensional space; and
- Useful for multimodal functions

Cons:

- lack of a clear trade-off between the quality of a solution and the time required to locate the solution, leading to longer computation time to converge
- converges slowly and it is difficult to find an appropriate stopping rule

Mechanism:

SA approaches the global maximum of a problem similar to using a bouncing ball that can bounce over mountains from the valley to the valley. It begins at a high temperature that enables the ball to bounce higher over any mountains to access any valley. As the temperature declines, the ball loses its bouncing power so it can settle in a relatively small

region of the valley. From the design objectives, possible valleys or states to be explored are generated. Acceptance criteria, based upon the difference between the depths of the presently explored valley and the last saved lowest valley, are used to determine probabilistically whether to stay in the new lower valley or to jump to another one. By carefully controlling the rate of cooling or the temperature, SA can effectively locate the global optimum over time.

Benchmark Tests: Alpine Function, Banana Function, Beak Function, Goldstein and Price Function, Branin Function, Schaffer's Function, Griewank Function, Generalized Polynomial Function, Shubert Function, and Six-hump Camel-back Function (SC)

Application Tests: travelling salesman problem, image reconstruction, integrated circuit (IC) designs; hybrid vehicles and many other applications

Code: In the library

T2.3. Particle Swarm Optimization (PSO)

Description:

- Global optimization algorithm
- Solves both constrained and unconstrained optimization problems
- Can handle high dimensional problems

Developer: *Kennedy and Eberhart* [3]

Pros:

- Simple concept;
- Owing the capacity of learning and memory, utilizing position and velocity;
- Easy to implement, apply, extend and hybridize;
- Can be used for optimization in continuous multi-dimensional space;
- Useful for multimodal functions; and
- Widely used in real life applications

Cons:

- May fall into local optimization solution; and
- low convergence velocity in the final stage

Mechanism:

To search for food, each member in a flock of birds determines its velocity based on their personal experience as well as information gained through interaction with other members of the flock. Each bird, a particle, flies through the solution space of the optimization problem searching for the optimum solution and its position represents a potential solution.

Benchmark Tests: Alpine Function, Banana Function, Beak Function, Goldstein and Price Function (GP), Branin Function, Schaffer's Function, and Six-hump Camel-back Function (SCF)

Application Tests: Automotive Magnetorheological Brake Design (MRB); Hybrid vehicles; and optimal tool size for NURBS profile milling efficiently

Code: In the library

T2.4. Dividing Rectangles (DIRECT)

Description:

- Global optimization method
- Can handle constrained optimization problems
- Introduced to solve difficult optimization problems

Developer*:* *D. Jones* [4]

Pros:

- Easy to understand and implement;
- Suitable for difficult optimization problems with bound constraints and a real-valued objective function;
- Less efficient than the gradient-based methods;
- Converging to a solution that may be the global optimum; and
- Used in many engineering applications;

Cons:

- Slow convergence

Mechanism:

The algorithm normalizes the search space to a unit hypercube, starts the search by sampling at the centre of the unit hypercube, and identifies the set of potentially optimal hyper-rectangles which are then sampled and subdivided until a pre-specified stopping criterion is achieved.

Benchmark Tests: SCF; Levy; shekel; and Hartmann H6

Application Tests: HEV power control strategy

Code: In the library

T2.5. Differential Evolution (DE)

Description:

- Global optimization method
- Can handle unconstrained and constrained optimization problems
- Can deal with higher-dimensional problems

Developer: *Storn and Price* (1997) [5]

Pros:

- Easy to understand and implement;
- Suitable for difficult optimization problems with bound constraints and a real-valued objective function;
- Good global convergence capability
- Widely used in many engineering applications;

Cons:

- Need more iteration when the objective is a multimodal problem.

Mechanism:

In evolutionary computation, **differential evolution** (**DE**) is a method that optimizes a problem by iteratively trying to improve a candidate solution with regard to a given measure of quality. Such methods are commonly known as metaheuristics as they make few or no assumptions about the problem being optimized and can search very large spaces of candidate solutions. However, metaheuristics such as DE do not guarantee an optimal solution is ever found.
DE is used for multidimensional real-valued functions but does not use the gradient of the problem being optimized, which means DE does not require for the optimization problem to be differentiable as is required by classic optimization methods such as gradient descent and quasi-newton methods. DE can therefore also be used on optimization problems that are not even continuous, are noisy, change over time, etc. DE optimizes a problem by maintaining a population of candidate solutions and creating new candidate solutions by combining existing ones according to its simple formulae, and then keeping whichever candidate solution has the best score or fitness on the optimization problem at hand. In this way, the optimization problem is treated as a black box that merely provides a measure of quality given a candidate solution and the gradient is therefore not needed.

Benchmark Tests: SCF; Levy; shekel; and Hartmann6, F16

Code: In the library

T2.6. Grey Wolf Optimization (GWO)

Description:

- Global optimization method
- Can handle unconstrained and constrained optimization problems
- Can deal with higher-dimensional problems

Developer*:* *Seyedali Mirjalili, Seyed Mohammad Mirjalili, Andrew Lewis* (2014) [6]

Pros:

- Easy to understand and implement;
- Suitable for difficult optimization problems with bound constraints and a real-valued objective function;
- Good global convergence capability
- Widely used in many engineering applications;

Cons:

- Need more iteration when the objective is a multimodal problem.

Mechanism:

This work proposes a new meta-heuristic called Grey Wolf Optimizer (GWO) inspired by grey wolves (Canis lupus). The GWO algorithm mimics the leadership hierarchy and hunting mechanism of grey wolves in nature. Four types of grey wolves such as alpha, beta, delta, and omega are employed for simulating the leadership hierarchy. In addition, the three main steps of hunting, searching for prey, encircling prey, and attacking prey, are implemented. The algorithm is then benchmarked on 29 well-known test functions, and the results are verified by a comparative study with Particle Swarm Optimization (PSO), Gravitational Search Algorithm (GSA), Differential Evolution (DE), Evolutionary Programming (EP), and Evolution Strategy (ES). The results show that the GWO algorithm is able to provide very competitive results compared to these well-known meta-heuristics. The paper also considers solving three classical engineering design problems (tension/compression spring, welded beam, and pressure vessel designs) and presents a real application of the proposed method in the field of optical engineering. The results of the classical engineering design problems and real application prove that the proposed algorithm is applicable to challenging problems with unknown search spaces.

Benchmark Tests: SCF; Levy; shekel; and Hartmann6, F16

Code: In the library

T2.7. Overview of Nature-inspired Global Optimization

Description:

- Comparison of recent Nature-inspired Global Optimization Methods
- Can handle unconstrained and constrained optimization problems
- Can deal with higher-dimensional problems

Developer*:* *Abdulbaset El Hadi Saad, Zuomin Dong and Meysam Karimi* (2017)

Pros:

- Easy to understand and compare;
- Suitable for difficult optimization problems with bound constraints and a real-valued objective function;
- Good global convergence capability
- Widely used in many engineering applications;

Cons:

- Hard to deal with computationally expensive problems.

Mechanism:

Advanced global optimization algorithms have been continuously introduced and improved to solve various complex design optimization problems for which the objective and constraint functions can only be evaluated through computation-intensive numerical analyses or simulations with a large number of design variables. The often implicit, multimodal, and ill-shaped objective and constraint functions in high-dimensional and "black-box" forms demand the search to be carried out using a smaller number of function evaluations with high search efficiency and good robustness. This work investigates the performance of six recently introduced, nature-inspired global optimization methods: Artificial Bee Colony (ABC), Firefly Algorithm (FFA), Cuckoo Search (CS), Bat Algorithm (BA), Flower Pollination Algorithm (FPA) and Grey Wolf Optimizer (GWO). These approaches are compared in terms of search efficiency and robustness in solving a set of representative benchmark problems in smooth-unimodal, non-smooth unimodal, smooth multimodal, and non-smooth multimodal function forms. In addition, four classic engineering optimization examples and a real-life complex mechanical system design optimization problem, floating offshore wind turbines design optimization, are used as additional test cases representing computationally-expensive black-box global optimization problems. Results from this comparative study show that the ability of these global optimization methods to obtain a good solution diminishes as the dimension of the problem or number of design variables increases. Although none of these methods is universally capable, the study finds that GWO and ABC are more efficient on average than the other four in obtaining high-quality solutions efficiently and consistently, solving 86% and 80% of the tested benchmark problems, respectively. The research contributes to future improvements of global optimization methods.

Benchmark Tests: High-dimensional benchmark functions (Dimensions from 25 to 50)

Code: In the library

T3. SURROGATE-BASED GLOBAL OPTIMIZATION ALGORITHMS

T3.1. Adaptive Response Surface Method (ARSM)

Description:

- Global optimization algorithm;
- Solves both constrained and unconstrained optimization problems; and
- Can handle high dimensional problems.

Developer: *Wang and Dong* (2001) [7]

Pros:

- Simple concept,
- Solves complex design problems.
- Independent of any commercial CAD/CAE packages.
- Could be used for optimization in continuous multi-dimensional space.
- Useful for multimodal functions
- Widely used in real-life applications

Cons:

- Might miss and not converge to the real global optimum.

Mechanism:

DOE is first applied to explore the unknown design space. A quadratic response function is introduced for model fitting. The global optimum of the fitted model is determined using a conventional global optimization algorithm. The real value of the design function at this obtained model optimum is calculated through another evaluation of the design function. After each iteration, a threshold, or cutting plane, is used to reduce the design space. The approach applies the response surface method iteratively with a progressively reduced design space that is determined by a varying design threshold until the design optimum is located.

Benchmark Tests: GP; SCF; Branin; GF; Rastrigin; Geometric Container function (GC); H6

Application Tests: Helicopter component design, industry silencer design, simple beam design, etc.

Code: In the library

T3.2. Mode Pursuing Sampling (MPS)

Description:

- Global optimization algorithm
- Designed for black-box functions
- Can handle constrained optimization problems

Developer: *L. Wang, S. Shan, and G. Wang* (2004) [8]

Pros:

- Applicable to both continuous and discontinuous problems
- Effective, efficient and robust

Cons:

- Might not be effective in high dimensional problems

Mechanism:

Based on a novel mode-pursuing sampling method that systematically generates more sample points in the neighbourhood of the function mode while statistically covers the entire search space, a quadratic regression is used to detect the region containing the global optimum. The sampling and detection process iterates until the global optimum is obtained.

Benchmark Tests: Six-hump Camel-back Function (SCF), Goldstein and Price Function (GP), Griewank Function (GN), Hartmann Function (H6 and H16)

Application Tests: Design of a two-member frame; and Design of a pressure vessel

Code: In the library

T3.3. Pareto Set Pursuing Method (PSP)

Description:

- Efficient multi-objective global optimization algorithm;
- Deals with continuous, discrete and mixed –variables optimization problems
- Designed for expensive black-box function

Developer: *Shan and Wang*, (2005) [9]

Pros:

- Performs well;
- Yields Pareto frontier with less number of function evaluations;
- Based on surrogate models

Cons:

- Cannot deal with constrained expensive black-box problems.

Mechanism:

Assuming at the first iteration we start from random sampling for the unknown problem, it is desirable at the next iteration to sample more points closer to the Pareto frontier than further away. If the trend continues, we can sample right on or very close to the frontier. A sampling guidance function to generate more sample points that conform to a given probability function PDF is used

and MPS used to construct an approximation function from few sample points and then used to generate a large number of points from the approximation model to design a CDF function. In each iteration, new sample points are combined with the good ones obtained in previous iterations until the Pareto frontier is identified.

Benchmark Tests: Mathematical formulas test problems

Application Tests: Fuel cell component design

Code: In the library

T3.4. Mixed Surrogates and Design Space Exploration (MSSE)

Description:

- Computationally intensive global design optimization problems.
- Good for constrained and unconstrained optimization problems.
- Useful in multi-dimensional space.
- Designed for black-box functions.

Developer: *Younis and Dong* (2009) [10]

Pros:

- Useful in multi-dimensional space.
- Dramatically reducing the number of function & constraint evaluation.
- Not expensive computationally if using the right sampling method.
- Efficient and robust.
- Promising for continuous optimization.
- Taking big advantage of meta-modelling.
- Successfully used in many applications.

Cons:

- Not suitable for very high dimensional problems

Mechanism:

The approach divides the field of interest into several unimodal regions; identifies and ranks the regions that likely contain the global minimum; fits a mixed surrogate models over each promising region with additional design experiments data points using Latin Hypercube Designs; identifies its minimum and removes the processed region, and moves to the next most promising region until all regions are processed and the global optimum is identified.

Benchmark Tests: SCF; Shubert; Levy; H6; Trid; and H16

Application Tests: Could be used in aerospace applications, robotics and other engineering applications

Code: In the library

T3.5. Space Exploration and Unimodal Region Elimination (SEUMRE)

Description:

- Global optimization algorithm
- Designed for black-box functions
- Can handle constrained optimization problems
- Good for high dimensional problems

Developer: *Younis and* Dong (2010) [11]

Pros:

- Useful in multi-dimensional space (tested up to 16 design variables).
- Reducing the number of design variables by dimensionality reduction.
- Reducing the design space by eliminating non-promising regions.
- Dramatically reducing the number of function & constraint evaluation.
- Not expensive computationally if using the right sampling method.
- Efficient and robust.
- Easy to understand and implement.
- Successfully used in many applications.

Cons:

- Cannot handle problems where the design variables are more than 60
- Requires efficient sampling techniques

Mechanism:

The approach divides the design space into several unimodal regions using design experiment data; identifies and ranks the regions that most likely contain the global minimum; fits a Kriging model with additional design experiments using Latin Hypercube designs over the most promising region; identifies its minimum, and moves to the next

most promising region. Step by step, the method identifies the global optimum by examining the most promising unimodal regions with additional design experiments.

Benchmark Tests: SCF; GP; Branin; Banana; Alpine; Beak; Schaffer's; GN; GF; Levy, Shekel; and Hartmann H6

Application Tests: High-Efficiency EV/PHEV/EREV Electric Mode Operations; and Automotive Magnetorheological Brake Design (MRB)

Code: In the library

T3.6. Hybrid and Adaptive Metamodel Based Global Optimization

Description:

- Computationally intensive global design optimization problems.
- Good for unconstrained optimization problems.
- Useful in multi-dimensional space.
- Designed for black-box functions.

Developer: *Gu, Li and Dong* (2011) [12]

Pros:

- Robust, highly efficient, and full automation in metamodel selection.

Cons:

- Sometimes might get stuck in local valleys on multimodal problems like Peaks, SE cases.
- Difficult to deal with high dimensional expensive black-box problems

Mechanism:

The program is a hybrid and adaptive metamodel-based global optimization method that can automatically select appropriate metamodelling techniques during the search process to improve search efficiency. The search initially applies three representative metamodels, Kriging, RBF and QRS, concurrently. Seven candidate point sets are created for selecting promising samples. Preference to better performing model is then introduced by selecting sample data points adaptively according to the calculated values of the three metamodels to improve modelling accuracy and better search efficiency. The method is particularly suitable for design problems involving computation-intensive, black-box analyses and simulations.

Benchmark Tests: SCF; GN, GP, Leon, HM, H6, and H16.

Application Tests: bumper crashworthiness simulation of passenger vehicles (3 and 6 variables)

Code: to be added.

Improvement: Gu and Ye have improved HAM respectively and put the improved version into this toolbox.

T3.7. Multi-start Space Reduction (MSSR) Surrogate-based Global Optimization Method

Description:

- Computationally expensive global design optimization problems.
- Good for constrained and unconstrained optimization problems.
- Useful in multi-dimensional space.
- Useful in multi-modal space.
- Designed for black-box functions.

Developer: *Huachao Dong and Zuomin Dong* (2016) [13]

Pros:

- Robust, highly efficient, and full automation.

Cons:

- Cost more time in high-dimensional problems.

Mechanism:

In this new algorithm, the design space is classified into: the original design space or global space (GS), the reduced medium space (MS) that contains the promising region, and the local space (LS) that is a local area surrounding the present best solution in the search. During the search, a kriging-based multi-start optimization process is used for local optimization, sample selection and exploration. In this process, Latin hypercube sampling is used to acquire the starting points and sequential quadratic programming (SQP) is used for local optimization. Based upon a newly introduced selection strategy, better sample points are obtained to supplement the kriging model, and the estimated mean square error of kriging is used to guide the search of the unknown areas. The multi-start search process is carried out alternately in GS, MS and LS until the global optimum is identified.

Benchmark Tests: Banana, Peaks, GP, SCF, Shubert, GF, HM, Leon, Shekel, Levy, H6, Trid6, Trid10, Sphere and H16.

Application Tests: G6 function, Himmelblau's nonlinear problems, Tension / Compression Spring Design (TSD), Welded Beam Design (WBD), Pressure Vessel Design (PVD), and Speed Reducer Design (SRD) (2 to 7variables; 2 to 11 constraints)

T3.8. Kriging-based multi-objective optimization (KMOO) for expensive black-box problem

Description:

- Computationally expensive multi-objective optimization problems.
- Good for constrained and unconstrained optimization problems.
- Useful in multi-dimensional space.
- Designed for black-box functions.

Developer: *Huachao Dong and Zuomin Dong* (2016, has not been published)

Pros:

- Robust, highly efficient, and full automation.

Cons:

- Hard to deal with some non-convex problems with the discrete Pareto frontiers.

Mechanism:

At the beginning, this algorithm employs kriging to construct an initial surrogate model that can predict response values. When the loop runs, the efficient NSGA2 optimizer is used to obtain the Pareto optimal set from the kriging model and then new samples are supplemented to reconstruct kriging. In each iteration, one important parameter, the number of new samples that are required to improve the predictive model affects the final computational cost. In order to find the optimal parameter of this algorithm, a new terminal criterion is presented. In addition, the proposed terminal criterion can also be widely used for the comparison of different algorithms in the multi-objective expensive black-box optimization field. For the complex constrained multi-objective problem, a clustering-based space reduction strategy is proposed to accelerate the convergence of this algorithm.

Benchmark Tests: SCH1, SCH2, PROB1, CONSTR, SRN, TNK, FON, FBT, OSY, ZDT2, ZDT1.

Application Tests: Welded Beam Design (WBD), Two-bar truss design (TBD), and Disk Brake Design (DBD) (2 to 4 variables; 1 to 5 constraints)

T3.9. Surrogate-based Optimization with Clustering-based Space Exploration (SOCE)

Description:

- Computationally expensive global design optimization problems.
- Good for constrained and unconstrained optimization problems.
- Useful in multi-dimensional space.

- Useful in multi-modal space.
- Designed for black-box functions.

Developer: *Huachao Dong and Zuomin Dong* (2017) [14]

Pros:

- Robust, highly efficient, wide applicability and full automation.

Cons:

- Hard to deal with high-dimensional multimodal expensive problems

Mechanism:

This method (SOCE) is presented to solve multimodal expensive black-box optimization problems (EBOPs) with or without expensive nonlinear constraints. Two approximation methods (kriging and quadratic response surfaces, QRS) are used to construct surrogate models, among which kriging can predict multiple promising local optima and QRS can reflect the overall trend of a true model. According to their characteristics, two different optimizers are employed to capture the promising samples on kriging and QRS, respectively. One is the nature-inspired algorithm "Grey wolf optimization (GWO)", which can efficiently find the global optimum of a QRS model. The other one is a multi-start optimization algorithm that can find several different local optimal locations from a kriging model. In addition, the complete optimization flow is presented and its detailed pseudo-code is given. In the presented optimization flow, if a proposed local convergence criterion is satisfied, sparsely sampled regions will be explored. Such a space exploration strategy is developed based on the k-means clustering algorithm, which can make the search jump out of a local optimal location and focus on unexplored regions. Furthermore, two penalty functions are proposed to make this algorithm applicable for constrained optimization. With tests on 15 bound-constrained and 7 nonlinear constrained benchmark examples, the presented algorithm shows remarkable capacity in dealing with multimodal EBOPs and constrained EBOPs.

Benchmark Tests: Shub, GW2, SE, Peaks, Beale, Alp, F1, Rast, Levy, Zakh, Shek10, HN6, GW10, Sphere, F16; G6, G7, G8, G9, G10

Application Tests: Welded Beam Design (WBD), Speed Reducer Design(SRD).

T3.10. Hybrid Surrogate-based Optimization using Space Reduction (HSOSR)

Description:

- Computationally expensive black-box global design optimization problems.
- Good for unconstrained optimization problems.
- Useful in multi-dimensional space.

- Useful in multi-modal space.
- Designed for black-box functions.

Developer: *Huachao Dong and Zuomin Dong* (2018)

Pros:

- Robust, highly efficient, wide applicability and full automation.

Cons:

- **Hard to deal with high-dimensional multimodal expensive problems**

Mechanism:

In this work, a surrogate-based global optimization algorithm HSOSR is presented, which can solve expensive black-box optimization problems with box constraints. In order to decrease the difficulty of the search in large-scale multimodal problems, a space reduction method based on hybrid surrogates is proposed. Kriging and Radial Basis Function (RBF) are employed to approximate the true expensive problems, respectively. A large number of samples are generated by Latin hypercube sampling to obtain the predictive values from the two surrogates. According to the size of these predictive values from kriging and RBF, all the samples are sorted, respectively. Subsequently, two potentially better regions from kriging and RBF are identified based on the ranks of these samples and two subspaces are also created. Since kriging and RBF models always produce multiple predictive optimal solutions, a multi-start optimization algorithm is proposed to capture the supplementary samples in the two subspaces alternately. Besides, the newly added samples need to satisfy a defined distance criterion for sampling diversity. Once the algorithm gets stuck in a local valley, the estimated mean square error of kriging is maximized by the multi-start optimization strategy to explore the sparsely sampled area. Eventually, 10 low-dimensional and 5 high-dimensional benchmark cases are used to test HSOSR. In addition, 5 surrogate-based global optimization algorithms are also tested as a contrast. Compared with the well-known efficient global optimization (EGO) method, HSOSR achieves an improvement of more than 50% on computational efficiency. To sum up, HSOSR has high efficiency and strong robustness in dealing with multimodal expensive black-box optimization problems.

Benchmark Tests: Ackley, GW, Peaks, ST, Alp, F1, Him, GF, Levy, HN6, Schw3, Trid10, Sums, F16, Sphere

T3.11. Surrogate Based Global Optimization Using Hierarchical Design Space Reduction (HDSR)

Description:

- Computationally expensive global design optimization problems.
- Good for unconstrained optimization problems.
- Useful in multi-dimensional space.

- Useful in multi-modal space.
- Designed for black-box functions.

Developer: *Pengcheng Ye and Zuomin Dong* (2018)

Pros:

- Accurate, highly efficient, robust and full automated.

Cons:

- Requiring more computation time in solving high-dimensional problems.
- Not good for constrained problems.

Mechanism:

In this new algorithm, TPSLE is employed to generate the initial sample points in the original global space for building three representative surrogate models containing PRS, RBF and KRG as well as the ensemble of surrogates with optimized weight factors. A hierarchical design space reduction method is introduced to define three different working spaces: OGS, PJS and ILS. The promising joint space is obtained by the fuzzy c-means clustering method. Similarly, a Point Selection Method (PSM) is introduced to identify the important local space. In order to further improve modelling accuracy, new sample points including approximate global optima of response surface and promising sample points in the sparse region are added to the sample set for adaptively updating the surrogate models. Many benchmark optimization problems and two engineering optimization problems are tested to demonstrate the accuracy, efficiency and robustness of the newly proposed global optimization method ESGO-HSR

Benchmark Tests: SCF, BR, GF, GP, RB, HM, CT, DW, LF3, AF4, GN4, HN6, TR6, GN8, TR10, SF, GN12, F16

Application Tests: I-Beam design and Pressure vessel design

T3.12. Kriging-Bat Algorithm (K-BA)

Description:

- For solving computationally expensive global design optimization problems
- Good for unconstrained optimization problems
- Designed for black-box objective functions

Developer: *Abdulbaset Saad and Zuomin Dong* (2018)

Pros:

- Accurate, highly efficient, robust and fully automated.

Cons:

- Requiring more function evaluations than other surrogate-based algorithms.

Mechanism:

Many global optimization (GO) algorithms have been introduced in recent decades to deal with computationally expensive black-box (CEBB) problems. The high number of objective function evaluations, required by conventional GO methods, is prohibitive or at least inconvenient for practical GO design applications. In this work, a new Kriging-Bat Algorithm (K-BA) is introduced for solving CEBB problems with further improved search efficiency and robustness. A Kriging surrogate model (SM) is integrated with the Bat Algorithm (BA) to find the global optimum using a substantially reduced number of function evaluations of the original objective function. The new K-BA algorithm is tested and compared with other well-known GO algorithms, using a set of standard benchmark problems with 2 to 16 design variables as well as real-life design optimization application, to determine its search capability and efficiency. The results of the statistical tests demonstrated the suitability and superior capability of the K-BA in solving complex CEBB.

Benchmark Tests: Banana, GP, SCF, Shubert, Peaks, Shekel, Dp, Powell, HM6, Leon, Alpine, Sphere, F16

Application Tests: Floating Wind Turbine Platform

T3.13. Reference to GO Programs from PDOL of SFU

Professor G. Gary Wang's Product Design and Optimization Lab (PDOL) and the research team at Simon Fraser University have developed an array of effective GO programs. We have included them here for the sake of convenience. The original web address and program download site is:

http://www.ensc.sfu.ca/~gwa5/index_files/software.htm

Adaptive Response Surface Method (ARSM)

ARSM is a global optimization scheme developed for design optimizations involving computation-intensive processes such as finite element analysis (FEA), computational fluid dynamics (CFD), simulation, and so on. For detailed information, one can download the papers (Wang et al. 2001) and (Wang 2003). ARSM is fully developed in the PDOL and its first version is completed in July 2001. It has been successfully applied to helicopter component design, industry silencer design, etc. ARSM then leads to the development of MPS as below.

Mode Pursuing Sampling (MPS) Method

As an improvement from ARSM, MPS is an efficient global optimization method for both constrained and unconstrained optimization problems (Wang et al. 2004). Its discrete-variable version was also developed (Sharif et al. 2008). The performance of MPS was studied in reference to genetic algorithms (Duan et al. 2008). MPS is considered a step-up from ARSM.

Pareto Set Pursuing (PSP) Method

PSP is an efficient multi-objective optimization (MOO) method. It deals with problems with continuous, discrete, and mixed-variables (Shan and Wang 2005). Its performance is also compared with other widely-used MOO methods such as multi-objective genetic algorithms (MOGA), NSGA-II, FastPGA, SPEA2, etc. It is found that for a limited number of function evaluations, PSP generates much better Pareto Frontier sets, as compared with others (Khokhar et al. 2010).

OPTIP

In summer 2010, MPS and its variation CiMPS, as well as PSP, are integrated into a new optimization tool, named Optimization Toolkit for Computationally Intensive Problems (OPTIP). This tool has a Graphic User Interface with many plots for the optimization process and outputs.

Others

Reliability-based Design Optimization

Collaboration Pursuing Method (CPM) for Multidisciplinary Design Optimization

T4. DEPENDANT OPTIMIZATION ALGORITHMS

T4.1. Sequential Quadratic Programming

Description:

- Global optimization algorithm.
- Used for low and high dimensional problems.
- Solves convex problems easily and non-convex problems with much difficulty.

Developer: *R. Wilson (1963)* [15]

Pros:

- Solving nonlinearly constrained optimization problems
- Robust and effective
- Easy to understand and implement

Cons:

- The success of SQP depends on the existence of rapid and accurate algorithms for solving quadratic programs.

Mechanism:

SQP method models an arbitrary nonlinear optimization problem using an approximate solution from a QP sub-problem and then uses the solution of this sub-problem to construct a better approximation. After a sequence of approximations, a solution is to be reached.

Benchmark Tests:

Application Tests: SQP algorithms have been developed and used to solve a remarkably large set of practical problems. Large scale versions of the algorithm have been devised and tested recently with promising results.

Code: In the library

The Linear and Quadratic MATLAB programs from Professors A. Antoniou and W.-S. Lu's book [16] on Practical Optimization: Algorithms and Engineering Applications [11] are included in this collection.

T5. BENCHMARK TEST PROBLEMS

The following are the mathematical formulas and the analytical global optimum solutions of the tested benchmark test problems: [17]

T5.1. Unconstrained Test Problems

1) **Banana Function, n=2:**

$$f(x) = 100(x_2 - x_1^2) + (1 - x_1)^2$$

Search Space: $-2 \le x_i \le 2, \quad i = 1,2.$

Global minimum: $x^* = (1, \dots, 1), \quad f(x^*) = 0$

2) **Beak Function, n=2:**

$$f(x_1, x_2) = 3(1 - x_1)^2 \mathrm{e}^{\left(-x_1^2 - (x_2+1)^2\right)} - 10\left(\frac{x_1}{5} - x_1^3 - x_2^5\right)\mathrm{e}^{\left(-x_1^2 - x_2^2\right)} - \frac{1}{3}\mathrm{e}^{\left(-(x_1+1)^2 - x_2^2\right)}$$

Search Space: $-3 \le x_1 \le 3 \quad -4 \le x_2 \le 4.$

Global minimum: $x^* = (0.2283, -1.6255), \quad f(x^*) = -6.5511$

3) **Branin Function, n=2:**

$$f(x) = \left(x_2 - \frac{5.1}{4\pi^2}x_1^2 + \frac{5}{\pi}x_1 - 6\right)^2 + 10\left(1 - \frac{1}{8\pi}\right)\cos x_1 + 10$$

Search Space: $-5 \le x_1 \le 0, \quad 10 \le x_2 \le 15.$

Global minimum: $x^* = (-\pi, 12.275), \; x^* = (\pi, \; 12.275), \; f(x^*) = 0.3978$

4) **Generalize Polynomial Function, n=2:**

$$f(x_1, x_2) = (1.5 - x_1(1 - x_2))^2 + (2.25 - x_1(1 - x_2^2))^2 + (2.625 - x_1(1 - x_2^3))^2$$

Search Space: $-2 \le x_1, x_2 \le 2$

Global minimum: $x^* = (2.0000, \; 0.1700), \; f(x^*) = 0.5233$

5) Goldstein and Price Function (GP), n=2:

$$f(x_1,x_2)=\left(1+(x_1+x_2+1)^2(19-14x_1+3x_1^2-14x_2+6x_1x_2+3x_2^2)\right)$$
$$\times\left(30+(2x_1-3x_2)^2(18-32x_1+12x_1^2+48x_2-36x_1x_2+27x_2^2)\right)$$

Search Space: $-2\le x_1,x_2\le 2$

Global minimum: $x^*=(0,-1),\ f(x^*)=3$

6) Griewank Function, n=2;

$$f(x_1,x_2)=\frac{x_1^2+x_2^2}{200}-\cos x_1\cos\left({x_2}/{\sqrt{2}}\right)+1$$

Search Space: $-100\le x_1,x_2\le 100$

Global minimum: $x^*=(0,0),\ f(x^*)=0$

7) Hartman Function (H6), n=6:

$$f_{HN}(x)=-\sum_{i=1}^{4}C_i exp\left(-\sum_{j=1}^{n}a_{ij}\left(x_j-p_{ij}\right)^2\right),$$

$$[a_{ij}]_{j=1,\cdots,6}=\begin{bmatrix}10 & 3 & 17 & 3.5 & 1.7 & 8\\ 0.05 & 10 & 17 & 0.1 & 8 & 14\\ 3 & 3.5 & 1.7 & 10 & 17 & 8\\ 17 & 8 & 0.05 & 10 & 0.1 & 14\end{bmatrix}$$

$$c=[1\quad 1.2\quad 3\quad 3.2]$$

$$[p_{ij}]_{j=1,\cdots,6}=\begin{bmatrix}0.1312 & 0.1696 & 0.5569 & 0.0124 & 0.8283 & 0.5886\\ 0.2329 & 0.4139 & 0.8307 & 0.3736 & 0.1004 & 0.9991\\ 0.2348 & 0.1451 & 0.3522 & 0.2883 & 0.3047 & 0.6650\\ 0.4047 & 0.8828 & 0.8732 & 0.5743 & 0.1091 & 0.0381\end{bmatrix}$$

Search space: $0\le x_i\le 1,\ \ i=1,\cdots,n$

Global minimum: $x^*=(0.02169,0.15001,0.47687,0.27533,0.31165,0.6573)$;
$f(x^*)=-3.3223$

8) Hartmann Function with 16 Design Variables (H16), n=16:

$$f(x)=\sum_{i=1}^{16}\sum_{j=1}^{16}a_{ij}\,(x_i^2+x_i+1)\left(x_j^2+x_j+1\right),\qquad i,j=1,2,\cdots,16$$

$$[a_{ij}]_{row1-8} = \begin{bmatrix} 1 & 0 & 0 & 1 & 0 & 0 & 1 & 1 & 0 & 0 & 0 & 0 & 0 & 0 & 0 & 1 \\ 0 & 1 & 1 & 0 & 0 & 0 & 1 & 0 & 0 & 1 & 0 & 0 & 0 & 0 & 0 & 0 \\ 0 & 0 & 1 & 0 & 0 & 0 & 1 & 0 & 1 & 1 & 0 & 0 & 0 & 1 & 0 & 0 \\ 0 & 0 & 0 & 1 & 0 & 0 & 1 & 0 & 0 & 0 & 1 & 0 & 0 & 0 & 1 & 0 \\ 0 & 0 & 0 & 0 & 1 & 1 & 0 & 0 & 0 & 1 & 0 & 1 & 0 & 0 & 0 & 1 \\ 0 & 0 & 0 & 0 & 0 & 1 & 0 & 1 & 0 & 0 & 0 & 0 & 0 & 0 & 1 & 0 \\ 0 & 0 & 0 & 0 & 0 & 0 & 1 & 0 & 0 & 0 & 1 & 0 & 1 & 0 & 0 & 0 \\ 0 & 0 & 0 & 0 & 0 & 0 & 0 & 1 & 0 & 1 & 0 & 0 & 0 & 0 & 1 & 0 \end{bmatrix}$$

$$[a_{ij}]_{row9-16} = \begin{bmatrix} 0 & 0 & 0 & 0 & 0 & 0 & 0 & 0 & 1 & 0 & 0 & 1 & 0 & 0 & 0 & 1 \\ 0 & 0 & 0 & 0 & 0 & 0 & 0 & 0 & 0 & 1 & 0 & 0 & 0 & 1 & 0 & 0 \\ 0 & 0 & 0 & 0 & 0 & 0 & 0 & 0 & 0 & 0 & 1 & 0 & 1 & 0 & 0 & 0 \\ 0 & 0 & 0 & 0 & 0 & 0 & 0 & 0 & 0 & 0 & 0 & 1 & 0 & 1 & 0 & 0 \\ 0 & 0 & 0 & 0 & 0 & 0 & 0 & 0 & 0 & 0 & 0 & 0 & 1 & 1 & 0 & 0 \\ 0 & 0 & 0 & 0 & 0 & 0 & 0 & 0 & 0 & 0 & 0 & 0 & 0 & 1 & 0 & 0 \\ 0 & 0 & 0 & 0 & 0 & 0 & 0 & 0 & 0 & 0 & 0 & 0 & 0 & 0 & 1 & 0 \\ 0 & 0 & 0 & 0 & 0 & 0 & 0 & 0 & 0 & 0 & 0 & 0 & 0 & 0 & 0 & 1 \end{bmatrix},$$

Search Space: $-1 \leq x_i \leq 1, \quad i = 1, \cdots, 16$

Global minimum: $f(x^*) = 25.875$

9) Levy Function, n=4:

$$f(x) = \sin^2(\pi y_1) + \sum_{i=1}^{n-1} \left((y_i - 1)^2 (1 + \sin^2(\pi y_i + 1))\right) + (y_n - 1)^2 (1 + 10 \sin^2(2\pi y_n)), y_i = 1 + \frac{x_i - 1}{4}, i = 1, \cdots, n$$

Search Space: $-10 \leq x_i \leq 10, \qquad i = 1, \cdots, n.$

Global minimum: $x^* = (1, \ldots, 1), \quad f(x^*) = 0$

10) Shekel Function, n=4:

$$f(x) = -\sum_{i=1}^{4} \alpha_i \, exp\left(-\sum_{j=1}^{6} B_{ij}(x_j - Q_{ij})^2\right),$$

$$\alpha = [1 \quad 1.2 \quad 3 \quad 3.2]^T,$$

$$B = \begin{bmatrix} 10 & 3 & 17 & 3.05 & 1.7 & 8 \\ 0.05 & 10 & 17 & 0.1 & 8 & 14 \\ 3 & 3.5 & 1.7 & 10 & 17 & 8 \\ 17 & 8 & 0.05 & 10 & 0.1 & 14 \end{bmatrix},$$

$$Q = 10^{-4} \times \begin{bmatrix} 1312 & 1696 & 15569 & 124 & 8283 & 5886 \\ 2329 & 4135 & 8307 & 03736 & 1004 & 9991 \\ 2348 & 1451 & 3522 & 2883 & 3047 & 6650 \\ 4047 & 8828 & 8732 & 5743 & 1091 & 381 \end{bmatrix}$$

Search Space: $0 \le x_i \le 1, \quad i = 1, \cdots, 6.$

Global minimum: $x^* = (4, 4, 4, 4), \quad f(x^*) = -10.1532$

11) Shubert Function, n=2:

$$f(x_1, x_2) = \left(\sum_{i=1}^{5} i \cos\big((i+1)x_1 + i\big)\right)\left(\sum_{i=1}^{5} i \cos\big((i+1)x_2 + i\big)\right),$$

Search Space: $-10 \le x_i \le 10, \quad i = 1, 2$

Global minimum: $x^* = (-1.4252, 5.4829), \ f(x^*) = -186.7309$

12) Sphere Function, n=10:

$$f(x) = \sum_{i=1}^{n} x_i^2,$$

Search Space: $-2.56 \le x_i \le 5.12, \quad i = 1, \cdots, n$

Global minimum: $x^* = (0, \dots, 0), \quad f(x^*) = 0$

13) Six-hump Camel-back Function (SCF), n=2:

$$f(x_1, x_2) = 4x_1^2 - 2.1x_1^4 + \frac{1}{3}x_1^6 + x_1 x_2 - 4x_2^2 + 4x_2^4$$

Search Space: $-2 \le x_1, x_2 \le 2,$

Global minimum: $x^* = (0.089842, -0.712656), x^* = (-0.089842, 0.712656)$

$$f(x^*) = -1.031628$$

14) Trid Function, n=10:

$$f(x) = \sum_{i=1}^{n} (x_i - 1)^2 - \sum_{i=2}^{n} x_i x_{i-1},$$

Search Space: $-n^2 \le x_i \le n^2, \qquad i = 1, \dots, n$

Global minimum: $x_i^* = i(7 - i), \quad i = 1, \dots, n, \ f(x^*) = -50$

T5.2. Constrained Test Problems

1) Problem C1:

$$min\ f(x_1, x_2) = (x_1 - 10)^3 + (x_2 - 20)^3$$

Subject to:

$$h_1(x) = (x_1 - 5)^2 + (x_2 - 5)^2 + 100 \le 0,$$

$$h_2(x) = (x_1 - 5)^2 + (x_2 - 5)^2 - 82.81 \le 0.$$

Search Space: $100 \le x_1 \le 13;\ \ 100 \le x_2 \le 0.$

Global minimum: $x^* = (14.095,\ 0.84296),\quad f(x^*) = -6961.81388$

2) Problem C2:

$$minf(x_1, x_2, x_3, x_4, x_5) = e^{x_1 x_2 x_3 x_4 x_5}$$

Subject to:

$$h_1(x) = x_1^2 + x_2^2 + x_3^2 + x_4^2 + x_5^2 - 10 = 0,$$
$$h_2(x) = x_2 x_3 - 5x_4 x_5 = 0,$$
$$h_3(x) = x_1^3 + x_2^3 + 1 = 0.$$

Search Space: $2.3 \le x_1, x_2 \le -2.3;\quad 3.2 \le x_3, x_4, x_5 \le -3.2$

Global minimum: $x^* = (-1.71714,\ 1.59571, 1.82724, -0.76364, -0.76364\ );$

$$f(x^*) = 0.0539498$$

3) Problem C3:

$$minf(x) = 5.3578547x_3^2 + 0.8356891x_1x_5 + 37.293239x_1 - 40792.141$$

Subject to:

$$h_1(x) = u(x) - 92 \le 0,$$
$$h_2(x) = -u(x) \le 0,$$
$$h_3(x) = v(x) - 110 \le 0,$$
$$h_4(x) = -v(x) + 90 \le 0,$$
$$h_5(x) = -w(x) + 20 \le 0,$$

where

$$u(x) = 85.334407 + 0.0056858x_2x_5 + 0.000626x_1x_4 - 0.0022053x_3x_5,$$
$$v(x) = 80.51249 + 0.007131x_2x_5 + 0.0029955x_1x_2 + 0.002183x_3^2,$$
$$w(x) = 9.300961 + 0.0047026x_3x_5 + 0.0012547x_1x_3 + 0.0019085x_3x_4.$$

Global minimum: $x^* = (78, 33, 29.9952, 45, 36.77581);\ f(x^*) = -30.665.539$

T6. BENCHMARK TEST CASES

T6.1. Design Optimization of Floating Offshore Wind Turbine Platform (FOWT)

Case Description:

FOWT is an effective means to utilize the vast space and wind resources in deep waters for generating electric power. However, the floating platform needs to be properly designed to

maintain a certain level of stability in the water and to prolong the operational life of the wind turbine. This section applies the new K-BA GO method to the FOWT design optimization application and also uses this application to test the search capability and performance of various GO search techniques. In this study, a ballast-stabilized platform with a deep draft, also called the spar buoy platform, as shown in Figure T - 1.

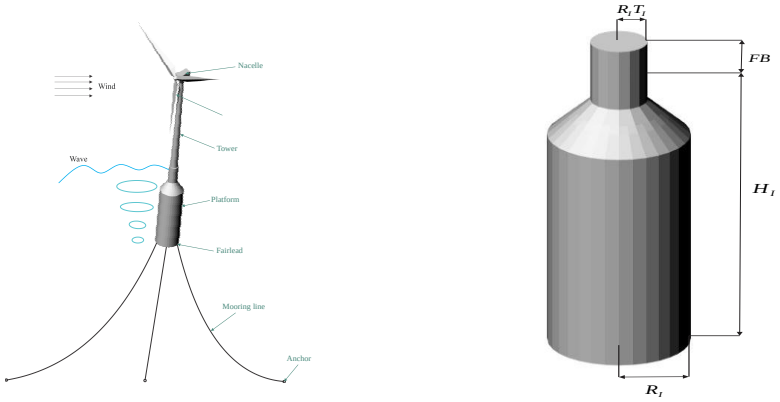

Figure T - 1FOWT

To evaluate the stability of the floating system in the given environmental condition, the linearized aerodynamic characteristics of the 5 MW wind turbine, and the linearized hydrodynamic characteristics of the platform and mooring line must be collected in a frequency domain dynamic model. The software tool FAST is used to calculate the linearized wind turbine mass, stiffness, and damping matrices for given wind speed. In addition, the platform added mass, damping and hydrostatics as well as mooring line stiffness are calculated using another design tool WAMIT and quasi-static mooring subroutine of the FAST, respectively. The linearity of the simplified dynamic system is exploited to define the response amplitude operator (RAO) of nacelle acceleration at each sea state condition based on the complex responses of the linearized frequency-domain equation of motion Eq. T6-30and T6-31.

$$-\omega^2 M_{total}(\omega)\hat{Z}(\omega) + i\omega B_{total}(\omega,\zeta)\hat{Z}(\omega) + C_{total}\hat{Z}(\omega) = \hat{X}(\omega) \qquad \text{(T6-30)}$$

$$[RAO_1(\omega) :: RAO_6(\omega)] = [-\omega^2 M_{total}(\omega) + i\omega B_{total}(\omega,\zeta) + C_{total}]^{-1}\hat{X}(\omega) \qquad \text{(T6-31)}$$

where, M_{total}, B_{total}, and C_{total} are the total mass matrix, damping matrix, and stiffness matrix of the FOWT respectively. $\hat{Z}(\omega)$ is the complex amplitude vector for the platform displacement and $\hat{X}(\omega)$ is the first-order wave excitation vector calculated by WAMIT. The complex form of nacelle acceleration *RAO* is given by Eq.T6-32. The performance metric for this study is defined as the standard deviation of nacelle acceleration Eq. T6-33.

$$\mathrm{RAO}_{a_{nac}}(\omega) = -\omega^2(\mathrm{RAO}_1(\omega) + \mathrm{RAO}_5(\omega)z_{nac}) \qquad \text{(T6-32)}$$

$$\sigma_{a_{nac}}(\omega) = \sqrt{\int_0^\infty |\mathrm{RAO}_{anac}(\omega)|^2 S(\omega)\,\mathrm{d}\omega} \qquad \text{(T6-33)}$$

where z_{nac} is the wind turbine hub height (90 m) and $S(\omega)$ is the spectral density of the waves at prescribed sea states. Note that $\mathrm{RAO}_{a_{nac}}(\omega)$ is the fore-aft response amplitude operator of nacelle acceleration and $\sigma_{a_{nac}}(\omega)$ is the standard deviation of this response.

In the current study, a number of design constraints are also applied to the objective function. To make sure about the stability of the platform and wind turbine, the standard deviation of the nacelle acceleration (performance metric) is limited to 1 m/s^2. Moreover, to avoid the over-turning of the platform, the steady-state pitch angle of the platform should be less than 10°. The expression of this constraint is given in the following equation.

$$\bar{\zeta}_5 = \frac{F_{hrust.z_{nac}} + M_{Mooring_5} - M_{ballast}}{\rho g \forall z_{CB} - M_t g z_{CG} + \rho g\, Ixx - C_{mooring_{5,5}} + C_{5,1} z_{\mathrm{fair}}} \qquad \text{(T6-34)}$$

where, F_{thrust} is the steady thrust load of the wind turbine, $M_{mooring5}$ is the mooring line pitching moment at the maximum wind turbine thrust; $M_{ballast}$ is the pitching moment due to stabilizing ballast mass; $\forall$ is the platform displacement; z_{CB} is the center of buoyancy location; M_t is the total mass of the system; z_{CG} is the center of gravity location; I_{xx} is the platform waterplane moment of inertia in pitch motion; $C_{mooring5,5}$ is the mooring lines stiffness in pitch motion; $C_{5,1}$ is the mooring line stiffness in pitch-surge motions; and z_{fair} is the fairlead depth in pitch motion.

The design optimization seeks the best performance of the wind turbine platform measured by the performance metric defined in Eq. T6-33 with respect to a number of key design variables: cylinder draft, H_I, cylinder radius, R_I, top tapper ratio, T_I, and a catenary mooring system, X_M. For the spar buoy platform, the freeboard (FB) of 5 m is considered. The mooring system design variable, X_M, defines three-angled taut line and slackline configurations for the spar buoy platform. The mass of support structure is determined using a wall thickness of 50 mm with a steel density of 8050 kg/m^3. Table T - 1 shows the comparison results.

Table T - 1 Geometric Design Variables of the Platform

Variable	Description	Min.	Max.
HI	Cylinder draft	2 m	150 m
RI	Cylinder radius	3 m	25 m
TI	Top taper ratio	0.2	2
XM	Mooring system	0	2

Case Results:

For this application, four decision variables were considered. Using this example application, the capability and the performance of the new K-BA method in solving real-life computationally expensive black-box optimization problems is demonstrated. The same optimization parameters were used with the population size set as 20. It can be seen from the statistical results presented in

Table T - 2 that the new K-BA method produced the best solution and with considerably lower NFE. The algorithm located the promising region with 100 NFE and quickly converged to the global optimum after only 480 NFEs, while the other four algorithms largely stopped at less accurate optima after 600 NFEs. The new K-BA also outperformed the original BA. The new K-BA algorithm has considerable robustness in handling the computationally expensive, real-life engineering application problem with consistent and reliable optimization results.

Table T - 2 Results of the Wind Turbine and Algorithm Performance

K-BA		BA		GA		SA		DE	
f^*	NFE	f^*	NFE	f^*	NFE	f^*	NFE	f^*	NFE
0.0012	540	0.0013	600	0.0013	600	0.0052	602	0.0013	600
x_1^*	149.7	x_1^*	147.5	x_1^*	148.1	x_1^*	148.1	x_1^*	149.1
x_2^*	23.98	x_2^*	23.95	x_2^*	23.58	x_2^*	24.11	x_2^*	23.68
x_3^*	0.30	x_3^*	0.19	x_3^*	0.38	x_3^*	0.31	x_3^*	0.29
x_4^*	1.97	x_4^*	1.92	x_4^*	1.89	x_4^*	1.37	x_4^*	1.71

T6.2. Generating Shortest Collision-free CNC Cutter Paths for Robotic Machining

Case Description:

Generation of shortest collision-free CNC Cutter Motion Paths for Robotic Machining/Inspection of Free-form Surfaces Using a Nested Global Optimization - In this case, the robot arm (RA) can be a rectangular parallelepiped (RP), cylinder, round table or cone, and the target object (TO) is a non-uniform rational basis spline (NURBS) surface. The shortest collision-free motion path can be obtained by the following steps.

(1) Give the beginning and ending locations of the RA.

(2) Select one dimension of the direction vector that is from the beginning location to the ending location. Give n locations that have the same interval with each other between the beginning and ending locations on this selected dimension.

(3) Each one from the n locations has the coordinate (x, y, z). Now, just two of them are regarded as variables. For example, if we have known the beginning and ending locations and then divide the interval between them on the dimension x, all the x coordinates of the n locations are confirmed. Hence, 2n design variables are defined.

(4) Construct the objective and constraint functions. The sum of the distances between the n locations is minimized and meanwhile, the RA on the n locations cannot touch the TO. The specific illustrations are shown in Figure T - 2.

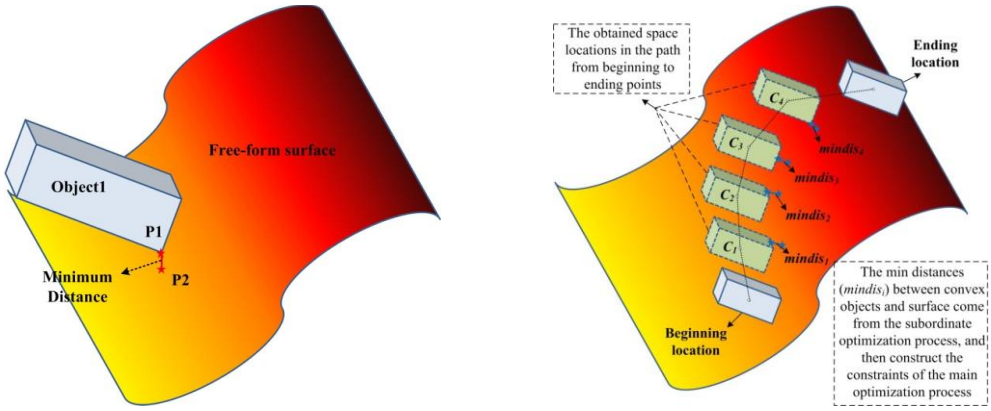

(a) subordinate optimization process (b) main optimization process

Figure T - 2 Generation of Shortest Collision-free Object Motion Path

The specific optimization expressions are formalized as follows.

The subordinate optimization is to calculate the minimum distance between the RA and TO.

$$Min\ dis = \|P_1(x_1, y_1, z_1) - P_2(x_2, y_2, z_2)\|$$

$$S.T. P_1 \in Object1 \quad P_2 \in Free\_form\ surface \tag{T6-35}$$

$$Here, dis = \sqrt{(x_1 - x_2)^2 + (y_1 - y_2)^2 + (z_1 - z_2)^2}$$

The main optimization is to get the shortest collision-free motion path.

$$Min\ Objective: Sum_{dis} = \sum_{i=0}^{n} \|C_i(x_i, y_i, z_i) - C_{i+1}(x_{i+1}, y_{i+1}, z_{i+1})\|$$

$$Nonlinear\ Constraints: Switch\ P(x, y, z)\ to\ p^i_{new}(x^i_{new}, y^i_{new}, z^i_{new})$$

$$mindis1 = Min(\ p^1_{new}(x^1_{new}, y^1_{new}, z^1_{new}) - Q(u, v, w)) \geq \varepsilon \tag{T6-36}$$

$$mindis2 = Min(\ p^2_{new}(x^2_{new}, y^2_{new}, z^2_{new}) - Q(u, v, w)) \geq \varepsilon$$

$$mindisn = Min(\ p^n_{new}(x^n_{new}, y^n_{new}, z^n_{new}) - Q(u, v, w)) \geq \varepsilon$$

$$Bound\ Constraints: C_i\ is\ in\ work\ space$$

In Eq. T6-36 , C_i is a location that the RA will move to, $mindis_i$ is the result of the subordinate optimization that is shown in Eq. T6-35 and Figure T - 2(a), and ε is a safety distance. In the main optimization process, design variables are the coordinates of C_i (y_i, z_i) that will be passed to the subordinate optimization program as translation coordinates. Since the subordinate optimization is carried out by global optimization, the main optimization process is an expensive optimization problem that includes expensive constraints.

Case Results:

The surrogate-based global optimization algorithm MSSR that can be found in this toolbox is used as the optimizer for the main optimization process. The specific results are shown in Figure T - 3 and Figure T - 4

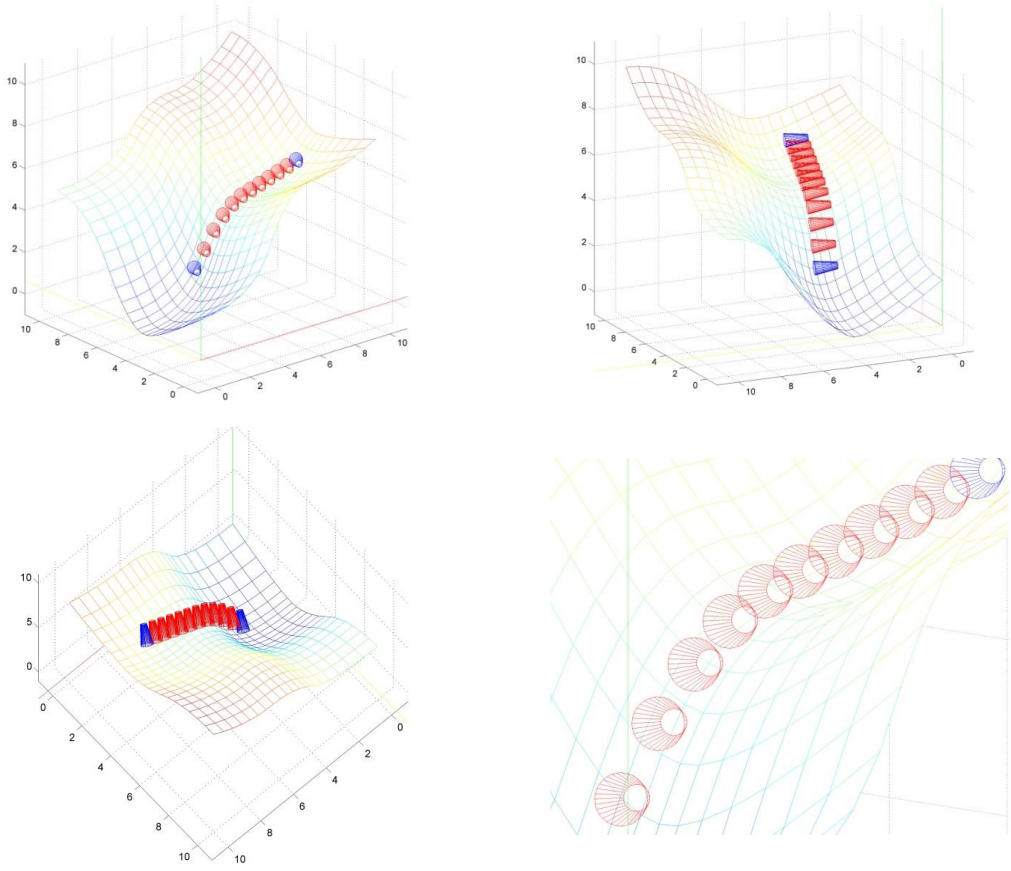

Figure T - 3 MSSR' results: Cylinder RA and NURBS TO with different viewing angles

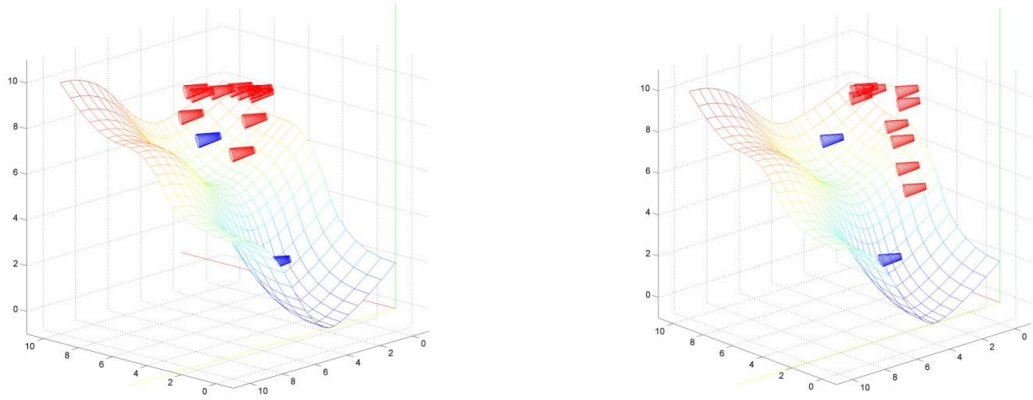

(a) GA's result on the same problem (b) GWO's result on the same problem

Figure T - 4 Comparison results with nature-inspired global optimization algorithms

The specific results of the three global optimization algorithms are listed in Table T - 3. It is clear that the surrogate-based global optimization algorithm MSSR is more appropriate than the nature-inspired global optimization algorithms, no matter on computational time or accuracy.

Table T - 3 Comparisons of three global optimization algorithms

Algorithms	Opt. values	CPU time/h	Iterations	NEFE	Feasible
GWO	14.3532	3.2731	30	1500	YES
GA	16.5328	3.8550	30	1550	YES
MSSR	6.8923	0.7228	30	154	YES

T6.3. Optimal Operation of Active Distribution Power Networks

Case Description:

Application and Comparison of Metaheuristic and New Metamodel Based Global Optimization Methods to the Optimal Operation of Active Distribution Network - As an imperative part of smart grids (SG) technology, the optimal operation of active distribution networks (ADNs) is critical to the best utilization of renewable energy and minimization of network power losses. However, the increasing penetration of distributed renewable energy sources with uncertain power generation and growing demands for higher quality power distribution are turning the optimal operation scheduling of ADN into complex and global optimization problems with non-unimodal, discontinuous and computation-intensive objective functions that are difficult to solve, constituting a critical obstacle to the further advance of SG and ADN technology. In this work, power generation from renewable energy sources and network load demands are estimated using probability distribution models to capture the variation trends of load fluctuation, solar radiation and wind speed, and probability scenario generation and reduction methods are introduced to capture uncertainties and to reduce computation. The Open Distribution System Simulator (OpenDSS) is used in modelling the ADNs to support quick changes to network designs and configurations. The optimal operation of the ADN is achieved by minimizing both network voltage deviation and power loss under the probability-based varying power supplies and loads. In solving the computation-intensive ADN operation scheduling optimization problem, several novel metamodel-based global optimization (MBGO) methods have been introduced and applied. A comparative study has been carried out to compare the conventional metaheuristic global optimization (GO) and MBGO methods to better understand their advantages, drawbacks and limitations, and to provide guidelines for subsequent ADN and smart grid scheduling optimizations. Simulation studies have been carried out on the modified IEEE 13, 33 and 123 node networks to represent ADN test cases. The MBGO methods were found to be more suitable for small- and medium-scale ADN optimal operation scheduling problems, while the metaheuristic GO algorithms are more effective in the optimal operation scheduling of large-scale ADNs with relatively straightforward objective functions that require limited computational time. This research provides a solution for ADN optimal operations and forms the foundation for ADN design optimization.

T6.4. Optimal Design of Integrated Energy Systems Using Nested Global Optimization

Case Description:

The case study is documented in one of our recent publication, "A Bi-Level Planning Approach for Integrated Energy Systems Incorporating Demand Response and Energy Storage under Uncertain Environment Using a Novel Metamodel Based Optimization Method". The planning of an integrated energy system (IES) is of great significance to promote the consumption of distributed renewable energy (DRE) and improve the overall energy efficiency of the energy system. With the increase of distributed generation (DG) penetration in IES, the power supply side and the load side of the IES are facing double high dimensional uncertainties, meanwhile, demand response (DR) and energy storage system (ESS) as important means of transferring energy across time intervals, have great potential for energy adjustment. However, the current IES planning method does not fully consider the uncertainties of DREs and loads, as well as the coordinated operation of DG-DR-ESS, which is far from optimal due to the large possible variations of system operations. In this paper, firstly, by considering the uncertainties of DREs and loads with the method of probability scenario, and taking full account of the coordinated operation and interaction of DG-DR-ESS under different configuration schemes, a bi-level stochastic scenario-based planning model for IES is established. In order to ensure the fast and efficient solution of the model, a two-stage iterative solution based on the newly metamodel based optimization method and the second-order cone optimization is proposed. The outer layer adopts the meta-model based optimization method to realize the fast solution of the black box and time-consuming optimization sizing model, the inner layer utilizes the second-order cone optimization to realize the quick solution of the optimal operation scheme for IES, the optimal planning capacity is then obtained through the interactive iteration of the two-layer model. The simulation has been carried out on an IES system modified from the IEEE 33-node distribution system. The simulation results show that the proposed method and model are effective.

T7. GLOBAL DESIGN OPTIMIZATION EXAMPLES

T7.1. Magnetorheological Brake Design

$$Minimize\ f(d) = k_w \frac{W}{W_{ref}} - k_t \frac{T_H}{T_{ref}}$$

where;

$$k_w + k_t = 1$$

subject to:

$$W < 150\ N, and\ \ d_{brake} < 240\ mm$$

T7.2. High-Efficiency EV/PHEV/EREV Electric Mode Operations

$$Maximize\ \ \eta = f(n, T, P_{MGB})$$

subject to:

$$0.8 \times P_{Battery\_Charging} \leq n \times T \leq -0.8 \times P_{Battery\_Discharging};$$

$$-P_{regen}(n_{MGB}) \leq P_{MGB} \leq P_{prop}(n_{MGB});$$

$$-P_{regen}(n_{RTM}) \leq P_{RTM} \leq P_{prop}(n_{RTM});$$

$$0 \leq n \leq 60$$

T8. LIST OF REVIEW PAPERS ON GLOBAL OPTIMIZATION

- Simpson T W, Peplinski J, Koch P N, et al. Metamodels for Computer-Based Engineering Design: Survey and Recommendations [J]. Engineering with Computers, 2001, 17(2): 129-150.
- Simpson T W, Booker A J, Ghosh D, et al. Approximation Methods in Multidisciplinary Analysis and Optimization: A Panel Discussion [J]. Structural and Multidisciplinary Optimization, 2004, 27(5): 302-313.
- Queipo N V, Haftka R T, Shyy W, et al. Surrogate-based analysis and optimization[J]. Progress in aerospace sciences, 2005, 41(1): 1-28.
- Wang G G, Shan S. Review of Metamodelling Techniques in Support of Engineering Design Optimization [J]. ASME Journal of Mechanical Design, 2007, 129(4): 370-380.
- Simpson T W, Toropov V, Balabanov V, et al. Design and Analysis of Computer Experiments in Multidisciplinary Design Optimization: A Review of How Far We Have Come or Not [C]. Victoria, BC, Canada: AIAA/ISSMO, 2008:1-22.
- Forrester A I J, Keane A J. Recent Advances in Surrogate-based Optimization [J]. Progress in Aerospace Sciences, 2009, 45: 50-79.
- Younis A, Dong Z. Trends, features, and tests of common and recently introduced global optimization methods[J]. Engineering Optimization, 2010, 42(8): 691-718.
- Shan S, Wang G G. Survey of modelling and optimization strategies to solve high-dimensional design problems with computationally-expensive black-box functions[J]. Structural and Multidisciplinary Optimization, 2010, 41(2): 219-241.
- Zang H, Zhang S, Hapeshi K. A review of nature-inspired algorithms[J]. Journal of Bionic Engineering, 2010, 7: S232-S237.
- Fister Jr I, Yang X S, Fister I, et al. A brief review of nature-inspired algorithms for optimization[J]. arXiv preprint arXiv:1307.4186, 2013.
- Haftka R T, Villanueva D, Chaudhuri A. Parallel surrogate-assisted global optimization with expensive functions–a survey[J]. Structural and Multidisciplinary Optimization, 2016, 54(1): 3-13.
- Liu H, Ong Y S, Cai J. A survey of adaptive sampling for global metamodelling in support of simulation-based complex engineering design[J]. Structural and Multidisciplinary Optimization, 2017: 1-24.

- Saad A E H, Dong Z, Karimi M. A Comparative Study on Recently-Introduced Nature-Based Global Optimization Methods in Complex Mechanical System Design[J]. Algorithms, 2017, 10(4): 120.

T9. SUMMARY

In summary, the Toolbox consists of three major components:

- Global optimization programs developed by our research team over the past years with a brief overview of the characteristics and unique capability of each of these programs and the research publications that present the algorithms behind and test results.
- Well-known and representative global optimization programs developed by other researchers, made available to us through open sources. Most of these programs have been tested and used as benchmarks in our previous research. We would like to acknowledge their contributions and willingness to share the codes.
- Special benchmark test cases and optimization application examples, which can be used to evaluate and compare the capability, performance and limitations of various global optimization algorithms and implementations.

REFERENCES

[1] J. Holland, in *Adaptation in Natural and Artificial Systems*, MIT, 1975.

[2] S., Kirkpatrick; C., Gelatt; M., Vecchi, "Optimization by Simulated Annealing," *Science*, pp. 671-680, 1983.

[3] J. Kennedy and R. Eberhart, "Particle Swarm Optimization," *Proceedings of IEEE International Conference on Neural Networks*, pp. 1942-1948, 1995.

[4] D. Jones, "The DIRECT Global Optimization Algorithm," *Encyclopedia of Optimization*, pp. 431-440.

[5] R. Storn; K. Price, "Differential evolution-- a simple and efficient heuristic for global optimization over continuous spaces," *Journal of global optimization*, pp. 341-359, 1997.

[6] S., Mirjalili; S. M., Mirjalili; A. Lewis, "Grey wolf optimizer," *Advances in Engineering Software*, pp. 46-61, 2014.

[7] G. Wang; Z. Dong; P. Aitchison, "Adaptive Response Surface Method-- A Global Optimization Scheme for Approximation--Based Design Problems," *Journal of Mechanical Engineering*, pp. 707-733, 2001.

[8] L., Wang; S. Shan; G., Wang, "Mode-Pursuing Sampling Method for Global Optimization on Expensive Black-Box Functions," *Engineering Optimization*, pp. 419-438, 2004.

[9] S. Shan; G. Wang, "An Efficient Pareto Set Identification Approach for Multi-objective Optimization on Black-Box Functions," *ASME*, pp. 866-874, 2005.

[10] A. Younis; Z. Dong, "Mixed Surrogate Models and Design Space Elimination Search Method for Global Optimization in Computation Intensive Designs," *Journal of Optimization theory and applications*, 2010.

[11] A. Younis; Z. Dong, "Metamodelling search using space exploration and unimodal region elimination for design optimization," *Engineering Optimization*, pp. 517-533, 2010.

[12] J. Gu; G. Y. Li; Z. Dong, "Hybrid and Adaptive Metamodel Based Global Optimization," *Engineering Optimization*, 2011.

[13] H. Dong; B. Song; Z. Dong, et. al., "Multi-start Space Reduction (MSSR) surrogate-based global optimization method," *Structural and Multidisciplinary Optimization*, 2016.

[14] H. Dong; B. Song; P. Wang; Z. Dong, "Surrogate-based optimization with clustering-based space exploration for expensive multimodal problems," *Structural and Multidisciplinary Optimiztaion*, 2017.

[15] R. B. Wilson, "A simplicial method for convex programming," *Harvard University*, 1963.

[16] A. Antoniou; W. S. Lu, Practical Optimization: Algorithms and Engineering Applications, Springer, 2007.

[17] A. Younis; Z. Dong, "Trends, Features, and Tests of Common and Recently Introduced Global Optimization Methods," *Engineering Optimization*, pp. 691-718, 2010.